BUREAU OF RECLAMATION

Technical Memorandum No. ENV-2021-001

West-Wide Climate and Hydrology Assessment




U.S. Department of the Interior

March 2021

Version 1.1

Mission Statements

The Department of the Interior (DOI) conserves and manages the Nation's natural resources and cultural heritage for the benefit and enjoyment of the American people, provides scientific and other information about natural resources and natural hazards to address societal challenges and create opportunities for the American people, and honors the Nation's trust responsibilities or special commitments to American Indians, Alaska Natives, and affiliated island communities to help them prosper.

The mission of the Bureau of Reclamation is to manage, develop, and protect water and related resources in an environmentally and economically sound manner in the interest of the American public.

Cover photographs (top left to right, bottom left to right): High alpine snowmelt flowing into a Western watershed; parched desert soil displaying increased drought across the West; a desert city representing increased populations in the West that augment demand for municipal and industrial water; irrigation water from a Reclamation Project supporting agriculture in Idaho.

BUREAU OF RECLAMATION

Technical Memorandum No. ENV-2021-001

West-Wide Climate and Hydrology Assessment

Primary Authors
Subhrendu Gangopadhyay, PE, PhD, Civil Engineer
Marketa McGuire, PE, Civil Engineer

Chapter 1
Subhrendu Gangopadhyay
Marketa McGuire
Avra Morgan

Chapter 2
Marketa McGuire
Subhrendu Gangopadhyay
In collaboration with:
Justin Martin
Greg Pederson
Connie Woodhouse
Jeremy Littell

Chapter 3
Subhrendu Gangopadhyay
Tom Pruitt
Marketa McGuire
In collaboration with:
Naoki Mizukami
Julie Vano
Ethan Gutmann
Andy Wood

Chapter 4
Subhrendu Gangopadhyay
Greg McCabe
Tom Pruitt
Brandon House

Chapter 5
Naresh Devineni
Upmanu Lall

Chapter 6
Marketa McGuire
Dan Broman
In collaboration with:
Lucas Barrett
Alan Butler
Jason Cameron
Melissa Estep
Scott Fennema
Jennifer Johnson
Jessie Khaya
Dagmar Llewellyn
Nancy Parker
James Prairie

Chapter 7
Justin Huntington
Chris Pearson
Dan Broman
Mark Spears

Chapter 8
Lindsay Bearup
Kristin Mikkelson
Subhrendu Gangopadhyay
In collaboration with:
Fred Tillman

Chapter 9
Marketa McGuire
Julie Vano
Rebecca Smith
Subhrendu Gangopadhyay

Bureau of Reclamation Technical Writer/Editor

Jesselyn Hamilton

Bureau of Reclamation Reviewers and Contributors in Alphabetical Order

Patrick Erger, Jen Johnson, Jobaid Kabir, Dagmar Llewellyn, Jeff Niehaus, Kenneth Nowak, James Prairie, David Raff, Eric Rothwell, Katie Schultz, Rebecca Smith, Jade Soddell, Mike Tansey, Jack Truax, Sophie Wilderotter

External Reviewers and Contributors in Alphabetical Order

Jeff Arnold, U.S. Army Corps of Engineers

Michelle Bushman, Western States Water Council

Rob Cifelli, National Oceanic and Atmospheric Administration

Naresh Devineni, City University of New York

Chris Frans, U.S. Army Corps of Engineers

Tim Green, U.S Department of Agriculture, Agricultural Research Service

Ethan Gutmann, National Center for Atmospheric Research

Steven Hostetler, U.S. Geological Survey

Justin Huntington, Desert Research Institute

Shih-Chieh Kao, Oak Ridge National Laboratories

Upmanu Lall, Columbia University

Patrick Lambert, U.S. Geological Survey

Jeremy Littell, U.S. Geological Survey

Justin Martin, U.S. Geological Survey

Greg McCabe, U.S. Geological Survey

Naoki Mizukami, National Center for Atmospheric Research

Chris Pearson, Desert Research Institute

Greg Pederson, U.S. Geological Survey

Adam Terando, U.S. Geological Survey

Fred Tillman, U.S. Geological Survey

Julie Vano, Aspen Global Change Institute

Andy Wood, National Center for Atmospheric Research

Connie Woodhouse, University of Arizona

Executive Summary

This 2021 West-Wide Climate and Hydrology Assessment (2021 Assessment) is the technical companion document to the Bureau of Reclamation's (Reclamation) 2021 SECURE[1] Water Act Report to Congress. The 2021 Assessment investigates changes in climate and hydrology across the West using approaches that align with Reclamation's 2011 and 2016 SECURE Water Act Reports and new techniques, data, and analyses that provide a broader assessment of future hydroclimate changes to support water management in the West. This work is performed by Reclamation's Technical Service Center in partnership with the United States Geological Survey (USGS), University of Arizona, Columbia University, Desert Research Institute, National Center for Atmospheric Research, Aspen Global Change Institute, and in collaboration with Reclamation regions and area offices.

The climate change analysis in the 2021 Assessment provides estimates of changes in temperature, precipitation, snowpack, and streamflow across the West using consistent methodology, including using statistically downscaled projections from the Coupled Model Intercomparison Project Phase 5 (CMIP5) climate model archive. The analysis approach to estimate changes for these hydroclimate variables followed methods similar to the 2011 and 2016 SECURE Water Act Reports. However, for the 2021 Assessment, additional data were used, and analyses performed to provide an assessment of hydroclimate changes to support water management in the West. Specifically, the following data and analyses are the newer aspects in the 2021 Assessment:

- Use of statistically downscaled CMIP5 projections for Representative Concentration Pathway (RCP) 4.5 ("lower scenario") and RCP8.5 ("higher scenario") developed using the LOcalized Constructed Analogs (LOCA) method (in short, CMIP5-LOCA) in the hydroclimate analysis.
- Use of paleohydrologic ("paleo") data—reconstructed streamflow and reconstructed drought index.
- Projections of drought index using the CMIP5-LOCA downscaled climate projection data.
- West-wide drought analysis with paleo-reconstructed and projected drought index data spanning 1473 to 2099.
- Data-driven reservoir performance risk quantification for five Reclamation reservoirs over a range of paleo-periods and recent historical periods.

[1] SECURE is the acronym for Science and Engineering to Comprehensively Understand and Responsibly Enhance.

- Planning and operations model-driven reservoir performance risk quantification over a range of paleo-period drought events and recent historical drought events on managed river systems in Reclamation's eight major river basins.
- Recent historical and future turfgrass water demands for major urban areas in the West.
- A synthesis of impacts of climate on groundwater recharge and discharge for eight case study areas.

This report is organized with the following chapters describing the data and analysis performed as part of the 2021 Assessment:

- Chapter 2: Background on the global climate projections used in the study, including the downscaled future climate projections, future hydrologic projections, and paleohydrology scenarios presented in this report.
- Chapter 3: Analysis of hydroclimate projections in the eight major Reclamation river basins, focused on annual climate projections and decadal changes in temperature and precipitation, April 1st snowpack, and mean monthly and mean seasonal runoff specific to each basin.
- Chapter 4: Analysis of the variability and characteristics of drought (duration, severity, and frequency) for historical (1473 to 2005) and future (2006 to 2099) projected climate conditions across the Western United States.
- Chapter 5: Quantification of risks to reservoir performance using drought indices that consider estimates of water demands and inflows into selected major reservoirs across the Western United States, including an implicit consideration of the reservoir operating rules used to approximate demands. The following five Reclamation reservoirs were studied: American Falls, Canyon Ferry, Lake Powell, Millerton Lake, and Shasta Lake.
- Chapter 6: Using consistent methodology, evaluation of observed historical drought events and drought events identified in paleo-reconstructed timeseries of streamflow (hereafter referred to as paleo droughts) on managed river systems in Reclamation's eight major river basins. Insights of system performance from the CMIP5-LOCA hydrology are also discussed.
- Chapter 7: Estimates of recent, historical, and future turfgrass water demands for major urban areas in the Western United States, as a complement to estimates of historical and future agricultural irrigation water demands developed in 2015 (Reclamation, 2015a).
- Chapter 8: Synthesis of impacts of climate change on groundwater recharge and discharge and summary of findings from recent studies conducted by Reclamation.
- Chapter 9: Uncertainties in the analysis presented throughout Chapters 2 through 8 and how these analyses may support risk-informed water management and planning even with associated uncertainties.

- Based on the data and analyses conducted across the chapters, the following are the key findings:
- Future projections show temperatures will continue to increase (see Chapter 3).
- Average annual precipitation is projected to increase in the north, particularly in the Columbia and Missouri River Basins, and decline in the south.
- Snow storage, as measured by snow water equivalents (the amount of water in snowpack) is projected to decline, with only a few locations showing some increases, likely due to increased precipitation.
- Climate model projections indicate an increase in average drought duration and an increase in the variability of drought duration for most of the Western United States in the future (see Chapter 4).
- Climate models also project future increases in average drought severity and in the variability of drought severity for most of the Western United States.
- The probability of severe drought is generally much higher in the paleohydrologic reconstructions than in the instrumental period for some of the reservoirs studied. However, given the high minimum active storage pool of the reservoirs selected for this study, the ability of the systems to avert a drought impact based on a prior reservoir refill cycle still relatively high in all of the five reservoirs studied (see Chapter 5).
- Analysis using water resources system models across the eight major Reclamation river basins showed the following (see Chapter 6):
    - In the Boise River basin, the paleo droughts were much more severe than the observed historical droughts. Future drought projections indicate the possibility of more severe, but shorter duration events as compared to the paleo events, or longer, but less severe events.
    - In the Klamath River Basin, the extended drought in the first half of the 1900s remains the most impactful drought when looking at historical and paleo droughts considered in this report. According to the analysis performed in this report, droughts of greater severity and of longer duration than those in the historical and paleo-reconstruction period are possible in the future.
    - In the Missouri River Basin, projected future droughts are generally comparable to the observed historical and paleo events, but suggest the possibility of moderate, but extremely long duration events.
    - In the Rio Grande Basin, future drought projections suggested droughts of greater severity and longer duration than any of the observed historical or paleo events.
    - In the Sacramento and San Joaquin River Basins, projected future droughts are generally of equal severity to observed historical or paleo events, but of greater length, or alternatively shorter in length and more severe.

  - In the Truckee River Basin, projected future droughts are generally comparable to observed historical or paleo events; however, longer duration droughts are possible.

- Projections of future evapotranspiration and net irrigation water requirements for urban turfgrass throughout the Western United States show substantial increases in water demands in the future. Sixty-eight urban demand areas were selected, and detailed results for specific seasonal turfgrass types covering a broad range of hydroclimates are given for three selected urban areas—Las Vegas, Nevada; Los Angeles, California; and Denver, Colorado (see Chapter 7).
- West-wide analyses of climate change impacts to groundwater recharge and discharge is not available, and only site-specific findings are documented in Chapter 8. However, for the Colorado River Basin—Upper Colorado River Basin and Lower Colorado River Basin—results from a multi-year collaboration effort with the USGS are available. This analysis was completed using the CMIP5 projections that were statistically downscaled using the Bias Correction and Spatial Disaggregation (BCSD) method. The key findings include:
  - Recharge projections in the Upper Colorado River Basin have considerable spatial heterogeneity throughout the basin and are seasonally variable.
  - With the combined projections of increased temperature (and increased evapotranspiration) and decreased precipitation, groundwater recharge is projected to be substantially less than historical levels in the Lower Colorado River Basin.

Drought analyses combined with projections of future hydroclimate conditions suggest that, overall, drought severity and duration will increase across the West in the coming century. However, in many locations in the West, variability in drought conditions will also increase, as climatic conditions evolve. Collectively, the impacts of climate change on water resources present challenges to operating Reclamation facilities to meet growing demands for water and hydropower now, and to upgrading and maintaining infrastructure to support operations in the future. The 2021 Assessment was conducted with a goal of providing quantitative information using diverse datasets (paleohydrologic, instrumental, and climate projections) to support future water management decisions across the West.

Acronyms and Abbreviations

AOP	Annual Operation Planning
ARBS	American River Basin Study
ASCE	American Society of Civil Engineers
ASCE-PM	American Society of Civil Engineers – Environmental and Water Resources Institute Standardized Penman-Monteith method
BCM	Basin Characterization Model
BCSD	Bias Correction and Spatial Disaggregation or bias-corrected and spatially downscaled
BIC	Bayesian Information Criteria
CA-DWR	California Department of Water Resources
CCWSC	Clark Canyon Water Supply Company
CD	cumulative deficit
CDD	Carson Division water demand of the Newlands Project
cfs	cubic feet per second
CMIP	Coupled Model Intercomparison Project (CMIP3 and CMIP5 are CMIP phases 3 and 5, respectively)
CO_2	carbon dioxide
CONUS	Contiguous United States (the United States excluding Alaska and Hawaii)
CRSS	Colorado River Simulation System
CVP	Central Valley Project
DCHP	Downscaled Climate and Hydrology Projections
deg F	degrees Fahrenheit
Delta	Sacramento-San Joaquin Rivers Delta
DMDU	decision making under deep uncertainty
DOE	Department of Energy
DOY	day of year
ET	evapotranspiration
ETact	evapotranspiration actual

ETbas	basal evapotranspiration
ETc	crop evapotranspiration
ETo	reference evapotranspiration based on the 0.12-meter cool season, clipped grass reference
EX	excess
exp	exponential (probability distribution)
FAO	Food and Agricultural Organization of the United Nations
FSID	Fort Shaw Irrigation District
gamma	gamma (probability distribution)
GCM	Global Climate Model
GH	Gumbel-Hougaard
GHG	Greenhouse Gas
GID	Greenfields Irrigation District
GIS	Geographic Information System
gumbel	Gumbel (probability distribution)
HCDN	Hydro-Climatic Data Network
HDe	ensemble-informed hybrid Delta (climate projection method)
HSPF	Hydrologic Simulation Program-Fortran
HUC	Hydrologic Unit Code
HUC-8s	Hydrologic Unit Code (eight digit) watershed boundaries
IPCC	Intergovernmental Panel on Climate Change
KBPM	Klamath Basin Planning Model
Kc	total crop coefficient curve
Kcb	basal crop coefficient
Ke	soil water evaporation coefficient
km	kilometer
KRBS	Klamath River Basin Study
LCRB	Lower Colorado River Basin
llog	log-logistic (probability distribution)
lnorm	log-normal (probability distribution)

LOCA	LOcalized Constructed Analogs
logis	logistic (probability distribution)
LSOCM	current end-of-month storage objective at Lahontan Reservoir
MACA	Multivariate Adaptive Constructed Analogs
MAF	million acre-feet
MODFLOW	United States Geological Survey Modular Ground-Water Flow Model
MODFLOW-NWT	Newton-Raphson formulation for MODFLOW (version 2005)
MODFLOW-OWHM	One-Water Hydrologic Model
mph	miles per hour
MTOM	Mid-Term probabilistic Operations Model
NARCCP	North American Regional Climate Change Assessment Program
NASA	National Aeronautics and Space Administration
NCA	National Climate Assessment
NCA4	Fourth National Climate Assessment
NIWR	net irrigation water requirements
NLDAS	North American Land Data Assimilation System
NOAA	National Oceanic and Atmospheric Administration
norm	normal (probability distribution)
NRCS	Natural Resources Conservation Service
PCA	Principal Component Analysis
PDFs	Probability Density Functions
PDSI	Palmer Drought Severity Index
PGMs	plant growth models
PM	Penman-Monteith (method of calculating evapotranspiration)
PM ETo or PMeto	Penman-Monteith reference evapotranspiration
PPT	precipitation
PRBM	Paso Robles Basin Model

PRIHM	Paso Robles Integrated Hydrologic Model
PRISM	Parameter-elevation Regressions on Independent Slopes Model
PRMS	Precipitation-Runoff Modeling System
q (lb/lb)	q is specific humidity, in pound of water per pound of dry air
RCP	Representative Concentration Pathways
RDD	Reservoir Drought Duration
RDI	Reservoir Drought Index
RDR	Reservoir Drought Recovery
RDS	Reservoir Drought Severity
Reclamation	Bureau of Reclamation
RED	Reservoir Excess Duration
REF	Reservoir Excess Fill-up
RMJOC	River Management Joint Operating Committee
Rs (ly/day)	solar radiation (Langleys per day)
SCRBS	Salinas and Carmel Rivers Basin Study
SECURE	Science and Engineering to Comprehensively Understand and Responsibly Enhance
SECURE Water Act	The 2009 Omnibus Public Land Management Act of 2009 (Public Law 111-11), Subtitle F of Title IX of the Act
SNWA	Southern Nevada Water Authority
SPARROW	SPAtially Referenced Regression On Watershed attributes
SVIHM	Salinas Valley Integrated Hydrologic Model
SVWM	Salinas Valley Watershed Model
SWA	SECURE Water Act
SWB	Soil Water Balance
SWE	Snow Water Equivalent
Tmean (F)	mean temperature (degrees Fahrenheit)
TROA Operations Model	Truckee River Operating Agreement Operations Model
TSC	Technical Service Center
UCRB	Upper Colorado River Basin

UMBIA	Upper Missouri Basin Impacts Assessment
URGWOM	Upper Rio Grande Water Operations Model
U.S.	United States
USGCRP	United States Global Change Research Program
USGS	United States Geological Survey
VIC	Variable Infiltration Capacity (hydrologic model)
WaterSMART	Water (Sustain and Manage America's Resources for Tomorrow)
WCRP	World Climate Research Programme
weibull	Weibull (probability distribution)
West	Western United States
WRIMS model engine, or WRIMS	Water Resource Integrated Modeling System
WWCRA	West-Wide Climate Risk Assessments
WWRA	West-Wide Risk Assessment
W/m^2	Watts per square meter
°	degree
°F	degrees Fahrenheit
%	percent
2021 Assessment	2021 West-Wide Climate and Hydrology Assessment (companion document to 2021 SECURE Water Act Report to Congress; this report)

Table of Contents

Figures

Tables

1 Introduction

The Bureau of Reclamation (Reclamation), established in 1902, is best known for the dams, powerplants, and canals it constructed within the 17 Western States of the United States. Reclamation's mission is to manage, develop, and protect water and related resources in an environmentally and economically sound manner in the interest of the American public. As the largest manager and wholesaler of Western water in the Nation, Reclamation has a responsibility to consider potential risks to water supplies, and to help implement measures that ensure water will be managed as effectively and sustainably as possible.

A growing risk to effective water management in the Western United States is climate change. In recent decades, climate science has highlighted a broad suite of future challenges for managing water, in addition to risks already posed by natural variations in climate and pressures associated with growing populations. These challenges include impacts to water supplies, water demands, and environmental conditions that may affect Reclamation's ability to fulfill its mission. In light of these challenges, Reclamation is working with its partners in the West to identify appropriate forward-looking adaptive actions that add resiliency and reliability to water management planning and practices.

The Omnibus Public Land Management Act of 2009 (Public Law 111-11) was enacted on March 30, 2009. Subtitle F of Title IX of that legislation, known as the SECURE[2] Water Act, recognizes that climate change poses a significant challenge to the protection of adequate and safe supplies of water, which are fundamental to the health, economy, security, and ecology of the United States. Section 9503 of the SECURE Water Act authorizes Reclamation to coordinate and partner with others to ensure the use of best available science; assess specific risks to water supply; analyze the extent to which water supply risks will impact various water-related benefits and services; develop appropriate mitigation strategies; and monitor water resources to support these analyses and assessments.[3]

Section 9503 (Reclamation's Climate Change and Water Program) authorizes Reclamation to assess climate change risks for water and environmental resources in the eight major Reclamation river basins. Section 9503 also includes the authorities to evaluate potential climate change impacts on water resource management, and to develop strategies to either mitigate for or adapt to impacts. The eight major Reclamation river basins listed within the SECURE Water Act include the Colorado, Columbia, Klamath, Missouri, Rio Grande, Sacramento, San Joaquin, and Truckee River Basins. The SECURE Water Act also directs Reclamation to submit reports to Congress 2 years after enactment and every 5 years thereafter to describe progress in carrying out those activities. This 2021 West-Wide Climate and Hydrology Assessment (2021

[2] SECURE is the acronym for Science and Engineering to Comprehensively Understand and Responsibly Enhance.

[3] The SECURE Water Act also authorizes the Department of Energy (Section 9505) and the Department of the Interior's United States Geological Survey (Sections 9507 and 9508) to assess and report on the impacts of climate change on national hydropower production and water data enrichment, respectively.

Assessment, or this report) is the technical companion document to the 2021 SECURE Water Act Report to Congress.

1.1 Reclamation's WaterSMART Programs and Activities Addressing the SECURE Water Act

WaterSMART (Sustain and Manage America's Resources for Tomorrow) was established in February 2010 by the Department of the Interior as a broad framework for Federal collaboration with States, Tribes, local governments, and non-governmental organizations to work toward a secure and sustainable water supply. Reclamation has implemented the climate change adaptation activities authorized under Section 9503 of the SECURE Water Act through the Basin Study Program, which is part of WaterSMART and supports President Biden's new Executive Order on Tackling the Climate Crisis at Home and Abroad.

The Basin Study Program includes a set of complementary activities that represent a comprehensive approach to incorporate the best available science into planning activities for climate change adaptation:

- **Basin Studies** – Reclamation partners with basin stakeholders to conduct comprehensive basin studies to define options for meeting future water demands in river basins in the West where imbalances in supply and demand exist or are projected as a result of climate change or other stressors. In response to the identified imbalances, the basin studies assess options and strategies for meeting future water demands. Partners can build on completed basin studies through Water Management Options Pilots to conduct deeper analysis of adaptation strategies, incorporate new science and data, or otherwise expand the analysis in the completed basin study.
- **West-Wide Risk Assessments (WWRAs)** – Through the WWRA activity, Reclamation develops key data on climate-induced risks and impacts to Reclamation's operations. Specifically, Reclamation has developed surface water hydrologic projections over the Western United States from contemporary climate projections. These projections provide risk assessment information for metrics described in the SECURE Water Act 9503(b)(2), including climate change risks to snowpack, changes in the timing of streamflow, and changes in the quantity of runoff. These data provide a foundation for future basin studies, as well as for project-specific applications and planning activities. Reclamation also coordinates with the United States Geological Survey (USGS), National Oceanic and Atmospheric Administration (NOAA), National Aeronautics and Space Administration (NASA), Department of Energy (DOE), and the Natural Resources Conservation Service (NRCS) on climate activities through the WWRA Implementation Team.
- **Applied Science Tools** – Reclamation also provides Basin Study Program funding on a competitive basis for projects to develop modeling, forecasting, and data-related tools to improve water management and operations. Funding is available for projects by non-

Federal entities and, separately, for projects by Reclamation staff that support technical capacity through the development of applied science tools and information.

- **Reservoir Operations Pilots** – Through Reservoir Operations Pilots, Reclamation identifies potential improvements to reservoir operations through the evaluation of operating alternatives and use of improved forecasts and modeling tools.
- **Science and Technology Program** – Reclamation is also actively engaged with research partners to develop and share information for a common understanding of climate change impacts to water resources in the West. The Science and Technology Program is a Reclamation-wide competitive, merit-based applied research and development program focused on innovative solutions for water and power challenges in the Western United States. Reclamation partners with the U.S. Army Corps of Engineers, USGS, NOAA, and others to identify mutual science needs for short-term water management decisions and long-term planning. These programs are fundamental to developing new information for adapting to climate change by assessing the current state of knowledge, identifying where gaps exist, and finding opportunities to address those gaps.

1.2 The 2011 SECURE Water Act Report

In 2011, Reclamation published the initial SECURE Water Act Section 9503(c) – Reclamation Climate Change and Water 2011 Report to Congress (Reclamation, 2011a). That report assessed climate change risks and how those risks could impact water operations, hydropower, flood control, and fish and wildlife in the Western United States. It represented the first consistent (with respect to methodology of analysis across the West) and coordinated assessment of risks to future water supplies across the eight major Reclamation river basins and identified several increased risks to water resources in the Western United States during the 21st century. The report noted that projected changes in temperature and precipitation are expected to impact the timing and quantity of streamflow in all Western river basins, which would impact the amount of water available for farms and cities, hydropower generation, fish and wildlife, and other uses, such as recreation.

1.3 The 2016 SECURE Water Act Report

The 2016 SECURE Water Act Report to Congress built upon the 2011 report and used the World Climate Research Programme (WCRP) global climate projections developed through its Coupled Model Intercomparison Project (CMIP), which are released roughly every 5 to 7 years. The companion technical assessment to the 2016 SECURE Water Act Report, the West-Wide Climate Risk Assessment, relied upon the most current climate projections featured in the Intergovernmental Panel on Climate Change's (IPCC) Fifth Assessment, which were developed as part of the WCRP CMIP Phase 5 and are referred to here as CMIP5 Projections.

1.4 The 2021 SECURE Water Act Report

This 2021 Assessment provides projections of future water supplies in the eight major Reclamation river basins listed in the SECURE Water Act, characterized in a manner consistent with the approach used in the 2016 SECURE Water Act Report. The evaluation includes an assessment of future climate conditions over the basin (i.e., precipitation and temperature), as well as the surface water hydrologic response (i.e., snow water equivalent, or the water available from snowpack) and runoff.

Reclamation operators and planners rely on information about temperature, precipitation (rainfall and snowfall), snowpack, streamflow, water demands, and groundwater to make informed decisions. As such, assessments of how these measures may change in the future are important to enable appropriate risk-informed decision-making, particularly in warmer, wetter, and drier periods. In 2011, and again in 2016, Reclamation conducted West-wide assessments of future temperature, precipitation, snowpack, and runoff changes.

Building on these prior efforts, Reclamation's 2021 Assessment provides supporting material for the 2021 SECURE Water Act Report using several complementary approaches that align with previous work and also promote innovations that allow a broader assessment of future change. Where appropriate, this report summarizes how hydroclimate projections developed since the 2016 Assessment align with previous projections. The 2021 Assessment was performed by Reclamation's Technical Service Center in partnership with the USGS, University of Arizona, Columbia University, Desert Research Institute, National Center for Atmospheric Research, Aspen Global Change Institute, and in collaboration with Reclamation Regions and Area Offices.

In this climate and hydrology assessment, in addition to using projections of future climate, Reclamation also incorporated paleohydrology to inform long-term planning. Paleohydrology uses tree-ring reconstructions of hydroclimate variables (e.g., precipitation, temperature, streamflow, etc.) to understand wet and dry conditions centuries before instrumentations (e.g., streamflow gages) were installed. As such, paleohydrology provides tools for water managers that complement and add value to contemporary projections of future climate and hydrology.

In particular, paleohydrology analysis provides new consistent information to water managers on the likelihood of drought. The term consistent refers to the same methodology across the Western United States. This is especially useful as instrumental records (stream gages), going back only a hundred years in most cases, capture a limited number of extreme events and may not contain the full range of variability (droughts and wet periods) that has occurred over past centuries. Using a longer record based in paleohydrology informs water managers whether droughts of the distant past were similar to or more severe than observed droughts. For example, as shown in the Colorado River Basin Study, paleohydrology reveals droughts hundreds of years ago (e.g., in the 1500s) that are more severe than any in the observed record. A longer record of past droughts can inform water managers about the types of droughts, and level of risk, to

consider in planning studies and can complement the use of future projections of how climate change may impact drought severity and duration.

Paleohydrology has been useful in informing water management and planning in watersheds as explored in earlier studies supported by Reclamation's WaterSMART Basin Studies Program, including the Colorado River Basin Water Supply and Demand Study (Reclamation, 2012b), the Upper Missouri Basin Impacts Assessment and Basin Study (Reclamation, 2018), and the Reservoir Operations Pilot Study for the Washita Project (Reclamation, 2018), among others. Further analysis of paleohydrology in other Reclamation basins and as a West-wide analysis allows water managers greater access to paleohydrology information, providing a longer history and consistent approach to evaluate risks with greater perspective across the entire West. New insights are shared in the West-wide Drought Analyses (spatial maps) and Water Supply Reliability Assessment chapters. Refer to Chapter 2 for a detailed discussion of the types of information leveraged and developed for the 2021 Assessment.

1.5 Report Organization

The focus of this report is to describe the development of hydroclimate projections and to provide a summary evaluation of climate change implications for water management in the eight major Reclamation river basins listed in the SECURE Water Act. The report is organized as follows:

Chapter 2 provides background on the global climate projections used in the study, including the downscaled future climate projections, future hydrologic projections, and paleohydrology scenarios presented in this report.

Chapter 3 presents an analysis of hydroclimate projections in the eight major Reclamation river basins. The overview focuses on annual climate projections and the decadal changes in temperature and precipitation, April 1st snowpack, and mean monthly and mean seasonal runoff specific to each basin.

Chapter 4 presents analyses of the variability and characteristics of drought (duration, severity, and frequency) for historical (1473 to 2005) and future (2006 to 2099) projected climate conditions across the Western United States.

Chapter 5 presents an approach to quantify reservoir performance risk using drought indices that consider estimates of water demands and inflows into five selected major reservoirs across the Western United States, including an implicit consideration of the reservoir operating rules used to approximate demands.

Chapter 6 presents a consistent West-wide evaluation of observed historical drought events and drought events identified in paleo-reconstructed timeseries of streamflow on managed river systems in Reclamation's eight major river basins. Insights of system performance from the CMIP5-LOCA hydrology are also discussed.

Chapter 7 provides estimates of historical and future turfgrass water demands for major urban areas in the Western United States as a complement to estimates of historical and future agricultural irrigation water demands developed in 2015 (Reclamation, 2015a).

Chapter 8 synthesizes impacts of climate on groundwater recharge and discharge and summarizes findings from recent studies conducted by Reclamation over approximately the last 5 years.

Chapter 9 summarizes uncertainties in the analysis presented throughout Chapters 2 through 8 and outlines how these analyses may support risk-informed water management and planning, even with associated uncertainties.

2 Background

This chapter describes the types of information leveraged and developed for the 2021 Assessment. This includes observed historical information, future hydroclimate projections using downscaled global climate model simulations, and paleohydrology information in the form of annual streamflow reconstructions. Further, an available gridded reconstruction of PDSI was used and compared against future projections of PDSI based upon downscaled climate projections.

2.1 Downscaled Global Climate Projections

Global Climate Models (GCMs) aim to simulate fundamental physical laws based on mass, energy, and momentum conservation in the coupled land-atmosphere-ocean system. Governing equations of these physical processes are solved numerically to provide a time evolution of state variables representing the Earth's climate. These simulations require vast computational resources. Thus, in practice, GCM simulations are performed at horizontal computational grid resolutions (about 100 kilometers (km)) that are nearly an order of magnitude greater than the spatial scale of interest for most regional climate impacts assessments (e.g., about 10 km or finer). Among other factors, the simulation of physical processes at a coarse spatial resolution leads to systematic discrepancies in comparisons between simulation results and observations. In order to obtain credible simulations of variables relevant to a climate impacts assessment, such as precipitation and temperature, among others, it is necessary to reduce or eliminate such model discrepancies.

Projections of future climate conditions have been developed by the climate modeling community using a wide range of GCMs forced with emissions scenarios. The emission scenarios encapsulate possible future trajectories of global greenhouse gas emissions and the corresponding atmospheric composition. The World Climate Research Programme established the Coupled Model Intercomparison Project (CMIP) in 1995 to facilitate broad analysis and application of GCMs. The CMIP framework provides standards for modeling and guidelines for comparing GCM results developed by the climate modeling community. The GCM simulations performed within the CMIP framework form the basis for periodic global and national climate impacts assessments. Examples of such climate impact assessments include the ones conducted by the Intergovernmental Panel on Climate Change, specifically the Third, Fourth, and Fifth Assessment Reports (IPCC 2001, 2007, and 2014). An example of a national assessment is the National Climate Assessment conducted every 4 years by the United States Global Change Research Program (USGCRP). In 2017, the USGCRP released the Fourth National Climate Assessment (NCA4). The USGCRP is mandated by Congress to coordinate Federal research and investments to understand the forces shaping the global environment.

To date, the contemporary climate assessments mentioned above use GCM-based climate projections from two CMIP phases: (1) CMIP Phase 3 (CMIP3) multi-model dataset completed in 2007, and (2) CMIP Phase 5 (CMIP5) multi-model dataset completed in 2013. Modeling experiments using CMIP Phase 6 (CMIP6) are currently underway.

For this report, no variables from these or other future climate projections were used directly from GCMs at their native geospatial scales. Because the GCMs are run to simulate climate over the whole Earth for 100 years or more, their geospatial scales are large—on the order of 100 to 200 km on a grid side. These native-scale outputs must be post-processed to make them useful at the finer spatial and temporal scales (e.g., daily) where assessment questions mostly arise.

The coarse GCM outputs must be downscaled to a spatial scale that is appropriate for impact assessment studies and to correct for inherent biases in GCM outputs. The downscaling process is a current area of active research, and there is a continuum of downscaling methods ranging from statistical approaches to physically oriented dynamic modeling methods. The climate projections used in the hydroclimate analysis for this report were derived from GCM projections that were downscaled using a statistical method referred to as LOcalized Constructed Analogs (LOCA) method of empirical-statistical downscaling (Pierce et al., 2014). In this approach, regional climate patterns are translated to local-scale through regional pattern matching. In regional pattern matching, the best-matching historical days (e.g., 30 days) are identified as compared to coarsened observations and they are used to describe the local scale spatial relationship for each grid point being downscaled. In addition, LOCA selects the single best analog based on the nearest grid cells from a pool of analogs selected based on the larger regional pattern. The CMIP5-LOCA projection set provides the primary source of downscaled projections presented in the Fourth National Climate Assessment (USGCRP, 2018) and Fourth California State Climate Assessment (Pierce et al., 2018).

The West-Wide Climate Risk Assessment of the 2016 SECURE Water Act Report (Reclamation, 2016c) was based on the monthly CMIP5 Bias Correction and Spatial Disaggregation (BCSD) climate projection dataset, whereas this report has been based on the daily CMIP5-LOCA climate projections. A brief description follows detailing the difference between the CMIP5-BCSD and CMIP5-LOCA climate projection datasets. Specifically, this description focuses on the climate projections that are provided through the Downscaled Climate and Hydrology Projections (DCHP) archive (Maurer et al., 2014). The DCHP archive has been the primary resource for Reclamation's WaterSMART studies.

The downscaled monthly CMIP5-BCSD climate projections available from the DCHP archive include results from 36 GCMs. Each of these GCMs was used for a minimum of four simulations, reflecting forcing of the climate system with four emission scenarios. The emissions scenarios in the CMIP5 archive are the same as those defined in the IPCC Fifth Assessment (IPCC, 2014) where they are referred to as Representative Concentration Pathways (RCPs). These scenarios are designated as RCP2.6, RCP4.5, RCP6.0, and RCP8.5. The numeric value for each RCP represents the possible range of radiative forcing values by the year 2100 relative to pre-industrial era (e.g., +2.6 Watts per square meter (W/m^2), +4.5 W/m^2, etc.). In this BCSD dataset, the observation dataset developed by Maurer et al. (2002) is used to develop

relationships between observed historical data and GCM-simulated historical data. The observation dataset has a grid spacing of 1/8th degree, about 12 km, and the training period used is 1950 to 1999. Relationships between observed historical and simulated historical climate are used to correct for systematic biases in the model simulations. To provide hydrologic variables such as snow water equivalent, evapotranspiration, and runoff, the downscaled climate information is used to run the Variable Infiltration Capacity (VIC; Liang et al., 1994; Liang et al., 1996; Njissen et al., 1997) hydrologic model, though these earlier datasets use an earlier VIC version 4.1.2 at 1/8th degree grid spacing.

The downscaled daily CMIP5-LOCA climate projections available from the DCHP archive include results from 32 GCMs. Each of these GCMs was used for two simulations, reflecting forcing of the climate system with RCP4.5 and RCP8.5. The NCA4 identified RCP4.5 and RCP8.5 as the core scenarios representing an appropriate range of future conditions, stating, "NCA4 focuses on RCP8.5 as a 'higher' scenario, associated with more warming, and RCP4.5 as a 'lower' scenario with less warming. Other RCP scenarios (e.g., RCP2.6, a 'very low' scenario) are used where instructive, such as in analyses of mitigation of science issues" (USGCRP, 2018). Reclamation has consistently relied on a broad range of possible climate scenarios when assessing the risks and impacts from climate change, considering each as equally likely to best characterize the range of possible futures. Scenarios contained within the West-Wide Climate Risk Assessment of the 2016 SECURE Water Act Report are incorporated in this report, which remains a state-of-the-art assessment of potential future climate and hydrology using RCP2.6 through RCP8.5. Additionally, this 2021 Assessment summarizes potential outcomes from RCP4.5 and RCP8.5, including additional downscaling methodologies as described in this report. Reclamation's use of a range of RCPs—without assigning probabilities to any individual climate modeling experiment—reflects Reclamation's commitment to understanding uncertainties associated with future projections and to identifying a fuller range of possible outcomes consistent with the current state of the practice in water resources climate impact assessments.

Figure 1 and Figure 2 show Coupled Model Intercomparison Project Phase 5 (CMIP5) projections using Bias Correction and Spatial Disaggregation (BCSD) and LOcalized Constructed Analogs (LOCA) distributions of annual mean temperature and total precipitation projections, respectively. These projections are shown for the range of Representative Concentration Pathways (RCPs) for key locations in the eight major Reclamation river basins. The key locations are as follows (see Table 1 for location latitude and longitude information):

- Colorado – Colorado River above Imperial Dam
- Columbia – Columbia River at The Dalles
- Klamath – Klamath River near Klamath
- Missouri – Missouri River at Omaha
- Rio Grande – Rio Grande at Elephant Butte Dam
- Sacramento-San Joaquin – Sacramento-San Joaquin Rivers at Delta
- Truckee – Truckee River at Nixon

In each sub-plot of Figure 1 and Figure 2, which represents a key location in one of the eight major Reclamation river basins listed above, the heavy line is the median value for each year across the range of projections. The shaded area is the annual time series of 10th to 90th percentiles. For CMIP5-BCSD, RCPs 2.6, 4.5, 6.0 and 8.5 are shown, and for CMIP5-LOCA, projections are shown for RCP4.5 and RCP8.5. The LOCA and BCSD ensemble presents a collective view of temperature and precipitation projections from the available full range of downscaled RCPs—2.6 through 8.5.

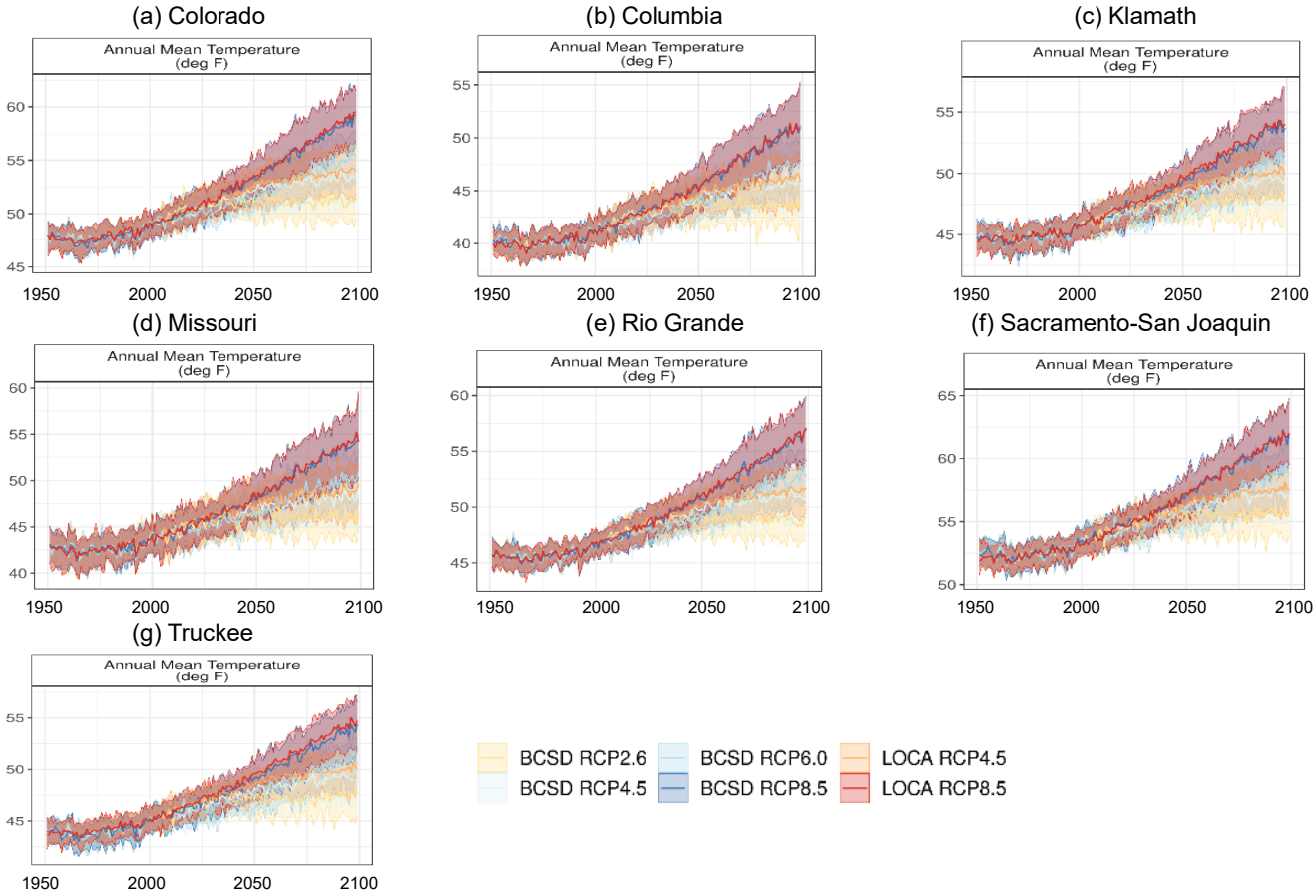

Figure 1. CMIP5 BCSD and LOCA distribution of annual mean temperature projections across RCPs.

Note: In each sub-plot, which represents a major Reclamation river basin location, the heavy line is the annual time series median value (i.e., median). The shaded area is the annual time series bounded by the 10th to 90th percentiles.

deg F = degrees Fahrenheit

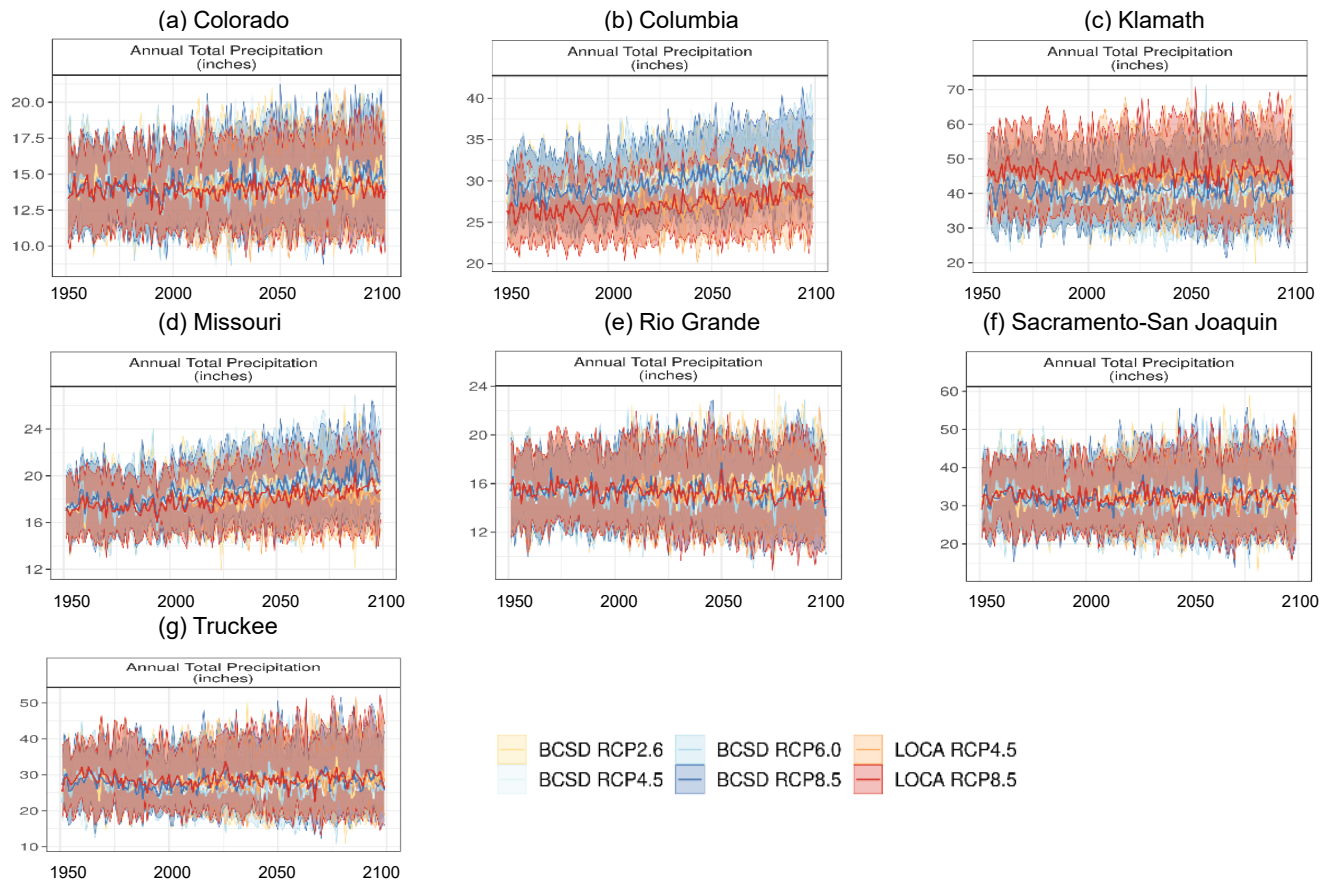

Figure 2. CMIP5 BCSD and LOCA distribution of annual total precipitation projections across RCPs.

Note: In each sub-plot, which represents a major Reclamation river basin location, the heavy line is the annual time series median value (i.e., median). The shaded area is the annual time series bounded by the 10th to 90th percentiles.

The historical dataset used for LOCA to develop relationships between observed historical climate and simulated historical climate by the GCMs was developed by Livneh et al. (2015), and the training period used is 1950 to 2005. In contrast, BCSD was trained on Maurer et al. (2002). These two observed datasets generally use the same approach for computing gridded climate fields from the station data available at the time they were developed; however, the Livneh et al. (2015) dataset has a higher resolution, leading to differences between it and the Maurer et al. (2002) dataset in local extremes and variability. The LOCA method uses local historical spatial patterns and has a bias correction method that includes a frequency-dependent correction to improve the simulation of natural climate variability and attempts to preserve the original GCM-predicted change in the bias-corrected result (Pierce et al., 2015). To provide hydrologic variables (including evapotranspiration, runoff, and snow water equivalent, among others), the downscaled precipitation and temperature are input into the VIC hydrologic model, version 4.2.c, at 1/16th degree grid spacing. The VIC hydrologic model configuration used was cited in Livneh et al. (2013), which used model parameters calibrated over many years on a 1/8th degree grid and moved them to a 1/16th degree grid with only a few modifications.

LOCA-downscaled climate and simulated hydrology were evaluated in this report as a set of two experiments—first as near-term projections of the next few decades through 2035, and second as the long-term projections through the end of the 21st century (Taylor et al., 2012). Additionally, a detailed comparison of CMIP5 climate projections based on the BCSD downscaling method and the LOCA downscaling method is presented by Vano et al. (2020).

The next section describes the development of hydrologic projections using the monthly CMIP5 projections in the DCHP archive.

2.2 Hydrologic Projections

In this report, projections of future climate and hydrology are summarized for each of the eight major Reclamation river basins, consistent with the past 2011 and 2016 SECURE Water Act hydroclimate reports. The projections are based on downscaled GCM climate projections as summarized in the previous section. Corresponding projections of streamflow were developed using methods summarized above and synthesized in the next section.

The methods used in the 2011 and 2016 West-Wide Climate Risk Assessments hydroclimate projections reports for developing hydrologic projections from climate projections were based on the macro-scale hydrologic model VIC (Liang et al., 1994; Liang et al., 1996; Nijssen et al., 1997). This current study is based on VIC model version 4.2.c. The VIC model is a gridded macro-scale (grid resolution greater than 1 km) hydrology model that is spatially distributed and solves the water balance at each model grid cell. The grid resolution for the VIC application is 1/16th degree latitude by 1/16th degree longitude (approximately 6 km by 6 km), which is the same grid resolution for the LOCA-downscaled CMIP5 climate projections. The model was initially developed as a land-surface model for direct integration with GCMs, but it now is run almost exclusively as a standalone hydrology model using a daily simulation timestep.

Future projections of snowpack (in the form of snow water equivalent, or SWE), as well as runoff and streamflow, are based on simulations using the VIC model with inputs of future climate projections (precipitation and temperature) described previously. The VIC model simulates runoff and streamflow that are unimpaired, meaning not affected by human influence (such as storage in dams or diversions for cities and irrigation networks). Further, the model is also based on an assumption of static land cover. Vano et al. (2020) describe in more detail the selected configuration of the VIC model for developing CMIP5-LOCA hydrology projections. Other surface hydrologic models may simulate dynamic vegetation and carbon dioxide effects on vegetation growth, but those were not considered in this report. Chapter 3 summarizes projected changes in snowpack, runoff, and streamflow based on the output from VIC model simulations. As was done in 2011 and 2016, routed streamflow was developed for the 43 selected locations given in Table 1. Analysis of the climate and streamflow data is presented in Chapter 3.

Table 1. Descriptions for the 43 West-wide reporting locations

River Basin(s)*	Site Name and Description	Latitude	Longitude	State(s)
Colorado	Colorado River at Lees Ferry	36.8647	–111.5875	AZ
	Colorado River above Imperial Dam	32.8834	–114.4685	CA-AZ
	Green River near Greendale	40.9086	–109.4224	UT
	Colorado River near Cameo	39.2392	–108.2656	CO
	Gunnison River near Grand Junction	38.9766	–108.4562	CO
	San Juan River near Bluff	37.1469	–109.8642	UT
Columbia	Snake River at Brownlee Dam	44.8389	–116.8995	ID
	Columbia River at Grand Coulee	47.9656	–118.9817	WA
	Columbia River at The Dalles	45.6075	–121.1722	OR
	Yakima River at Parker	46.5061	–120.4519	WA
	Deschutes River near Madras	44.7261	–121.2465	OR
	Snake River near Heise	43.6128	–111.6600	ID
	Flathead River at Columbia Falls	48.3619	–114.1839	MT
Klamath	Williamson R. below the Sprague River	42.5577	–121.8442	OR
	Klamath River below Iron Gate Dam	41.9281	–122.4431	CA
	Klamath River near Seiad Valley	41.8529	–123.2311	CA
	Klamath River at Orleans	41.3036	–123.5336	CA
	Klamath River near Klamath	41.5111	–123.9783	CA
Missouri	Missouri River at Canyon Ferry Dam	46.6494	–111.7275	MT
	Milk River at Nashua	48.1297	–106.3639	MT
	South Platte River near Sterling	40.6192	–103.1886	CO
	Missouri River at Omaha	41.2589	–95.9222	NE
	Bighorn River at Yellowtail Dam	45.3079	–107.9567	MT
	North Platte River at Lake McConaughy	41.2145	–101.6434	NE
Rio Grande	Rio Grande near Lobatos	37.0786	–105.7564	CO
	Rio Chama near Abiquiu	36.3183	–106.5972	NM
	Rio Grande near Otowi	35.8762	–106.1433	NM
	Rio Grande at Elephant Butte Dam	33.1563	–107.1905	NM

River Basin(s)*	Site Name and Description	Latitude	Longitude	State(s)
	Pecos River at Damsite No. 3 near Carlsbad	32.5114	–104.3342	NM
Sacramento-San Joaquin	Sacramento River at Freeport	38.4561	–121.5003	CA
	Sacramento River at Bend Bridge near Red Bluff	40.2642	–122.2219	CA
	Feather River at Oroville	39.5217	–121.5467	CA
	San Joaquin River near Vernalis	37.6761	–121.2653	CA
	Stanislaus River at New Melones Dam	37.9472	–120.5292	CA
	Sacramento-San Joaquin Rivers at Delta	38.0645	–121.8567	CA
	San Joaquin River at Millerton Lake (Friant Dam)	36.9981	–119.7066	CA
	American River at Fair Oaks	38.6366	–121.2284	CA
	Tulare-Buena Vista Lakes	36.0524	–119.7187	CA
Truckee	Little Truckee River below Boca Dam	39.3883	–120.0950	CA
	W.F. Carson River at Woodfords	38.7697	–119.8328	CA
	Truckee River at Farad Gage (just above CA State line)	39.4540	–120.0063	CA
	Truckee River at Nixon Gage	39.7780	–119.3392	NV
	Carson River at Fort Churchill Gage	39.3272	–119.1508	NV

* Note: The Pecos, Tulare, and Carson are not SECURE Water Act (SWA) River Basins, but are included respectively under the Rio Grande, Sacramento and San Joaquin, and Truckee River Basins because they are of interest from a water operations standpoint.

Further, in this report, future projections of a common drought index, Palmer Drought Severity Index (PDSI; Palmer, 1965), have been developed to provide additional context to the variability of future water supply. This information is introduced in the next section.

2.3 Reconstructed and Projected Drought Index

Knowing more about the occurrence of drought events will help stakeholders prepare and subsequently adapt to changing hydroclimate conditions. In this report, Reclamation has developed a risk-informed framework to support water management decisions by way of a range of data and tools based on current science.

One component of that framework is a dataset to explore drought events that leverages existing information, as well as encompasses newly developed information. Reclamation and study partners developed tools and information based on paleohydrology reconstructions to evaluate dry and wet period characteristics and analyze probabilities of shifting between a wet state or dry

state (regime shifts). A West-wide analysis of drought and hydrologic regime shifts using PDSI are described in Chapter 4 of this report.

The analyses are performed using the PDSI (Palmer, 1965) to define drought events. The advantage of using PDSI to define droughts is that it focuses explicitly on droughts driven by hydroclimate variability (see Section 9.3 for more on advantages and disadvantages of different drought measures). The historical period used in this analysis includes the years 1473 to 2005, which encompasses the beginning of the available PDSI reconstruction to 2005, which is the end of the historical period over which climate projections were trained. The PDSI data for this period were leveraged from the Cook et al. (2010) PDSI dataset, which provides tree-ring based reconstructions of average June-July-August PDSI on a 0.5-degree (°) latitude by 0.5° longitude spatial resolution for the years 0 to 2017 (see Section 4.1 for more details regarding PDSI data).

Future projections of PDSI were developed based on CMIP5-LOCA climate projections using the Wells (2003) model for computing PDSI. Thus, time series of PDSI data covering the period 1473 to 2099 was developed for use in the analyses. The PDSI model (Wells, 2003) was run using projected temperature and precipitation for each available CMIP5-LOCA projection to calculate gridded monthly PDSI values, again for each projection, for each of the $1/16^{th}$ degree grid cells for the period 1950 to 2099. Subsequently, for each projection, the monthly PDSI magnitudes were averaged to summer (June-July-August average) values for consistency with the historical PDSI analysis. As a final step, the summer season PDSI values for the $1/16^{th}$ degree grid cells then were aggregated to the 1,255 USGS eight-digit Hydrologic Unit Codes (HUC-8s).

2.4 Streamflow Reconstructions and Drought Definition

Additional analyses in this report use water-year annual streamflow reconstructions based on tree-rings. In recent years, tree-ring based reconstructions of streamflow have been increasingly used to evaluate how well water systems throughout the West would manage if droughts like those that have occurred in the distant past were to occur today. More specifically, they have been used to broaden the perspective of long-term water supplies in multiple Reclamation basins via their incorporation into the Basin Study Program (Reclamation, 2012b; Reclamation, 2018). In ideal situations, reconstructions can extend annual estimates of past streamflow at key monitoring locations by up to 1,000 years or more. Due to their great length, these records can: (1) help characterize the long-term patterns of variability that influence drought and flood risk over time (Gangopadhyay et al., 2019); (2) provide greater perspective on the likelihood of particularly challenging wet and dry periods that have posed historical challenges for water management (Meko et al., 2007; Woodhouse et al., 2010; Martin et al., 2020); and (3) establish a robust baseline of natural internal climate variability from which to estimate future change (Prairie et al., 2008). The extreme wet and dry conditions often represented in reconstructions, but which are lacking in the short instrumental record, also help managers test infrastructure and operational strategies under these stressful conditions using model simulations.

The basic process of reconstructing streamflow from tree-rings relies first on the science of dendrochronology in which the growth rings of trees are accurately dated by calendar year and measured for growth characteristics (Douglass, 1941; Stokes and Smiley, 1968; Fritts, 1976). Because the annual growth of many trees is largely a function of climate conditions prior to and during the growing season, the long growth records of older trees can serve as valuable "proxy" records of inter-annual climate variability over the entire lifespan of a tree (Fritts, 1976). Tree rings are used to develop chronologies, or timescale information about wet years and dry years. The steps in developing the chronologies include, selecting appropriate sites for trees, developing the tree-ring chronologies from the sampled trees' annual tree-rings, and developing the empirical (statistical) models between chronologies and annual flows. Since inter-annual streamflow variability is also closely related to climatic conditions over the course of the water year, tree-rings record valuable information on the drivers of streamflow that can be used to estimate streamflow variability over time. There is a fundamental question about how a changing climate may impact the relationships between tree rings and streamflow, and whether the hydroclimate conditions of the distant past are informative for the future. This is a question not easily answered, particularly because relationships in the current form typically rely on a century of instrumental records and climate change has been observed over that same duration, confounding analysis. Still, hydroclimate conditions have occurred in the paleo-reconstructed period that have not been observed in the instrumental record and these conditions are valuable to consider in an assessment of water management risks.

The general approach to reconstructing streamflow involves the statistical correlation of growth patterns in tree-rings to variability in an observed streamflow record. This allows for the development of a statistical reconstruction model that can then be used to estimate annual flow from annual growth rings. Most often, the approach takes the form of a multiple linear regression model based directly on composite tree-ring records called chronologies. Chronologies are developed from multiple trees for multiple sites (Meko and Graybill, 1995; Woodhouse et al., 2006; Woodhouse, 2001), but may use larger pools of tree-ring data via the principal components (i.e., a statistical summary of common variance) of numerous chronologies (Hidalgo et al., 2000; Littell et al., 2016), or may employ other non-parametric or Bayesian network models (Gangopadhyay et al., 2009; Ravindranath et al., 2019). The skill of the tree-ring data is assessed in terms of variance explained. The accuracy of the reconstruction is also tested against the observed record using the process of cross-validation—a process that quantifies predicted streamflow from the statistical model against observed data not used in the calibration process, or an independent dataset (Fritts, 1976; Briffa et al., 1988).

Fundamentally, there is uncertainty associated with correlating tree-rings with annual streamflow using a statistical model. Probabilistic interpretations of flow reconstructions are needed because of uncertainty stemming from limitations of the basic data, from the reconstruction process itself, and from the choice of analytical methods. Important differences in these reconstructions can largely be traced to differences in basic tree-ring data, hydrologic data, and modeling choices. Section 9.2 further describes the steps in developing streamflow reconstructions and important uncertainties to consider. This uncertainty stems from methodological choices inherent to the

techniques, as well as a limited understanding of how past variability characteristics will persist under changing future climate conditions.

The 2021 Assessment used 152 streamflow reconstructions for various gaging locations across the eight major Reclamation river basins (refer to Figure 3) and focused on records at 10 key locations across the West for incorporation into river management system modeling exercises (Chapter 6). This allowed for a continuous estimate of streamflow variability across Reclamation's full operational area from 1685 to 1977, which provides an assessment period of over 300 years when combined with existing observational streamflow records.

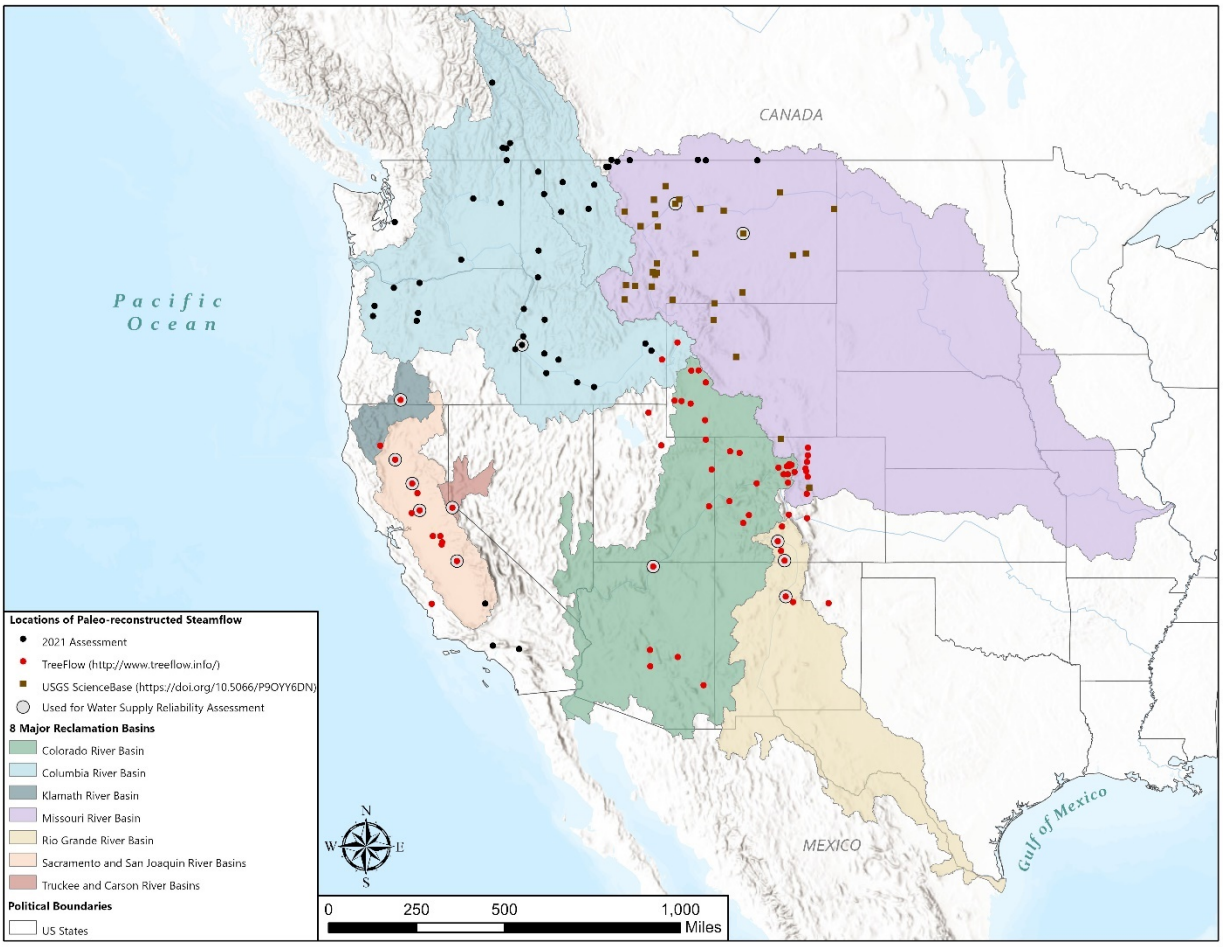

Figure 3. Locations of available 152 streamflow reconstructions.

Note: The brown filled squares represent sites referenced by ScienceBase, red filled circles represent sites compiled in TreeFlow, and black filled circles represent sites that were developed as part of this report. Sites surrounded by larger open circles were used as part of the Water Supply Reliability Analysis (Chapter 6).

Table 2 provides a list of 47 additional streamflow reconstruction locations beyond the 105 that were already cited by Gangopadhyay et al. (2019).

Table 2. Additional 47 streamflow reconstruction locations beyond the 105 that were already cited by Gangopadhyay et al. (2019)

Reconstruction Name	Nearest Stream Gage ID*	Reclamation River Basin	State or Province	Start Date	End Date
Columbia River at the Dalles	14105700	Columbia	OR	1685	1977
Boise River at Boise	13202000	Columbia	ID	1450	2001
Crooked River below Opal Springs near Culver	14087400	Columbia	OR	1450	1998
Deschutes River near Madras	14092500	Columbia	OR	1500	1980
Green River at Auburn	12113000	Columbia	WA	1500	1980
Kootenay River at Glade	08NJ001	Columbia	BC	1500	1980
Kootenay Lake Outflow near Corra Linn	08NJ158	Columbia	BC	1500	1980
Kootenai River below Libby Dam near Libby	12301933	Columbia	MT	1486	1982
Kootenai River at Bonners Ferry	12309500	Columbia	ID	1500	1980
Brownlee Res at Brownlee Dam	13289710	Columbia	ID	1500	1980
North Fork Clearwater River at Ahsahka	13341000	Columbia	ID	1451	1982
Salmon River at White Bird	13317000	Columbia	ID	1451	2006
Columbia River at Grand Coulee	12436500	Columbia	WA	1486	1983
North Fork Payette River at Cascade	13245000	Columbia	ID	1451	2006
Clark Fork at Whitehorse Rapids near Cabinet	12392000	Columbia	ID	1451	2003
Flathead River near Polson	12372000	Columbia	MT	1486	1982
Clark Fork near Plains	12389000	Columbia	MT	1500	1980
Pend Oreille River near Waneta Dam	Not applicable	Columbia	NA	1437	1982
Sandy River below Bull Run	14142500	Columbia	OR	1437	1982
Spokane River at Long Lake	12433000	Columbia	WA	1500	1980
Columbia River at Birchbank	08NE049	Columbia	BC	1497	1983
Columbia River above Steamboat Rapids	08ND011	Columbia	BC	1391	1996
South Fork Boise River at Anderson Ranch	13190500	Columbia	ID	1500	1980
Snake River at CJ Strike Dam	13171620	Columbia	ID	1500	1980
Snake River at Milner	13087995	Columbia	ID	1485	1983
Owyhee Reservoir Inflow	13183000	Columbia	OR	1500	1980
Boise River near Parma	13213000	Columbia	ID	1500	1980
Payette River near Payette	13251000	Columbia	ID	1450	1998
Henrys Fork near Rexburg	13056500	Columbia	ID	1489	1985
Owyhee River near Rome	13183000	Columbia	OR	1500	1980
Teton River at Mouth	Not applicable	Columbia	ID	1440	1983
Snake River near Heise	13037500	Columbia	ID	1500	1980

Reconstruction Name	Nearest Stream Gage ID*	Reclamation River Basin	State or Province	Start Date	End Date
Willamette River at Albany	14174000	Columbia	OR	1500	1980
Willamette River at Salem	14191000	Columbia	OR	1500	1980
Yakima River at Kiona	12510500	Columbia	WA	1451	1982
Flathead River at Hungry Horse	12362500	Columbia	MT	1450	1980
Arroyo Seco River at Pasadena	11098000	NA	CA	1404	2016
Santa Ana River near Mentone	11051500	NA	CA	1404	2016
Kern River below Isabella	11191000	San Joaquin	CA	1404	2016
Swiftcurrent Creek at Sherburne	05016000	Missouri	MT	1026	2008
St. Mary River near Babb	05017500	Missouri	MT	1026	2000
St Mary River near International Boundary	05020500	Missouri	MT	1026	1999
North Fork Milk River above St. Mary Canal near Browning	06133500	Missouri	MT	1347	2006
Milk River at Western Crossing of International Boundary	06133000	Missouri	MT	1018	1999
Frenchman River at International Boundary	06164000	Missouri	MT	1741	2008
Lodge Creek at International Boundary	06144500	Missouri	MT	1581	2000
Battle Creek at International Boundary	06149500	Missouri	MT	1730	2005

* Streamflow gages with alphanumeric ID are located in Canada.

To estimate the risks associated with future drought and pluvial events, it is necessary to quantify the long-term likelihood of such events through both their magnitudes and durations over time. This information allows managers to improve strategies for mitigating the unwanted effects of too much or too little water and provides a baseline assessment of risk on which to project estimates of changing future water supplies. The first step in describing drought and pluvial dynamics over time is to develop a definition for what constitutes a drought or pluvial event. Definitions useful to management are often tied to the types of events that represent risks to infrastructure or operations. For the purpose of this work, a drought or (pluvial) event is defined as:

> An event beginning with, and including, two or more consecutive years of streamflow below (above) the median flow level that is ended only by, and excludes, two or more consecutive years of streamflow above (below) the median flow level. An event may include one or more individual wet (dry) years within the drought (pluvial) only when bounded on both sides by dry (wet) years.

The median flow is computed over the duration of the paleo-reconstructed streamflow record. As an example, drought events in the paleo-reconstructed period are defined for the Missouri River at Toston, Montana, and illustrated in the upper panel of Figure 4 by brown-shaded regions. The lower panel of Figure 4 illustrates the drought definition for a single drought in the observed

historical period—the Dust Bowl drought of the 1930s. The same definition was applied to each of the 152 streamflow reconstruction locations identified previously (Figure 3).

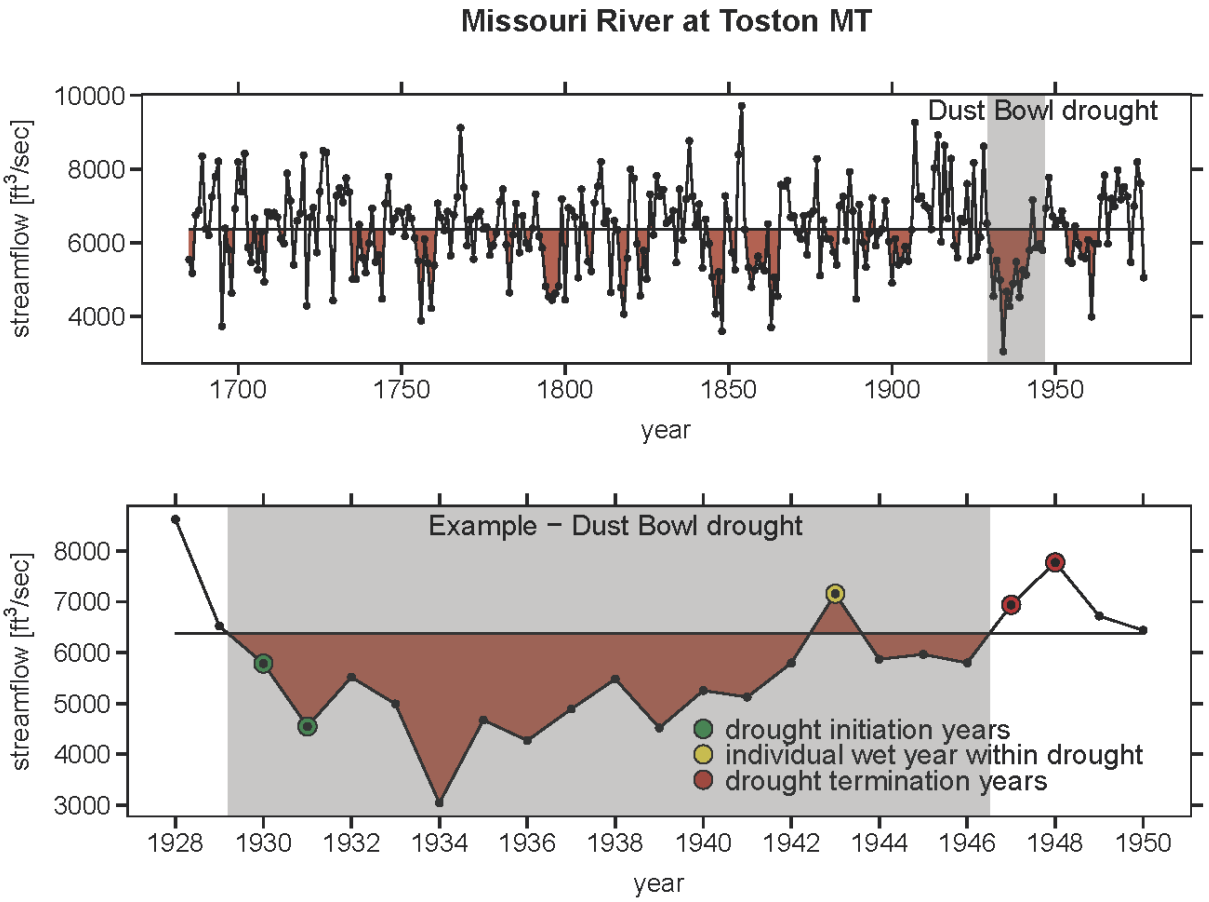

Figure 4. Illustration of drought definition used in the example in Chapter 6 shown for Missouri River at Toston, Montana.

Note: Black horizontal line shows the median flow for the period of record, and the brown shading highlights the classified drought years

ft^3/sec = cubic feet per second

This drought definition captures the prolonged nature of potentially challenging wet and dry periods and recognizes that such events generate cumulative water deficits and surpluses, despite the brief cessation of difficult conditions that may occur during a single intervening wet or dry year. The second step in describing drought and pluvial dynamics over time is to quantify the magnitude and duration of each event. This can be accomplished in many ways; however, for the purpose of this work, five measures of magnitude and/or duration were determined for each event. These included the event duration (measured in years), the intensity (measured as the average annual flow deficit/surplus over the length of the event), the cumulative deficit/surplus (measure as the sum of annual deficits/surpluses over the length of the event), the variability (measured as the variance of annual flows over the length of the event), and how quickly the event developed (assessed as the lowest/highest value averaged over the first 5 years of the drought/pluvial event).

As an example, Figure 5 illustrates the maximum cumulative deficit (in acre-feet) for each of the 152 locations illustrated in Figure 3, calculated using the above drought definition over the period 1685 to 1977. The largest cumulative deficits appear in the wettest parts of the Western United States, namely the Pacific Northwest and California. Cumulative deficit is highly correlated with the average magnitude of streamflow, so regions with large deficits generally have higher average streamflow.

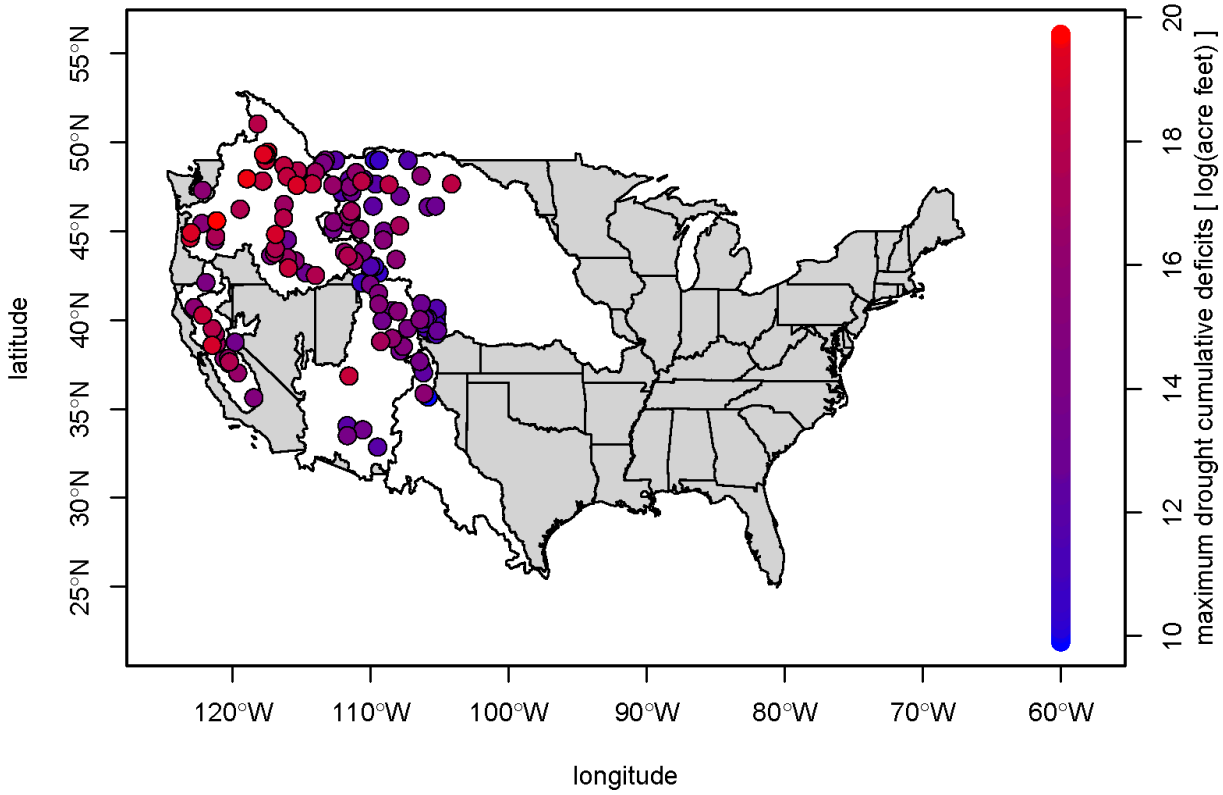

Figure 5. Drought events with maximum cumulative deficit (in acre-feet) over common years 1685 to 1977 for 152 streamflow locations.

Note: Drought events with maximum cumulative deficit as calculated using the selected drought definition for this analysis for each of 152 streamflow reconstruction locations.

As another example, Figure 6 illustrates the maximum drought length (in years) for each of the 152 locations illustrated in Figure 3, calculated using the same drought definition and time period. The longest droughts have also appeared in the Pacific Northwest; however, long droughts of 40 years or more did occur throughout the Western United States.

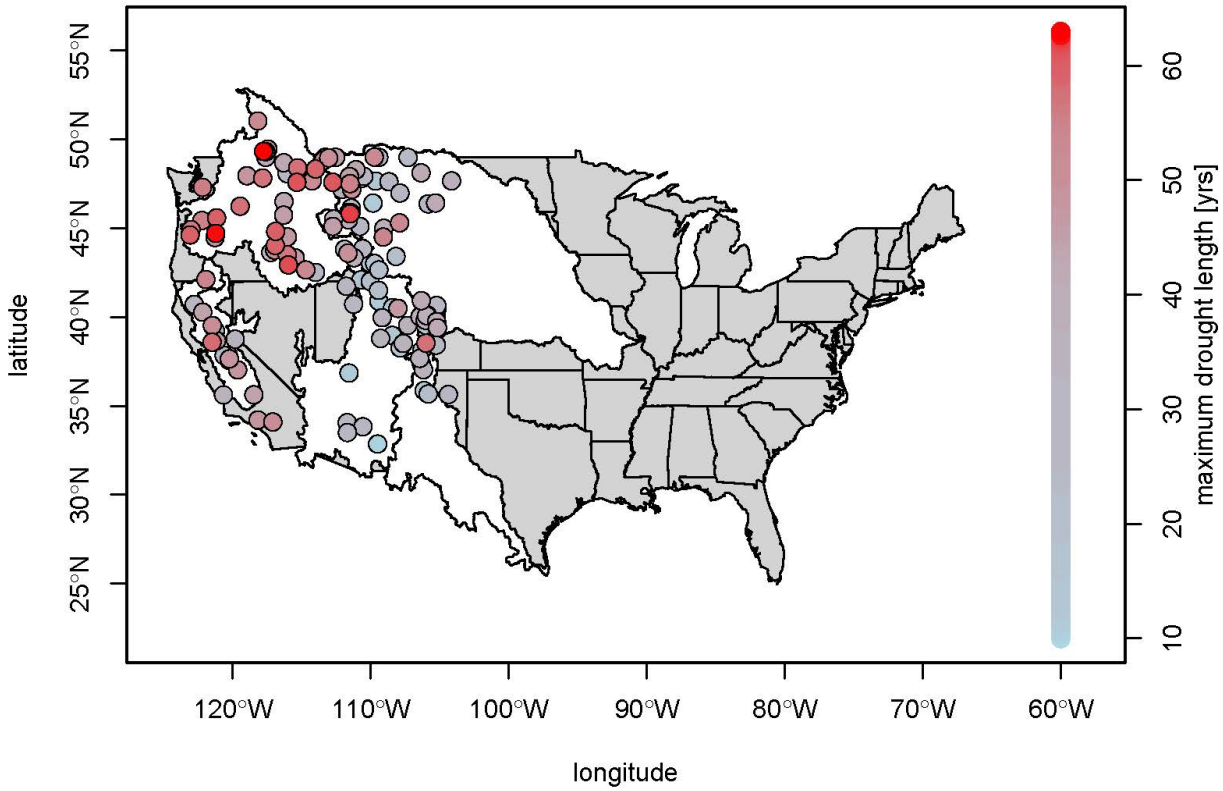

Figure 6. Drought events with maximum drought length (in years) over common years 1685 to 1977 for 152 streamflow locations.

Note: Drought events with maximum drought length as calculated using the selected drought definition for this analysis over common years 1685 to 1977 for each of the 152 streamflow reconstruction locations.

Droughts with the largest cumulative deficit are further investigated in Chapter 6. Ten of the 152 streamflow reconstructions were used to develop inputs to river systems models to evaluate how these drought events impact water management.

The choice of drought definition and the choice of paleo-reconstruction period of analysis can have important implications for the identification of drought events. These methodological choices introduce uncertainty into the analysis and results need to be examined with a full understanding of the choices made and the limitations introduced when selecting drought events. An illustration of this point is discussed below with respect to the Colorado River Basin, where several streamflow reconstructions exist for the Colorado River at Lees Ferry location over different time periods in the paleo record and allow for an evaluation of differences in identified drought events. Similar uncertainty exists in all basins, though it may not be possible to directly examine given the more limited paleo-reconstructions available.

Streamflow reconstructions for the Colorado River at Lees Ferry have been previously used in the Colorado River Basin Water Supply and Demand Study (Reclamation, 2012b), as well as other water planning and management efforts within the basin.

The Woodhouse et al. (2006) streamflow reconstruction (Lees-B) has a record of 1490 to 1997. A subset of that record (1685 to 1977) was used to inform the storage-deficit ratio analysis (Chapter 5) and water supply reliability evaluation in this report (Chapter 6). A reconstruction was also developed by Meko et al. (2007) over a longer period, 762 to 2005. More recently, yet another reconstruction at the same location was developed for the California Department of Water Resources (CDWR) and spans 1116 to 2015 (described in Lukas et al., 2020).

An analysis was performed to understand the sensitivity of identified drought events to the reconstruction record used to inform them. For example, droughts further investigated in Chapter 6 were identified using the Woodhouse et al. (2006; Lees-B) reconstruction over the period 1685 to 1977. Had the full Lees-B reconstruction been used, this median flow level would have increased by just under 150,000 acre-feet (from 14,604,117 acre-feet to 14,752,460 acre-feet). Further, if the Meko 2007 reconstruction had been used, this median flow level would have increased slightly more (14,833,860 acre-feet).

To illustrate how the median flow impacts the identification of drought that would have been used in Chapter 6 had the full Lees-B reconstruction been used, droughts were identified using both the full median flow for 1490 to 1998 and the common period median flow (1685 to 1977) over the full reconstruction length.

The analysis found that one drought is affected by choice of median flow. This indicates that the drought definition is relatively insensitive to moderate changes in the long-term median flow level for the Woodhouse et al. (2006; Lees-B) reconstruction. Perhaps more informative, the analysis revealed that there were drought events in the full Woodhouse et al. (2006; Lees-B) record (i.e., prior to 1685) that ranked higher in terms of cumulative deficit than the droughts used in this report. The other two reconstructions (Meko et al., 2007 and CDWR, 2017) both extend further back in time than Lees-B and identify additional droughts that exceed the droughts considered in this report. Available information developed for the Colorado River Basin illustrates that methodological choices related to drought definition and data used may impact the selection of drought scenarios used in assessments such as this one.

2.5 Storyline of Analyses for Risk-Informed Decision-Making

As previously discussed, the 2021 Assessment provides additional information beyond hydroclimate projections and analysis provided in the 2011 and 2016 assessment reports. Hydroclimate analysis provides valuable information on projected changes in temperature, precipitation, and simulated natural streamflow that would occur in the absence of water management. The West-wide drought analysis, presented in Chapter 4 of this report, offers context by evaluating droughts of the distant past through quantification of a common drought measure (PDSI) based on hydroclimate variability. The frequency and duration of droughts characterized by natural conditions (i.e., with consideration of evapotranspiration demands from the natural landscape, but not from the human-altered landscape such as agricultural fields) provides information to understand the variability of drought and pluvial (wet) events over long

time scales. It also allows for evaluation of the same information into the future using climate projections.

The analyses performed in Chapter 5 offer a purely data driven evaluation of drought impacts on five managed river systems based on observed historical records and paleo-reconstructed streamflow records. Water demands are implicitly incorporated into this data-driven approach through use of observed data that reflects diversions, return flows, storage, and losses. Although this approach requires simplifying assumptions on river operations, it offers a broad view of drought impacts without the investment of detailed water supply reliability assessments, which were performed and summarized in Chapter 6 of this report. The data-driven approach provides a high-level view of water supply availability compared to demands over time.

The analysis in Chapter 6 may be thought to build upon that presented in Chapter 5 in terms of complexity of approach. Chapter 6 analyses are based on detailed water supply reliability assessments conducted in case study river basins. Each individual case study analysis requires detailed input data of inflows and water demands, as well as a robust modeling framework to account for river operations, infrastructure, and management constraints. In this report, water supply reliability analyses were performed using the observed historical record and drought events from the paleo-reconstructed period.

Together, these analyses provide a sample of approaches that facilitate understanding of the frequency, severity, and variability of past and potential future droughts. They may also offer a road map for further exploration into droughts.

2.6 Water Management with Uncertainty

This chapter discusses the wealth of analysis and understanding that led up to and includes this report with respect to future climate projections, future hydrologic projections, and paleohydrology (in the form of PDSI reconstructions and annual streamflow reconstructions). It is important to acknowledge that a diversity of techniques collectively provides a more robust analysis, especially when different techniques reveal similar conclusions. For example, even with advances in models of the Earth System and downscaling techniques, all future climate projections indicate climate will continue to warm beyond what humans have experienced, despite the uncertainty in the precise trajectory of greenhouse gas concentrations. Moreover, paleo analysis and analysis using future projections both reveal scenarios and likelihoods which extend understanding, allow for a more risk-informed decision-making framework, and can help promote more resilient planning.

Uncertainties associated with approaches described in this chapter in part stem from an evolving understanding of complex system processes and imperfect representation of those processes in models. These uncertainties are reducible to some extent with improved knowledge and computing power. Uncertainties also stem from the chaotic nature of the climate system, which is not reducible. As research continues to characterize and, where possible, reduce uncertainties inherent in projecting hydroclimate impacts of climate change, the water resources management

community should also be aware that future conditions are ultimately deeply uncertain. This means that risk-informed analyses alone may not provide appropriate practical information for planning, and that bottom-up approaches using decision-making under deep uncertainty (DMDU) methods should continue to be explored. Such methods can help identify system vulnerabilities and improve understanding of what conditions make a system most vulnerable.

There is no single approach that provides a full understanding of climate change impacts on the managed river systems in the West. Top-down approaches that translate climate projections to impacts on watersheds may be applied in concert with bottom-up approaches such as those DMDU methods to provide the broadest insights.

While it is important to acknowledge limitations in the analyses presented in this report and to make an initial effort to fully characterize and better reveal that uncertainty space, the information presented in the remaining chapters offers an assessment and illustration of new and updated tools that water managers may use to explore their decision-making space. Further acknowledgement and discussion of uncertainties associated with the range of analyses conducted in this report is provided in Chapter 9.

3 Hydroclimate Projections for Major Reclamation River Basins

This chapter presents hydroclimate projections for the eight major Reclamation river basins. The variables illustrated in this report are precipitation, mean temperature, snow water equivalent, and runoff. The evaluation approach for the hydroclimate projections from CMIP5-LOCA is first presented in Section 3.1. Results from the evaluation for each of the eight major Reclamation river basins are presented in Sections 3.2 to 3.8. To provide context and to develop an expanded understanding, Section 3.9 summarizes a comparison of CMIP5-LOCA streamflow projections presented in this report and CMIP5-BCSD streamflow projections reported in the West-Wide Climate Risk Assessment of the 2016 SECURE Water Act Report (Reclamation, 2016c). A summary of projected hydroclimate changes from this assessment is presented in Section 3.10 for each basin. Finally, a broad list of potential impacts for future water management is given in Section 3.11.

3.1 Evaluation Approach

The figures and analysis for each basin are grouped under two sections. The first section provides an assessment of projections for a set of hydroclimate variables in each basin. The second section presents climate change impacts on annual runoff, seasonal cycles, and shifts in annual runoff timing for selected runoff locations within each of the basins. Runoff impacts are reported at 43 locations (refer to Table 1) covering the eight major Reclamation river basins. Under the hydroclimate projections section, four sets of plots are presented for each major river basin. These include:

- Time series plots of six hydroclimate variables.
- Spatial plots showing the spatial distribution of
    - temperature;
    - precipitation; and
    - April 1st snow water equivalent (SWE)[4].

[4] All references to SWE (snow water equivalent) in this report correspond to April 1st SWE values.

3.1.1 Hydroclimate Projections

3.1.1.1 Time Series Plots

Basin- and projection-specific annual time series plots are presented for six hydroclimate indicator variables covering the period 1950 to 2099 as follows:

- Annual total precipitation
- Annual mean temperature
- April 1st snow water equivalent
- Annual runoff
- December-through-March runoff
- April-through-July runoff

Three variables—annual total precipitation, annual mean temperature, and April 1st snow water equivalent—vary spatially (at 1/16th degree or about 6-kilometer (km) grid resolution) across the basins. To estimate total annual precipitation for a given basin, basinwide average precipitation (averaged across the grid cells in the basin) was first calculated for each month of the years 1950 to 2099. These monthly precipitation values then were summed for each year (1950 to 2099) to obtain the annual total precipitation.

To estimate basin mean temperature, average temperature was calculated from all the grid cells in the basin for each month of the years 1950 to 2099. Next, these monthly temperatures for any given year were averaged to estimate the basinwide annual mean temperature.

SWE on April 1st of a given year is a widely used measure to assess snowpack and subsequent spring-summer runoff conditions in the snowmelt-dominated basins of the Western United States. SWE is a state variable that is output from the VIC hydrology model. For each of the simulation years, 1950 to 2099, April 1st SWE was saved from the simulations for the model grid cells in a given basin. This gridded SWE on April 1st was averaged over all the grid cells for the given basin to calculate the basinwide April 1st SWE in each of the simulation years, 1950 to 2099.

Runoff for each of the locations listed in Table 1 was calculated for the annual timescale and for two seasonal timescales, December-through-March total runoff conditions and April-through-July total runoff conditions. For the VIC model, the term "total runoff" signifies the sum of VIC's surface runoff and baseflow variables, which, when combined, represent stream channel input that can be routed to estimate streamflow at a particular location. For each of the simulation years 1950 to 2099, monthly total runoff was aggregated on a water year[5] basis to

[5] Water year *t* is defined as the period from October 1 of year *t–1* to September 30 of year *t*. For example, water year 1951 spanned from October 1950 through September 1951. So, there are 149 water years spanning the calendar years 1950 to 2099. For time series plotting, values from water year 1951 were repeated for 1950.

calculate water year-specific total annual runoff, December-through-March runoff, and April-through-July runoff.

The annual time series plots for the six hydrologic indicator variables for all the projections were calculated, and the results are presented to reflect ensemble central tendency and ensemble spread. The central tendency is measured using the ensemble median, and the 10th and 90th percentile bounds from the 64 projections provides the lower and upper bounds in the envelope of hydroclimatic possibility through time.

3.1.1.2 Spatial Plots

The second sets of plots presented in this report include spatial plots of decade-mean precipitation, temperature, and April 1st SWE. These plots show the spatial distribution for the variables across the contributing basins in each of the eight major Reclamation river basins (a total of seven locations[6]). The spatial plots are developed on a water year basis (affecting calculations for only precipitation and temperature averaging) for the reference decade of the 1990s (water years 1990 to 1999).

The spatial distribution of temperature for the 1990s is presented as an ensemble median of the 64 projections. At each grid cell in a given basin and for each of the 64 selected projections, the mean annual temperature is first calculated from the 12 monthly values for each of the 10 water years 1990 to 1999. Next, for each grid cell, the ensemble median of the decade average mean temperature was calculated and used in developing the spatially varying temperature plots.

Temperature changes in each of the future decades were estimated as follows. At each grid cell in a given basin and for each of the 64 projections, the decade-mean temperature changes were calculated by averaging the mean annual temperature from the 10 water years in each of the respective future decades. Then, for a given projection and at a given grid cell, the difference (in degrees Fahrenheit) between a given future decade's mean annual temperature and the reference decade's mean annual temperature was calculated. The uncertainty in the distribution of the change in decade-mean temperature for the 2020s, 2050s, and 2070s is presented using the 25th and 75th percentile, and the median (50th percentile) represents the central tendency of change in decade-mean temperature distribution.

The calculations for decade-mean precipitation and April 1st SWE distribution follow steps similar to the ones used for deriving the temperature distributions. The spatial distribution of precipitation for the 1990s is presented as an ensemble median of the 64 projections. At each grid cell in a given basin and for each of the 64 projections, average total precipitation for the 1990s was calculated first. Next, for each grid cell, the ensemble median of the average total precipitation for each of the future decades was calculated and used in developing the spatially varying precipitation plots. A positive magnitude change implies wetter conditions and a negative change implies drier conditions, relative to the 1990s. The uncertainty in the distribution of the change in decade-mean precipitation for the future decades is presented using

[6] Seven locations result from the eight major Reclamation basins because the Sacramento-San Joaquin Rivers Delta inflow location combines flows from two river basins—Sacramento and San Joaquin.

the 25th and 75th percentile, and the median (50th percentile) represents the central tendency of change in decade-mean precipitation distribution.

The spatial distribution of April 1st SWE for the reference decade is also presented as an ensemble median of the 64 projections. The VIC macro-scale hydrology model was used to simulate snow dynamics, when applicable, for grid cells in the basin. Typically, snow is present in only a subset of grid cells in a basin, and VIC simulated snow accumulation and melt dynamics are only for these grid cells. At each of these grid cells in the basin and for each of the 64 projections, the average April 1st SWE for the 1990s was calculated first. Next, the ensemble median of the average April 1st SWE for each of the future decades was calculated and used in developing the spatially varying SWE plots.

SWE changes in each of the future decades were estimated as follows. For the relevant grid cells (i.e., grid cells with snow present) in a given basin and for each of the 64 projections, average April 1st SWE was calculated by averaging SWE values from the 10 water years in the decade. Then, for a given projection and at a given grid cell, the difference in average April 1st SWE between a given future decade and the reference decade was calculated. A positive magnitude change implies an increase in the SWE value, and a negative change implies a decrease in SWE, relative to the reference decade. The uncertainty in the distribution of the change in decade-mean SWE for the future decades is presented using the 25th and 75th percentile, and the median (50th percentile) represents the central tendency of change in decade-mean SWE distribution.

3.1.2 Impacts on Streamflow Annual and Seasonal Cycles

This section presents impacts on streamflow for selected subbasin river locations within the eight major Reclamation basins. Streamflow is calculated (Vano et al., 2020) using a network routing scheme (Mizukami et al., 2016) that uses the USGS geospatial fabric (Viger, 2014).

In the river basin sections that follow, the first set of plots for each basin demonstrates annual cycle variation and climate change impacts on the annual cycle at each of the selected locations for the three future periods. The second set of plots presents the uncertainty information in the flow projections using box-and-whisker plotting symbols (or boxplots for short). The box in the boxplot corresponds to the inter-quartile range (i.e., the lower bound of the box corresponds to the 25th percentile, and the upper bound corresponds to the 75th percentile). The horizontal line within the box corresponds to the median value of the change estimated from the 64 flow simulations. The whiskers correspond to the 5th and 95th percentiles of the runoff magnitude change estimated from the 64 flow simulations. For each future decade, three boxplots are presented, corresponding to the annual runoff and the December-through-March and April-through-July seasonal runoff.

The third set of plots shows the shift in timing of the annual runoff volumes as boxplots. For each projection, the shift in runoff timing was estimated to be the difference in the centroid dates, which corresponds to the timing of the center of mass of annual flow (i.e., half of the annual flow) between the mean annual hydrographs of the future decade and the reference decade. A negative shift means that the future decade will have an earlier centroid date and that more of the

annual runoff will occur earlier in the year. A positive shift indicates that more of the runoff will happen later in the year. Finally, these shifts in annual runoff timing are presented as separate boxplots for each of the three future decades. The boxplots show the uncertainty in the distribution of the shift in runoff timing estimated from the 64 projections.

The plots described here are presented in the subsequent Sections 3.2 through 3.8. The results for the eight major Reclamation river basins are presented in the following order:

- Colorado River Basin (Section 3.2)
- Columbia River Basin (Section 3.3)
- Klamath River Basin (Section 3.4)
- Missouri River Basin (Section 3.5)
- Rio Grande Basin (Section 3.6)
- Sacramento and San Joaquin River Basins (Section 3.7)
- Truckee and Carson River Basins (Section 3.8)

3.2 Colorado River Basin

The Colorado River Basin, located in the Southwestern United States, occupies an area of approximately 250,000 square miles. The Colorado River is approximately 1,400 miles long. It originates along the Continental Divide in Rocky Mountain National Park, Colorado, and ends where it meets the Gulf of California in Mexico. The Colorado River is a critical resource in the West because seven basin States (Arizona, California, Colorado, Nevada, New Mexico, Utah, and Wyoming) depend on it for water supply, hydropower production, recreation, fish and wildlife habitat, and other benefits. Although agricultural uses account for 70 percent of Colorado River water use, between 35 and 40 million people rely on the same water for some or all of their municipal needs. Moreover, the United States also has a delivery obligation to Mexico for some of the Colorado River waters pursuant to a 1944 treaty.

3.2.1 Hydroclimate Projections

Figure 7 shows six plots of hydroclimate indicators for the Colorado River above Imperial Dam: annual total precipitation (top left), annual mean temperature (top right), April 1st SWE (middle left), annual runoff (middle right), December-through-March runoff (bottom left), and April-through-July runoff (bottom right). The heavy black line is the median value (50th percentile) of the annual time series of the 64 projections. The shaded area is the annual time series of the 10th to 90th percentiles.

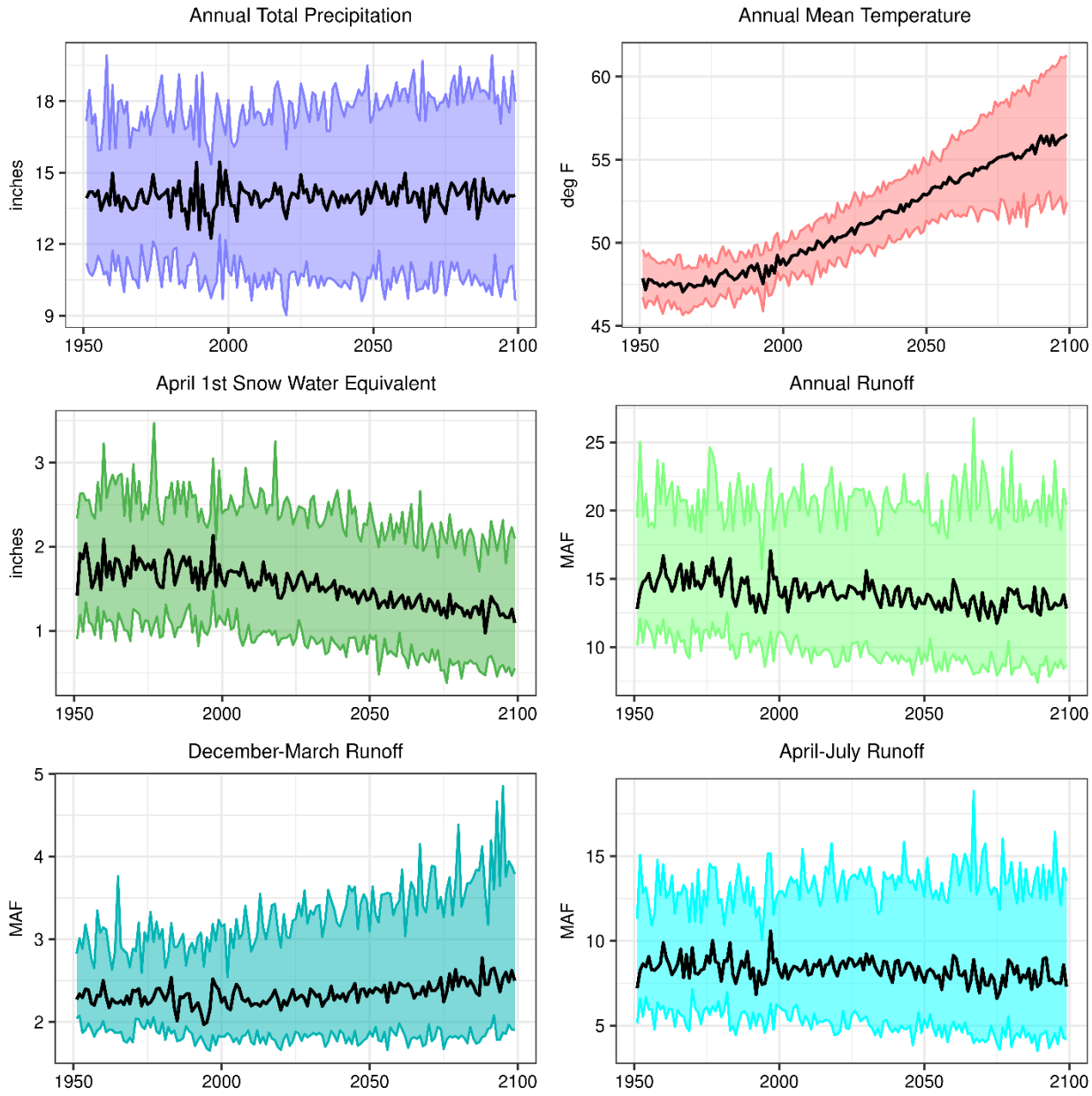

Figure 7. Colorado River Basin – Time series plots for six projected hydroclimate indicators.

Note: The heavy black line is the annual time series median value (i.e., median). The shaded area is the annual time series of 10th to 90th percentiles.

MAF = million acre-feet; deg F = degrees Fahrenheit

Total annual precipitation (median value) throughout the basin is shown to be largely constant over time. The ensemble spread appears to be somewhat widening, implying that, there is some increase in the range of values for total annual precipitation magnitudes through time. The mean annual temperature (median value) throughout the basin shows an increase over time and a widening ensemble spread, implying that, there is some increase in the range of mean annual temperature values over time. April 1st SWE (median value) shows a decrease over time. The annual runoff (median value) shows a decrease over time. The December-through-March runoff

volume shows an increase over time, and the April-through-July runoff shows a decrease over time. For additional discussions and information regarding currently ongoing studies in the basin, see Sections 3.9 and 3.9.1.1.

Figure 8, Figure 9, and Figure 10 show the spatial distribution of simulated decade-mean temperatures, precipitation, and April 1st SWE, respectively, in the Colorado River Basin above Imperial Dam. In each figure, the simulated 1990s distribution of median decadal mean condition for the variable of interest is shown in the upper middle plot, and changes in the decadal mean condition are shown below for three future periods (2020s, 2050s, and 2070s relative to the 1990s) at three change percentiles within the range of projections (25th, 50th, and 75th percentiles).

In Figure 8, the median change for the three future decades relative to the 1990s indicates increasing temperatures throughout the basin. In Figure 9, the median change in precipitation for the future decades indicates a wet pattern, particularly in the upper portions of the basin (Upper Colorado River Basin). In Figure 10, the spatial plots generally indicate a reduced snowpack.

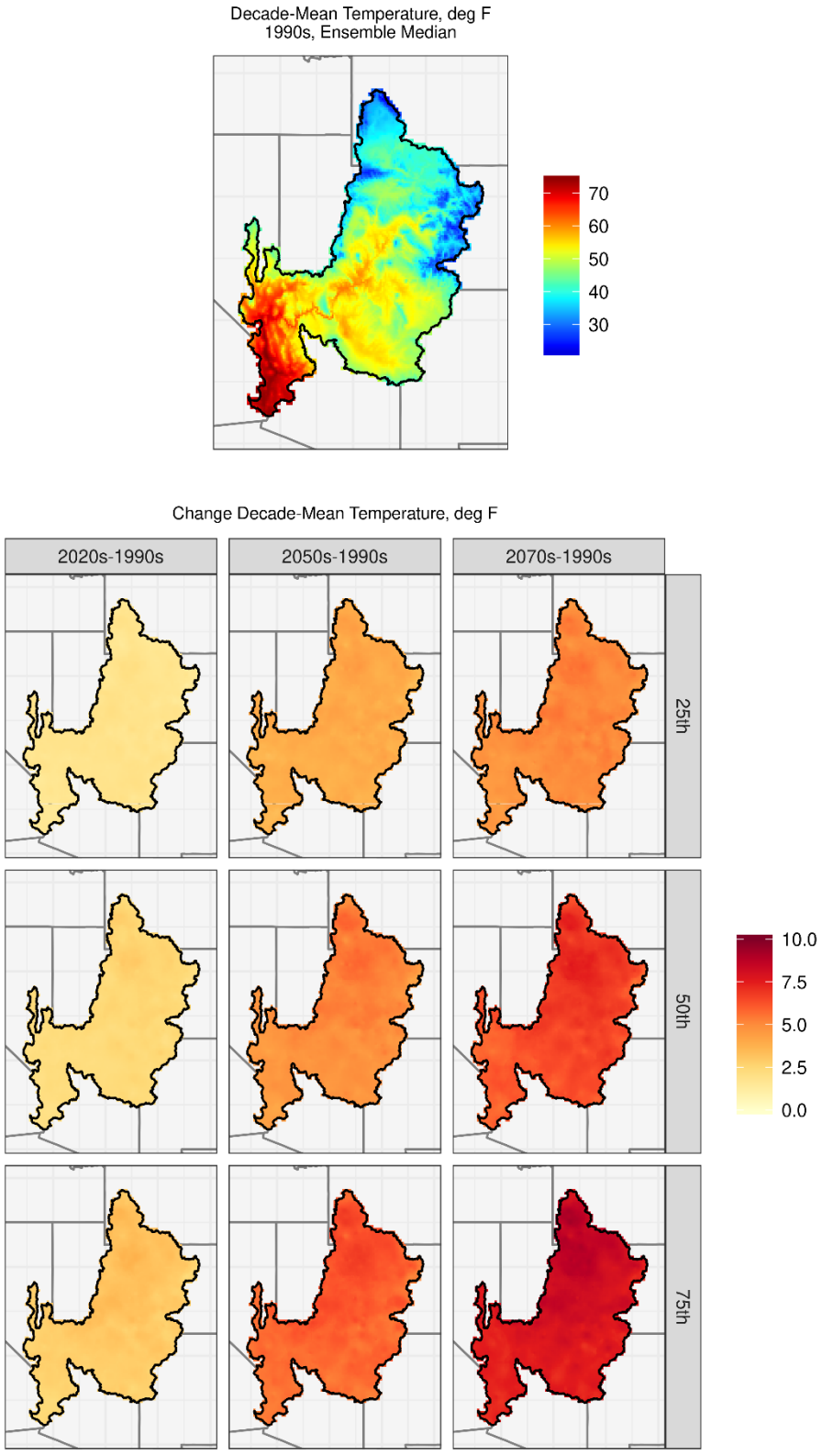

Figure 8. Colorado River Basin – Spatial distribution of simulated decadal temperature changes.

Note: deg F = degrees Fahrenheit

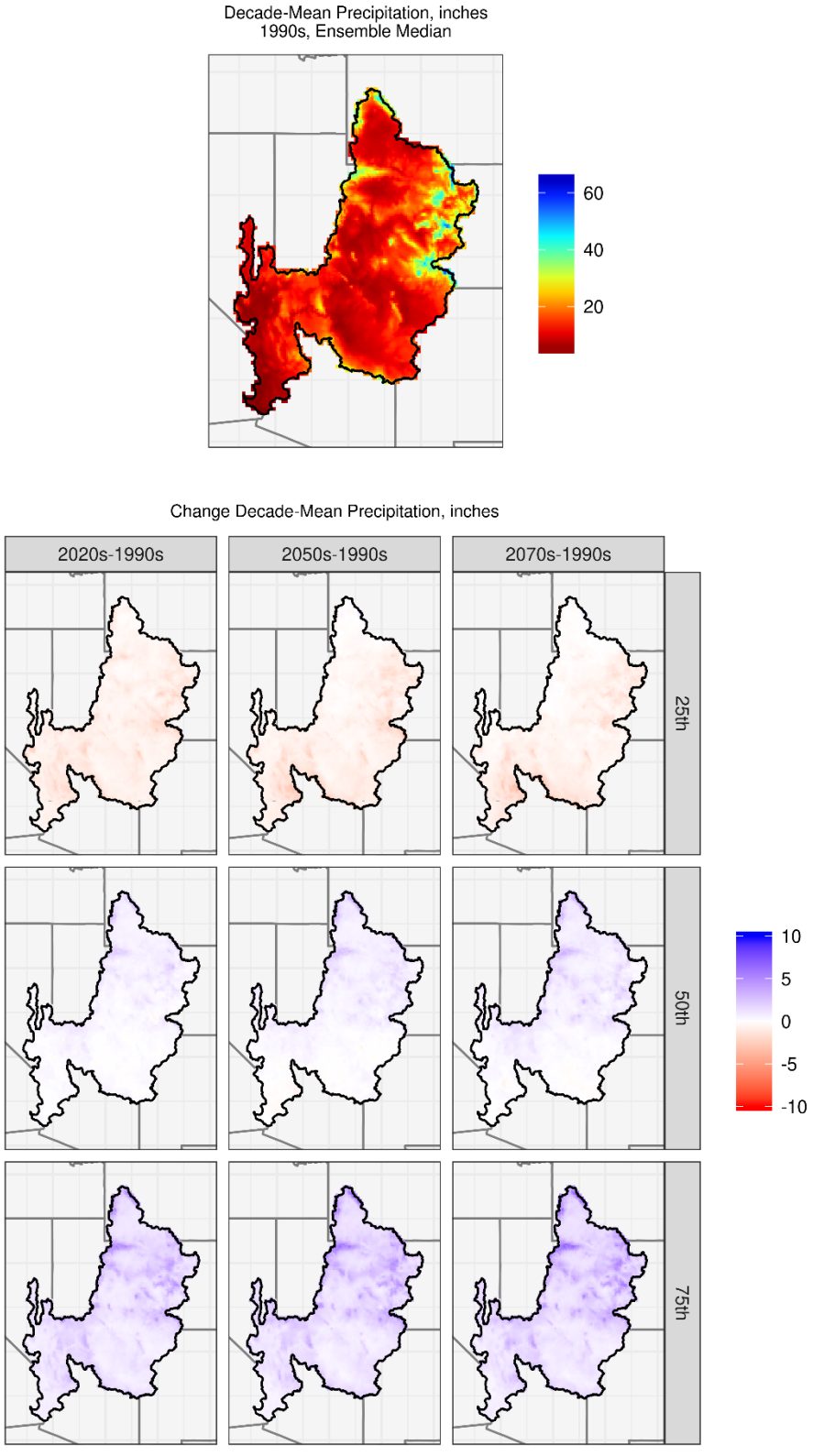

Figure 9. Colorado River Basin – Spatial distribution of simulated precipitation changes.

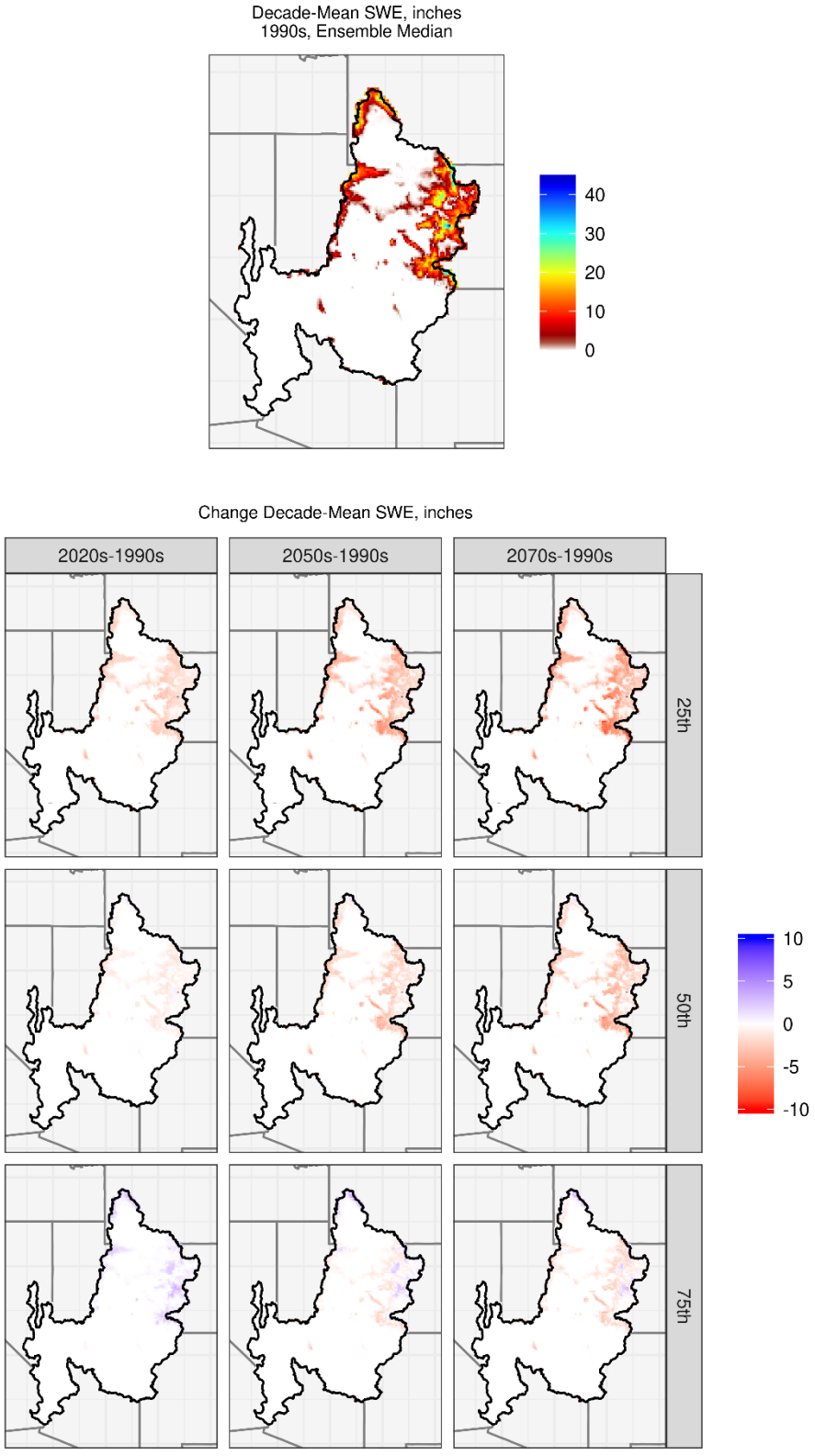

Figure 10. Colorado River Basin – Spatial distribution of simulated decadal April 1st SWE changes.

3.2.2 Impacts on Streamflow Annual and Seasonal Cycles

Figure 11 shows the mean monthly streamflow values for the 1990s, 2020s, 2050s, and 2070s in six Colorado River subbasins. Overall, there is a shift to earlier runoff peaks, which is most prominent in the 2070s for all the subbasins. Also, the magnitude of the peaks varies across the subbasins in the future decades in comparison to the reference 1990s decade.

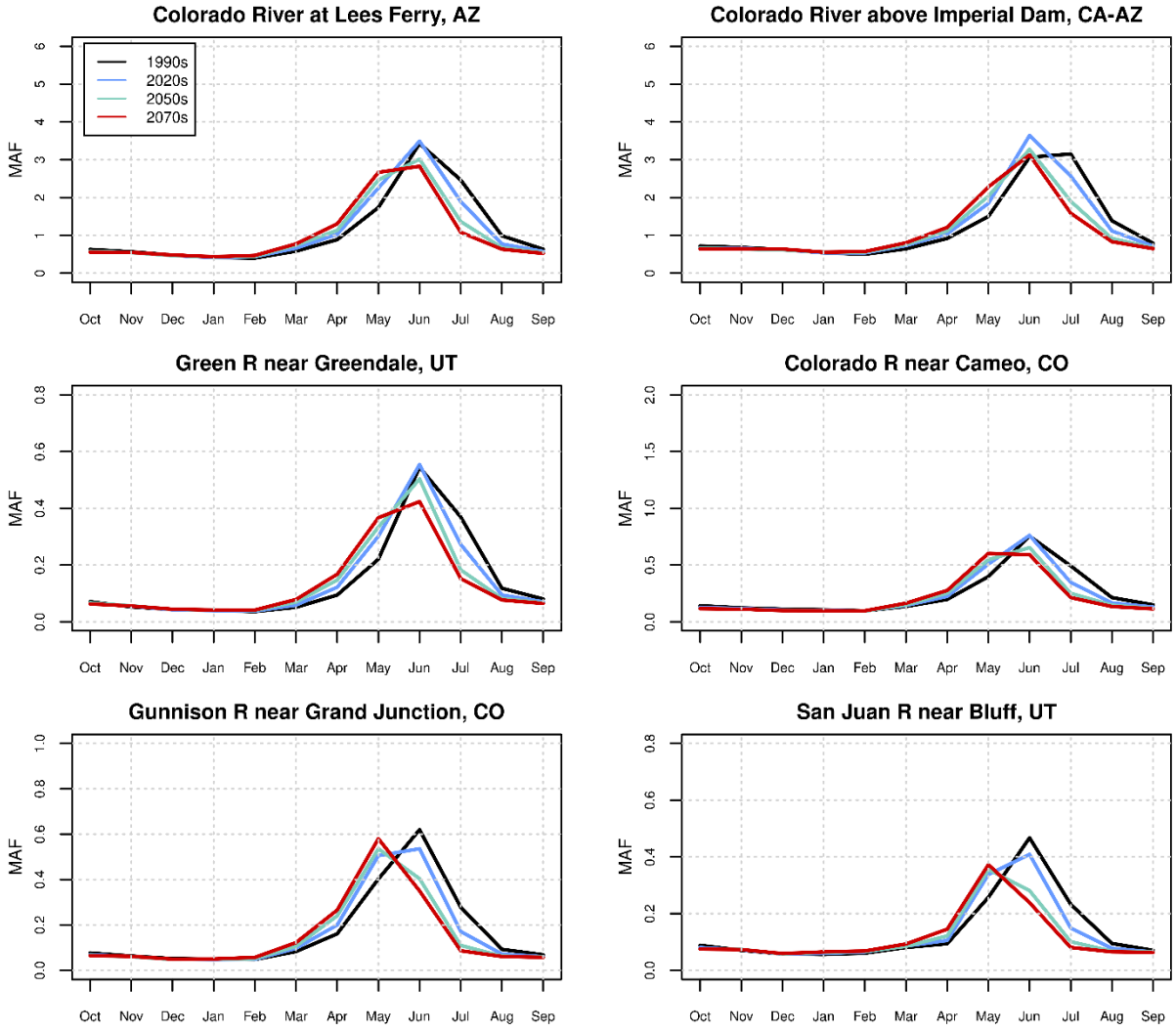

Figure 11. Colorado River Basin – Simulated mean monthly streamflow for various subbasins.

Note: MAF = million acre-feet

Figure 12 shows boxplots of the distribution of simulated changes in runoff magnitude for annual, December-through-March, and April-through-July runoff in the six Colorado River subbasins. The median change for the December-through-March period in all three decades is generally positive, indicating an increase in runoff. Also, see Figure 7 (bottom left panel) for an example of the December-through-March runoff time series for the Colorado River above Imperial Dam subbasin, which shows an increase over time in runoff for this season. The median annual streamflow change, both at Lees Ferry and at Imperial Dam, shows practically no change

for the 2020s, but decreases for the 2050s and 2070s from the 1990s reference. Overall, in the 2020s, the median annual flow is largely unchanged from the 1990s for most of the subbasins. However, for the 2050s and 2070s, a decline in the median annual flows is indicated for all subbasins (except for Green River near Greendale, UT which shows minor flow increases in the 2050s). Finally, in interpreting these change results, it is important to recognize the uncertainty in the change magnitude and direction.

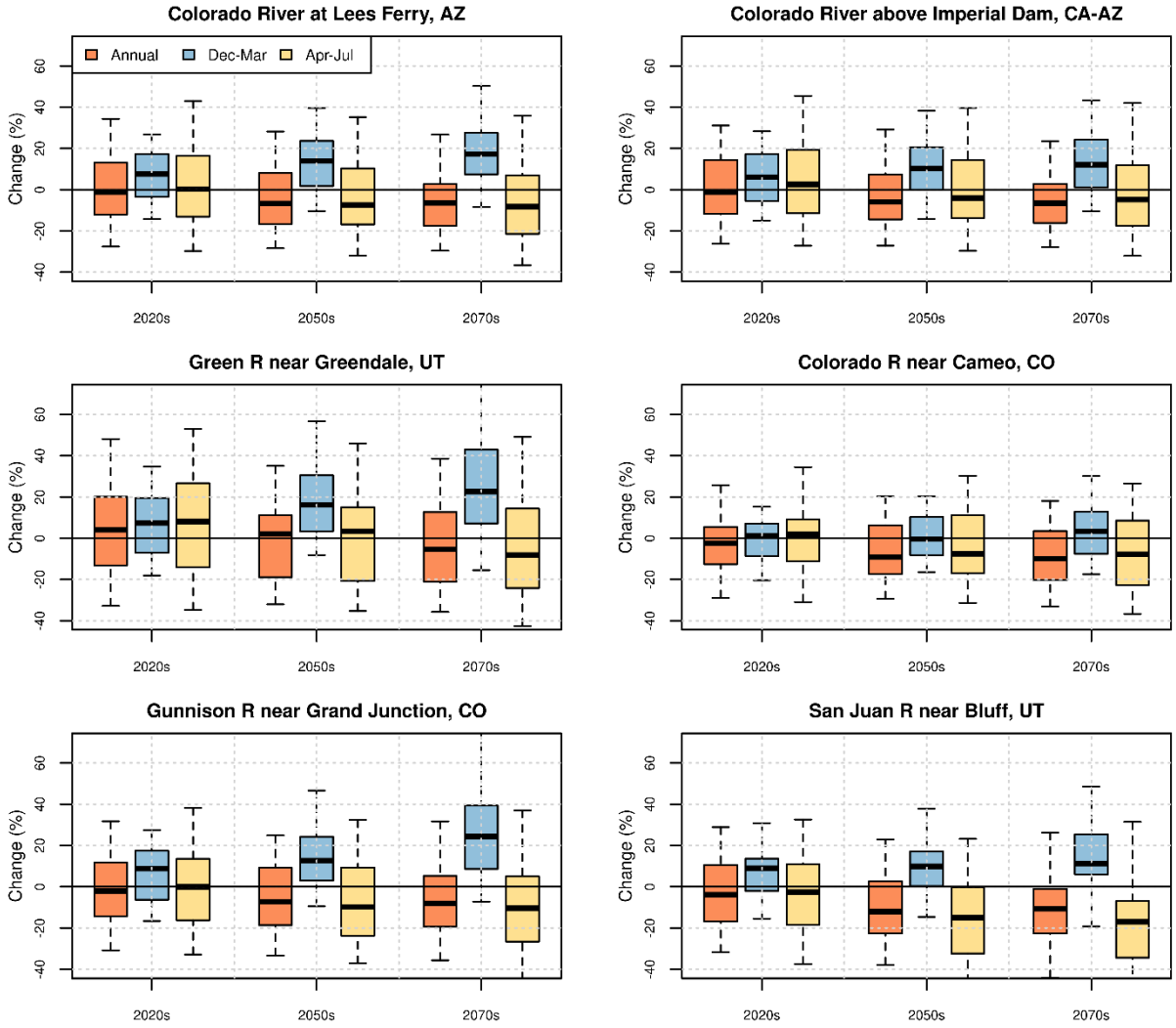

Figure 12. Colorado River Basin – Simulated change in streamflow magnitude for various subbasins.

Figure 13 shows the simulated shift in runoff timing for the various subbasins. The analysis shows that for all three future periods—2020s, 2050s, and 2070s—nearly half of the projections (i.e., the median value in the boxplots) show that the timing of the center of mass of annual flow (i.e., half of the annual flow) will occur earlier than in the 1990s. As an example, for the Colorado River at Lees Ferry, this shift in early runoff timing will be about 6 days, 9 days, and 11 days respectively for the 2020s, 2050s, and 2070s decades. Overall, nearly all projections are pointing towards an early runoff in the future relative to the 1990s.

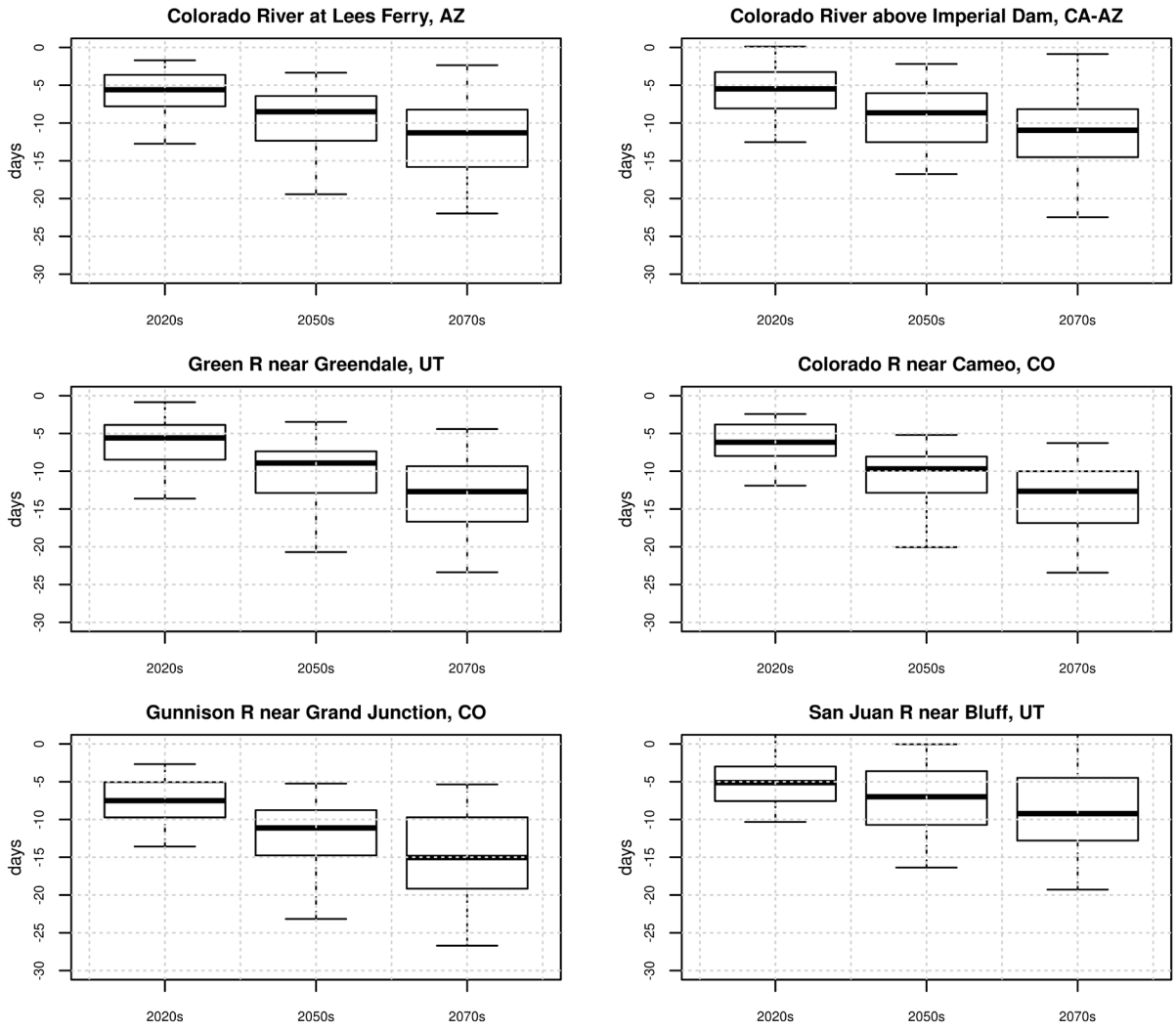

Figure 13. Colorado River Basin – Simulated shift in streamflow timing for various subbasins; negative values denote earlier runoff relative to the 1990s.

3.3 Columbia River Basin

The Columbia River is the fourth largest river in North America. It rises in the Rocky Mountains of British Columbia, Canada, and flows 1,243 miles to the Pacific Ocean through Washington and Oregon. The Columbia River Basin occupies an area of approximately 258,000 square miles and spans seven States (Idaho, Montana, Nevada, Oregon, Utah, Washington, and Wyoming) and one Canadian province (British Columbia). The river system has more than 400 dams, which provide hydroelectricity, irrigation, flood control, operations for fish and wildlife, streamflow regulation, and storage and delivery of water. Dams in the Columbia River Basin and lower Snake River basin also provide operations for navigation. Collectively, Columbia River system dams provide up to 80 percent of the electrical needs in the Northwest; 39.7 million acre-feet of storage space for flood control; locks and other infrastructure for navigation of 17 million tons of

cargo annually; irrigation for 7.8 million acres of land; and recreational opportunities for hundreds of thousands of Americans.

3.3.1 Hydroclimate Projections

Figure 14 shows six hydroclimate indicators for the Columbia River at The Dalles: annual total precipitation (top left), annual mean temperature (top right), April 1st SWE (middle left), annual runoff (middle right), December-through-March runoff (bottom left), and April-through-July runoff (bottom right). The heavy black line is the median value (50th percentile) of the annual time series of the 64 projections. The shaded area is the annual time series of the 10th to 90th percentiles.

Total annual precipitation (median value) throughout the basin is shown to be increasing over time. The ensemble spread appears to be somewhat widening, implying that, there is some increase in the range of values for total annual precipitation magnitudes through time. The mean annual temperature (median value) throughout the basin shows an increase over time and a widening ensemble spread, implying that, there is some increase in the range of mean annual temperature values over time. April 1st SWE (median value) shows a decrease over time. The annual runoff (median value) shows some decrease over time (for additional discussions, see Sections 3.9 and 3.9.1.2). The December-through-March runoff volume shows an increase over time, and the April-through-July runoff shows a decrease over time.

Figure 15, Figure 16, and Figure 17 show the spatial distribution of simulated decade-mean temperatures, precipitation, and April 1st SWE, respectively, in the Columbia River above The Dalles. In each figure, the simulated 1990s distribution of median decadal mean condition for the variable of interest is shown in the upper middle plot, and changes in the decadal mean condition are shown below for the three future periods and at three change percentiles within the range of projections (25th, 50th, and 75th percentiles).

In Figure 15, the median change for the three future decades relative to the 1990s indicates increasing temperatures throughout the basin. In Figure 16, the median change in precipitation for the future decades indicates a wet pattern in the basin. In Figure 17, the spatial plots indicate the basin is projected to have generally reduced snowpack (April 1st SWE). Analyses of results from Figure 14 through Figure 17 indicate that warming is projected to lead to precipitation falling as rain instead of snow, leading to decreased snowpack in the basin and shifts in runoff seasonality.

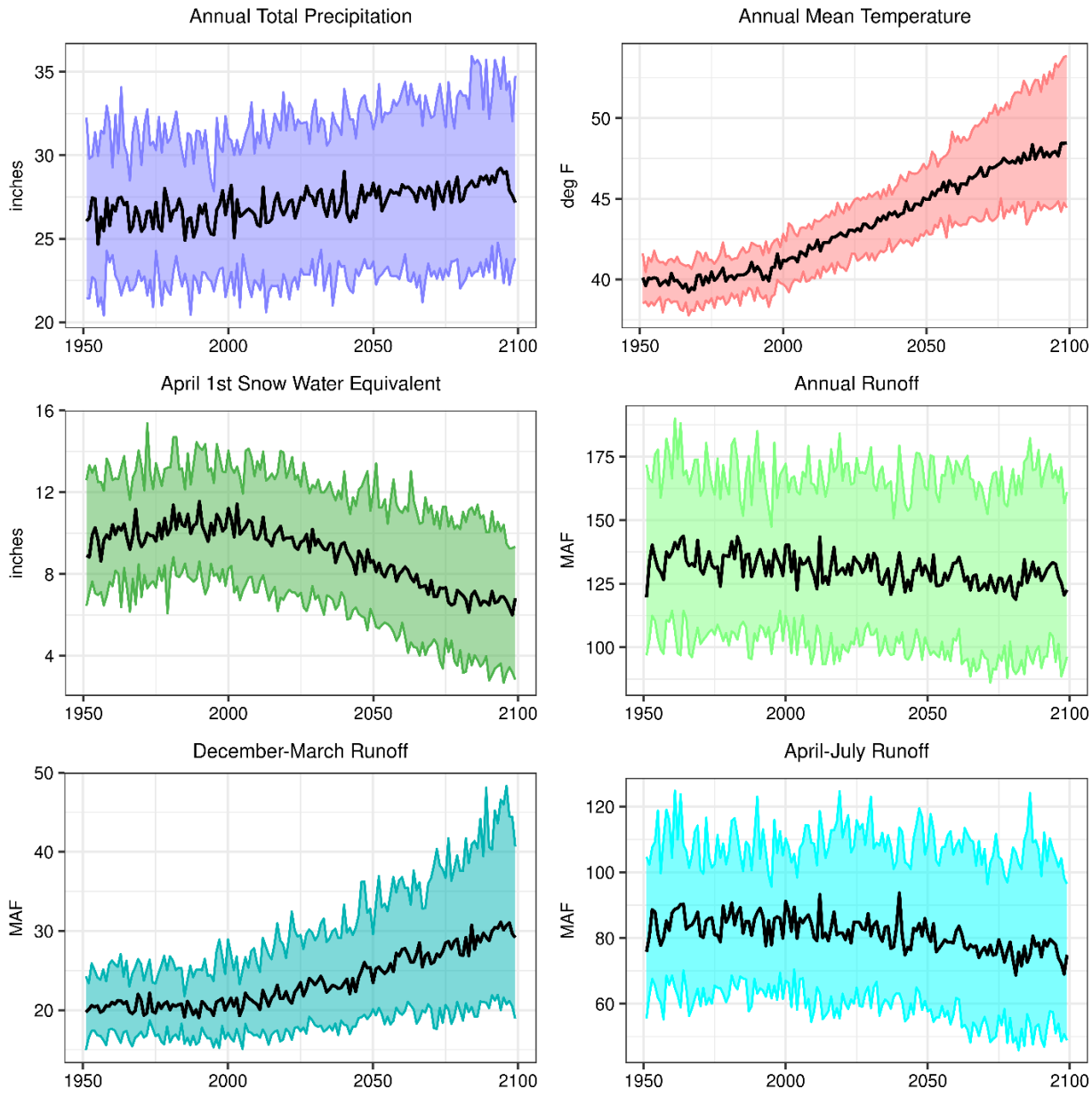

Figure 14. Columbia River Basin – Time series plots for six projected hydroclimate indicators.

Note: The heavy black line is the annual time series median value (i.e., median). The shaded area is the annual time series of 10th to 90th percentiles.

MAF = million acre-feet; deg F = degrees Fahrenheit

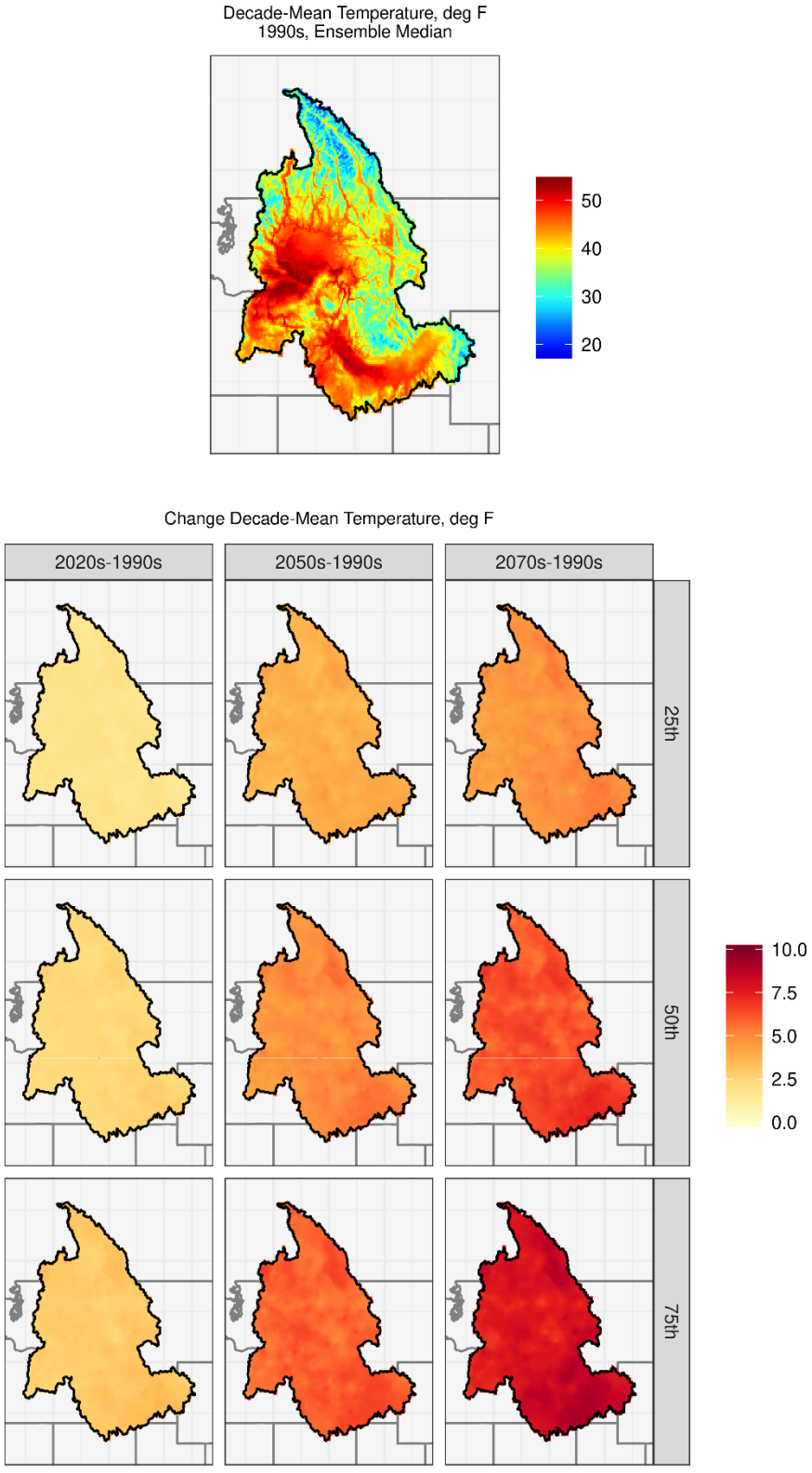

Figure 15. Columbia River Basin – Spatial distribution of simulated decadal temperature changes.

Note: deg F = degrees Fahrenheit

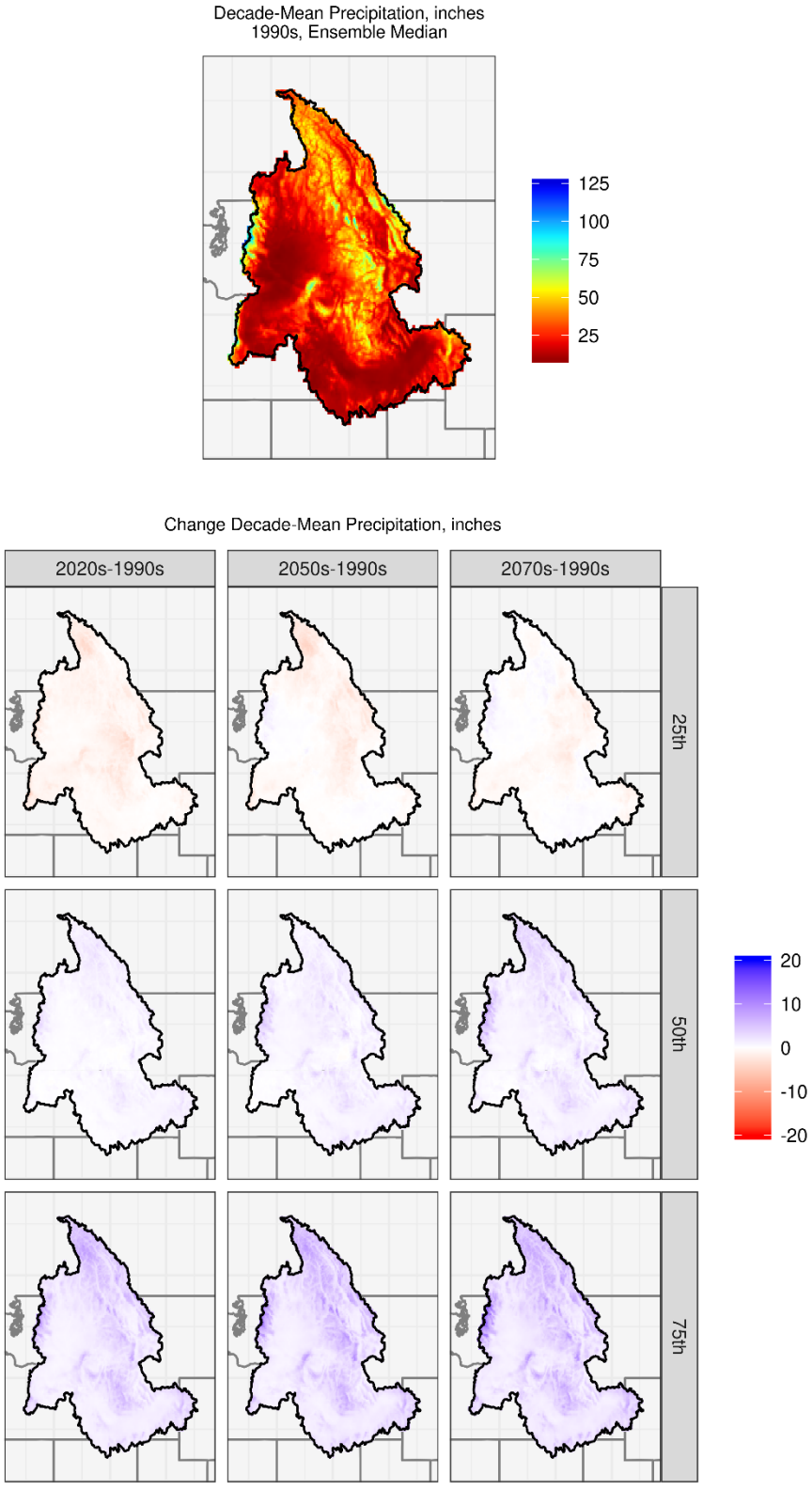

Figure 16. Columbia River Basin – Spatial distribution of simulated precipitation changes.

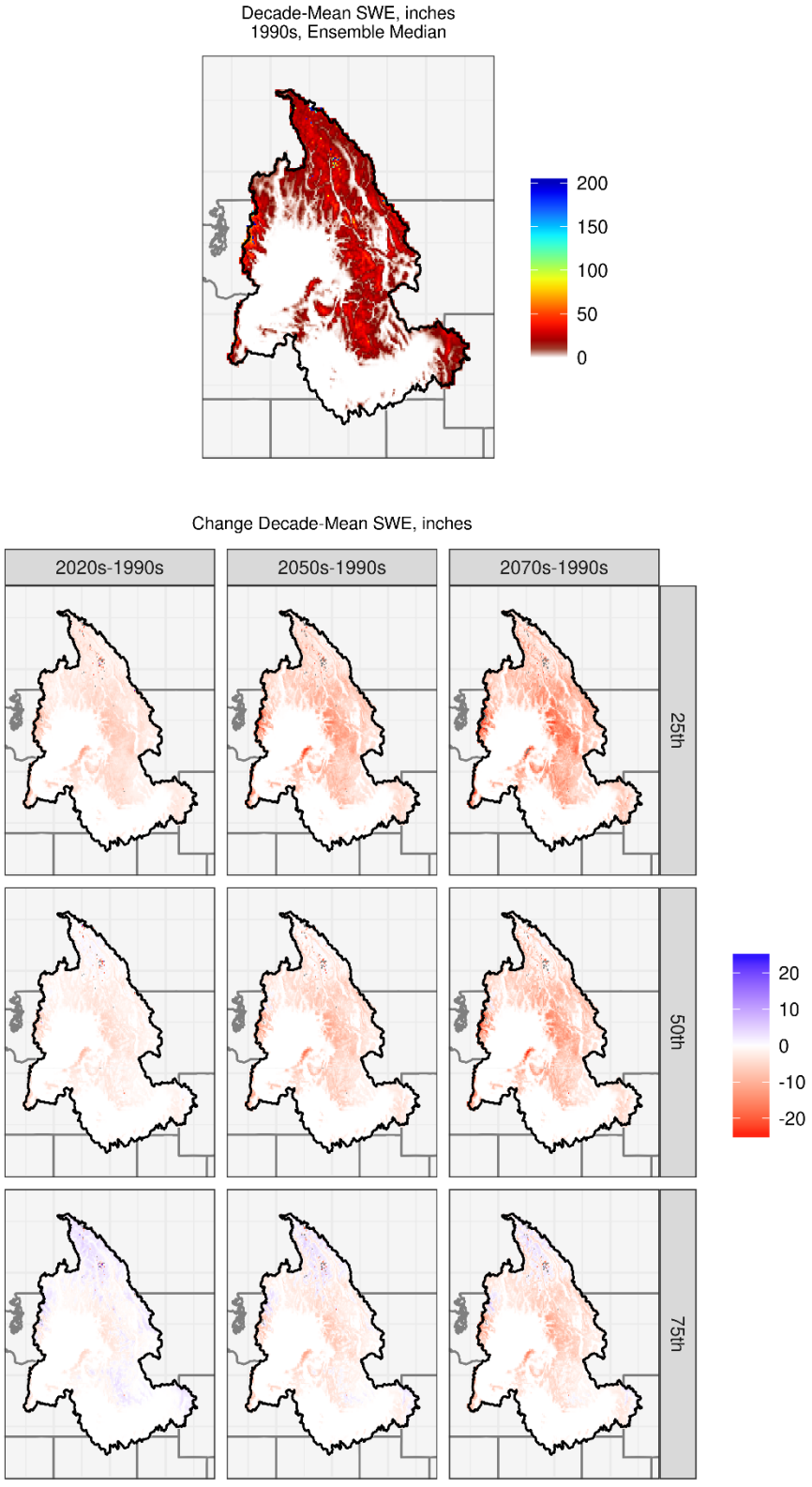

Figure 17. Columbia River Basin – Spatial distribution of simulated decadal April 1st SWE changes.

3.3.2 Impacts on Streamflow Annual and Seasonal Cycles

Figure 18 shows the mean monthly streamflow values for the 1990s, 2020s, 2050s, and 2070s in seven Columbia River subbasins. Overall, there does not appear to be much of a shift in the peak runoff timing from the reference 1990s decade to the 2020s and 2050s. For the 2070s, however, all the subbasins show a noticeable early shift in peak flow. Furthermore, the peaks are generally the same or somewhat lower in the 2020s and 2050s, but consistently lower in the 2070s across all subbasins from the 1990s reference.

Figure 19 shows boxplots of the distribution of simulated changes in streamflow magnitude for annual, December-through-March, and April-through-July runoff in the seven Columbia River subbasins. For most of the subbasins, in all three future decades the median change for the December-through-March runoff is positive, indicating an increase in streamflow during this season. Also, see Figure 14 (bottom left panel) for an example of the December-through-March runoff time series for the Columbia River at The Dalles subbasin, which shows an increase in runoff over time for this season. The April-through-July median streamflow shows declines in the 2050s and 2070s relative to the 1990s across the subbasins. In addition, see Figure 14 (bottom right panel) for an example of the April-through-July runoff time series for the Columbia River at The Dalles subbasin, which shows a decrease in runoff over time for this season.

Figure 20 shows the simulated shift in streamflow timing for the various subbasins. For all the subbasins in all three future decades, the median value of the change in runoff timing is negative. This implies that half of the annual flow occurs sooner than it did in the 1990s. For example, for the Columbia River at The Dalles, the earlier shift is about 5, 9, and 11 days, respectively, in the 2020s, 2050s, and 2070s relative to the 1990s.

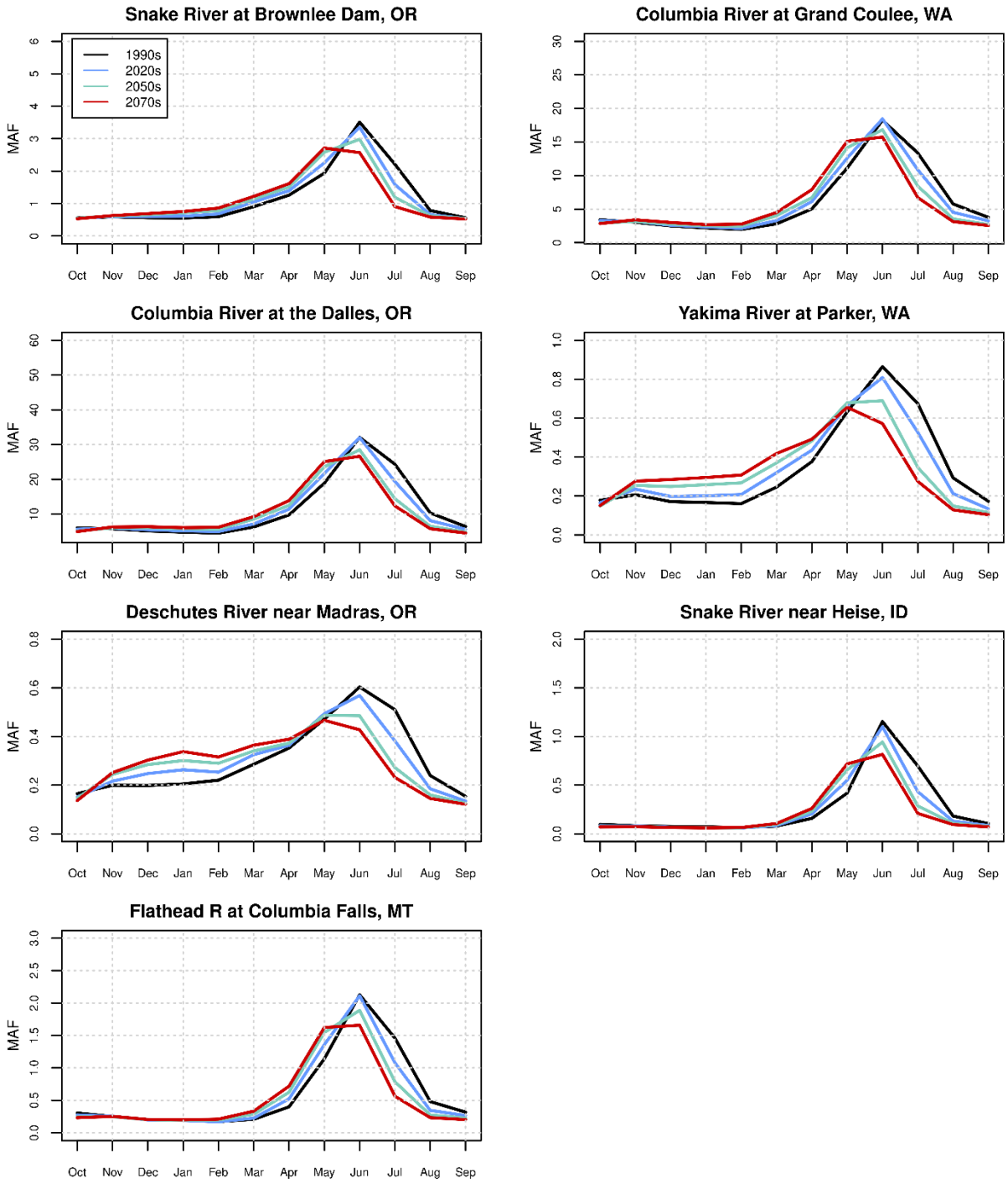

Figure 18. Columbia River Basin – Simulated mean monthly streamflow for various subbasins.

Note: MAF = million acre-feet

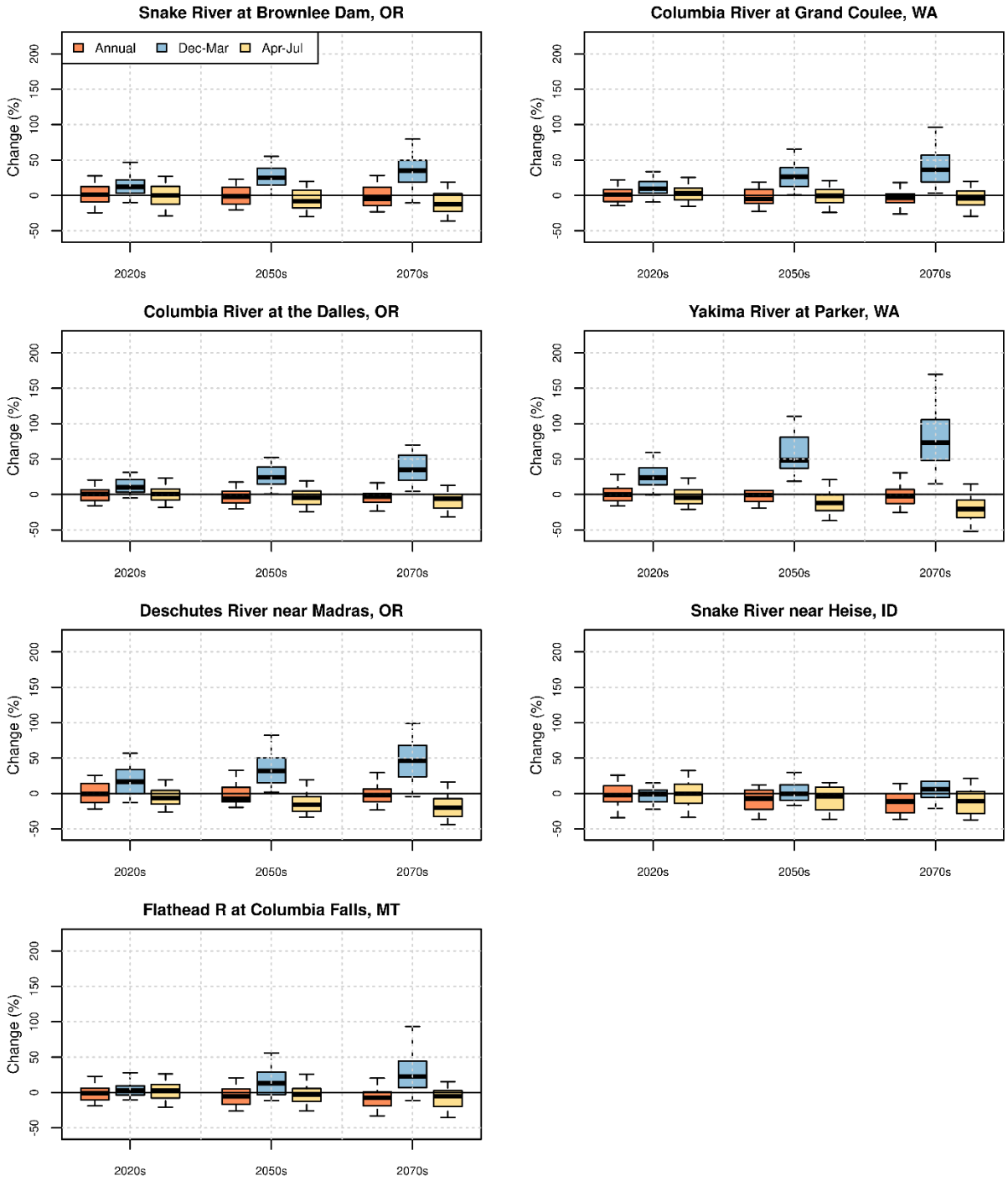

Figure 19. Columbia River Basin – Simulated change in streamflow magnitude for various subbasins.

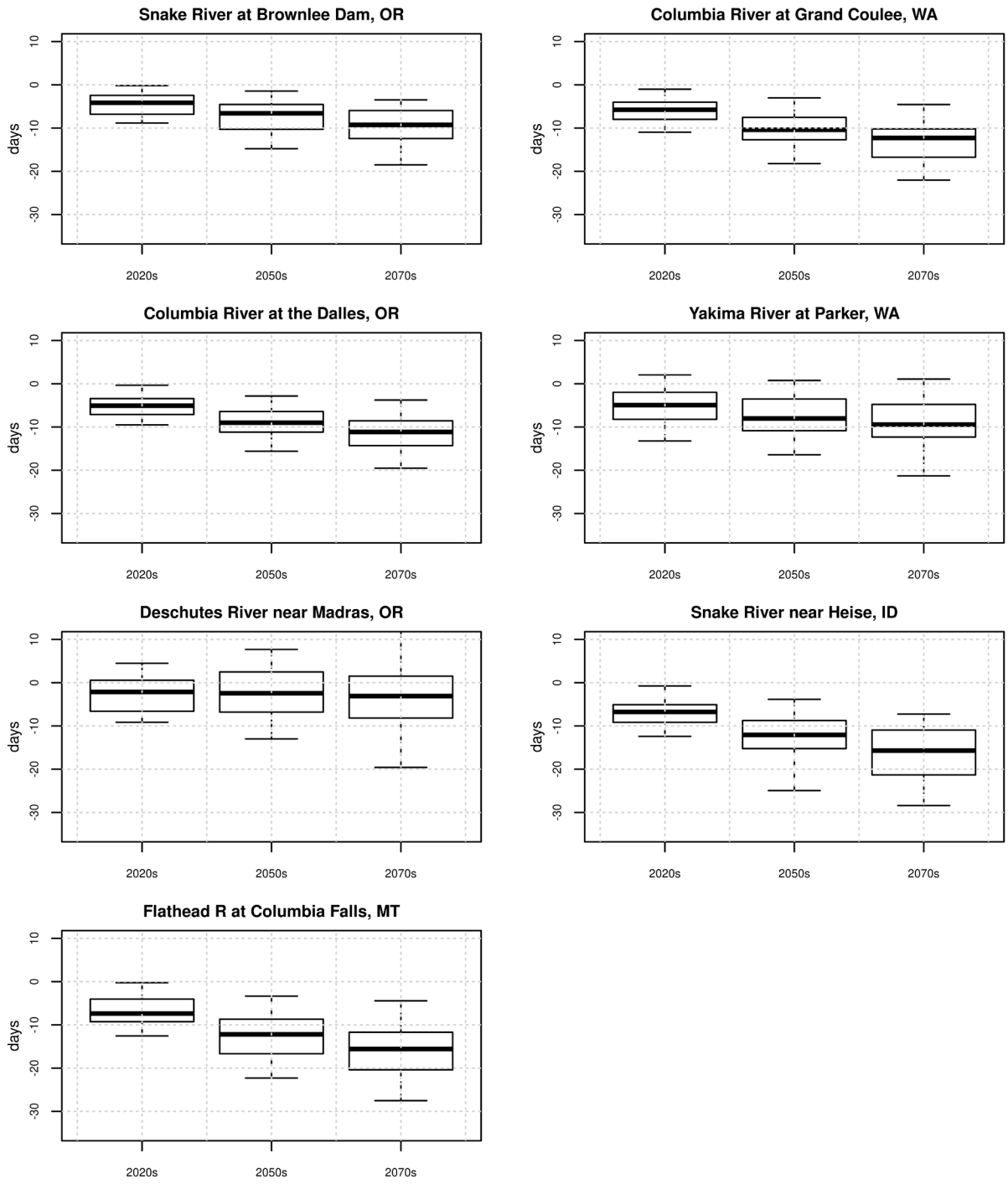

Figure 20. Columbia River Basin – Simulated shift in streamflow timing for various subbasins; negative values denote earlier runoff relative to the 1990s.

3.4 Klamath River Basin

The Klamath River originates in headwater streams of south-central Oregon. It eventually flows southwest through the Cascade Range and picks up runoff from the Shasta, Scott, Salmon, and Trinity Rivers in California before flowing to the Pacific Ocean. The length of the Klamath River is approximately 254 miles and the Klamath River Basin covers an area of approximately 15,700 square miles. Reclamation's Klamath Project provides irrigation water for approximately 210,000 acres of cropland and is an important recreation area for residents of northern California and southern Oregon, providing myriad boating, water skiing, fishing, hunting, camping, and picnicking opportunities.

3.4.1 Hydroclimate Projections

Figure 21 shows six hydroclimate indicators for the basin above the Klamath River near Klamath gaging station: annual total precipitation (top left), annual mean temperature (top right), April 1st SWE (middle left), annual runoff (middle right), December-through-March runoff (bottom left), and April-through-July runoff (bottom right). The heavy black line is the median value (50th percentile) of the annual time series of the 64 projections. The shaded area is the annual time series of the 10th to 90th percentiles.

Total annual precipitation (median value) throughout the basin is shown to be largely constant over time. The ensemble spread appears to be somewhat widening, implying that, there is some increase in the range of values for total annual precipitation magnitudes through time. The mean annual temperature (median value) throughout the basin shows an increase over time and a widening ensemble spread, implying that, there is some increase in the range of mean annual temperature values over time. April 1st SWE (median value) shows a decrease over time. The annual runoff (median value) shows some decrease over time (for additional discussions, see Sections 3.9 and 3.9.1.3). The December-through-March runoff volume shows an increase over time, and the April-through-July runoff shows a decrease over time.

Figure 22, Figure 23, and Figure 24 show the spatial distribution of simulated decade-mean temperatures, precipitation, and April 1st SWE, respectively, in the basin above the Klamath River near Klamath gaging station. In each figure, the simulated 1990s distribution of median decadal mean condition for the variable of interest is shown in the upper middle plot, and changes in the decadal mean condition are shown below for the three future periods and at three change percentiles within the range of projections (25th, 50th, and 75th percentiles).

In Figure 22, the median change for the three future decades relative to the 1990s indicates increasing temperatures throughout the basin. In Figure 23, the median change in precipitation for the future decades indicates a slightly wetter pattern in the lower portions of the basin. In Figure 24, the spatial plots indicate that a reduced snowpack is projected throughout the basin.

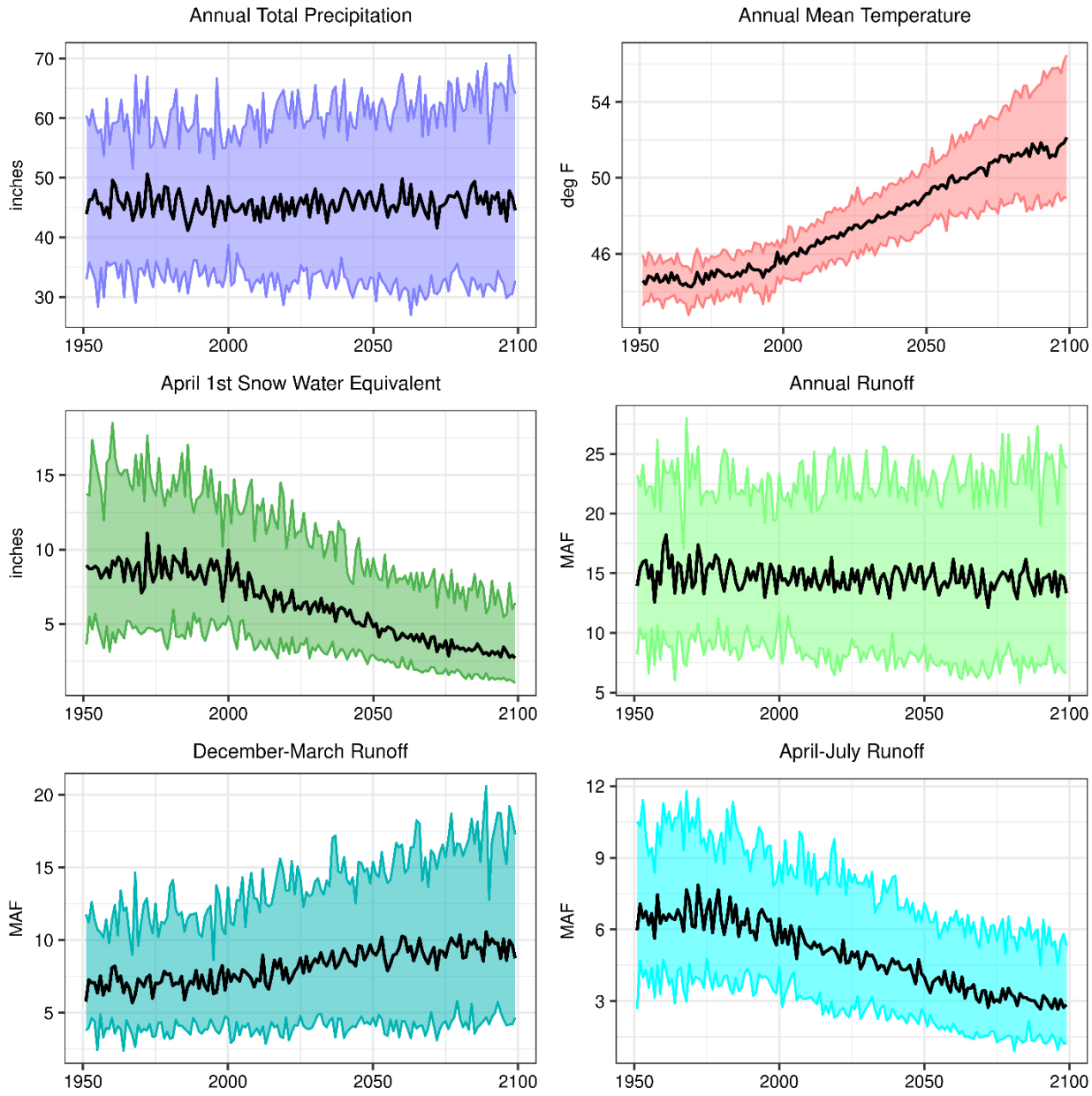

Figure 21. Klamath River Basin – Time series plots for six projected hydroclimate indicators.

Note: The heavy black line is the annual time series median value (i.e., median). The shaded area is the annual time series of 10th to 90th percentiles.

MAF = million acre-feet; deg F = degrees Fahrenheit

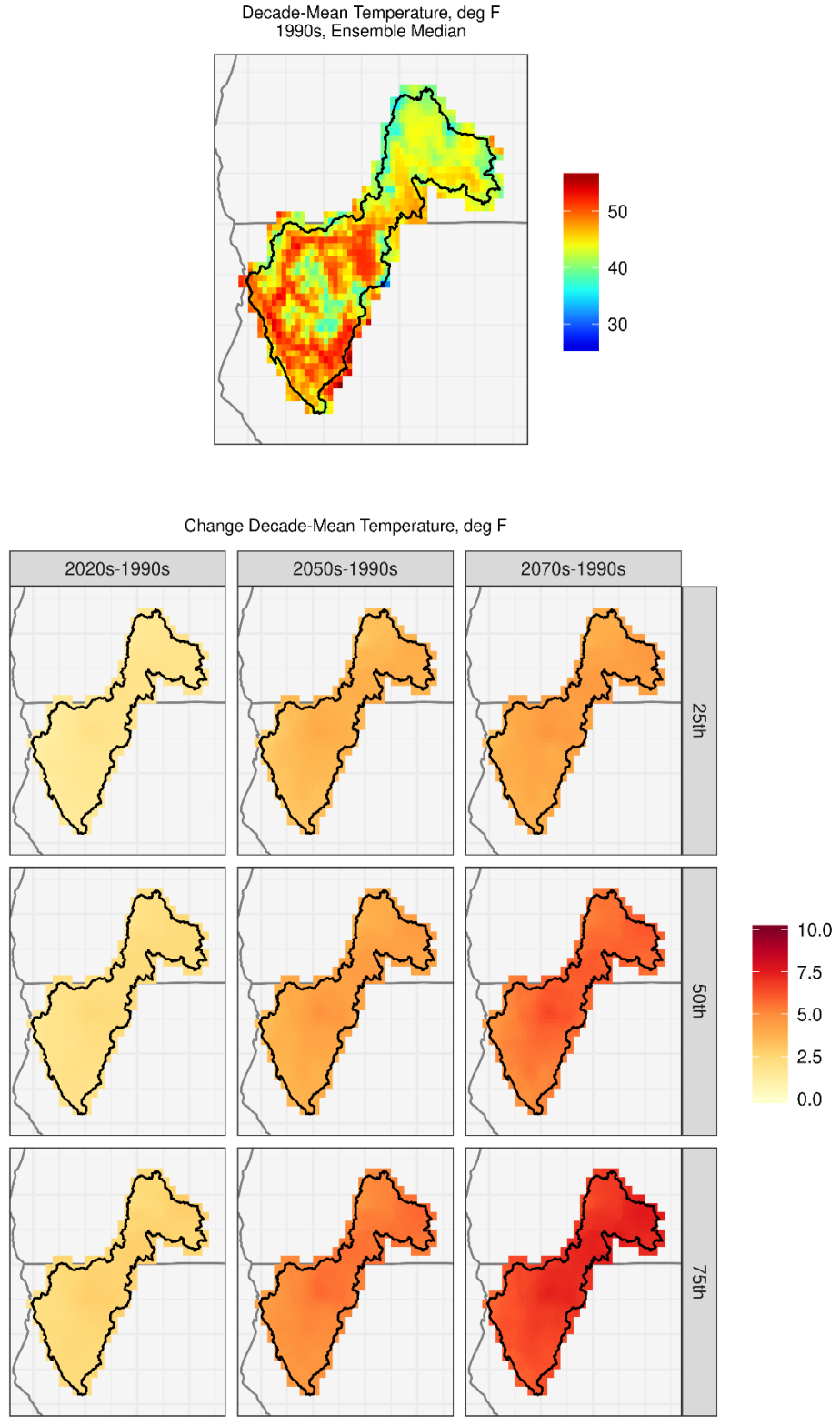

Figure 22. Klamath River Basin – Spatial distribution of simulated decadal temperature changes.

Note: deg F = degrees Fahrenheit

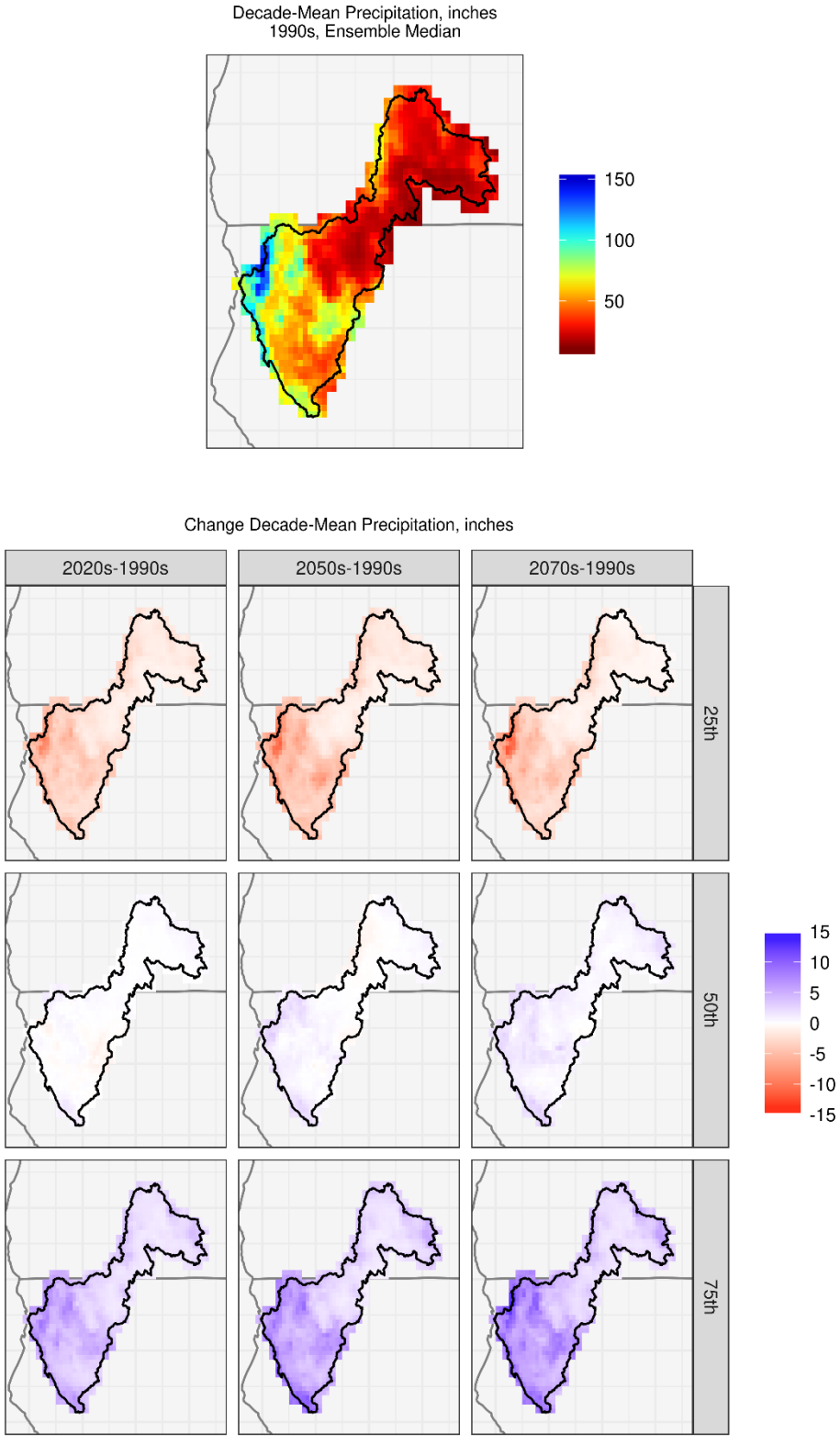

Figure 23. Klamath River Basin – Spatial distribution of simulated precipitation changes.

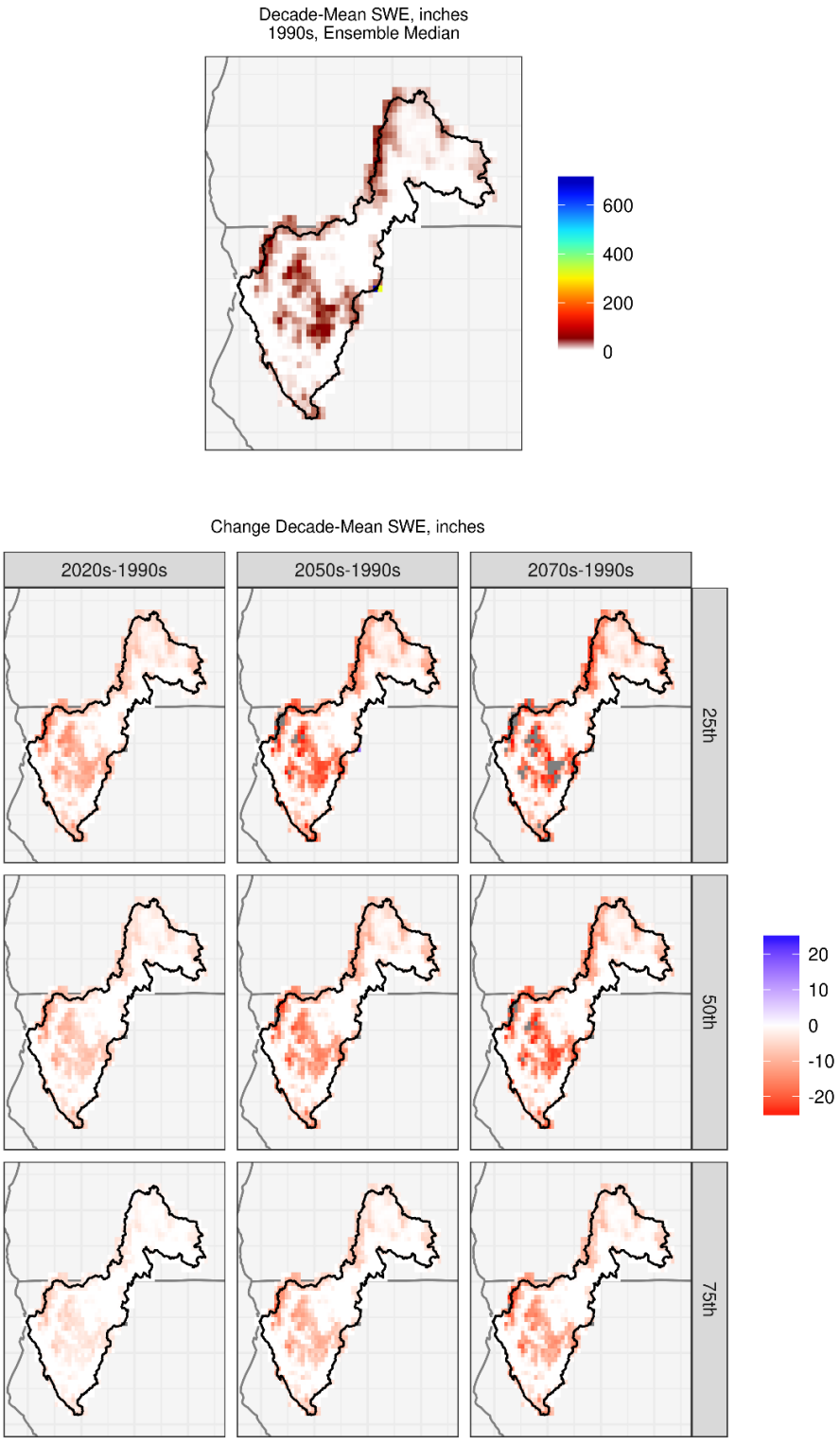

Figure 24. Klamath River Basin – Spatial distribution of simulated decadal April 1st SWE changes.

Note: The gray pixels within the basin boundary indicate reduction of SWE beyond the color scale range.

3.4.2 Impacts on Streamflow Annual and Seasonal Cycles

Figure 25 shows mean monthly streamflow values for the 1990s, 2020s, 2050s, and 2070s in five Klamath River subbasins. For the five sites in this basin, the shift in peak runoff in all future decades is clearly visible and fairly pronounced for the 2070s relative to the 1990s.

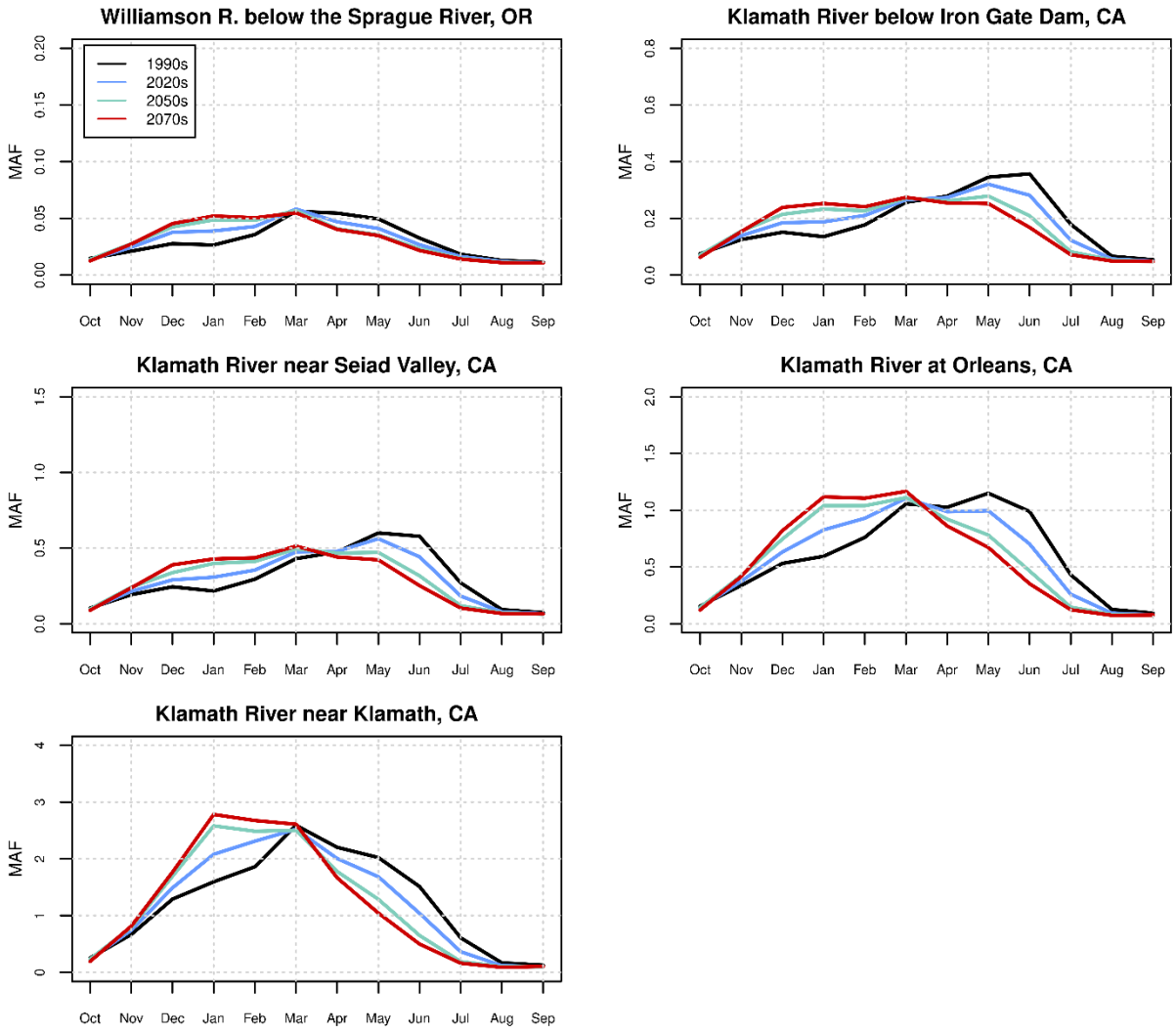

Figure 25. Klamath River Basin – Simulated mean monthly streamflow for various subbasins.

Note: MAF = million acre-feet

Figure 26 shows boxplots of the distribution of changes in runoff magnitude for annual, December-through-March, and April-through-July runoff in the five Klamath River subbasins. For all the subbasins, in all three future decades the median change for the December-through-March runoff is positive, indicating an increase in runoff during this season. Also, see Figure 21 (bottom left panel) for an example of the December-through-March runoff time series for the Klamath River near Klamath subbasin, which shows an increase in runoff over time for this season. However, the April-through-July median runoff shows declines in the 2020s, 2050s, and 2070s relative to the 1990s across all of the subbasins. In addition, see Figure 21 (bottom right

panel) for an example of the April-through-July runoff time series for the Klamath River near Klamath subbasin, which shows a decrease in runoff over time for this season. The median annual runoff largely shows no change in any of the subbasins in any of the three future periods.

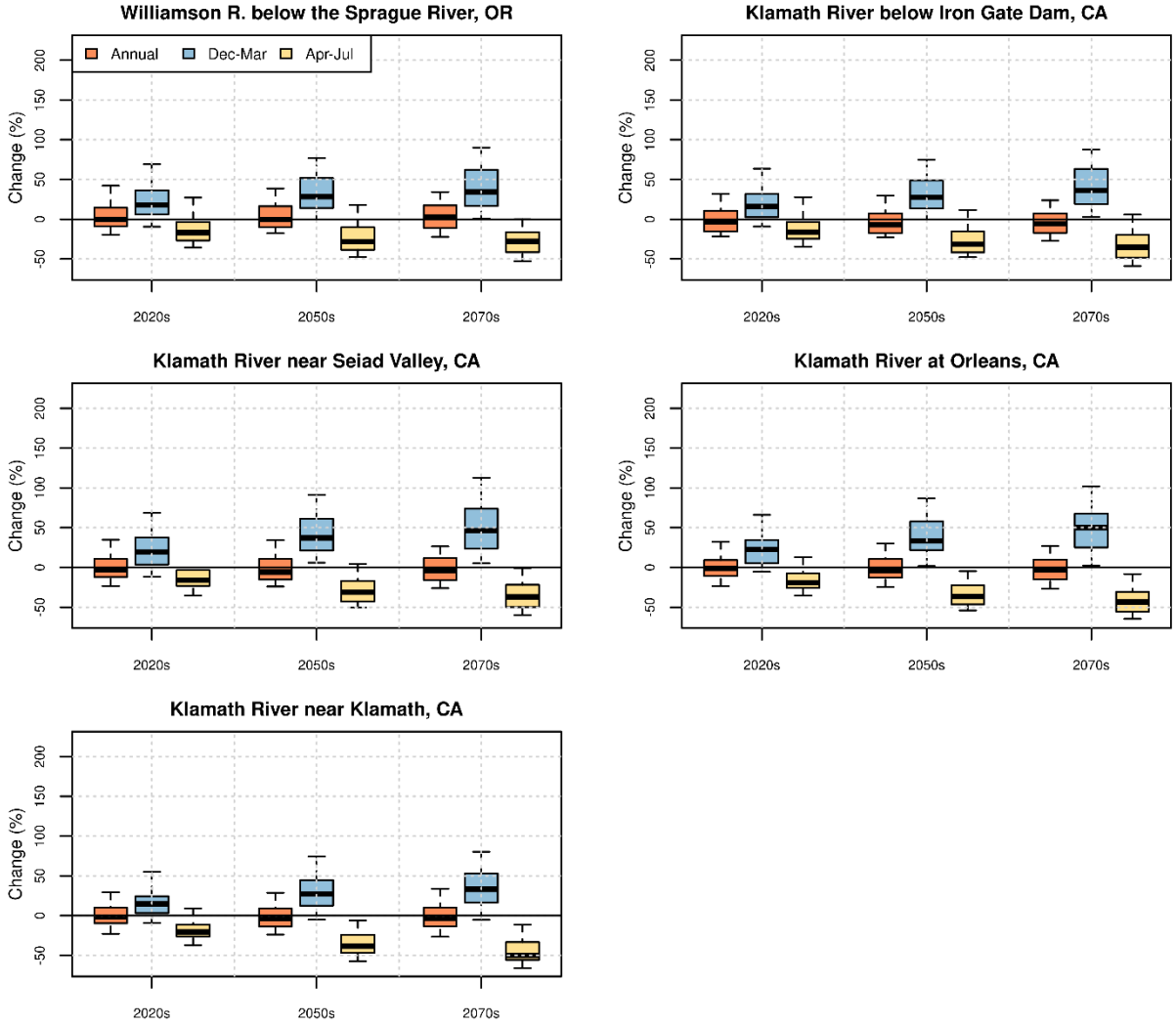

Figure 26. Klamath River Basin – Simulated change in streamflow magnitude for various subbasins.

Figure 27 shows the simulated shift in runoff timing for the various subbasins. For all the subbasins in all three future decades, the median value of the change in runoff timing varies from near zero to a positive value. Positive values imply that about half of the annual flow occurs later than it did in the 1990s. As an example, for the location Klamath River near Klamath, the median shift for the 2020s and 2050s practically shows no change, but for the 2070s decades, it is about 4 days later than from the 1990s.

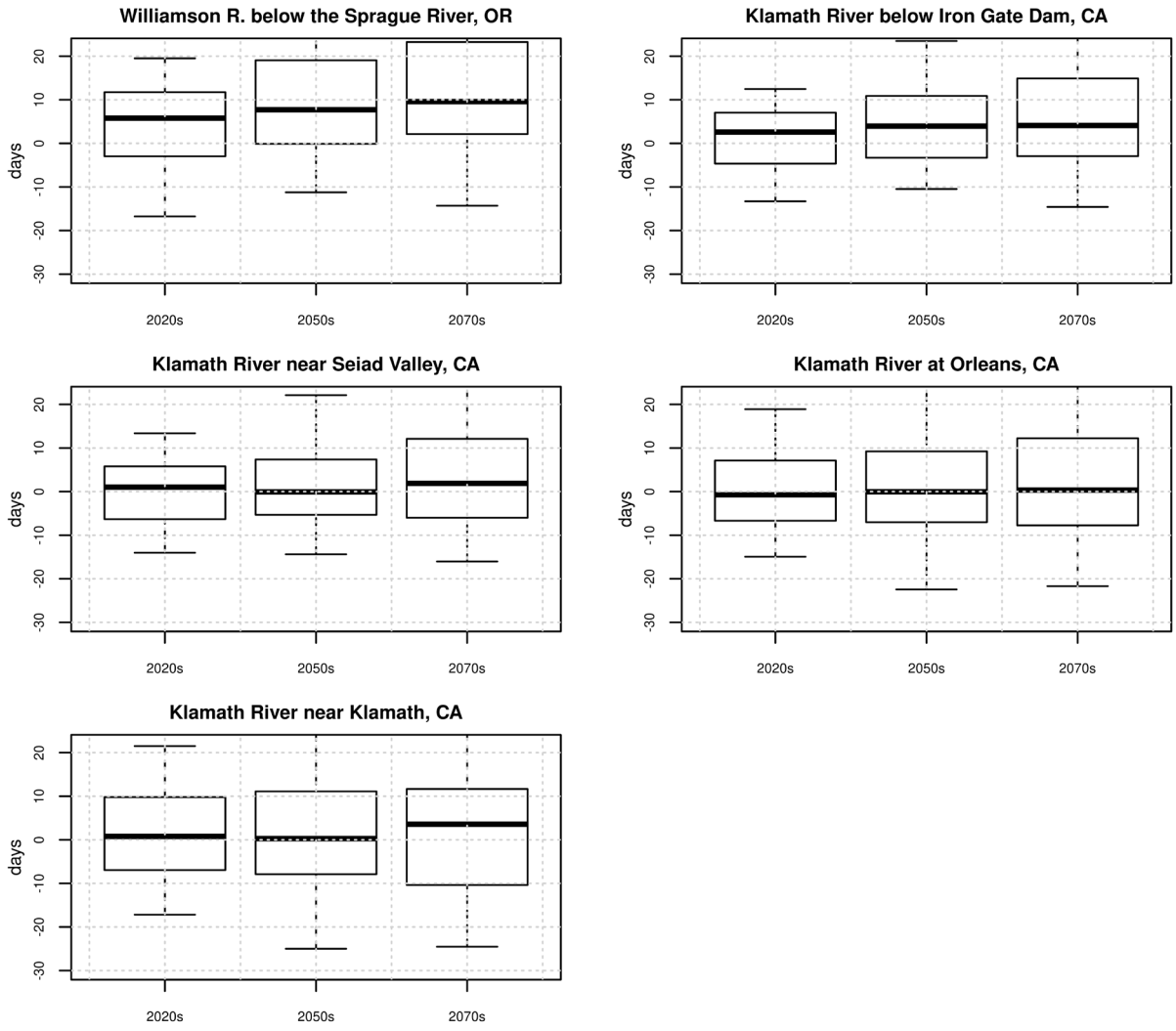

Figure 27. Klamath River Basin – Simulated shift in streamflow timing for various subbasins; negative values denote earlier runoff relative to the 1990s.

3.5 Missouri River Basin

The Missouri River is the longest river in the United States. It has a watershed of more than 500,000 square miles, which includes portions of ten States (Montana, North Dakota, South Dakota, Wyoming, Colorado, Nebraska, Iowa, Kansas, Missouri, and Minnesota) and two Canadian provinces (Alberta and Saskatchewan) and encompasses approximately one-sixth of the entire lower 48 United States. The Missouri River drains the largest watershed within the United States and produces annual yields of nearly 40 million acre-feet. Reclamation has constructed more than 40 dams on Missouri River tributaries that have helped with agricultural development in the basin. The facilities in the basin also provide benefits including flood control, navigation, irrigation, hydropower, water supply, recreation, fish and wildlife, and water quality.

Navigation is important in the lower basin States, while reliable water delivery for agriculture and municipal, rural, and industrial use is important in the upper basin States.

3.5.1 Hydroclimate Projections

Figure 28 shows six hydroclimate indicators for the Missouri River Basin above Omaha: annual total precipitation (top left), annual mean temperature (top right), April 1st SWE (middle left), annual runoff (middle right), December-through-March runoff (bottom left), and April-through-July runoff (bottom right). The heavy black line is the median value (50th percentile) of the annual time series of the 64 projections. The shaded area is the annual time series of the 10th to 90th percentiles.

Total annual precipitation (median value) throughout the basin is shown to be increasing over time. The ensemble spread appears to be somewhat widening, implying that, there is some increase in the range of values for total annual precipitation magnitudes through time. The mean annual temperature (median value) throughout the basin shows an increase over time and a widening ensemble spread, implying that, there is some increase in the range of mean annual temperature values over time. April 1st SWE (median value) shows a decrease over time. The December-through-March runoff volume shows a general increase over time, and the April-through-July runoff shows an increase over time. However, largely, there are no changes in annual runoff, in spite of increased seasonal flows. This likely points to losses attributable to other hydrologic processes, such as increased evapotranspiration or losses to the sub-surface. For additional discussions, see Sections 3.9 and 3.9.1.4.

Figure 29, Figure 30, and Figure 31 show the spatial distribution of simulated decade-mean temperatures, precipitation, and April 1st SWE, respectively, in the Missouri River Basin. In each figure, the simulated 1990s distribution of median decadal mean condition for the variable of interest is shown in the upper middle plot, and changes in the decadal mean condition are shown below for the three future periods and at three change percentiles within the range of projections (25th, 50th, and 75th percentiles).

In Figure 29, the median change for the three future decades relative to the 1990s indicates increasing temperatures throughout the basin. In Figure 30, the median change in precipitation for the future decades indicates a wetter pattern. In Figure 31, the spatial plots indicate the basin is projected to have generally reduced snowpack. Analyses of the results from Figure 28 through Figure 31 indicate that warming is projected to lead to precipitation falling as rain instead of snow and, consequently, to decreased snowpack in the basin. However, due to projected increases in precipitation, runoff is expected to increase mostly over the April-through-July season.

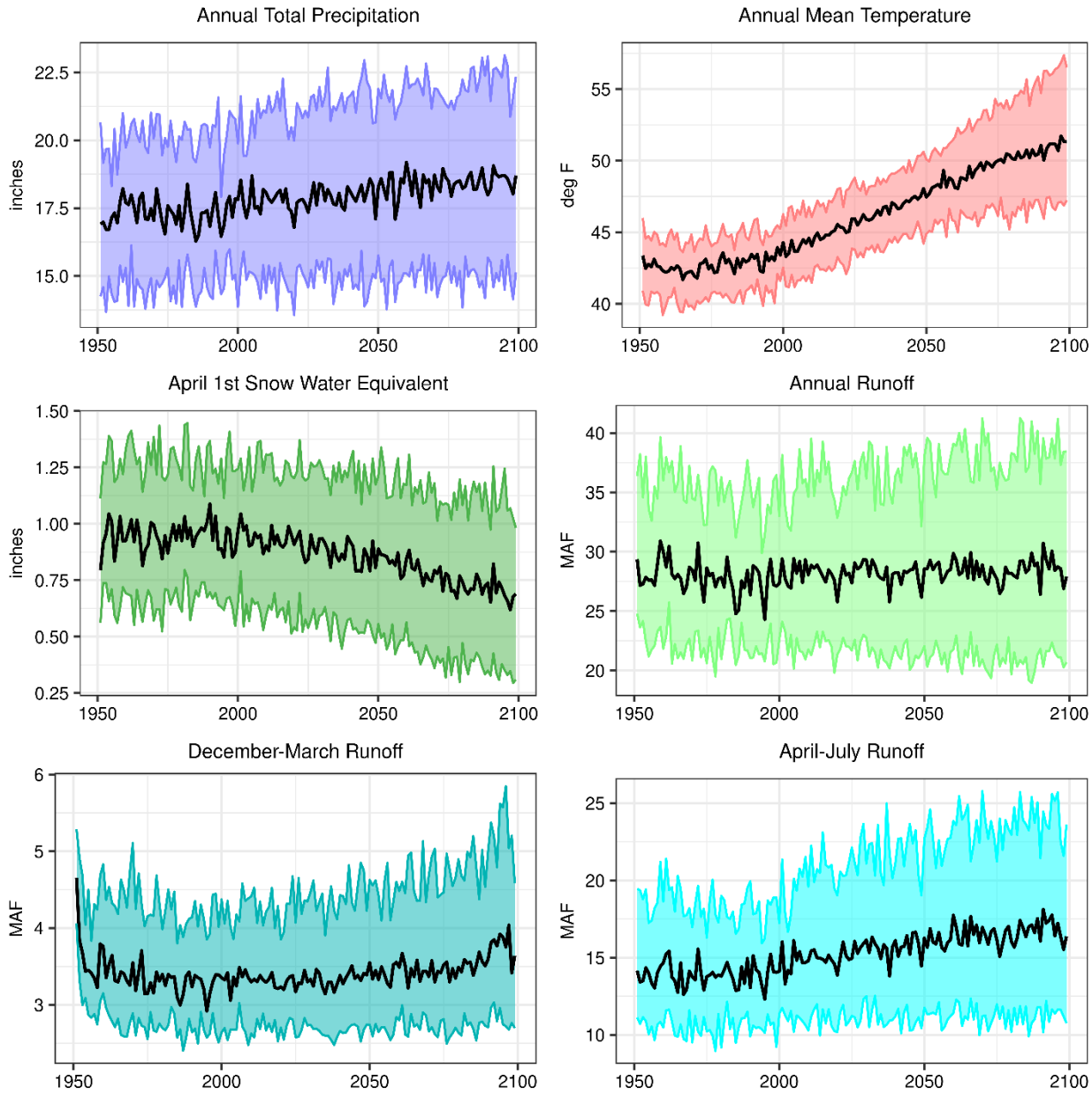

Figure 28. Missouri River Basin – Time series plots for six projected hydroclimate indicators.

Note: The heavy black line is the annual time series median value (i.e., median). The shaded area is the annual time series of 10th to 90th percentiles.

MAF = million acre-feet; deg F = degrees Fahrenheit

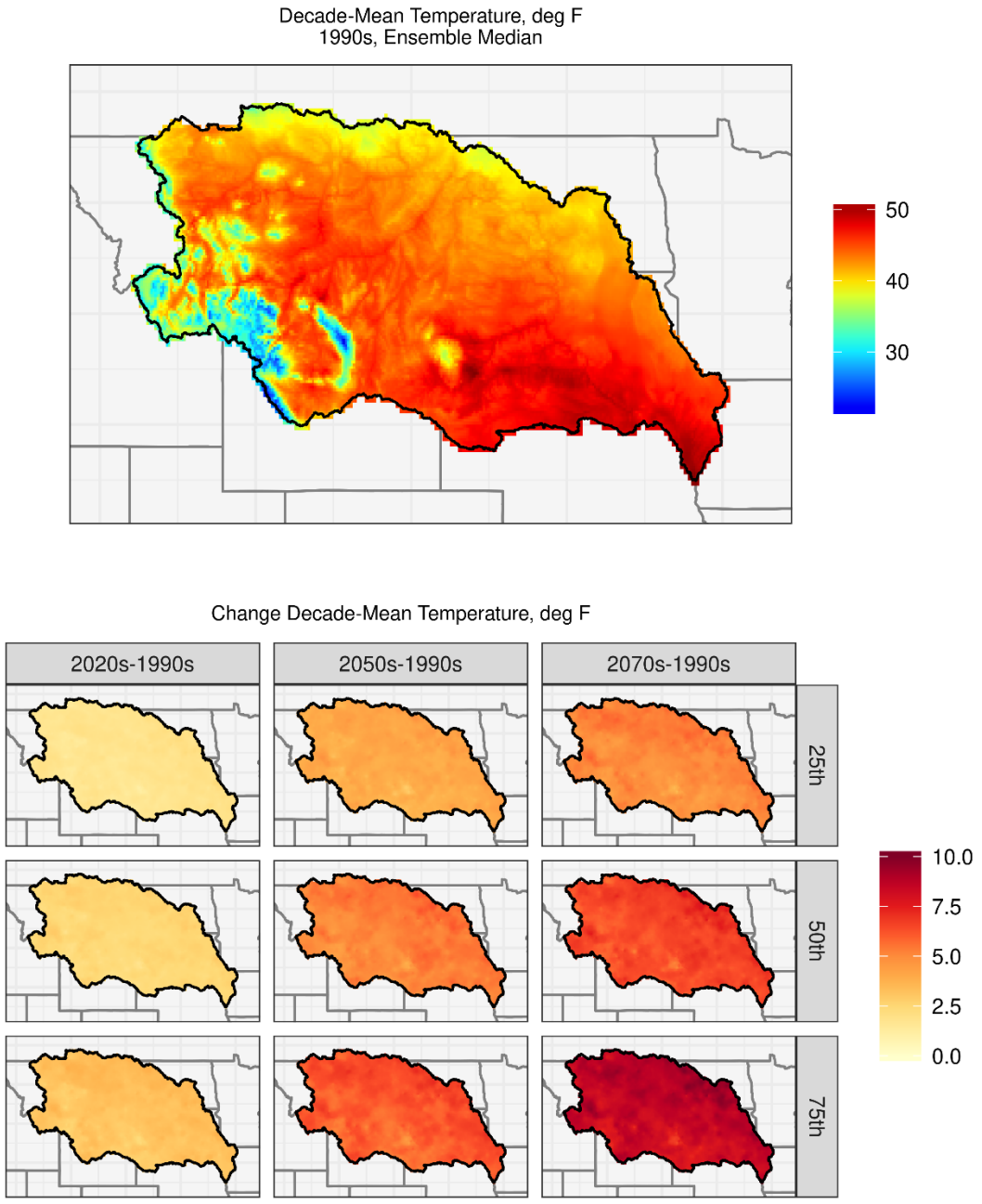

Figure 29. Missouri River Basin – Spatial distribution of simulated decadal temperature changes.

Note: deg F = degrees Fahrenheit

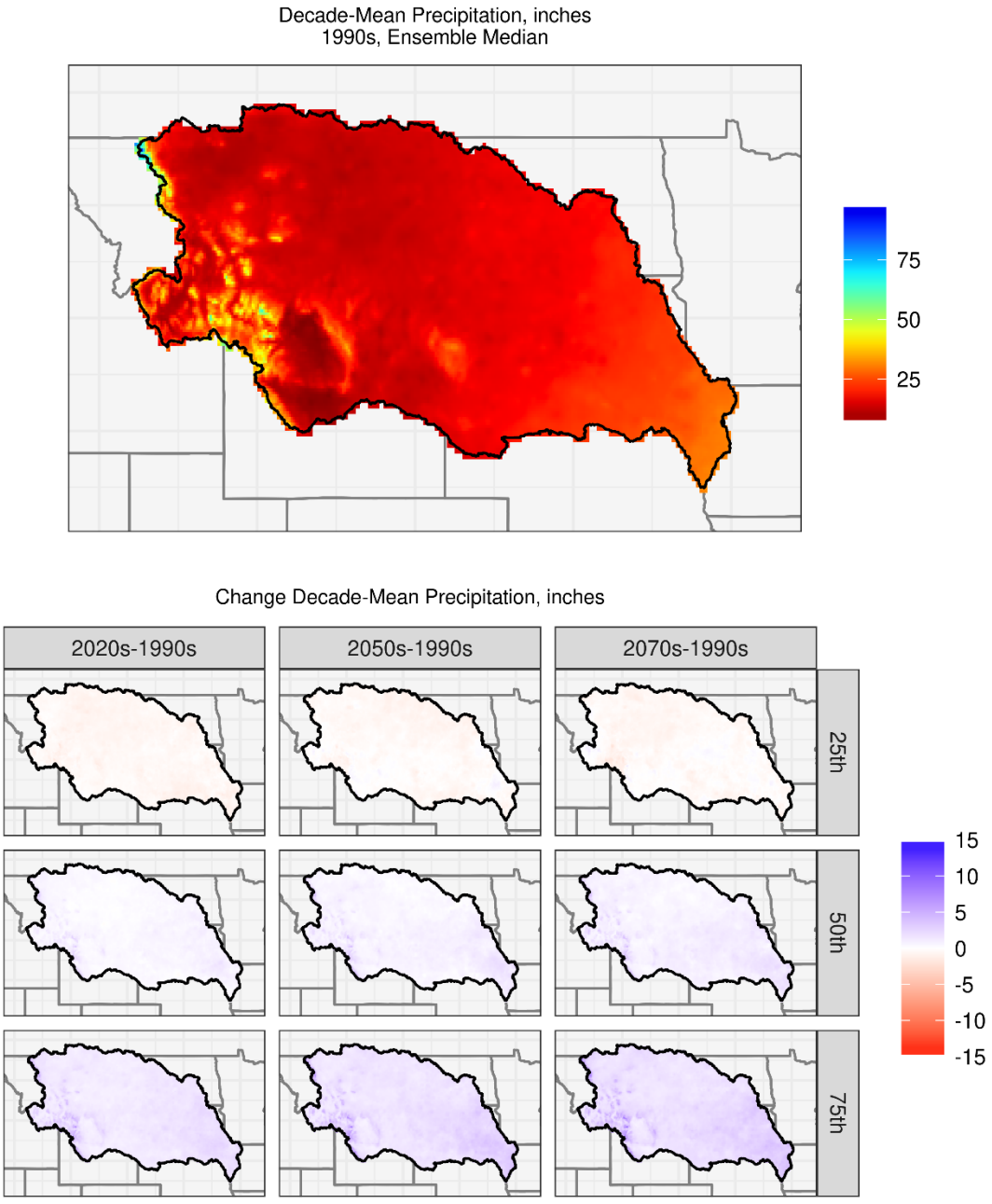

Figure 30. Missouri River Basin – Spatial distribution of simulated precipitation changes.

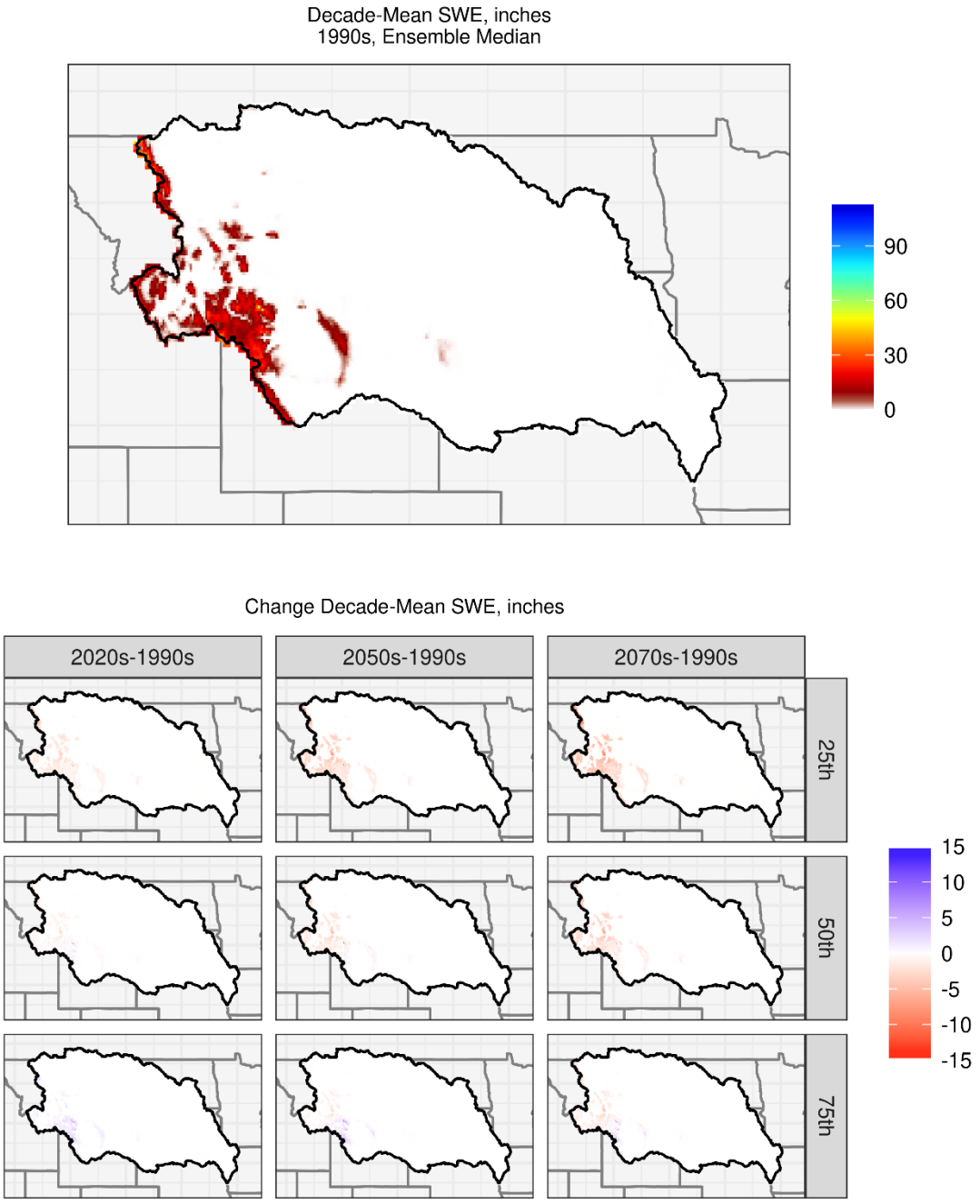

Figure 31. Missouri River Basin – Spatial distribution of simulated decadal April 1st SWE changes.

3.5.2 Impacts on Streamflow Annual and Seasonal Cycles

Figure 32 shows the mean monthly streamflow values for the 1990s, 2020s, 2050s, and 2070s in six Missouri River subbasins. For several subbasins (e.g., Bighorn River at Yellowtail Dam, Missouri River at Omaha, and North Platte River at Lake McConaughy) the hydrograph peak is higher in all the future decades from the 1990s reference. Also, there is an earlier shift in peak runoff timing from the 1990s decade for many of the subbasins, and it is apparent over the 2070s (e.g., Missouri River at Canyon Ferry Dam, Missouri River at Omaha, and Bighorn River at Yellowtail Dam).

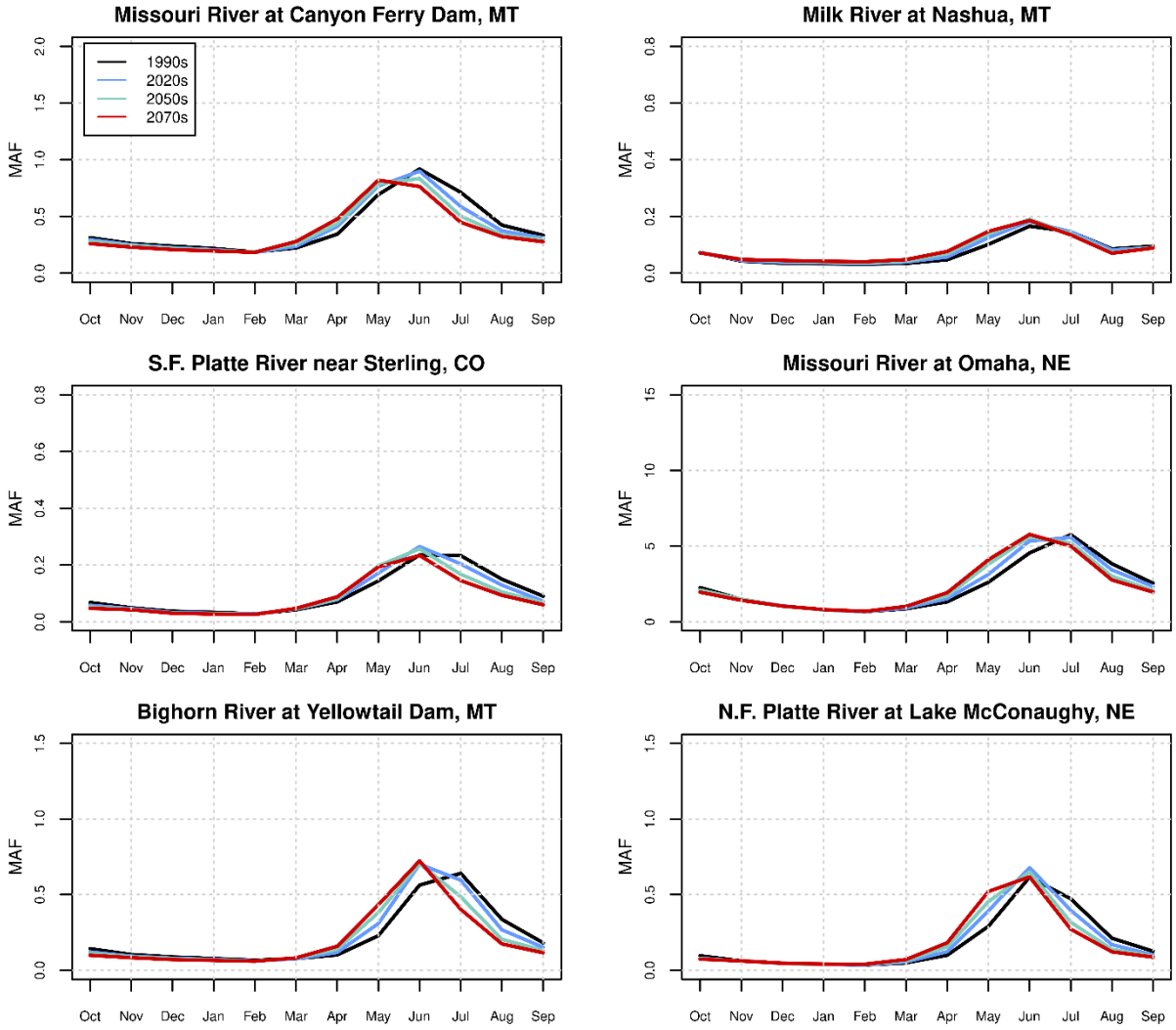

Figure 32. Missouri River Basin – Simulated mean monthly streamflow for various subbasins.

MAF = million acre-feet

Figure 33 shows boxplots of the distribution of changes in runoff magnitude for annual, December-through-March, and April-through-July runoff in the six Missouri River subbasins. Overall, the median change for the annual and seasonal runoffs vary across the subbasins. Changes to both annual and December-through-March streamflow in the 2020s and 2050s

relative to the 1990s are variable ranging from no change (e.g., North Fork of Platte River at Lake McConaughy), to decrease in runoff (e.g., South Fork of Platte River near Sterling), and increase in runoff (e.g., Missouri River at Omaha). However, the April-through-July runoff largely shows an increase across the subbasins in all three future decades relative to the 1990s reference. This increase in April-through-July runoff is also evident from the example time series plot (Figure 28, bottom right panel) for the subbasin, Missouri River at Omaha.

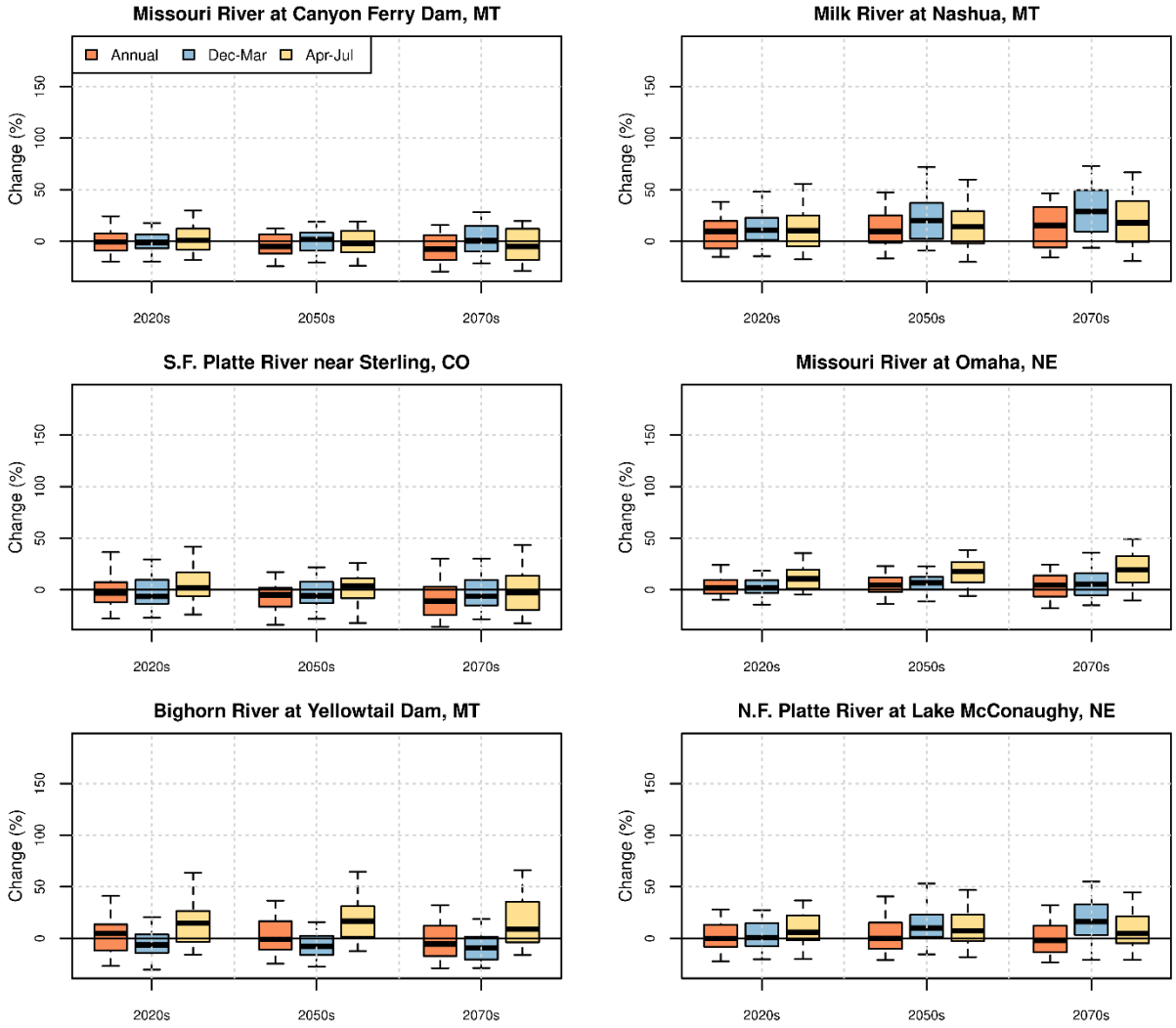

Figure 33. Missouri River Basin – Simulated change in streamflow magnitude for various subbasins.

Figure 34 shows the simulated shift in runoff timing for the various subbasins. In all the subbasins, the analysis shows that for each future decade, the median value of the change in runoff timing is negative. This implies that half of the annual flow occurs earlier in the three future decades (2020s, 2050s, and 2070s) relative to the 1990s reference. As an example, for the location Missouri River at Omaha, the earlier shift is about 5, 9, and 12 days, respectively, for the 2020s, 2050s, and 2070s decade, as compared to the 1990s decade.

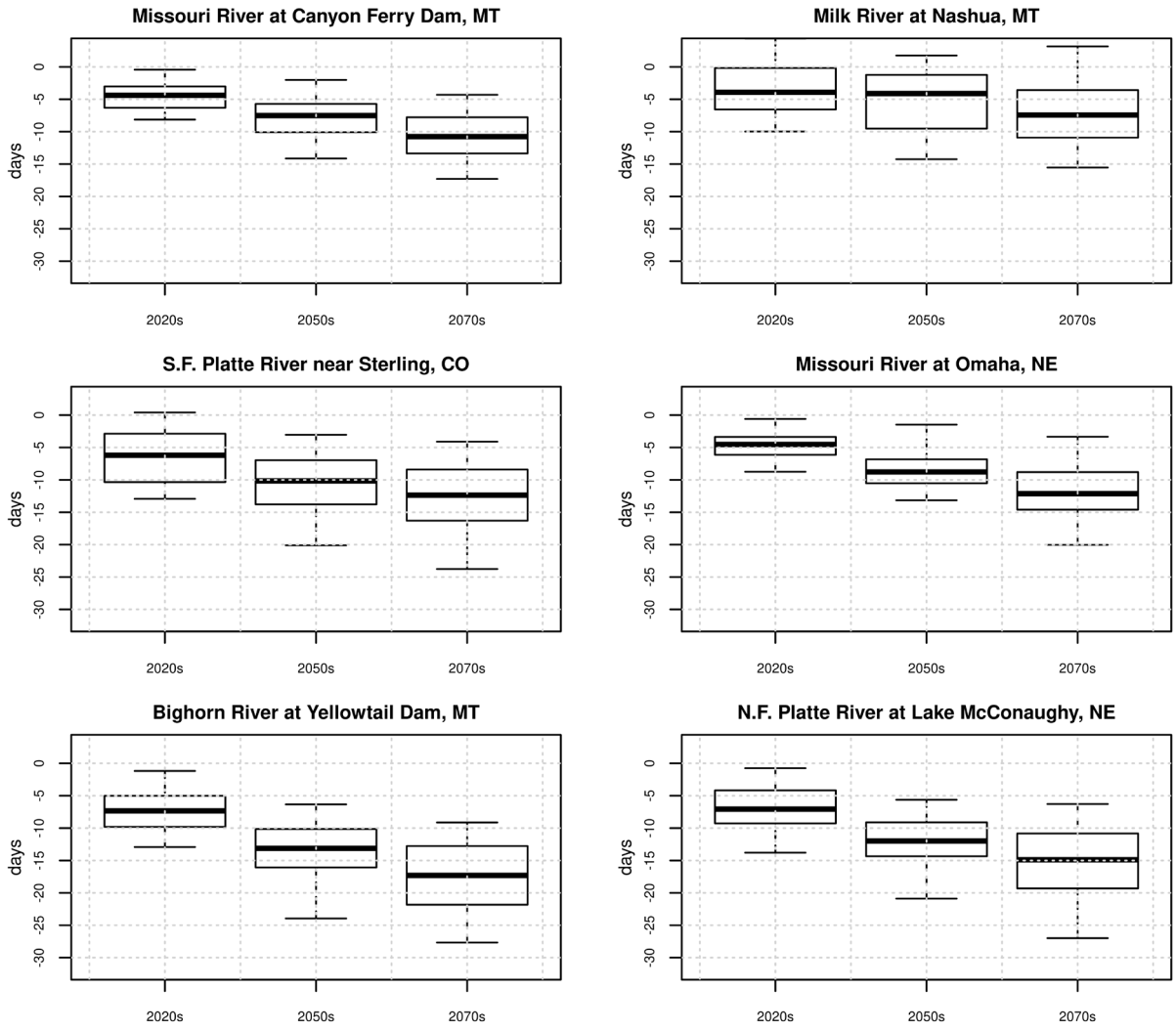

Figure 34. Missouri River Basin – Simulated shift in streamflow timing for various subbasins; negative values denote earlier runoff relative to the 1990s.

3.6 Rio Grande Basin

The Rio Grande Basin, located in the Southwestern United States, provides water for irrigation, residential, environmental, and recreational uses in Colorado, New Mexico, and Texas, as well as Mexico. The Rio Grande is approximately 1,896 miles long and drains a basin about 182,200 square miles in area across both countries—the United States and Mexico. Reclamation Projects within the basin include the Closed Basin Project, Colorado; the San Juan-Chama Trans-mountain Diversion Project, between Colorado and New Mexico; the Middle Rio Grande Project, New Mexico; and the Rio Grande Project, in New Mexico and Texas. These Projects provide water for municipalities, Tribes, and industry, and support approximately 200,000 acres of irrigated agriculture, which produces alfalfa, cotton, vegetables, pecans, and grain. Reclamation's facilities provide critical water and power for industry and communities,

including Albuquerque and Las Cruces, New Mexico; El Paso, Texas; and Ciudad Juarez, Mexico. This analysis presents results for the upper portion of the basin above the Rio Grande at Elephant Butte Dam.

3.6.1 Hydroclimate Projections

Figure 35 shows six hydroclimate indicators for the upper portion of the basin above the Rio Grande at Elephant Butte Dam: annual total precipitation (top left), annual mean temperature (top right), April 1st SWE (middle left), annual runoff (middle right), December-through-March runoff (bottom left), and April-through-July runoff (bottom right). The heavy black line is the median value (50th percentile) of the annual time series of the 64 projections. The shaded area is the annual time series of the 10th to 90th percentiles.

Total annual precipitation (median value) throughout the upper basin is shown to be nominally decreasing over time. The ensemble spread appears to be somewhat widening, implying that, there is some increase in the range of values for total annual precipitation magnitudes through time. The mean annual temperature (median value) throughout the basin shows an increase over time and a widening ensemble spread, implying that, there is some increase in the range of mean annual temperature values over time. April 1st SWE (median value) shows a decrease over time. The annual runoff (median value) shows a decrease over time. The December-through-March runoff volume is largely constant over time until around 2050 and post-2050 it nominally increases over time. The April-through-July runoff shows a decrease over time.

Figure 36, Figure 37, and Figure 38 show the spatial distribution of simulated decade-mean temperatures, precipitation, and April 1st SWE, respectively, in the Rio Grande Basin above Elephant Butte Dam. In each figure, the simulated 1990s distribution of median decadal mean condition for the variable of interest is shown in the upper middle plot, and changes in the decadal mean condition are shown below for the three future periods and at three change percentiles within the range of projections (25th, 50th, and 75th percentiles).

In Figure 36, the median change for the three future decades relative to the 1990s indicates increasing temperatures throughout the basin. In Figure 37, the median change in precipitation for the future decades indicates a slightly wet pattern primarily in the highest elevations (headwater areas) of the basin. In Figure 38, the spatial plots indicate the median basin snowpack (April 1st SWE) is projected to decrease.

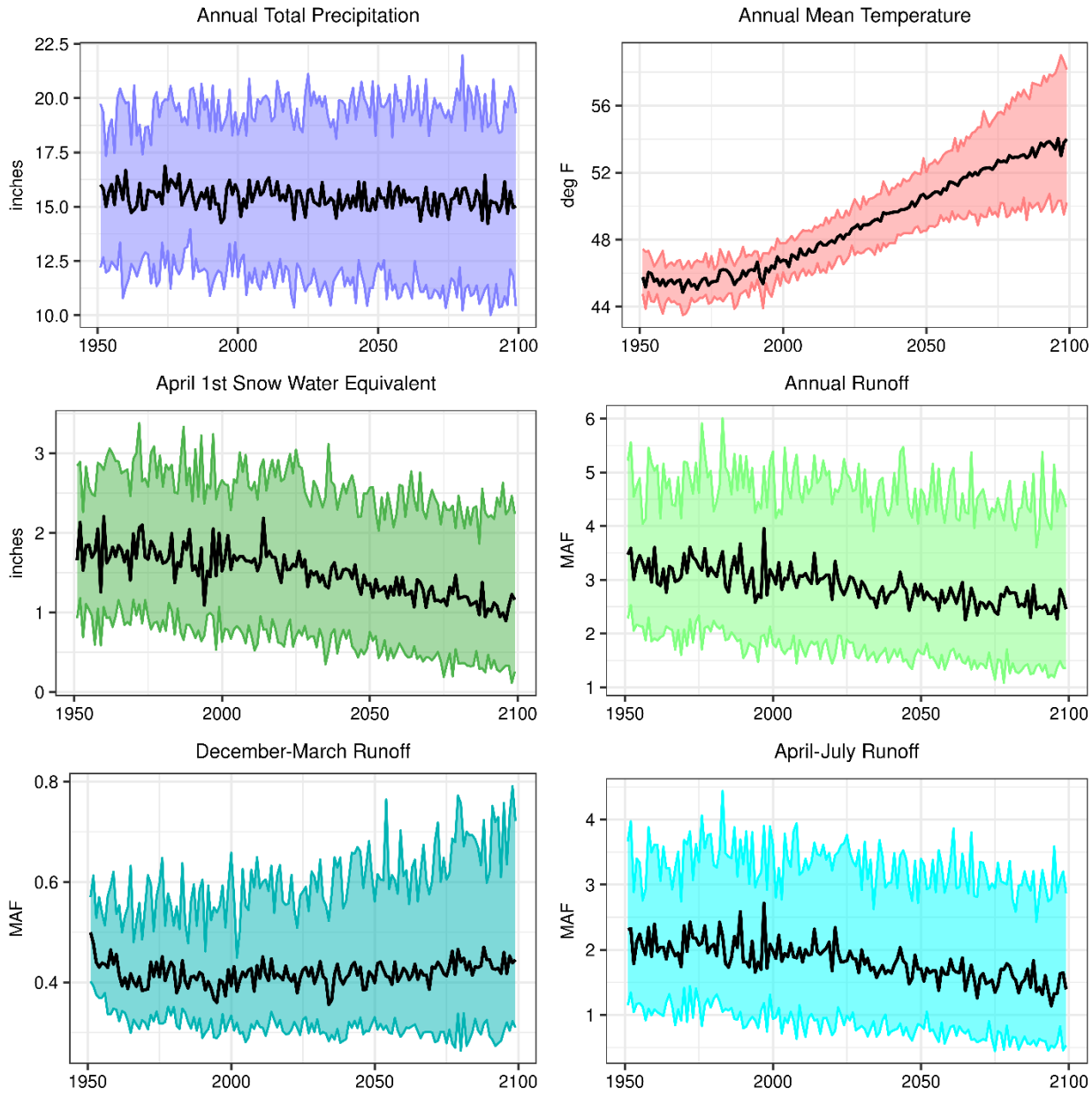

Figure 35. Rio Grande Basin – Time series plots for six projected hydroclimate indicators.

Note: The heavy black line is the annual time series median value (i.e., median). The shaded area is the annual time series of 10th to 90th percentiles.

MAF = million acre-feet; deg F = degrees Fahrenheit

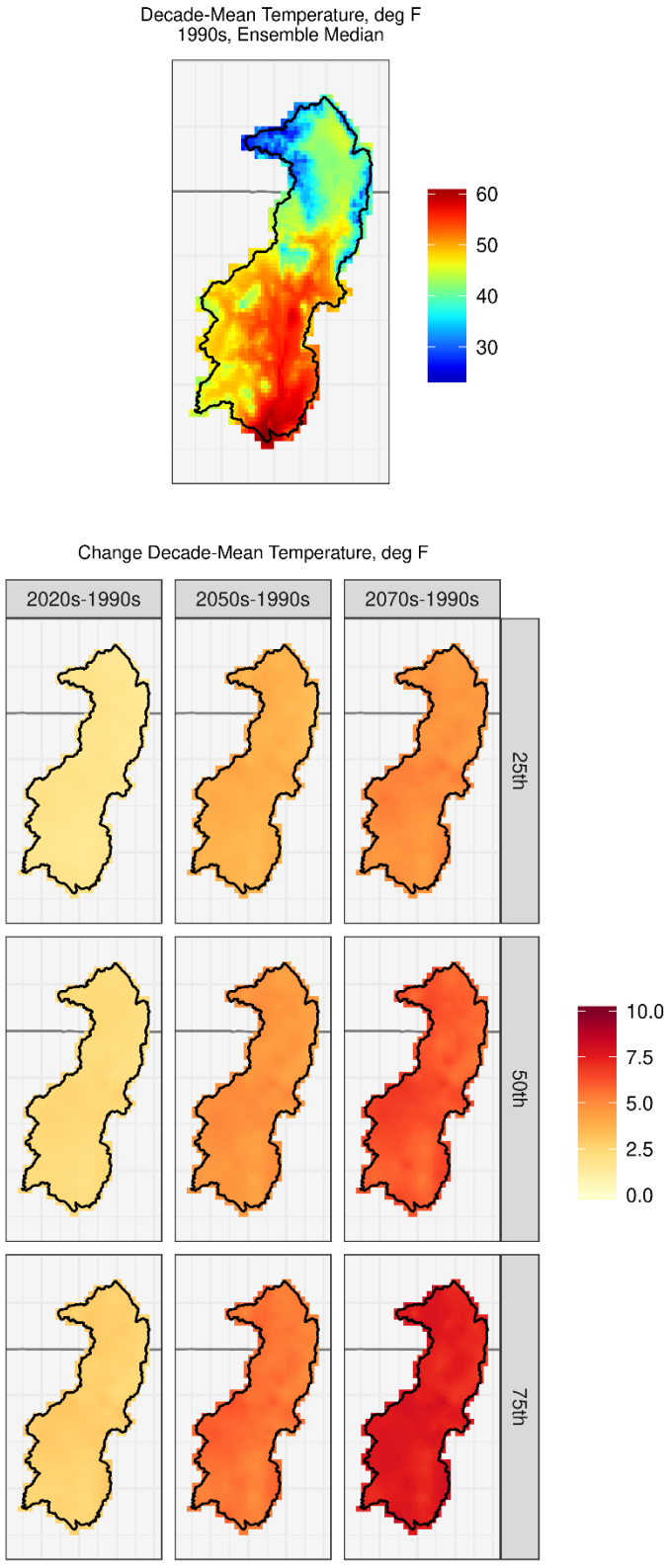

Figure 36. Rio Grande Basin – Spatial distribution of simulated decadal temperature changes.

Note: deg F = degrees Fahrenheit

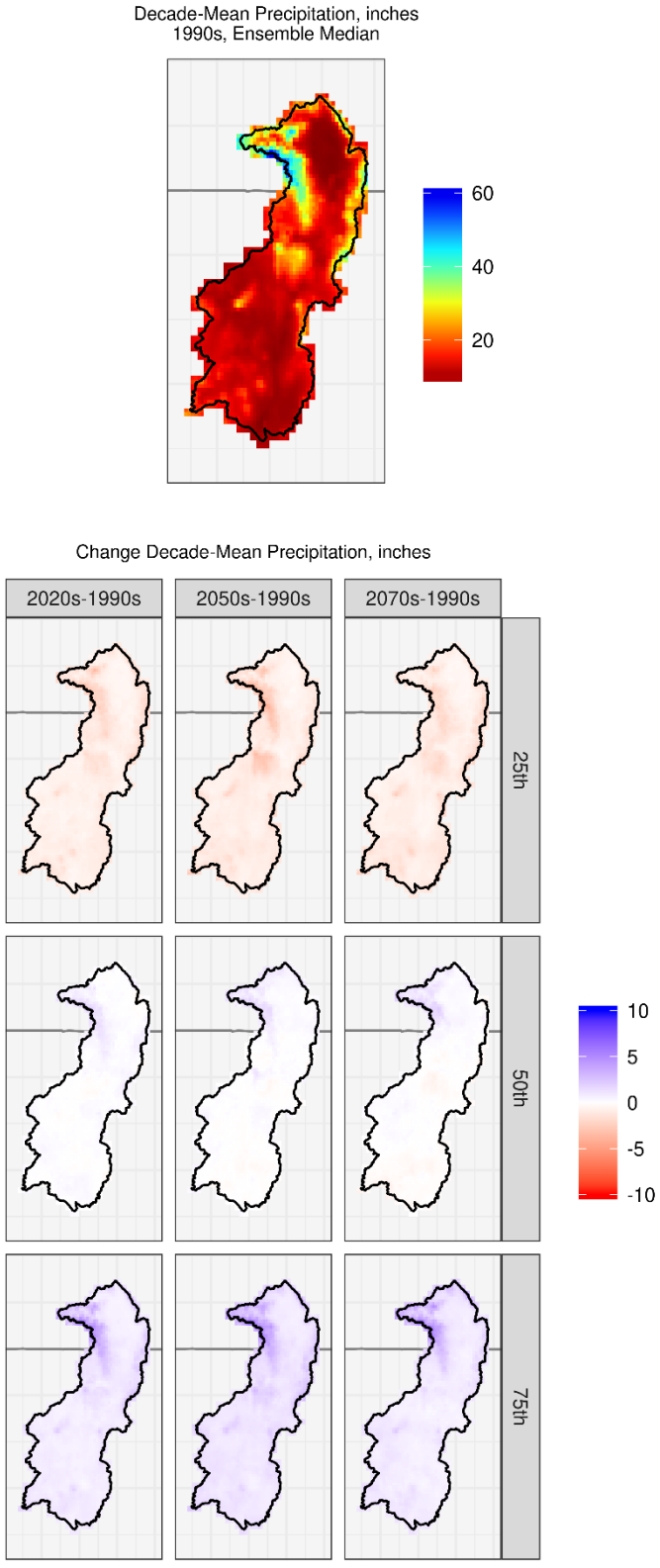

Figure 37. Rio Grande Basin – Spatial distribution of simulated precipitation changes.

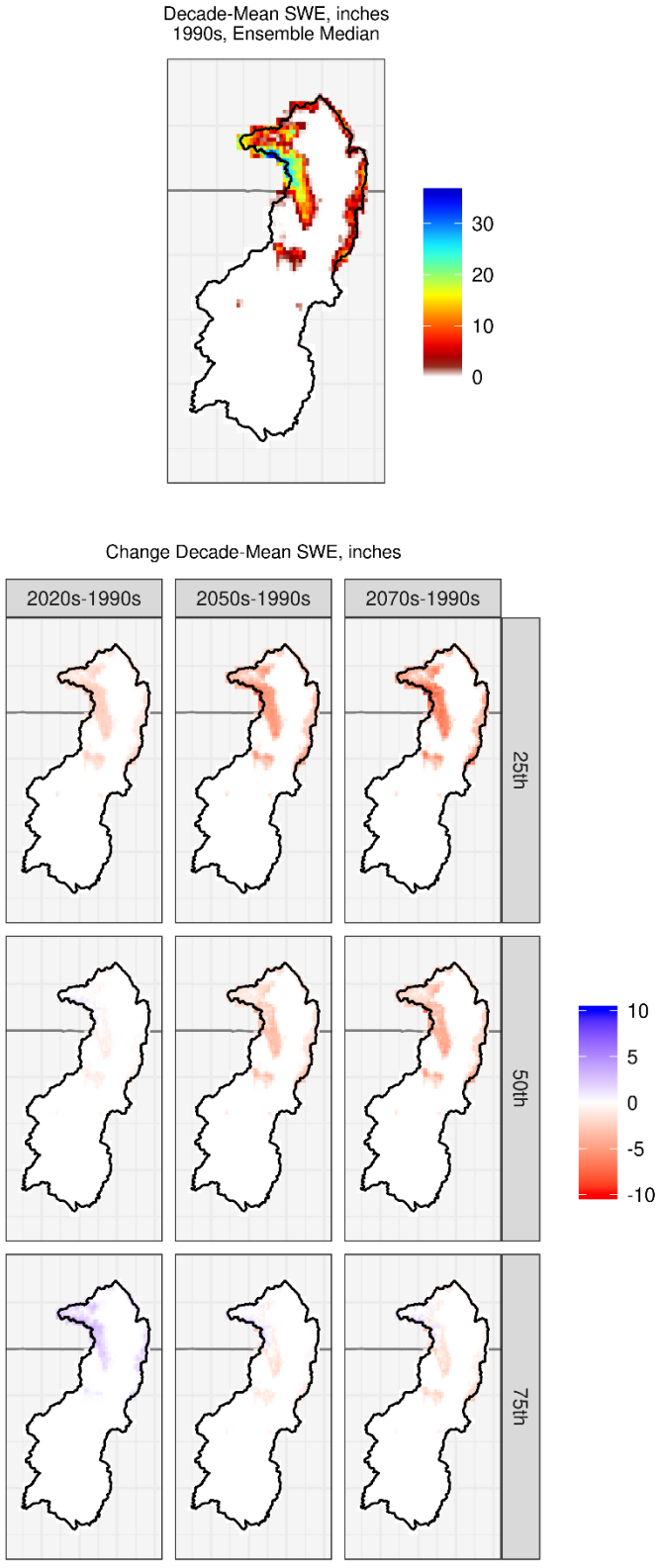

Figure 38. Rio Grande Basin – Spatial distribution of simulated decadal April 1st SWE changes.

3.6.2 Impacts on Streamflow Annual and Seasonal Cycles

Figure 39 shows the mean monthly streamflow values for the 1990s, 2020s, 2050s, and 2070s in five Upper Rio Grande subbasins. For most locations in this basin, relative to the 1990s, the runoff peaks appear to be occurring earlier in the spring during the later decade (2070s) than the earlier decade (2020s). The exception to this is the Pecos River near Carlsbad where the hydrograph peak around August is attributed to summer monsoon runoff events.

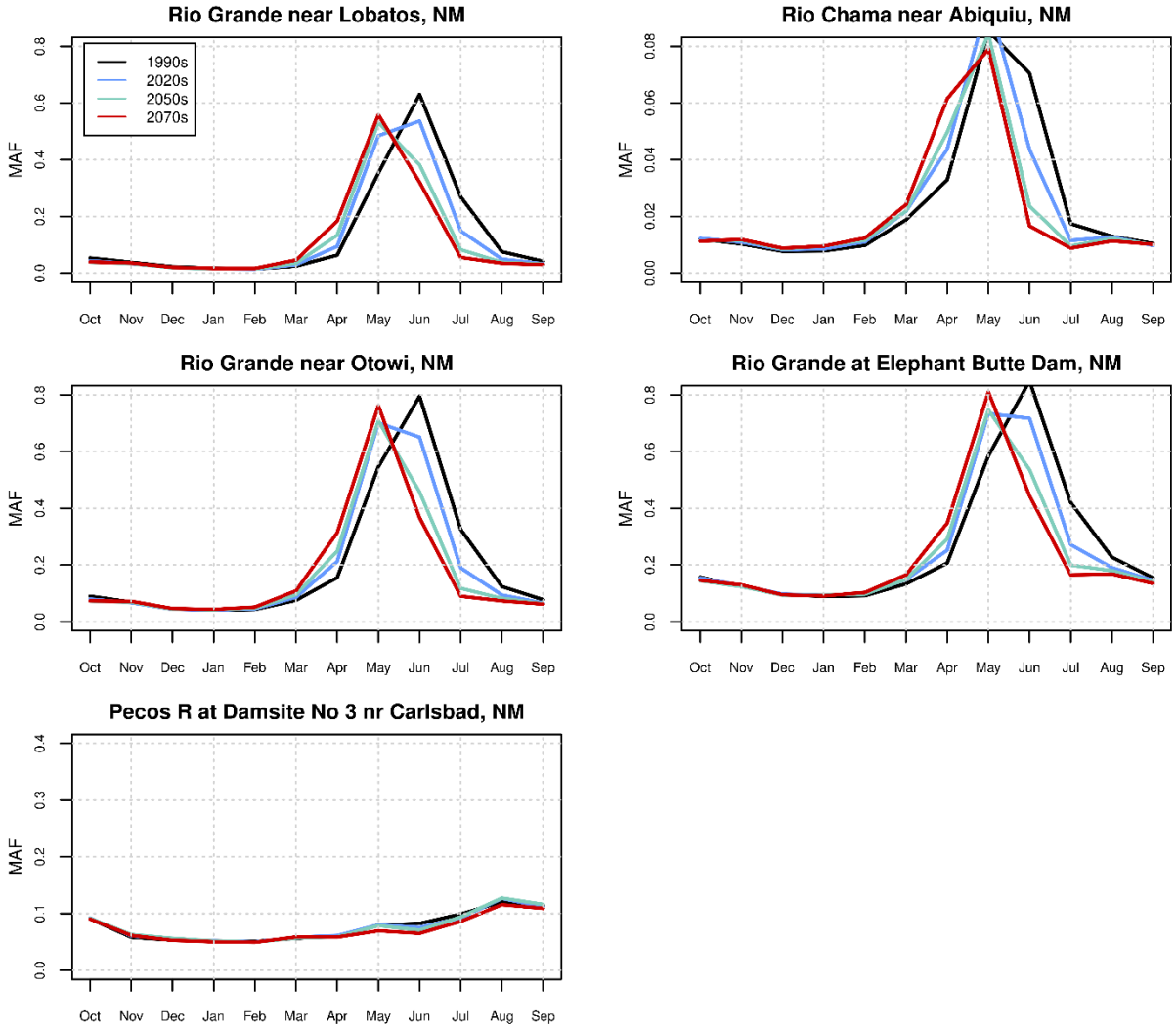

Figure 39. Rio Grande Basin – Simulated mean monthly streamflow for various subbasins.

MAF = million acre-feet

Figure 40 shows boxplots of the distribution of simulated changes in runoff magnitude for annual, December-through-March, and April-through-July runoff in the five Upper Rio Grande subbasins. Across the subbasins, the median annual flow, relative to the 1990s reference, shows practically no change in the 2020s for all subbasins, but largely shows a decrease in the 2050s decade. By the 2070s, median annual flow shows a decrease for all the subbasins. The median December-through-March runoff, except for the Pecos River site, shows an increase in the three

future decades relative to the 1990s reference. As an example, a nominal increase in the median December-through March runoff for the Rio Grande at Elephant Butte Dam can be also be seen in Figure 35 (bottom left panel). The median April-through-July runoff for all locations, relative to the 1990s, generally shows no change in the 2020s, but shows a decrease in the 2050s and 2070s decade. This decrease is illustrated, for example, in the time series plot for the Rio Grande Basin at Elephant Butte Dam (Figure 35, bottom right panel), which generally shows a decrease in the median April-through-July runoff over time.

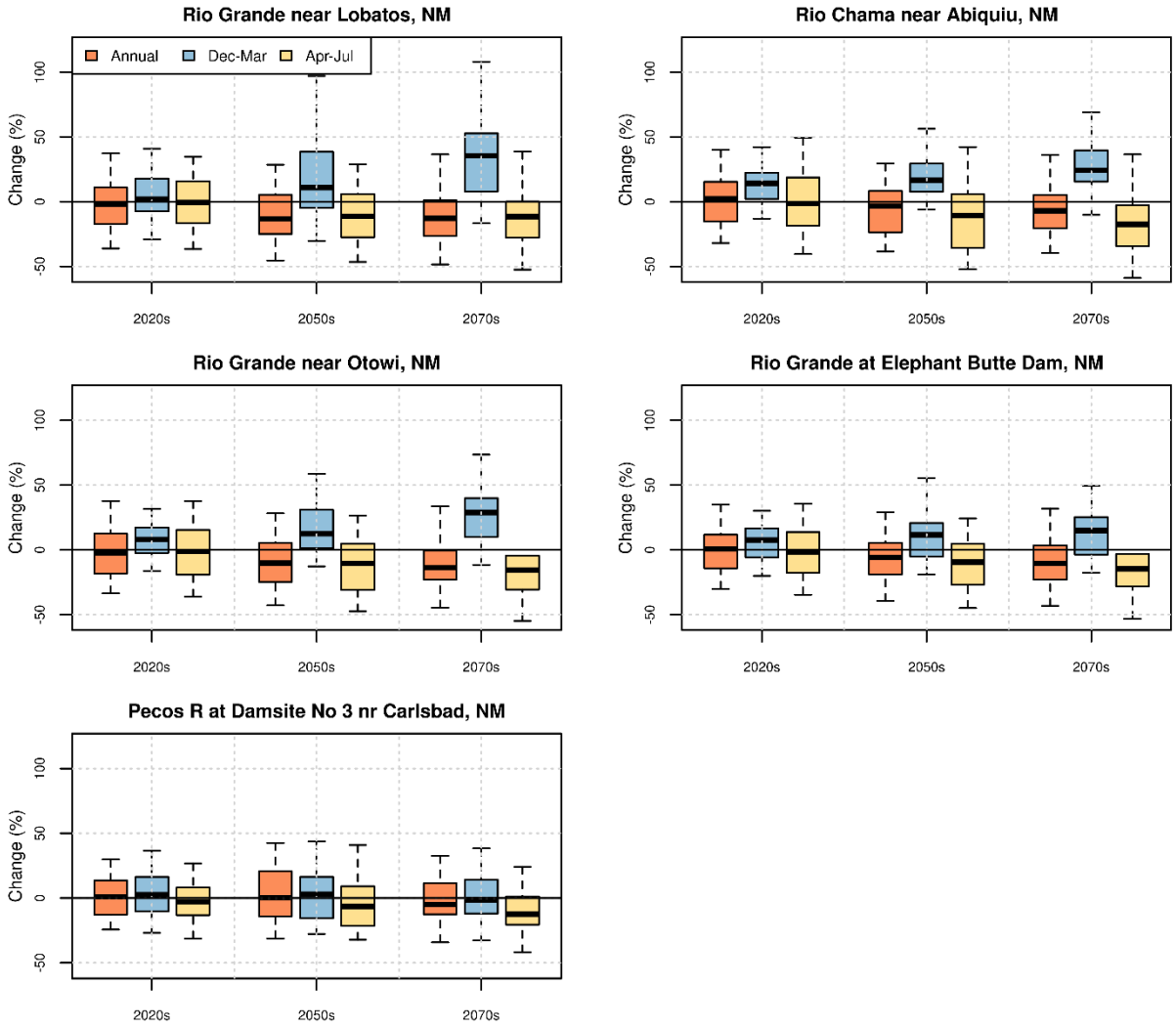

Figure 40. Rio Grande Basin – Simulated change in streamflow magnitude for various subbasins.

Figure 41 shows the simulated shift in runoff timing for the various subbasins. The Pecos River location shows positive value (i.e., late) of the median change in runoff timing in all of the three future decades 2020s (1 day), 2050s (3 days), and 2070s (3 days) relative to the 1990s. For all the other Upper Rio Grande locations, the analysis shows that for each future decade the median value of the change in runoff timing is negative. This implies that half of the annual flow occurs sooner than it did in the 1990s. For example, for the Rio Grande at the Elephant Butte Dam, the

earlier shift is approximately 6, 8, and 9 days, respectively, in the 2020s, 2050s, and 2070s relative to the 1990s.

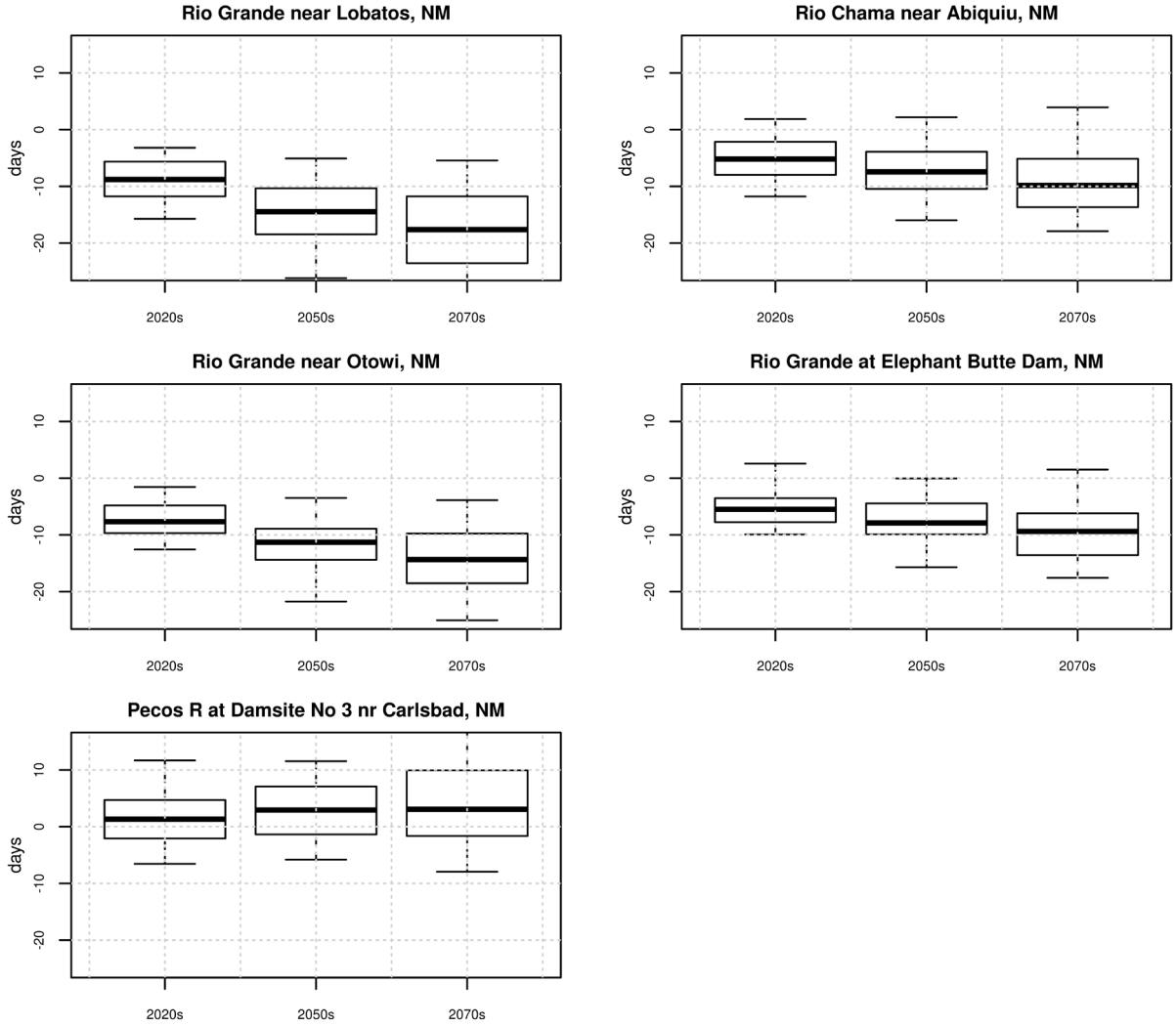

Figure 41. Rio Grande Basin – Simulated shift in streamflow timing for various subbasins; negative values denote earlier runoff relative to the 1990s.

3.7 Sacramento and San Joaquin River Basins

The Sacramento and San Joaquin River Basins include three major Central Valley watersheds—the Sacramento River in the north, and the San Joaquin River and Tulare Lake Basins in the south. The combined watersheds extend nearly 500 miles from northwest to southeast and range from 60 to 100 miles wide. The Sacramento and San Joaquin Rivers are the two largest rivers in California with lengths of 445 miles and 366 miles, respectively. These two rivers have a combined drainage area of about 60,000 square miles and meet in the Sacramento-San Joaquin Rivers Delta, the largest estuary on the West Coast and the hub of California's complex water

supply system. The rivers play a key role in supporting California's economy by providing water for many of the agricultural counties in the Nation's leading farm State. In addition to water for farms, homes, and industry in California's Central Valley and major urban centers in the San Francisco Bay and Central Coast areas, the rivers sustain aquatic and terrestrial habitats, along with numerous managed waterfowl refuges.

3.7.1 Hydroclimate Projections

Figure 42 shows six hydroclimate indicators for the basin above the Sacramento and San Joaquin Rivers at the Delta: annual total precipitation (top left), annual mean temperature (top right), April 1st SWE (middle left), annual runoff (middle right), December-through-March runoff (bottom left), and April-through-July runoff (bottom right). The heavy black line is the median value (50th percentile) of the annual time series of the 64 projections. The shaded area is the annual time series of the 10th to 90th percentiles.

Total annual precipitation (median value) throughout the basin is shown to be largely constant over time. The ensemble spread appears to be somewhat widening, implying that, there is some increase in the range of values for total annual precipitation magnitudes through time. The mean annual temperature (median value) throughout the basin shows an increase over time and a widening ensemble spread, implying that, there is some increase in the range of mean annual temperature values over time. April 1st SWE (median value) shows a decrease over time. The annual runoff (median value) shows a nominal decrease over time. The December-through-March runoff volume shows an increase over time, and the April-through-July runoff shows a decrease over time.

Figure 43, Figure 44, and Figure 45 show the spatial distribution of simulated decade-mean temperatures, precipitation, and April 1st SWE, respectively, in the Sacramento and San Joaquin River Basins above the Delta. In each figure, the simulated 1990s distribution of median decadal mean condition for the variable of interest is shown in the upper middle plot, and changes in the decadal mean condition are shown below for the three future periods and at three change percentiles within the range of projections (25th, 50th, and 75th percentiles).

In Figure 43, the median change for the three future decades relative to the 1990s indicates increasing temperatures throughout the basin. In Figure 44, the median change in precipitation for the future decades indicates a slightly wetter pattern, mostly in the mountainous regions of the basin. In Figure 45, the spatial plots indicate the median basin snowpack (April 1st SWE) is projected to decrease.

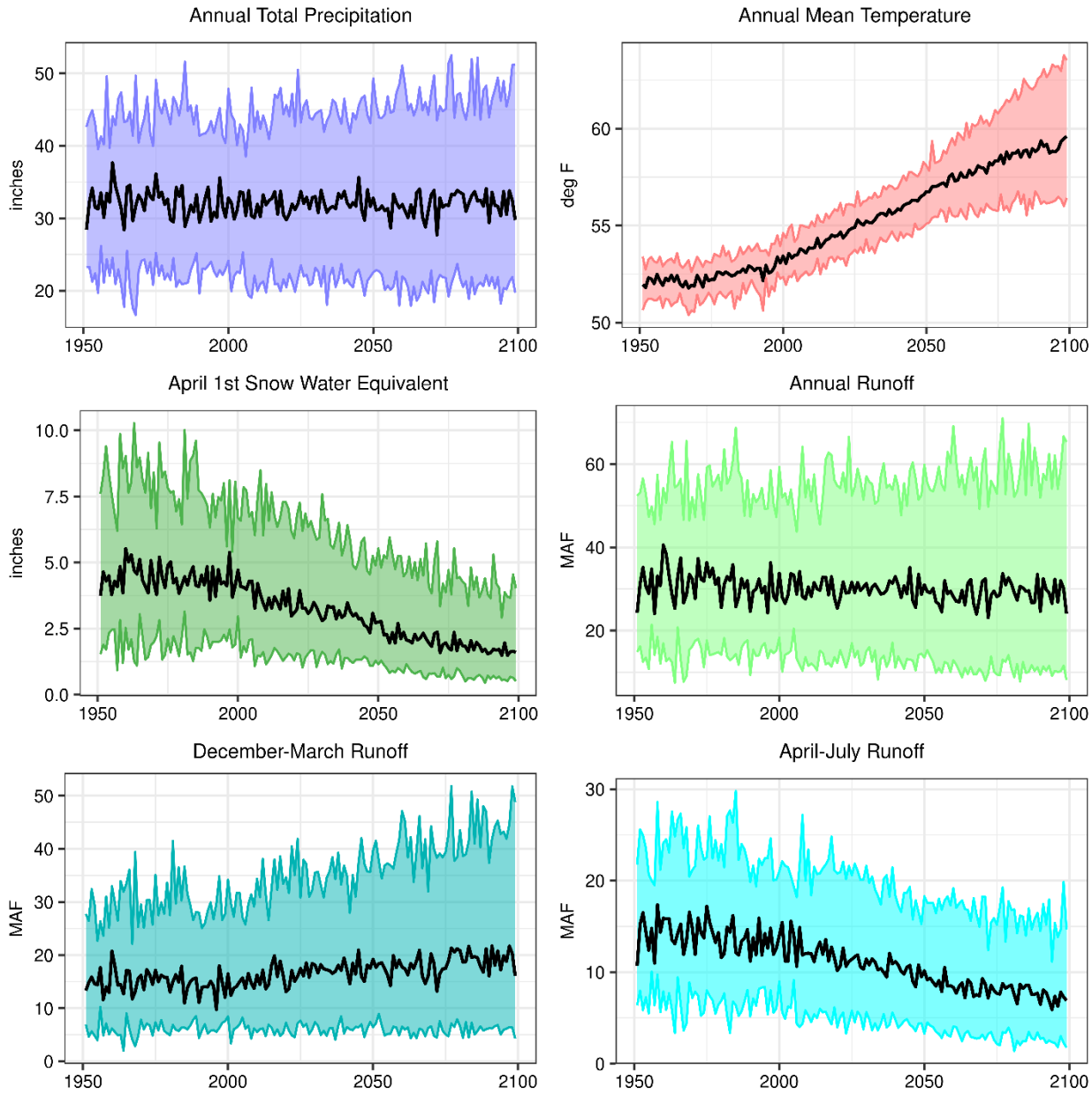

Figure 42. Sacramento and San Joaquin River Basins – Time series plots for six projected hydroclimate indicators.

Note: The heavy black line is the annual time series median value (i.e., median). The shaded area is the annual time series of 10th to 90th percentiles.

MAF = million acre-feet; deg F = degrees Fahrenheit

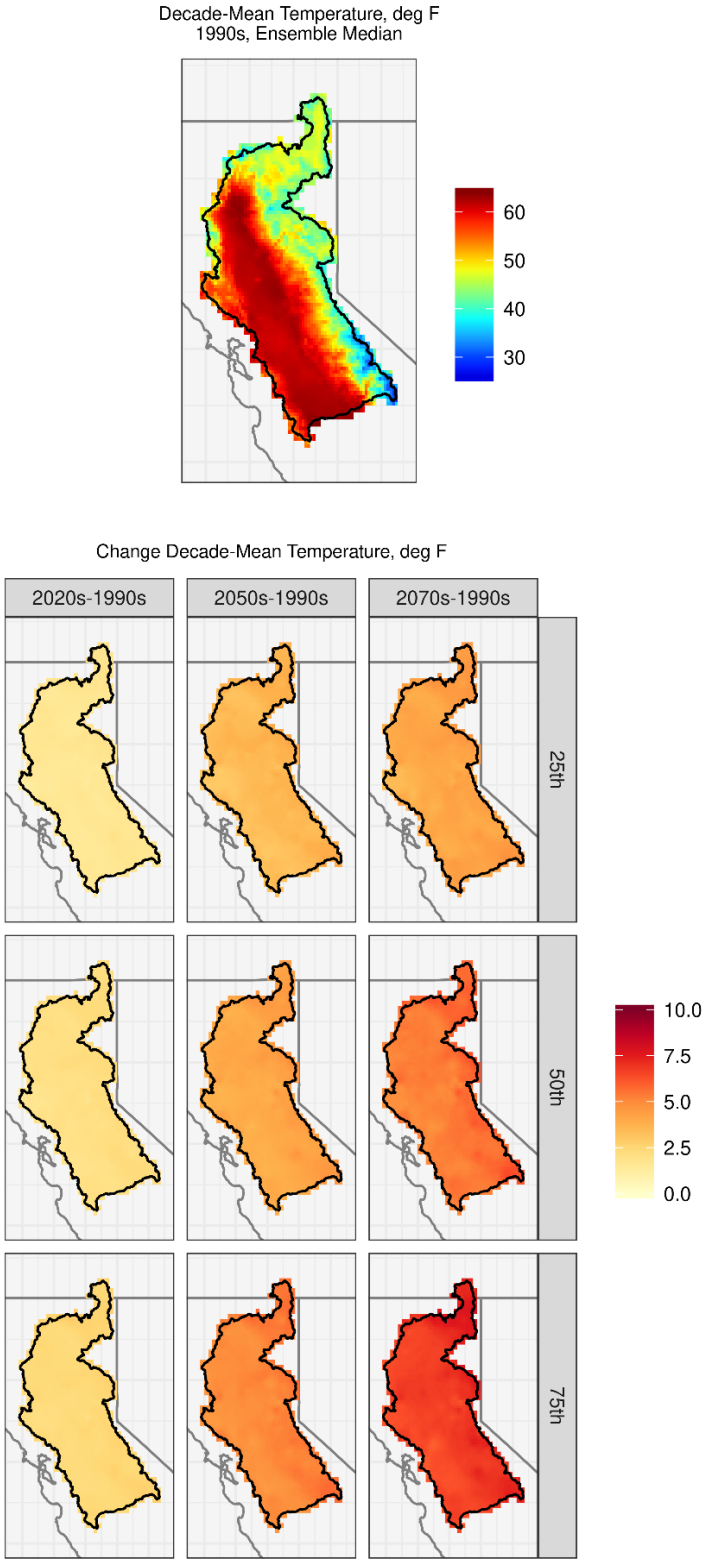

Figure 43. Sacramento and San Joaquin River Basins – Spatial distribution of simulated decadal temperature changes.

Note: deg F = degrees Fahrenheit

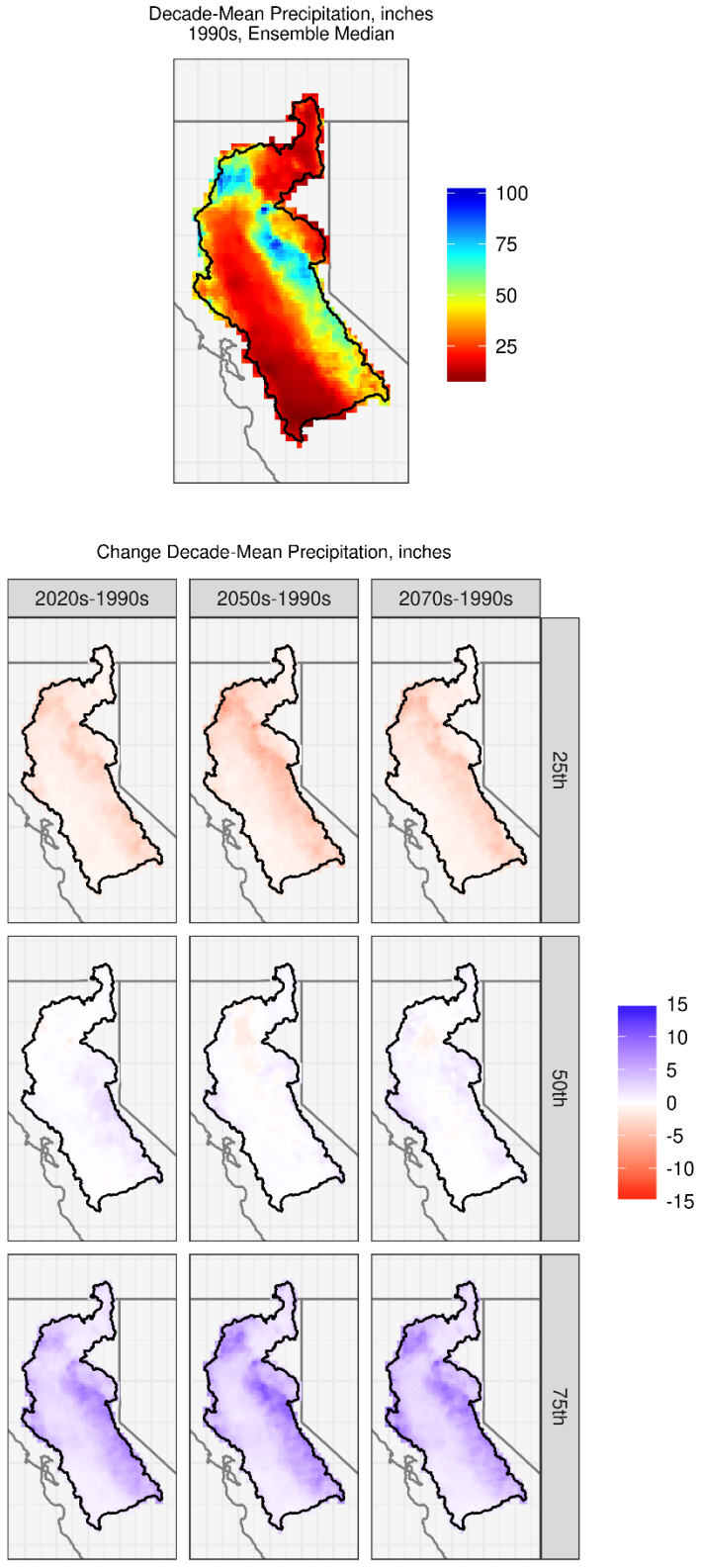

Figure 44. Sacramento and San Joaquin River Basins – Spatial distribution of simulated precipitation changes.

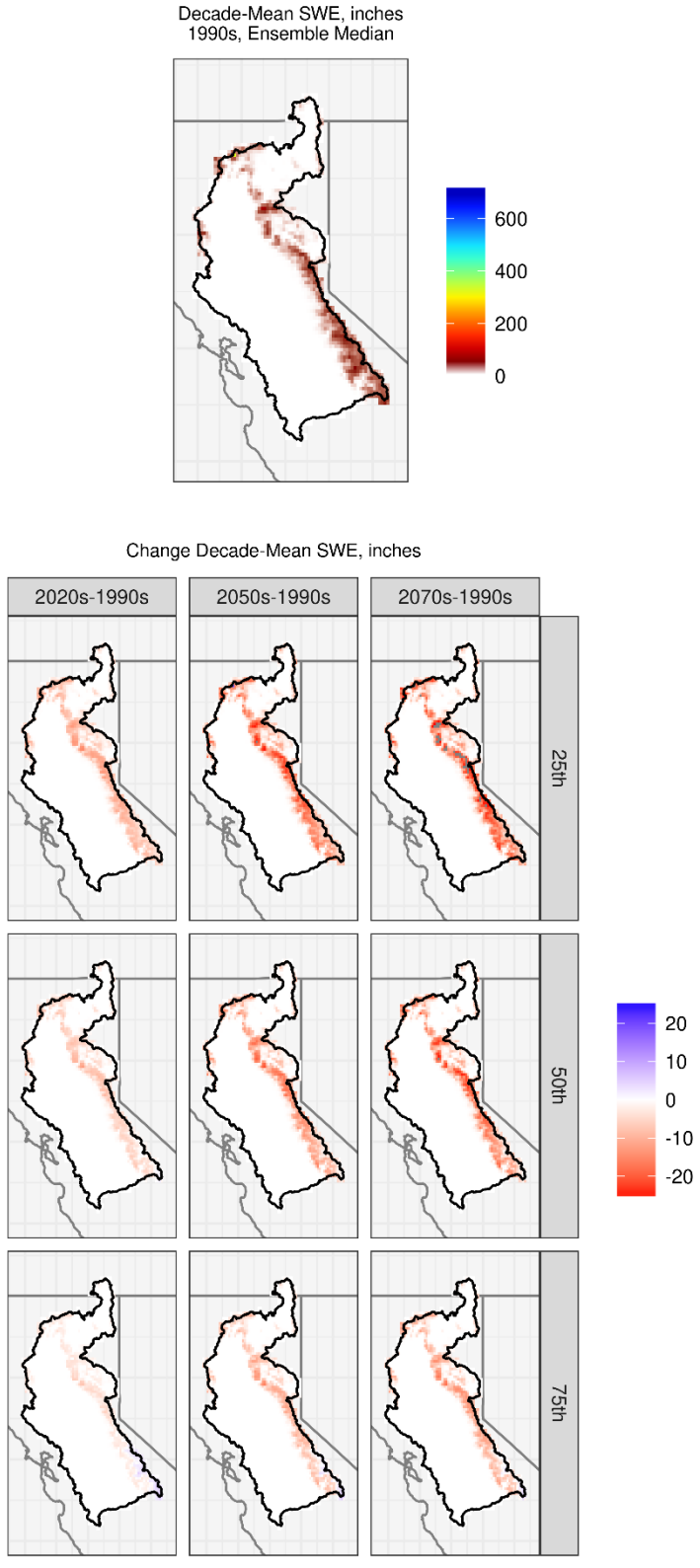

Figure 45. Sacramento and San Joaquin River Basins – Spatial distribution of simulated decadal April 1st SWE changes.

3.7.2 Impacts on Streamflow Annual and Seasonal Cycles

Figure 46 shows the mean monthly streamflow values for the 1990s, 2020s, 2050s, and 2070s in eight Sacramento and San Joaquin River subbasins and the Tulare basin. For all the locations, there appears to be an earlier shift in runoff peak.

Figure 47 shows boxplots of the distribution of simulated changes in runoff magnitude for annual, December-through-March, and April-through-July runoff in the eight Sacramento and San Joaquin River subbasins and the Tulare basin. Overall, the analysis shows that there is an increase in the median December-through-March runoff and decrease in the April-through-July runoff in all three future decades, with nominal changes in the ensemble-median annual runoff magnitudes. These changes in streamflow seasonality are evident in the time series plots for the basin above the Sacramento and San Joaquin Rivers at the Delta. In addition, in Figure 42, the bottom left panel shows an increase over time in the median December-through-March runoff and the bottom right panel shows a decrease over time in the median April-through-July runoff.

Figure 48 shows the simulated shift in runoff timing for the various subbasins. For all the subbasins, the shift represented by the ensemble median shows that half of the annual flow volume will occur earlier in the future decades relative to the 1990s decade. Also, it appears from the analysis that this earlier shift grows for some of the subbasins in the three future decades relative to the 1990s decade. For example, for the Delta inflow, the earlier shift is about, 4, 7, and 9 days, respectively, in the 2020s, 2050s, and 2070s relative to the 1990s.

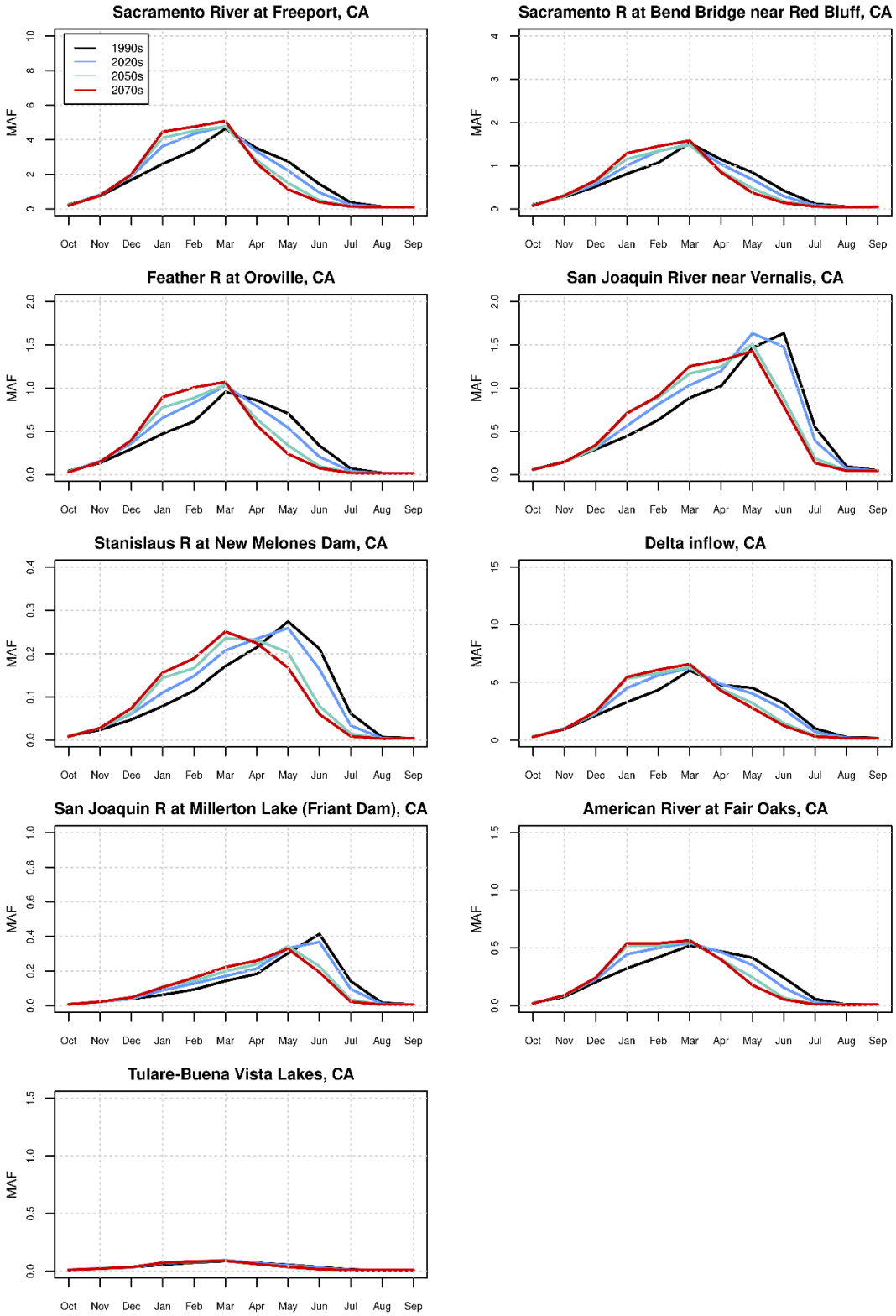

Figure 46. Sacramento and San Joaquin River Basins – Simulated mean monthly streamflow for various subbasins.

Note: MAF = million acre-feet

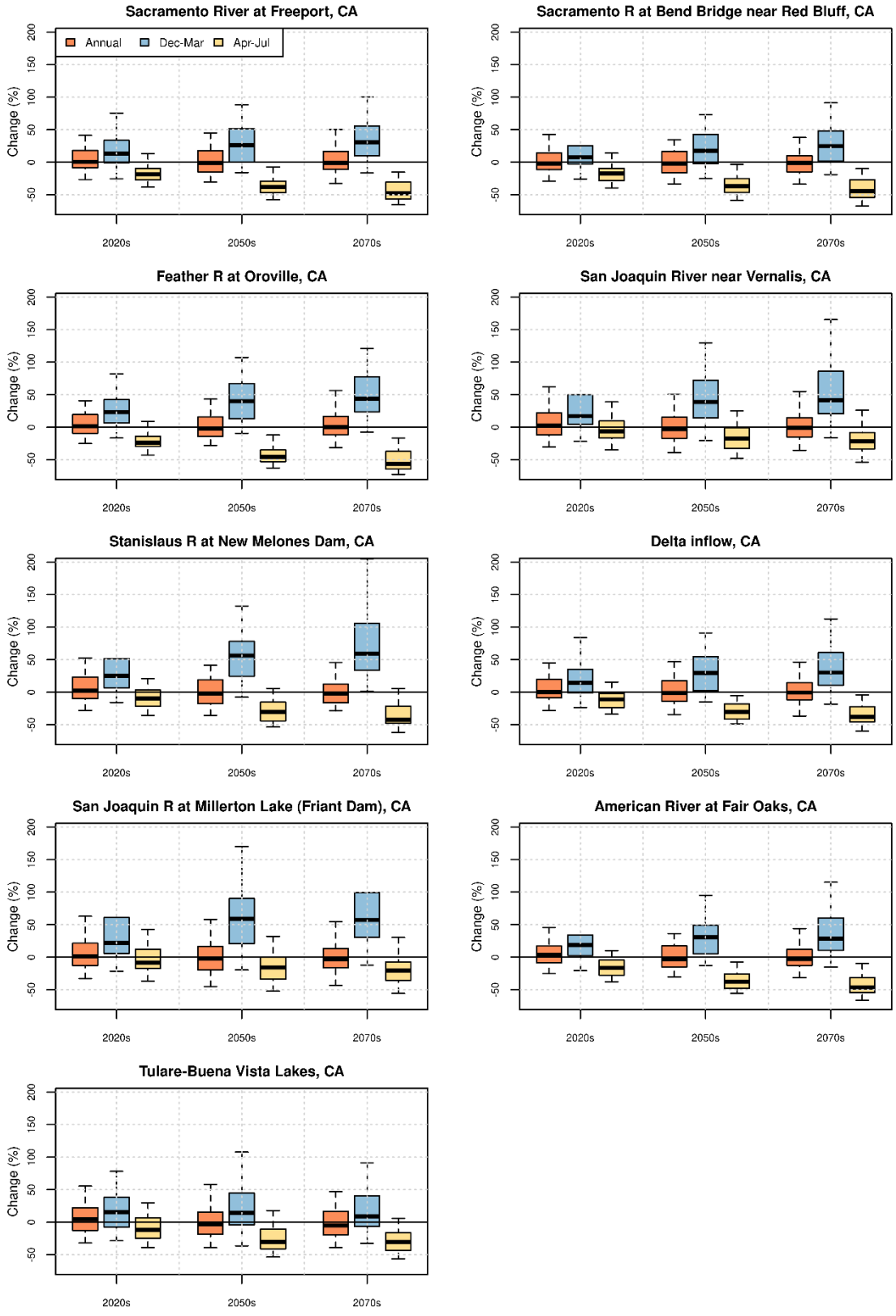

Figure 47. Sacramento and San Joaquin River Basins – Simulated change in streamflow magnitude for various subbasins.

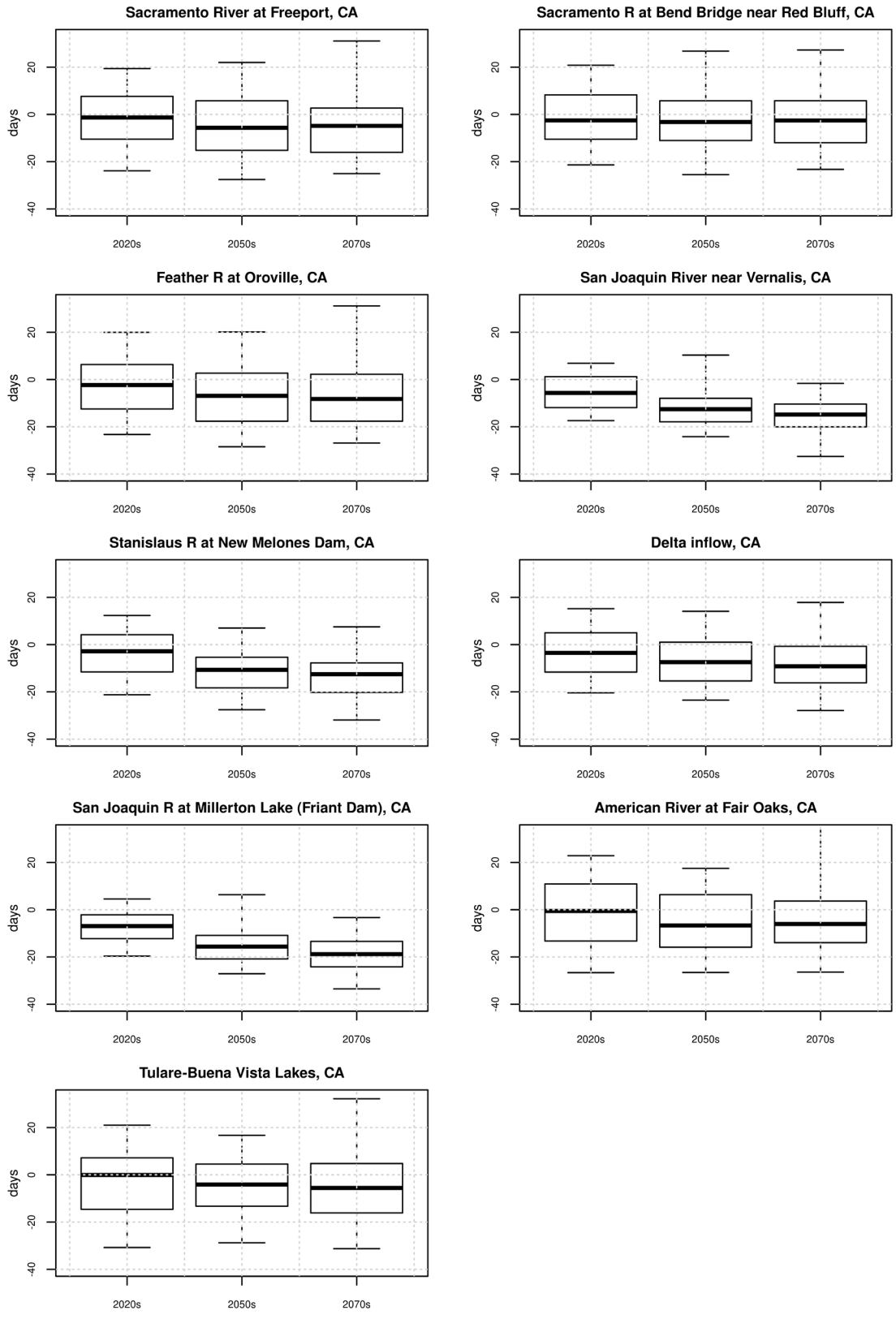

Figure 48. Sacramento and San Joaquin River Basins – Simulated shift in streamflow timing for various subbasins; negative values denote earlier runoff relative to the 1990s.

3.8 Truckee and Carson River Basins

The Truckee River originates at Lake Tahoe in California and flows for nearly 119 miles north and east into Nevada, where it terminates in Pyramid Lake. The Truckee River Basin encompasses an area of approximately 3,060 square miles in the States of California (760 square miles) and Nevada (2,300 square miles). The Truckee River is a major source of water for western Nevada, including the cities of Reno and Sparks. Along with the Carson River, the Truckee River supplies irrigation water to Reclamation's Newlands Project for approximately 57,000 acres of cropland. The Truckee River is also an important recreation resource for residents in California and Nevada, providing boating, rafting, kayaking, fishing, hunting, and camping opportunities.

3.8.1 Hydroclimate Projections

Figure 49 shows six hydroclimate indicators for the basin above the Truckee River at Nixon gage: annual total precipitation (top left), annual mean temperature (top right), April 1st SWE (middle left), annual runoff (middle right), December-through-March runoff (bottom left), and April-through-July runoff (bottom right). The heavy black line is the median value (50th percentile) of the annual time series of the 64 projections. The shaded area is the annual time series of the 10th to 90th percentiles.

Total annual precipitation (median value) throughout the basin is shown to be largely constant over time. The ensemble spread appears to be somewhat widening, implying that, there is some increase in the range of values for total annual precipitation magnitudes through time. The mean annual temperature (median value) throughout the basin shows an increase over time and a widening ensemble spread, implying that, there is some increase in the range of mean annual temperature values over time. April 1st SWE (median value) shows a decrease over time. The annual runoff (median value) shows a nominal decrease over time. The December-through-March runoff volume shows an increase over time, and the April-through-July runoff shows a decrease over time.

Figure 50, Figure 51, and Figure 52 show the spatial distribution of simulated decade-mean temperatures, precipitation, and April 1st SWE, respectively, in the basin above the Truckee River at Nixon gage. In each figure, the simulated 1990s distribution of median decadal mean condition for the variable of interest is shown in the upper middle plot, and changes in the decadal mean condition are shown below for the three future periods and at three change percentiles within the projections (25th, 50th, and 75th percentiles).

In Figure 50, the median change for the three future decades relative to the 1990s indicates increasing temperatures throughout the basin. In Figure 51, the median change in precipitation for the future decades indicates a slightly wetter pattern, mostly in the mountainous regions of the basin. In Figure 52, the spatial plots indicate the median basin snowpack (April 1st SWE) is projected to decrease.

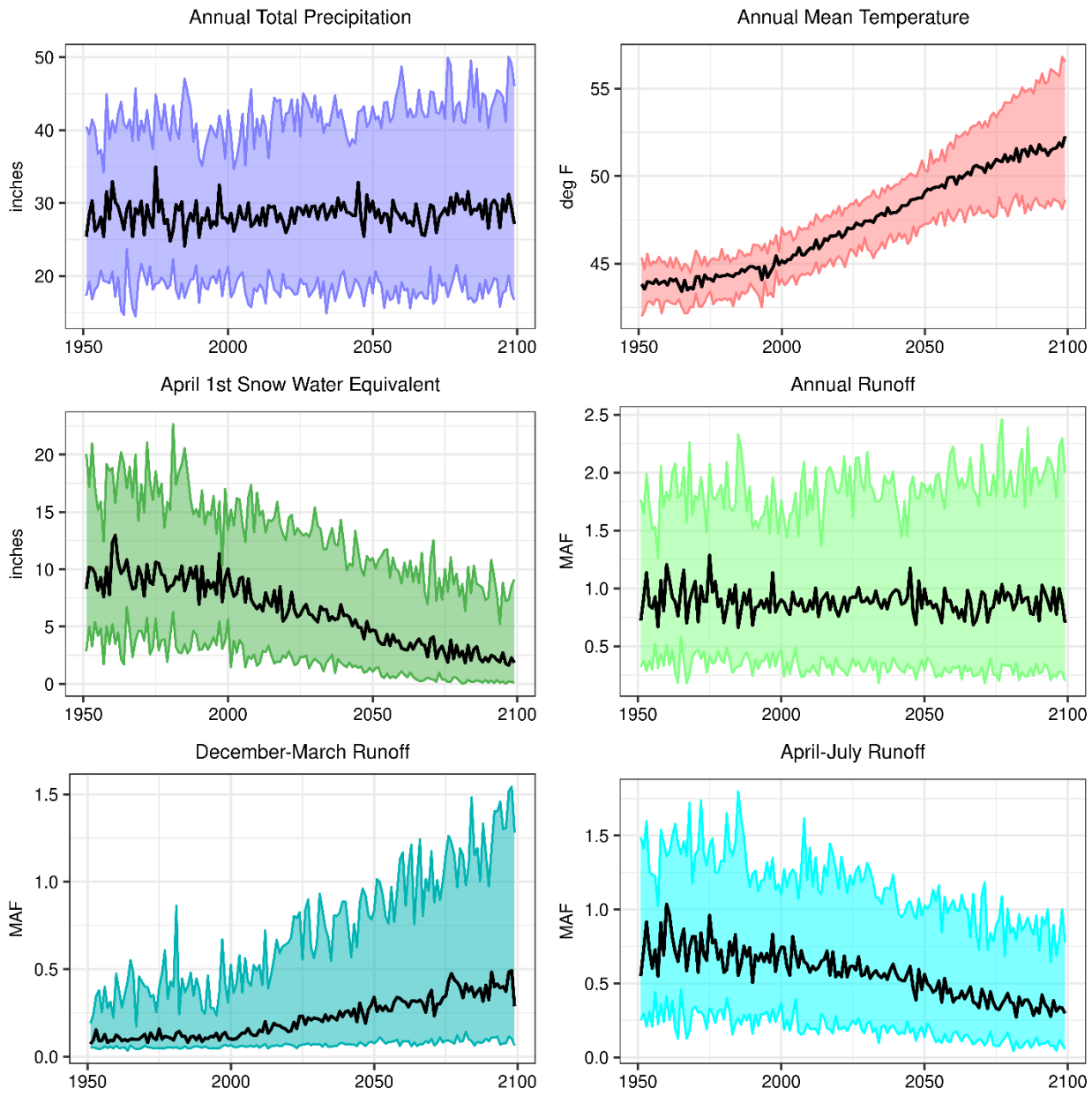

Figure 49. Truckee and Carson River Basins – Time series plots for six projected hydroclimate indicators.

Note: The heavy black line is the annual time series median value (i.e., median). The shaded area is the annual time series of 10th to 90th percentiles.

MAF = million acre-feet; deg F = degrees Fahrenheit

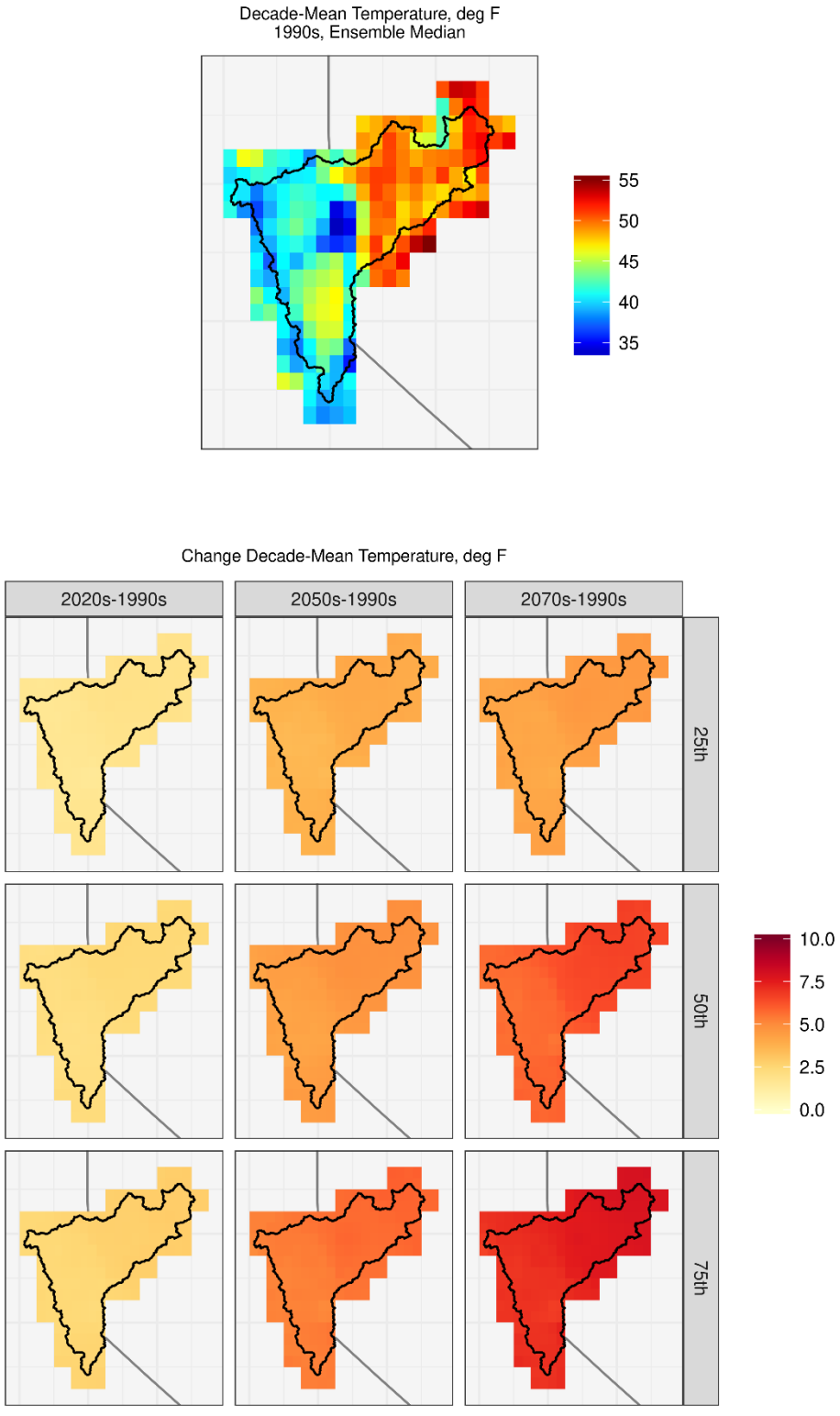

Figure 50. Truckee and Carson River Basins – Spatial distribution of simulated decadal temperature changes.

Note: deg F = degrees Fahrenheit

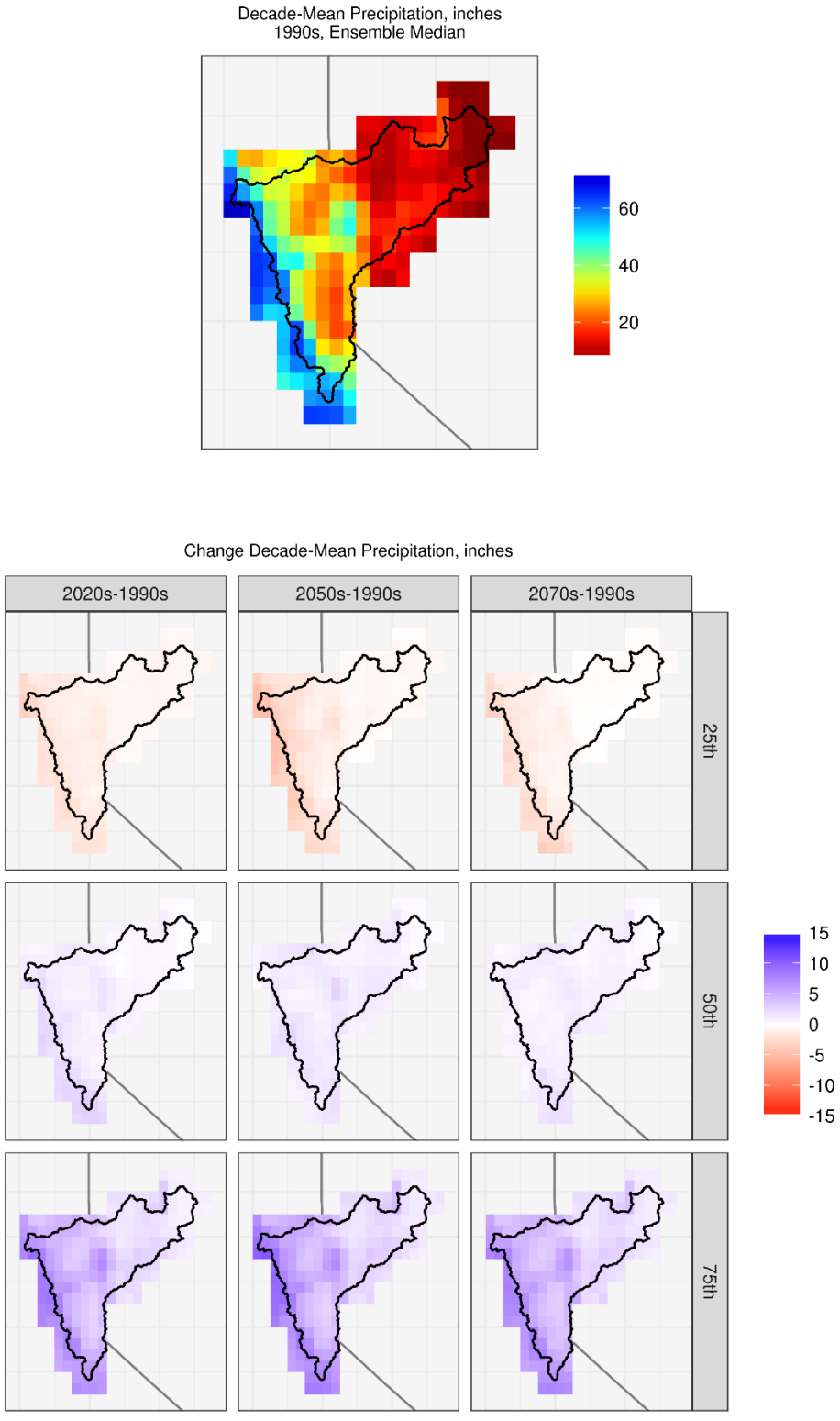

Figure 51. Truckee and Carson River Basins – Spatial distribution of simulated precipitation changes.

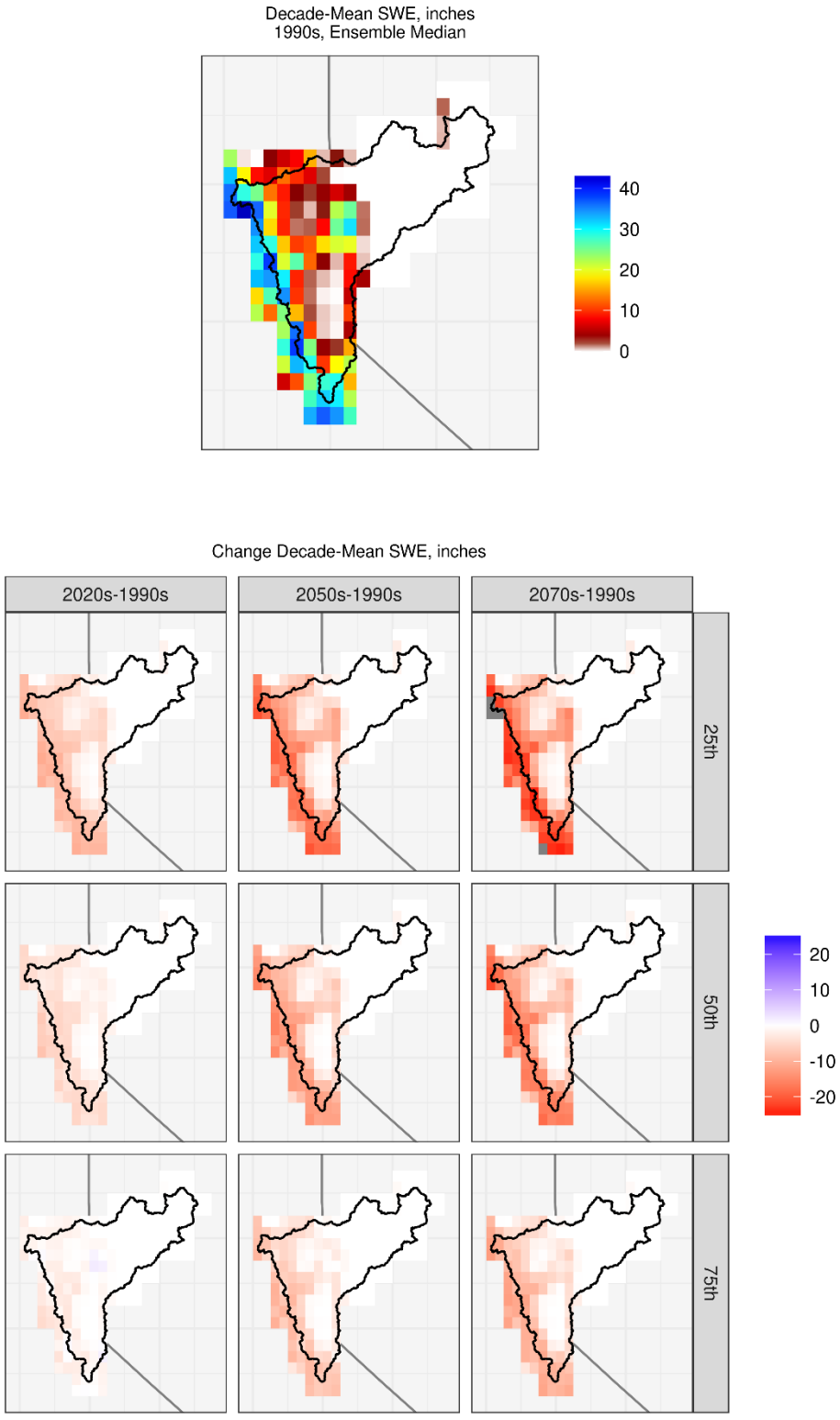

Figure 52. Truckee and Carson River Basins – Spatial distribution of simulated decadal April 1st SWE changes.

3.8.2 Impacts on Streamflow Annual and Seasonal Cycles

Figure 53 shows the mean monthly streamflow values for the 1990s, 2020s, 2050s, and 2070s in four Truckee River subbasins and the Carson River Basin. There are noticeable shifts in the distribution of monthly flow in the future decades relative to the 1990s reference, but, there do not appear to be large shifts in the peak runoff timing except for the 2070s.

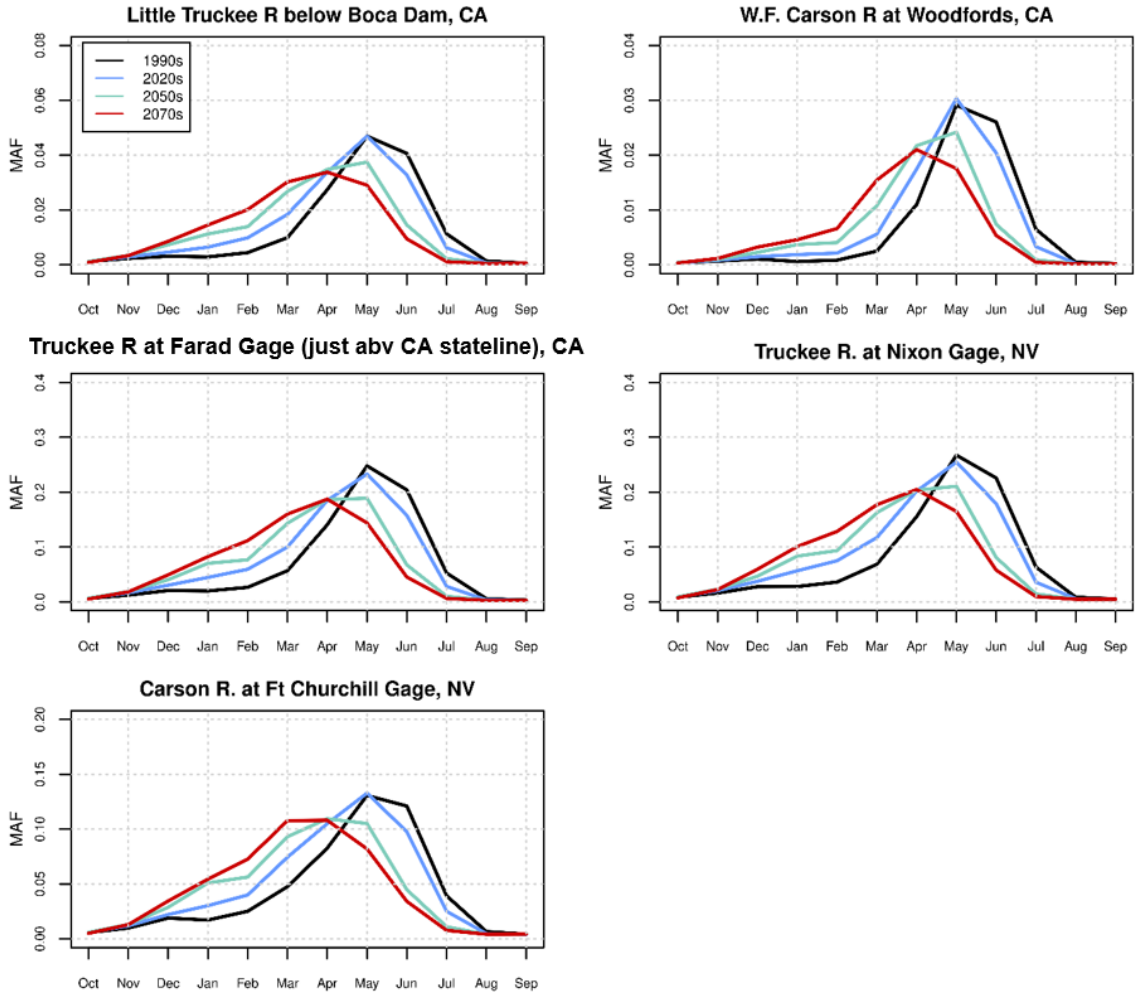

Figure 53. Truckee and Carson River Basins – Simulated mean monthly streamflow for various subbasins.

Note: MAF = million acre-feet

Figure 54 shows boxplots of the distribution of simulated changes in runoff magnitude for annual, December-through-March, and April-through-July runoff in the four Truckee River subbasins and the Carson River Basin. Overall, the analysis shows that there is an increase in the ensemble-median December-through-March runoff and a decrease in the April-through-July runoff in all three future decades, with nominal changes in the ensemble-median annual runoff magnitudes. These changes in streamflow seasonality are evident in the time series plots for the basin above the Truckee River at Nixon gage. In Figure 49, the bottom left panel shows an

increase over time in the median December-through-March runoff and the bottom right panel shows a decrease over time in the median April-through-July runoff.

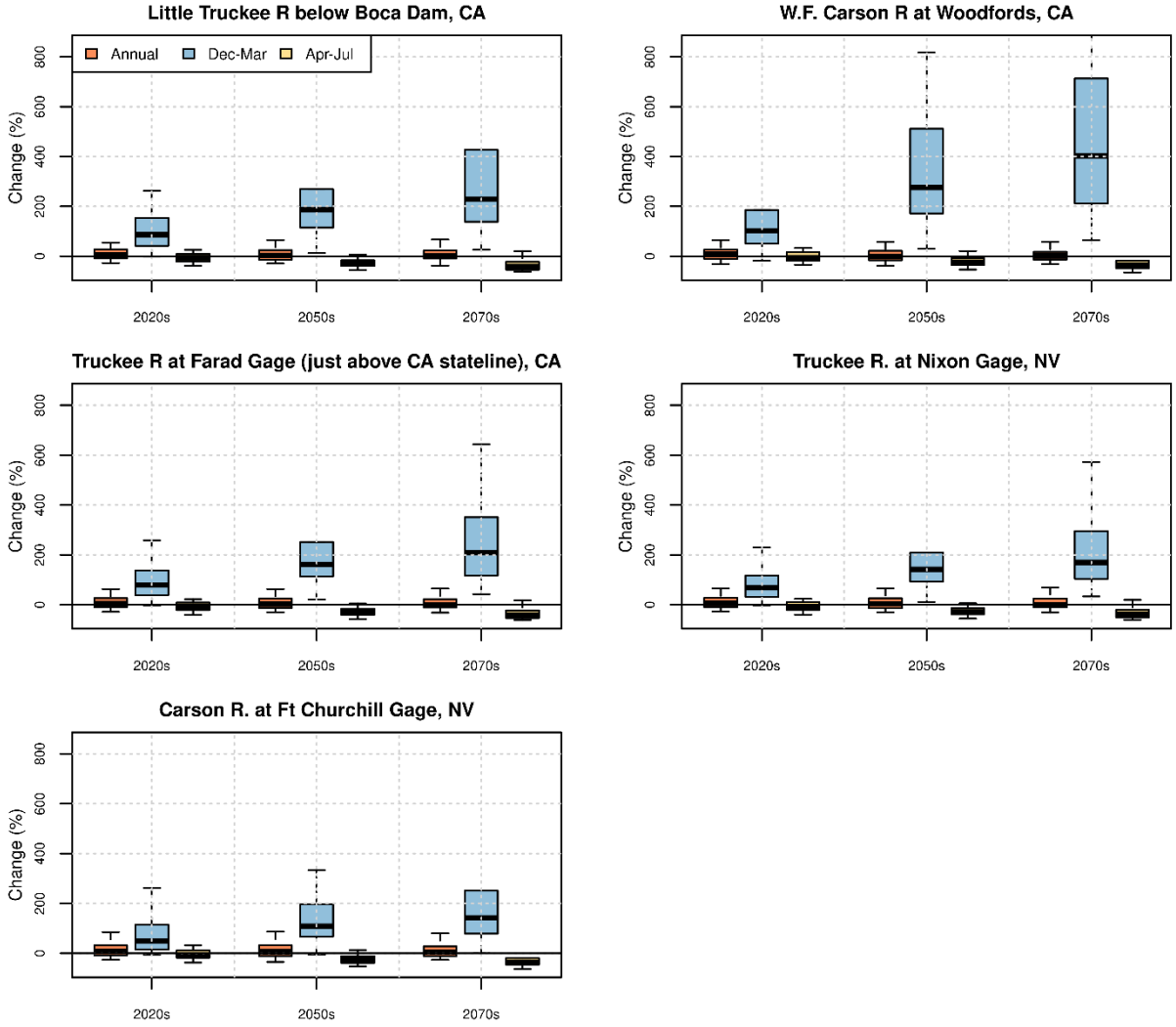

Figure 54. Truckee and Carson River Basins – Simulated change in streamflow magnitude for various subbasins.

Figure 55 shows the simulated shift in runoff timing for the various subbasins. For all of the subbasins, the shift represented by the ensemble median shows that half of the annual flow volume will occur earlier in the future decades relative to the 1990s decade. Also, it appears from the analysis that, for some of the subbasins, this earlier shift grows in the three future decades (2020s, 2050s, and 2070s) relative to the 1990s decade. For example, for the Truckee River at the Nixon gage, the earlier shift is about 9, 18, and 20 days, respectively, in the 2020s, 2050s, and 2070s relative to the 1990s.

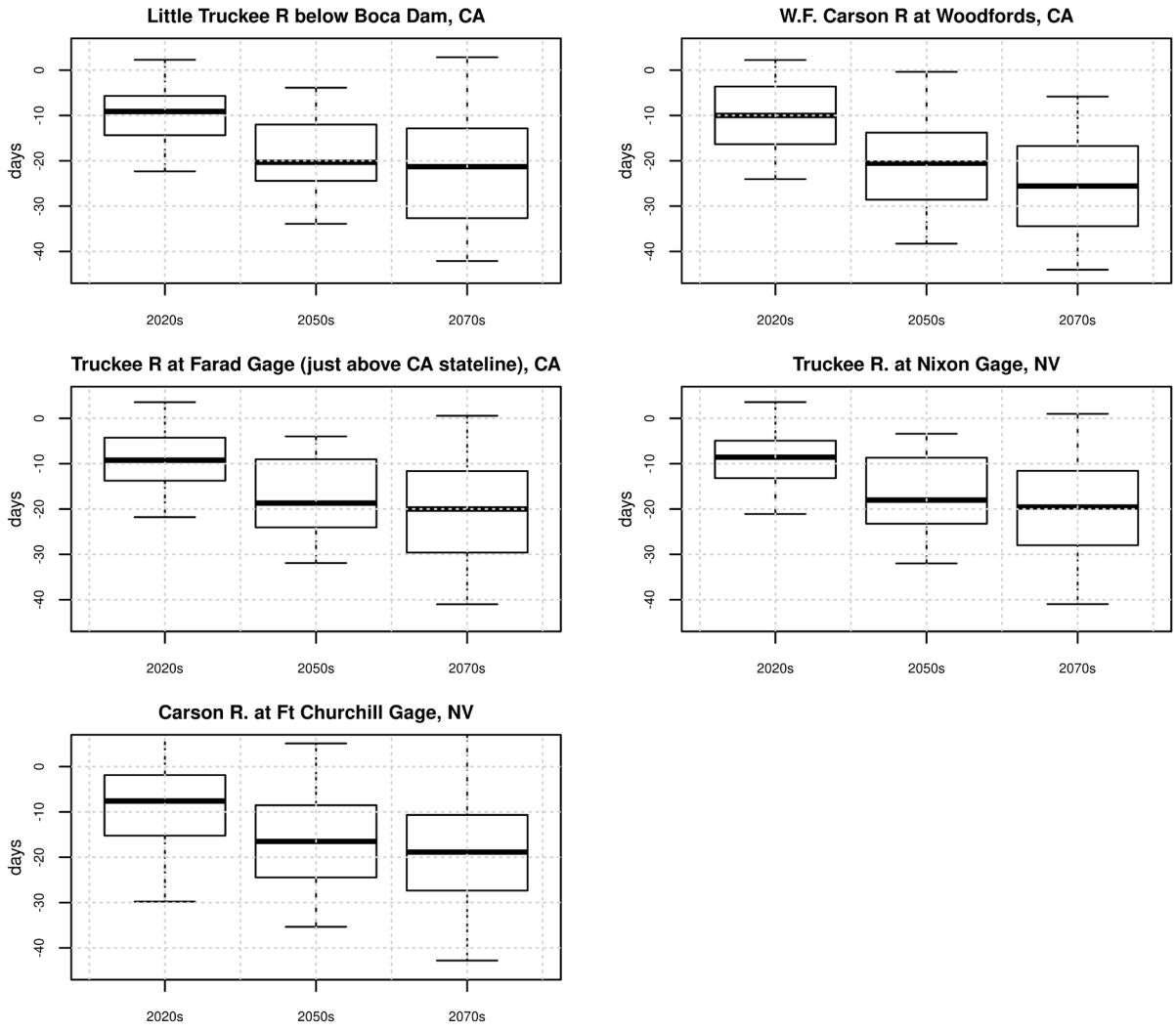

Figure 55. Truckee and Carson River Basins – Simulated shift in streamflow timing for various subbasins; negative values denote earlier runoff relative to the 1990s.

3.9 Expanding Understanding of Streamflow Simulations

To expand understanding of the LOCA streamflow projections described above (Sections 3.2 through 3.8), this section highlights comparisons of these streamflow projections with streamflow projections from BCSD reported in the West-Wide Climate Risk Assessment of the 2016 SECURE Water Act Report (Reclamation, 2016c). In addition, streamflow projection information used in other Reclamation regional climate impact studies are also discussed to provide context for the current LOCA streamflow projections. The discussions in this section are focused only on streamflow simulations as it is the primary variable of interest for use in any subsequent water resources system modeling to support water allocation decisions.

Though the GCM projections from the CMIP5 experiment were used both in the 2021 and 2016 assessments, there are some key differences as to how the hydrologic projections were developed in these two assessments. These include:

- Use of different statistical downscaling techniques—LOCA (this report) and BCSD (2016 Assessment)—to develop the climate projections.
    - The LOCA and BCSD methods use different climate observation datasets in their training step to develop the transfer function relationships that are subsequently used in the downscaling step.
- Different configurations of the VIC hydrology model—including model version, model grid resolution, and flow routing scheme—were used in this report and 2016 Assessment.
- Some differences in basin contributing area were also noted in the flow routing schemes used in this report and 2016 Assessment.

These differences in the choice of downscaling techniques and hydrology model configurations can lead to substantial differences in natural (i.e., unimpaired) streamflow simulations. In fact, some substantial differences were found between the CMIP5-LOCA (this report) and CMIP5-BCSD (2016 Assessment) streamflow simulations. To illustrate this, a comparison of LOCA and BCSD streamflow simulations over the historical period—water years 1951 to 1999 at selected key gage locations in the eight major Reclamation river basins—is presented in Figure 56. Note that, the comparisons are based on VIC simulated natural flows only and do not involve any post-processing of these simulated flows (e.g., secondary bias-corrections). Typically, additional post-processing would be done prior to use of the information as input to a river systems model, for example.

For each location, the comparison is based on the respective (LOCA or BCSD) ensemble median of mean annual flows calculated over the historical period water years 1951 to 1999. In the case of LOCA, the total number of streamflow projections over this historical period, water years 1951 to 1999, is 32 as the RCP4.5 and RCP8.5 streamflow projections are identical over this historical period (recall, the total number of projections from CMIP5-LOCA is 64, which includes 32 for RCP4.5 and 32 for RCP8.5). In the case of BCSD, the total number of CMIP5 streamflow projections over this historical period, water years 1951 to 1999, is 97 and includes

RCPs 2.6, 4.5, 6.0 and 8.5 (Reclamation, 2016c). This difference in which scenarios and GCMs are used, is another reason why future streamflow projections could differ (in addition to downscaling and hydrologic model configuration).

Simulated annual flow for a given projection over water years 1951 to 1999 was used to first calculate the mean annual flow for the projection. This step to calculate mean annual flow was repeated with each projection in the respective set—32 projections in the case of LOCA; 97 projections in the case of BCSD—resulting in an ensemble of mean annual flows for LOCA and BCSD projections. The median of each ensemble was then calculated to obtain the ensemble median mean annual flow. The ensemble median of mean annual flow over water years 1951 to 1999 for key gage locations from LOCA and BCSD simulations is presented in Figure 56 for the same key locations presented in Section 2.1 of this report. Simulated flows based on LOCA and BCSD projections are presented in units of million acre-feet (MAF).

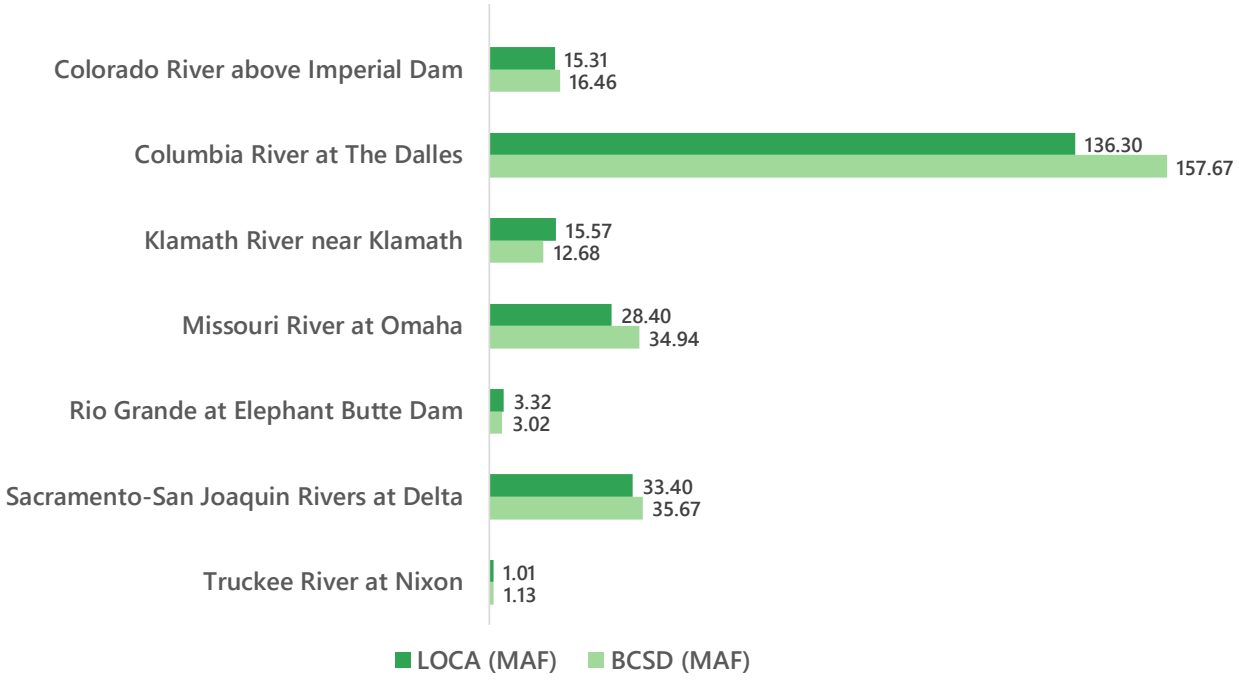

Figure 56. Comparison of ensemble median of mean annual flow between LOCA and BCSD over water years 1951 to 1999 for key gage locations.

Note: Simulated flows (ensemble median of mean annual flow over water years 1951 to 1999) in million acre-feet (MAF) comparing CMIP5-LOCA and BCSD results is shown adjacent to each bar plot.

The comparison presented in Figure 56 shows that, generally, the LOCA streamflow simulations are biased low relative to the BCSD streamflow simulations. However, for two locations—Klamath River near Klamath and Rio Grande at Elephant Butte Dam—the LOCA simulated flows are higher than the BCSD simulated streamflow. This difference in ensemble median of mean annual flow magnitude over water years 1951 to 1999 between LOCA and BCSD simulations for the key gage locations is presented in Figure 57. For each gage location, the difference is expressed in terms of a percentage difference of the LOCA simulated flows from the BCSD simulated flows shown in Figure 56.

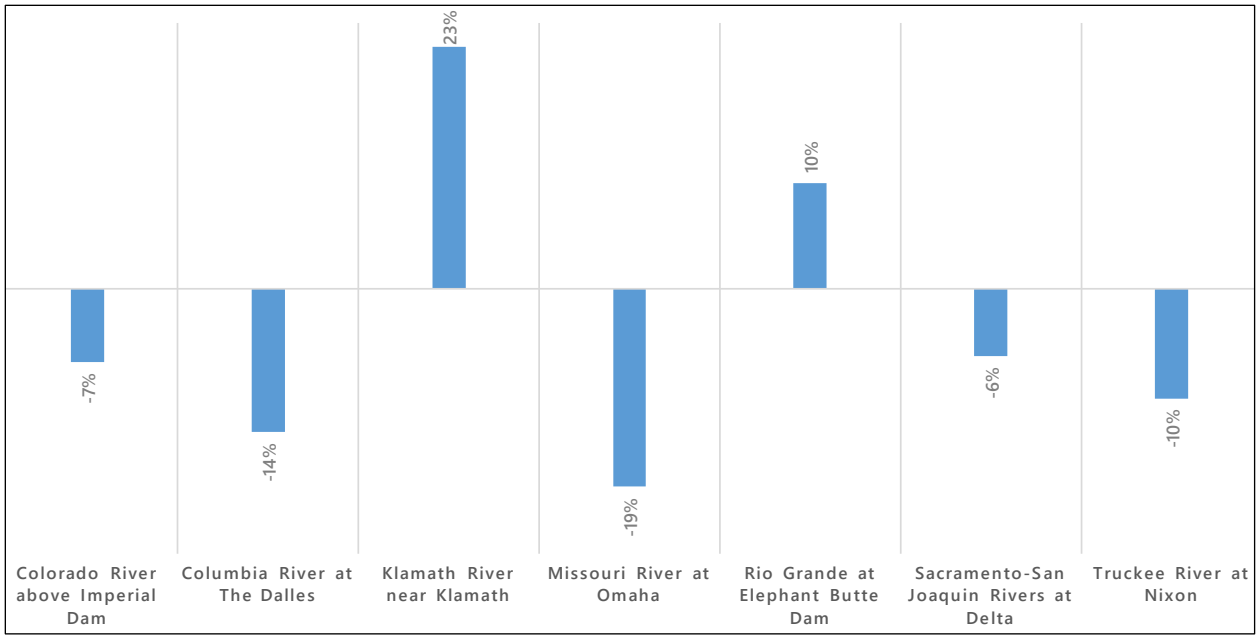

Figure 57. Percentage difference in ensemble median of mean annual flow magnitude between LOCA and BCSD simulations over water years 1951 to 1999 for key gage locations.

Note: The difference is expressed in terms of a percentage difference (rounded to the nearest integer) of the LOCA simulated flows from the BCSD simulated flows (ensemble median of mean annual flow over water years 1951 to 1999; refer to Figure 56 for flow magnitudes). For a given gage location, negative (positive) percentage value implies that LOCA simulated flow is lower (higher) than BCSD simulated flow.

This comparison of LOCA and BCSD flow simulations and the differences shown over the historical period—water years 1951 to 1999 (see Figure 56 and Figure 57, respectively)—persists into the future as well. To illustrate differences over historical and projected future periods, LOCA and BCSD simulated flows over the full simulation period—water years 1951 to 2099—are presented in Figure 58 through Figure 64. Specifically, for each location, ensemble median flow (50th percentile) along with the lower (10th percentile) and upper (90th percentile) confidence limits are shown for the LOCA and BCSD simulations separately, and then the LOCA and BCSD ensembles were combined to develop an ensemble from which the median and confidence limits were calculated. The ensemble median and confidence limits calculated from the combined LOCA and BCSD ensembles are shown using heavy colored lines in the time-series plots. The combined LOCA and BCSD streamflow ensemble thus presents the collective view of streamflow projections from these two sets of projections with the available full range of downscaled RCPs—2.6 through 8.5[7].

[7] BCSD projections include RCP 2.6, 4.5, 6.0, and 8.5. LOCA projections include RCP 4.5 and 8.5.

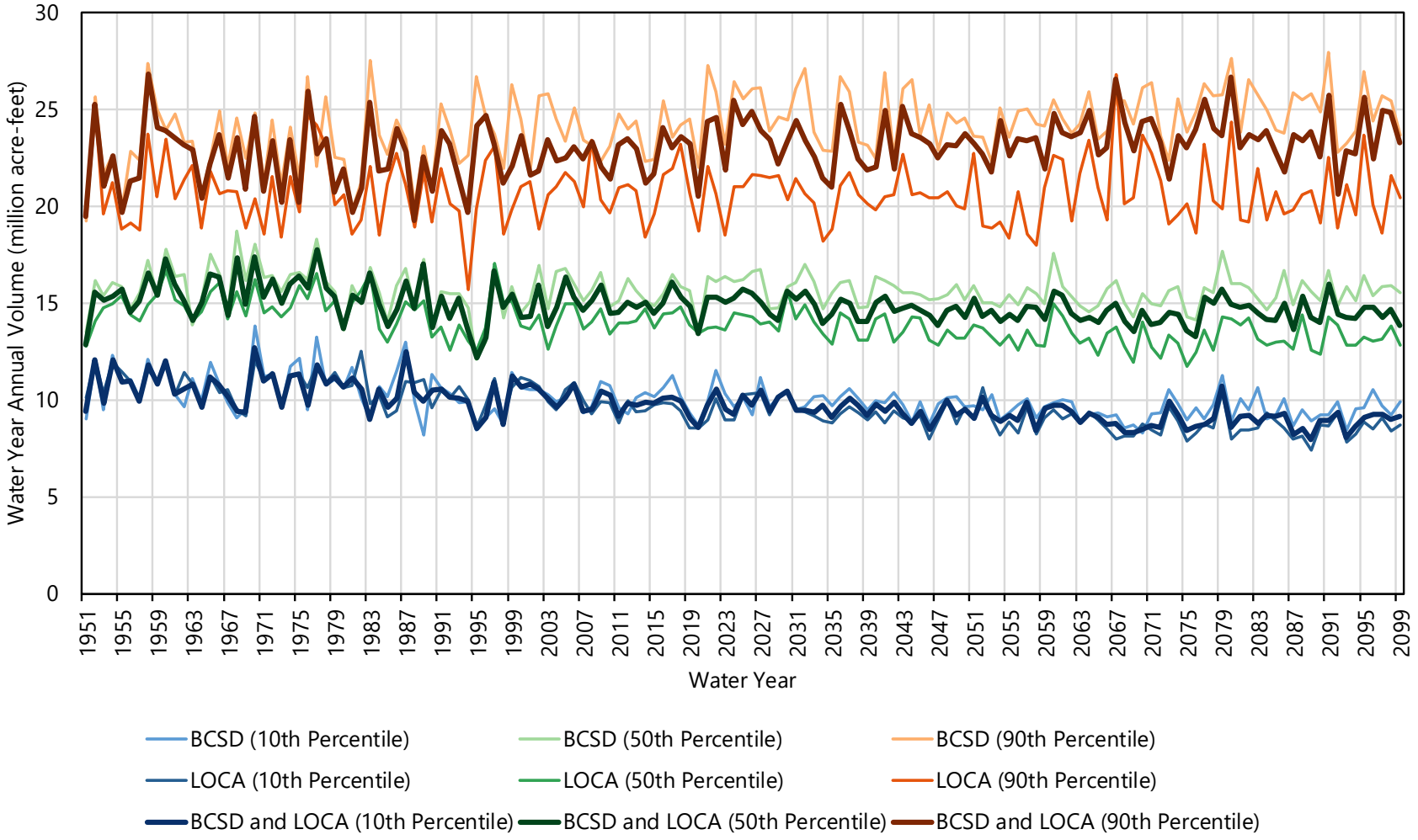

Figure 58. Simulated flows for Colorado River above Imperial Dam from BCSD, LOCA, and combined BCSD and LOCA projections.

Note: Ensemble median (50th percentile), lower (10th percentile), and upper (90th percentile) confidence limits are shown in the figure.

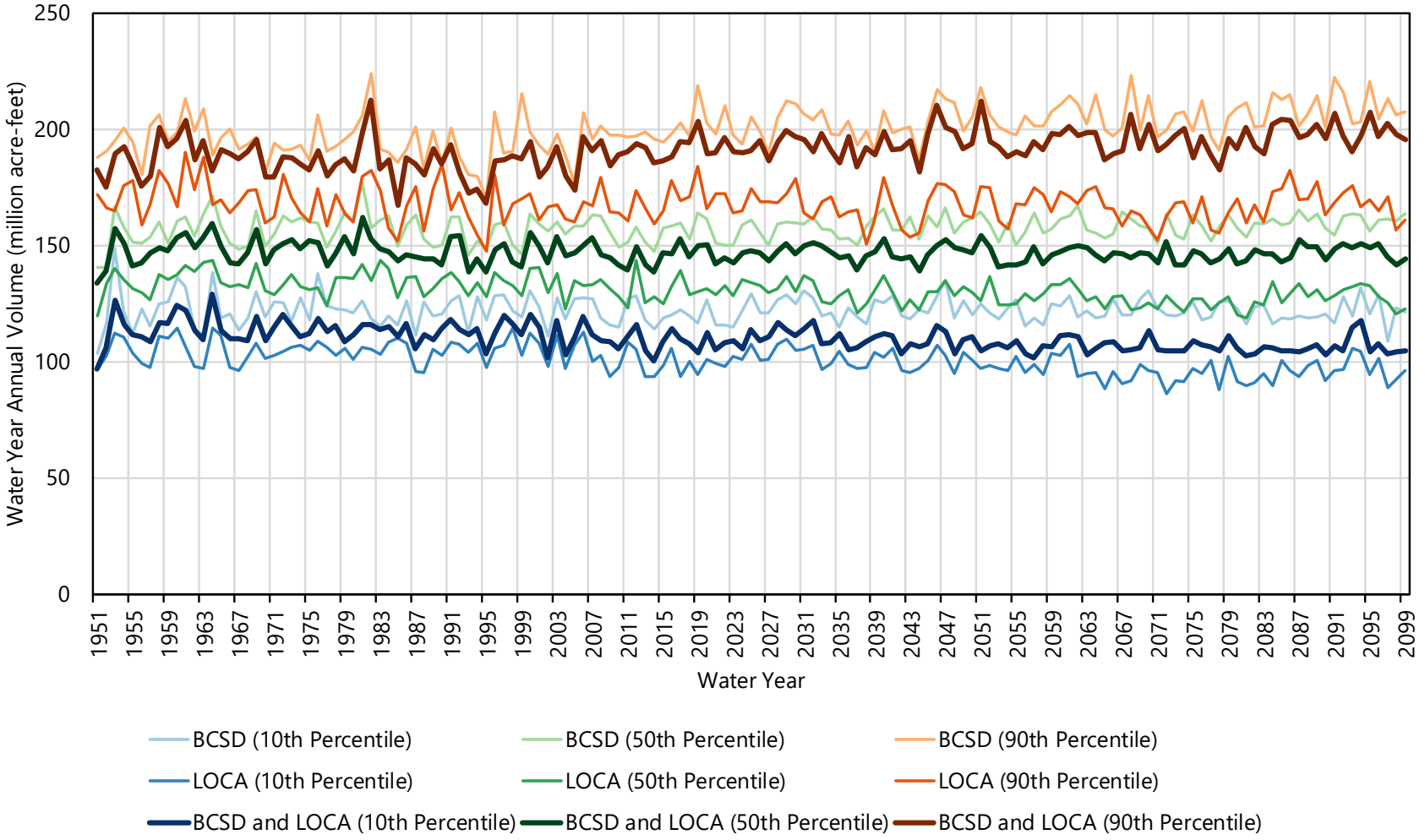

Figure 59. Simulated flows for Columbia River at The Dalles from BCSD, LOCA, and combined BCSD and LOCA projections.

Note: Ensemble median (50th percentile), lower (10th percentile), and upper (90th percentile) confidence limits are shown in the figure.

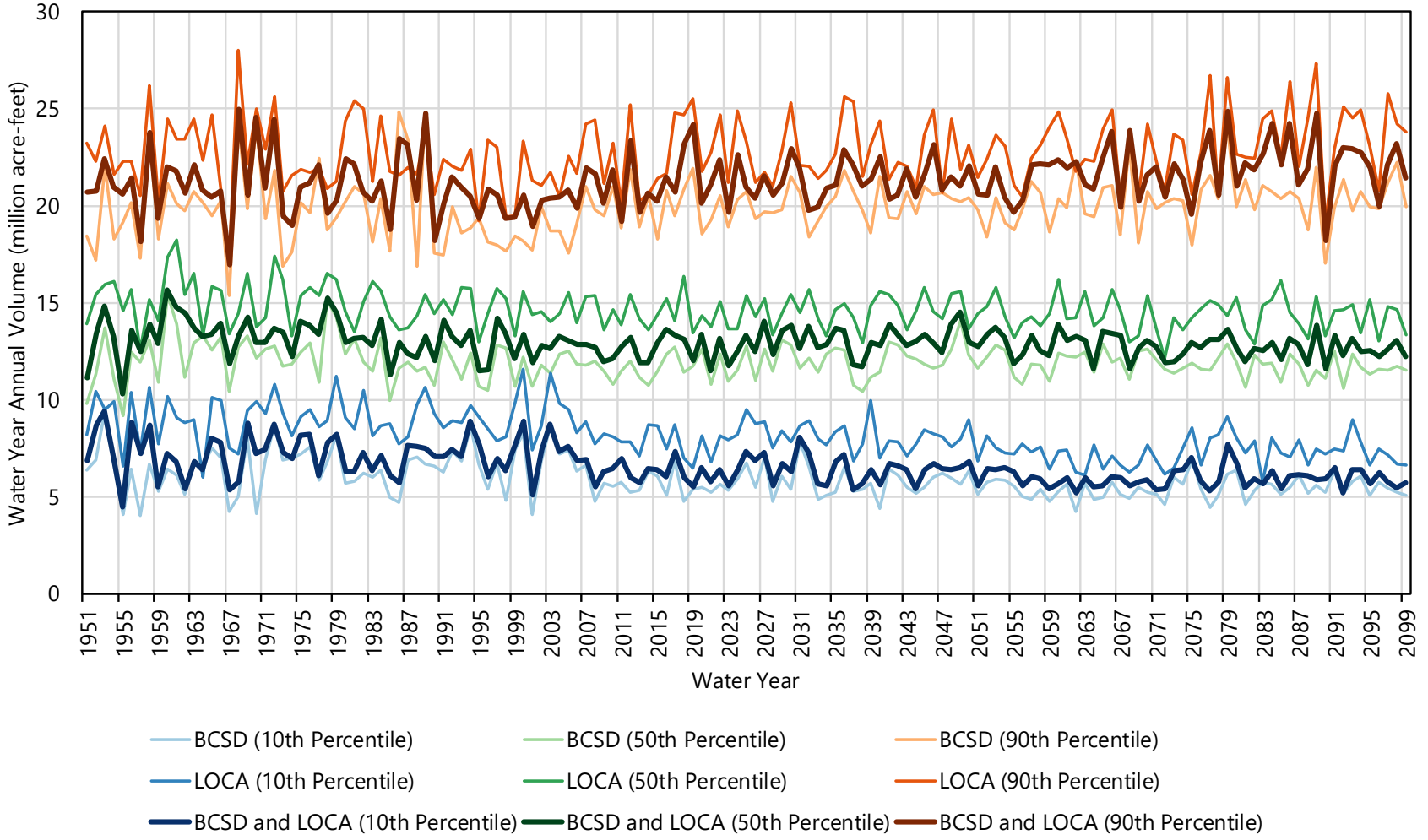

Figure 60. Simulated flows for Klamath River near Klamath from BCSD, LOCA, and combined BCSD and LOCA projections.

Note: Ensemble median (50th percentile), lower (10th percentile), and upper (90th percentile) confidence limits are shown in the figure.

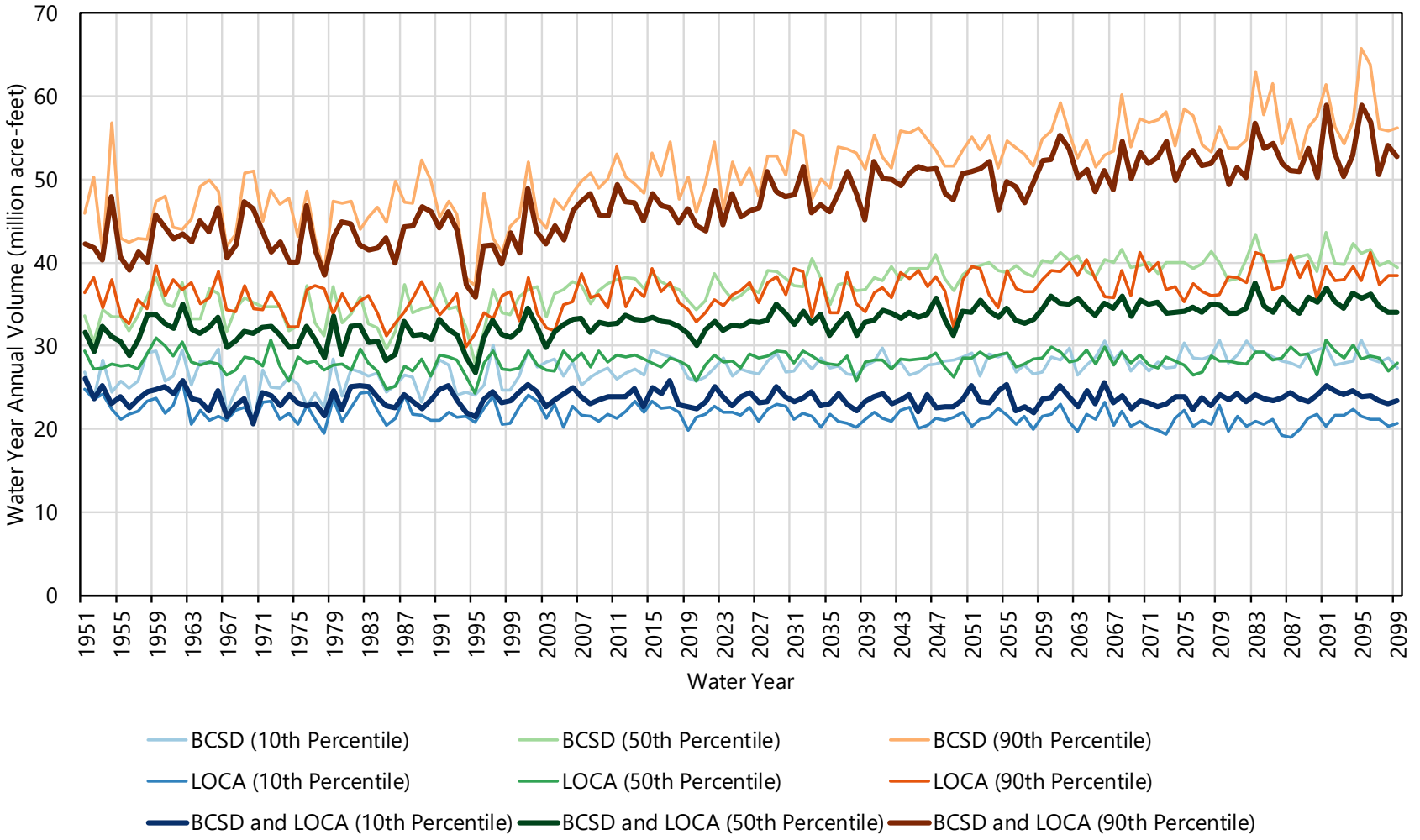

Figure 61. Simulated flows for Missouri River at Omaha from BCSD, LOCA, and combined BCSD and LOCA projections.

Note: Ensemble median (50th percentile), lower (10th percentile), and upper (90th percentile) confidence limits are shown in the figure.

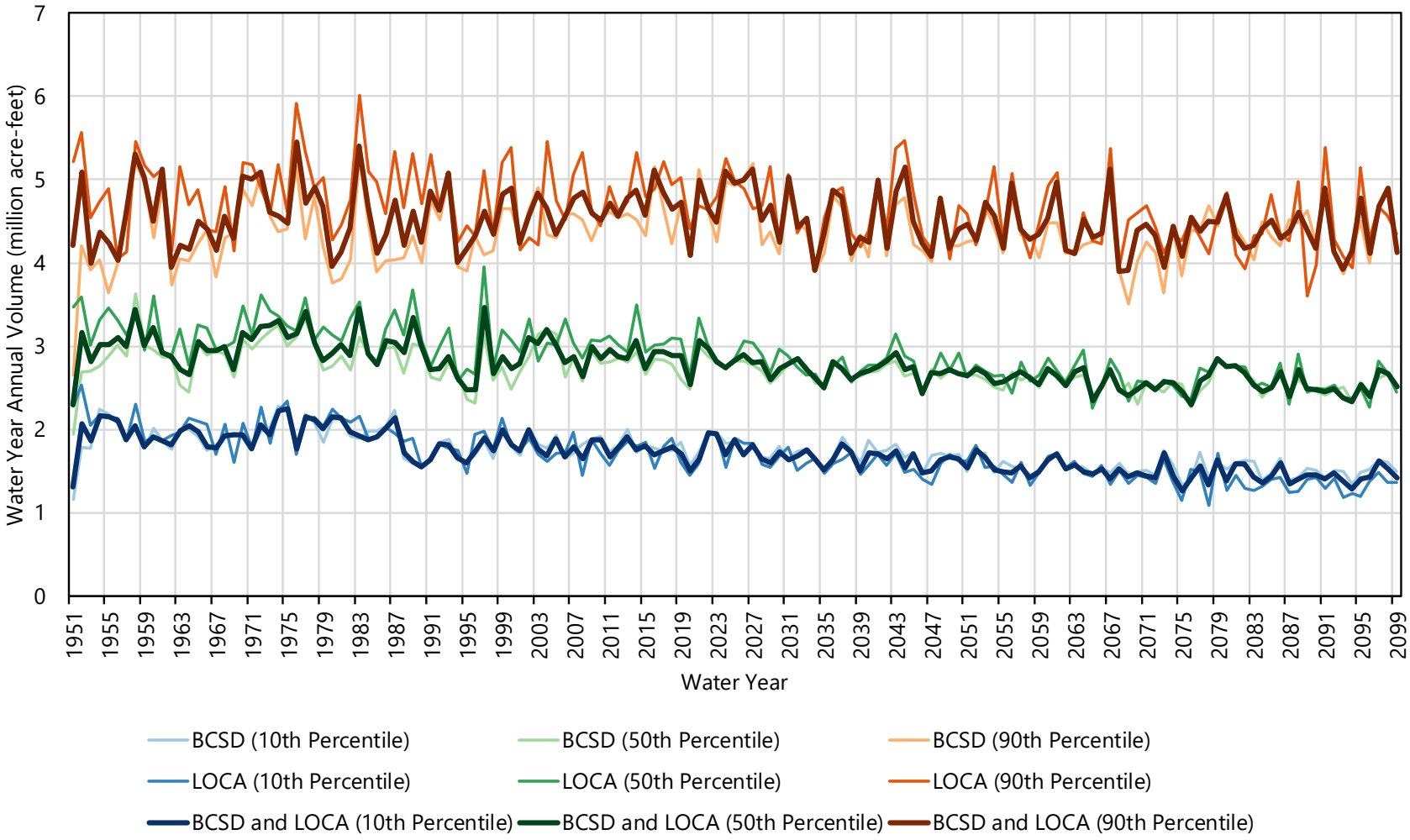

Figure 62. Simulated flows for Rio Grande at Elephant Butte Dam from BCSD, LOCA, and combined BCSD and LOCA projections.

Note: Ensemble median (50th percentile), lower (10th percentile), and upper (90th percentile) confidence limits are shown in the figure.

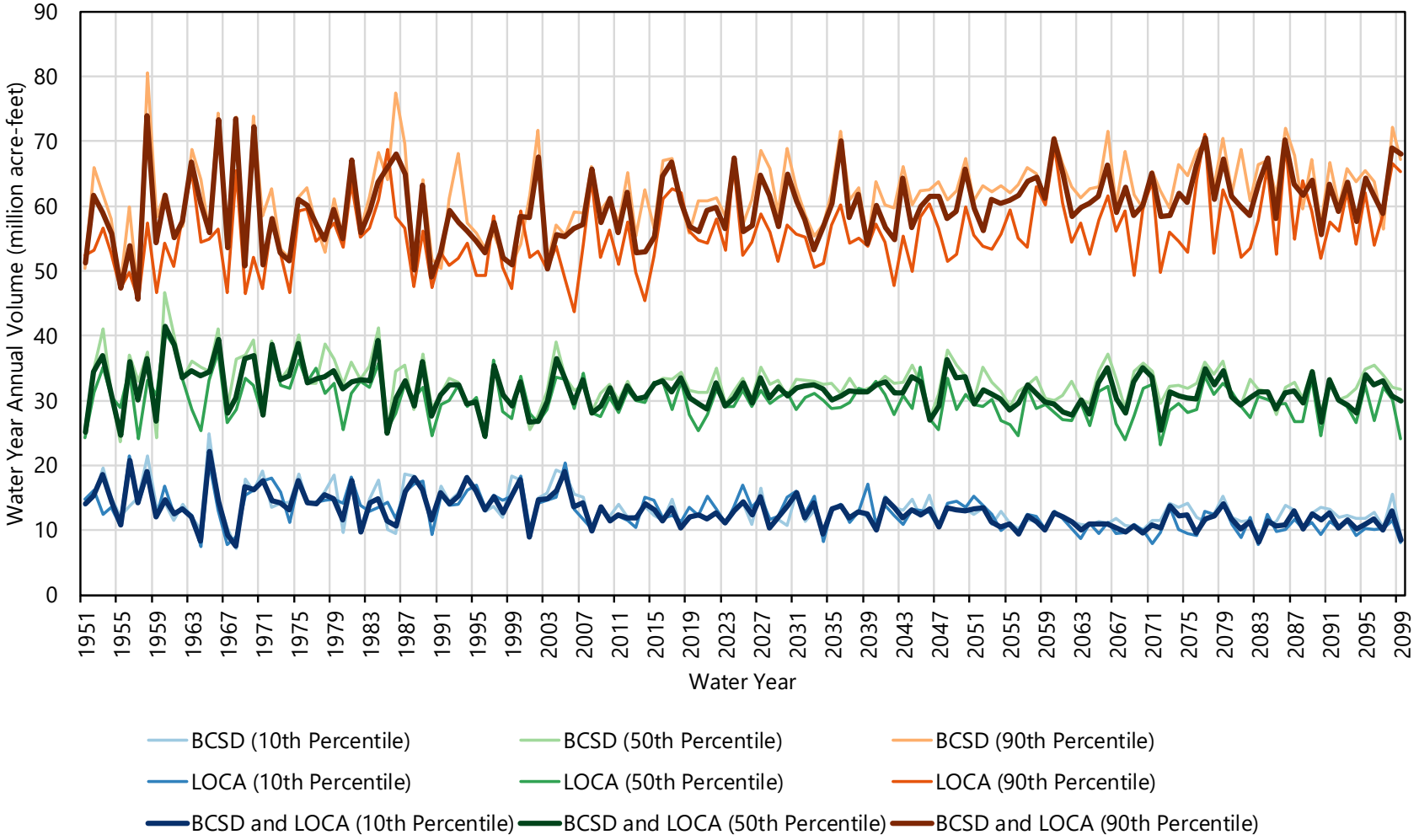

Figure 63. Simulated flows for Sacramento-San Joaquin Rivers at Delta from BCSD, LOCA, and combined BCSD and LOCA projections.

Note: Ensemble median (50th percentile), lower (10th percentile), and upper (90th percentile) confidence limits are shown in the figure.

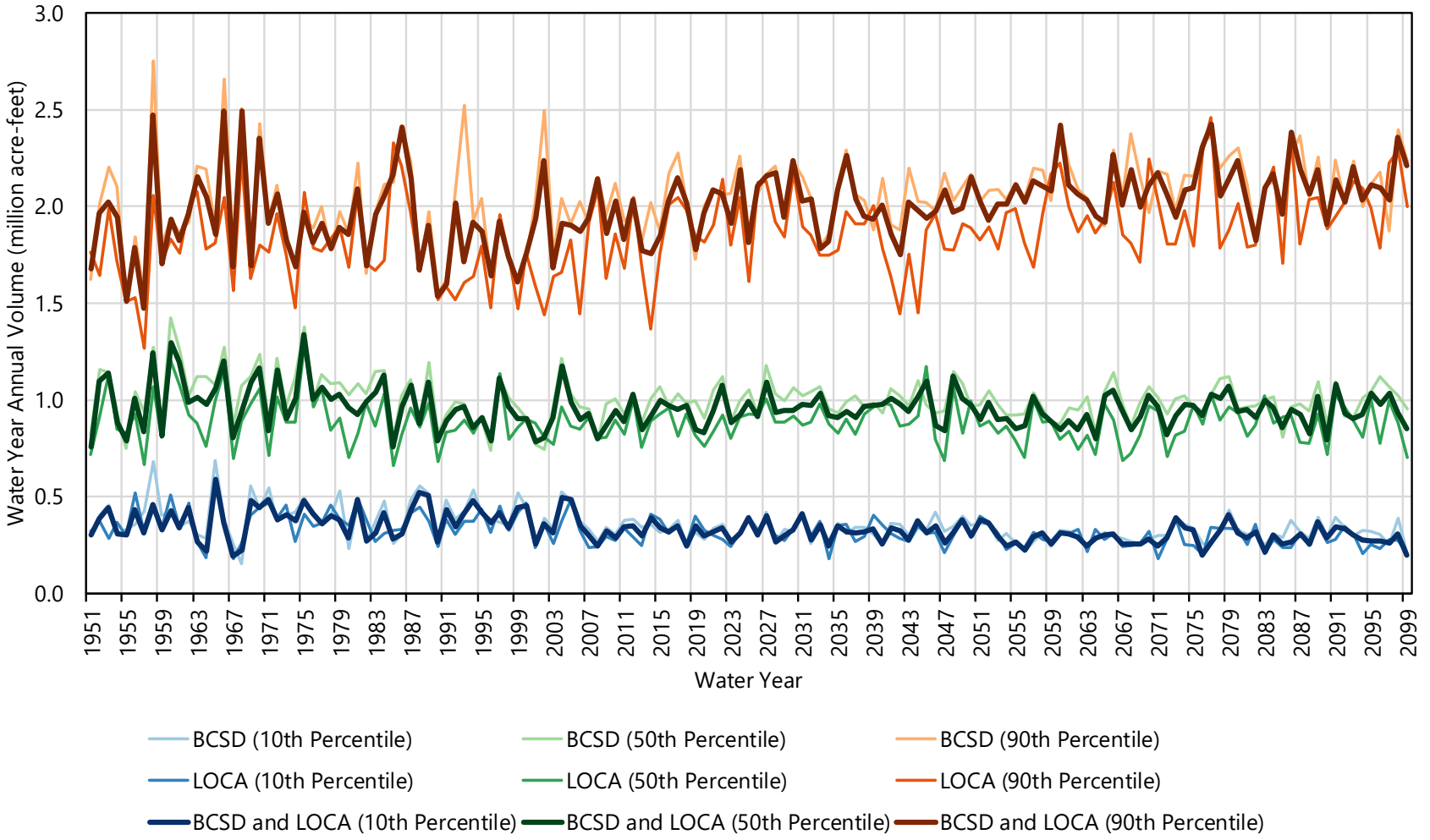

Figure 64. Simulated flows for Truckee River at Nixon from BCSD, LOCA, and combined BCSD and LOCA projections.

Note: Ensemble median (50th percentile), lower (10th percentile), and upper (90th percentile) confidence limits are shown in the figure.

Overall, Figure 58 through Figure 64 show that the bias between LOCA and BCSD flow simulations identified over the historical period (water years, 1951 to 1999; see Figure 57) persists into the future streamflow simulations. Comparison of changes in annual and seasonal streamflow values for the key gage locations from the LOCA and BCSD simulations are presented in Table 3. To be consistent with the LOCA analysis presented in Sections 3.2 through 3.8 and the BCSD analysis findings reported in the West-Wide Climate Risk Assessment of the 2016 SECURE Water Act Report (Reclamation, 2016c; see Tables 8, 9 and 10), comparison of LOCA and BCSD streamflow change information is presented using the 1990s reference decade (water years 1990 to 1999) for the three future decades, 2020s (water years 2020 to 2029), 2050s (water years 2050 to 2059), and 2070s (water years 2070 to 2079). Results (percentage change) are shown as inter-quartile range—25th percentile to 75th percentile—for annual and seasonal changes for the selected key gage locations. In interpreting this change information, it is important to note the hydroclimate conditions in the basin for the reference 1990s decade—i.e., in the reference decade (1990s), a basin could be, for example, in either dry, average, or wet state.

Table 3. Comparison of LOCA and BCSD annual and seasonal streamflow projection changes for selected key gage locations

Location	Projection*	2020s			2050s			2070s		
		Annual (%)	Dec-Mar (%)	Apr-Jul (%)	Annual (%)	Dec-Mar (%)	Apr-Jul (%)	Annual (%)	Dec-Mar (%)	Apr-Jul (%)
Colorado River above Imperial Dam	LOCA	-11.8 to 14.4	-5.4 to 17.2	-11.5 to 19.2	-14.4 to 7.4	-0.2 to 20.6	-13.7 to 14.4	-16.1 to 2.8	1.1 to 24.3	-17.6 to 11.8
	BCSD	-6.6 to 19.5	-7.4 to 17.7	-3.6 to 25.1	–11.0 to 15.9	–6.3 to 22.9	–8.4 to 21.2	–12.6 to 18.7	–0.8 to 25.0	–10.1 to 25.3
Columbia River at The Dalles	LOCA	-8.5 to 6.2	3.0 to 21.2	-7.7 to 7.8	-11.7 to 4.7	14.5 to 39.0	-14.1 to 5.0	-11.2 to 1.5	20.2 to 55.6	-19.3 to 0.4
	BCSD	-2.5 to 8.7	2.0 to 31.1	-4.4 to 10.5	–5.2 to 11.4	10.3 to 43.4	–7.6 to 9.9	–2.2 to 11.0	16.0 to 54.4	–10.2 to 5.7
Klamath River near Klamath	LOCA	-9.7 to 10.1	3.1 to 24.4	-26.2 to -11.4	-13.9 to 9.1	12.5 to 44.7	-47.0 to -24.2	-13.7 to 10.2	16.2 to 53.1	-55.9 to -33.3
	BCSD	-9.8 to 14.7	5.5 to 28.0	-27.5 to -11.2	–9.5 to 12.5	21.7 to 45.4	–47.0 to –17.7	–8.5 to 18.2	23.6 to 68.8	–54.9 to –22.9

Location	Projection*	2020s			2050s			2070s		
		Annual (%)	Dec-Mar (%)	Apr-Jul (%)	Annual (%)	Dec-Mar (%)	Apr-Jul (%)	Annual (%)	Dec-Mar (%)	Apr-Jul (%)
Missouri River at Omaha	LOCA	-4.0 to 9.5	-3.3 to 9.1	1.3 to 19.7	-2.1 to 12.1	0.5 to 12.4	7.3 to 26.7	-6.7 to 13.9	-5.2 to 15.9	7.0 to 32.8
	BCSD	2.6 to 18.6	2.2 to 26.5	4.5 to 22.7	6.5 to 25.1	15.6 to 44.6	8.6 to 32.0	7.0 to 34.5	13.8 to 59.0	13.1 to 41.7
Rio Grande at Elephant Butte Dam	LOCA	-14.2 to 11.7	-5.6 to 16.8	-17.9 to 13.6	-18.9 to 5.3	-5.1 to 20.8	-26.7 to 4.7	-22.9 to 3.4	-3.6 to 25.3	-28.3 to -3.2
	BCSD	-7.8 to 17.6	-8.2 to 16.0	-9.2 to 25.1	–16.2 to 7.3	–12.1 to 11.7	–18.5 to 9.7	–20.5 to 8.9	–15.4 to 15.0	–22.2 to 11.2
Sacramento-San Joaquin Rivers at Delta	LOCA	-8.7 to 19.9	-0.6 to 35.5	-23.5 to -1.7	-14.1 to 17.6	2.6 to 54.6	-41.5 to -17.7	-11.5 to 14.9	10.6 to 61.1	-45.2 to -22.1
	BCSD	-8.2 to 24.8	-1.5 to 42.8	-25.0 to -0.1	–11.0 to 26.1	5.8 to 51.0	–40.9 to –14.0	–12.0 to 24.6	6.3 to 56.8	–43.8 to –14.7

Location	Projection*	2020s			2050s			2070s		
		Annual (%)	Dec-Mar (%)	Apr-Jul (%)	Annual (%)	Dec-Mar (%)	Apr-Jul (%)	Annual (%)	Dec-Mar (%)	Apr-Jul (%)
Truckee River at Nixon	LOCA	-9.2 to 27.3	31.8 to 117.4	-21.4 to 9.8	-13.4 to 26.1	93.2 to 208.7	-38.6 to -14.0	-9.8 to 24.9	104.3 to 295.8	-50.7 to -21.1
	BCSD	-8.1 to 28.7	27.3 to 156.6	-22.8 to 11.8	–13.1 to 22.1	76.8 to 242.6	–38.1 to –4.6	–13.0 to 24.2	111.2 to 316.4	–49.9 to –13.8

* Note: The BCSD projections (Reclamation, 2016c) include RCP 2.6, 4.5, 6.0, and 8.5 (total, 97 projections). LOCA projections (this report) include RCPs 4.5 and 8.5 (total, 64 projections). The LOCA RCP4.5 and RCP8.5 streamflow projections are identical over the period, 1950 to 2005.

Again, the combined LOCA and BCSD streamflow ensemble presents a collective view of streamflow projections and reflects the various sources of uncertainties involved in the steps to develop these projections.

A range of climate and hydrology projection information has been used in other Reclamation regional climate impact studies. It is, therefore, important to acknowledge and provide context for these streamflow projections for some of these studies. The following sub-section provides a listing of regional studies in selected major Reclamation river basins[8]. Further, it provides context around the hydroclimate projections summarized in this report in relation to existing regional studies.

3.9.1 Streamflow Projections and Regional Studies

3.9.1.1 Colorado River Basin

Currently, Reclamation together with Scripps Institution of Oceanography, are completing a study that explores future water supply projections in the Colorado River Basin developed based on CMIP5, and comparing them to previously developed CMIP3 projections, across 48 metrics that provide an overall quality ranking for each model. Similar to this report, the study also evaluates the effects of BCSD and LOCA downscaling techniques on the CMIP5 projections. Additionally, the study further uses the VIC hydrologic model to explore the Colorado River Basin's hydroclimatic sensitivity to future warming.

Preliminary findings show similar results to what has been discussed in this report with respect to the evaluation of the CMIP projections and that the choice of downscaling techniques, either BCSD or LOCA, influence results. Further findings show that, as a group, the CMIP5 models are better performing than CMIP3 models at reproducing historical regional atmospheric circulation, but not temperature or precipitation metrics. However, some individual CMIP3 models did perform better than some individual CMIP5 models. In addition, it was shown that, independent of precipitation, the warming trends in the CMIP5 projections could reduce future streamflows in the Colorado River Basin.

3.9.1.2 Columbia River Basin

Recently, the River Management Joint Operating Committee (RMJOC) consisting of the U.S. Army Corps of Engineers, Bonneville Power Administration, and Bureau of Reclamation, together with the University of Washington, completed the second edition of a comprehensive study on climate change in the region known as RMJOC-II (RMJOC, 2018). Like this report, it evaluated two different downscaling techniques, BCSD and Multivariate Adaptive Constructed Analogs (MACA), but also evaluated different versions of the hydrologic models, Variable Infiltration Capacity (VIC) and Precipitation-Runoff Modeling System (PRMS). The RMJOC-II

[8] The major Reclamation river basins where selected studies are discussed are the ones where, based on the analysis of annual flows over the historical period—water years 1951 to 1999 (refer to Figure 57)—the absolute percentage difference in ensemble median of mean annual flow magnitude between LOCA and BCSD simulations was greater than 10. In addition, the Colorado River Basin is also included.

study concluded that both the variation in downscaling technique and hydrologic model can influence the results of the streamflow outputs, which is further reflected in this evaluation of the LOCA downscaling technique. Differences in the results of this report and the RMJOC-II study can be attributed to the effects of different downscaling techniques and versions of hydrologic models used.

3.9.1.3 Klamath River Basin

In the Klamath River Basin, Reclamation partnered with the California Department of Water Resources and the Oregon Water Resources Department to conduct the Klamath River Basin Study, which was completed in 2016. The study relied on CMIP5-BCSD hydroclimate projections as well as CMIP3-BCSD hydroclimate projections that were summarized in the West-Wide Climate Risk Assessment of the 2011 SECURE Water Act Report (Reclamation, 2011b). At the time of the Klamath River Basin Study, CMIP5-BCSD projections were novel and not well understood and the basin study offered an opportunity to better understand differences between CMIP3 and CMIP5 hydroclimate projections. Results of this report largely coincide with results summarized in the Klamath River Basin Study. However, with the addition of CMIP5-LOCA hydroclimate projections, a few notable differences ought to be made apparent.

One notable difference in streamflow projections presented in Figure 60 is partly due to the watershed boundary used in calculating streamflow from runoff across the landscape. The CMIP5-LOCA modeling sequence utilized a contributing area approximately 30 percent larger than the CMIP5-BCSD modeling sequence. This largely accounts for the approximately 23 percent difference between mean annual flow at Klamath River at Klamath, California over the historical period, illustrated in Figure 57 (i.e., where CMIP5-LOCA results in higher mean annual flow than CMIP5-BCSD). Additional differences are apparent in projections of change in runoff volume, which may be attributed to other methodological choices previously described.

3.9.1.4 Missouri River Basin

For the Missouri River at Omaha, the ensemble median of mean annual streamflow calculated using the CMIP5-LOCA suite of models and approaches over the historical time period is 19 percent lower than that using the CMIP5-BCSD suite of models and approaches (refer to Figure 57). In other words, over the historical comparison period (water years, 1951 to 1999), the simulated streamflow from the CMIP5-BCSD suite of models are generally higher than the simulated streamflow from the CMIP5-LOCA suite of models. Figure 61 shows that CMIP5-BCSD mean annual streamflow are higher than CMIP5-LOCA mean annual flow at corresponding percentiles of the ensembles. This difference corresponds with historical and future projections of precipitation as well. Observed precipitation from the two different datasets used in these approaches (Maurer et al., 2002 for CMIP5-BCSD and Livneh et al., 2013 for CMIP5-LOCA) over the historical period are largely consistent, but differences are apparent in the future projections, which becomes greater closer to 2100. CMIP5-LOCA precipitation projections are drier in the northern Rocky Mountains than the CMIP5-BCSD projections. The comparison of these two datasets summarized by Vano et al. (2020) shows that CMIP5-BCSD

projections indicate larger changes in the ensemble mean streamflow, which is consistent with projected changes summarized in Table 3.

Streamflow projections presented in this report encompass a vast watershed—over 233,000 square miles. Investigation of differences between the CMIP5-BCSD and CMIP5-LOCA datasets in smaller watersheds within the greater Missouri River Basin illustrate similar differences, although to varying degrees. Further, previous existing studies that may provide insights into the differences in mean annual streamflow between CMIP5-BCSD and CMIP5-LOCA have been conducted over smaller watersheds within the Missouri River Basin, for example the Upper Missouri Basin Impacts Assessment (Reclamation, 2020c), which encompasses the Upper Missouri River upstream of Fort Peck Reservoir. Streamflow projections from that study relied on CMIP5-BCSD projections and are consistent with other analyses using the same projections in this region.

This 2021 Assessment report highlights one challenge of using one consistent approach for climate impact assessment across the West, as the Missouri River Basin spans diverse geography, topography, climate, and hydrological processes. For example, the northern latitudes of the basin encompass the Prairie Potholes Region, notable for its complex groundwater and surface water interactions and vast small depression storage basins. Further regional investigations would be required to fully understand the methodological choices that may cause the differences in projected annual streamflow seen in the Missouri River Basin.

3.10 Summary of Hydroclimate Changes

This section provides a West-wide summary of the findings from the hydroclimate analyses for the changes in precipitation, temperature, snow condition, streamflow, runoff magnitude, and runoff seasonality (including shifts to annual runoff timing) for each of the major Reclamation river basins described in Sections 3.2 through 3.8 above.

Results from the analyses are presented for the 43 West-wide reporting locations (see Table 1) in a set of tables. In each table, change information for the hydroclimate variable of interest (e.g., temperature, precipitation, runoff, etc.) is presented as inter-quartile range (referred to as "range" hereafter). In other words, every entry in the table corresponds to a set of two values, where the first value corresponds to the 25th percentile and the second value corresponds to the 75th percentile estimates. This change information is calculated from the 1990s reference decade for the three future decades, 2020s, 2050s, and 2070s for the 64 (32 for RCP4.5 and 32 for RCP8.5) LOCA downscaled projections. The listed summary tables include:

- Projected range of temperature change (Table 4)
- Projected range of precipitation change (Table 5)
- Projected range of April 1st SWE change (Table 6)
- Projected range of annual runoff change (Table 7)

- Projected range of December-through-March runoff change (Table 8)
- Projected range of April-through-July runoff change (Table 9)
- Projected range of annual runoff timing shift (Table 10)

Table 4. Projected range of temperature change for the 43 West-wide reporting locations

River Basin*	Site Name and Description	Projected Range[1] of Temperature Change (degrees Fahrenheit)		
		2020s	2050s	2070s
Colorado	Colorado River at Lees Ferry	1.8 to 3.1	3.9 to 6.1	5.2 to 8.1
	Colorado River above Imperial Dam	1.8 to 2.9	3.9 to 6.0	5.2 to 7.7
	Green River near Greendale	1.8 to 3.3	4.2 to 6.3	5.1 to 8.6
	Colorado River near Cameo	1.7 to 2.9	3.9 to 5.8	4.8 to 7.8
	Gunnison River near Grand Junction	1.8 to 2.9	4.0 to 5.8	5.0 to 7.9
	San Juan River near Bluff	1.8 to 2.9	4.0 to 5.8	5.1 to 7.5
Columbia	Snake River at Brownlee Dam	1.7 to 3.2	4.0 to 6.1	4.9 to 8.5
	Columbia River at Grand Coulee	1.9 to 3.0	3.8 to 5.8	4.8 to 8.0
	Columbia River at The Dalles	1.8 to 2.9	3.8 to 5.8	4.9 to 7.9
	Yakima River at Parker	1.8 to 2.8	3.6 to 5.6	4.2 to 7.4
	Deschutes River near Madras	1.7 to 2.7	3.5 to 5.4	4.2 to 7.2
	Snake River near Heise	1.6 to 3.0	4.1 to 5.9	4.9 to 8.2
	Flathead River at Columbia Falls	1.8 to 2.9	3.7 to 5.6	4.7 to 8.0
Klamath	Williamson R. below the Sprague River	1.8 to 2.6	3.8 to 5.6	4.4 to 7.4
	Klamath River below Iron Gate Dam	1.8 to 2.7	3.7 to 5.4	4.3 to 7.2
	Klamath River near Seiad Valley	1.8 to 2.7	3.7 to 5.3	4.3 to 7.1
	Klamath River at Orleans	1.8 to 2.7	3.7 to 5.3	4.3 to 7.0
	Klamath River near Klamath	1.7 to 2.6	3.6 to 5.2	4.2 to 6.8

River Basin*	Site Name and Description	Projected Range[1] of Temperature Change (degrees Fahrenheit)		
		2020s	2050s	2070s
Missouri	Missouri River at Canyon Ferry Dam	1.8 to 3.1	4.1 to 6.2	5.1 to 8.5
	Milk River at Nashua	1.8 to 3.4	4.1 to 6.4	5.4 to 8.8
	South Platte River near Sterling	1.7 to 3.0	3.7 to 5.6	4.8 to 7.7
	Missouri River at Omaha	1.8 to 3.2	4.1 to 6.0	5.0 to 8.6
	Bighorn River at Yellowtail Dam	1.7 to 3.1	4.0 to 5.9	5.0 to 8.4
	North Platte River at Lake McConaughy	1.6 to 3.0	3.7 to 5.5	4.7 to 8.0
Rio Grande	Rio Grande near Lobatos	1.7 to 2.8	3.8 to 5.5	4.7 to 7.5
	Rio Chama near Abiquiu	1.9 to 2.8	3.8 to 5.6	4.8 to 7.3
	Rio Grande near Otowi	1.8 to 2.7	3.8 to 5.5	4.7 to 7.4
	Rio Grande at Elephant Butte Dam	1.8 to 2.8	3.8 to 5.7	4.8 to 7.4
	Pecos R at Damsite No. 3 near Carlsbad	1.8 to 2.7	3.8 to 5.4	4.9 to 7.5
Sacramento–San Joaquin	Sacramento River at Freeport	1.7 to 2.5	3.6 to 5.2	4.3 to 6.9
	Sacramento River at Bend Bridge near Red Bluff	1.7 to 2.5	3.6 to 5.2	4.3 to 7.0
	Feather River at Oroville	1.7 to 2.5	3.7 to 5.3	4.3 to 7.0
	San Joaquin River near Vernalis	1.6 to 2.5	3.5 to 5.2	4.3 to 6.8
	Stanislaus River at New Melones Dam	1.7 to 2.6	3.6 to 5.3	4.2 to 7.0
	Sacramento-San Joaquin Rivers at Delta	1.6 to 2.4	3.6 to 5.1	4.3 to 6.8
	San Joaquin River at Millerton Lake (Friant Dam)	1.7 to 2.7	3.8 to 5.5	4.6 to 7.2
	American River at Fair Oaks	1.6 to 2.5	3.6 to 5.3	4.2 to 6.8

River Basin*	Site Name and Description	Projected Range[1] of Temperature Change (degrees Fahrenheit)		
		2020s	2050s	2070s
	Tulare-Buena Vista Lakes	1.5 to 2.4	3.2 to 5.0	4.2 to 6.6
Truckee	Little Truckee River below Boca Dam	1.7 to 2.5	3.7 to 5.4	4.2 to 7.1
	W.F. Carson River at Woodfords	1.8 to 2.7	3.8 to 5.4	4.3 to 7.2
	Truckee River at Farad Gage (just above CA State line)	1.7 to 2.5	3.7 to 5.4	4.2 to 7.1
	Truckee River at Nixon Gage	1.8 to 2.7	3.8 to 5.5	4.4 to 7.4
	Carson River at Fort Churchill Gage	1.8 to 2.8	4.0 to 5.6	4.5 to 7.4

* Note: The Pecos, Tulare, and Carson are not SWA river basins, but are included under the Rio Grande, Sacramento and San Joaquin, and Truckee, respectively, as these locations are of interest from a water operations standpoint.

[1] Ranges of projected temperatures are the 25th to 75th percentile change of the 64 projections.

Table 5. Projected range of precipitation change for the 43 West-wide reporting locations

River Basin*	Site Name and Description	Projected Range[1] of Precipitation Change (%)		
		2020s	2050s	2070s
Colorado	Colorado River at Lees Ferry	-3.2 to 10.6	-3.4 to 12.0	-1.7 to 12.0
	Colorado River above Imperial Dam	-3.8 to 10.2	-4.5 to 10.7	-1.2 to 11.0
	Green River near Greendale	-2.2 to 12.8	0.0 to 14.4	0.5 to 16.9
	Colorado River near Cameo	-3.9 to 8.0	-4.0 to 9.0	-3.0 to 10.1
	Gunnison R. near Grand Junction	-4.0 to 7.9	-2.8 to 9.5	-2.5 to 9.4
	San Juan River near Bluff	-4.6 to 8.7	-5.4 to 9.4	-1.4 to 8.4

River Basin*	Site Name and Description	Projected Range[1] of Precipitation Change (%)		
		2020s	2050s	2070s
Columbia	Snake River at Brownlee Dam	-1.4 to 9.6	1.7 to 12.2	1.7 to 12.4
	Columbia River at Grand Coulee	-2.2 to 8.8	-1.5 to 11.7	1.0 to 9.7
	Columbia River at The Dalles	-1.3 to 7.2	-0.7 to 11.1	2.3 to 10.9
	Yakima River at Parker	-3.0 to 8.9	0.5 to 10.8	0.1 to 14.8
	Deschutes River near Madras	-7.3 to 8.5	-5.0 to 8.9	-3.3 to 9.8
	Snake River near Heise	-1.6 to 9.7	-1.0 to 11.5	-2.3 to 13.8
	Flathead River at Columbia Falls	-3.1 to 8.4	-3.1 to 10.0	-0.7 to 10.9
Klamath	Williamson River below the Sprague River	-7.1 to 10.2	-7.0 to 13.9	-3.3 to 14.0
	Klamath River below Iron Gate Dam	-6.8 to 8.4	-6.9 to 9.5	-3.8 to 10.0
	Klamath River near Seiad Valley	-6.1 to 8.2	-6.0 to 9.8	-4.6 to 10.2
	Klamath River at Orleans	-6.0 to 8.7	-6.7 to 9.2	-5.0 to 10.0
	Klamath River near Klamath	-5.0 to 7.7	-6.6 to 10.0	-4.9 to 10.1
Missouri	Missouri River at Canyon Ferry Dam	-2.0 to 7.6	-1.0 to 9.5	-0.4 to 12.2
	Milk River at Nashua	-3.6 to 9.7	-3.8 to 13.0	-3.8 to 14.1
	South Platte River near Sterling	-0.2 to 6.5	-1.6 to 8.8	-1.7 to 7.9
	Missouri River at Omaha	-0.5 to 5.9	1.2 to 8.6	0.4 to 12.0
	Bighorn River at Yellowtail Dam	-0.3 to 10.7	0.7 to 12.5	-0.6 to 14.7
	North Platte River at Lake McConaughy	-2.2 to 8.7	-2.0 to 9.8	-0.8 to 10.6

River Basin*	Site Name and Description	Projected Range[1] of Precipitation Change (%)		
		2020s	2050s	2070s
Rio Grande	Rio Grande near Lobatos	-4.8 to 6.8	-4.2 to 9.0	-3.9 to 8.7
	Rio Chama near Abiquiu	-5.3 to 6.7	-7.0 to 8.7	-4.7 to 5.7
	Rio Grande near Otowi	-5.8 to 6.4	-4.4 to 9.5	-4.2 to 7.2
	Rio Grande at Elephant Butte Dam	-5.0 to 5.6	-5.2 to 8.8	-4.8 to 6.3
	Pecos River at Damsite No. 3 near Carlsbad	-7.0 to 5.9	-8.7 to 8.6	-10.3 to 3.8
Sacramento–San Joaquin	Sacramento River at Freeport	-4.1 to 7.7	-6.7 to 10.0	-4.2 to 12.2
	Sacramento River at Bend Bridge near Red Bluff	-4.5 to 6.3	-5.8 to 10.4	-4.0 to 11.4
	Feather River at Oroville	-4.8 to 10.2	-6.2 to 12.3	-4.3 to 11.4
	San Joaquin River near Vernalis	-5.6 to 12.0	-6.4 to 13.3	-5.2 to 11.4
	Stanislaus R. at New Melones Dam	-5.4 to 12.3	-7.7 to 13.4	-5.8 to 11.2
	Sacramento-San Joaquin Rivers at Delta	-4.3 to 9.6	-6.4 to 11.5	-4.7 to 9.8
	San Joaquin River at Millerton Lake (Friant Dam)	-6.7 to 12.0	-8.1 to 12.9	-6.1 to 12.5
	American River at Fair Oaks	-3.4 to 10.2	-7.1 to 12.9	-5.5 to 10.3
	Tulare-Buena Vista Lakes	-8.0 to 11.4	-9.6 to 10.0	-10.0 to 11.2
Truckee	Little Truckee R. below Boca Dam	-4.2 to 13.9	-6.7 to 16.7	-3.7 to 13.2
	W.F. Carson River at Woodfords	-4.3 to 14.0	-4.1 to 14.0	-3.3 to 12.9
	Truckee River at Farad Gage (just above CA State line)	-3.9 to 13.4	-5.9 to 15.0	-3.4 to 12.6
	Truckee River at Nixon Gage	-4.4 to 14.9	-5.9 to 15.6	-3.5 to 13.4

River Basin*	Site Name and Description	Projected Range[1] of Precipitation Change (%)		
		2020s	2050s	2070s
	Carson River at Fort Churchill Gage	-4.2 to 15.5	-4.0 to 16.2	-1.8 to 14.6

* Note: The Pecos, Tulare, and Carson are not SWA river basins, but are included under the Rio Grande, Sacramento and San Joaquin, and Truckee, respectively, as these locations are of interest from a water operations standpoint.

[1] Ranges of projected precipitation are the 25th to 75th percentile change of the 64 projections.

Table 6. Projected range of April 1st SWE change for the 43 West-wide reporting locations

River Basin*	Site Name and Description	Projected Range[1] of April 1st SWE Change (%)		
		2020s	2050s	2070s
Colorado	Colorado River at Lees Ferry	-17.2 to 5.2	-27.2 to -5.5	-33.3 to -13.3
	Colorado River above Imperial Dam	-17.7 to 4.6	-28.4 to -6.4	-34.3 to -13.4
	Green River near Greendale	-13.7 to 10.0	-18.0 to 3.3	-21.5 to -1.1
	Colorado River near Cameo	-13.5 to 7.2	-21.2 to 0.2	-25.2 to -6.1
	Gunnison R. near Grand Junction	-17.2 to 8.4	-27.5 to -3.1	-34.9 to -6.0
	San Juan River near Bluff	-17.4 to 8.2	-35.2 to -5.7	-42.4 to -8.3
Columbia	Snake River at Brownlee Dam	-18.2 to 0.2	-30.5 to -9.3	-44.4 to -17.5
	Columbia River at Grand Coulee	-14.9 to 0.9	-29.1 to -10.1	-43.5 to -19.8
	Columbia River at The Dalles	-13.9 to -0.7	-31.2 to -10.8	-44.6 to -17.9
	Yakima River at Parker	-19.9 to -1.9	-46.3 to -20.0	-61.9 to -33.6
	Deschutes River near Madras	-7.3 to 9.2	-21.3 to 8.3	-38.2 to 1.0
	Snake River near Heise	-11.5 to 7.5	-16.6 to -1.1	-23.6 to -6.4
	Flathead River at Columbia Falls	-10.3 to 3.8	-21.4 to -5.0	-35.8 to -12.6

River Basin*	Site Name and Description	Projected Range[1] of April 1st SWE Change (%)		
		2020s	2050s	2070s
Klamath	Williamson River below the Sprague River	-59.8 to -22.5	-83.1 to -51.7	-91.0 to -59.5
	Klamath River below Iron Gate Dam	-39.7 to -17.8	-62.9 to -34.3	-74.4 to -44.0
	Klamath River near Seiad Valley	-26.9 to -6.3	-45.3 to -17.5	-54.9 to -24.4
	Klamath River at Orleans	-32.7 to -11.2	-52.4 to -23.8	-63.0 to -32.0
	Klamath River near Klamath	-35.6 to -12.6	-57.1 to -28.2	-67.7 to -36.7
Missouri	Missouri River at Canyon Ferry Dam	-15.3 to 3.5	-29.6 to -7.3	-40.1 to -12.5
	Milk River at Nashua	-17.0 to 2.7	-28.1 to -10.8	-36.9 to -16.3
	South Platte River near Sterling	-11.1 to 9.6	-19.2 to 2.7	-24.8 to 0.6
	Missouri River at Omaha	-13.0 to 3.5	-19.9 to -2.7	-32.5 to -8.5
	Bighorn River at Yellowtail Dam	-8.9 to 8.6	-10.2 to 9.6	-16.2 to 2.7
	North Platte River at Lake McConaughy	-12.2 to 11.2	-17.2 to 8.6	-23.3 to 0.5
Rio Grande	Rio Grande near Lobatos	-13.2 to 12.3	-30.2 to 0.9	-34.7 to -5.3
	Rio Chama near Abiquiu	-18.5 to 10.6	-37.4 to -7.6	-47.1 to -13.2
	Rio Grande near Otowi	-15.2 to 13.0	-34.1 to -2.6	-39.7 to -7.7
	Rio Grande at Elephant Butte Dam	-15.7 to 12.4	-35.1 to -3.0	-40.3 to -7.8
	Pecos River at Damsite No. 3 near Carlsbad	-27.4 to 7.1	-55.6 to -17.7	-67.1 to -30.9

River Basin*	Site Name and Description	Projected Range[1] of April 1st SWE Change (%)		
		2020s	2050s	2070s
Sacramento–San Joaquin	Sacramento River at Freeport	-37.6 to -14.0	-59.2 to -31.4	-70.8 to -38.7
	Sacramento River at Bend Bridge near Red Bluff	-30.1 to -3.8	-45.2 to -15.5	-56.4 to -22.3
	Feather River at Oroville	-44.4 to -20.6	-71.2 to -44.0	-82.9 to -51.6
	San Joaquin River near Vernalis	-23.4 to 1.9	-42.6 to -14.8	-48.9 to -19.3
	Stanislaus R. at New Melones Dam	-30.2 to -2.8	-54.6 to -21.6	-63.9 to -32.2
	Sacramento-San Joaquin Rivers at Delta	-32.1 to -8.9	-51.0 to -25.0	-62.2 to -34.4
	San Joaquin River at Millerton Lake (Friant Dam)	-20.2 to 5.0	-37.8 to -10.4	-41.7 to -14.8
	American River at Fair Oaks	-39.8 to -16.6	-69.9 to -39.8	-80.9 to -45.7
	Tulare-Buena Vista Lakes	-25.5 to 4.9	-42.4 to -13.5	-46.6 to -20.1
Truckee	Little Truckee R. below Boca Dam	-33.9 to -10.0	-62.7 to -31.4	-75.4 to -40.4
	W.F. Carson River at Woodfords	-33.1 to -4.2	-62.3 to -28.9	-75.4 to -39.3
	Truckee River at Farad Gage (just above CA State line)	-32.6 to -10.1	-62.0 to -31.7	-73.5 to -38.5
	Truckee River at Nixon Gage	-33.1 to -10.1	-62.3 to -31.9	-73.7 to -39.0
	Carson River at Fort Churchill Gage	-32.0 to -2.3	-58.2 to -24.6	-69.1 to -35.3

* Note: The Pecos, Tulare, and Carson are not SWA river basins, but are included under the Rio Grande, Sacramento and San Joaquin, and Truckee, respectively, as these locations are of interest from a water operations standpoint.

[1] Ranges of projected April 1st SWE are the 25th to 75th percentile change of the 64 projections.

Table 7. Projected range of annual runoff change for the 43 West-wide reporting locations

River Basin*	Site Name and Description	Projected Range[1] of Annual Runoff Change (%)		
		2020s	2050s	2070s
Colorado	Colorado River at Lees Ferry	-12.1 to 13.2	-16.6 to 8.0	-17.5 to 2.7
	Colorado R. above Imperial Dam	-11.8 to 14.4	-14.4 to 7.4	-16.1 to 2.8
	Green River near Greendale	-13.1 to 20.1	-18.9 to 11.2	-21.0 to 12.7
	Colorado River near Cameo	-12.6 to 5.5	-17.3 to 6.2	-20.3 to 3.5
	Gunnison R. near Grand Junction	-14.4 to 11.8	-18.7 to 9.3	-19.5 to 5.3
	San Juan River near Bluff	-16.8 to 10.6	-22.6 to 2.6	-22.7 to -1.1
Columbia	Snake River at Brownlee Dam	-8.9 to 12.2	-12.5 to 11.7	-14.1 to 11.8
	Columbia River at Grand Coulee	-8.7 to 8.2	-11.2 to 8.8	-10.3 to 2.2
	Columbia River at The Dalles	-8.5 to 6.2	-11.7 to 4.7	-11.2 to 1.5
	Yakima River at Parker	-8.8 to 8.7	-10.0 to 5.7	-12.7 to 7.1
	Deschutes River near Madras	-12.9 to 13.9	-11.5 to 8.5	-11.6 to 6.3
	Snake River near Heise	-12.0 to 10.8	-22.6 to 4.7	-27.2 to -0.4
	Flathead River at Columbia Falls	-10.5 to 6.3	-16.7 to 4.9	-19.0 to 0.8
Klamath	Williamson River below the Sprague River	-9.0 to 14.4	-10.0 to 16.3	-10.8 to 17.5
	Klamath R. below Iron Gate Dam	-15.4 to 10.8	-17.4 to 7.3	-17.1 to 7.2
	Klamath River near Seiad Valley	-12.2 to 10.8	-15.3 to 10.8	-15.7 to 11.6
	Klamath River at Orleans	-10.8 to 9.3	-12.8 to 10.5	-15.1 to 9.9
	Klamath River near Klamath	-9.7 to 10.1	-13.9 to 9.1	-13.7 to 10.2

River Basin*	Site Name and Description	Projected Range[1] of Annual Runoff Change (%)		
		2020s	2050s	2070s
Missouri	Missouri R. at Canyon Ferry Dam	-9.0 to 7.4	-11.9 to 6.6	-17.9 to 6.0
	Milk River at Nashua	-7.0 to 19.6	-1.3 to 25.2	-6.1 to 33.4
	South Platte River near Sterling	-12.2 to 7.3	-16.6 to 1.9	-24.4 to 3.1
	Missouri River at Omaha	-4.0 to 9.5	-2.1 to 12.1	-6.7 to 13.9
	Bighorn River at Yellowtail Dam	-11.7 to 13.4	-11.0 to 16.7	-17.2 to 12.1
	North Platte River at Lake McConaughy	-8.2 to 13.1	-10.3 to 15.2	-13.6 to 12.1
Rio Grande	Rio Grande near Lobatos	-17.2 to 10.9	-24.9 to 5.4	-26.5 to 0.9
	Rio Chama near Abiquiu	-15.3 to 15.3	-23.6 to 8.2	-20.5 to 5.1
	Rio Grande near Otowi	-18.3 to 12.5	-24.7 to 5.5	-23.1 to -0.3
	Rio Grande at Elephant Butte Dam	-14.2 to 11.7	-18.9 to 5.3	-22.9 to 3.4
	Pecos River at Damsite No. 3 near Carlsbad	-12.8 to 13.7	-14.1 to 20.7	-12.6 to 11.4
Sacramento–San Joaquin	Sacramento River at Freeport	-8.5 to 18.2	-14.7 to 17.7	-11.0 to 16.8
	Sacramento River at Bend Bridge near Red Bluff	-11.1 to 14.4	-16.1 to 16.7	-14.8 to 10.1
	Feather River at Oroville	-9.2 to 19.6	-14.1 to 16.0	-11.3 to 16.6
	San Joaquin River near Vernalis	-11.7 to 22.0	-16.8 to 15.5	-14.8 to 14.8
	Stanislaus River at New Melones Dam	-9.8 to 23.5	-17.6 to 19.3	-16.2 to 12.7
	Sacramento-San Joaquin Rivers at Delta	-8.7 to 19.9	-14.1 to 17.6	-11.5 to 14.9
	San Joaquin River at Millerton Lake (Friant Dam)	-12.7 to 21.6	-19.7 to 16.4	-16.2 to 13.5

River Basin*	Site Name and Description	Projected Range[1] of Annual Runoff Change (%)		
		2020s	2050s	2070s
	American River at Fair Oaks	-8.6 to 17.2	-14.7 to 17.4	-12.5 to 12.2
	Tulare-Buena Vista Lakes	-12.6 to 22.4	-18.6 to 15.7	-19.0 to 16.9
Truckee	Little Truckee R. below Boca Dam	-8.7 to 27.8	-14.5 to 24.6	-9.0 to 22.6
	W.F. Carson River at Woodfords	-10.4 to 26.1	-16.2 to 21.7	-13.5 to 17.8
	Truckee River at Farad Gage (just above CA State line)	-9.5 to 26.4	-13.3 to 25.3	-11.0 to 22.3
	Truckee River at Nixon Gage	-9.2 to 27.3	-13.4 to 26.1	-9.8 to 24.9
	Carson R. at Fort Churchill Gage	-8.3 to 31.3	-10.5 to 31.5	-10.6 to 27.4

* Note: The Pecos, Tulare, and Carson are not SWA river basins, but are included under the Rio Grande, Sacramento and San Joaquin, and Truckee, respectively, as these locations are of interest from a water operations standpoint.

[1] Ranges of projected annual runoff are the 25th to 75th percentile change of the 64 projections.

Table 8. Projected range of December-through-March runoff change for the 43 West-wide reporting locations

River Basin*	Site Name and Description	Projected Range[1] of Dec–Mar Runoff Change (%)		
		2020s	2050s	2070s
Colorado	Colorado River at Lees Ferry	-3.5 to 17.3	1.7 to 23.7	7.5 to 27.5
	Colorado River above Imperial Dam	-5.4 to 17.2	-0.2 to 20.6	1.1 to 24.3
	Green River near Greendale	-7.1 to 19.4	3.3 to 30.5	7.2 to 42.9
	Colorado River near Cameo	-8.6 to 7.1	-8.2 to 10.2	-7.6 to 12.9
	Gunnison River near Grand Junction	-6.3 to 17.4	2.9 to 24.3	8.6 to 39.3
	San Juan River near Bluff	-2.1 to 13.6	0.3 to 17.2	6.0 to 25.4

River Basin*	Site Name and Description	Projected Range[1] of Dec–Mar Runoff Change (%)		
		2020s	2050s	2070s
Columbia	Snake River at Brownlee Dam	3.1 to 22.0	14.6 to 38.1	18.9 to 49.5
	Columbia R. at Grand Coulee	3.0 to 19.4	12.4 to 39.1	19.1 to 57.0
	Columbia River at The Dalles	3.0 to 21.2	14.5 to 39.0	20.2 to 55.6
	Yakima River at Parker	13.4 to 37.7	37.0 to 80.8	48.1 to 105.6
	Deschutes River near Madras	-0.5 to 34.0	14.9 to 50.3	23.6 to 68.1
	Snake River near Heise	-11.9 to 5.0	-9.9 to 12.4	-5.6 to 17.3
	Flathead R. at Columbia Falls	-3.7 to 9.5	-3.0 to 29.0	6.7 to 44.3
Klamath	Williamson River below the Sprague River	6.1 to 36.4	14.1 to 51.8	16.5 to 62.2
	Klamath River below Iron Gate Dam	2.5 to 31.7	13.5 to 48.7	19.2 to 63.4
	Klamath River near Seiad Valley	3.6 to 37.6	21.1 to 61.3	23.8 to 73.7
	Klamath River at Orleans	5.1 to 34.6	21.8 to 57.6	25.2 to 67.6
	Klamath River near Klamath	3.1 to 24.4	12.5 to 44.7	16.2 to 53.1
Missouri	Missouri River at Canyon Ferry Dam	-6.9 to 6.4	-9.2 to 8.3	-9.9 to 14.7
	Milk River at Nashua	1.2 to 22.8	2.2 to 37.0	9.3 to 49.4
	South Platte River near Sterling	-13.6 to 9.8	-13.1 to 7.6	-15.1 to 9.7
	Missouri River at Omaha	-3.3 to 9.1	0.5 to 12.4	-5.2 to 15.9
	Bighorn River at Yellowtail Dam	-14.1 to 3.7	-16.2 to 2.4	-20.6 to 1.5
	North Platte River at Lake McConaughy	-7.5 to 14.6	1.1 to 22.8	3.3 to 33.0

River Basin*	Site Name and Description	Projected Range[1] of Dec–Mar Runoff Change (%)		
		2020s	2050s	2070s
Rio Grande	Rio Grande near Lobatos	-7.5 to 17.8	-4.9 to 38.4	7.8 to 52.8
	Rio Chama near Abiquiu	2.1 to 22.4	7.5 to 29.4	15.4 to 39.6
	Rio Grande near Otowi	-2.4 to 17.2	1.1 to 30.9	9.9 to 39.9
	Rio Grande at Elephant Butte Dam	-5.6 to 16.8	-5.1 to 20.8	-3.6 to 25.3
	Pecos River at Damsite No. 3 near Carlsbad	-10.4 to 16.4	-15.7 to 16.4	-12.0 to 14.2
Sacramento–San Joaquin	Sacramento River at Freeport	-0.6 to 33.7	0.5 to 51.6	10.0 to 55.9
	Sacramento River at Bend Bridge near Red Bluff	-2.5 to 25.3	-2.0 to 42.7	1.9 to 48.5
	Feather River at Oroville	6.4 to 42.6	12.9 to 67.2	23.7 to 77.5
	San Joaquin River near Vernalis	4.5 to 49.9	14.6 to 72.5	20.8 to 86.2
	Stanislaus River at New Melones Dam	6.8 to 51.7	24.7 to 78.1	33.7 to 105.6
	Sacramento-San Joaquin Rivers at Delta	-0.6 to 35.5	2.6 to 54.6	10.6 to 61.1
	San Joaquin River at Millerton Lake (Friant Dam)	5.9 to 61.1	20.9 to 90.3	30.6 to 99.3
	American River at Fair Oaks	2.9 to 33.9	5.2 to 49.4	10.6 to 60.5
	Tulare-Buena Vista Lakes	-7.4 to 38.3	-4.1 to 44.8	-6.6 to 40.3
Truckee	Little Truckee River below Boca Dam	41.6 to 153.7	114.3 to 269.0	138.1 to 426.5
	W.F. Carson R. at Woodfords	50.6 to 185.4	171.9 to 511.2	211.6 to 713.2
	Truckee River at Farad Gage (just above CA State line)	38.6 to 137.7	113.3 to 251.7	116.9 to 351.5

River Basin*	Site Name and Description	Projected Range[1] of Dec–Mar Runoff Change (%)		
		2020s	2050s	2070s
	Truckee River at Nixon Gage	31.8 to 117.4	93.2 to 208.7	104.3 to 295.8
	Carson River at Fort Churchill Gage	14.5 to 114.7	66.8 to 196.2	78.7 to 251.3

* Note: The Pecos, Tulare, and Carson are not SWA river basins, but are included under the Rio Grande, Sacramento and San Joaquin, and Truckee, respectively, as these locations are of interest from a water operations standpoint.

[1] Ranges of projected December-through-March runoff are the 25th to 75th percentile change of the 64 projections.

Table 9. Projected range of April-through-July runoff change for the 43 West-wide reporting locations

River Basin*	Site Name and Description	Projected Range[1] of Apr–Jul Runoff Change (%)		
		2020s	2050s	2070s
Colorado	Colorado River at Lees Ferry	-13.1 to 16.4	-16.9 to 10.4	-21.5 to 7.0
	Colorado River above Imperial Dam	-11.5 to 19.2	-13.7 to 14.4	-17.6 to 11.8
	Green River near Greendale	-14.1 to 26.7	-20.7 to 15.1	-24.2 to 14.3
	Colorado River near Cameo	-11.0 to 9.1	-17.1 to 11.2	-22.8 to 8.5
	Gunnison River near Grand Junction	-16.3 to 13.6	-23.7 to 9.3	-26.6 to 5.0
	San Juan River near Bluff	-18.4 to 11.0	-32.4 to -0.2	-34.4 to -6.9
Columbia	Snake River at Brownlee Dam	-12.6 to 13.0	-17.8 to 7.5	-22.7 to 2.7
	Columbia River at Grand Coulee	-6.5 to 10.1	-10.4 to 8.1	-13.7 to 6.0
	Columbia River at The Dalles	-7.7 to 7.8	-14.1 to 5.0	-19.3 to 0.4
	Yakima River at Parker	-12.8 to 6.6	-22.9 to -0.9	-32.7 to -8.0
	Deschutes River near Madras	-15.1 to 4.2	-25.3 to -4.4	-32.7 to -7.2
	Snake River near Heise	-13.6 to 13.4	-23.3 to 9.0	-28.4 to 2.8
	Flathead R. at Columbia Falls	-7.9 to 11.3	-12.5 to 5.6	-19.7 to 2.6

River Basin*	Site Name and Description	Projected Range[1] of Apr–Jul Runoff Change (%)		
		2020s	2050s	2070s
Klamath	Williamson River below the Sprague River	-26.6 to -3.4	-38.5 to -10.3	-41.6 to -16.2
	Klamath River below Iron Gate Dam	-24.4 to -3.3	-41.6 to -15.6	-48.2 to -19.7
	Klamath River near Seiad Valley	-23.2 to -3.5	-42.7 to -17.0	-49.9 to -21.9
	Klamath River at Orleans	-25.9 to -7.5	-46.5 to -22.4	-55.7 to -30.7
	Klamath River near Klamath	-26.2 to -11.4	-47.0 to -24.2	-55.9 to -33.3
Missouri	Missouri River at Canyon Ferry Dam	-8.0 to 12.2	-10.8 to 10.3	-18.1 to 12.1
	Milk River at Nashua	-4.9 to 24.9	-2.0 to 29.3	-0.6 to 38.9
	S. Platte River near Sterling	-6.1 to 16.8	-8.3 to 11.3	-19.8 to 13.6
	Missouri River at Omaha	1.3 to 19.7	7.3 to 26.7	7.0 to 32.8
	Bighorn River at Yellowtail Dam	-3.4 to 26.6	1.4 to 31.0	-3.9 to 35.3
	North Platte River at Lake McConaughy	-2.0 to 22.0	-2.7 to 22.8	-4.8 to 21.1
Rio Grande	Rio Grande near Lobatos	-16.8 to 15.7	-27.5 to 5.7	-27.7 to 0.1
	Rio Chama near Abiquiu	-18.5 to 18.6	-35.8 to 5.7	-34.4 to -2.7
	Rio Grande near Otowi	-19.2 to 15.5	-31.0 to 4.9	-30.6 to -4.6
	Rio Grande at Elephant Butte Dam	-17.9 to 13.6	-26.7 to 4.7	-28.3 to -3.2
	Pecos River at Damsite No. 3 near Carlsbad	-13.2 to 8.1	-21.3 to 9.1	-20.5 to 1.2

River Basin*	Site Name and Description	Projected Range[1] of Apr–Jul Runoff Change (%)		
		2020s	2050s	2070s
Sacramento–San Joaquin	Sacramento River at Freeport	-27.2 to -9.2	-46.8 to -28.8	-56.6 to -30.4
	Sacramento River at Bend Bridge near Red Bluff	-28.2 to -9.3	-46.1 to -25.2	-53.8 to -26.9
	Feather River at Oroville	-29.6 to -13.6	-52.7 to -34.7	-64.4 to -37.1
	San Joaquin River near Vernalis	-16.5 to 9.7	-32.6 to -0.5	-33.1 to -7.9
	Stanislaus River at New Melones Dam	-21.4 to 3.2	-43.9 to -15.3	-47.7 to -21.3
	Sacramento-San Joaquin Rivers at Delta	-23.5 to -1.7	-41.5 to -17.7	-45.2 to -22.1
	San Joaquin River at Millerton Lake (Friant Dam)	-17.2 to 12.2	-33.8 to -0.2	-35.4 to -7.2
	American River at Fair Oaks	-27.6 to -4.4	-47.6 to -26.1	-54.5 to -31.3
	Tulare-Buena Vista Lakes	-24.3 to 6.8	-40.8 to -10.5	-43.3 to -16.1
Truckee	Little Truckee River below Boca Dam	-21.4 to 9.0	-38.6 to -16.1	-53.8 to -22.6
	W.F. Carson R. at Woodfords	-18.2 to 15.8	-35.9 to -8.0	-47.3 to -17.5
	Truckee River at Farad Gage (just above CA State line)	-21.5 to 9.1	-40.0 to -15.8	-53.0 to -22.2
	Truckee R. at Nixon Gage	-21.4 to 9.8	-38.6 to -14.0	-50.7 to -21.1
	Carson River at Fort Churchill Gage	-17.4 to 11.1	-38.5 to -11.9	-45.2 to -19.9

* Note: The Pecos, Tulare, and Carson are not SWA river basins, but are included under the Rio Grande, Sacramento and San Joaquin, and Truckee, respectively, as these locations are of interest from a water operations standpoint.

[1] Ranges of projected April-through-July runoff are the 25th to 75th percentile change of the 64 projections.

Table 10. Projected range of annual runoff timing shift for the 43 West-wide reporting locations

River Basin*	Site Name and Description	Projected Range[1] of Annual Runoff Timing Shift (day)		
		2020s	2050s	2070s
Colorado	Colorado River at Lees Ferry	-7.8 to -3.6	-12.3 to -6.4	-15.8 to -8.2
	Colorado River above Imperial Dam	-8.1 to -3.3	-12.5 to -6.1	-14.5 to -8.2
	Green River near Greendale	-8.5 to -3.9	-12.9 to -7.4	-16.7 to -9.3
	Colorado River near Cameo	-8.0 to -3.8	-12.8 to -8.1	-16.8 to -10.0
	Gunnison River near Grand Junction	-9.7 to -5.1	-14.8 to -8.8	-19.2 to -9.7
	San Juan River near Bluff	-7.6 to -3.0	-10.7 to -3.6	-12.8 to -4.5
Columbia	Snake River at Brownlee Dam	-6.8 to -2.4	-10.3 to -4.5	-12.4 to -5.9
	Columbia River at Grand Coulee	-8.0 to -4.0	-12.7 to -7.5	-16.7 to -10.2
	Columbia River at The Dalles	-7.1 to -3.4	-11.2 to -6.4	-14.3 to -8.6
	Yakima River at Parker	-8.2 to -2.0	-10.9 to -3.5	-12.3 to -4.8
	Deschutes River near Madras	-6.6 to 0.6	-6.8 to 2.5	-8.2 to 1.5
	Snake River near Heise	-9.2 to -5.1	-15.2 to -8.8	-21.3 to -11.0
	Flathead R. at Columbia Falls	-9.3 to -4.0	-16.7 to -8.7	-20.4 to -11.7
Klamath	Williamson River below the Sprague River	-3.0 to 11.7	-0.1 to 19.1	2.1 to 23.3
	Klamath River below Iron Gate Dam	-4.7 to 7.0	-3.3 to 10.9	-2.9 to 14.9
	Klamath River near Seiad Valley	-6.3 to 5.8	-5.3 to 7.4	-6.0 to 12.1
	Klamath River at Orleans	-6.7 to 7.1	-7.0 to 9.2	-7.8 to 12.2

River Basin*	Site Name and Description	Projected Range[1] of Annual Runoff Timing Shift (day)		
		2020s	2050s	2070s
	Klamath River near Klamath	-6.9 to 9.8	-7.9 to 11.1	-10.4 to 11.7
Missouri	Missouri River at Canyon Ferry Dam	-6.3 to -3.0	-10.1 to -5.7	-13.4 to -7.8
	Milk River at Nashua	-6.6 to -0.2	-9.5 to -1.2	-10.9 to -3.6
	S. Platte River near Sterling	-10.3 to -2.9	-13.8 to -7.0	-16.3 to -8.4
	Missouri River at Omaha	-6.1 to -3.4	-10.5 to -6.8	-14.6 to -8.8
	Bighorn River at Yellowtail Dam	-9.8 to -5.0	-16.1 to -10.1	-21.8 to -12.8
	North Platte River at Lake McConaughy	-9.3 to -4.2	-14.3 to -9.1	-19.3 to -10.8
Rio Grande	Rio Grande near Lobatos	-11.8 to -5.6	-18.5 to -10.3	-23.5 to -11.8
	Rio Chama near Abiquiu	-8.0 to -2.1	-10.5 to -3.9	-13.7 to -5.1
	Rio Grande near Otowi	-9.7 to -4.8	-14.4 to -8.9	-18.5 to -9.8
	Rio Grande at Elephant Butte Dam	-7.8 to -3.5	-9.9 to -4.4	-13.6 to -6.2
	Pecos River at Damsite No. 3 near Carlsbad	-2.1 to 4.7	-1.4 to 7.1	-1.6 to 9.9
Sacramento–San Joaquin	Sacramento River at Freeport	-10.5 to 7.6	-15.2 to 5.8	-16.0 to 2.7
	Sacramento River at Bend Bridge near Red Bluff	-10.5 to 8.3	-11.0 to 5.7	-12.0 to 5.8
	Feather River at Oroville	-12.5 to 6.3	-17.6 to 2.7	-17.6 to 2.2
	San Joaquin River near Vernalis	-11.9 to 1.2	-17.9 to -7.9	-20.0 to -10.4
	Stanislaus River at New Melones Dam	-11.6 to 4.2	-18.3 to -5.3	-20.2 to -7.7

River Basin*	Site Name and Description	Projected Range[1] of Annual Runoff Timing Shift (day)		
		2020s	2050s	2070s
	Sacramento-San Joaquin Rivers at Delta	-11.6 to 5.0	-15.4 to 1.0	-16.2 to -0.7
	San Joaquin River at Millerton Lake (Friant Dam)	-12.2 to -2.2	-20.8 to -10.9	-24.2 to -13.4
	American River at Fair Oaks	-13.2 to 10.9	-15.9 to 6.4	-13.9 to 3.7
	Tulare-Buena Vista Lakes	-14.6 to 7.2	-13.3 to 4.6	-16.1 to 4.8
Truckee	Little Truckee River below Boca Dam	-14.4 to -5.7	-24.4 to -12.0	-32.7 to -12.9
	W.F. Carson R. at Woodfords	-16.3 to -3.6	-28.6 to -13.8	-34.4 to -16.7
	Truckee River at Farad Gage (just above CA State line)	-13.7 to -4.3	-24.1 to -9.0	-29.6 to -11.6
	Truckee R. at Nixon Gage	-13.2 to -4.9	-23.2 to -8.7	-28.0 to -11.6
	Carson River at Fort Churchill Gage	-15.2 to -1.9	-24.5 to -8.5	-27.3 to -10.7

* Note: The Pecos, Tulare, and Carson are not SWA river basins, but are included under the Rio Grande, Sacramento and San Joaquin, and Truckee, respectively, as these locations are of interest from a water operations standpoint.

[1] Ranges of projected annual runoff (half of the annual flow volume) timing shift are the 25th to 75th percentile change of the 64 projections. Negative values denote earlier runoff relative to the 1990s; whereas, positive values denote later runoff relative to the 1990s.

3.11 Implications for Future Water Management

Based on the hydroclimate analysis presented in this chapter, a listing of potential implications for future water management is presented. Specific analysis related to hydroclimate impacts, such as droughts and performance metrics of water resources systems (e.g., storage at the end of a drought cycle), are described in subsequent chapters of this report and are referenced here, as applicable. Furthermore, potential hydroclimate impacts are outlined here. However, for details on basin-specific impacts, the pertinent WaterSMART reports, such as those from basin studies, should be referenced. The following is a broad list of potential impacts for future water management:

- Projected increases in temperatures, decreases in snowpack, and runoff occurring earlier in the year, with a corresponding reduction in supply in summer months, can make supplies less predictable and water deliveries more difficult to manage.
- With projected increases in temperature and variable precipitation, more frequent and more severe droughts can be anticipated. Chapter 4 provides a West-wide drought analysis to quantify such impacts (i.e., changes in drought characteristics—duration, severity, and frequency).
- As shown in the hydroclimate analysis, with the shifts toward earlier timing and volume of spring runoff largely projected in the eight major Reclamation river basins, hydropower production will likely be impacted. A generally decreasing pattern in April to July streamflow (except for the Missouri River Basin) and projected higher temperatures in the subsequent summer will likely add to hydropower production challenges from these two aspects—decreasing water supplies in summer months for hydropower generation and increasing power needs to meet cooling demands.
- Changes in projected flow dynamics, such as shifts in the flow seasonality (substantial runoff occurring earlier in the year) and drought characteristics, can lead to reduced end-of-water-year reservoir levels and river flows. This can have negative implications for flow and water-dependent recreational activities. An analysis of reservoir performance using a range of metrics for selected reservoirs is presented in Chapter 6.
- In addition, changes in projected flow dynamics coupled with increasing temperatures and variable precipitation will likely impact water quality and present challenging ecosystem conditions.

4 West-wide Drought Analysis

This chapter describes analyses of the variability and characteristics of drought for historical and future projected climate conditions across the Western United States. The analyses are performed using the Palmer Drought Severity Index (PDSI; Palmer, 1965) to define drought events. The advantage of using PDSI to define droughts is that it focuses explicitly on droughts driven by hydroclimate variability. The PDSI does not include anthropogenic effects, such as water management, including the effects of reservoirs and diversions. Thus, PDSI is well-suited to examine natural climate-driven drought characteristics (i.e., drought duration, severity, and frequency).

The next section (Section 4.1) describes the PDSI dataset and how it is used in the analyses. Section 4.2 describes the methodologies used to identify and analyze drought events. Section 4.3 presents results, along with considerations regarding the interpretations of the results. Summary and next steps emerging from the analyses are described in Section 4.4. Lastly, a listing of key findings is given in Section 4.5.

4.1 Data

The PDSI data used in the analyses contains two time periods: (1) the historical period, which includes the years 1473 to 2005; and (2) the projection period, which comprises the years 2006 to 2099. The PDSI data collated from various sources to cover these two time periods were aggregated to a common spatial resolution of U.S. Geological Survey (USGS) eight-digit Hydrologic Unit Codes (HUC-8s; Seaber et al. 1987). Figure 65 shows the distribution of HUC-8s across the Western United States (including portions of Canada in the north and Mexico in the south) and covering the eight major Reclamation river basins. The region shown in Figure 65 consists of a total of nearly 1,316 HUC-8s, but analysis was largely constrained to HUC-8s within the boundaries of the United States, resulting in a total of 1,255 HUC-8s with complete PDSI data covering the time periods used in the analysis.

Furthermore, eight HUC-8s, one for each of the eight major Reclamation river basins, are highlighted in Figure 65. These specific HUC-8s are used for focused analyses. Metadata for these eight selected HUC-8s is given in Table 11. The spatial resolutions of the source PDSI data used are discussed within the respective time period sections—Section 4.1.1 (historical period PDSI) and Section 4.1.2 (projection period PDSI). Thus, time series of PDSI data covering the period 1473 to 2099 for each of the 1,255 HUC-8s was developed for use in the analyses. Note, all PDSI values referenced here are the summer (June-July-August) averaged PDSI values.

4.1.1 Historical Period (1473 to 2005) PDSI

The historical period used in this analysis includes the years 1473 to 2005. The PDSI data for this period were obtained from the Cook et al. (2010) PDSI dataset which provides tree-ring based reconstructions of PDSI on a 0.5°latitude-by-0.5°longitude spatial resolution for the years 0 to 2017 (note that the Cook et al. paper was published in 2010, but the PDSI data have been updated). The Cook et al. (2010) PDSI data were aggregated to the 1,255 HUC-8s using area-weighted averaging. A PDSI value was not calculated for a HUC-8 where the gridded area value was less than 50 percent of the HUC-8 area. This largely happens in areas where a HUC-8 straddles cells with and without data (e.g., HUC-8s straddling the northern and southern United States borders). These HUC-8s were assigned a missing value. The aggregation of the Cook et al. (2010) PDSI data to the HUC-8s resulted in complete time series for all 1,255 HUC-8s starting in the year 1473. Thus, 1473 was selected as the first year for the analyses of the historical PDSI dataset. The last year selected for the historical PDSI time series was 2005. This date was selected because the CMIP5 climate projections begin in the following year. Statistically downscaled CMIP5 projections of monthly precipitation and temperature time series from 1950 to 2099 were used to compute PDSI time series for the projection period, which is described in the next section.

4.1.2 Projection Period (2006 to 2099) PDSI

Future projections of PDSI were developed based on CMIP5-LOCA climate projections, using the Wells (2003) model for computing PDSI. The input data requirements to develop monthly PDSI time series (Wells, 2003) are: (1) average monthly temperature, (2) total monthly precipitation, (3) monthly normal or average temperature for a period of record, and (4) a parameter set consisting of two values—the first value is the soil water capacity (also referred to as the available water holding capacity, or root zone water holding capacity) and the second value is the latitude of the site (e.g., a meteorological station or the centroid of a grid cell for a gridded dataset). All PDSI calculations for a given projection were computed for the $1/16^{th}$ degree (latitude-by-longitude) grid.

The first three inputs required to calculate PDSI were developed by aggregating the LOCA precipitation and temperature time series to monthly values for each $1/16^{th}$ degree grid cell. The soil water storage capacity data were derived by re-gridding (using bilinear interpolation) the 1-degree global soil texture and derived water-holding capacities dataset (Webb et al., 2000) to the $1/16^{th}$ degree grid resolution. The site latitude value was the centroid of the $1/16^{th}$ degree grid cell.

With this set of inputs developed for each projection, the PDSI model (Wells, 2003) was run to calculate gridded monthly PDSI values for each climate model projection for each of the $1/16^{th}$ degree grid cells for the period 1950 to 2099. Subsequently, for each projection, the monthly PDSI magnitudes were averaged to summer (June-July-August average) values. Additionally, PDSI values (e.g., Dai and NCAR, 2019) greater than +10 (wet) or less than -10 (dry) were replaced with a missing value and removed in subsequent calculations. As a final

step, the summer PDSI values for the 1/16th degree grid cells then were aggregated to the 1,255 HUC-8s.

The period 1950 to 2005 is a period common to both the historical data and the climate model simulated PDSI data sets. This common period (1950 to 2005) was used to compare drought characteristics— duration, severity, and interarrival times (see Figure 67 for definitions) computed using climate model data with drought characteristics computed using historical data. For other analyses, the "projection period" includes the years 2006 to 2099. Thus, three periods will be mentioned in the analyses that follow: (1) the historical period (1473 to 2005), (2) the common period (1950 to 2005), and (3) the projection period (2006 to 2099). As mentioned earlier, the computation of PDSI requires a long-term normal (average) temperature for each site. For the common period analyses the long-term normal temperature was computed for 1950 to 2005, and for the climate model projection analyses the long-term normal temperature was computed for 1950 to 2099.

Additionally, the Cook et al. (2010) PDSI data for the common period (i.e., 1950 to 2005) will be used to represent measured or observed PDSI for this period and will be referred to as observed data for analyses for the common period.

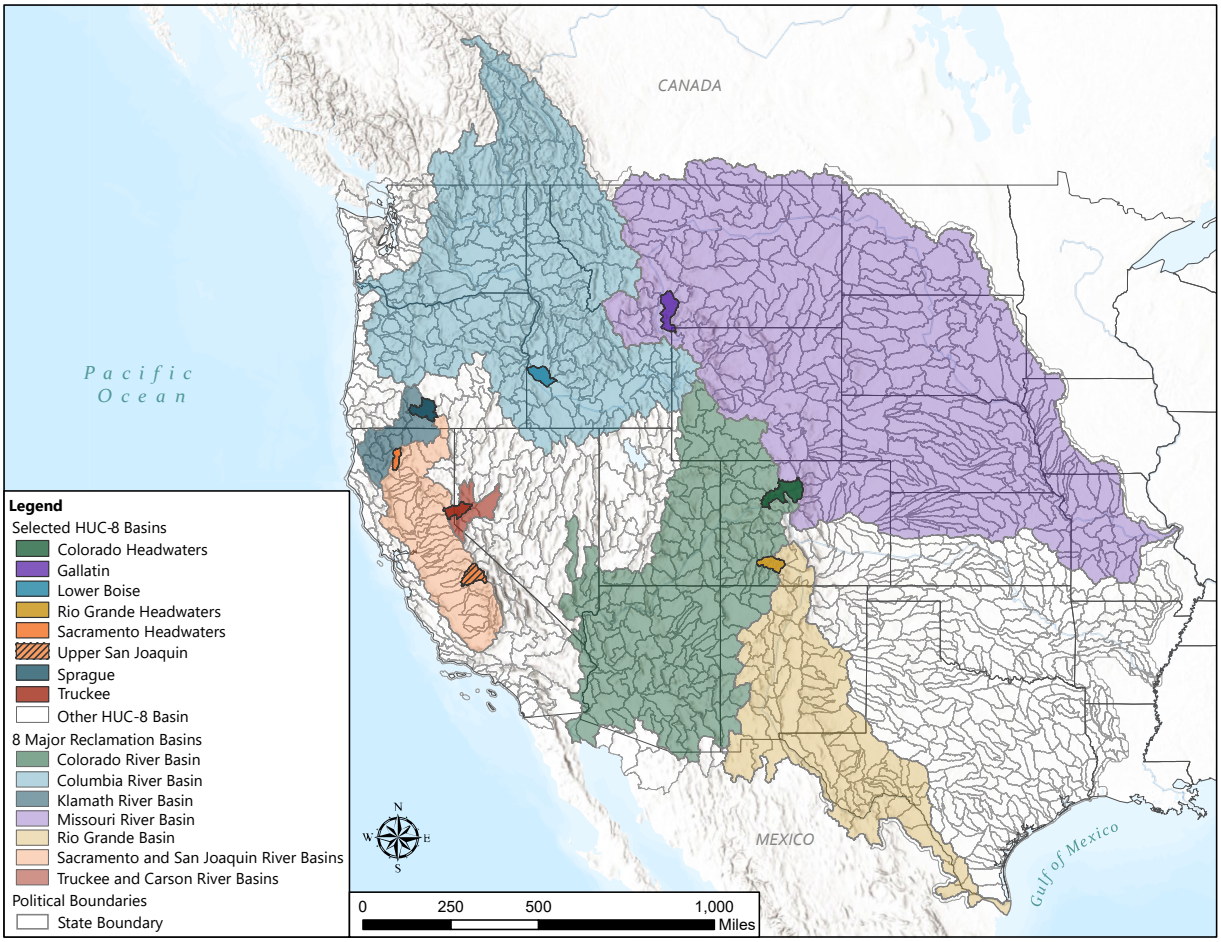

Figure 65. HUC-8s across the Western United States with select HUC-8s highlighted that were used for focused analyses.

Note: Metadata for the eight selected HUC-8s across the eight major Reclamation river basins are provided in Table 11.

Table 11. Select eight-digit Hydrologic Unit Codes (HUC-8) in the eight major Reclamation river basins used to present study results

River Basin	HUC-8 ID	HUC-8 Name	State(s)	HUC-8 Centroid		Drainage Area (square miles)
				Latitude	Longitude	
Colorado	14010001	Colorado Headwaters	CO	40.0040	-106.4111	2,902
Columbia	17050114	Lower Boise	ID	43.6040	-116.4098	1,329
Klamath	18010202	Sprague	OR	42.5638	-121.2062	1,610
Missouri	10020008	Gallatin	MT-WY	45.4972	-111.1727	1,847
Rio Grande	13010001	Rio Grande Headwaters	CO	37.7278	-106.9285	1,381
Sacramento	18020005	Sacramento Headwaters	CA	41.0691	-122.3794	592
San Joaquin	18040006	Upper San Joaquin	CA	37.3375	-119.2087	1,639
Truckee	16050102	Truckee	CA-NV	39.4459	-119.8722	1,217

4.2 Methodology

4.2.1 Drought Definitions

The time series of summer PDSI for 1,255 HUC-8s were used to identify drought events for historical and projection periods. Two methods were used to identify drought periods, both based on PDSI values moving below or above a PDSI value of zero (i.e., zero cross-over). Using the first method, a drought event occurs when a summer PDSI value drops below the zero threshold and ends when a summer PDSI value moves above the zero threshold (Figure 66a). Using this method, a drought as short as 1 year is possible.

The second method uses 3-year moving averages of summer PDSI to identify drought events. A 3-year moving average was used to remove high frequency variability in PDSI. For this method, a drought event occurs when the 3-year moving average summer PDSI value drops below the zero threshold and ends when the 3-year moving average summer PDSI value moves above the zero threshold (Figure 66b).

In general, the first method used to identify drought events results in more frequent and shorter droughts than the second method (compare Figure 66a and Figure 66b).

Once drought events were identified for each HUC-8 and for the historical and projection periods, several drought characteristics were computed—drought duration (in years), drought severity (mean PDSI for the drought event), and drought inter-arrival time (the number of years from the beginning of one drought to the beginning of the successive drought) (Figure 67). The number of droughts for the historical and projection periods also were computed for each HUC-8. Probability distributions were developed using the drought duration and drought severity data and were used in conjunction with the expected value of drought interarrival times to develop return period estimates of selected drought events.

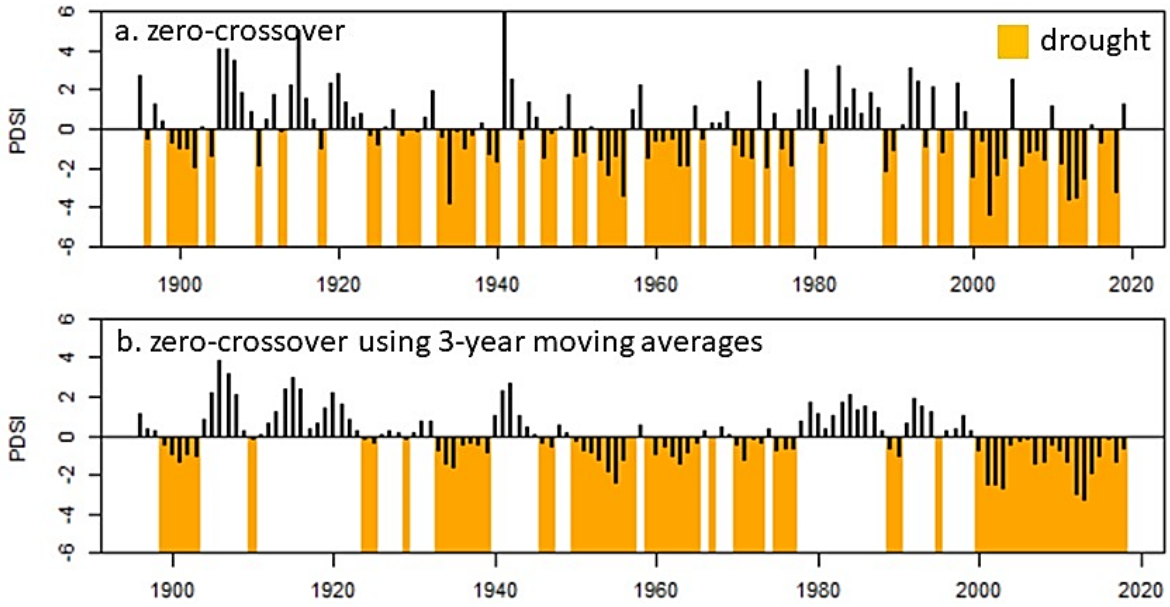

Figure 66. Illustration of droughts using zero-crossover of PDSI values.

Note: Droughts are identified using (a) zero-crossover of yearly PDSI values, and (b) zero-crossover using 3-year moving averages of yearly PDSI values.

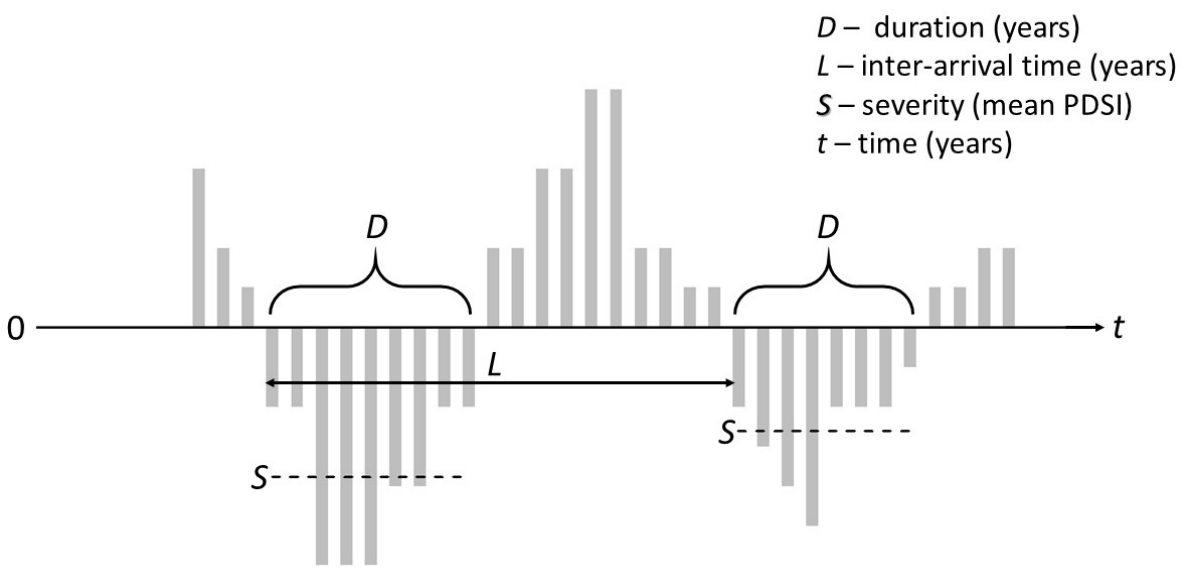

Figure 67. Generalized drought definition and characteristics.

Note: Drought characteristics include drought duration (D, years), severity (S, mean PDSI calculated over a drought event), and inter-arrival times (L, years).

4.2.2 Marginal Distributions of Drought Duration and Severity

Using the drought duration and severity datasets from the historical (1473 to 2005) period and projection period (2006 to 2099), probability distributions[9] (marginal probability distributions), were developed for drought duration and drought severity. These marginal distributions were developed for each of the 1,255 HUC-8s in the domain.

The historical period, which is 533-years long, had a sufficient number of events (≥ 30; sample size) for each HUC-8 using either drought definition to develop the marginal distributions of duration and severity. Table 12 presents a summary of the sample size ranges from all the 1,255 HUC-8s used to fit the marginal distributions over the historical period for each drought definition.

[9] These probability distributions are referred to as marginal distributions when used in a joint probability analysis, which is subsequently conducted (refer to Sections 4.2.3 and 4.2.5) to estimate drought return periods.

Table 12. Range of sample size by drought definition from all 1,255-HUC8s used in distribution fitting over the historical period (1473 to 2005)

Drought Definition	Sample Size Range*
Zero-crossover of yearly PDSI values	62 to 154 (12% to 29%)
Zero-crossover using 3 year moving averages of yearly PDSI values	38 to 89 (7% to 17%)

* Note: The sample size percentages given in parenthesis are calculated as a fraction of the total length of the historical period time series, 533 years.

However, for the projection period, which is only 94 years long, the number of drought events for any single projection and HUC-8 is limited. Thus, for any HUC-8, the number of drought events for a climate model projection can range from zero to only a single exceptionally long drought event over this period. Due to these limitations, the 32 projections for each of the RCPs (RCP4.5 and RCP8.5) were pooled to ensure that enough drought events were available to develop the marginal distributions. Furthermore, the pooling of drought duration and severity data from the RCP projections provides a robust representation of the underlying probability distributions of drought duration and severity by accounting for the wide range of variability provided by the climate model projections. A summary of the sample size ranges from all 1,255 HUC-8s and 32 projections (in each RCP case, RCP4.5 and RCP8.5) used to fit the marginal distributions over the projection period and for each drought definition is given in Table 13.

Furthermore, the range of sample size percentages calculated as a fraction of the total time series length in the two periods—historical period (Table 12) and the projection period (Table 13) are very comparable. This fraction is directly comparable for the drought definition of zero-crossover of yearly PDSI values because of the binary drought description where any year can either be in drought or not.

For the second drought definition, zero-crossover using 3-year moving averages of yearly PDSI values, the comparison of sample size fraction is somewhat indirect since the PDSI time series is first smoothed before identifying the drought events. However, the full time series length is used to make the comparison. Since this approach is used for both the historical and projection period, the sample size fractions are comparable in a relative sense between these two time periods.

Table 13. Range of sample size by drought definition from all 1,255-HUC8s used in distribution fitting over the projection period (2006 to 2099)

Drought Definition	Sample Size Range*	
	RCP4.5	RCP8.5
Zero-crossover of yearly PDSI values	375 to 685 (12% to 23%)	318 to 647 (11% to 22%)
Zero-crossover using 3-year moving averages of yearly PDSI values	189 to 358 (6% to 12%)	154 to 333 (5% to 11%)

* Note: The sample size percentages given in parenthesis are calculated as a fraction of the total length of the projection period time series, (32 x 94 years).

A set of eight different probability distributions for both drought duration and severity were tested for each HUC-8 to identify the best-fit distribution. The eight different probability distributions tested were: (1) log-normal (*lnorm*), (2) log-logistic (*llog*), (3) gamma (*gamma*), (4) logistic (*logis*), (5) exponential (*exp*), (6) normal (*norm*), (7) Gumbel (*gumbel*), and (8) Weibull (*weibull*)[10]. All distribution fitting and testing was conducted using the R statistical computing environment (R Core Team, 2019)[11]. Furthermore, distribution fitting was performed using maximum likelihood estimation of distribution parameters with R function *fitdist* from the R library, *fitdistrplus*. Standard error estimates for the fitted distribution parameters also were calculated and can be used to test the effects of distribution parameter uncertainty on results, such as changes in return period estimates.

The best-fit distribution was selected using the Bayesian Information Criteria (BIC). BIC provides a score for each of the fitted distributions, and the distribution with the minimum BIC value was selected to be the best-fit distribution. In addition, further statistical tests (NIST, 2012)—Chi-squared, Kolmogorov-Smirnov, Cramer-von Mises, and Anderson-Darling—also were conducted to evaluate the fitted distributions. The performance of these statistical tests varied widely primarily because, among other test-specific assumptions, statistical tests are sensitive to methods used in estimating distribution parameters. The method of maximum likelihood used here in parameter estimation is a well-founded approach in statistical literature and generally estimates unbiased distribution parameters over other approaches, such as the method of moments. However, other distribution parameter estimation methods, such as probability weighted moments or L-moments exist (Hosking and Wallis, 1997), but those methods were not used in the analysis here. The rationale being that many distributions (total, eight) were tested and a ranking scheme following the BIC scores was used to select the best-fit

[10] R function names for the respective distributions are given in the parenthesis in italics font.

[11] Any use of trade, firm, or product names is for descriptive purposes only and does not imply endorsement by the United States Government.

distribution from this pool of distributions. The selected best-fit distribution fits the time series data the “best” (minimum BIC value) relative to the pool of distributions tested. Finally, note that, with the distribution fitting of drought severity, which are negative PDSI values, the values were converted to positive magnitudes and, since log-transform distributions are undefined for zero PDSI values, a nominal value of 0.001 was used for these cases. The selected best-fit distribution counts (i.e., the number of HUC-8s) for the two drought definitions for drought duration and drought severity for historical and projection period (by RCP) are given in Table 14 and Table 15.

Table 14. Best-fit distribution count across the domain (1,255 HUC-8s) of drought duration and drought severity for the drought definition "zero-crossover of yearly PDSI values" for historical and projection period (by RCP)

Drought Characteristic	Best-fit Distribution	HUC-8 Count		
		Historical	RCP4.5	RCP8.5
Duration	Log-normal	1253	1255	1252
	Log-logistic	2	0	3
	Gamma	0	0	0
	Logistic	0	0	0
	Exponential	0	0	0
	Normal	0	0	0
	Gumbel	0	0	0
	Weibull	0	0	0
Severity	Log-normal	0	0	0
	Log-logistic	7	0	0
	Gamma	50	0	2
	Logistic	9	1	0
	Exponential	5	0	0
	Normal	55	243	22
	Gumbel	142	30	6
	Weibull	987	981	1225

Table 15. Best-fit distribution count across the domain (1,255 HUC-8s) of drought duration and drought severity for the drought definition "zero-crossover using 3-year moving averages of yearly PDSI values" for historical and projection period (by RCP)

Drought Characteristic	Best-fit Distribution	HUC-8 Count		
		Historical	RCP4.5	RCP8.5
Duration	Log-normal	846	1248	1255
	Log-logistic	21	0	0
	Gamma	343	7	0
	Logistic	0	0	0
	Exponential	0	0	0
	Normal	0	0	0
	Gumbel	0	0	0
	Weibull	45	0	0
Severity	Log-normal	0	0	0
	Log-logistic	0	0	0
	Gamma	23	0	27
	Logistic	6	0	0
	Exponential	36	0	155
	Normal	107	76	0
	Gumbel	66	25	3
	Weibull	1017	1154	1070

Based on Table 14 and Table 15, the dominant best-fit distribution for drought duration is the log-normal distribution, and for drought severity it is the Weibull distribution for both of the drought definitions. It is important to note that the predominant distributions—log-normal for drought duration and Weibull for drought severity—are the same for both the historical period and the projection period. This result provides a level of robustness indicating that the underlying stochastic processes generating drought characteristics are fundamentally the same under

historical and projected climate conditions though the parameters of the individual distributions are different.

4.2.3 Joint Distributions of Drought Duration and Drought Severity

With the marginal distributions established for each HUC-8, joint distributions were developed using copulas. Several families of copulas are reported in the hydrologic literature. In this study, the Gumbel-Hougaard (GH) copula, specific to the Archimedean family of copulas that are generally used to model extreme value type processes, was used. Also, the parameter estimation for the GH copula was done using inverse Kendall tau. Kendal tau is a measure of correlation between the two variables used here—drought duration and drought severity. A closed-form relationship exists between the GH copula parameter (θ) and Kendall tau (τ)[12], which couples (hence the name copula) the marginal distributions of drought duration and drought severity to form the joint distribution[13].

A copula parameter was calculated, along with its 95 percent confidence interval, for each of the 1,255 HUC-8s in the domain using the combination of the pertinent time series discussed previously (Sections 4.1 and 4.2.2). For example, the historical time series of drought duration and drought severity were used to develop the set of copula parameters for the historical period (1473 to 2005). Similarly, for the projection period (2006 to 2099), copula parameters were calculated using the pooled time series data for the respective climate projections—RCP4.5 and RCP8.5. The estimated GH copula parameter for the historical and projection period RCPs (RCP4.5 and RCP8.5) for the two drought definitions ("zero-crossover of yearly PDSI values" and "zero-crossover using 3-year moving averages of yearly PDSI values") are shown in Figure 68 and Figure 69 respectively.

The copula parameter provides a measure of the degree of association between drought duration and drought severity. With the first drought definition ("zero-crossover of yearly PDSI values"), the copula parameter distribution given in Figure 68 shows, for the historical period (1473 to 2005), a greater association between drought duration and drought severity over portions of the Missouri River Basin (values between 1.5 to 2.0; or Kendall tau values between 0.33 and 0.50), and a weaker relationship across the remainder of the domain (copula parameter values below 1.5; or Kendall tau values below 0.33). Note that, the copula parameter distribution uses the full historical period and does not account for any non-stationarity in the parameter estimation and, thus, can be viewed here as an estimate of the long-term mean parameter. For the projection period (2006 to 2099), the degree of association between drought duration and drought severity increases and expands spatially for the RCP8.5 projections compared with the RCP4.5 projections.

[12] $\theta = 1/(1 - \tau)$; $\tau \geq 0$. For $\tau < 0$, $\theta = 1$, i.e., independent copula. Range of τ, [-1, 1]. Refer to R library *copula* (Kojadinovic and Yan, 2010).

[13] Copulas are functions that join or "couple" marginal distribution functions to form multivariate distribution functions.

For the second drought definition ("zero-crossover using 3-year moving averages of yearly PDSI values"; Figure 69), a stronger association between drought duration and severity generally is seen for both the historical and projection periods compared with the first method of drought definition (see Figure 68). In the case of the RCP8.5 projections, the relationship between drought duration and severity becomes substantially stronger (copula parameter values between 3.0 and 4.0, or Kendall tau values between 0.67 and 0.75) for HUC-8s in the Colorado, Columbia, Rio Grande, and Missouri River Basins.

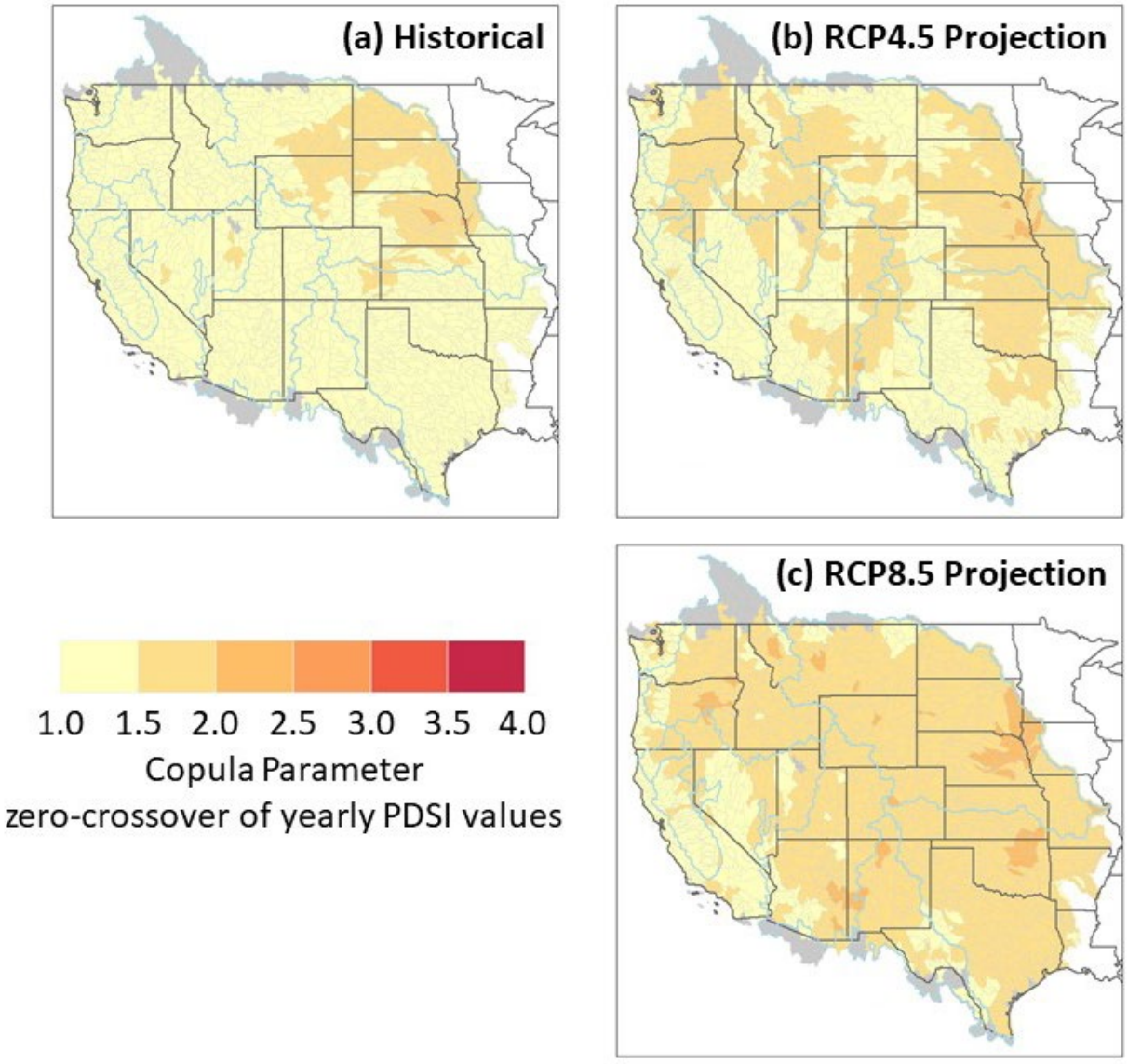

Figure 68. (a to c) Copula parameter for drought definition "zero-crossover of yearly PDSI values."

Note: Copula parameter shown for drought definition "zero-crossover of yearly PDSI values" for (a) historical (1473 to 2005), (b) simulations from RCP4.5 climate models (2006 to 2099), and (c) simulations from RCP8.5 climate models (2006 to 2099).

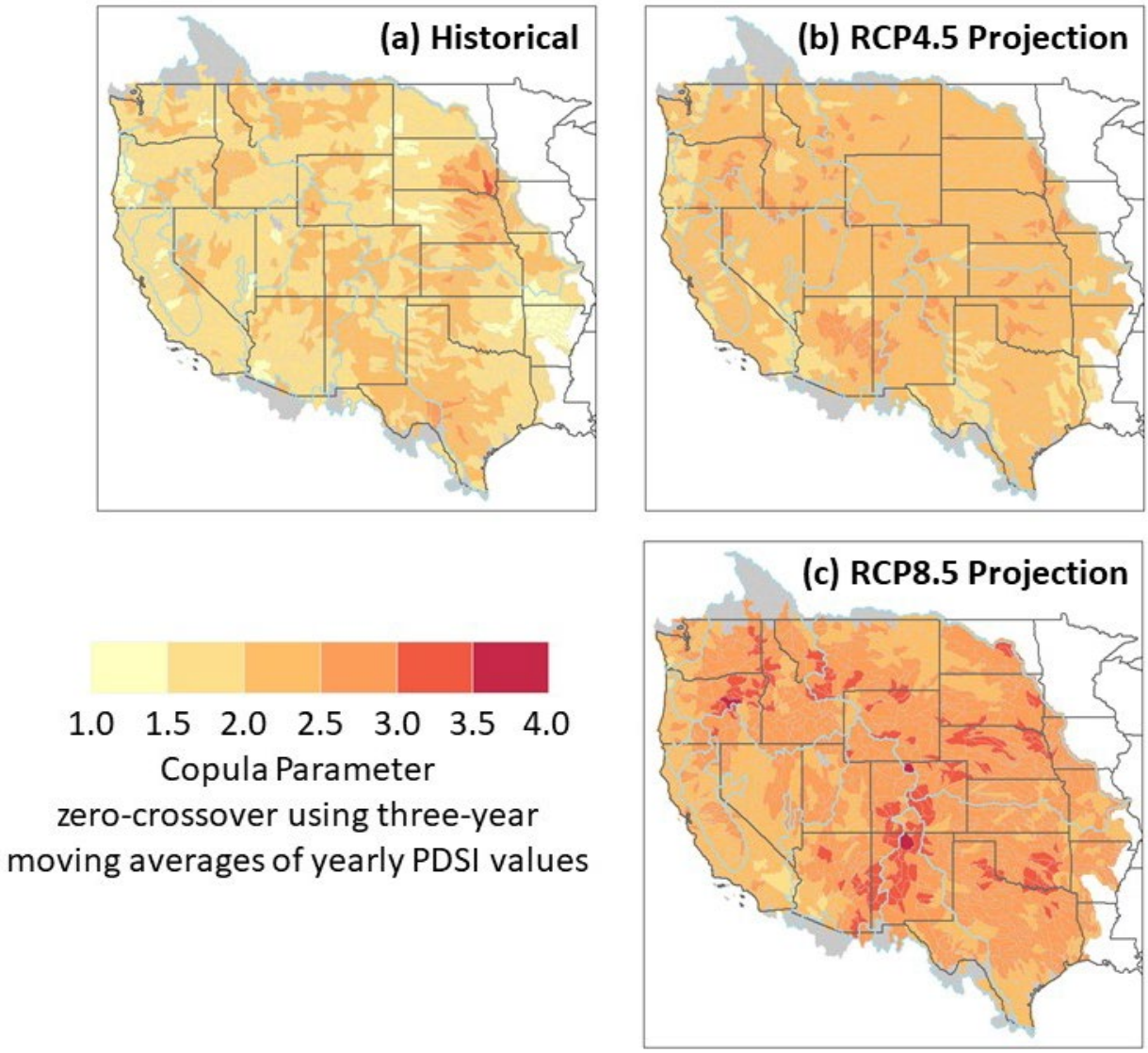

Figure 69. (a to c) Copula parameter for drought definition "zero-crossover using 3-year moving averages of yearly PDSI values."

Note: Copula parameter for drought definition "zero-crossover using 3-year moving averages of yearly PDSI values" for (a) historical (1473 to 2005), (b) simulations from RCP4.5 climate models (2006 to 2099), and (c) simulations from RCP8.5 climate models (2006 to 2099).

4.2.4 Drought Interarrival Time

The drought interarrival time is the time between the start of two successive drought events. The expected value (or, mean/average value) of drought interarrival time for each HUC-8 for the historical period (1473 to 2005), and the projection period (2006 to 2099) is used in the following calculations of return periods for selected drought events.

For the historical period (1473 to 2005), the calculation of the expected drought interarrival time for a HUC-8 is largely straightforward. Using the drought events identified over this period for a given HUC-8, the time interval between two successive drought events was calculated, and this set of interarrival time values was averaged to obtain the expected drought interarrival time for the HUC-8.

For the projection period (2006 to 2099), and for each RCP (RCP4.5 and RCP8.5), the ensemble mean drought interarrival time for the 32 projections was calculated for the domain (1,255 HUC-8s). For a given projection and given HUC-8, the identified drought events over the projection period were used to calculate the interarrival times and then averaged to obtain a mean interarrival time for the given HUC-8 and projection. Note, in some cases, a projection will only identify a single drought event for the projection period and, in such cases, the interarrival time was identified as a missing value. The ensemble-mean interarrival time for a given HUC-8 was calculated using the mean interarrival times from the 32 projections after excluding missing mean interarrival time values.

The distribution of mean interarrival time for the historical period (1473 to 2005), and the ensemble mean interarrival time for the projection period (2006 to 2099) for RCP4.5 and RCP8.5 are shown in Figure 70 for drought definition "zero-crossover of yearly PDSI values," and Figure 71 for drought definition "zero-crossover using 3-year moving averages of yearly PDSI values."

For the first drought definition (Figure 70), both for the historical and projection periods, most of the domain indicates return periods between 3 to 7 years. However, the historical period (1473 to 2005) shows large portions of the domain with mean interarrival times between 3 to 5 years, and portions of the Missouri River Basin with interarrival times between 7 to 10 years. Note that, for the projections, it is the ensemble mean interarrival times that are shown (Figure 70b and Figure 70c).

For the second drought definition ("zero-crossover using 3-year moving averages of yearly PDSI values"), the smoothing of the PDSI values used in this drought definition result in generally longer drought interarrival times compared with the first drought definition. For the historical period (Figure 71a), most of the domain shows drought interarrival times between 7 to 10 years, with shorter interarrival times in the Central Valley of California (between 5 to 7 years) and large portions of the Missouri River Basin indicating interarrival times between 10 to 15 years. Though with a somewhat different spatial distribution (e.g., portions of the Colorado River and Lower Rio Grande Basins) between RCP4.5 (Figure 71b) and RCP8.5 (Figure 71c), the ensemble mean interarrival times are between 7 to 10 years for the projection period for this drought definition.

In addition to calculating the ensemble mean interarrival times using all projections (32 per RCP), the lower (5th percentile) and upper (95th percentile) bounds of the mean interarrival times were calculated for each RCP as an indicator of uncertainty associated with the mean interarrival times. These distributions of uncertainty in drought interarrival time are shown in Figure 72 for drought definition "zero-crossover of yearly PDSI values" and Figure 73 for drought definition "zero-crossover using 3-year moving averages of yearly PDSI values."

For the first drought definition (Figure 72), the lower bound (5th percentile) of the mean drought interarrival time for both the projections (RCP4.5, Figure 72a; RCP8.5, Figure 72c) is between 3 to 5 years. The upper bound (95th percentile) of the mean drought interarrival time for both the projections (RCP4.5, Figure 72b; RCP8.5, Figure 72d) is between 5 to 10 years.

For the second drought definition (Figure 73), the lower bound (5th percentile) of the mean drought interarrival time for both the projections (RCP4.5, Figure 73a; RCP8.5, Figure 73c) is between 5 to 10 years. The upper bound (95th percentile) of the mean drought interarrival time for both the projections (RCP4.5, Figure 73b; RCP8.5, Figure 73d) is between 10 to 30 years.

In all cases, both drought definitions (Figure 72 and Figure 73), the respective uncertainty bounds (lower, 5th percentile; upper, 95th percentile) across the RCP projections (RCP4.5 and RCP8.5) show largely similar spatial patterns of uncertainty in mean drought interarrival times.

The mean (for the projections this mean is an ensemble mean of RCP projections) drought interarrival time is an input variable that is used to calculate drought event return periods (see next section, Section 4.2.5), and are used to provide bounds to return period estimates discussed in the results section (Section 4.3.4).

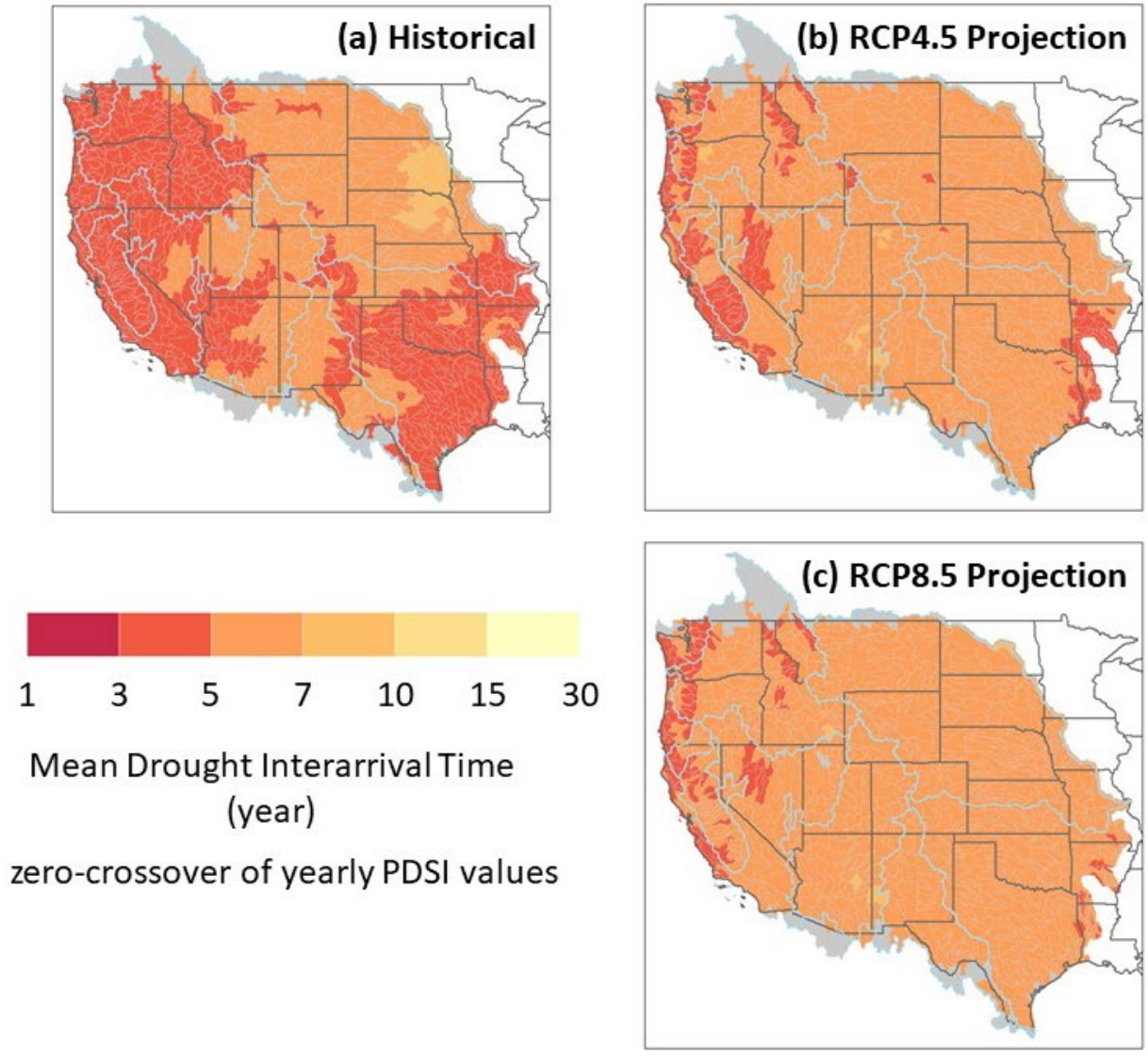

Figure 70. (a to c) Mean drought interarrival time for drought definition "zero-crossover of yearly PDSI values."

Note: Mean drought interarrival time shown for (a) historical (1473 to 2005) and ensemble mean drought interarrival time shown for the projection period (2006 to 2099), (b) RCP4.5, and (c) RCP8.5.

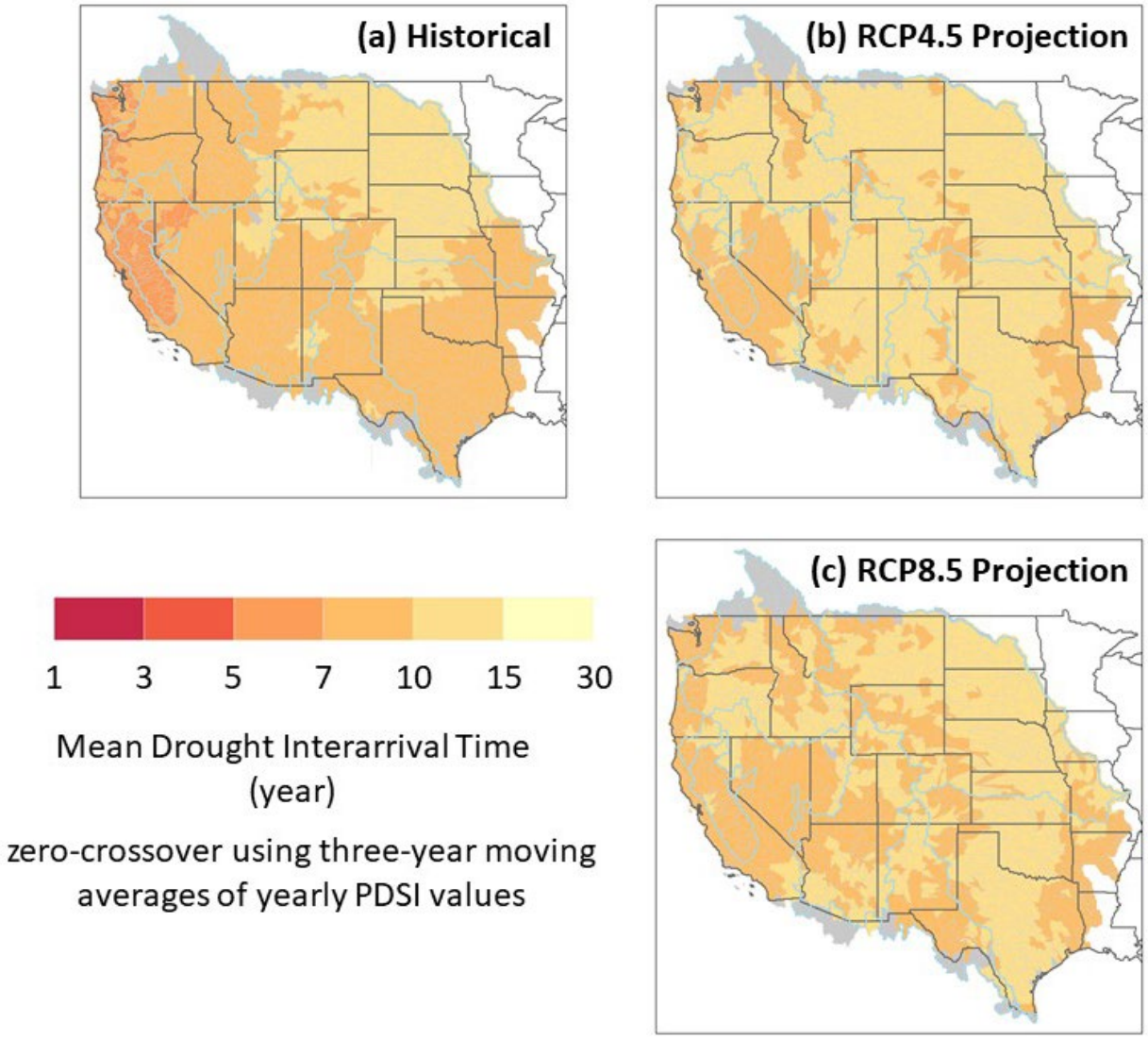

Figure 71. (a to c) Mean drought interarrival time for drought definition "zero-crossover using 3-year moving averages of yearly PDSI values."

Note: Mean drought interarrival time shown for (a) historical (1473 to 2005) and ensemble mean drought interarrival time shown for the projection period (2006 to 2099), (b) RCP4.5, and (c) RCP8.5.

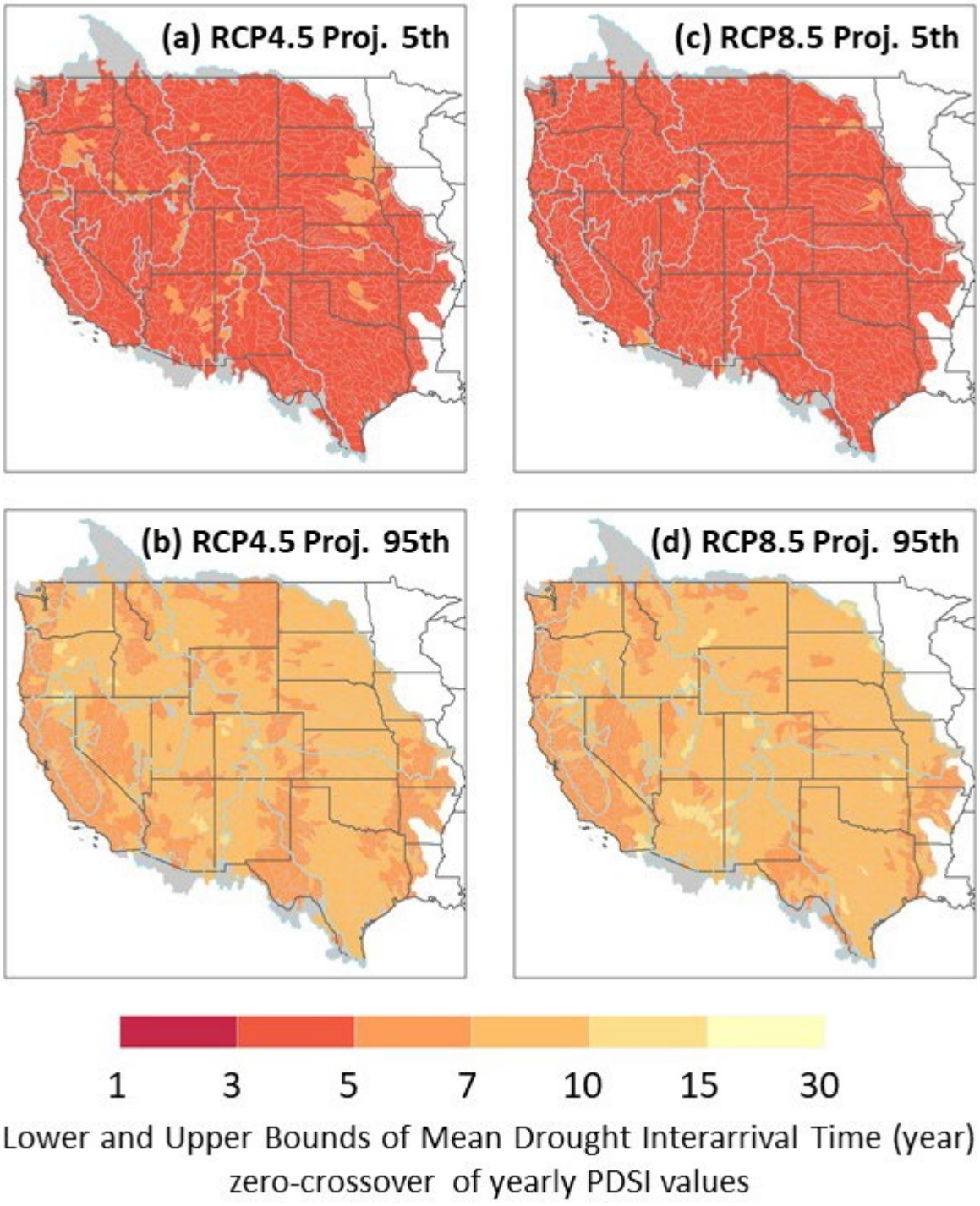

Figure 72. (a to d) Lower (5th percentile) and upper (95th percentile) bounds of mean drought interarrival time for drought definition "zero-crossover of yearly PDSI values."

Note: Left column plots – RCP4.5 projections, (a) lower bound (5th percentile) and (b) upper bound (95th percentile). Right column plots – RCP8.5 projections, (c) lower bound (5th percentile) and (d) upper bound (95th percentile).

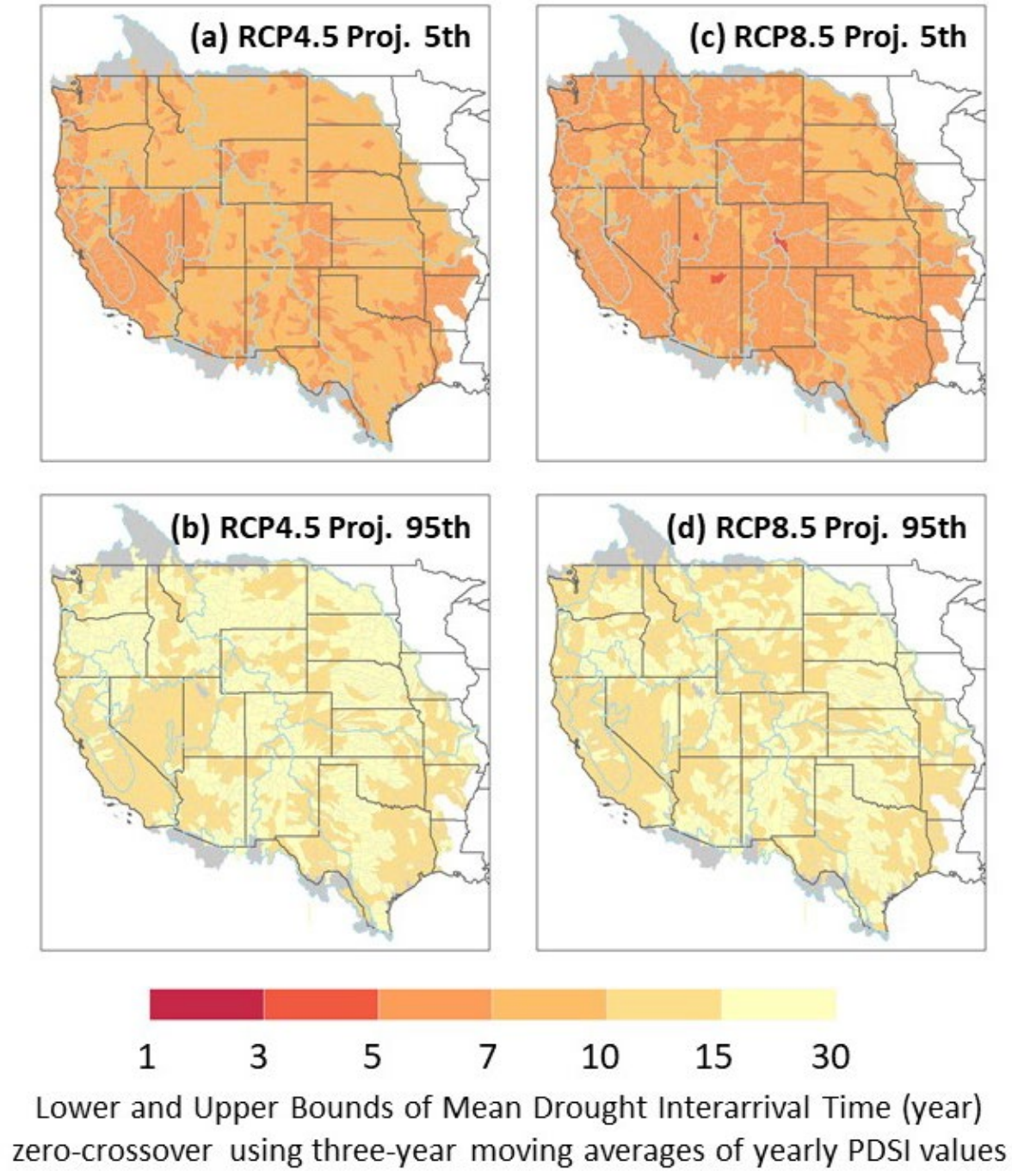

Figure 73. (a to d) Lower (5th percentile) and upper (95th percentile) bounds of drought interarrival time for drought definition "zero-crossover using 3-year moving averages of yearly PDSI values."

Note: Left column plots – RCP4.5 projections, (a) lower bound (5th percentile) and (b) upper bound (95th percentile). Right column plots – RCP8.5 projections, (c) lower bound (5th percentile) and (d) upper bound (95th percentile).

4.2.5 Joint Drought Return Periods

The marginal distributions of drought duration and drought severity (see Section 4.2.2) in conjunction with the joint distribution from the copula analysis (see Section 4.2.3) and the mean drought interarrival times (see Section 4.2.4) are used to develop return period estimates of selected drought events for the two drought definitions: (1) zero-crossover of yearly PDSI values, and (2) zero-crossover using 3-year moving averages of yearly PDSI values.

The methodology to calculate drought return periods is described in Shiau (2006) and Kwon and Lall (2016) and provides an application of the Shiau (2006) methodology to estimate drought return periods. The joint analysis of drought duration and drought severity as outlined in Shiau (2006)[14] provides two cases as follows:

The first case "*and"* (AND) case (Shiau, 2006; p. 810, equation 22), denotes the joint return period for drought duration (D) equaling or exceeding a specified drought duration threshold (d), i.e., $D \geq d$ ***and*** drought severity (S) equaling or exceeding a specified drought severity threshold (s), i.e., $S \geq s$.

The second case "*or"* (OR) case (Shiau, 2006; p. 810, equation 23), denotes the joint return period for drought duration (D) equaling or exceeding a specified drought duration threshold (d), i.e., $D \geq d$ ***or*** drought severity (S) equaling or exceeding a specified drought severity threshold (s), i.e., $S \geq s$.

From these formulations (Shiau, 2006), it is evident that the "*and"* case is a more extreme case of events over the "*or"* case. Thus, it is expected that the estimated drought return periods for the "*and"* case will be longer than those estimated for the "*or"* case.

Results using the Shiau (2006) methodology for selected droughts—i.e., events with specified drought durations (d) and severity (s) for the two drought definitions for the historical and projection periods—are discussed in Section 4.3.4. This approach allows comparison of changes in drought return periods between the historical and projection period of a given drought event and using a specific drought definition.

4.2.6 Regime Shift Analysis

The regime shift analysis conducted here follows the methodology published in Gangopadhyay and McCabe (2010)[15]. The GM10 methodology was first developed and applied to reconstructed streamflows in the Colorado River Basin at Lees Ferry. Application of the GM10 method to reconstructed streamflows at multiple sites across the West is documented in Gangopadhyay et al. (2019). Regime shift analysis provides an approach to develop decadal to multi-decadal outlooks for likelihoods of shift in the hydroclimate state of a system. It helps to answer questions, such as, if a basin has been under drought conditions for a certain period of time, what

[14] Refer to equations (22) and (23) in Shiau (2006), page 810.

[15] The publication Gangopadhyay and McCabe (2010) is abbreviated as GM10 hereafter in the report.

is the chance (probability) that it will shift to wetter conditions in the next 5, 10, or even 20 years?

PDSI values over the historical period, 1473 to 2005, were used to develop estimates of probabilities of regime shifts for the domain, 1,255 HUC-8s. Note that, this analysis also is valid not only for transitions from dry to wet, but also from wet to dry conditions for a given HUC-8.

To be consistent with the published GM10 method, the data used were from the first drought definition only (i.e., zero-crossover of yearly PDSI values) over the historical period of record, 1473 to 2005 (533 years). Projection period (2006 to 2099) PDSI data were not used in this analysis because the projection period is only 94 years long and is not long enough for this type of analysis. In particular, the projection period is not of sufficient length to capture low frequency components in the climate system that largely modulate regime shift behaviors (e.g., Gangopadhyay et al., 2019). Thus, only data for the historical period—PDSI values over the period 1473 to 2005 (533 years)—for the 1,255-HUC8s were used.

4.3 Results

4.3.1 Common Period (1950 to 2005) Analysis

Prior to analyzing changes in drought characteristics (duration, severity, and interarrival times of droughts), an evaluation of the performance of the climate models to simulate drought characteristics was performed for the common period (i.e., 1950 to 2005). Evaluating the performance of climate models to simulate drought characteristics is important for the interpretation of subsequent results. This analysis is based on droughts identified using "zero-crossover of yearly PDSI values" (refer to illustration shown in Figure 66a).

To perform this evaluation, plots of the spatial distributions of mean drought duration, mean drought severity, and mean drought interarrival time were developed. These drought characteristics were calculated for the 1950 to 2005 common period with two datasets—the Cook et al. (2010) PDSI time series (referred to as observations for the common period) and PDSI estimates developed from downscaled climate model projections of precipitation and temperature (referred to as simulations for the common period). The downscaled climate projections of precipitation and temperature from LOCA are identical over this common period for RCP4.5 and RCP8.5. As the precipitation and temperature projections are identical, only one set of 32 projections (recall, the total number of projections from LOCA is 64, which includes 32 for RCP4.5 and 32 for RCP8.5) was necessary for the common period analyses.

Next, a set of statistics is presented to compare the drought characteristics between observed and simulated values for the domain (1,255 HUC-8s), analyze bias, and consider performance across selected HUC-8s in the domain (see Figure 65 and Table 11). An evaluation of these three drought characteristics is discussed in the following sub-sections.

4.3.1.1 Mean Drought Duration

Figure 74 shows the spatial distribution of mean drought duration. For each HUC-8, the mean duration was calculated as the average of all the individual drought events that occurred for the given HUC-8 over the period 1950 to 2005. Figure 74a shows the distribution of observed mean drought duration, and Figure 74b shows the simulated mean drought duration from the climate model simulations (total, 32 projections). Note that, in the case of the climate model simulations, the mean drought duration is an ensemble mean of this statistic calculated in each case from the respective climate model projections. From Figure 74a, the observed mean drought duration for the study domain approximately ranges between 1.4 and 3.8 years, and the simulated mean (ensemble mean; Figure 74b) drought duration calculated from the climate projections approximately ranges between 2.1 and 3.8 years.

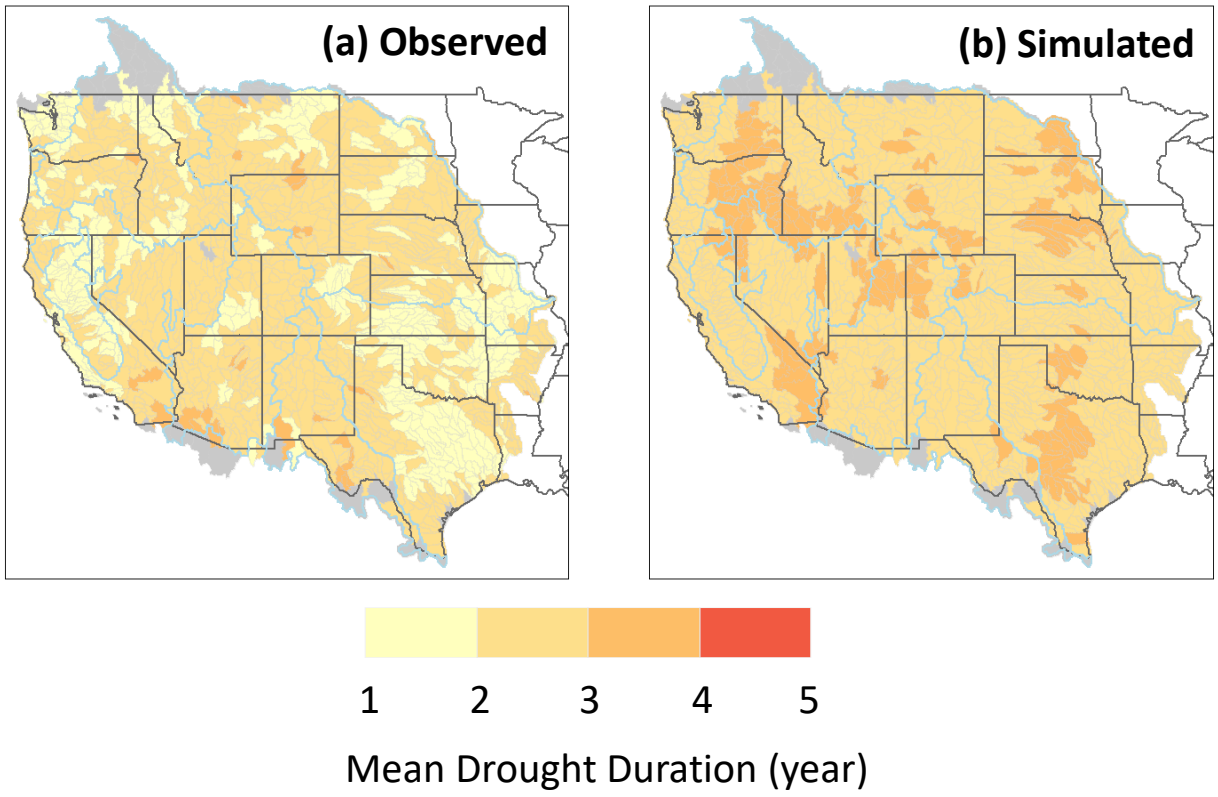

Figure 74. Mean drought duration for (a) observed and (b) climate model simulations during 1950 to 2005.

Note: Mean drought duration shown for the common period (1950 to 2005) for (a) observed, (b) simulations from climate models.

Figure 75a provides an overview summary for this statistic. The boxplots compare the distribution of mean drought duration across the 1,255 HUC-8s for the observations and climate model simulations. The median of the mean drought duration estimated for the observed is about 2.14 years, and the median of the ensemble mean from the climate model simulations is about 2.75 years. These median values present an overall comparison of the mean drought duration statistics for the study domain.

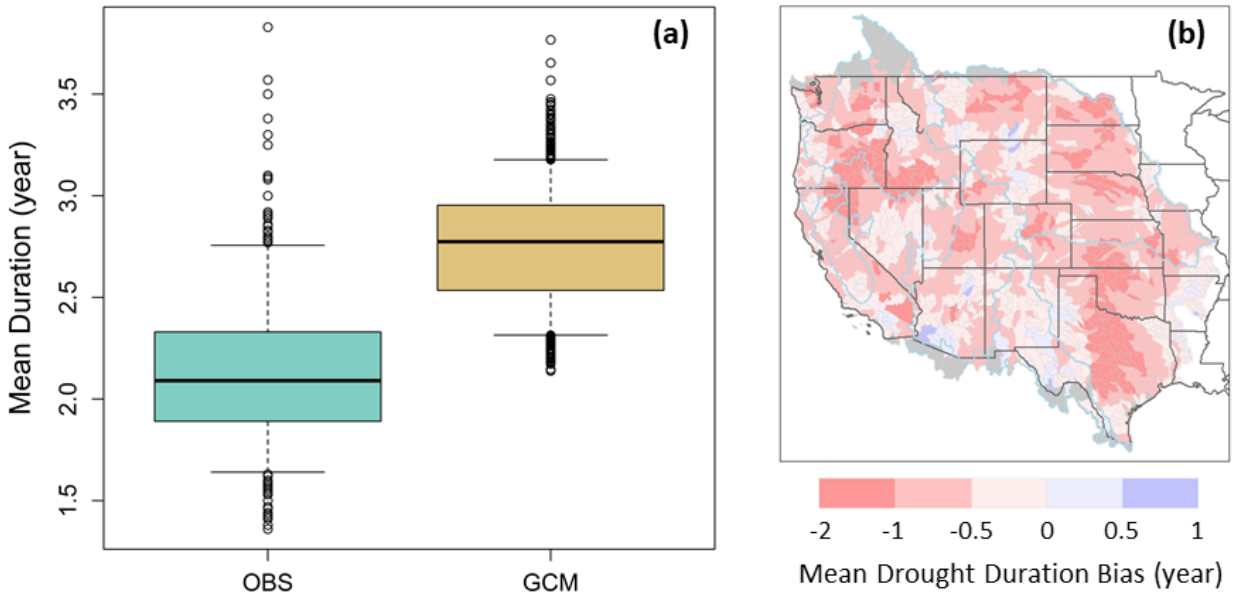

Figure 75. (a) Distribution and (b) bias of mean drought duration for observed and climate model simulations during 1950 to 2005.

Note: Mean drought duration, (a) boxplot of observed and GCM simulations, (b) spatial distribution of bias—see text for description.

The climate model simulations show somewhat greater drought durations for the study domain over the observations—the GCM boxplot is positioned higher than the observed boxplot of mean drought duration (Figure 75a). Though the boxplots provide an overall comparison of the performance of the climate model simulations, the bias—defined here as the difference between the observed estimate and the simulated estimate—specifically, observed mean drought duration minus simulated ensemble mean drought duration, is spatially distributed. The spatial distribution of mean drought duration bias for each of the 1,255 HUC-8s is shown in Figure 75b.

A negative bias value for a given HUC-8 means that the simulated drought duration is greater than the observed drought duration for that HUC-8. Nearly 94 percent of the domain show that the simulated mean (ensemble mean) drought duration is greater than the observed mean drought duration, and distribution of the bias is spatially heterogeneous. To further explore this spatial distribution of bias, it is illustrated using selected HUC-8s—one HUC-8 in each of the eight major Reclamation river basins (see Figure 65 and Table 11). Figure 76 shows results as a set of box and whisker plots (boxplots) of mean drought duration for these selected HUC-8s.

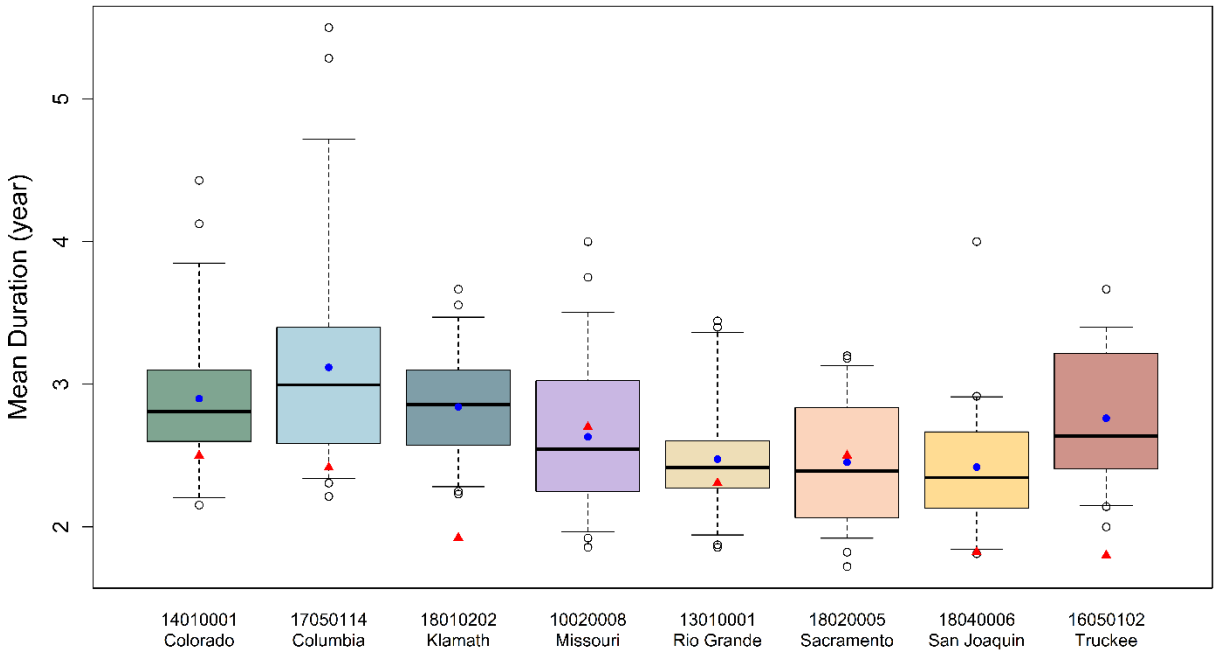

Figure 76. Boxplots of mean drought duration from climate model simulations and ensemble mean for climate model simulations and observed mean drought durations for selected HUC-8s.

Note: The box in the box and whisker plots (boxplots) correspond to the 25th percentile (lower edge of the box) and 75th percentile (upper edge of the box) of the mean drought duration from climate model simulations during 1950 to 2005. The horizontal solid line in the box is the median (50th percentile) value and the lower and upper whiskers respectively extend to the 5th and 95th percentile values. Outliers are shown with open circles. The ensemble mean drought durations from climate model simulations are shown with blue filled circles. Observed mean drought durations during 1950 to 2005 are shown with red filled triangles.

The boxplot for each HUC-8 shows the distribution of mean drought duration from the 32 climate model projections and demonstrates the range of simulated mean drought duration magnitudes from the climate models. The ensemble mean from this set of projections is shown with a blue filled circle, and the observed mean drought duration during 1950 to 2005 is shown with a red filled triangle. As an example, for the Colorado River Basin HUC-8, the ensemble mean drought duration is about 2.9 years, and the observed mean drought duration is about 2.5 years. Thus, the observed drought duration is somewhat lower (0.4 year) than the ensemble mean estimated from the climate model simulations. This comparison indicates that the model simulations are biased high in the example of the Colorado River Basin HUC-8. Table 16 provides a listing of the observed and simulated mean drought duration for the selected HUC-8s shown in Figure 76.

Table 16. Observed and simulated mean drought duration for the selected HUC-8s in the eight Reclamation river basins

River Basin	Mean Drought Duration (year)		
	Observed	Simulated	Bias
Colorado	2.50	2.90	-0.40
Columbia	2.42	3.12	-0.70
Klamath	1.92	2.84	-0.92
Missouri	2.70	2.63	0.07
Rio Grande	2.31	2.47	-0.16
Sacramento	2.50	2.45	0.05
San Joaquin	1.82	2.42	-0.60
Truckee	1.80	2.76	-0.96

For most of the river basins (selected HUC-8s) listed in Table 16, the observed drought duration is lower than the ensemble mean estimated from the climate model simulations. This indicates that the model simulations are biased high (longer drought duration than observed). This is largely the case for the study domain and the bias (observed mean drought duration minus simulated ensemble mean drought duration) ranges between -1.68 to 0.62 years (see Figure 75b). Negative bias values imply that the simulated drought duration is greater than the observed drought duration—climate model simulations are biased high.

4.3.1.2 Mean Drought Severity

Figure 77 shows the spatial distribution of mean drought severity. For each HUC-8, the mean severity was calculated as the average PDSI of all the individual drought events that occurred for the given HUC-8 over the period 1950 to 2005. Figure 77a shows the distribution of observed mean drought severity, and Figure 77b shows the simulated mean drought severity from the climate model projections (total, 32 projections). Note that, in the case of the climate model simulations, the mean drought severity is an ensemble mean of this statistic calculated in each case from the respective climate model projections. From Figure 77a, the observed mean drought duration for the study domain approximately ranges between PDSI values of -0.8 and -2.5, and the simulated mean (ensemble mean; Figure 77b) drought severity calculated from the climate projections approximately ranges between PDSI values of -1.2 and -2.5.

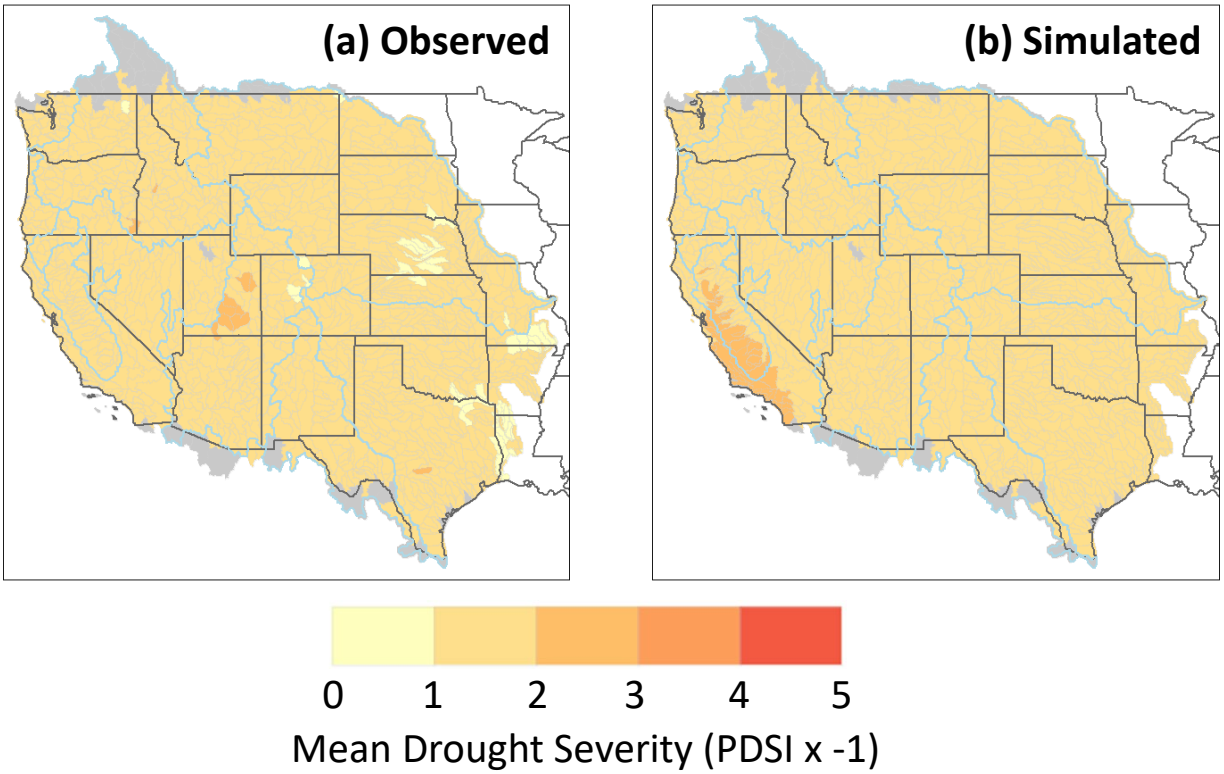

Figure 77. Mean drought severity for (a) observed and (b) climate model simulations during 1950 to 2005.

Note: Mean drought severity shown for the common period (1950 to 2005) for (a) observed, (b) simulations from climate models.

Figure 78a provides an overview summary for this statistic. The boxplots compare the distribution of mean drought severity across the 1,255 HUC-8s for the observations and climate model simulations. The median of the mean drought severity estimated for the observed is a PDSI value of about -1.42, and the median of the ensemble mean from the climate model simulations is a PDSI value of about -1.62. These median values present an overall comparison of the mean drought duration statistics for the study domain.

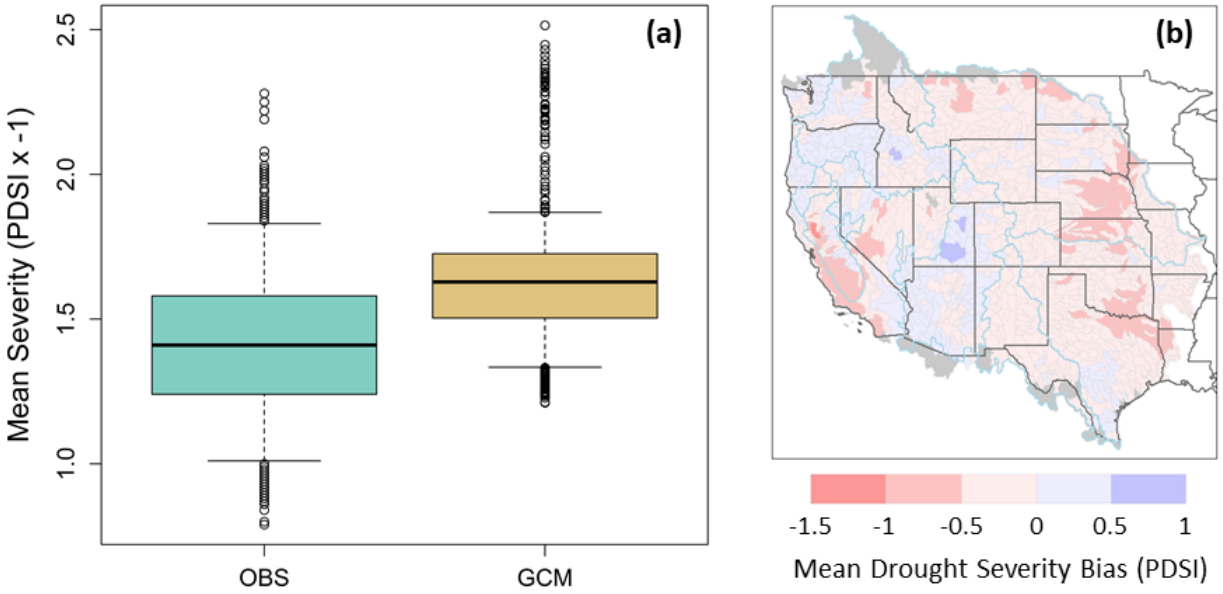

Figure 78. (a) Distribution and (b) bias of mean drought severity for observed and climate model simulations during 1950 to 2005.

Note: Mean drought severity, (a) boxplot of observed and GCM simulations, (b) spatial distribution of bias—see text for description.

The climate model simulations show nominally greater drought severity for the domain over the observations (Figure 78a). Though the boxplots provide an overall comparison of the performance of the climate model simulations, the bias—defined here as the difference between the observed estimate and the simulated estimate—specifically, absolute value of observed mean drought severity minus absolute value of simulated ensemble mean drought severity, is spatially distributed. Since higher negative values of PDSI imply greater drought severity, absolute PDSI values were used to calculate drought severity bias—to aid in the interpretation of results in the following discussions.

The spatial distribution of mean drought severity bias for each of the 1,255 HUC-8s is shown in Figure 78b. A negative bias value for a given HUC-8 means that the simulated drought severity is greater than the observed drought severity for that HUC-8. Nearly 76 percent of the domain show that the simulated mean (ensemble mean) drought severity is greater than the observed mean drought severity, and distribution of the bias is spatially heterogeneous. To further explore this spatial distribution of bias, it is illustrated using selected HUC-8s—one HUC-8 in each of the eight major Reclamation river basins (see Figure 65 and Table 11). Figure 79 shows results as a set of box and whisker plots (boxplots) of mean drought severity for these selected HUC-8s.

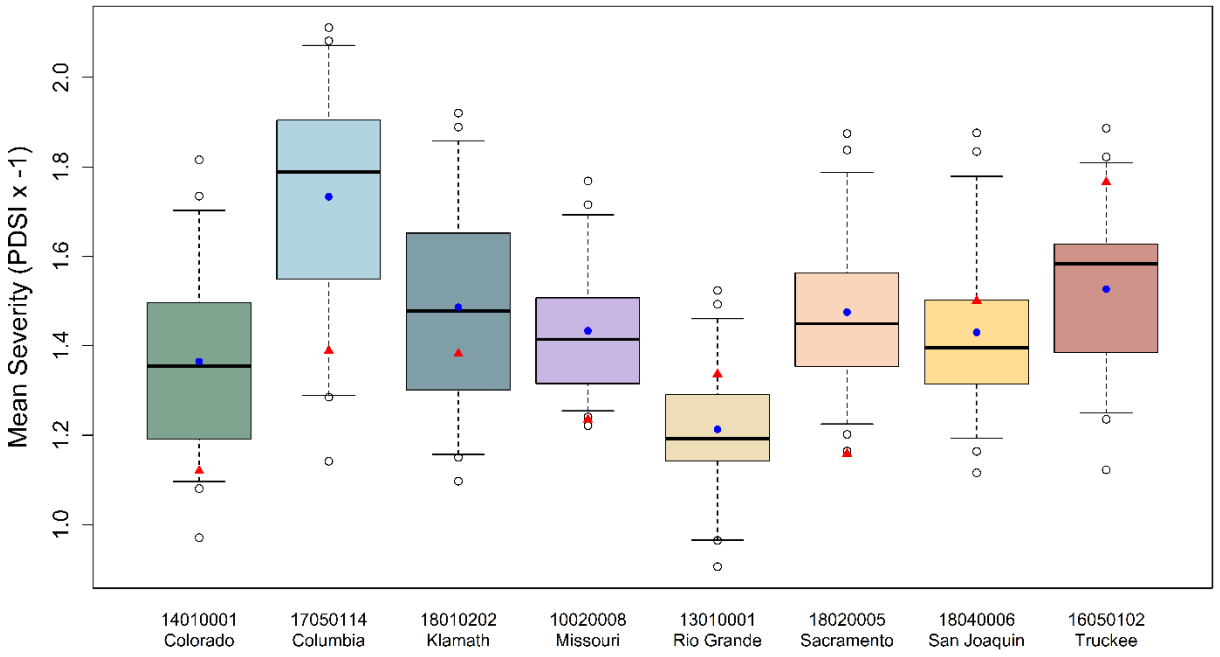

Figure 79. Boxplots of mean drought severity from climate model simulations and ensemble mean from climate model simulations and observed mean drought severity for selected HUC-8s.

Note: The box in the box and whisker plots (boxplots) correspond to the 25th percentile (lower edge of the box) and 75th percentile (upper edge of the box) of the mean drought severity from climate model simulations during 1950 to 2005. The horizontal solid line in the box is the median (50th percentile) value and the lower and upper whiskers respectively extend to the 5th and 95th percentile values. Outliers are shown with open circles. The ensemble mean drought severity from climate model simulations are shown with blue filled circles. Observed mean drought severity during 1950 to 2005 are shown with red filled triangles.

The boxplot for each HUC-8 shows the distribution of mean drought severity from the 32 climate model projections and demonstrates the range of simulated mean drought severity magnitudes from the climate models. The ensemble mean from this set of projections is shown with a blue filled circle, and the observed mean drought severity during 1950 to 2005 is shown with a red filled triangle. As an example, for the Colorado River Basin HUC-8, the ensemble mean drought severity has a PDSI value of -1.36, and the observed mean drought severity has a PDSI value of -1.12. Thus, the observed drought severity is somewhat lower (absolute magnitude difference in PDSI, 0.24) than the ensemble mean estimated from the climate model simulations. This comparison indicates that the model simulations are biased high in the example of the Colorado River Basin HUC-8, i.e., simulated drought severity is greater than the observed drought severity. Table 17 provides a listing of the observed and simulated mean drought severity for the selected HUC-8s shown in Figure 79.

Table 17. Observed and simulated mean drought severity for the selected HUC-8s in the eight Reclamation river basins

River Basin	Mean Drought Severity (PDSI)		
	Observed	Simulated	Bias*
Colorado	-1.12	-1.36	-0.24
Columbia	-1.39	-1.73	-0.34
Klamath	-1.38	-1.49	-0.11
Missouri	-1.24	-1.43	-0.19
Rio Grande	-1.34	-1.21	0.13
Sacramento	-1.16	-1.48	-0.32
San Joaquin	-1.50	-1.43	0.07
Truckee	-1.77	-1.53	0.24

* Note: Bias is calculated as the absolute value of observed mean drought severity minus absolute value of simulated ensemble mean drought severity.

For most of the river basins (selected HUC-8s) listed in Table 17, the observed drought severity is lower than the ensemble mean estimated from the climate model simulations—indicating that the model simulations are biased high (drier than observed). This is largely the case for the study domain, and the bias (absolute value of observed mean drought severity minus absolute value of simulated ensemble mean drought severity) ranges between PDSI values of -1.03 and 0.73 (see Figure 78b). Negative bias values imply that the simulated drought severity is greater than the observed drought severity. However, because the range of the bias is essentially within one PDSI category increment (e.g., Palmer, 1965), the climate model simulations and the observed values practically indicate the same drought conditions.

4.3.1.3 Mean Drought Interarrival Time

Figure 80 shows the spatial distribution of mean drought interarrival time. For each HUC-8, the mean drought interarrival time was calculated as the average of all (less one[16]) of the individual drought event interarrival times that occurred for the given HUC-8 over the period 1950 to 2005. Figure 80a shows the distribution of observed mean drought interarrival time, and Figure 80b shows the simulated mean drought interarrival time from the climate model projections (total, 32 projections). Note that, in the case of the climate model simulations, the mean drought interarrival time is an ensemble mean of this statistic calculated in each case from the respective climate model projections. From Figure 80a, the observed mean drought interarrival time for the study domain approximately ranges between 2.8 and 9.6 years, and the simulated mean (ensemble mean; Figure 80b) drought interarrival time calculated from the climate projections approximately ranges between 4 and 6.5 years.

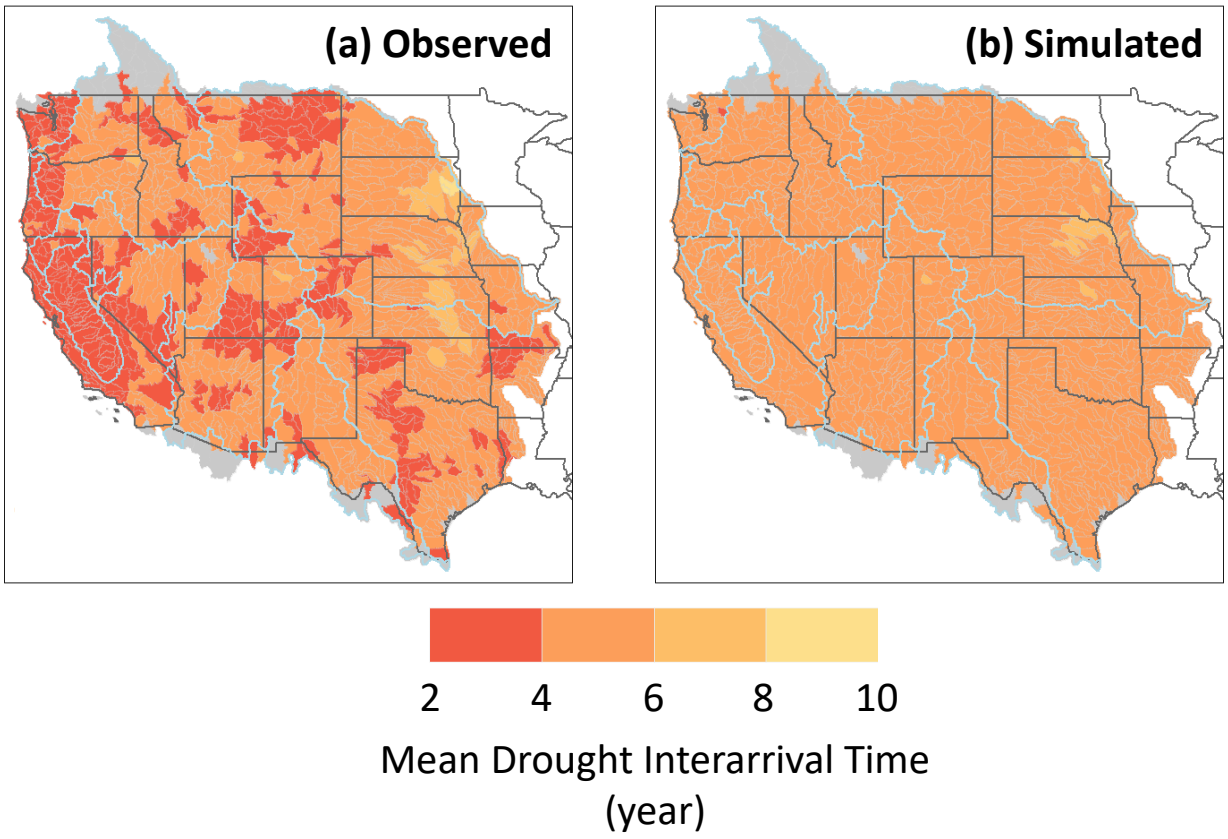

Figure 80. Mean drought interarrival time for (a) observed and (b) climate model simulations during 1950 to 2005.

Note: Mean drought interarrival time shown for the common period (1950 to 2005) for (a) observed, (b) simulations from climate models.

[16] Since the interarrival time measures the time between the start of two successive drought events (see Figure 67), the number of events used in averaging is the total number of drought events minus one.

Figure 81a provides an overview summary for this statistic. The boxplots compare the distribution of mean drought interarrival time across the 1,255 HUC-8s for the observations and climate model simulations. The median of the mean drought duration estimated for the observed is about 4.39 years, and the median of the ensemble mean from the climate model simulations is about 4.93 years. These median values present an overall comparison of the mean drought interarrival time statistics for the study domain.

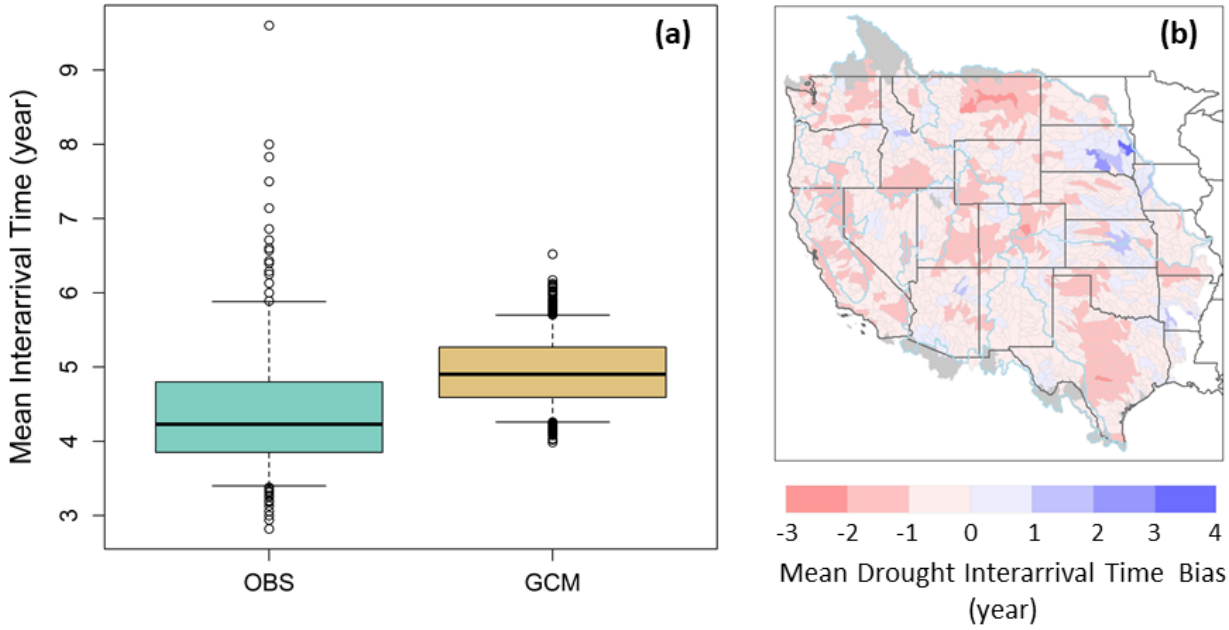

Figure 81. (a) Distribution and (b) bias of mean drought interarrival time for observed and climate model simulations during 1950 to 2005.

Note: Mean drought interarrival time, (a) boxplot of observed and GCM simulations, (b) spatial distribution of bias—see text for description.

The climate model simulations show somewhat greater drought interarrival for the study domain over the observations—the GCM boxplot is positioned higher than the observed boxplot of mean drought interarrival time (Figure 81a). Though the boxplots provide an overall comparison of the performance of the climate model simulations, the bias—defined here as the difference between the observed estimate and the simulated estimate—specifically, observed mean drought interarrival time minus simulated ensemble mean drought interarrival time, is spatially distributed. The spatial distribution of mean drought interarrival time bias for each of the 1,255 HUC-8s is shown in Figure 81b.

A negative bias value for a given HUC-8 means that the simulated drought interarrival time is greater than the observed drought interarrival time for that HUC-8. Nearly 82 percent of the domain show that the simulated mean (ensemble mean) drought interarrival time is greater than the observed mean drought interarrival time, and distribution of the bias is spatially heterogeneous. To further explore this spatial distribution of bias, it is illustrated using selected HUC-8s—one HUC-8 in each of the eight major Reclamation river basins (see Figure 65 and

Table 11). Figure 82 shows results as a set of box and whisker plots (boxplots) of mean drought interarrival time for these selected HUC-8s.

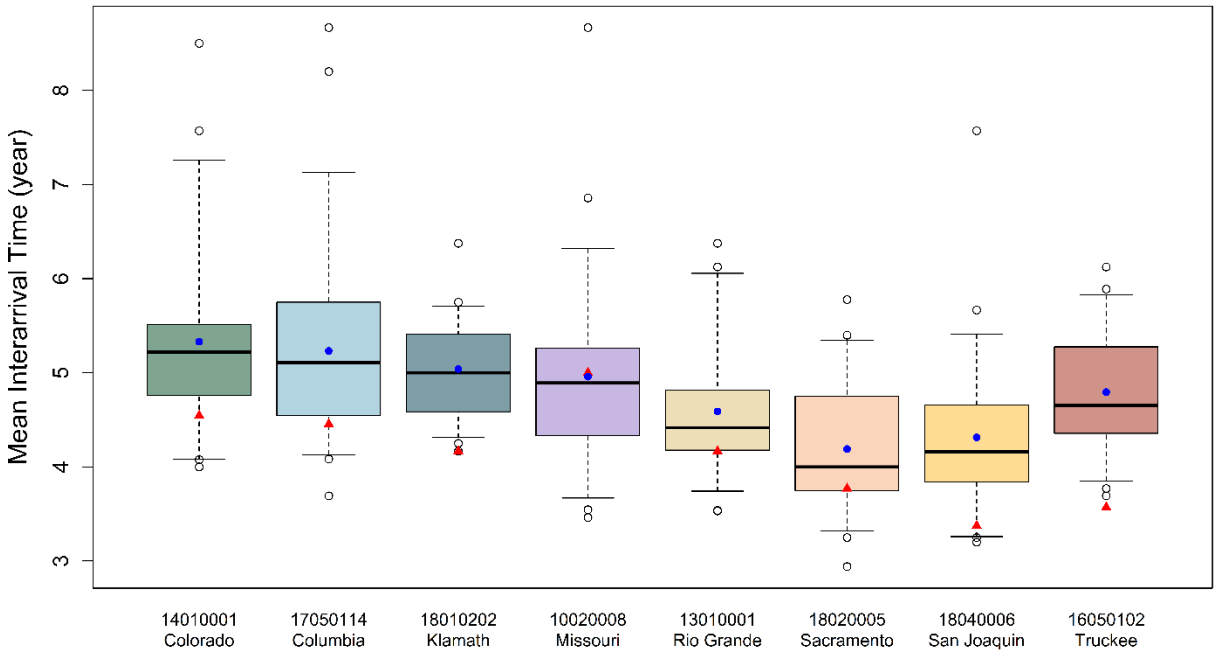

Figure 82. Boxplots of mean drought interarrival time from climate model simulations and ensemble means from climate model simulations and observed means for selected HUC-8s.

Note: The box in the box and whisker plots (boxplots) correspond to the 25th percentile (lower edge of the box) and 75th percentile (upper edge of the box) of the mean drought interarrival time from the climate model simulations during 1950 to 2005. The horizontal solid line in the box is the median (50th percentile) value and the lower and upper whiskers respectively extend to the 5th and 95th percentile values. Outliers are shown with open circles. The ensemble mean drought interarrival time from climate model simulations are shown with blue filled circles. Observed mean drought interarrival time during 1950 to 2005 are shown with red filled triangles.

The boxplot for each HUC-8 shows the distribution of mean drought interarrival time from the 32 climate model projections and demonstrates the range of simulated mean drought interarrival time magnitudes from the climate models. The ensemble mean from this set of projections is shown with a blue filled circle, and the observed mean drought severity during 1950 to 2005 is shown with a red filled triangle. As an example, for the Colorado River Basin HUC-8, the ensemble mean drought interarrival time has a value of 5.33 years, and the observed mean drought interarrival time has a value of 4.55 years. Thus, the observed drought interarrival time is somewhat lower (0.78 year) than the ensemble mean estimated from the climate model simulations. This comparison indicates that the model simulations are biased high in the example of the Colorado River Basin HUC-8 (i.e., simulated drought interarrival time is greater than the observed drought interarrival time). Table 18 provides a listing of the observed and simulated mean drought interarrival time for the selected HUC-8s shown in Figure 82.

Table 18. Observed and simulated mean drought interarrival time for the selected HUC-8s in the eight Reclamation river basins

River Basin	Mean Drought Interarrival Time (year)		
	Observed	Simulated	Bias
Colorado	4.55	5.33	-0.78
Columbia	4.45	5.23	-0.78
Klamath	4.17	5.04	-0.87
Missouri	5.00	4.96	0.04
Rio Grande	4.17	4.59	-0.42
Sacramento	3.77	4.19	-0.42
San Joaquin	3.38	4.31	-0.93
Truckee	3.57	4.80	-1.23

For most of the river basins (selected HUC-8s) listed in Table 18, the observed drought interarrival time is lower than the ensemble mean estimated from the climate model simulations. This indicates that the model simulations are biased high (longer drought interarrival times). This is largely the case for the study domain and the bias (observed mean drought interarrival time minus simulated ensemble mean drought interarrival time) ranges between values of -2.20 and 3.61 years (see Figure 81b). Negative bias values imply that the simulated drought interarrival time is greater than the observed drought interarrival time—climate model simulations are biased high.

In summary, the climate model simulations generally have a somewhat dry bias—drought severity drier than observed, longer drought duration than observed coupled with longer drought interarrival times (the time between the start of two successive drought events) implying shorter wet spells. Furthermore, in an analysis such as this, it is typical to see regional bias signatures for drought characteristics (refer to Figure 75b, Figure 78b, and Figure 81b). Nevertheless, the climate model simulated drought characteristics over the common period (1950 to 2005) largely show that climate models encompass the observed drought characteristics and provide comparable results (summarized in Table 19). Based on these findings, it is concluded that the climate model simulations are useful for the study of droughts under future conditions across the Western United States.

Table 19. Summary of observed and climate model simulated drought characteristics for the study domain in the common period, 1950 to 2005

Drought Characteristic	Study Domain Median Value	
	Observed Mean	Simulated Ensemble Mean
Duration (year)	2.14	2.75
Severity (PDSI)	-1.42	-1.62
Interarrival Time (year)	4.39	4.93

Analysis of changes in drought duration and drought severity between the full historical period (1473 to 2005) and the projection period (2006 to 2099) are presented in the next two sub-sections (duration, Section 4.3.2; severity, Section 4.3.3). Changes to select drought event return periods, which involves mean drought interarrival times, is presented in Section 4.3.4.

4.3.2 Changes in Drought Duration

Changes in mean drought duration and variability of drought duration are analyzed between the historical period (1473 to 2005) and the projection period (2006 to 2099) using the first drought definition of "zero-crossover of yearly PDSI values." The historical mean drought duration for each HUC-8 was calculated using all the drought events identified over the 1473 to 2005 period. The mean drought duration for the study domain (1,255 HUC-8s) is shown in Figure 83a. Over the historical period, most of the domain show a mean drought duration between 2 to 3 years. For the coastal regions, the mean drought duration is between 1 to 2 years. In portions of the Missouri River Basin, longer droughts with mean duration between 3 to 4 years is seen. Note that these are mean drought durations and provide an estimate of the average drought lengths (duration) for the domain. It is of interest to know the maximum drought duration for the domain as well.

The maximum drought duration for a given HUC-8 was first calculated as the maximum drought duration length from all the drought events that occurred during 1473 to 2005 for each HUC-8. The range of maximum drought durations for the domain was calculated to be between 5 and 20 years during the historical period. Droughts of decadal and longer durations in the Western United States are well documented in the paleohydrology literature (e.g., Woodhouse et al., 2010) and this analysis includes droughts from the historical data (starting in 1473) used in many of the paleohydrology analyses.

For the projection period, 2006 to 2099, mean drought durations are shown for the two sets of climate model runs—RCP4.5 (Figure 83b) and RCP8.5 (Figure 83d). Results from both RCPs show an increase in mean drought duration consistently throughout the domain with RCP8.5 models projecting more increases in drought duration than the RCP4.5 models.

In the case of the RCP4.5 projections (Figure 83b), most of the domain shows a mean drought duration between 3 to 4 years (compared to 1 to 2 years for the historical period) with some regions showing an increase in mean drought duration varying between 4 to 5 and 5 to 6 years. These regional changes are notable in portions of the Colorado, Rio Grande, Columbia, and Missouri River Basins. For the RCP8.5 projections (Figure 83d), most of the domain shows a mean drought duration between 4 to 5 years, which is 1 to 2 years longer than mean drought duration for the historical period. More areas of the domain show droughts with mean duration between 5 to 6 years and even between 6 to 7 years under RCP8.5.

Figure 83c and Figure 83e show the changes in mean drought duration from the historical period for the RCP4.5 and RCP8.5 projections, respectively. A positive change (shown as percentage [%] change) implies an increase in mean drought duration length from the historical period, and a negative value implies a decrease in mean drought duration length from the historical period. The changes in mean drought duration in the domain are overwhelmingly positive for both of the RCPs and suggests an increase in mean drought duration for the projection period (2006 to 2099) compared with the historical period (1473 to 2005). Overall, the RCP8.5 changes are greater than the changes projected by the RCP4.5 models. The changes are most prominent for portions of the Colorado, Rio Grande, Columbia, and Klamath River Basins.

This discussion of changes in mean drought duration broadly shows an increase in mean drought duration across the Western United States with varying degrees depending on a given climate model and region in the study domain. An increase or positive shift in the mean of a distribution also is associated with an increase in the maximum drought duration. For the historical period, the range of maximum drought duration for the domain was calculated to be between 5 and 20 years; the range for RCP4.5 projections was calculated to be between 11 and 57 years, and between 19 and 74 years for RCP8.5 projections.

Along with an understanding of how mean drought duration may change in the future, it is important to understand the changes in the variability of drought duration. Variability in drought duration is described using the standard deviation of drought durations. Higher values of standard deviation imply a greater variability.

During the historical period (Figure 84a), for most of the study domain the standard deviation of drought duration ranged between 1 to 2 years. For portions of the Colorado and Rio Grande River Basins, the variability in drought duration ranged between 2 to 3 years. The Missouri River Basin showed a wider range, with some portions of the basin indicating a standard deviation between 3 to 5 years. Both the projections, RCP4.5 (Figure 84b) and RCP8.5 (Figure 84d), show an increase in the variability of drought duration, with the RCP8.5 projections showing larger increases in variability than the RCP4.5 projections. For the RCP4.5 projections, the majority of the domain shows a standard deviation of drought duration between 3 to 5 years, whereas the RCP8.5 projections indicate a substantial portion of the domain with standard deviations in drought duration of 5 to 8 years. Figure 84c and Figure 84e show the changes from the historical in the standard deviation of drought duration for RCP4.5 and RCP8.5 projections, respectively.

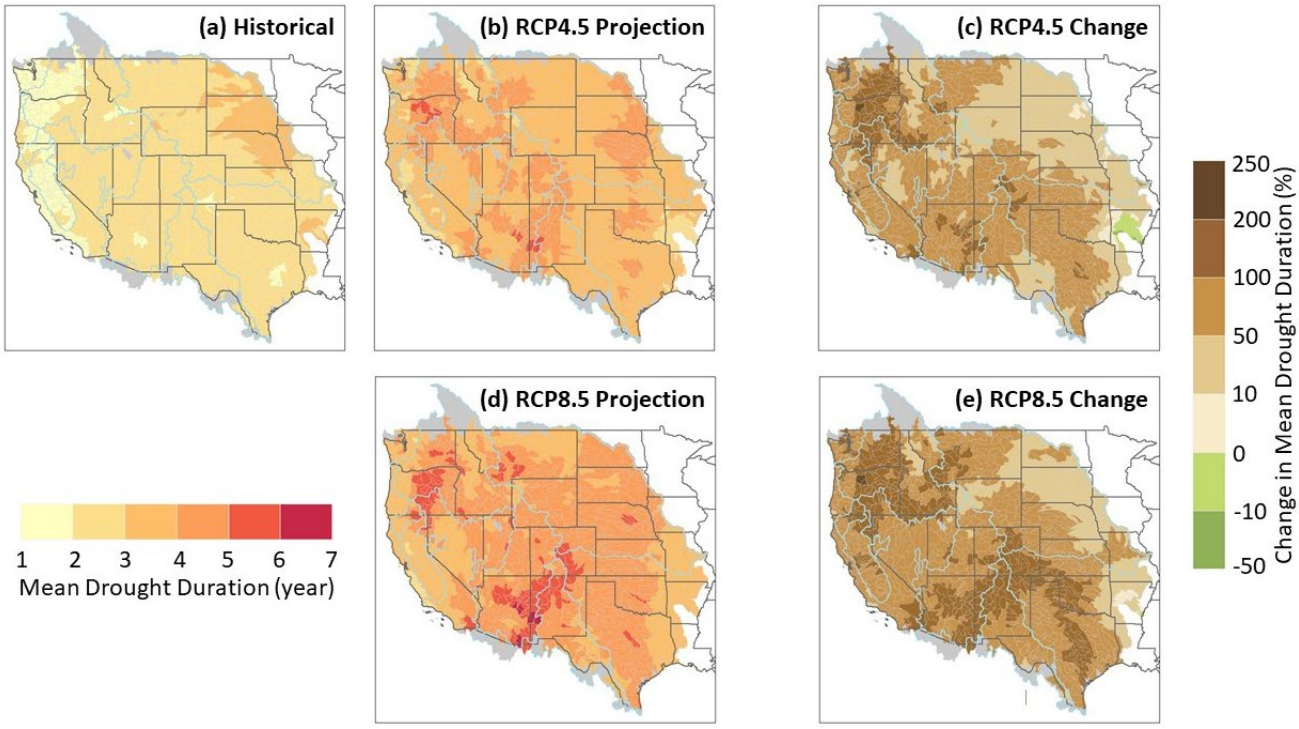

Figure 83. Mean drought duration for (a) historical (1473 to 2005), (b and d) climate model simulations (2006 to 2099), (c and e) and projected changes.

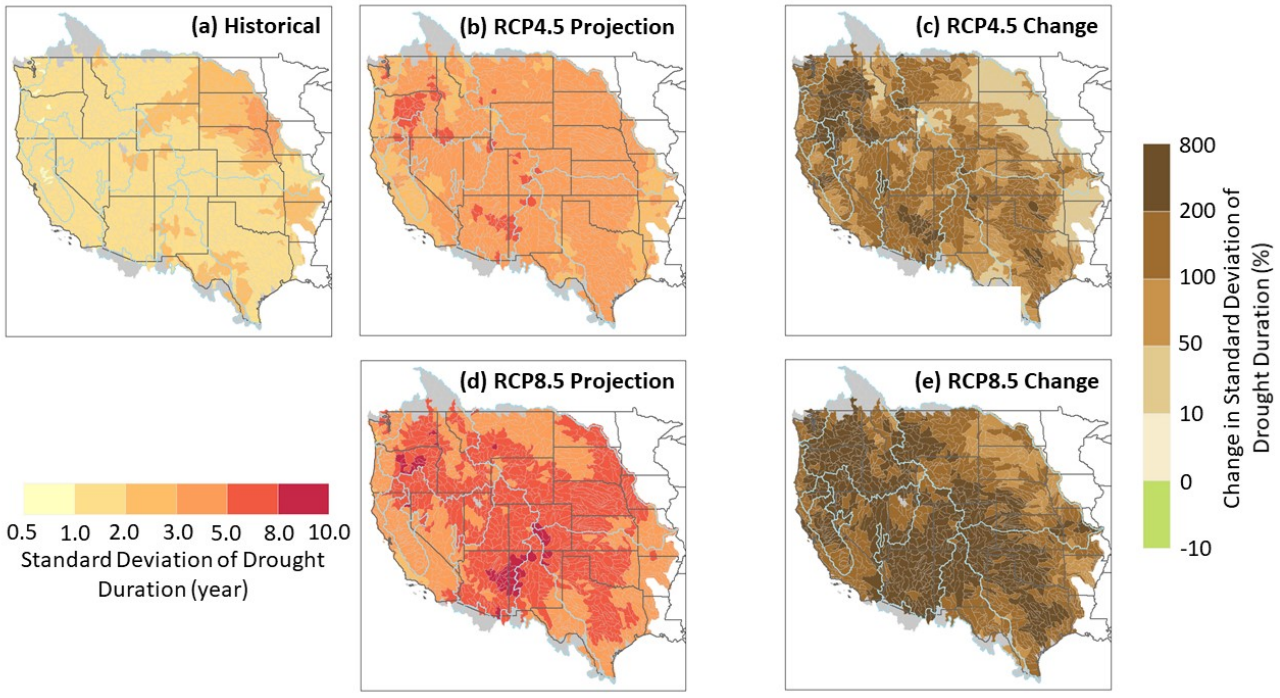

Figure 84. Standard deviation of drought duration for (a) historical (1473 to 2005), (b and d) climate model simulations (2006 to 2099), and (c and e) projected changes.

4.3.3 Changes in Drought Severity

Changes in mean drought severity and variability of drought severity also is analyzed between the historical period (1473 to 2005) and the projection period (2006 to 2099) using the first drought definition of "zero-crossover of yearly PDSI values."

The historical mean drought severity (i.e., mean PDSI for a drought) for each HUC-8 was calculated using all the drought events identified over the 1473 to 2005 period. The mean drought severity for the study domain (1,255 HUC-8s) is shown in Figure 85a. Over the historical period, all of the domain uniformly shows a mean drought severity with PDSI values between -1 to -2, or mild to moderate drought severities. However, the maximum drought severity PDSI values over the historical period range between -2.4 and -9.4, implying that some mean drought severities varied from moderate to extreme severity.

For the projection period, 2006 to 2099, mean drought severity values are shown for the two sets of climate model runs—RCP4.5 (Figure 85b) and RCP8.5 (Figure 85d). Results for both of the RCPs show an increase in mean drought severity in portions of the domain. It is interesting to note that the mean drought severity for both RCP4.5 and RCP8.5 show similar distributions that point to increases in water-limited conditions in the future. Mean drought severity under both RCP4.5 and RCP8.5 projections show an increase in drought severity from the historical period with PDSI values ranging from -2 to -3, or moderate to severe droughts. The increase in drought severity is seen mostly for the High Plains, Central Valley, and the Great Basin regions.

Figure 85c and Figure 85e show the changes in mean drought severity for the RCP4.5 and RCP8.5 projections, respectively. A positive value (shown as a percentage change) implies an increase in mean drought severity from the historical period, and a negative value implies a decrease in drought severity. The changes in mean drought severity in the domain are overwhelmingly positive for both RCPs and suggests an increase in mean drought severity for the projection period (2006 to 2099) from the historical period (1473 to 2005). The maximum drought severity for both RCPs indicate a range of PDSI values from -3.6 to -9.0, which indicates severe to extreme drought severity. Thus, at the lower end, the maximum severity is projected to increase from moderate (historical PDSI value, -2.4) to severe (projected PDSI value, about -3.6) droughts.

During the historical period (Figure 86a), for most of the study domain the standard deviation of PDSI ranges between -0.75 and -1.00[17]. Higher standard deviation values are seen in some regions of the domain, such as the Central Valley of California, portions of the Columbia River Basin, and in sections of Kansas, Oklahoma, and Texas. Both projections, RCP4.5 (Figure 86b) and RCP8.5 (Figure 86d), generally show an increase in variability (higher standard deviation values). The increases in the variability of drought severity are generally larger for the RCP8.5 projections than for the RCP4.5 projections; however, there are some portions of the domain where variability decreases for both RCP projections (e.g., areas around northern California)

[17] Standard deviation by definition is a positive value and always represented using the same unit as the variable being analyzed. Note, drought severity is represented using negative PDSI values, and hence the negative PDSI range for standard deviation is presented here.

(Figure 86c and Figure 86e). The areas around northern California under both sets of projections are showing a decrease in variability and the conditions may likely be further exacerbated with an increase in mean drought severity (see Figure 85c and Figure 85e), likely suggesting persistent drought conditions for the region.

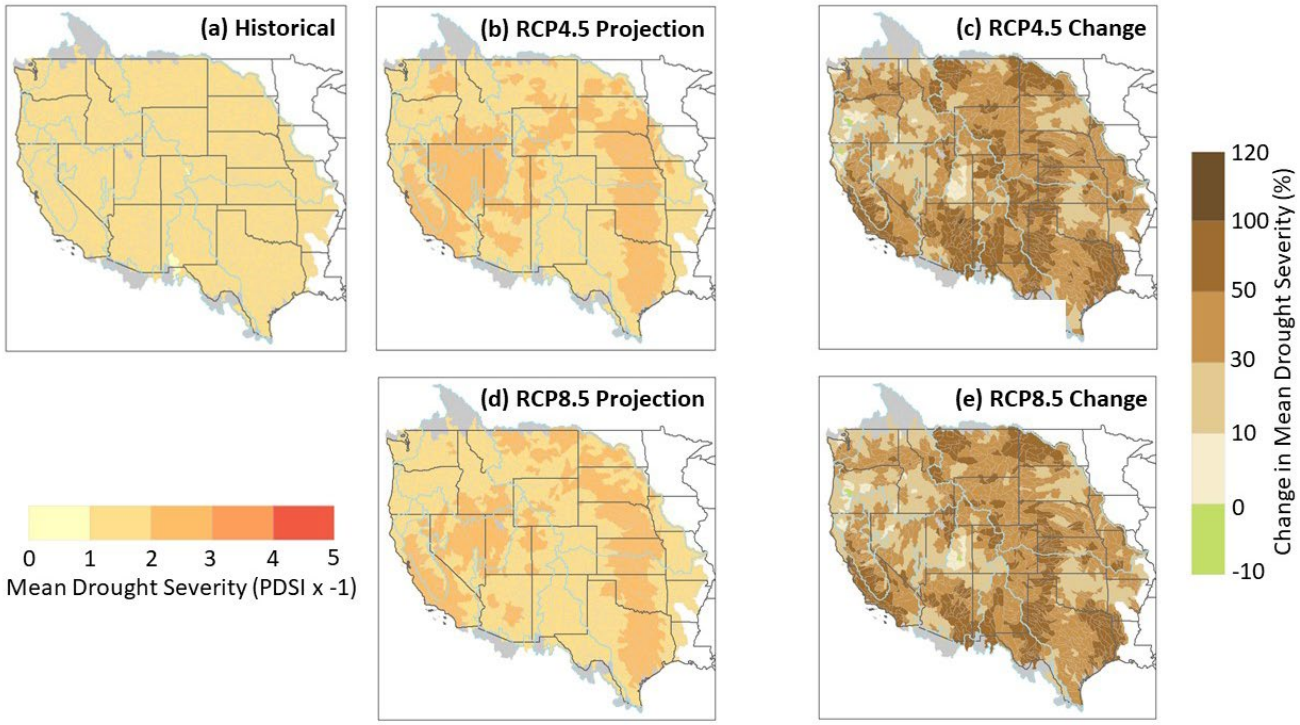

Figure 85. Mean drought severity for (a) historical (1473 to 2005), (b and d) climate model simulations (2006 to 2099), and (c and e) projected changes.

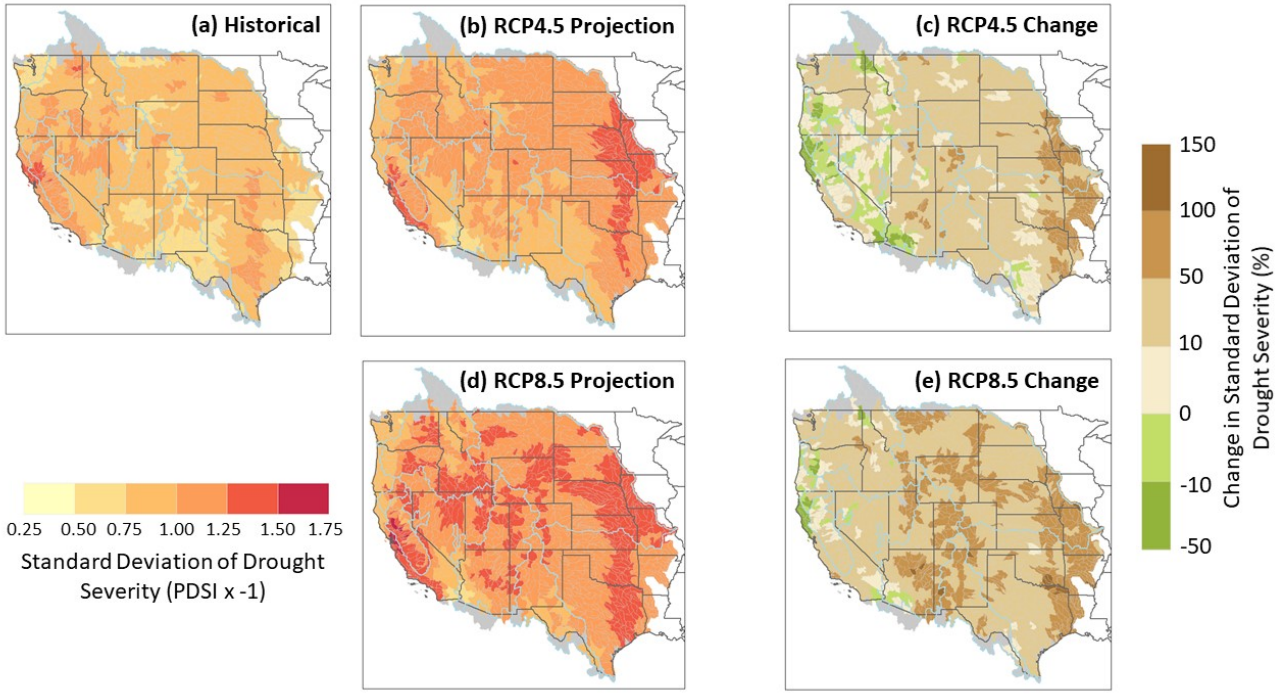

Figure 86. Standard deviation of drought severity for (a) historical (1473 to 2005), (b and d) climate model simulations (2006 to 2099), and (c and e) projected changes.

4.3.4 Changes in Joint Drought Return Periods

Joint drought return periods were estimated for two specifications of drought duration and severity and with the two drought definitions (i.e., "zero-crossover of yearly PDSI values" and "zero-crossover using 3-year moving averages of yearly PDSI values").

The first drought considered is based on a drought duration of 4 years and severity with a PDSI value of -2.5. Furthermore, return periods were estimated for the AND and OR cases. For this drought specification, the calculated return periods for the **AND case** means estimated joint return periods for drought duration equaling or exceeding the specified drought duration threshold of 4 years, ***and*** drought severity equaling or exceeding the specified drought severity threshold of PDSI equal to -2.5 (note, exceeding here should be interpreted as lower PDSI values as droughts are indicated by negative PDSI values). The **OR case** provides estimates of joint return periods for drought duration equaling or exceeding the specified drought duration threshold of 4 years, ***or*** drought severity equaling or exceeding the specified drought severity threshold of PDSI equal to -2.5.

Results of estimated joint drought return periods for these drought specifications and using the first drought definition (i.e., "zero-crossover of yearly PDSI values") are shown in Figure 87. This selection represents a drought where the duration is at least 4 years in length and the average severity (PDSI) during this time is -2.5. Note that, this is an average PDSI value over the duration of the drought (for a single year, however, a PDSI value of -2.5 will be classified as a moderate drought year according to the Palmer drought classification (Palmer, 1965)) and individual drought years within the drought spell can have PDSI values greater or smaller than this average severity (see Figure 67).

Furthermore, the first definition ("zero-crossover of yearly PDSI values") used here is associated with larger variability in drought events compared with the second drought definition ("zero-crossover using 3-year moving averages of yearly PDSI values"). Also, the projection period estimates are based on the ensemble mean drought interarrival times. Overall, these specific drought conditions can be considered to represent extreme conditions, particularly the AND case.

Figure 87 (top row) shows the joint return periods for these specified drought conditions estimated for the historical period (1473 to 2005) and the projection period (2005 to 2099) and for the two RCPs (RCP4.5 and RCP8.5). During the historical period, this event (duration $\geq$ 4 years *and* PDSI $\leq$ -2.5) was expected to occur for the major portion of the domain, on average, once in 100 to 500 years. For portions of the Missouri River Basin, this event was expected to occur, on average, once in 50 to 100 years. For portions of the Pacific Northwest, this event was expected to occur, on average, once in 500 to 1,000 years.

For the projections of future climate, this event is shown to occur, on average, once in 25 to 50 years. It is interesting to note that the joint return periods are similar for both the RCP4.5 and RCP8.5 projections and suggest that water-limited conditions likely will be reached under RCP4.5 projections.

The OR case, Figure 87 (bottom row), shows the joint return periods estimated for the historical period (1473 to 2005) and the projection period (2005 to 2099) and for the two RCPs (RCP4.5

and RCP8.5). During the historical period, this event (duration ≥ 4 years *or* PDSI ≤ -2.5) was expected to occur, on average, once in 10 to 25 years across the High Plains, Central Valley of California, Great Basin, and portions of the Upper Colorado River Basin; and, on average, once in 25 to 50 years in the Rio Grande Basin, and in portions of the Lower Colorado River Basin, Missouri River Basin, and Pacific Northwest.

For the projections of future climate, this event is shown to occur, on average, once in 10 to 25 years for practically the entire domain; except, in portions of the Central Valley of California this event is projected to occur, on average, once in 2 to 10 years. Similar to the AND case, it is interesting to note that the joint return periods are similar for both the RCP4.5 and RCP8.5 projections, again suggesting that water-limited conditions likely will be reached under RCP4.5 projections.

As discussed earlier in Section 4.2.5, the OR case provides a situation of more frequent events (shorter return periods) compared with the AND case (events with longer return periods or rarer events). This is demonstrated with the results presented here. In interpreting these results, it is important to note the uncertainties in the estimation process. The sources of uncertainties include the parameters of the underlying marginal distributions fitted to drought duration and severity data. Developing the joint distributions using copulas also includes uncertainty associated with the fitted copula parameter. Choosing specific distributional models and copulas add to the uncertainty pool.

An important question is, which uncertainty sources are most important and have the greatest impact on results. Based on the common period analysis (refer to Section 4.3.1), the drought interarrival time (see Section 4.3.1.3) was generally identified as a relatively larger source of uncertainty in comparison to drought duration and drought severity. During the analyses, all distributional model parameter estimates and associated standard errors or confidence bounds of model parameters were saved and can be used to further explore uncertainties in future studies. Here, only the drought interarrival time is used to show its impact on joint return period estimates.

As mentioned earlier, the projection period estimates (Figure 87 plots for RCP4.5 and RCP8.5) are based on the ensemble mean drought interarrival times. However, with the 32 projections for each RCP, it is also possible to obtain the 5^{th} and 95^{th} percentiles of the mean drought interarrival times, which can then be used to provide an estimate of the 90 percent confidence interval of the joint drought return periods for each case. Results for selected HUC-8s, along with results for the second drought definition ("zero-crossover using 3-year moving averages of yearly PDSI values"), are given in Table 20 for the AND case, and Table 21 for the OR case. The second drought definition was included to evaluate the sensitivity of selecting one drought definition over another.

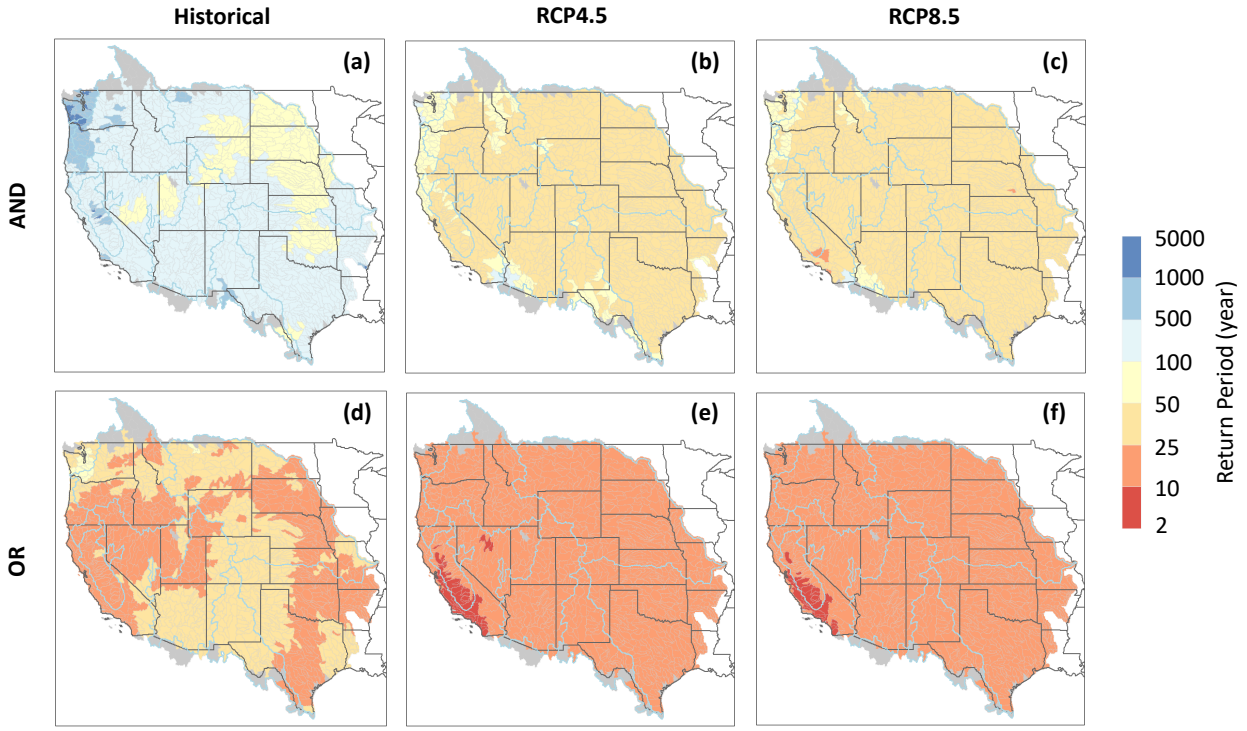

Figure 87. Joint drought return periods for drought with specified duration of 4 years and severity (PDSI) of -2.5 using the drought definition "zero-crossover of yearly PDSI values", (a to c) AND case; (d to f) OR case.

Note: Results of estimated joint drought ("zero-crossover of yearly PDSI values") return periods for drought specified with duration of 4 years and severity (PDSI) of -2.5 for the historical (1473 to 2005) and projection (2006 to 2099) periods. Top row (a to c) is the AND case (duration ≥ 4 years *and* PDSI ≤ -2.5) and the bottom row (d to f) is the OR case (duration ≥ 4 years *or* PDSI ≤ -2.5). The projection period return periods are calculated using the ensemble mean drought interarrival time from the climate model projections.

As an example, for the selected HUC-8 in the Colorado River Basin (14010001), for the first drought definition ("zero-crossover of yearly PDSI values"), the return period for the event (duration ≥ 4 years *and* PDSI ≤ -2.5) was estimated to be ~298 years (Table 20). For the second drought definition ("zero-crossover using 3-year moving averages of yearly PDSI values"), this event was estimated to have a return period of ~528 years.

For the RCP4.5 projections, the drought definitions provide estimates of return periods for the HUC-8 in the Colorado River Basin as follows (Table 20):

- Using the first drought definition ("zero-crossover of yearly PDSI values"), the 5th percentile return period is 28 years and the 95th percentile return period is 50 years, resulting in a 90 percent confidence interval of 28 to 50 years.
- Using the second drought definition ("zero-crossover using 3-year moving averages of yearly PDSI values"), the 5th percentile return period is 66 years and the 95th percentile return period is 164 years, resulting in a 90 percent confidence interval of 66 to 164 years.

For the RCP8.5 projections, the drought definitions provide estimates of return periods for the HUC-8 in the Colorado River Basin as follows (Table 20):

- Using the first drought definition ("zero-crossover of yearly PDSI values"), the 5th percentile return period is 24 years and the 95th percentile return period is 51 years, resulting in a 90 percent confidence interval of 24 to 51 years.
- Using the second drought definition ("zero-crossover using 3-year moving averages of yearly PDSI values"), the 5th percentile return period is 46 years and the 95th percentile return period is 99 years, resulting in a 90 percent confidence interval of 46 to 99 years.

Similar results are shown for the other HUC-8 basins (Table 20). Since the second drought definition uses a smoothed PDSI time series, the estimated return periods for the AND case are longer, and the 90 percent confidence intervals also are wider (greater uncertainty) when compared with the first drought definition. For the OR case (Table 21), the joint return periods are similar for both drought definitions.

To provide another example of application for this approach, results also were computed for a second drought with conditions defined by a duration of 2 years and a severity with a PDSI value equal to -1.25. These drought conditions are half the duration and severity of the first drought specification discussed above.

Results for this second drought specification are presented for the AND case in Table 22, and the OR case in Table 23. This drought specification is less severe than the first and, as expected, the joint return periods are shorter when compared with the return periods for the first drought specification. Similar to the first drought specification, for the OR case, the joint return periods are similar for both drought definitions. It should be noted that the 90 percent confidence interval is based only on considering the effects of uncertainty of the mean interarrival time and does not include any other uncertainty sources.

Table 20. Return periods for historical and projected droughts with specified duration of 4 years AND severity (PDSI) of -2.5

River Basin (HUC-8 ID)	Drought Defn.*	Return Periods for Drought with Duration ≥ 4 years *and* Severity (PDSI) ≤ -2.5 AND Case						
		Historical (year)	RCP4.5 (year)			RCP8.5 (year)		
		Mean	5th percentile	Ensemble mean	95th percentile	5th percentile	Ensemble mean	95th percentile
Colorado (14010001)	I	298	28	38	50	24	37	51
	II	528	66	102	164	46	70	99
Columbia (17050114)	I	158	22	31	45	19	27	38
	II	863	47	70	120	39	53	77
Klamath (18010202)	I	237	25	35	52	24	32	41
	II	2338	48	75	133	43	69	102
Missouri (10020008)	I	130	33	44	63	28	37	49
	II	966	80	131	202	43	74	114
Rio Grande (13010001)	I	224	41	50	63	36	47	68
	II	1184	115	153	211	73	133	214
Sacramento (18020005)	I	394	47	62	82	36	44	52
	II	>5000[1]	226	317	455	135	167	197
San Joaquin (18040006)	I	419	40	49	58	31	40	51
	II	>5000[1]	160	230	338	72	110	169
Truckee (16050102)	I	325	29	39	49	26	36	45
	II	4881	81	120	190	56	85	124

* Note: (I) corresponds to droughts defined by "zero-crossover of yearly PDSI values," and (II) corresponds to droughts defined by "zero-crossover using 3-year moving averages of yearly PDSI values."

[1] These results (low confidence) show values exceeding 5,000 years and are listed for reference purposes only. This is likely related to numerical instabilities resulting from distributional fitting with smaller sample sizes for the second drought definition and probability estimations subsequently used to estimate joint return periods. This issue was observed mostly for the historical period with the second drought definition for the event under the AND case.

The historical period includes years 1473 to 2005 and projection period includes years 2006 to 2099 for RCP4.5 and RCP8.5, along with uncertainty bounds.

Table 21. Return periods for historical and projected droughts with specified duration of 4 years OR severity (PDSI) of -2.5

River Basin (HUC-8 ID)	Drought Defn.*	Return Periods for Drought with Duration ≥ 4 years *or* Severity (PDSI) ≤ -2.5 OR Case						
		Historical (year)	RCP4.5 (year)			RCP8.5 (year)		
		Mean	5th percentile	Ensemble mean	95th percentile	5th percentile	Ensemble mean	95th percentile
Colorado (14010001)	I	36	11	16	20	10	15	21
	II	20	12	19	30	11	17	23
Columbia (17050114)	I	19	9	12	18	9	13	18
	II	22	13	19	33	12	17	24
Klamath (18010202)	I	21	11	15	23	11	15	19
	II	25	13	20	35	12	20	29
Missouri (10020008)	I	23	12	15	22	12	15	20
	II	20	12	19	29	10	18	27
Rio Grande (13010001)	I	30	13	17	21	12	16	23
	II	28	13	17	24	10	19	31
Sacramento (18020005)	I	20	10	14	18	11	14	16
	II	19	14	19	27	14	17	20
San Joaquin (18040006)	I	23	11	14	16	11	14	17
	II	27	12	18	26	12	18	28
Truckee (16050102)	I	20	10	14	17	10	14	17
	II	22	13	19	30	11	17	25

* Note: (I) corresponds to droughts defined by "zero-crossover of yearly PDSI values," and (II) corresponds to droughts defined by "zero-crossover using 3-year moving averages of yearly PDSI values."

The historical period includes years 1473 to 2005 and projection period includes years 2006 to 2099 for RCP4.5 and RCP8.5, along with uncertainty bounds.

Table 22. Return periods for historical and projected droughts with specified duration of 2 years AND severity (PDSI) of -1.25

River Basin (HUC-8 ID)	Drought Defn.*	Return Periods for Drought with Duration ≥ 2 years *and* Severity (PDSI) ≤ -1.25 AND Case						
		Historical (year)	RCP4.5 (year)			RCP8.5 (year)		
		Mean	5th percentile	Ensemble mean	95th percentile	5th percentile	Ensemble mean	95th percentile
Colorado (14010001)	I	28	9	13	17	9	13	19
	II	70	17	25	41	17	26	36
Columbia (17050114)	I	17	8	11	16	8	11	16
	II	44	14	22	37	15	20	29
Klamath (18010202)	I	20	9	13	19	10	13	17
	II	65	16	24	43	16	26	39
Missouri (10020008)	I	18	9	13	18	10	13	17
	II	48	16	27	41	16	27	42
Rio Grande (13010001)	I	22	10	13	16	10	13	19
	II	57	20	26	36	17	31	49
Sacramento (18020005)	I	20	8	11	15	9	11	13
	II	97	22	31	44	21	26	31
San Joaquin (18040006)	I	27	10	12	14	10	12	16
	II	103	21	30	43	18	27	42
Truckee (16050102)	I	20	8	11	14	9	12	15
	II	70	17	25	40	16	24	35

* Note: (I) corresponds to droughts defined by "zero-crossover of yearly PDSI values," and (II) corresponds to droughts defined by "zero-crossover using 3-year moving averages of yearly PDSI values."

The historical period includes years 1473 to 2005 and the projection period includes years 2006 to 2099 for RCP4.5 and RCP8.5, along with uncertainty bounds.

Table 23. Return periods for historical and projected droughts with specified duration of 2 years OR severity (PDSI) of -1.25

River Basin (HUC-8 ID)	Drought Defn.*	Return Periods for Drought with Duration ≥ 2 years *or* Severity (PDSI) ≤ -1.25 OR Case						
		Historical (year)	RCP4.5 (year)			RCP8.5 (year)		
		Mean	5th percentile	Ensemble mean	95th percentile	5th percentile	Ensemble mean	95th percentile
Colorado (14010001)	I	9	6	8	10	6	8	12
	II	12	9	13	22	8	12	17
Columbia (17050114)	I	6	5	7	10	5	7	10
	II	11	9	14	24	9	12	17
Klamath (18010202)	I	6	6	8	12	6	8	11
	II	11	9	14	26	9	14	21
Missouri (10020008)	I	7	6	8	11	6	8	11
	II	12	9	14	21	7	13	20
Rio Grande (13010001)	I	8	6	7	9	5	7	10
	II	12	9	11	16	7	13	21
Sacramento (18020005)	I	5	4	6	7	5	6	7
	II	9	9	12	18	9	11	13
San Joaquin (18040006)	I	7	5	6	7	5	7	9
	II	11	8	12	17	8	12	19
Truckee (16050102)	I	6	5	7	8	5	7	9
	II	10	9	13	21	8	12	18

* Note: (I) corresponds to droughts defined by "zero-crossover of yearly PDSI values," and (II) corresponds to droughts defined by "zero-crossover using 3-year moving averages of yearly PDSI values."

The historical period includes years 1473 to 2005 and the projection period includes years 2006 to 2099 for RCP4.5 and RCP8.5, along with uncertainty bounds.

4.3.5 Regime Shift Analysis

The regime shift analysis provides an approach to develop decadal to multi-decadal outlooks for likelihoods of shifts in the hydroclimate state of a system. Figure 88 shows the results of regime shift analyses using the PDSI data for the historical period (1473 to 2005) for 5-year and 10-year outlooks for the study domain (1,255 HUC-8s). Figure 88a and Figure 88b shows regime shift probabilities for 5-year outlooks when the Western United States has been under drought for 5 and 20 years, respectively.

The 5-year outlook (probability) of a regime shift (i.e., moving to a wetter state) with time in drought for 5-years (Figure 88a) for most of the domain is between 50 to 60 percent. Somewhat higher regime shift probabilities—60 percent to 70 percent—are found for portions of the Lower Colorado River Basin, Rio Grande Basin, and Central Valley of California. However, lower probabilities (< 50 percent) of regime shifts are seen for portions of the Upper Colorado, Upper Missouri, and Columbia River Basins.

Figure 88b shows the 5-year outlook of a regime shift when the Western United States has been under drought conditions for 20 years (rather than 5 years as in Figure 88a). As expected, the probabilities of a shift to wetter conditions are higher across the domain given that drought has persisted for 20 years. However, results indicate that, even after being in drought for 20 years, substantial portions of the domain still indicate less than a 100 percent probability of transitioning to a wet state. For example, portions of the Upper Colorado River Basin only show regime shift probabilities between 60 to 80 percent. In contrast, transition to wet conditions is more likely (regime shift probability between 90 to 100 percent) for the Central Valley of California.

The 10-year outlook for the Western United States following 20 years in drought (Figure 88c) indicates a high likelihood that the entire domain will transition to a wet state (regime shift probability between 90 to 100 percent). Note that the discussions here are focused on dry to wet transition, but the approach also is applicable for wet to dry transition. Finally, it is important to take into consideration that the method is based on historical PDSI data over the 1473 to 2005 period with a specific drought definition, “zero-crossover of yearly PDSI values.” It also does not answer how long a dry or wet regime is going to last and only provides an estimate of the likelihood of a regime shift given the length of time in a specific regime (wet or dry) and the length of time into the future.

Even though the regime shift analysis is based on historical PDSI data (1473 to 2005), in conjunction with the information presented here for projected changes to mean drought duration, drought duration variability, and mean interarrival times, the regime shift analysis here can be used to guide and monitor projected shifts in regime shift probabilities.

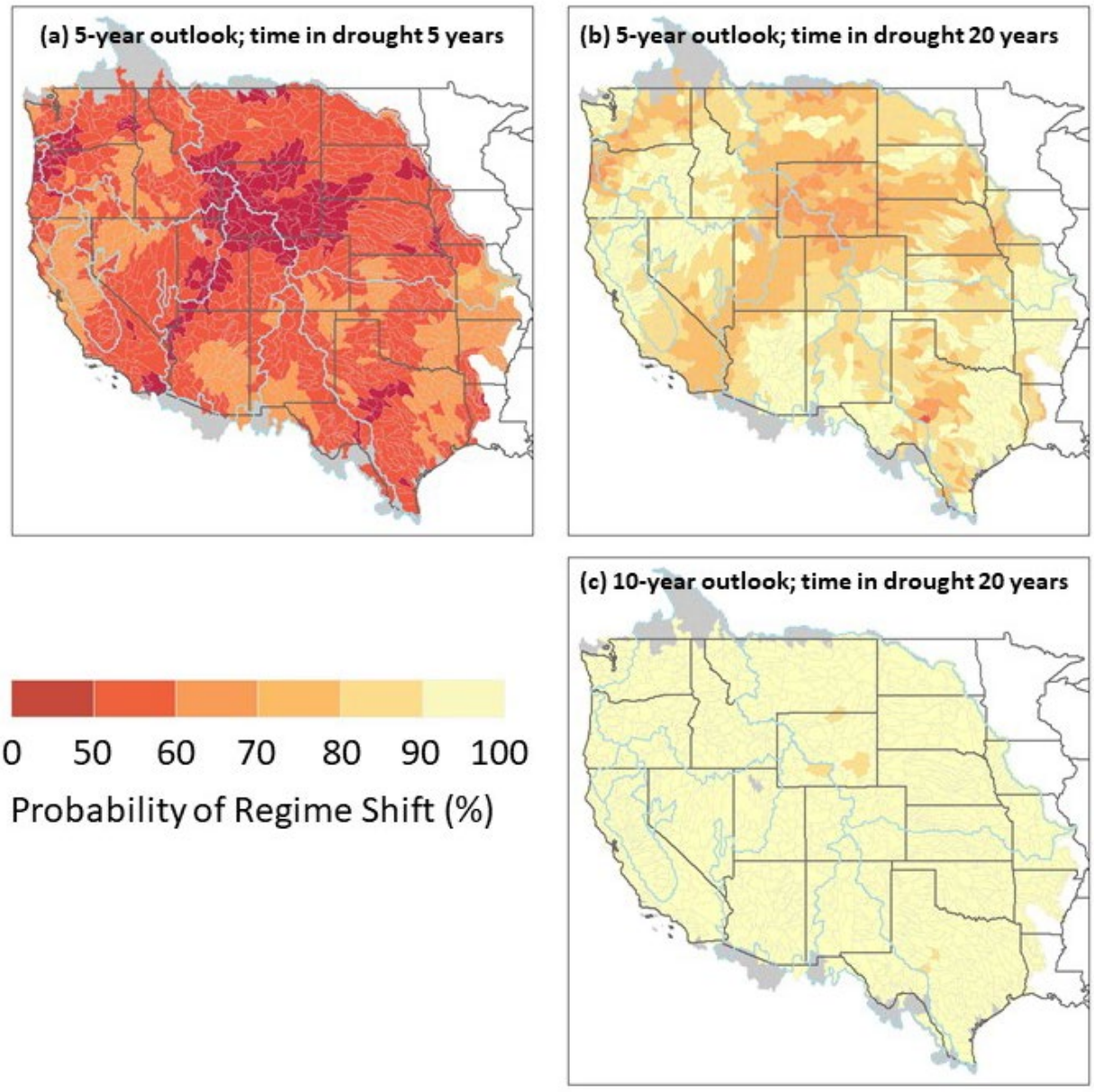

Figure 88. (a to c) Probability of regime shift using historical (1473 to 2005) PDSI data.

4.4 Summary and Next Steps

West-wide drought analyses were conducted to understand changes in drought variability and drought characteristics (duration, severity, and frequency/interarrival times/return periods) for historical and future projected climate conditions across the Western United States using the PDSI. Summer season (June-July-August) PDSI resulting in a single PDSI value per year was used to define droughts. Two separate drought definitions were developed. The first drought definition used "zero-crossover of yearly PDSI values," and the second definition used "zero-crossover of a smoothed (3-year moving averaged) PDSI time series." Use of the first definition

to identify drought events results in more frequent and shorter droughts than does the second definition. The PDSI data used in the analyses spanned the period 1473 to 2099 and a few different sub-periods of this long time period were used for the analyses. The period 1473 to 2005 was referred to as the historical period and consists of reconstructed PDSI and instrumental observations. The period 1950 to 2005 was considered to be a common period, which is an overlapping period between instrumental observations of PDSI and simulated PDSI values from climate models. The period 2006 to 2099 was considered to be the projection period for the climate models forced with RCP4.5 and RCP8.5 emissions projections. All PDSI data were aggregated to USGS eight-digit Hydrologic Unit Code (HUC-8) resulting in a total of 1,255 HUC-8s for the study domain.

With the drought events identified using the two separate drought definitions, characteristics of drought events (duration, severity, and interarrival times) were computed. Subsequently, marginal probability distributions were fitted to drought duration and drought severity for the historical and projection period with distribution parameters estimated using the maximum likelihood parameter estimation method. The predominant distributions were log-normal for drought duration and Weibull for drought severity for both the historical period and the projection period, and for both drought definitions. This provides a level of robustness such that the underlying stochastic processes generating drought characteristics are fundamentally the same under historical and projected climate conditions.

Following the development of marginal distributions, joint probability distributions were developed using copulas, specifically, Gumbel-Hougaard copulas were fitted to the respective drought duration and severity time series data with the copula parameter in each case estimated using the analytical relationship with inverse Kendall tau.

Prior to analyzing changes in drought characteristics, an evaluation of the performance of the ability of the climate models to simulate drought characteristics was performed for the common period (i.e., 1950 to 2005). This analysis was based on droughts identified using zero-crossover of yearly PDSI values. Evaluations were performed for drought duration, severity, and drought interarrival times. The climate model simulated drought characteristics over the common period (1950 to 2005) largely show that climate models encompass the observed drought characteristics and provide comparable results. Thus, it was concluded that the climate model simulations are useful for the study of droughts under future conditions across the Western United States.

Changes in drought duration and severity based on the climate model projections were then conducted. The results section is focused on change in drought characteristics using the first drought definition. Climate model projections indicate an increase in drought duration and an increase in the variability of drought duration for most of the Western United States in the future. Climate models also project future increases in drought severity and in the variability of drought severity for most of the Western United States.

Additionally, changes in joint drought return periods using two drought specifications were evaluated. One drought specification with relatively severe drought characteristics (duration of 4 years; severity, PDSI of -2.5) was compared with a second less severe drought specification (duration of 2 years; severity, PDSI of -1.25). This evaluation included both

drought definitions and two event types—the AND case (resulting in more severe events), and the OR case (resulting in less severe events).

Furthermore, the joint return periods for the AND case using the first drought definition ("zero-crossover of yearly PDSI values") are shorter than the joint return periods estimated using the second drought definition ("zero-crossover using 3-year moving averages of yearly PDSI values"). For the OR case, both drought definitions resulted in similar joint return periods. Finally, the 90 percent confidence intervals of joint return periods also were calculated by considering the uncertainty of the mean interarrival time. This estimation of confidence interval did not include any other uncertainty sources except for the uncertainty in mean interarrival time. This choice was guided from the common period evaluation of climate model performance.

In addition to evaluating changes in drought characteristics, a regime shift analysis using the historical period (1473 to 2005) PDSI data was conducted. This analysis provided the ability to estimate outlooks of the likelihood of shifts in hydroclimate state (from dry to wet or vice-versa) given the number of years in a particular state (dry or wet). The 10-year outlook for the Western United States following 20 years in drought indicates that most of the domain is likely to shift to a wet state (regime shift probability between 90 to 100 percent).

The analyses conducted here should provide water managers with a set of data, information, and tools to support water management decisions across the Western United States. As part of the next steps in a West-wide drought analysis, it will be important to consider the multiple sources of uncertainty (e.g., distribution parameter uncertainties) in the analysis steps used to estimate joint drought return periods. Ault (2020) provides a list of potential topics related to the future of drought research.

4.5 Key Findings

A listing of key findings from the West-wide drought analyses are given below:

- Climate model projections indicate an increase in drought duration and an increase in the variability of drought duration for most of the Western United States in the future.
- Climate models also project future increases in drought severity and in the variability of drought severity for most of the Western United States.
- Underlying stochastic processes generating drought characteristics are fundamentally the same under historical and projected climate conditions.
- CMIP5 climate model projections adequately capture the broad observed drought characteristics (duration, severity, interarrival times) during the common overlap period, 1950 to 2005.
- Joint return periods of drought duration and severity for more severe drought events, in comparison to less severe and frequent drought events, are sensitive to the drought definition used.

- Given the length of time in a specific hydroclimatic regime (i.e., wet period or dry period), the probability of a shift to a different regime can be estimated for time periods into the future.
- Using reconstructed and observed summer season (June-July-August) PDSI over the 1473 to 2005 period, the 10-year outlook for the Western United States following 20 years in drought shows the domain to transition to a wet state, but duration of the wet spells are projected to be more variable in the future in comparison to the historical period (1473 to 2005).

5 Storage-Deficit Ratios and Risk Analysis

A set of reservoir drought indices that consider water demands and inflows into the reservoir, including a consideration of the reservoir operating rules to estimate non-drought demand from the reservoir implicitly, are presented in this chapter. Broadly, these indices capture the storage (surplus/deficit) behavior of reservoirs as a function of inflows and demand and using the minimum active storage pool as an operations guide to estimate supply-demand imbalances and subsequent drought risks.

Unlike commonly used drought measures, such as PDSI, which only consider hydroclimate variability, the indices developed here include a direct consideration of reservoir demand and inflows; the duration and severity of drought and surplus periods; and the ability of the system to likely avert a drought impact based on a prior reservoir refill cycle, or to recover from a drought-induced failure in the subsequent period of surplus.

Seasonal (flash droughts) and multi-year sustained droughts were identified through indices for drought duration, severity, recovery, and prior period surplus duration and volume. The indices were derived for five large reservoirs in Reclamation's management area across the Western United States. These indices were then applied using both instrumental and tree-ring reconstructed streamflow data.

For each of these five reservoirs, both univariate and multivariate drought statistics for the instrumental period based on the observed streamflow record and for the paleo-reconstructed period based on tree-ring reconstructed streamflow are presented. Two probability measures, the probability of long-duration and high-stress droughts (severe sustained droughts), and the probability of flash-drought (seasonal or short duration) failure are derived from the drought events for the instrumental period and the paleo-reconstructed period.

The next section (Section 5.1) summarizes the reservoir inflow, outflow, and storage data for the instrumental period, and the inflow data for the paleo period used in the analyses. Section 5.2 describes the methodology. The results are presented in Section 5.3, along with findings and considerations to interpret the results. Summary and next steps from the analysis are described in Section 5.4 and key findings are listed in Section 5.5.

5.1 Data

Five large reservoirs in the Western United States in Reclamation's management area were selected as case studies to develop a set of reservoir drought indices. Their geographic locations are shown in Figure 89. Data on daily reservoir inflow and outflow rates and storage volumes were acquired from Reclamation offices for each of these five reservoirs. For the American Falls Reservoir, the streamflow data at the immediate downstream gage was used as a proxy for reservoir release. Reconstructed streamflow data from tree-ring reconstructions were available at

the monthly time scale and are based on prior studies across the Western United States. For all the variables (inflow, outflow, and storage), the daily data for the instrumental period was converted to monthly totals. Missing values at the monthly level (<1 percent) were imputed using random simulations from climatological mean and standard deviation. Table 24 provides the list of these reservoirs, along with the name of the respective dam, storage information (storage capacity and minimum active storage pool), their available records of years, and the streamflow reconstruction location (nearest USGS stream gage ID; refer to Section 2.4).

5.2 Methodology

The reservoir drought index and associated metrics for drought duration, severity, recovery, and excess duration and volume are introduced in this section. Given a sequence of monthly reservoir inflow and outflow, a monthly deficit is calculated as the difference between demand (outflow) and supply (inflow). These deficits, or monthly water shortages, could be met at least partially by the storage in the reservoir at that time. The accumulation of this shortage over time represents the storage drawdown, while an accumulation of negative deficits (or surpluses) represents reservoir fill-up. A fixed annual cycle of demand (i.e., a static 12-month demand profile with time varying reservoir inflows) was considered. Several metrics of supply-demand imbalance were then derived.

In the absence of detailed demand data for the reservoirs, a procedure by which non-drought period releases could be used to estimate the "normal" demand from the reservoir on a monthly basis was first developed. The rationale was that releases in non-drought months would meet the allocated demand, as well as any spills from the reservoir. The allocated demands would include hydropower, irrigation, municipal and industrial demands, as well as required ecosystem maintenance flows. Consequently, under non-drought conditions, the minimum release for each calendar month could then be considered as the demand as it would not represent any spills or excess releases for that calendar month. For each reservoir, the monthly demand profile was derived as follows:

- The minimum active storage (i.e., the volume at the minimum operating level) was first identified and assumed as a "proxy" reservoir rule curve.
- The months when the available storage is not below this minimum active storage level were next identified. These are the months when the assumed rule curve is not triggered and are considered as "non-trigger events."
- The monthly distributions of the outflow data during these "non-trigger events" from the last 30 years (water years 1990 to 2019) were then selected. The minimum outflow for each calendar month from this distribution was considered as the minimum demand for that month. It should be noted that, over the past 30 years, operations may have changed (e.g., month-to-month release patterns) and demands have likely grown. As such, these minimum demand values are likely to be low when aggregated to an annual release.

Table 24. Location and data for five selected reservoirs in the Western United States in Reclamation's management area

Reservoir	Dam	Latitude	Longitude	Storage Capacity (acre-feet)	Minimum Active Storage (acre-feet)	Data Availability (Water Year)			Streamflow Reconstruction Location*
						Inflow	Outflow	Storage	
American Falls	American Falls	42.95	-112.83	1,672,590	490,000	1927 to 2019	1908 to 2019	1926 to 2019	13077000 and Reclamation Hydromet[1]
Canyon Ferry	Canyon Ferry	46.65	-111.73	1,891,888	396,031	1953 to 2019	1953 to 2019	1953 to 2019	06054500
Lake Powell	Glen Canyon	37.00	-111.49	27,000,000	3,997,163	1963 to 2019	1963 to 2019	1963 to 2019	09380000
Millerton Lake	Friant	37.00	-119.71	520,500	135,000	1995 to 2019	1988 to 2019	1985 to 2019	11250100
Shasta Lake	Shasta	40.71	-122.42	4,552,000	1,900,000	1922 to 2019	1988 to 2019	1985 to 2019	11377100

* Notes: For a given reservoir, the streamflow reconstruction location is the nearest USGS stream gage ID (refer to Section 2.4) unless otherwise noted. Also, the period of record used in the paleohydrology analysis is 1685 to 1977 (refer to Section 2.4) and excludes drought events in the paleo-reconstructions prior to 1685.

[1] The Bureau of Reclamation operates a network of automated hydrologic and meteorologic monitoring stations located throughout the Pacific Northwest. This network and its associated communications and computer systems are collectively called Hydromet; https://www.usbr.gov/pn/hydromet/. Site ID for American Falls Reservoir inflow and storage is AMF. USGS gage 13077000 Snake River at Neeley, ID is used to represent outflow.

Figure 89. Five selected Reclamation reservoirs shown with their maximum storage capacity and dams.

The basic concepts of the approach are illustrated in Figure 90 for a simplified, but representative, case where the demand is constant over time, and the supply varies as is typical of inflow time series (Figure 90, top panel). For each month, the deficit and the surplus are computed. If a new deficit occurs, a calculation of a potential drought is initiated, and the cumulative deficit (red bars in Figure 90, lower panel) is computed for each subsequent month and recorded.

The number of consecutive months up to the maximum cumulative deficit in that sequence is recorded as the drought duration. The drought recovery period is the time from the peak of the cumulative deficit sequence for the event to the time when the cumulative deficit becomes zero. The subsequent period is one of surplus and the excess (blue bars in Figure 90, lower panel) is computed. An example of a reservoir drawdown-from and recovery-to a given storage level, and subsequent fill-up (a full reservoir cycle) is shown with a grey-shaded box in the lower panel of Figure 90. A full reservoir cycle begins with a drought and ends with a fill-up of the reservoir.

Based on this illustration of a reservoir cycle (see gray-shaded box in Figure 90, lower panel), the following reservoir indices are defined:

- Reservoir Drought Severity (RDS) is the maximum value of the cumulative deficit (CD) within a reservoir cycle.
- Reservoir Drought Duration (RDD) is the amount of elapsed time from the beginning of the reservoir cycle to the point when CD peaks.
- Reservoir Drought Recovery (RDR) is the amount of time that is required from the peak severity to the end of the dry regime. This is similar to the reservoir filling up to the level from where it started depleting.
- Reservoir Excess Fill-up (REF) is the sum of the excess (EX) during the cycle.
- Reservoir Excess Duration (RED) is the amount of time that elapses from onset of the excess (EX) to its conclusion.
- Reservoir Drought Index (RDI) for a given month is defined as either the cumulative deficit or excess within a reservoir cycle. RDI time series results are presented here as a percent of active storage, where active storage for a reservoir is defined as the difference between the storage capacity and minimum active storage pool (see Table 24).

Together, RDD, RDS, RDR, RED, and REF constitute the reservoir drought metrics for one reservoir cycle. Multiple such events allow inference as to the multivariate probability distribution of these metrics. RDI and the respective metrics (RDD, RDS, RDR, RED, and REF) were calculated for both the instrumental period and the paleo-reconstructed period based on the estimated static 12-month demand profile.

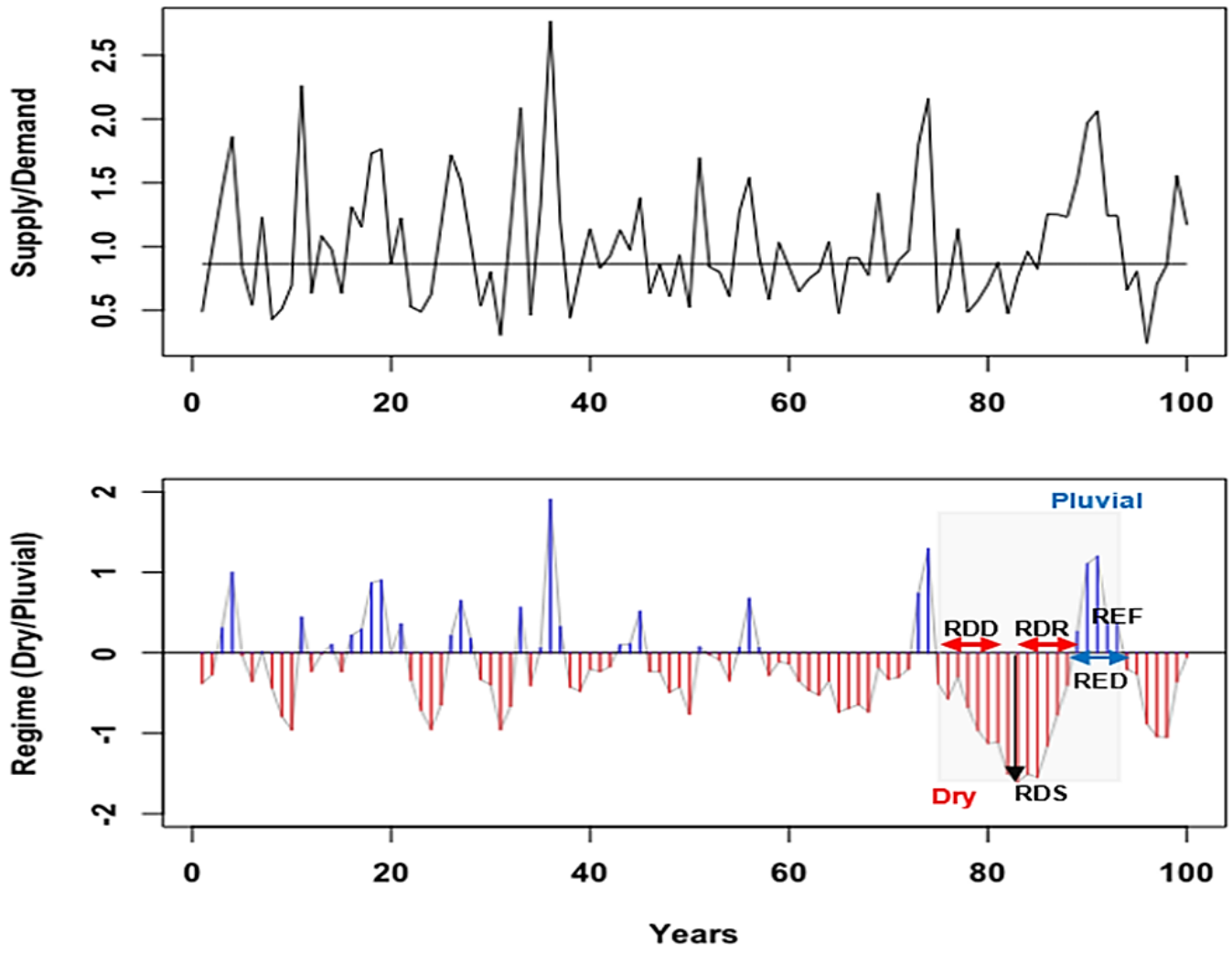

Figure 90. An illustration of the reservoir cycle and corresponding drought metrics.

Note: The top panel shows a synthetic reservoir inflow time series and the horizontal line represents constant reservoir demand. The bottom panel shows the various drought metrics. In addition, it shows an example of a reservoir drawdown-from and recovery-to a given storage level, and subsequent fill-up (a full reservoir cycle) is shown in the gray-shaded box.

Once the RDI and the related indices are computed, several types of droughts can be analyzed using the drought and surplus events. A visual presentation of these drought types is shown in Figure 91.

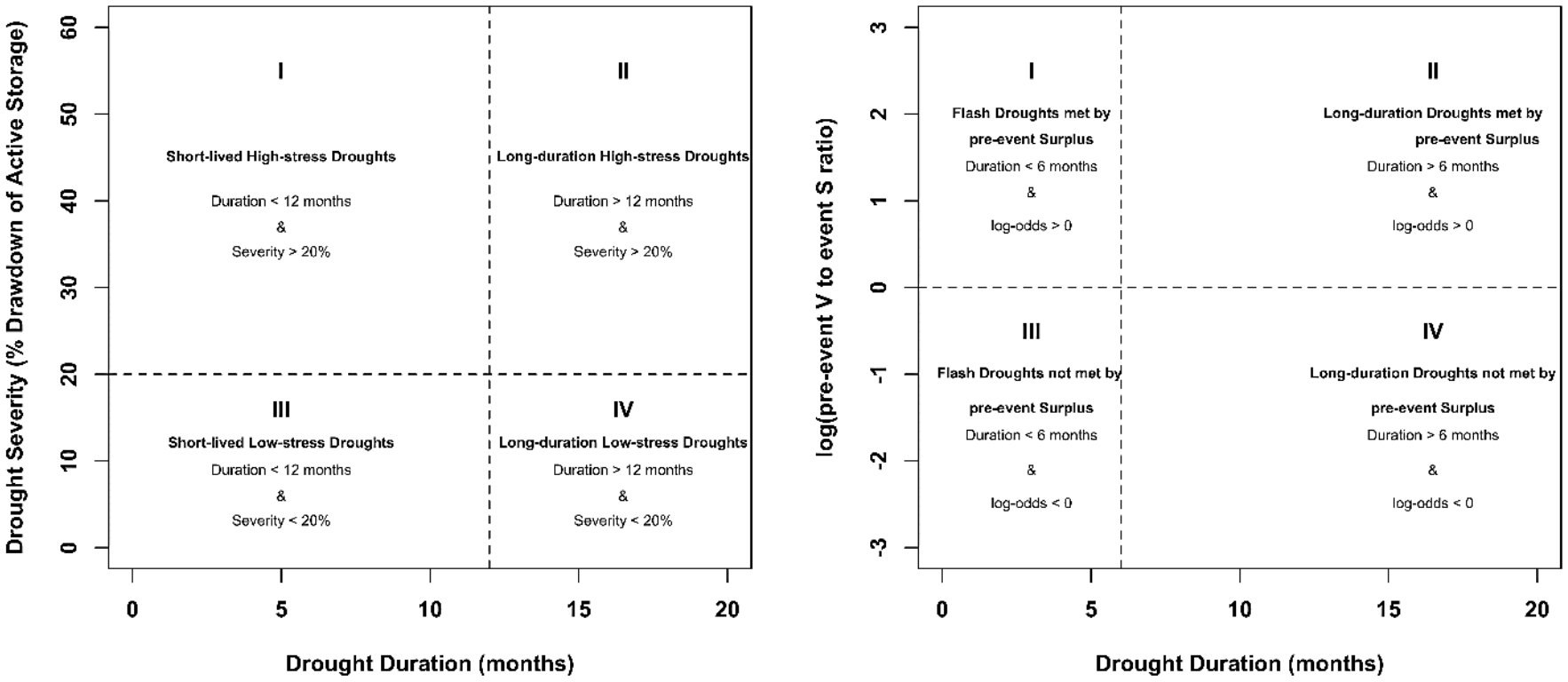

Figure 91. Drought types based on drought metrics.

Note: The different drought types described in the text are shown in the quadrants labeled I through IV in the left and right panels. The drought duration in months (horizontal axis) may vary with the reservoirs analyzed.

A total of eight different drought types is shown in Figure 91 between the left and right panels. Both panels in Figure 91 consider drought events as a multivariate distribution with drought duration on the horizontal axis as one of its variables to define the drought types; however, the second variable given in the vertical axis is defined differently between the two panels. The left panel considers the overall impact of a drought event on the reservoir's active storage. The right panel considers the effects of pre-event reservoir fill-up, and the ability of this pre-event reservoir storage to mitigate drought impacts across a range of drought durations.

The left panel of Figure 91 shows reservoir drought duration in months on the horizontal axis and reservoir drought severity as a percentage-drawdown of the active storage capacity of the reservoir on the vertical axis. Vertical and horizontal separators (dashed lines) are shown at RDD = 12 months and RDS = 20 percent to broadly separate severe sustained droughts from short-lived (1-year or less) droughts resulting in quadrants labeled I through IV for this panel.

- Quadrant I represents short-lived, high-stress droughts defined by events where RDD < 12 and RDS > 20 percent
- Quadrant II represents long-duration, high-stress droughts defined by events where: RDD > 12 and RDS > 20 percent
- Quadrant III represents short-lived, low-stress droughts defined by events where: RDD < 12 and RDS < 20 percent
- Quadrant IV represents long-duration, low-stress droughts defined by events where: RDD > 12 and RDS < 20 percent

The right-panel of Figure 91 shows reservoir drought duration in months on the horizontal axis and a term referred to as the log-odds ratio in the vertical axis. The term log-odds ratio (or "log-odds" in short) on the vertical axis is defined by: $\log\left(\frac{\mathrm{REF_{i-1}}}{\mathrm{RDS_i}}\right)$; $\mathrm{REF_{i-1}}$ is the preceding event's (i-1; where, i is the current event) storage fill; $\mathrm{RDS_i}$ is the current event's (event, i) maximum deficit. Vertical and horizontal separators (dashed lines) are shown at RDD = 6 months and log-odds = 0[18] resulting in quadrants labeled I through IV for this panel. Furthermore, droughts less than 6 months in duration are referred to as "flash drought" to characterize short-duration (sub-annual – RDD ≤ 6 months) drought events.

- Quadrant I represents flash drought events that can be met by pre-event reservoir fill-up where: RDD < 6 and log-odds > 0
- Quadrant II represents longer-duration droughts that can be met by pre-event fill-up where: RDD > 6 and log-odds > 0
- Quadrant III represents flash droughts that cannot be met by pre-event reservoir fill-up where: RDD < 6 and log-odds < 0

[18] The ratio, log-odds is equal to 0 when $\mathrm{REF_{i-1}} = \mathrm{RDS_i}$; where i is the current event. The notation *log(x)* means the logarithm (logarithm to the base 10) of *x*; *x>0*.

- Quadrant IV represents longer-duration droughts that cannot be met by pre-event reservoir fill-up where: RDD > 6 and log-odds < 0

Amongst all the drought events described here (total of 8), of particular interest are:

- Long-duration, high-stress droughts (Figure 91, left panel, quadrant II)
- Flash droughts that cannot be met by pre-event reservoir fill-up (Figure 91, right panel, quadrant III)
- Longer-duration droughts that cannot be met by pre-event reservoir fill-up (Figure 91, right panel, quadrant IV)

Drought events and statistics for the five case study reservoirs are presented in the next section.

5.3 Results

The reservoir drought index, the multivariate distributions of the RDI statistics, and selected events for each of the five reservoirs are discussed in the following sections. The results for each reservoir are presented using a set of three figures (with multiple panels or sub-plots) shown in the following order.

- First figure: In this figure, the RDI time series normalized (divided) by the reservoir's active storage and expressed as a percentage for the paleo-reconstructed period and the instrumental period are shown.
- Second figure: In this figure, the multivariate distributions (refer to Figure 91) showing the results for drought events in the paleo-reconstructed and instrumental periods are given. The top three worst drought events in the paleo-reconstructed period and the worst event in the instrumental period are also highlighted. The severity of the events is defined by the magnitude of RDS.
- Third figure: In this figure, the RDI time series of the top three worst events in the paleo-reconstructed period and the worst event in the instrumental period are shown to demonstrate the reservoir cycles (refer to Figure 90 lower panel gray-shaded box region).

Further descriptions for the figures are given below.

In the first figure, the top (paleo-reconstructed period) and the bottom (instrumental period) panels show the RDI time series. Reservoir drawdown-from CD is shown in red, and fill-up EX is shown in blue. The scale used for the RDI is in percent of active storage for the reservoir. The zero-line represents the reservoir storage level at the beginning of the period. Reservoir storage in million acre-feet (MAF) is indicated on the secondary ordinate axis, along with indicators (dashed lines) at the reservoir's minimum active storage pool and storage capacity. In the bottom panel, which presents the RDI for the instrumental period, the reservoir's actual storage time series is shown on the secondary ordinate axis (using a light gray line). This comparison provides an evaluation of the RDI in filling and depleting the reservoir and serves as a validation for the

index. When there is a storage depletion, the periods should naturally correspond to greater negative RDI or cumulative deficit periods.

In the second figure, the multivariate distribution of the drought duration and drought severity (RDS, as a percentage of active storage) is shown in the left panel. The joint distribution of the drought duration and the log-odds (i.e., the pre-event reservoir fill-up ratio to current event severity) is shown in the right panel. Paleo-reconstructed drought events are presented with filled (orange) squares, and the instrumental period's events are presented with filled (gray) circles. The top three worst paleo-reconstructed drought events and the worst event in the instrumental period (both defined by the magnitude of RDS) are highlighted using larger-sized red, orange, and yellow squares, and gray circles. The year of occurrence is indicated against the points.

In the left panel, vertical and horizontal dashed lines are provided at a duration of 12 months and severity of 20 percent, respectively, to broadly separate severe sustained droughts from short-lived droughts (see Figure 91 for definitions). The number indicated inside the larger squares or the larger circle is the recovery period for that drought. In the right panel, vertical and horizontal dashed lines are provided at a duration of 6 months and log-odds of 0. Events below a log-odds ratio of zero (negative scale) are those whose current excess demands cannot be met through pre-event excess storage. Events on the positive scale are those whose excess demand in a drought period can be fully supplied by the excess storage from the immediately preceding event. The numbers in the top three worst paleo-reconstructed drought events and the worst event in the instrumental period indicate the pre-event's reservoir excess duration (RED_{i-1}).

Finally, the third figure shows the time series view of the first figure for the top three worst events in the paleo-reconstructed period and the worst event in the instrumental period. These events are arranged in a time order where the earliest of the top three worst events in the paleo-reconstructed drought events is shown in sub-plot (a), followed by the second earliest in sub-plot (b), and the latest event in sub-plot (c). The worst instrumental period event is shown in sub-plot (d), and it naturally follows the order of the most recent time. RDI 12 months before and after the events are also shown. The actual event is highlighted in red for CD and blue for EX.

Discussion of results using these figures are presented next for the five reservoirs.

5.3.1 American Falls

Drought statistics for the American Falls Reservoir are shown in Figure 92, Figure 93, and Figure 94. Given its relatively small storage and high minimum active storage, the American Falls reservoir cycles rapidly with drawdowns and fill-ups both in the instrumental and paleo period (Figure 92). Multiple events where the RDI was in excess of 100 percent of active storage capacity were noted in both the instrumental and paleo period. A severe drought was seen during the 1860s that was worse than any in the instrumental period.

The left panel of Figure 93 (drought duration versus drought severity) reinforces this observation. Additional long-duration, high-stress droughts were noted in the paleo period, whereas no such events occurred in the instrumental period. These long-duration, high-stress droughts (i.e., a drought with a duration greater than 12 months and severity in excess of

20 percent active storage drawdown) typically recovered within 5 to 18 months. It is also noteworthy that these long-duration, high-stress events also have a log-odds close to or less than zero, indicating that the deficit during the drought period could not have been met through pre-event excess storage (Figure 93, right panel).

The chances of long-duration, high-stress drought was negligible in the instrumental period, but, was high in the paleo period as all the events that have a drought that exceeds 12 months were also severe. Several of the high-stress droughts were short-lived (less than 6 months). The probability of flash drought failure was 31 percent for both the instrumental and paleo periods, reinforcing that the primary difference informed by the paleo period pertains to severe sustained droughts with the criteria used in the analysis.

Figure 94 shows the RDI for the top events highlighted in Figure 93. The worst event in the paleo-reconstructed period occurred during 1863 to 1865. The duration of this drought was 14 months, with a recovery period of 18 months. The severity was 221 percent of the active storage capacity of the reservoir. The worst event in the instrumental period occurred during 1935 to 1936 with 6 months to peak severity, and a recovery of 19 months. The severity was on the order of 163 percent of the active storage capacity.

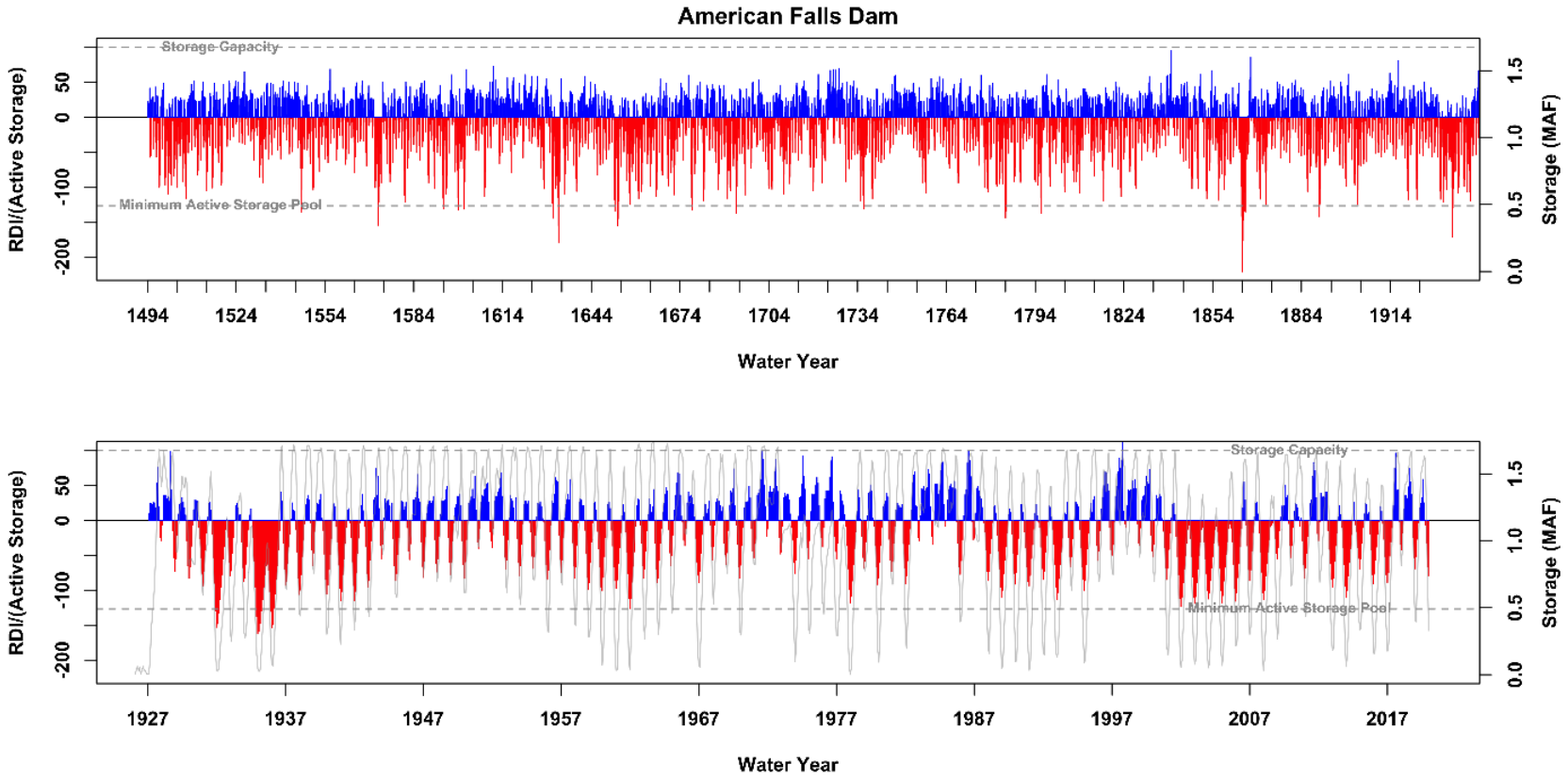

Figure 92. Drought types based on drought metrics.

Note: Normalized RDI time series (percentage of active storage) for the paleo-reconstructed period (top panel) and the instrumental period (bottom panel). For the instrumental period, the reservoir's actual storage time series is shown using a light gray line. Storage capacity and minimum active storage pool in both panels are shown with dashed gray lines.

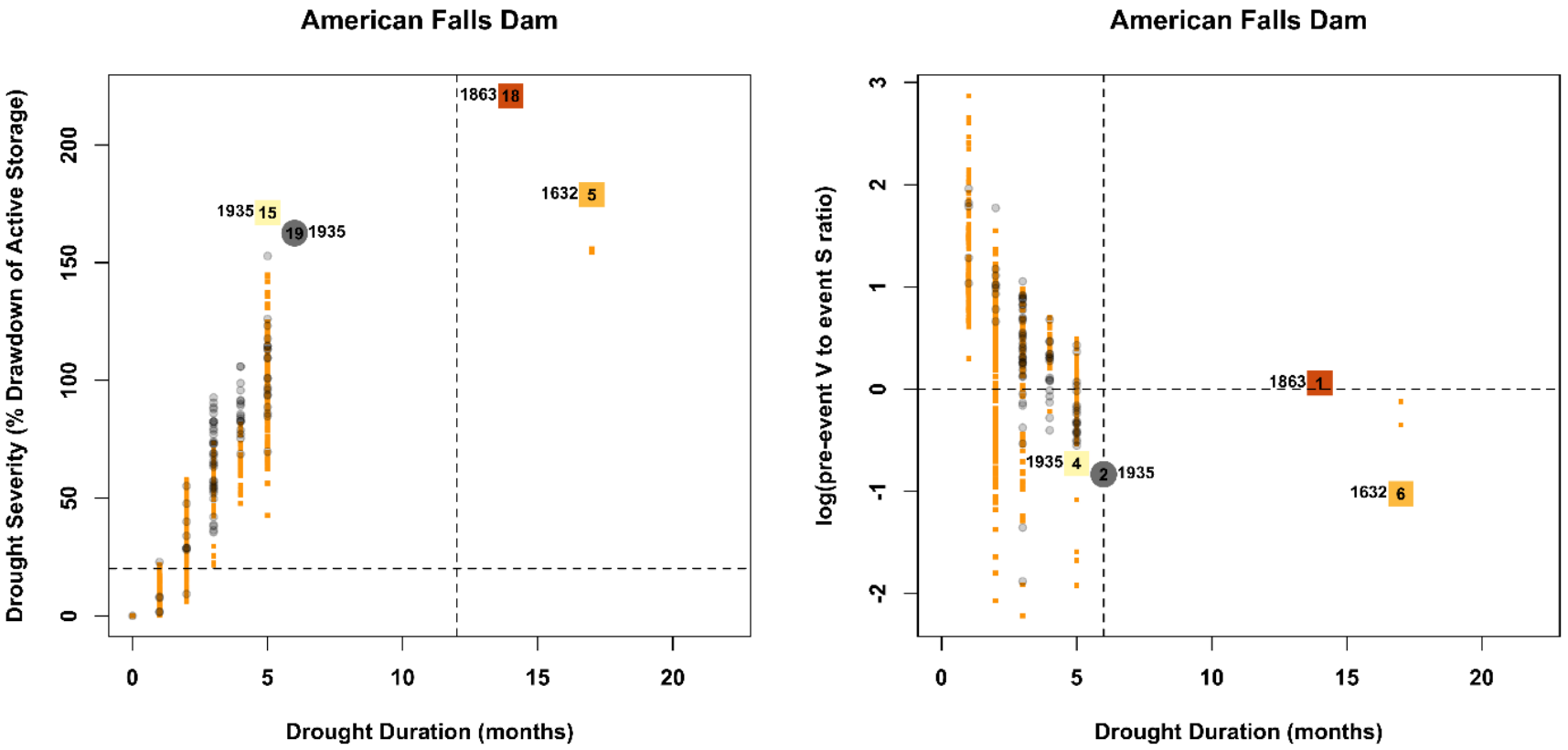

Figure 93. Multivariate distribution of drought events for American Falls Reservoir.

Note: Multivariate distribution of drought events with paleo-reconstructed drought events shown with filled (orange) squares, and the instrumental period's events shown with filled (gray) circles. The top three worst paleo-reconstructed drought events and the worst event in the instrumental period are highlighted using larger-sized red, orange, and yellow squares, and gray circles. The year of occurrence is indicated against the points. The number indicated inside the larger squares or the larger circle is the reservoir drought recovery in months for that drought event. Dashed lines are used to define drought event thresholds (refer to text for details).

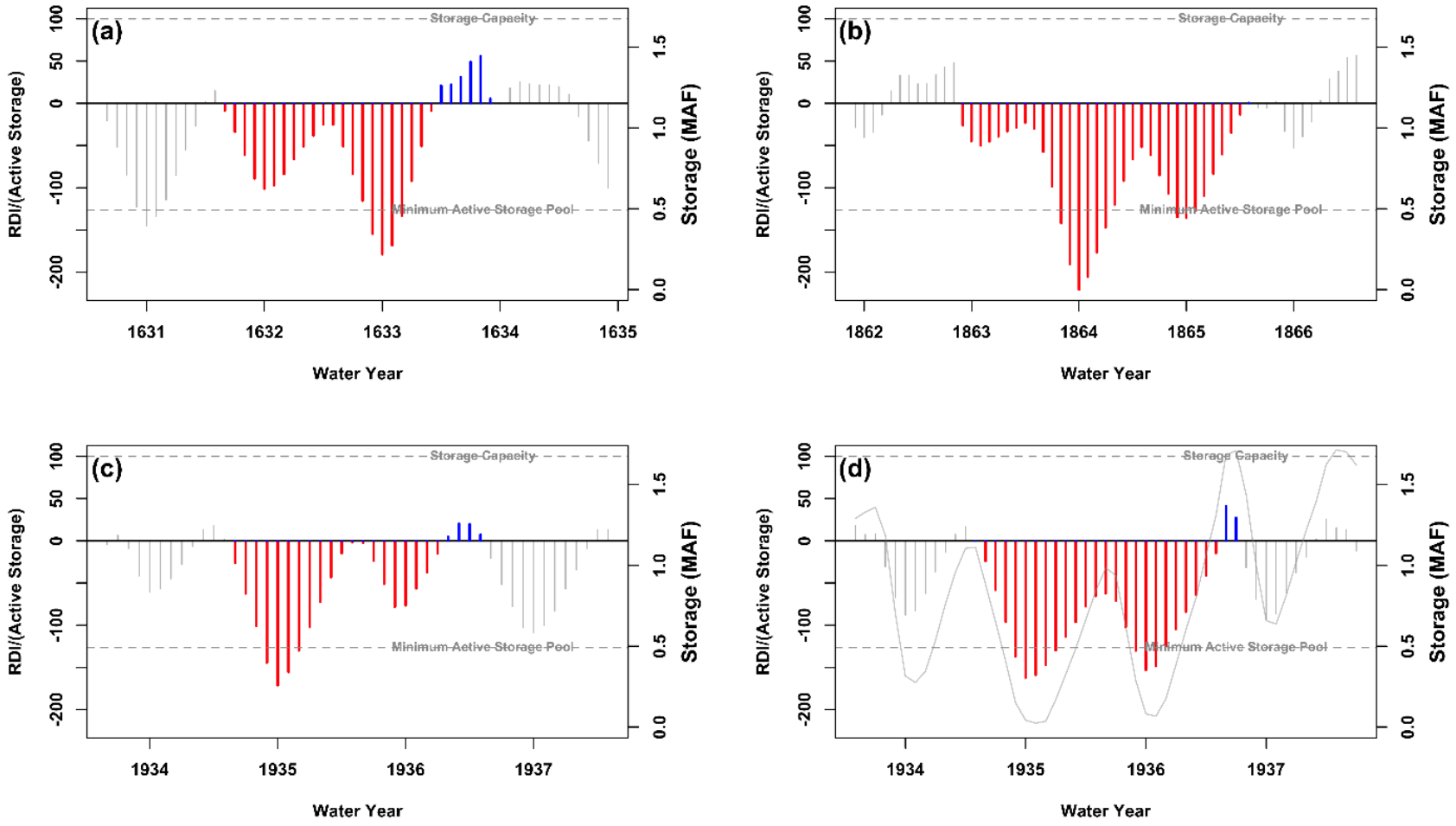

Figure 94. Normalized RDI time series for selected events for American Falls Reservoir.

Note: Sub-plots (a) through (c) are in time order for the three worst paleo-reconstructed droughts and the worst instrumental period drought event is shown in sub-plot (d)

.

5.3.2 Canyon Ferry

Drought statistics for Canyon Ferry Reservoir are shown in Figure 95, Figure 96, and Figure 97. The Canyon Ferry Reservoir was dominated by pluvial events, with a few intervening short droughts during the instrumental period. This pattern was similar in the paleo-period. The observed storage fits well with the deficit periods, indicating that the RDI algorithm efficiently tracks reservoir depletion and could provide a proxy for storage analysis. The initial low storage in the 1950s corresponds to the first fill after its construction. In both the instrumental and the paleo-reconstructed period, the RDI has been less than 50 percent of active storage capacity.

The worst event in the instrumental period corresponds to an 8-month drought with 20 percent of active storage depletion and 2 months to recover. Except for this, there were a few events in the short-lived, high-stress category during the paleo-reconstructed period during 1744, 1756, 1783, 1797, 1865, and 1935. There is one event (around 1845 to 1846) in the long-duration, high-stress category. These events had quick recoveries (between 2 to 6 months). The probability of flash drought failure is estimated to be very low.

Figure 97 shows the RDI for the top events highlighted in Figure 96. The worst event in the paleo-reconstructed period occurred during 1936. The duration of this drought was 9 months, with a recovery period of 2 months. The severity was 38 percent of the active storage capacity of the reservoir. Interestingly, the second-worst drought (severity of 33 percent), had a much longer duration (15 months). The worst event in the instrumental period occurred during 1989, 8 months to peak severity, and a recovery of 2 months. The severity was nearly 23 percent of the active storage capacity.

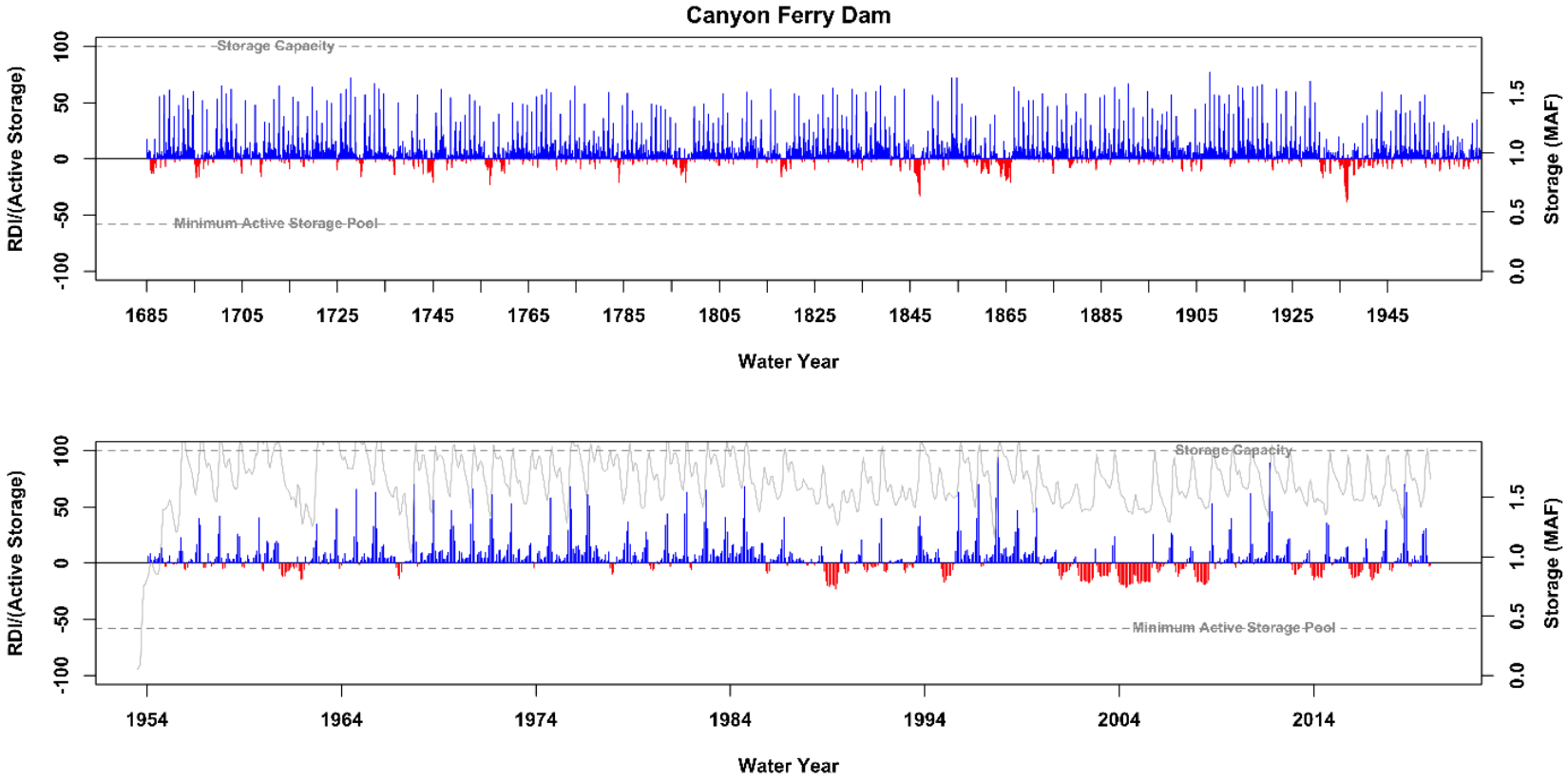

Figure 95. RDI time series normalized by active storage for Canyon Ferry Reservoir.

Note: Normalized RDI time series (percentage of active storage) for the paleo-reconstructed period (top panel) and the instrumental period (bottom panel). For the instrumental period, the reservoir's actual storage time series is shown using a light gray line. Storage capacity and minimum active storage pool in both panels are shown with dashed gray lines.

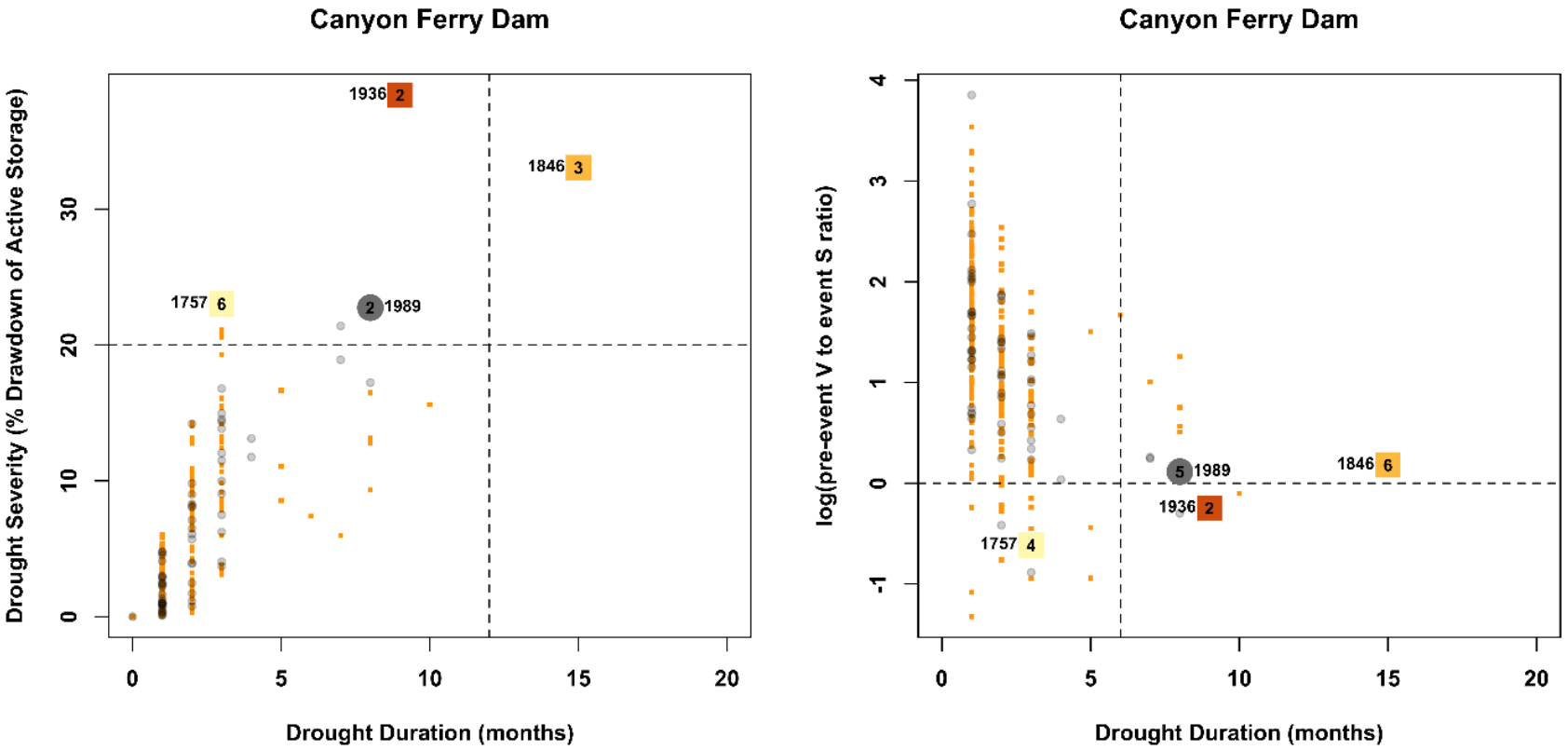

Figure 96. Multivariate distribution of drought events for Canyon Ferry Reservoir.

Note: Multivariate distribution of drought events with paleo-reconstructed drought events shown with filled (orange) squares, and the instrumental period's events shown with filled (gray) circles. The top three worst paleo-reconstructed drought events and the worst event in the instrumental period are highlighted using larger-sized red, orange, and yellow squares, and gray circles. The year of occurrence is indicated against the points. The number indicated inside the larger squares or the larger circle is the reservoir drought recovery in months for that drought event. Dashed lines are used to define drought event thresholds (refer to text for details).

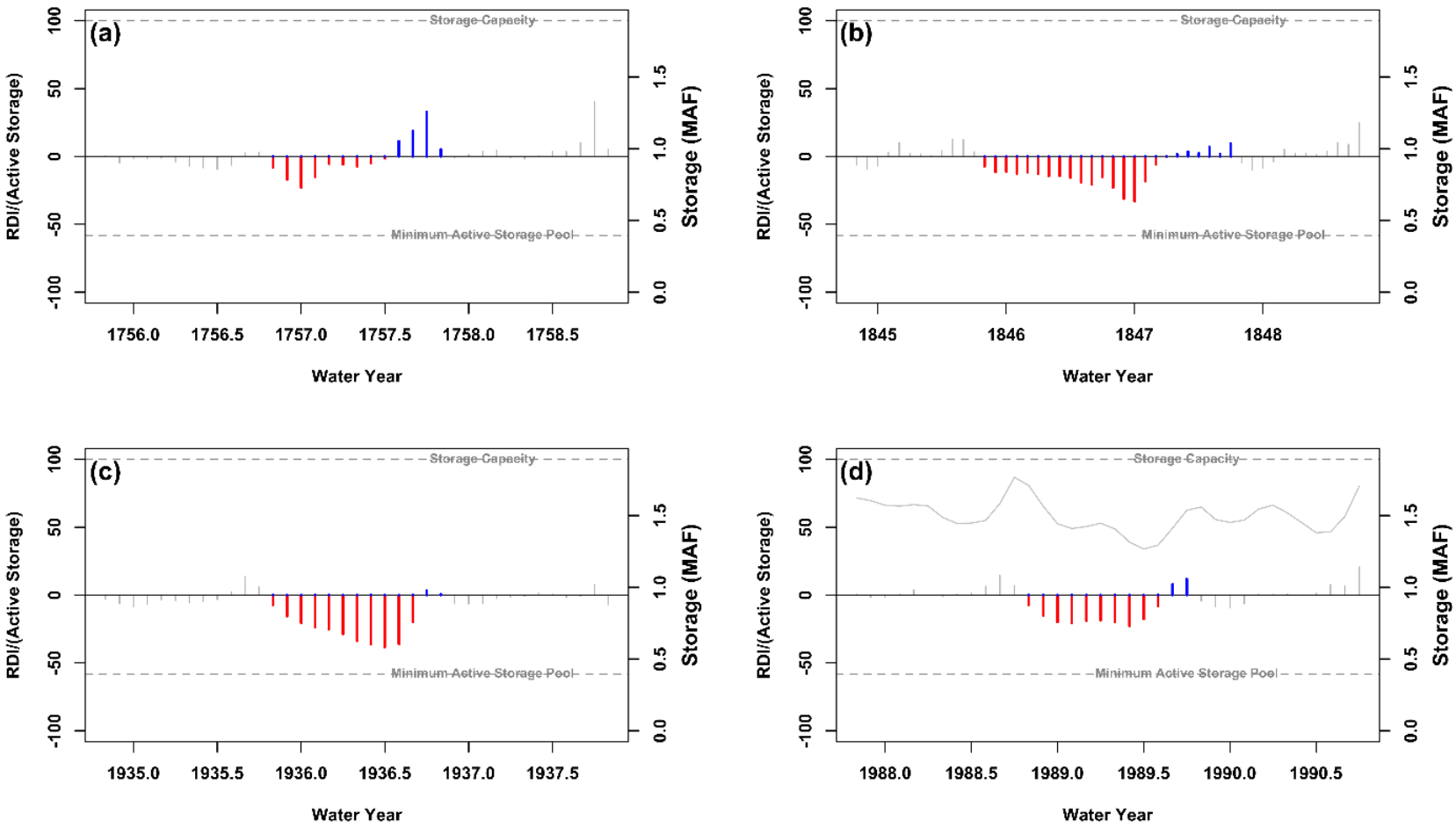

Figure 97. Normalized RDI time series for selected events for Canyon Ferry Reservoir.

Note: Sub-plots (a) through (c) are in time order for the three worst paleo-reconstructed droughts and the worst instrumental period drought event is shown in sub-plot (d)

.

5.3.3 Lake Powell

Drought statistics for Lake Powell are shown in Figure 98, Figure 99, and Figure 100. For Lake Powell, the worst droughts occurred in the instrumental period, most notably in the 2000s and 1980s. The RDI during these droughts was up to 40 percent of active reservoir storage capacity. The droughts in the paleo period were short-lived and less intense compared to the instrumental period. Observed storage depicts a long period of initial fill up since construction of Glen Canyon Dam, subsequent moderate drawdown and fill up, and the recent depletion. This is reflected in the cumulative deficit curve.

Figure 99 reveals that several droughts in the instrumental and paleo period were longer than 12 months in duration, but generally less severe in the paleo period. The probability of severe sustained drought was around 50 percent in the instrumental period and much lower (15 percent) in the paleo period. The probability of flash drought failure was 11 percent in the instrumental and 19 percent in the paleo period.

Figure 100 shows the RDI for the top events highlighted in Figure 99. The worst event in the paleo-reconstructed period occurred during 1702 to 1704, according to this analysis which relies on the Woodhouse et al. (2006) streamflow reconstruction. Note, this result is based on the analysis period 1685 to 1977 (also refer to Section 2.4) and does not include information from extended paleo-reconstructions. For example, the 1100s drought highlighted in Meko et al. (2007) is not included, nor are other notable droughts seen in the paleo-reconstructions prior to 1685. The duration of this drought was 31 months, with a recovery period of 3 months. The severity was 25 percent of the active storage capacity of the reservoir. The worst event in the instrumental period occurred during 2001 to 2008 with 57 months to peak severity, and a recovery of 37 months. The severity was nearly 37 percent of the active storage capacity.

.

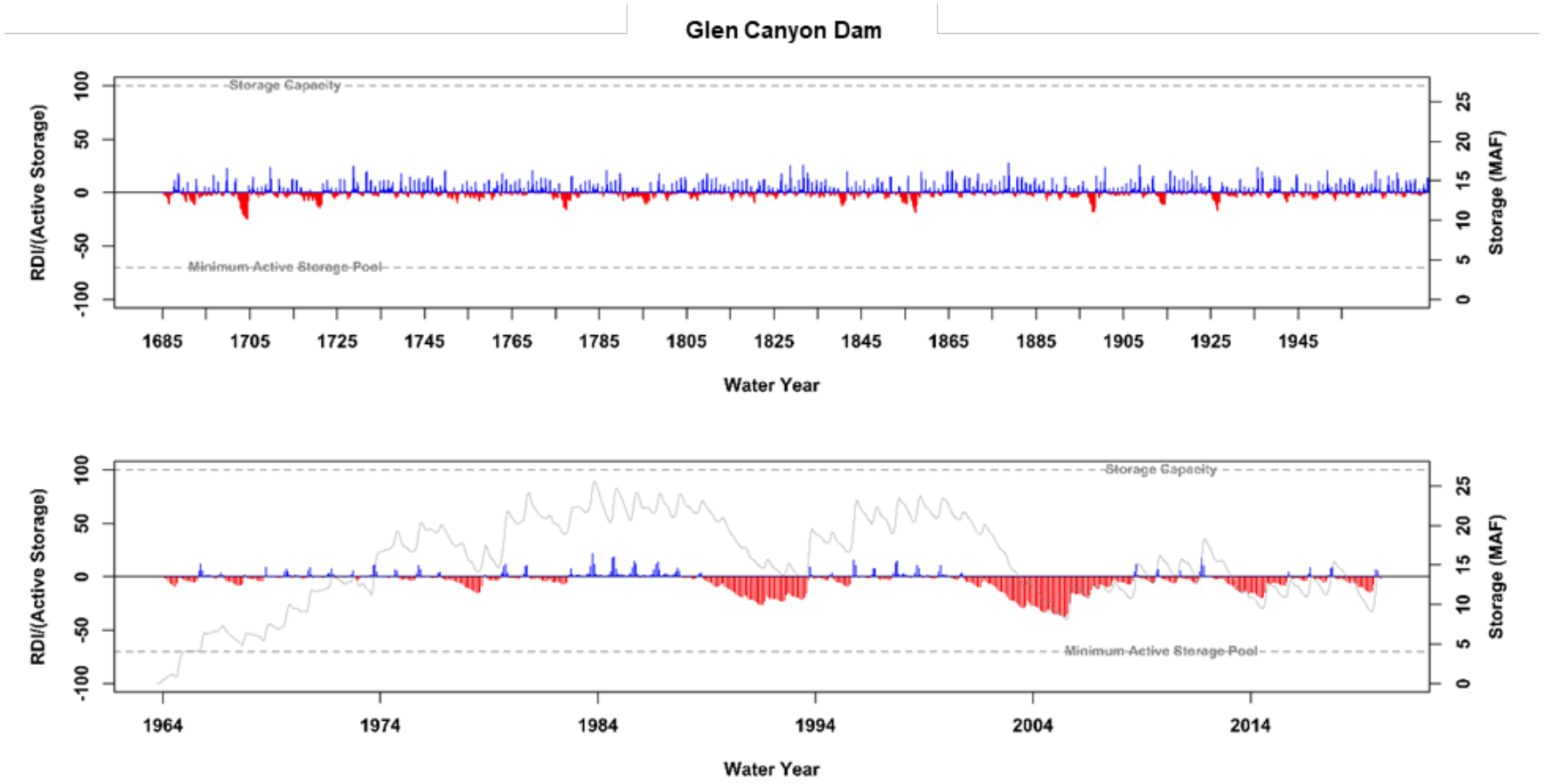

Figure 98. RDI time series normalized by active storage for Lake Powell.

Note: Normalized RDI time series (percentage of active storage) for the paleo-reconstructed period (top panel) and the instrumental period (bottom panel). For the instrumental period, the reservoir's actual storage time series is shown using a light gray line. Storage capacity and minimum active storage pool in both panels are shown with dashed gray lines.

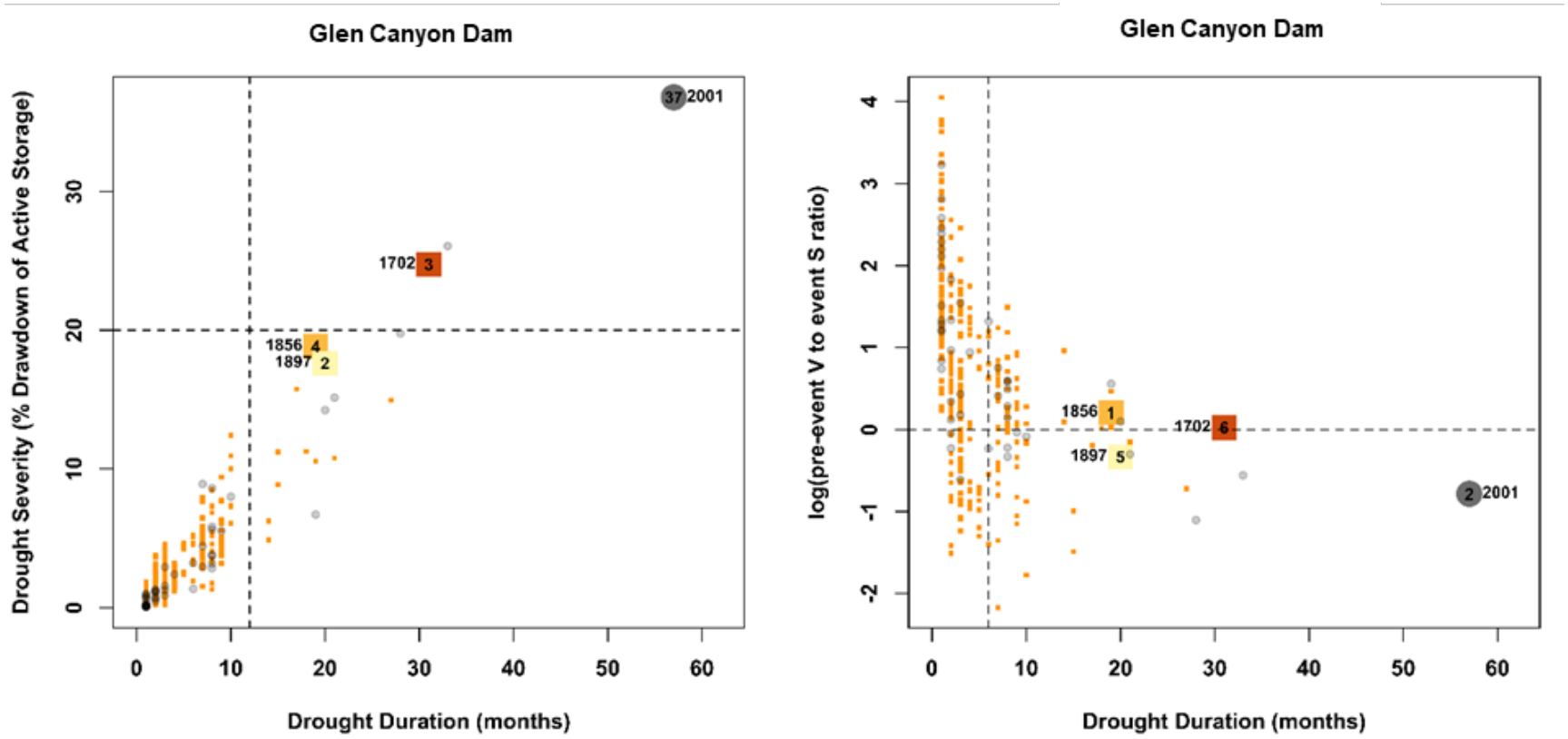

Figure 99. Multivariate distribution of drought events for Lake Powell.

Note: Multivariate distribution of drought events with paleo-reconstructed drought events shown with filled (orange) squares, and the instrumental period's events shown with filled (gray) circles. The top three worst paleo-reconstructed drought events and the worst event in the instrumental period are highlighted using larger-sized red, orange, and yellow squares, and gray circles. The year of occurrence is indicated against the points. The number indicated inside the larger squares or the larger circle is the reservoir drought recovery in months for that drought event. Dashed lines are used to define drought event thresholds (refer to text for details).

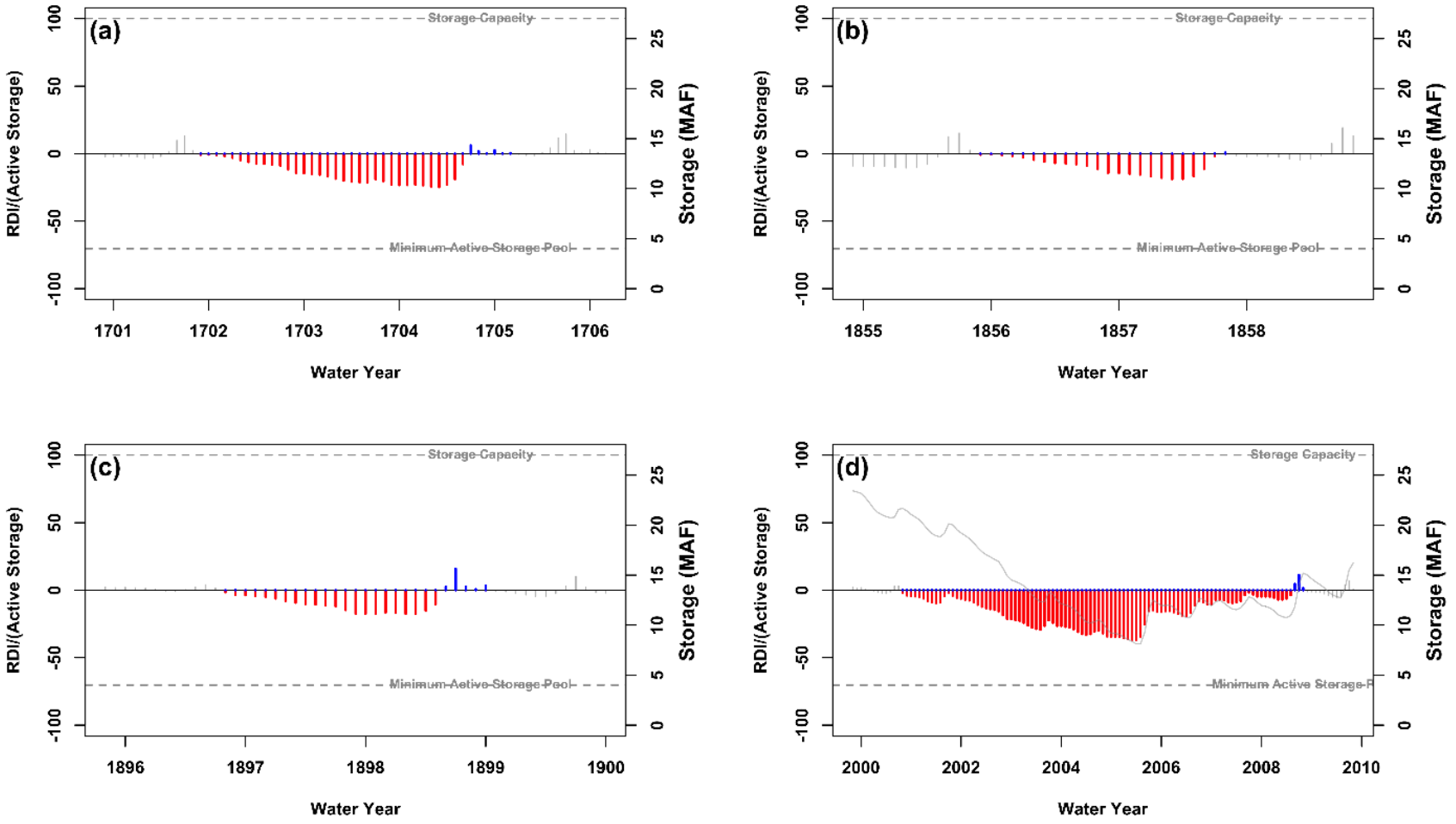

Figure 100. Normalized RDI time series for selected events for Lake Powell.

Note: Sub-plots (a) through (c) are in time order for the three worst paleo-reconstructed droughts and the worst instrumental period drought event is shown in sub-plot (d)

5.3.4 Millerton Lake

Drought statistics for Millerton Lake are shown in Figure 101, Figure 102, and Figure 103. A severe sustained drought around 2012 was noted for Millerton Lake during the instrumental period, and this is the drought of record based on the paleo-reconstructed and the instrumental periods. Except for this event, much of the instrumental period was dominated by wet periods. The same pattern was seen in the paleo period—pluvial events interspersed with short bursts of intense droughts. Interestingly, the severity of the 4-month droughts were always greater than 20 percent of the active reservoir storage, and recovery happened within 5 months. About half of these droughts could have been alleviated with pre-event pluvial volume storage. No severe, sustained droughts were noted in the paleo period.

Figure 103 shows the RDI for the top events highlighted in Figure 102. The worst event in the paleo-reconstructed period occurred during 1796. The duration of this drought was 4 months, with a recovery period of 5 months. The severity was 68 percent of the active storage capacity of the reservoir. The worst event in the instrumental period occurred during 2015 to 2016, 17 months to peak severity, and recovery of 4 months. The severity was nearly 95 percent of the active storage capacity.

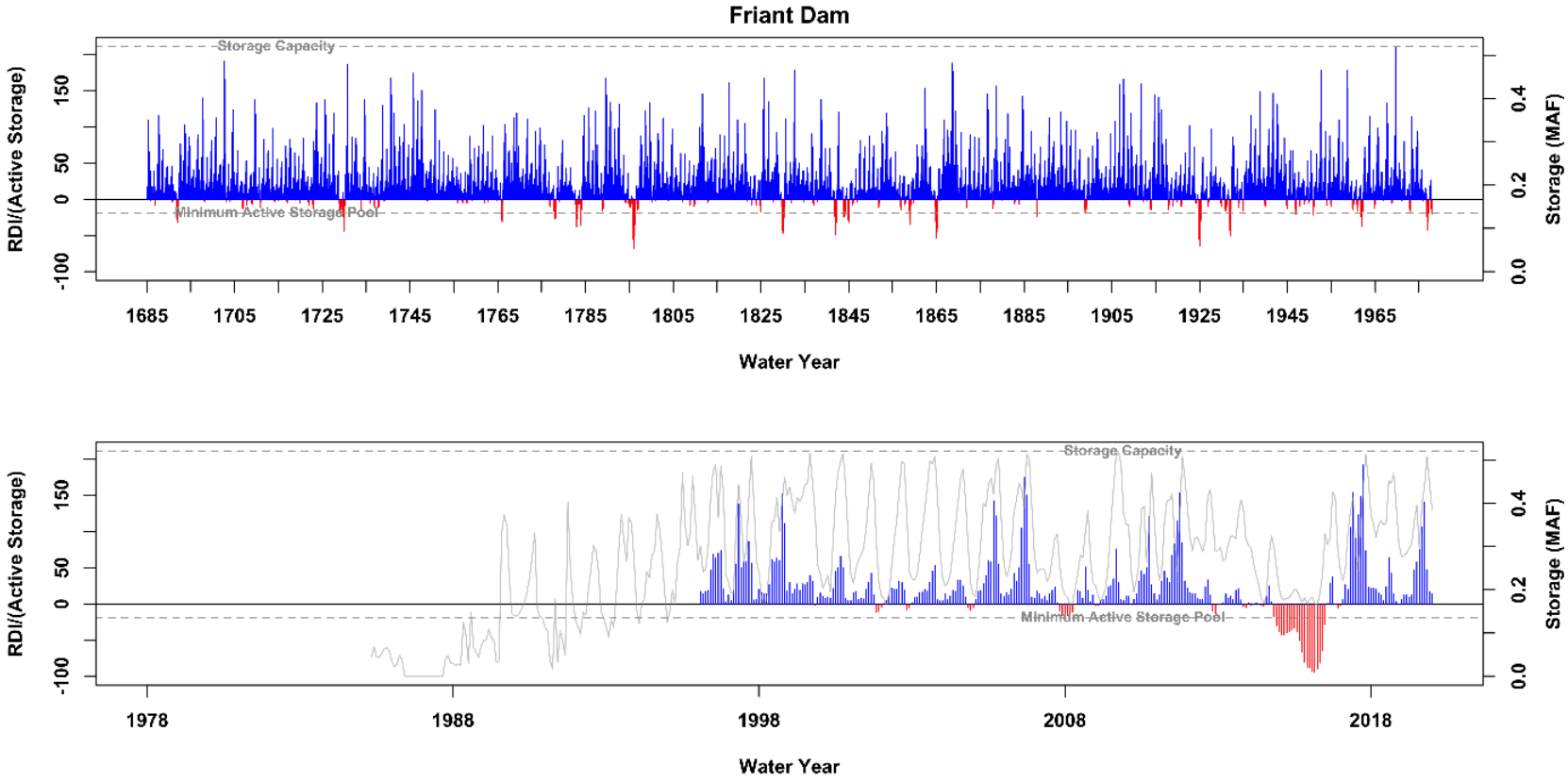

Figure 101. RDI time series normalized by active storage for Millerton Lake.

Note: Normalized RDI time series (percentage of active storage) for the paleo-reconstructed period (top panel) and the instrumental period (bottom panel). For the instrumental period, the reservoir's actual storage time series is shown using a light gray line. Storage capacity and minimum active storage pool in both panels are shown with dashed gray lines.

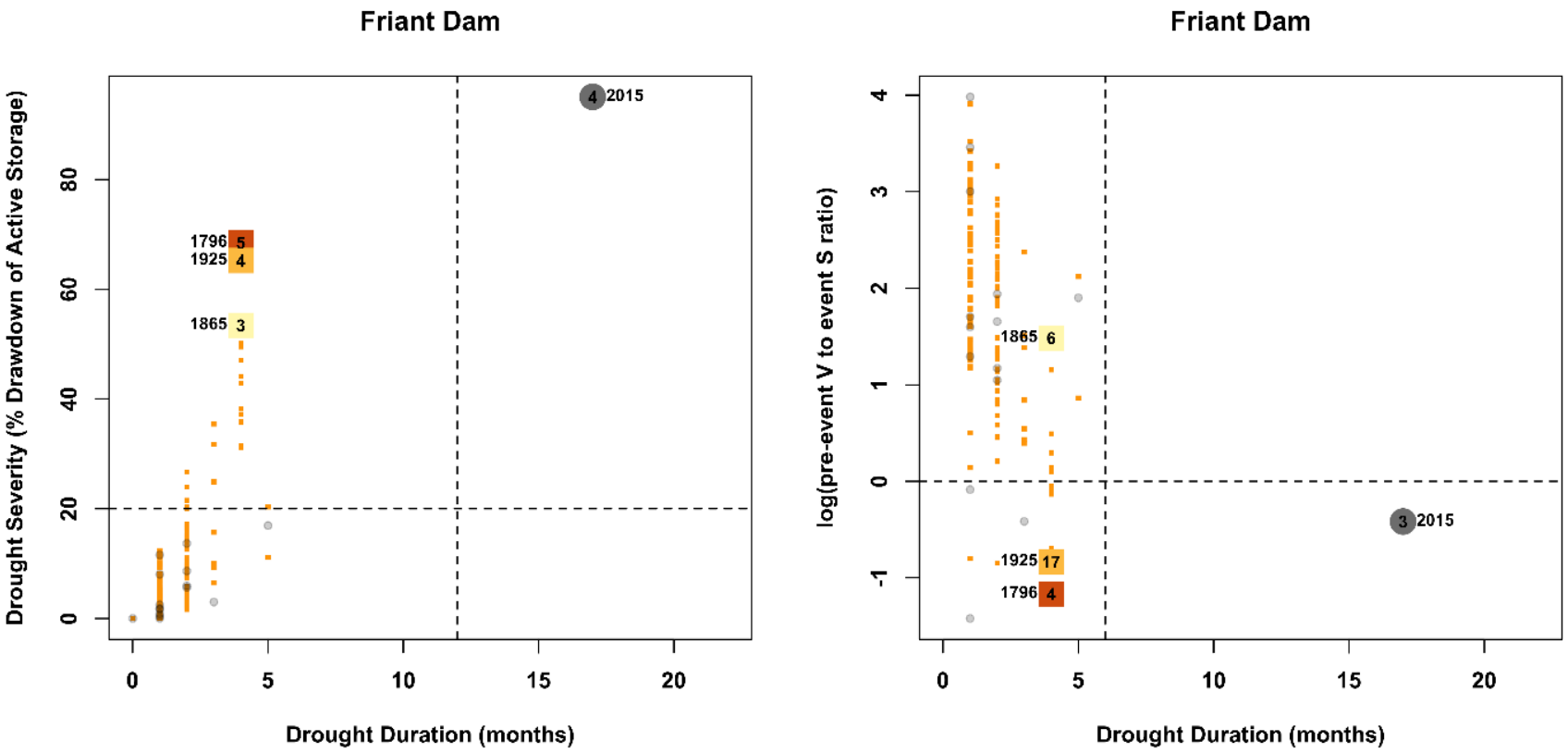

Figure 102. Multivariate distribution of drought events for Millerton Lake.

Note: Multivariate distribution of drought events with paleo-reconstructed drought events shown with filled (orange) squares, and the instrumental period's events shown with filled (gray) circles. The top three worst paleo-reconstructed drought events and the worst event in the instrumental period are highlighted using larger-sized red, orange, and yellow squares, and gray circles. The year of occurrence is indicated against the points. The number indicated inside the larger squares or the larger circle is the reservoir drought recovery in months for that drought event. Dashed lines are used to define drought event thresholds (refer to text for details).

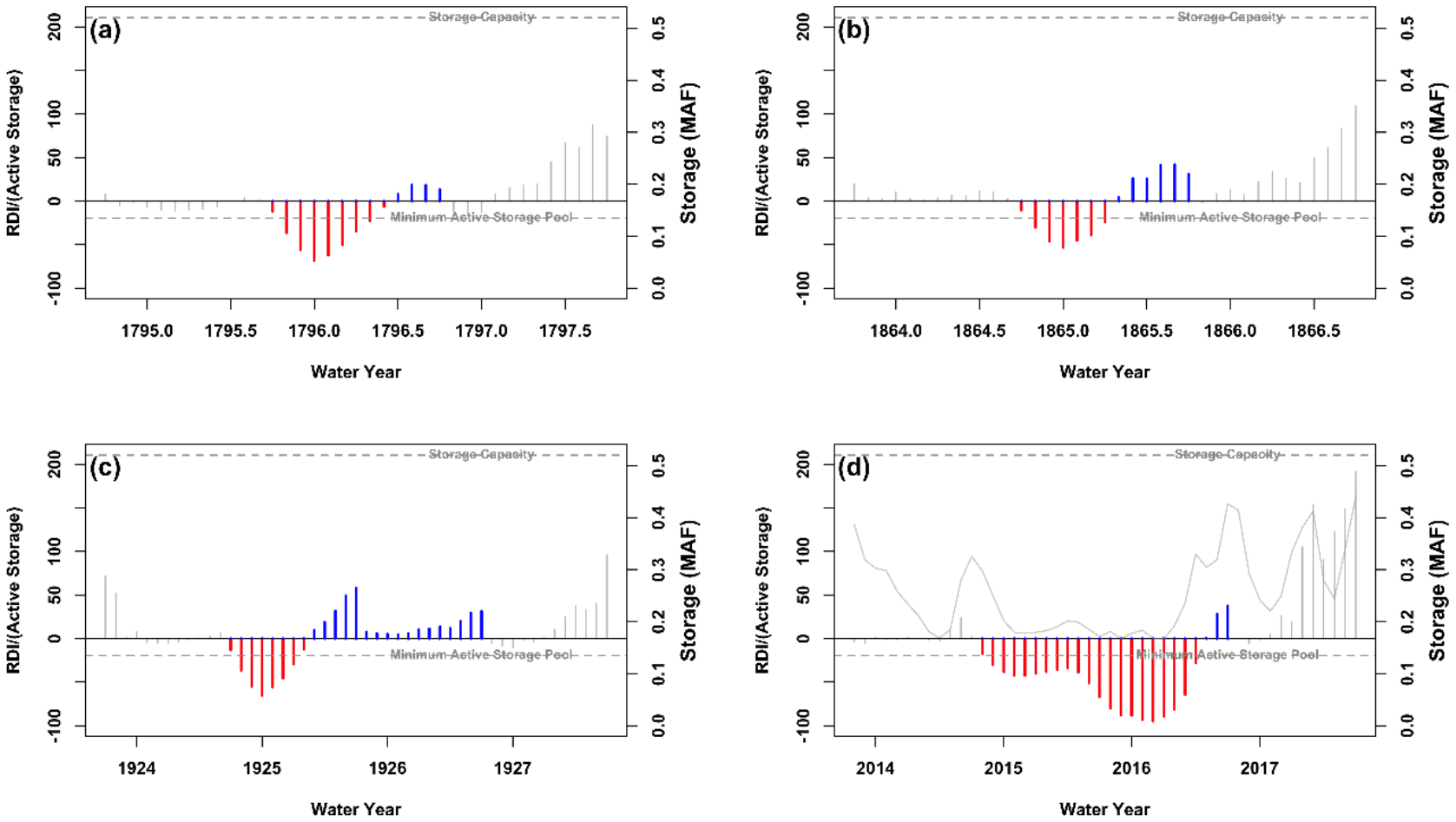

Figure 103. Normalized RDI time series for selected events for Millerton Lake.

Note: Sub-plots (a) through (c) are in time order for the three worst paleo-reconstructed droughts and the worst instrumental period drought event is shown in sub-plot (d).

5.3.5 Shasta Lake

Results for Shasta Lake are shown in Figure 104, Figure 105, and Figure 106. The RDI behavior of Shasta Lake is similar to that of American Falls Reservoir. It exhibits cyclicity in droughts and pluvial, both in the instrumental and paleo-reconstructed periods. Severe sustained droughts in both the instrumental and paleo period were noted, but the recovery from these longer droughts was typically within 5 months. The short-lived droughts (both in the instrumental and paleo period) had a severity between 20 to 50 percent of the active storage. The flash drought failure probability was low in both of the periods (less than 10 percent). Most of these short-lived droughts can be alleviated using pre-event reservoir fill-ups.

Figure 106 shows the RDI for the top events highlighted in Figure 105. The worst event in the paleo-reconstructed period occurred during 1924 to 1925. The duration of this drought was 17 months, with a recovery period of 3 months. The severity was 67 percent of the active storage capacity of the reservoir. The worst event in the instrumental period occurred during 1931 to 1932, 19 months to peak severity, and recovery of 5 months. The severity was nearly 56 percent of the active storage capacity.

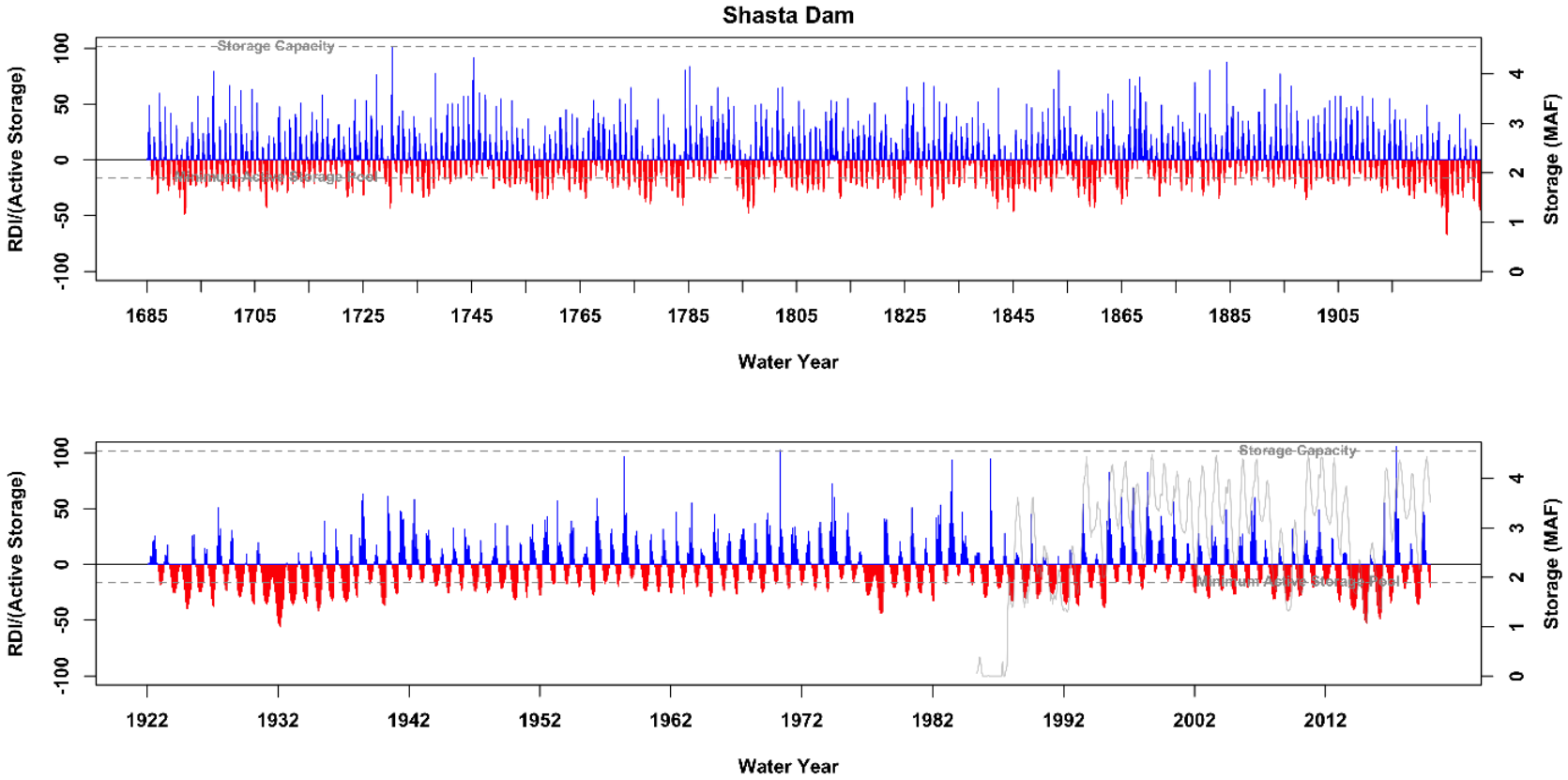

Figure 104. RDI time series normalized by active storage for Shasta Lake.

Note: Normalized RDI time series (percentage of active storage) for the paleo-reconstructed period (top panel) and the instrumental period (bottom panel). For the instrumental period, the reservoir's actual storage time series is shown using a light gray line. Storage capacity and minimum active storage pool in both panels are shown with dashed gray lines.

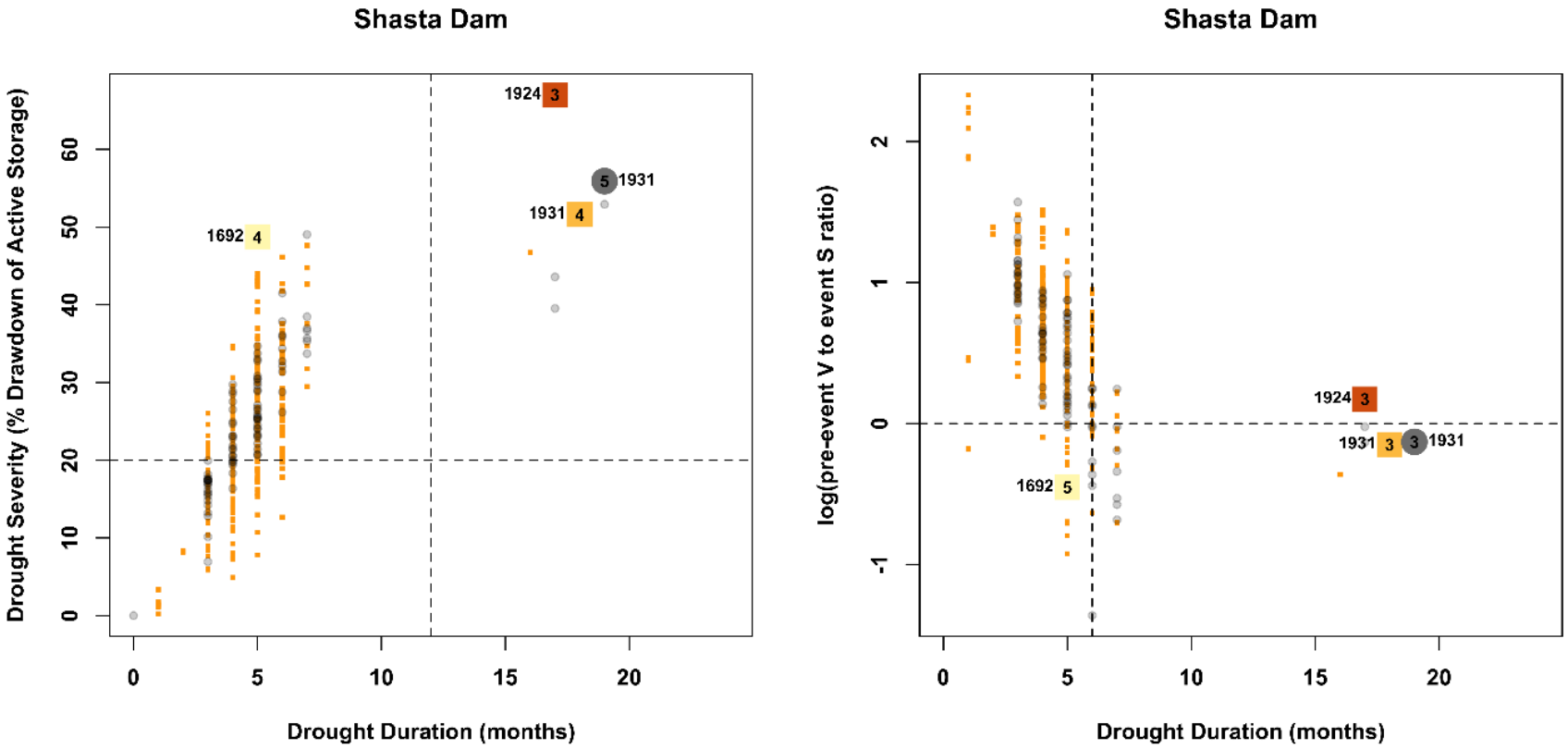

Figure 105. Multivariate distribution of drought events for Shasta Lake.

Note: Multivariate distribution of drought events with paleo-reconstructed drought events shown with filled (orange) squares, and the instrumental period's events shown with filled (gray) circles. The top three worst paleo-reconstructed drought events and the worst event in the instrumental period are highlighted using larger-sized red, orange, and yellow squares, and gray circles. The year of occurrence is indicated against the points. The number indicated inside the larger squares or the larger circle is the reservoir drought recovery in months for that drought event. Dashed lines are used to define drought event thresholds (refer to text for details).

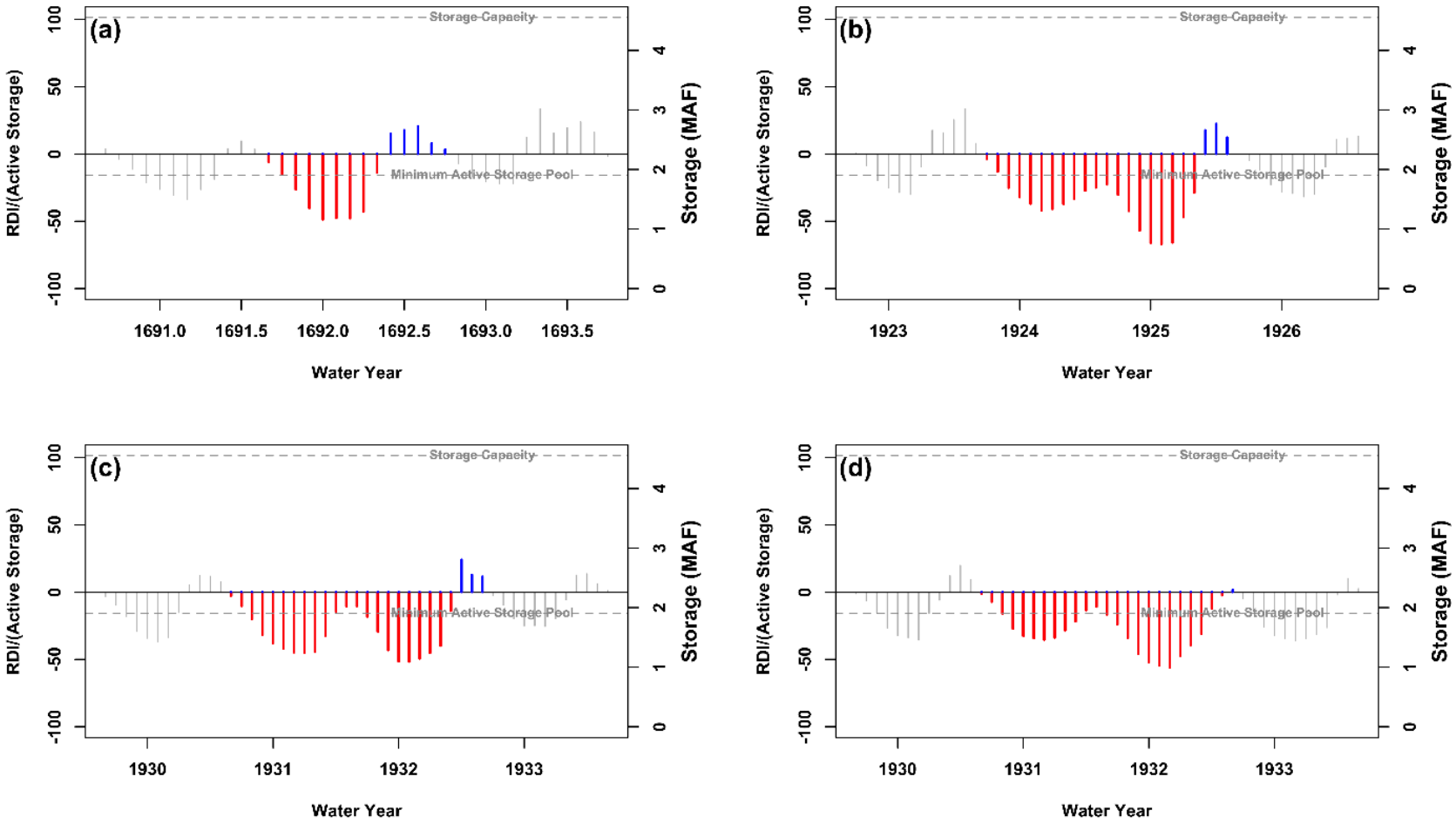

Figure 106. Normalized RDI time series for selected events for Shasta Lake.

Note: Sub-plots (a) through (c) are in time order for the three worst paleo-reconstructed droughts and the worst instrumental period drought event is shown in sub-plot (d).

Finally, a summary of the five drought statistics (RDD, RDS, RDR, RED, and REF) for the top three worst events in the paleo-reconstructed period and the worst event in the instrumental period for all five reservoirs is presented in Table 25. Lake Powell has the most prolonged drought durations among the five reservoirs. American Falls Reservoir has the most severe droughts, and the droughts in this reservoir took the longest time to recover. Millerton Lake has the most excess period fill-up durations and volumes among the five reservoirs. Except for a few occasions, there is no common overlapping period for the time of occurrence of these events, indicating that the reservoir stress can be evaluated relatively independently across the five reservoirs analyzed.

Table 25. Summary of five drought statistics for the five reservoirs

Reservoir	Event		RDD (month)	RDS (percent of active storage)	RDR (month)	RED (month)	REF (percent of active storage)
	Type[1]	Year					
American Falls	Paleo.	1863	14	221	18	1	0.39
		1632	17	179	5	6	184
		1935*	5	171	15	4	52
	Inst.	1935	6	163	19	2	68
Canyon Ferry	Paleo.	1936	9	38	2	2	4
		1846	15	33	3	6	26
		1757	3	23	6	4	68
	Inst.	1989	8	23	2	2	20
Lake Powell	Paleo.	1702	31	25	3	6	11
		1856	19	19	4	1	1
		1897	20	18	2	5	25
	Inst.	2001	57	37	37	3	17
Millerton Lake	Paleo.	1796	4	68	5	4	58
		1925	4	65	4	17	325
		1865	4	53	3	6	171

Reservoir	Event		RDD (month)	RDS (percent of active storage)	RDR (month)	RED (month)	REF (percent of active storage)
	Type[1]	Year					
	Inst.	2015	17	95	4	3	67
Shasta Lake	Paleo.	1924	17	67	3	3	52
		1931*	18	52	4	3	48
		1692	5	49	4	5	65
	Inst.	1931	19	56	5	1	2

* Note: Based on reconstructed streamflow used for reservoir inflows. These years also appear in the instrumental period and the calculated drought statistics are practically the same using the reconstructed inflows ("paleo-period") and the measured inflows ("instrumental period").

[1] Two types of drought event: paleo-reconstructed (labeled as "Paleo.") and instrumental (labeled as "Inst."). The top three worst paleo-reconstructed drought events and the worst event in the instrumental period are listed.

5.4 Summary and Next Steps

Reservoirs are designed to buffer the effect of droughts and capture surplus flows during wet epochs. Paleo-reconstructed streamflow records are potentially useful to provide information on wet and dry periods with severity and duration that may not have been seen during the 20th century and beyond the instrumental record. The work presented in this chapter aimed to put these paleo-reconstructions in the context of reservoir supply and demand, such that the potential imbalances in and failure statistics of reservoir storage could be compared on a common footing. A detailed modeling of reservoir operation rules and water rights would be an ideal approach for such an evaluation and comparison. However, given practical time and resource constraints, a more simplified approach that could be readily applied to multiple reservoirs to gain insights was taken in this work.

The first step was to develop a reasonable proxy for calendar month water demand from each reservoir that is respectful of the operational rule curve for the reservoir and covers all possible uses. This was done for all the reservoirs, with a check of how reasonable this approach was for some of the reservoirs where some additional data was available. The consistency of the resulting depletion and fill statistics with the actual reservoir storage time series for each of the reservoirs provides confidence that the approximation was comparable for the purpose of assessing drought statistics. The methodology may underestimate the drought statistics if the assumption of minimum demand during "non-trigger" events is quite different than the actual demands for the reservoir.

The assessment of drought severity-duration-recovery considering estimated demands and inflows is usually only a first step in the development of a management process for adaptation and risk mitigation. The risk indices developed here can serve as performance indicators for a proposed management strategy for climate risk mitigation. Climate risk mitigation needs to integrally consider information from climate change simulations (future trends), and from the instrumental and paleoclimate periods (the nature of persistence in climate variability and its predictability). The importance of such a consideration to identify the timing and nature of specific adaptation actions is highlighted by Doss-Gollin et al. (2019) and Doss-Gollin (2020).

Adaptation strategies to increasing drought (and flood) risk in the future may entail changes in operational strategies to address changes in the seasonality of inflows and demands that include changes in the rule curves based on seasonal to decadal climate forecasts that leverage the predictability of the climate system at these time scales (e.g., Rajagopalan et al., 2019; Erkyihun et al., 2016; Yeager et al., 2018).

They may also include structural changes, such as considerations for increasing water storage as climate model results show a shift in runoff seasonality. Finally, it is inevitable that a changing climate will lead to changes in water demand. This is an area that so far has not seen nearly as much attention as the generation of inflow and climate scenarios. Changes in demand may come from changes in population; crops; cropped area and irrigation technologies; environmental flow demands to address ecosystem needs under warming conditions; and demand for hydropower

and pumped storage as the Nation considers a greater emphasis on renewable energy sources. It is inevitable that these factors will pressure the existing system of surface and groundwater rights and reservoir operation in the Western United States. There is impetus for market-based mechanisms and the introduction of financial mechanisms for risk mitigation through water futures trading (CME, 2020). The integration of these factors into the consideration for an adaptation strategy is important. Reclamation is appropriately placed to play a leadership role in the integrated scientific analysis of the options. Further, Reclamation is well-placed to develop recommendations as to how the evolution of water allocation and system operation could be conjunctively analyzed to demonstrate how equity and value considerations can be best informed across the region.

5.5 Key Findings

A listing of key findings from the reservoir drought index and related drought metrics capturing storage-deficit and reservoir performance are given below:

- From the five reservoirs analyzed, the minimum active storage pool at which restrictions are imposed is generally a large fraction of the active storage capacity. This may represent a strategy that tries to hedge against droughts; however, this analysis does not consider other constraints on reservoir storage—non-structural constraints (e.g., environmental flows), and structural constraints (e.g., outlet capacity).
- For some of the reservoirs, the probability of severe sustained drought indicated is generally much higher in the paleo-reconstructed period than in the instrumental period. However, given the high minimum active storage pool, the ability of the system to avert a drought impact based on a prior reservoir refill cycle still relatively high in all five cases.
- The estimated static demand considered here may belie the actual allocated water from the reservoir considering all uses and environmental flows and, if this is the case, then the likelihood of severe sustained drought may be understated by this analysis.
- The results for Glen Canyon Dam (Lake Powell) are notable since, in this analysis, the severity and duration of droughts in the observed historical period is unmatched in the paleo-reconstructed period. However, the length of the paleo-reconstructed streamflow record used in this analysis does not capture the severe and long-duration drought events documented over the 1100s through the late 1500s, as described in Chapter 2. In other words, the major “megadroughts” in the paleo-reconstructed streamflow records were not analyzed.

6 Water Supply Reliability Assessment

6.1 Background

Repeated years of above- or (especially) below-average streamflow can challenge water managers and users since both infrastructure and management protocols are generally designed around average hydrologic conditions. The accumulation of water deficits (droughts) or, to a lesser degree, surpluses (pluvial events) over prolonged periods can force both managers and water users into sub-optimal modes of operation. For example, sustained drought may deplete reservoir storage, forcing shortages in water deliveries to end-users or may impact hydropower generation. Repeated flood episodes, however, may impact regional economies since flood damage to infrastructure may outpace maintenance and repair.

Use of paleohydrology scenarios in water management and planning allows for broad understanding of possible future conditions based on known historical drought or pluvial events from the distant past. This chapter of the report summarizes water supply reliability under observed historical conditions and paleohydrology scenarios. Paleohydrology scenarios are scenarios of river inflow developed using streamflow reconstructions based on tree-ring data (i.e., paleo-reconstructions of streamflow). Scenarios may be input to a river systems model to evaluate major drought and pluvial events from the distant past. Paleo-reconstructions of streamflow that informed this analysis are introduced in Chapter 2. Similarly, Chapter 2 also describes the definition of drought that was used to identify major events in the reconstructed streamflow record. This analysis was performed in each of the eight major Reclamation river basins to demonstrate how this approach may be applied across these basins.

This evaluation builds on existing studies that have been completed under Reclamation's WaterSMART Basin Studies Program to evaluate water reliability under scenarios based on paleohydrology. Examples of existing studies include the Colorado Supply and Demand Study (Reclamation, 2012b), the Upper Missouri Basin Impacts Assessment and Missouri Headwaters Basin Study (Reclamation, 2020c), and the Reservoir Operations Pilot Study for the Washita Project (Reclamation, 2018). These studies, as well as the West-wide analysis summarized in this chapter, offer a broader look at the impact of droughts and pluvial events on water management than is typically considered when only examining historical events.

This information may help water managers better understand potential worst-case scenarios using paleo-reconstructed streamflow to "stress test" their operational decisions. For many basins, the observed historical period does not encompass the full range of variability in conditions that occurred over a much longer historical period. In this study, paleo-reconstructed streamflow dating back to 1685 was used because 1685 to 1977 is the common time period across all the reconstructions considered. Individual reconstructions may go back even further in time, for example to about 762 in the Colorado River Basin (Meko et al., 2007).

This chapter summarizes methods used and resulting impacts to rivers and reservoirs using paleo-reconstructed streamflow information based on tree-rings.

6.1.1 River Basin Identification

This report of water supply reliability considered each of the eight major Reclamation river basins outlined in the SECURE Water Act, namely the Colorado River Basin, the Columbia River Basin, the Klamath River Basin, the Missouri River Basin, the Rio Grande Basin, the Sacramento and San Joaquin River Basins, and the Truckee and Carson River Basins. For the Columbia River Basin, this analysis focuses on the Boise River basin. For the Missouri River Basin, this analysis focuses on the Upper Missouri River upstream of Fort Peck Reservoir. For Truckee River Basin, the Carson River basin is also considered as part of the analysis because these rivers are co-managed. Figure 107 illustrates the river basins considered in this analysis.

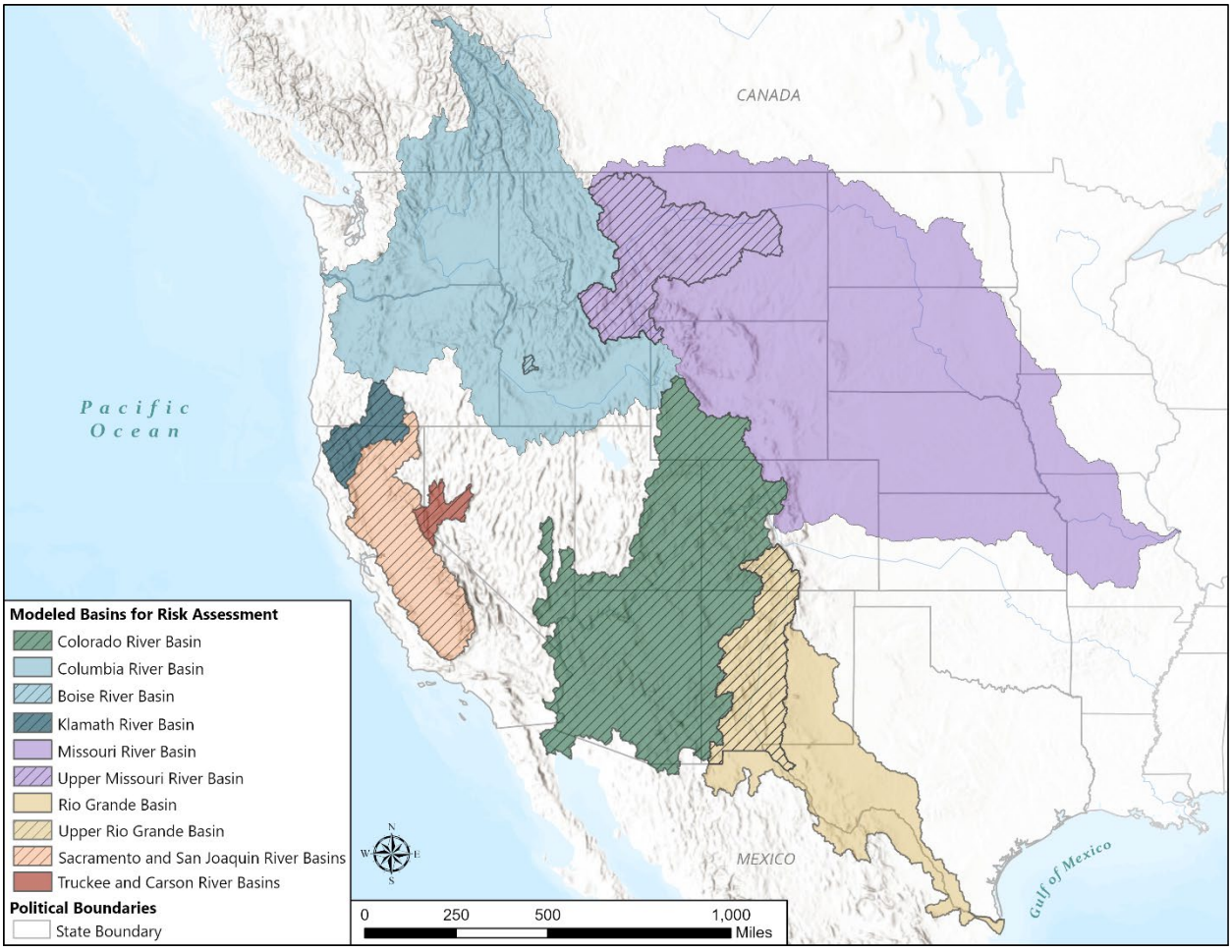

Figure 107. River basins used in this water supply reliability assessment.

6.1.2 Overview of Analysis Methods

For each of the basins selected for analysis, there is an existing river systems model used for long-term planning. In some cases, the same model is also used for daily operations. Table 26 summarizes the river systems models used to simulate each system and key information about each model. It also identifies the observed historical period used as a baseline for analysis.

The development of model inputs, model simulations, and analysis of model outputs were performed collaboratively among Reclamation staff at the Technical Service Center and Reclamation's Region and Area Offices.

Table 26. Models used to simulate water management in each basin

River Basin	Model	Software	Time Step	Observed Historical Period used as Baseline
Columbia	Boise RiverWare Planning Model	RiverWare	Daily	10/01/1980-09/30/2018
Colorado	Colorado River Simulation System (CRSS)	RiverWare	Monthly	10/01/1905-09/30/2018
Klamath	Klamath River Basin Study (KRBS) RiverWare Model	RiverWare	Daily	10/01/1960-09/30/2013
Missouri	Upper Missouri Basin Impacts Assessment (UMBIA) RiverWare Model	RiverWare	Daily	10/01/1950-09/30/1999
Rio Grande	Upper Rio Grande Water Operations Model (URGWOM)	RiverWare	Daily	01/01/1950-12/31/2015
Sacramento and San Joaquin	CalSim 2	WRIMS	Monthly	10/1921-09/2003
Truckee and Carson	Truckee River Operating Agreement Planning Model	RiverWare	Daily	10/01/1901-12/31/2015

This analysis sought to evaluate managed river conditions using the models identified above under an observed historical baseline period, notable historical drought events, and identified drought events from the distant past using streamflow reconstructions. Drought events from the distant past are called paleohydrology scenarios. As case studies, pluvial events were also evaluated in the Boise River basin and Truckee and Carson River Basins. The following sections describe notable historical droughts in the observed period that are relevant in the minds of water

managers. The following sections also generally describe the approach used to develop paleohydrology scenarios from streamflow reconstructions.

Managed river conditions were evaluated for selected metrics. These metrics generally include storage in key reservoirs in the basin, as well as managed streamflow at key locations. Additional metrics were identified that are specific to each basin and are described in each basin subsection.

In this report, projected future scenarios were not simulated by river systems models to evaluate future water management impacts. Typically, assessments of future impacts on water management have been performed through basin studies and other long-term planning studies. Application of models and tools that perhaps more appropriately represent physical hydrology in a specific river basin may be preferred for an analysis of climate change impacts. As discussed in Chapter 3, choices in methods for performing impacts assessments can lead to different outcomes. A single West-wide analysis using a consistent set of methodological choices (e.g., surface hydrology model) has advantages for making comparisons across basins and also may have limitations by not representing the hydrologic complexities of a river basin. Moreover, where possible, this chapter refers to existing basin-specific studies to discuss local impacts.

For each river basin evaluated in this chapter, however, paleo drought events are compared with observed historical droughts and future droughts identified for each future CMIP5-LOCA streamflow projection under RCP4.5 and RCP8.5 emissions scenarios. The drought events were identified under unmanaged conditions and, despite the conditions being unmanaged, this provides information about the severity and duration of drought events. These results are discussed in the basin sections within this chapter.

It should be noted that future projected drought events are identified using streamflow simulated using the Variable Infiltration Capacity (VIC) hydrologic model (e.g., Vano et al., 2020), which may be un-calibrated or partially calibrated in each of the river basins evaluated in this chapter. Because drought events identified from simulated streamflow are compared with events based on historical and paleo-reconstructed streamflow, which are based on observations, a step was performed to remove systematic biases in the simulated streamflow, therefore making events between record types comparable.

6.1.3 Observed Historical Events

Historical drought events provide information on how these relatively recent events affected a managed river system of interest. Drought events from the paleo-reconstructed period can be simulated in the same way and compared to those from the observed historical period. Water managers, stakeholders, and the general public have familiarity with observed historical events that can provide a tangible benchmark against which to compare impacts of events from the more distant past. Historical events are also often used by water managers in developing risk-informed operating decisions. Table 27 summarizes observed historical and paleo drought events evaluated in this chapter.

Table 27. Selected drought events from the observed historical period and paleo-reconstructed period

River Basin	Relevant Reconstruction(s)	Drought	Start Year	End Year	Length
Colorado	Colorado River at Lees Ferry, AZ	Historical Drought 1	1953	1964	12
		Historical Drought 2	2000	2020[1]	21[1]
		Paleo Drought 1	1772	1783	12
		Paleo Drought 2	1845	1848	4
		Paleo Drought 3	1873	1883	11
Columbia	Boise River nr Parma, ID	Historical Drought 1	1930	1942	13
		Historical Drought 2	1987	1995	9
		Paleo Drought 1	1878	1907	30
		Paleo Drought 2	1729	1745	17
		Paleo Drought 3	1813	1819	7
Klamath	Klamath River at Keno, OR	Historical Drought 1	1917	1934	18
		Historical Drought 2	1990	1995	6
		Historical Drought 3	2000	2005	6
		Paleo Drought 1	1774	1787	14
		Paleo Drought 2	1843	1856	14
		Paleo Drought 3	1732	1746	15
Missouri	Missouri River at Fort Benton, MT; Musselshell River at Mosby, MT	Historical Drought 1	1930	1946	17
		Historical Drought 2	1954	1964	11
		Historical Drought 3	1985	1992	8
		Paleo Drought 1	1793	1809	17
		Paleo Drought 2	1844	1852	9
		Paleo Drought 3	1855	1865	11

River Basin	Relevant Reconstruction(s)	Drought	Start Year	End Year	Length
Rio Grande	Rio Grande at Otowi Bridge, NM; Conejos River near Mogote, CO; Rio Grande near Del Norte, CO	Historical Drought 1	1950	1956	8
		Historical Drought 2	2011	2015	6
		Paleo Drought 1	1870	1883	15
		Paleo Drought 2	1772	1782	12
		Paleo Drought 3	1728	1737	11
Sacramento and San Joaquin	Sacramento River at Bend Bridge, CA; Feather River at Oroville, CA; American River at Fair Oaks, CA; San Joaquin River at Millerton, CA	Historical Drought 1	1928	1934	7
		Historical Drought 2	1987	1992	6
		Paleo Drought 1	1776	1783	8
		Paleo Drought 2	1753	1765	13
		Paleo Drought 3	1833	1846	14
		Paleo Drought 1	1776	1783	8
		Paleo Drought 2	1833	1846	14
		Paleo Drought 3	1753	1766	14
		Paleo Drought 1	1776	1783	8
		Paleo Drought 2	1840	1851	12
		Paleo Drought 3	1753	1765	13
		Paleo Drought 1	1776	1783	8
		Paleo Drought 2	1840	1846	7
		Paleo Drought 3	1793	1796	4

River Basin	Relevant Reconstruction(s)	Drought	Start Year	End Year	Length
Truckee and Carson	Carson River at Fort Churchill, NV	Historical Drought 1	1923	1936	14
		Historical Drought 2	2012	2016	5
		Paleo Drought 1	1841	1851	11
		Paleo Drought 2	1776	1783	8
		Paleo Drought 3	1856	1865	10

[1]The 2000 to 2020 drought in the Colorado River Basin is currently ongoing

[2]The 1976 to 1977 drought and 2013 to 2015 drought were also historic droughts in California, but were not considered in this analysis. In the future, the approaches presented in this report may be used to evaluate the implications of these drought events as well.

6.1.4 Paleohydrology Scenario Development

Paleo-reconstructed streamflow timeseries (reconstructions) were collected at a total of 152 locations. The reconstructions and their source information are further discussed in Chapter 2. As discussed in Chapter 2, drought events may be defined many ways. Also, the characteristics of droughts may vary geographically, leading to use of different drought definitions in different parts of the West. Based on the selected definition for this analysis, droughts with the overall largest cumulative deficit compared with the long-term median were evaluated.

In each of the river basins, select streamflow reconstructions were used to develop inputs for river systems models in those basins. The individual reconstructions that informed each basin analysis are listed in Table 27 and are also illustrated in Figure 3. To develop streamflow inputs that correspond with the inflow locations of the river systems models and at the needed timestep (typically daily), the paleo-reconstructed streamflow timeseries were spatially and temporally disaggregated using a similar approach to that developed by Nowak et al. (2010). For some models, a single streamflow reconstruction was used to inform inflow development for all locations in the model (e.g., Truckee and Carson River Basins). For other models, multiple reconstructions were mapped to appropriate inflow locations in the river systems model (e.g., Sacramento and San Joaquin River Basins).

Water year annual timestep paleo-reconstructed streamflow was disaggregated to either a daily or monthly timestep (depending on the river system model) using the pattern of available observed or modeled streamflow (depending on the location), adjusted to ensure the summed water year annual flows match the streamflow reconstruction.

Based on the variety of drought events identified, the three drought events with the largest cumulative deficit, in other words those events with the largest overall volume below the long-term median, were run through the river systems models and evaluated, along with the notable drought events in the observed historical period (refer to Table 27). The Paleo Drought 1

is the largest drought according to this definition while Paleo Drought 3 is the third largest. These three droughts represent three of the most severe droughts to occur during the 1685 to 1977 period, which is the time period common to all available streamflow reconstructions.

6.1.5 Evaluating Impacts to Water Management Metrics

Water managers commonly consider metrics as indicators of the success of achieving certain management objectives. There are metrics that are common across river basins, such as reservoir storage. However, there are metrics that are unique to each basin. For example, a managed river may have minimum instream flow requirements to accommodate fish and wildlife habitat unique to that river.

In this chapter, common metrics are identified that were evaluated for each modeled river basin and drought event. Common reservoir metrics that were quantified in each river basin include:

- Daily or monthly storage at major reservoirs during identified drought events
- Average percent of days over drought below minimum managed pool elevation
- Average percent of days over drought reservoir refills to top of managed pool
- Average percent of capacity at the end of the water year (September 30)

It should be noted that these select metrics may not illustrate the implications of drought length on the river systems. To this end, each basin evaluation discussed in the following sections provides timeseries illustrations of reservoir storage to offer complementary information on the impacts due to drought length, in addition to the average metrics over each drought event. Basin-specific metrics beyond those listed above, and that are unique to individual river systems, are described in respective subsections below.

When evaluating reservoir metrics, such as the average percent capacity at the end-of-water-year (September 30), it is important to consider reservoir storage as a function of mean annual inflow because some reservoirs may hold more water than can be accumulated in one year. For example, Lake Mead and Lake Powell can hold multiple years of reservoir inflow to allow for capture of water in wet years that may be used to meet demands in dry years. Other reservoirs may have limited capacity compared with mean annual inflow. Therefore, percent of reservoir capacity at the end of the water year may have unique meaning for each reservoir. Table 28 summarizes total reservoir capacity relative to mean annual inflow. This information is referred to in following discussions of the impacts of drought events on reservoir storage.

Table 28. Mean annual inflow and capacity for evaluated reservoirs

River Basin	Reservoir Name	Total Reservoir Capacity (acre-feet)	Mean Annual Inflow (acre-feet)[1]	Ratio (capacity / inflow)
Colorado	Lake Mead	27,620,000[2]	10,881,113 (1976-2019)	2.7
	Lake Powell	24,322,000[3]	10,292,224 (1963-2019)	2.4
Columbia[4]	Anderson Ranch	474,900	671,821 (1981-2018)	0.71
	Lucky Peak	264,400	1,888,263 (1981-2018)	0.16
Klamath	Upper Klamath Lake	515,408	1,190,327 (1961-2013)	0.43
Missouri	Canyon Ferry	1,992,977	3,697,270 (1953-2019)	5.4
Rio Grande	Elephant Butte	2,010,900	444,071 (2002-2019)	4.5
Sacramento and San Joaquin	Millerton	611,500	1,756,393 (1994-2019)	0.35
	Lake Shasta	4,552,000	5,603,984 (1990-2019)	0.81
Truckee	Lahontan	309,917	318,070 (1901-2017)	1.0
	Lake Tahoe	756,960	165,336 (1901-2017)	4.6

[1] Mean annual reservoir inflow was computed over water years based on available observed data.

[2] Reservoir capacity represents active capacity (not including dead pool) and not total capacity.

[3] Reservoir capacity represents active capacity (not including dead pool) and not total capacity.

[4] Anderson Ranch Reservoir is upstream of and contributes flow to Lucky Peak Reservoir. Therefore, some of the inflow to Lucky Peak Reservoir is storage release from Anderson Ranch Reservoir.

6.2 Colorado River Basin

The Colorado River Basin extends across seven basin States of the United States and into Mexico. Colorado River Basin water is shared among these seven States and Mexico in accordance with the "Law of the River"—a collection of compacts, Federal and State statutes, court decisions and decrees, international treaties, regulations, and other legal agreements—which began with the 1922 Colorado River Compact. The river provides irrigation water to 4.5 million acres and water supply to between 35 and 40 million people (Reclamation, 2015b). In addition, reservoirs in the Colorado River Basin are managed for hydropower, flooding, and to meet obligations under the Endangered Species Act.

Since 2000, the Colorado River Basin has experienced a historic drought impacting water supply, hydropower production, recreation, and ecologic services. Inflows into reservoirs in the basin are the lowest in over 100 years of record keeping and, in 2016, Lake Mead reached its lowest storage since it first filled in the mid-1930s.

The analysis of water supply risks related to drought events was performed by identifying notable historic drought events, as well as drought events in the paleo-reconstructed period, and comparing the managed system, under current operations and demands, with an observed historical baseline period. Two drought periods from the observed historical period were selected for analysis—the "Mid-20th Century Drought" lasting 12 years from 1953 to 1964 (Historical Drought 1), and the ongoing "Millennium Drought" spanning so far 21 years from 2000 to 2020 (Historical Drought 2). Hydrologic conditions beyond 2018 were not simulated due to data constraints, but, from observations, the period 2000 to 2020 is the lowest 21-year period since the closure of Glen Canyon Dam in 1963. Had the simulations used hydrologic conditions from 2019 and 2020, the Historical Drought 2 would have extended an additional 2 years and, if dry conditions continue to persist in the basin, could continue even longer.

6.2.1 Paleohydrology Scenario Development

Paleohydrology scenarios for the Colorado River Basin were developed using the Lees-B annual streamflow reconstruction for the Colorado River at Lees Ferry, AZ (USGS ID 09380000). Multiple streamflow reconstructions have been developed for this location and additional information including references for these reconstructions can be found in Chapter 2. Figure 108 shows the paleo-reconstructed naturalized (i.e., unimpaired) streamflow for the Colorado River at Lees Ferry, AZ (Lees-B) for the period 1685 to 1977, and naturalized streamflow over the observed historical period from 1906 to 2018.

Annual paleo-reconstructed streamflow is shown in black, with the historical streamflow shown in blue. Drought events of interest are shaded and include the three "largest cumulative deficit" droughts from the paleo-reconstructed period—Paleo Drought 1 which spans 12 years from 1772 to 1783; Paleo Drought 2 which spans 4 years from 1845 to 1848; and, Paleo Drought 3 which spans 11 years from 1873 to 1883. These three drought events were identified using the drought definition described in Section 2.4. This approach, along with sub-setting the reconstruction to the West-wide common paleo-reconstruction period, limited the selection of droughts examined in this analysis. For example, the 1100s drought highlighted in Meko et al.

(2007) is not included, nor are other notable droughts seen in the paleo-reconstructions prior to 1685, the start of the common period. Additional discussion of these earlier droughts, a comparison of different reconstructions, and the sensitivity of drought definition to the selected period can be found in Chapter 2.

Together, these five drought events—two from the observed historical period and three from the paleo-reconstruction period—were used to investigate impacts to reservoir storage in Lake Mead and Lake Powell.

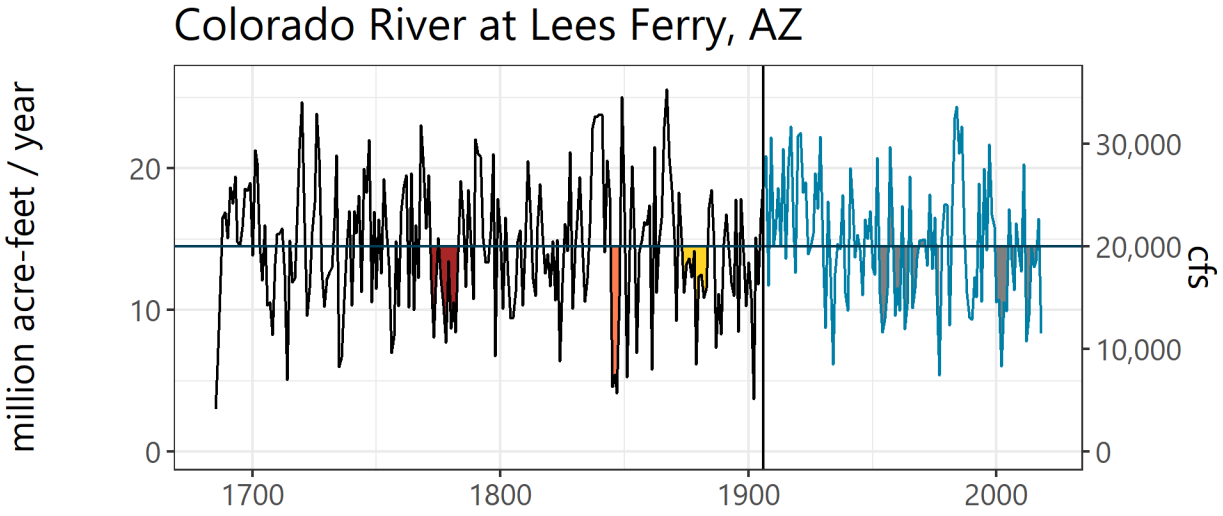

Figure 108. Annual streamflow for the Colorado River at Lees Ferry, AZ showing droughts in the paleo-reconstructed and observed historical periods.

Note: Paleo-reconstructed streamflow is in black and historical streamflow is in blue. The horizontal line shows long-term median streamflow. Drought events are shaded (red, orange, and yellow for Paleo Droughts 1, 2, and 3, respectively, and gray for historical droughts).

cfs = cubic feet per second

6.2.2 River Systems Model Overview

The Colorado River Simulation System (CRSS) is a monthly timestep river systems model that has been used for decades to support mid-term and long-term planning in the Colorado River Basin. For example, it was used as the basis for the Colorado Water Supply and Demand Study (Reclamation, 2012b) and to support development of the 2007 Interim Guidelines for Lower Basin Shortages and the Coordinated Operations for Lake Powell and Lake Mead (Reclamation, 2007).

The model version used in this report was CRSS.V4.5.0.2021.Apr2020, with policy ruleset CRSS.Baseline.2027IGDCP.v4.4.2. These are important to note for potential further exploration into results beyond the scope of this study. The CRSS model was run for each paleohydrology scenario with the framing of: "*What would happen if the drought started tomorrow?"* Initial conditions for all scenarios in the CRSS model simulations were end-of-calendar-year

projections from April 2020 Mid-Term probabilistic Operations Model (MTOM) Most Probable run. The operational policy set corresponds with the 2007 Interim Guidelines and Drought Contingency Plan which are assumed to extend through the end of the simulation period for modeling purposes. Model demands are based on official projections from the Upper Colorado River Commission (2007) held constant at 2018 levels.

Baseline conditions were based on CRSS model simulations using historical 1906 to 2018 hydrology where 112 different hydrology traces were modeled by starting hydrology in each year from 1906 to 2018.

6.2.3 Water Resource Metrics

Water supply reliability metrics examined using CRSS are shown in Table 29. These metrics focused on impacts to the two major storage reservoirs in the basin, Lake Powell and Lake Mead, as well as their ability to deliver water to downstream water users. For each reservoir, two critical thresholds were identified. At Lake Powell, these were 3,525 feet, below which Lake Powell enters into the Lower Elevation Balancing Tier, as specified in the 2007 Interim Guidelines; and elevation 3,490 feet, which is the minimum power pool. In the Lower Elevation Balancing Tier, releases from Lake Powell are made to balance contents between Lake Powell and Lake Mead subject to minimum and maximum release constraints of 7.0 and 9.5 million acre-feet, respectively. Below the minimum power pool, hydropower can no longer be produced. At Lake Mead, the first critical elevation threshold is 1,025 feet, below which Lake Mead is in the Third Shortage Tier where deliveries to the Lower Division States and Mexico are reduced by a total of 1,375,000 acre-feet. Additionally, below this elevation, the Secretary of the Interior, in consultation with basin States, can consider hydrologic conditions and anticipated deliveries and enact additional measures to try and keep Lake Mead from falling below 1,000 feet. The lower critical elevation threshold is 1,000 feet, below which Intakes 1 and 2 are inoperable. These intakes are used by the Southern Nevada Water Authority (SNWA) to provide water to their service area that includes Las Vegas, Nevada. SNWA can still operate Intake 3 below this elevation.

The final two metrics are related to water delivery. The first quantifies the 10-year total release from Lake Powell, which is representative of the 1922 Colorado River Compact article III.d that quotes, “The States of the Upper Division will not cause the flow of the river at Lee[s] Ferry to be depleted below an aggregate of 75,000,000 acre-feet for any period of ten consecutive years…”, and the second quantifies water deliveries to Lower Division States and Mexico.

Table 29. Metrics for quantifying water supply reliability in the Colorado River Basin

Pool Elevation Metrics
Percent of years Lake Powell elevation falls below 3,525 feet
Percent of years Lake Powell elevation falls below 3,490 feet
Percent of years Lake Mead elevation falls below 1,025 feet
Percent of years Lake Mead elevation falls below 1,000 feet
Other Metrics
10-year release from Lake Powell
Average lower basin deliveries (to Lower Division States plus Mexico)

6.2.4 Summary

Consistent with the approach for other basins, drought events from the observed historical period and the 1685 to 1977 paleo-reconstruction period were evaluated to gain a broad understanding of drought events across the West and their relative impacts on regional water management. Paleo drought events have been studied before in the Colorado River Basin, more so than in other Western river basins. Several streamflow reconstructions exist for the Colorado River at Lees Ferry including Lees-B (Woodhouse et al., 2006), Meko 2007 (Meko et al., 2007), and CA DWR 2017 (described in Lukas et al., 2020). This report used the Lees-B reconstruction, which encompasses over 500 years from 1490 to 1997, and it has been an integral dataset for previous studies. This reconstruction was subset to the West-wide common paleo-reconstruction period. Several paleo droughts of record can be found in the Colorado River at Lees Ferry paleo-reconstructions prior to 1685. These include the major 1100s drought identified in Meko (2007). Additional discussion about uncertainty regarding paleo-reconstructions and specific differences across reconstructions for the Colorado River at Lees Ferry can be found in Chapter 2.

The following figures illustrate how drought events may affect Lake Mead and Lake Powell reservoir elevation under the paradigm of: *"What would happen if the drought started tomorrow?"* Figure 109 illustrates monthly Lake Powell pool elevation for each of the five identified drought events. The two horizonal lines show elevation 3,525 feet, below which Lake Powell enters into the Lower Elevation Balancing Tier, as specified in the 2007 Interim Guidelines; and elevation 3,490 feet, which is the minimum power pool.

Each figure begins at January 1, 2021 initial reservoir conditions and then applies one of the five drought events to simulate reservoir conditions. Applying Historical Drought 1, pool elevation dropped below the higher 3,525-foot threshold in two periods—one near the start of the drought and another near the end—but remained above the lower 3,490 foot threshold over the duration of the drought. Applying Historical Drought 2, Lake Powell pool elevation dropped below the lower 3,490-foot threshold in the mid-2000s, recovered with slowly increasing elevations until

2012, and then declined to just above the 3,490-foot threshold until 2018 when it again dropped below this threshold. In Paleo Drought 1, lake elevations remained above both thresholds for 7 years before declining around 1780 and remaining below 3,490 feet until 1784. Paleo Drought 2 shows a much shorter-duration drought where lake elevations steadily decline from the start of the drought in 1845 to the end of the drought in 1848. For two of those years, 1847 and 1848, lake elevation remains below 3,490 feet, but rapidly recovers following the conclusion of the drought. Paleo Drought 3 is a longer-lasting, but less severe drought than the first two paleo droughts, with lake elevation remaining above both thresholds for the first 7 years before dropping below 3,525 feet, and only slightly falling below 3,490 feet in 2 years at the end of the drought.

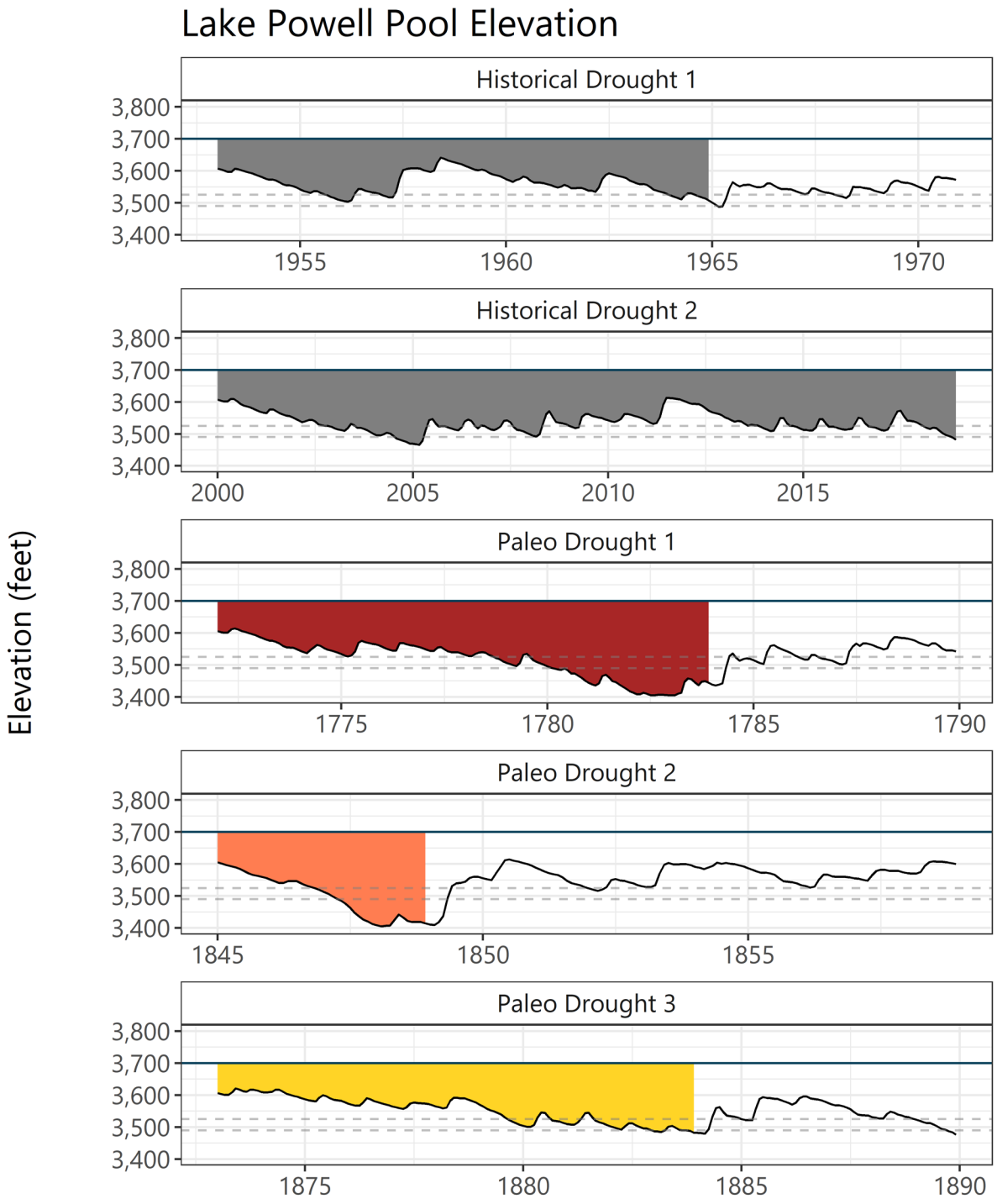

Figure 109. Monthly modeled reservoir pool elevation for Lake Powell for each drought event (panels).

Note: The solid horizontal lines show full pool elevation (3,700 feet) and the dashed horizontal lines show critical elevations (3,525 feet and 3,490 feet). Drought events are shaded.

Figure 110 illustrates monthly Lake Mead pool elevation for each of the five identified drought events. The two horizontal dashed lines show elevations 1,025 feet, below which Lake Mead is in the Third Shortage Tier; and 1,000 feet, below which Intakes 1 and 2 that provide water to Las Vegas, Nevada, are inoperable. In a shortage condition where pool elevation is below 1,025 feet, deliveries to Lower Division States and Mexico are reduced by a total of 1,375,000 acre-feet, and additional measures can be enacted as determined by the Secretary of the Interior, in consultation with the basin States.

Historical Drought 1 shows a steady decline in Lake Mead elevation to just below 1,025 feet, a slight increase in elevation in the middle of the drought, followed by a slight decline to below 1,025 feet at the end of the drought. At no point does Lake Mead fall below 1,000 feet in this drought. It is interesting to note that Lake Mead elevation following the end of the drought remains at or just above 1,025 feet.

Historical Drought 2 shows Lake Mead elevation dropping to a low point just below the lower threshold of 1,000 feet, before remaining between 1,000 feet and 1,025 feet for the remainder of the drought. Historical Drought 2 examines how the basin would respond if hydrologic conditions from 2000 to 2018 were to occur again with the reservoir starting at near-present day conditions.

Paleo Drought 1 shows a steady decrease in Lake Mead elevation for the first 12 years of the drought. Lake elevation falls below 1,025 feet after the first 6 years, and below 1,000 feet after the first 9 years. Elevation remains significantly below 1,000 feet for 3 years and even after the end of the drought. Similar to Historical Drought 1, lake elevation only returns to around 1,025 feet in the years following the end of the drought.

The two remaining paleo droughts, Paleo Drought 2 and Paleo Drought 3, show similar relative behavior to Lake Powell—with Lake Mead elevation dropping to below the lower threshold in Paleo Drought 2 before recovering, and dropping to just at the lower threshold and remaining steady in Paleo Drought 3. In these two droughts, lake elevation remains close to 1,025 feet following the end of the drought and does not substantially recover.

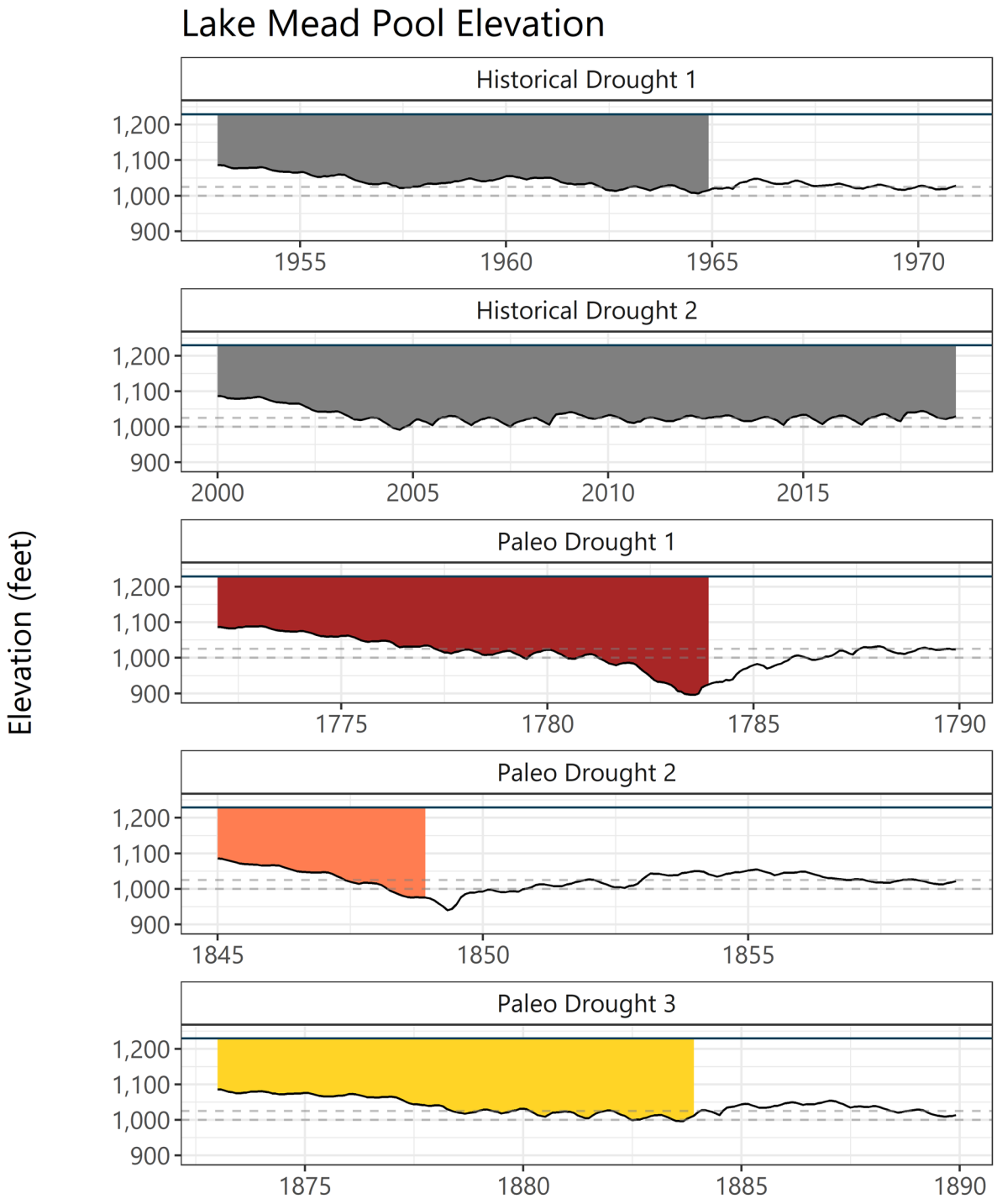

Figure 110. Monthly modeled reservoir pool elevation for Lake Mead for each drought event (panels).

Note: The solid horizontal lines show full pool elevation (1,229 feet) and the dashed horizontal lines show critical elevations (1,025 feet and 1,000 feet). Drought events are shaded.

Figure 111 shows the water management metrics identified for the Colorado River Basin and how they perform over the 1906 to 2018 baseline period and over each of the historical and paleo drought events. To restate, baseline conditions reflect system performance when historical hydrology is run with near-present day starting initial conditions using an ensemble of the historical hydrology, and drought events reflect how the system would respond if the drought started with near-present day initial conditions. In addition to the percent of years below the two pool elevation thresholds each for Lake Powell and Lake Mead, this figure also shows the 10-year average release from Lake Powell and the average annual delivery of water to the lower basin, including Lower Division States and Mexico. These are metrics that water managers consider in operation of the Colorado River Basin.

Figure 111 shows the percent of years that have at least 1 month below relevant pool elevation thresholds. At Lake Powell, over the baseline period, Lake Powell is below 3,525 feet in 28 percent of years (32 out of 113 years), and below 3,490 feet in 4 percent of years (5 out of 113 years). For the two historical droughts, Lake Powell pool elevation is below 3,525 feet 33 percent of years (6 out of 18 years) during Historical Drought 1 and 73 percent of years (14 out of 19 years) during Historical Drought 2. Lake Powell was also below 3,490 feet 5 percent of years (1 out of 18 years) during Historical Drought 1 and was below this same threshold 16 percent of years (3 out of 19 years) during Historical Drought 2. For the paleo droughts, the percent of years Lake Powell pool elevation fell below 3,525 ranged from 36 percent of years during Paleo Drought 3 (8 out of 17 years) to 56 percent of years (10 out of 18 years) during Paleo Drought 1. Similarly, the percent of years below 3,490 ranged from 18 percent (3 out of 17 years) in Paleo Drought 3 to 28 percent (5 out of 18 years) in Paleo Drought 1.

For Lake Mead, in the historical baseline period, pool elevation falls below 1,025 feet in 33 percent of years (37 out of 113 years), and below 1,000 feet 4 percent in of years (5 out of 113 years). For the historical droughts, these percentages increase to 44 percent of years below 1,025 feet (8 out of 18 years) and no years below 1,000 feet during Historical Drought 1, and 84 percent below 1,025 feet (16 out of 19 years) and 5 percent below 1,000 feet during Historical Drought 2. Interestingly, in the paleo droughts, the percentage of years below 1,025 feet is less than the historical droughts, which ranged from 53 percent (9 out of 17 years) to 72 percent (13 out of 18 years), but the percentage of years below 1,000 feet is much greater than the historical droughts, ranging from 12 percent (2 out of 17 years) to 44 percent (8 out of 18 years).

Total delivery to the Lower Division States and Mexico over the baseline period averaged 8.79 million acre-feet, just under the 9.0 million acre-feet delivery obligation under the 1922 Colorado River Compact. The average delivery was reduced for all drought events, averaging 8.15 million acre-feet under Historical Drought 1, 8.06 million acre-feet under Historical Drought 2, and between 7.96 million acre-feet and 8.19 million acre-feet for the paleo droughts. The 10-year average release from Lake Powell was also reduced. The 10-year average release was 93 million acre-feet over the historical baseline period. Under Historical Drought 1, the average release was reduced to 82 million acre-feet, and under Historical Drought 2, reduced to 83 million acre-feet. For the three paleo droughts these average releases ranged from 80 to 83.9 million acre-feet.

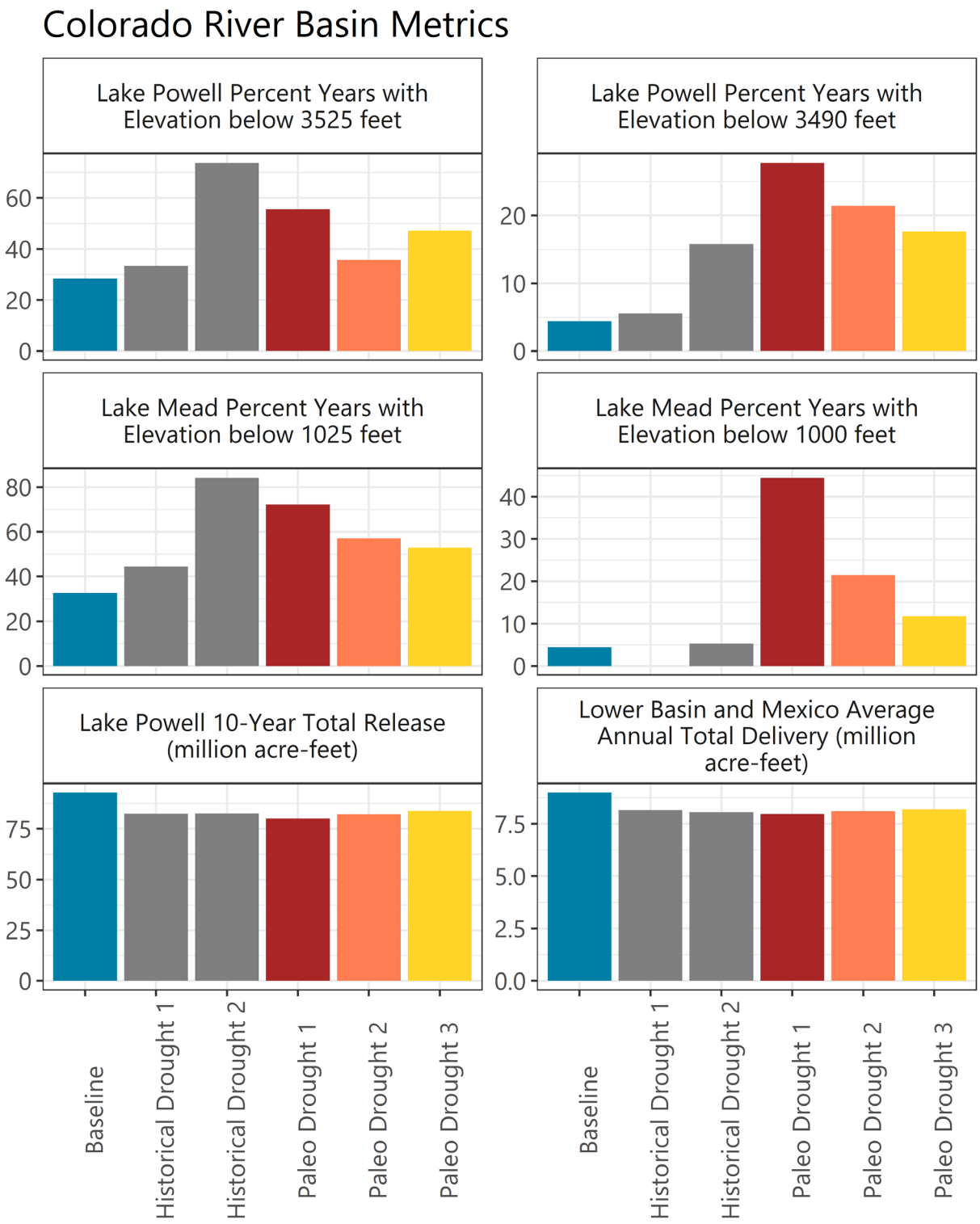

Figure 111. Colorado River Basin metrics showing mean baseline conditions (blue), historical droughts (gray), and paleo droughts (red, orange, and yellow).

To explore how more recent historical and paleo drought events may be different from projected drought events using the CMIP5-LOCA RCP4.5 and RCP8.5 hydrologic traces from 2006 to

2099, average annual deficit by volume (acre-feet) and duration (length in years) are plotted for the drought events discussed in this section (drought events in the observed historical period and the paleo-reconstructed period), as well as for the largest cumulative deficit events for each projected hydrology trace. Figure 112 illustrates these events relative to each other.

The grey circles represent Historical Drought 1 and Historical Drought 2. The colored diamonds represent the three largest paleo drought events. The green triangles represent the drought events for each future hydrologic projection. These droughts are based on natural streamflow for the Colorado River at Lees Ferry, AZ and do not reflect water management effects. The figure illustrates that the paleo drought events were moderately to substantially more severe than the historical droughts, but of shorter duration. Paleo Drought 2 by far is the most severe event as measured by average annual deficit, however, only lasts for 4 years. The future droughts indicate the possibility of droughts of similar severity to Paleo Drought 1, and more severe than the two historical droughts, but much longer lasting, up to 91 years. They also indicate the possibility of droughts with average annual deficits 2.5 to 3 times those of the two historical droughts and lasting for similar or slightly longer durations.

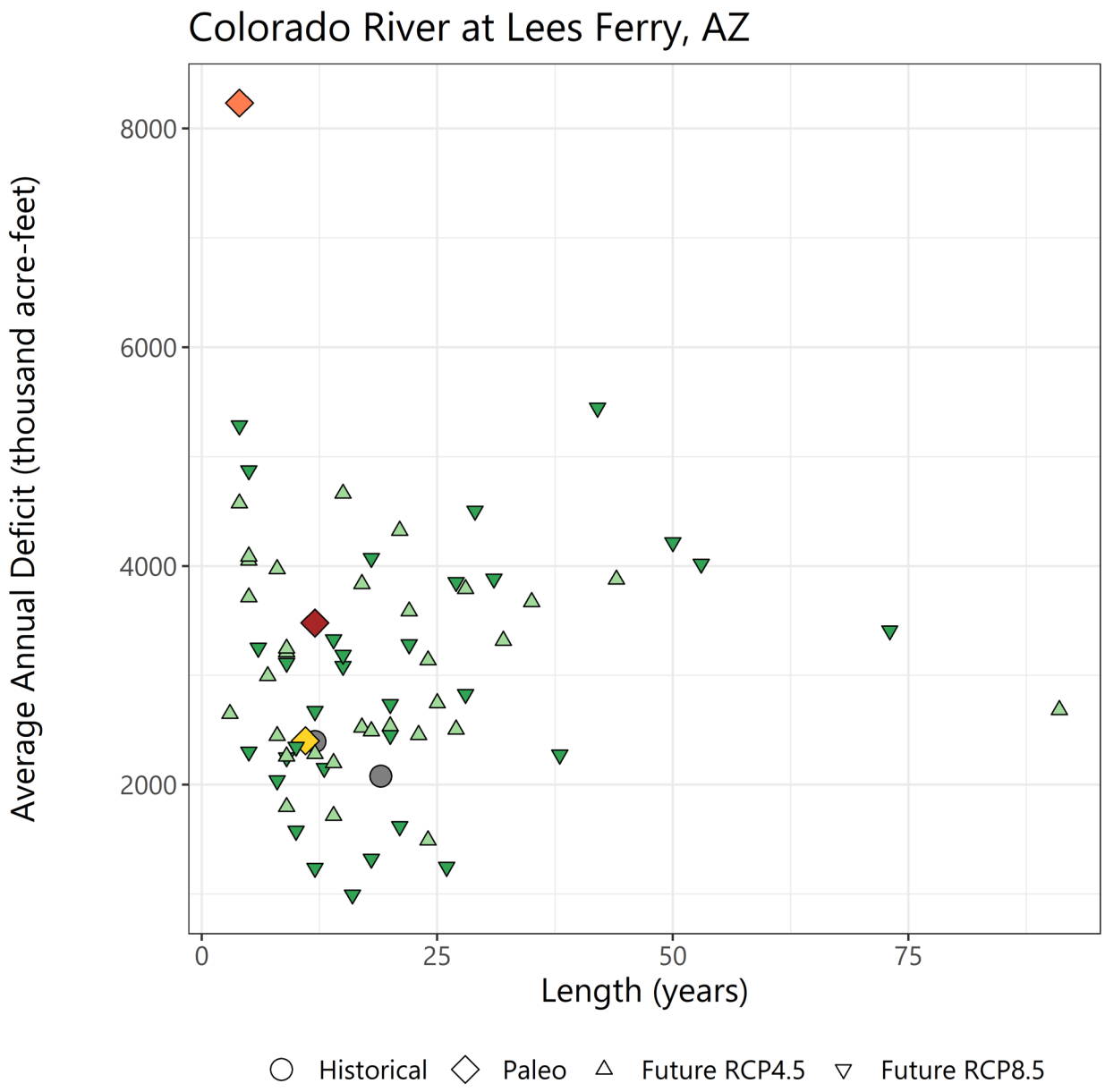

Figure 112. Drought length and average annual drought deficit for drought events at the Colorado River at Lees Ferry, AZ.

Note: Circles represent historical droughts, diamonds represent paleo droughts, and triangles represent the largest drought from each projection in the LOCA dataset for RCP4.5 and RCP8.5.

6.3 Columbia River Basin (Boise)

The Columbia River Basin contributes streamflow to the fourth largest river in the United States by mean annual streamflow volume. Evaluation of drought scenarios across the entire river basin would be complex. This report focuses on the Boise River basin, which is a subbasin of the Snake River, one of the Columbia River's primary tributaries. The Boise River basin is

illustrated in Figure 107 while the main features of the Columbia River Basin are illustrated in the Columbia River Basin document of the Water Reliability in the West – 2021 SECURE Water Act Report.

The Boise Project was one of the first irrigation projects constructed by Reclamation and currently supplies irrigation water to 224,000 acres and supplemental water supply to an additional 173,000 acres in southwest Idaho and eastern Oregon. The Project has two divisions, the Payette Division and the Arrowrock Division, which are the focus of this risk analysis (Figure 107). The Boise RiverWare Planning Model was developed using the RiverWare software package (Zagona et al., 2001) and encompasses the Boise River from Arrowrock Dam to the river's confluence with the Snake River near Parma, Idaho. Three reservoirs are included in the model: Anderson Ranch Reservoir and Arrowrock Reservoir owned by Reclamation, and Lucky Peak Reservoir, which is owned by the U.S. Army Corps of Engineers and operated jointly by the two agencies. These reservoirs provide flood risk management benefits and store water for irrigation supply and hydropower generation. Additionally, these reservoirs are managed to support recreation.

Almost 40 percent of Idaho residents live in the Boise River watershed, with one-sixth of the population of the State residing in the floodplain. The Boise River watershed has recently experienced the most substantial growth in the State and continuing to meet current and future water needs is a major concern for residents and State and local officials. For example, in 2017, the Boise River saw an annual (October through September) runoff of 184 percent of normal (3,442,000 acre-feet) that caused flooding through the City of Boise for 101 days.

The analysis of water supply risks related to drought events was performed by identifying notable historical drought events, as well as drought events in the paleo-reconstructed period, and comparing the managed system, under current operations and demands, with an observed historical baseline period. Two drought periods from the observed historical period were selected for analysis in the Boise River basin—the first lasting 13 years from 1930 to 1942 (Historical Drought 1), and the second lasting 9 years from 1987 to 1995 (Historical Drought 2). Analysis of managed streamflow and reservoir storage for these drought periods were compared with results for an overall historical baseline simulation period, in this case, water years 1981 to 2018. Additionally, results were compared with those from paleohydrology scenarios, which are described in the next section.

6.3.1 Paleohydrology Scenario Development

Paleohydrology scenarios for the Boise River were developed using the annual streamflow reconstruction for the Boise River near Parma, ID (USGS ID 13213000). Additional information including references for these reconstructions can be found in Chapter 2.

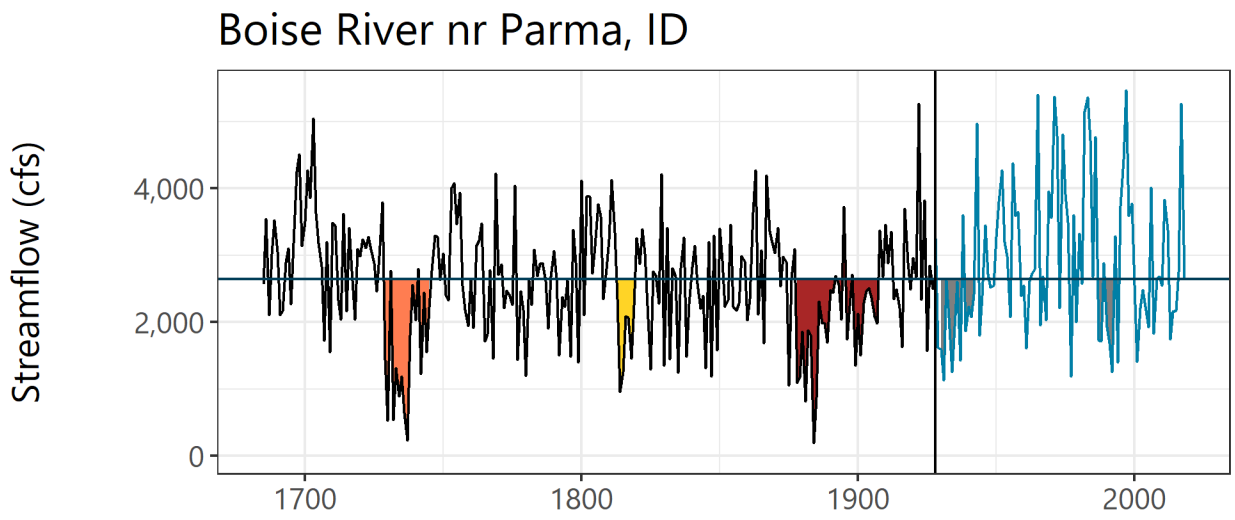

Figure 113. Annual streamflow for the Boise River nr Parma, ID showing droughts in the paleo-reconstructed and observed historical periods.

Note: Paleo-reconstructed streamflow is in black and historical streamflow is in blue. The horizontal line shows long-term median streamflow. Drought events are shaded (red, orange, and yellow for Paleo Droughts 1, 2, and 3, respectively, and gray for historical droughts).

cfs = cubic feet per second

Figure 113 shows this reconstruction in black, with the historical naturalized streamflow over the observed historical period shown in blue. Drought events of interest are shaded and include the three "largest cumulative deficit" droughts from the paleo-reconstructed period—the 1930s dustbowl drought and the late 1980s to 1990s drought from the observed historical period. These five drought events were used to investigate impacts to reservoir storage in Anderson Ranch Reservoir and Lucky Peak Reservoir.

6.3.2 River Systems Model Overview

The Boise RiverWare model was used to conduct the risk assessment for the Boise River. The model was developed as part of the larger Upper Snake RiverWare model used for the Modified Flows analysis (https://www.bpa.gov/p/Power-Products/Historical-Streamflow-Data/streamflow/Reclamation%20Upper%20Snake%20Modified%20Flows.pdf)." Additional model documentation may be found in Reclamation (2020d).

October 1, 1980, through September 30, 2018, was selected as the observed historical period (i.e., baseline) because this period has the most widely available observed data and is quality assured. Water user demand inputs represent current condition demands from 2008 to 2018 and were developed from the Modified Flows process used in Reclamation's Columbia-Pacific Northwest Region (https://www.bpa.gov/p/Power-Products/Historical-Streamflow-Data/streamflow/Reclamation%20Upper%20Snake%20Modified%20Flows.pdf). This process developed three different patterns of demands by classifying each year between 2008 and 2018 into dry, medium, or wet conditions.

To determine model initial conditions, inflows were corrected to remove the influence of groundwater returns from irrigation and the model was set to "spin-up" to get the groundwater effects to a current level. For the most part, the reservoirs in the Boise River basin fill within a couple of years. Consequently, up to about the first 2 years of simulated data were ignored in the analysis of output.

6.3.3 Water Resource Metrics

The Boise RiverWare model encompasses the Boise River from Anderson Ranch Reservoir to the river's confluence with the Snake River near Parma, ID. It includes Arrowrock Reservoir and Lucky Peak Reservoir, diversions to water users, and representation of the policy used to manage the river. This policy contains water management objectives that can be used to assess risk to the system. Table 30 lists the water supply reliability metrics examined using the Boise RiverWare model. These include how often Lucky Peak Lake reaches near full capacity between May 31 and September 1 to support recreation on the lake, how often the Boise River at Glenwood exceeds the Flood Action Flow, and how often winter and summer streamflow targets below Anderson Ranch Dam are met.

Table 30. Metrics for quantifying water supply reliability in the Boise River basin

Storage Metrics
Average percent of years Lucky Peak Lake reaches top of active capacity (264,400 acre-feet)
Average percent of days Lucky Peak Lake meets summer recreation target storage (264,400 acre-feet from May 31 to September 1 for recreation)
Average percent of days Lucky Peak Lake falls below conservation pool (28,730 acre-feet)
Average percent of capacity on September 30 for Lucky Peak Lake
Average percent of years Anderson Ranch Reservoir reaches top of active capacity (413,074 acre-feet)
Average percent of capacity on September 30 for Anderson Ranch Reservoir
Flow Metrics
Boise River between Lucky Peak Dam and Glenwood streamflow below 6,500 cubic feet per second (cfs) (Flood Action Flow)
Boise River below Anderson Ranch Dam minimum streamflow target (300 cfs from September 15 to March 31 and 600 cfs from April 1 to September 14)

6.3.4 Summary

Drought events from the observed historical period and the paleo-reconstruction period were selected to examine water resource metrics in the Boise River basin. The two droughts identified in the historical period represent two of the most severe droughts to occur in the Boise River basin, as evaluated by streamflow records for the Boise River near Parma, ID.

Three droughts from the paleo-reconstruction period were also selected to examine their impact on water resources metrics relative to the observed historical droughts. These paleo droughts were identified using the "largest cumulative deficit" drought definition and represent the top three ranked droughts using this definition. These three droughts represent three of the most severe droughts to occur in the Boise River basin in the 1685 to 1977 paleo-reconstruction period.

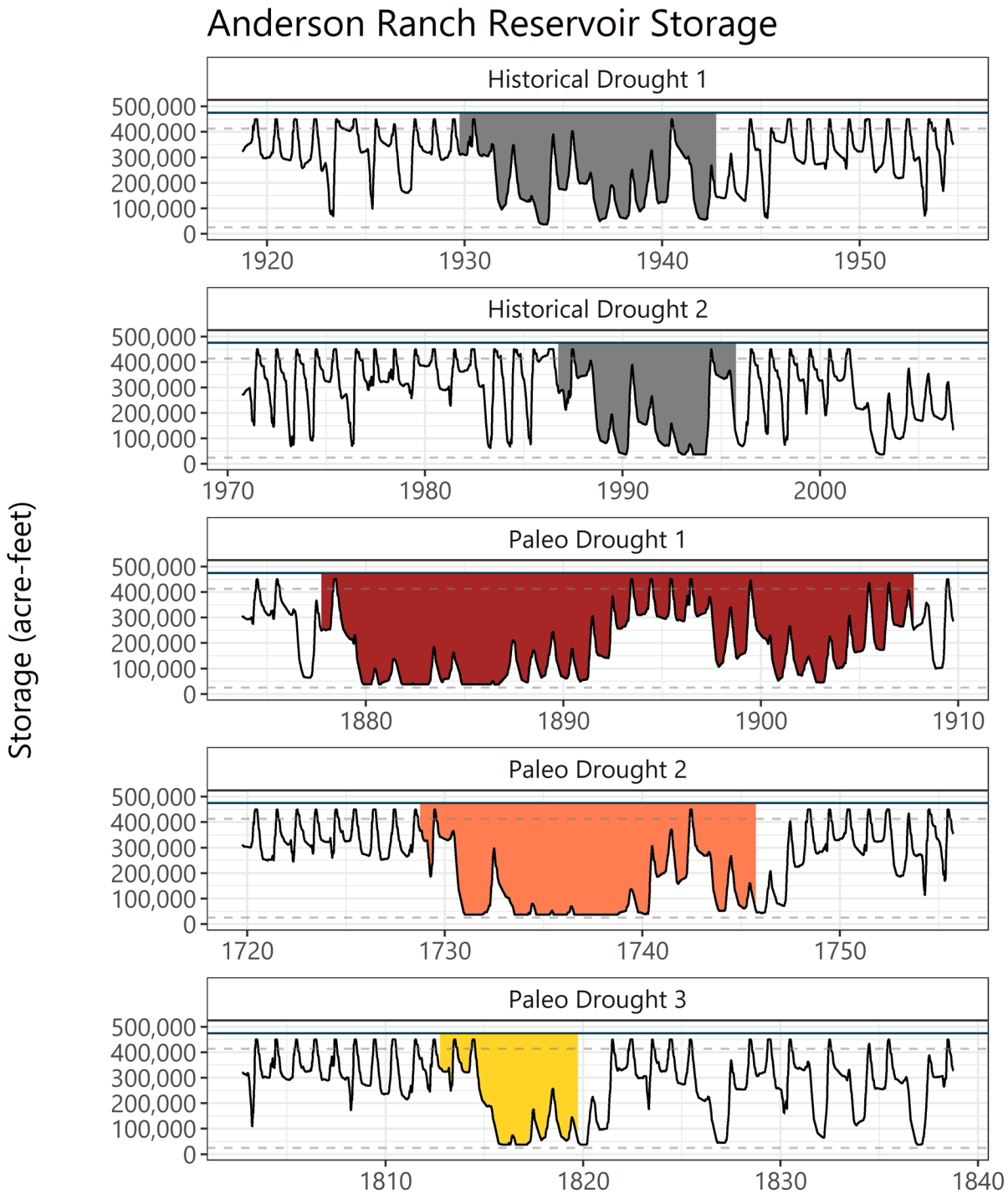

Figure 114. Daily modeled storage for Anderson Ranch Reservoir for each drought event (panels).

Note: The solid horizontal line shows full pool (474,900 acre-feet) and the dashed horizontal lines shows the top of active storage (413,074 acre-feet) and bottom of conservation pool (24,044 acre-feet) storages. Dead pool storage of 35,956 acre-feet is not modeled. Drought events are shaded.

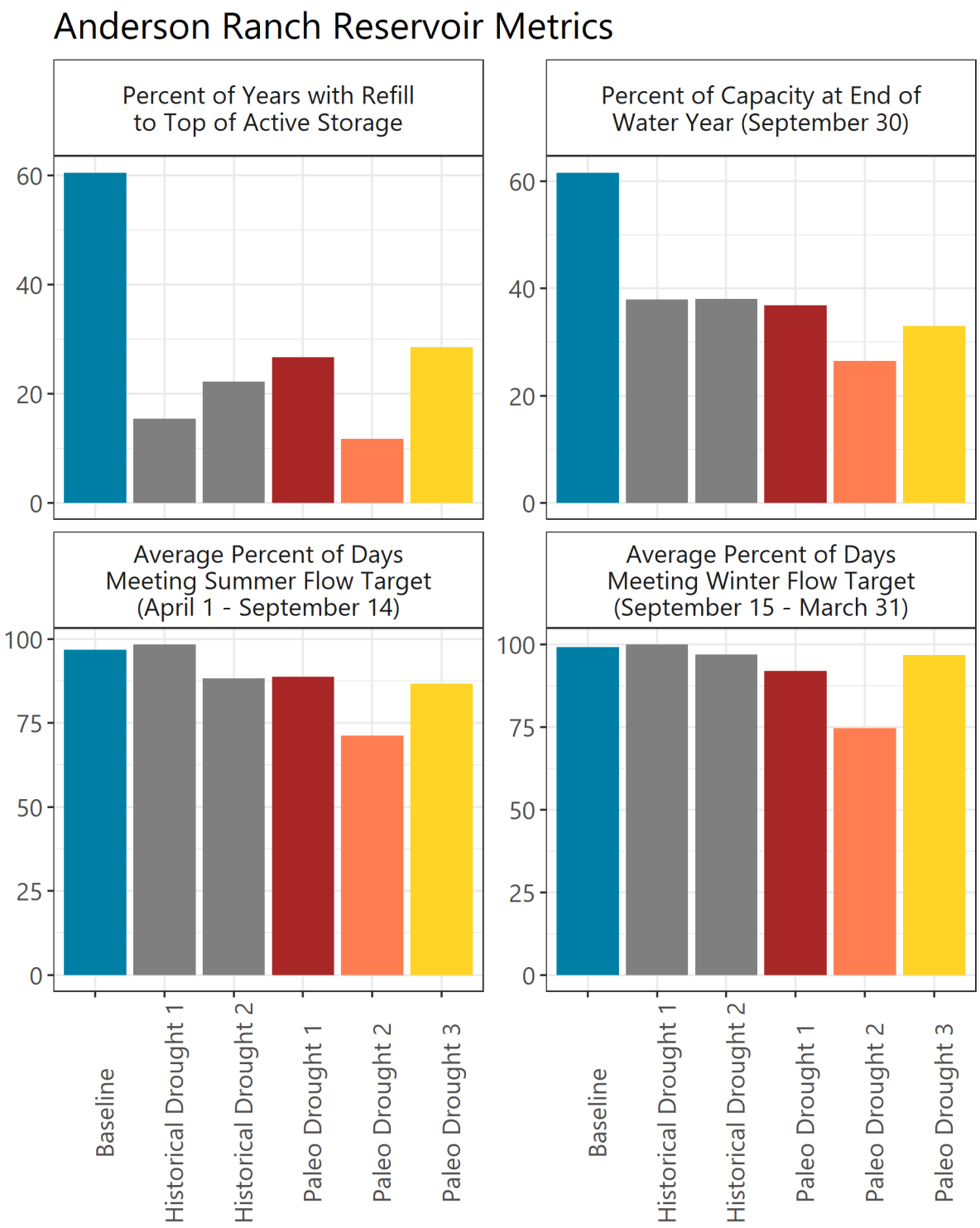

Figure 115. Anderson Ranch Reservoir storage and downstream streamflow metrics showing mean baseline conditions (blue), historical droughts (gray), and paleo droughts (red, orange, and yellow).

Figure 114 shows the timeseries of storage at Anderson Ranch Reservoir for the two historical droughts and three paleo droughts. The lower dashed line shows the bottom of conservation pool at 25,000 acre-feet, as represented in the RiverWare model. The actual bottom of conservation pool is 62,000 acre-feet, but this includes dead pool storage, which is not represented in the model. Similarly, the upper dashed line shows the top of active storage at 413,074 acre-feet, as modeled, which also does not include dead pool storage. Overall, storage during drought events does not fall below the bottom of conservation pool, but does fall to this minimum and remain there for periods during each drought event. For close to a decade between 1880 and 1890, storage remains at or close to the bottom of conservation pool during Paleo Drought 1. Between 1731 and 1740 in Paleo Drought 2, storage also remains close to the bottom of conservation pool. Storage drops to this level in Historical Drought 1 and Historical Drought 2, but for much shorter periods of time.

Figure 115 shows reservoir metrics summarized over the historical baseline period and over each of the drought events. Anderson Ranch Reservoir refilled to the top of active storage 61 percent of years over the baseline period (water years 1981 through 2018). This refill percentage greatly decreased for each of the drought events—with the worst performance seen during Paleo Drought 2 where the reservoir refilled 11 percent of years (2 out of 17 years). During Historical Drought 1 the reservoir refilled 15 percent of years (2 out of 13 years), and during Historical Drought 2 it refilled 22 percent of years (2 out of 9 years). There are similar results for the percent capacity at the end of the water year. Over the baseline period, Anderson Ranch is 62 percent full on average on September 30, with decreases in all droughts. Droughts, however, appear to have less of an impact on the ability to meet instream flow targets. There are summer and winter streamflow targets downstream of Anderson Ranch Reservoir, and for most drought events these targets are met as frequently as for the baseline period. For both streamflow targets, Paleo Drought 2 has the greatest impact on meeting these targets—75 percent of summer days (April 1 to September 14) during the drought for the summer target, and 71 percent of winter days (September 15 to March 31) during the drought for the winter target.

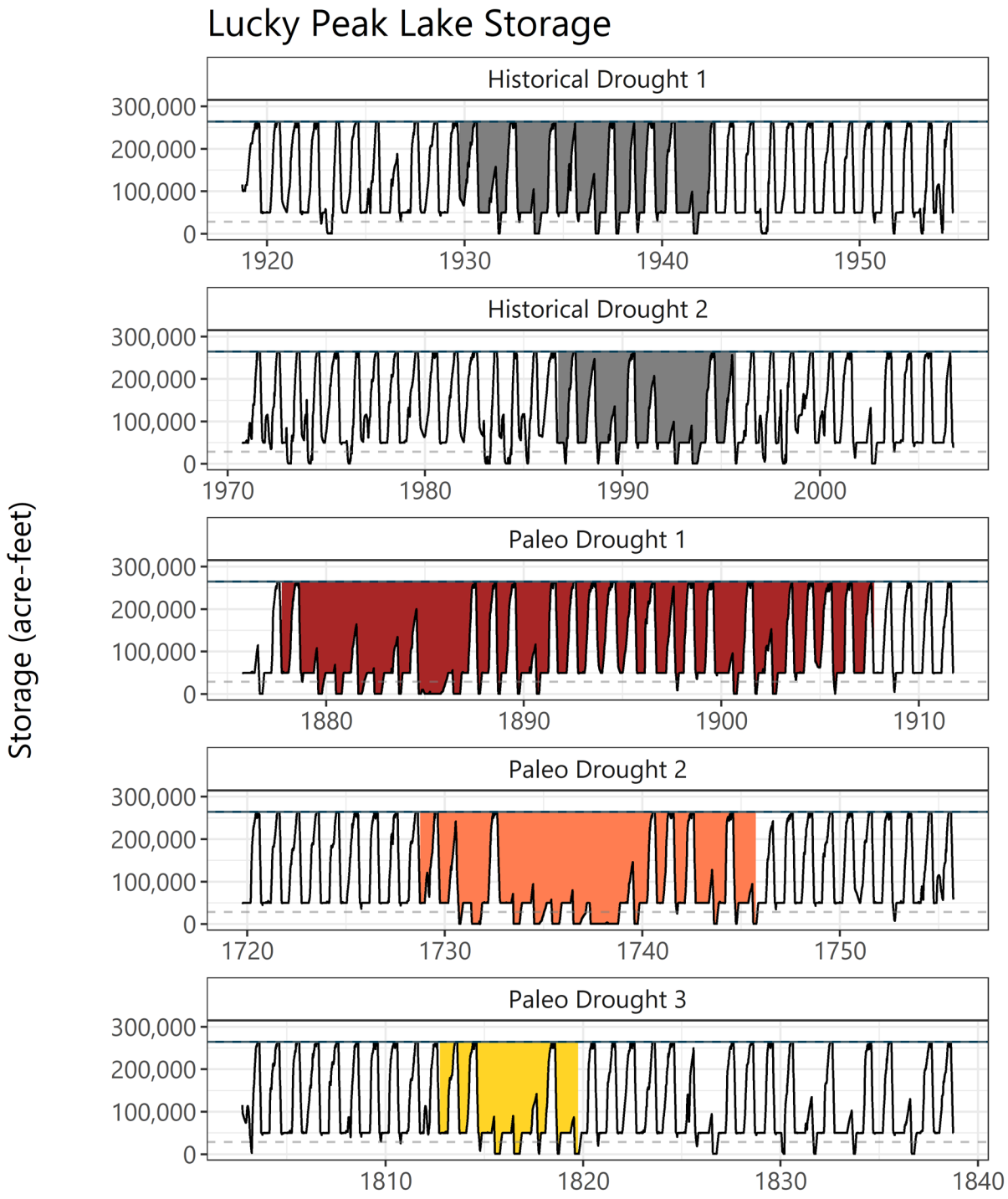

Figure 116. Daily modeled storage for Lucky Peak Lake for each drought event (panels).

Note: The solid horizontal line shows the top of total storage (264,440 acre-feet) and the dashed horizontal line shows the bottom of conservation pool storage (28,730 acre-feet). Drought events are shaded.

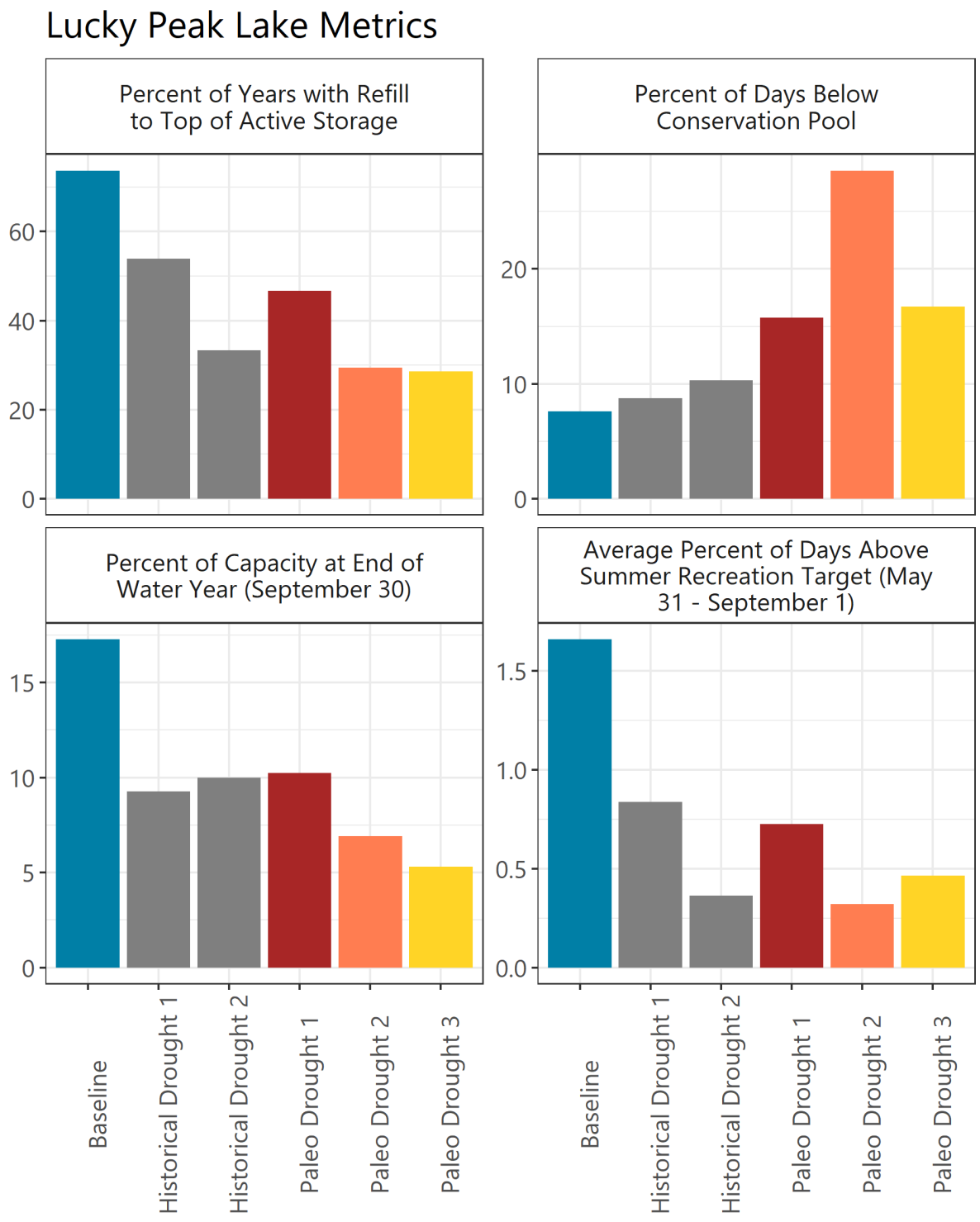

Figure 117. Lucky Peak Lake storage and downstream streamflow metrics showing mean baseline conditions (blue), historical droughts (gray), and paleo droughts (red, orange, and yellow).

Figure 116 shows the timeseries of storage at Lucky Peak Lake for the two historical droughts and three paleo droughts. The dashed line shows the bottom of conservation pool storage (28,730 acre-feet). The solid line shows the top of total storage (264,400 acre-feet). For the two historical droughts, Lucky Peak Lake is able to refill to the top of total storage with regularity and does not fall below the bottom of conservation pool storage often or for long durations. This contrasts with the paleo droughts, where in a long period in Paleo Drought 1, beginning in 1878 and extending to 1887, storage remains well-below full storage, and for 2 years between 1876 and 1877 storage remains below the bottom of conservation pool. The middle of Paleo Drought 2 also shows this behavior, with storage remaining below full storage from 1733 to 1741, and a 2-year period with storage below the bottom of conservation pool.

Figure 117 shows Lucky Peak Lake metrics that are similar to those described for Anderson Ranch Reservoir. Over the historical baseline period, Lucky Peak Lake refilled to the top of active storage in 74 percent of years. For the two historical droughts, the reservoir refilled to the top of active storage in 54 percent of years for Historical Drought 1 (7 out of 13 years), and 33 percent of years for Historical Drought 2 (3 out of 9 years). For the paleo droughts, the reservoir refilled between 29 percent and 47 percent of years. As illustrated in Figure 116 for Paleo Drought 1, hydrologic conditions allowed for Lucky Peak reservoir to refill for several years in the middle of the drought, despite its duration of 30 years. Together, these figures illustrate that a single metric may not provide a full understanding of the severity of a drought on the managed Boise River system. Although Paleo Drought 1 does not appear as impactful as other drought events in terms of reservoir refill, there were more than 10 consecutive years where Lucky Peak was not able to refill over the course of a 30-year drought. Consideration of various aspects of drought, including severity and duration, are particularly important for understanding the potential water management impacts.

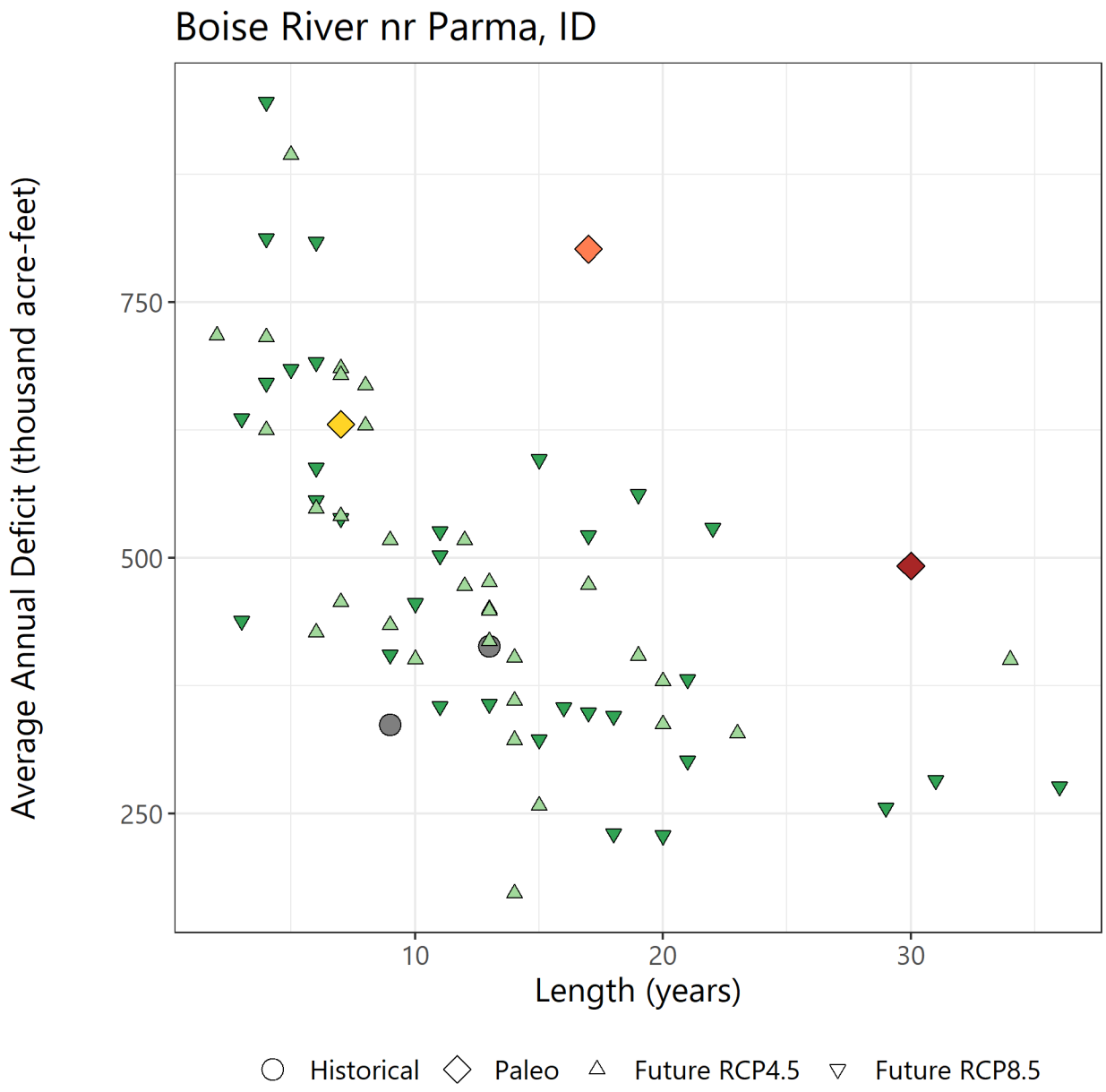

Figure 118. Drought length and average annual drought deficit for drought events at the Boise River near Parma, ID.

Note: Circles represent historical droughts, diamonds represent paleo droughts, and triangles represent the largest drought from each projection in the LOCA dataset for RCP4.5 and RCP8.5.

To explore how more recent historical and paleo drought events may be different from projected drought events using the CMIP5-LOCA RCP4.5 and RCP8.5 hydrologic traces from 2006 to 2099, average annual deficit by volume (acre-feet) and duration (length in years) are plotted for the drought events discussed in this section (drought events in the observed historical period and the paleo-reconstructed period), as well as for the largest cumulative deficit events for each projected hydrology trace. Figure 118 illustrates these events relative to each other.

The grey circles represent notable droughts in the instrumental record identified by Reclamation's regional partners. The colored diamonds represent the three largest paleo drought events. The green triangles represent the drought events for each future hydrologic projection. These droughts are based on natural streamflow for the Boise River near Parma, ID and do not reflect water management effects. The figure illustrates that the paleo drought events were substantially more severe, and in the case of Paleo Drought 1, a substantially longer duration. With an average annual deficit of just under 500,000 acre-feet, Paleo Drought 1 is substantially longer than any of the historical or future droughts with similar deficits—at 30 years in length, the next closest drought is from the future droughts with an average annual deficit of just over 500,000 acre-feet and a length of 21 years.

6.3.4.1 Analysis of Flood Events – Case Study for the Boise River Basin

The Boise River flows directly through Boise, Idaho, and flooding is an important consideration in managing the Boise River. A Flood Action Flow of 6,500 cubic feet per second (cfs) exists for the Boise River at Glenwood Bridge, ID (USGS ID 13206000). Historic notable flood events occurred in 1972, 1974, 1997, and 2017 and were identified by regional water managers as important for context setting along with identified wet periods in the paleohydrology period. Figure 119 shows daily modeled streamflow for the Boise River at Glenwood Bridge, ID for these four historic flood events, as well as for 3 years in the paleo record that also experienced flood events.

Figure 120 shows the percent of time the Boise River at Glenwood Bridge, ID was above the Flood Action Flow of 6,500 cfs on average over the baseline historical period as compared to the historical and paleo flood events. Over the historical baseline period, the Boise River exceeds 6,500 cfs 2.4 percent of days during the event. Out of the four historical flood events, the two most severe were in 2017 when streamflow was above 6,500 cfs 21.1 percent of the days, and in 1997 when streamflow was above 6,500 cfs 19.7 percent of the days. While below the historical flood events, the three paleo floods examined still substantially exceeded this threshold, between 9.9 percent and 12.9 percent of the days during the event.

Interestingly, in 1997 there were two substantial flood events, the first being a winter flood with 1-day peak discharge of 24,052 cfs on January 2, 1997, and 10 days with daily streamflow more than 5,000 cfs. This event was notable at many other Reclamation dams throughout the West (Lahontan, Shasta, Trinity, and Folsom Dams for example). The second event was a spring snowmelt flood with 1-day discharge of 22,157 cfs on May 16, 1997, and 105 days with daily streamflow more than 5,000 cfs.

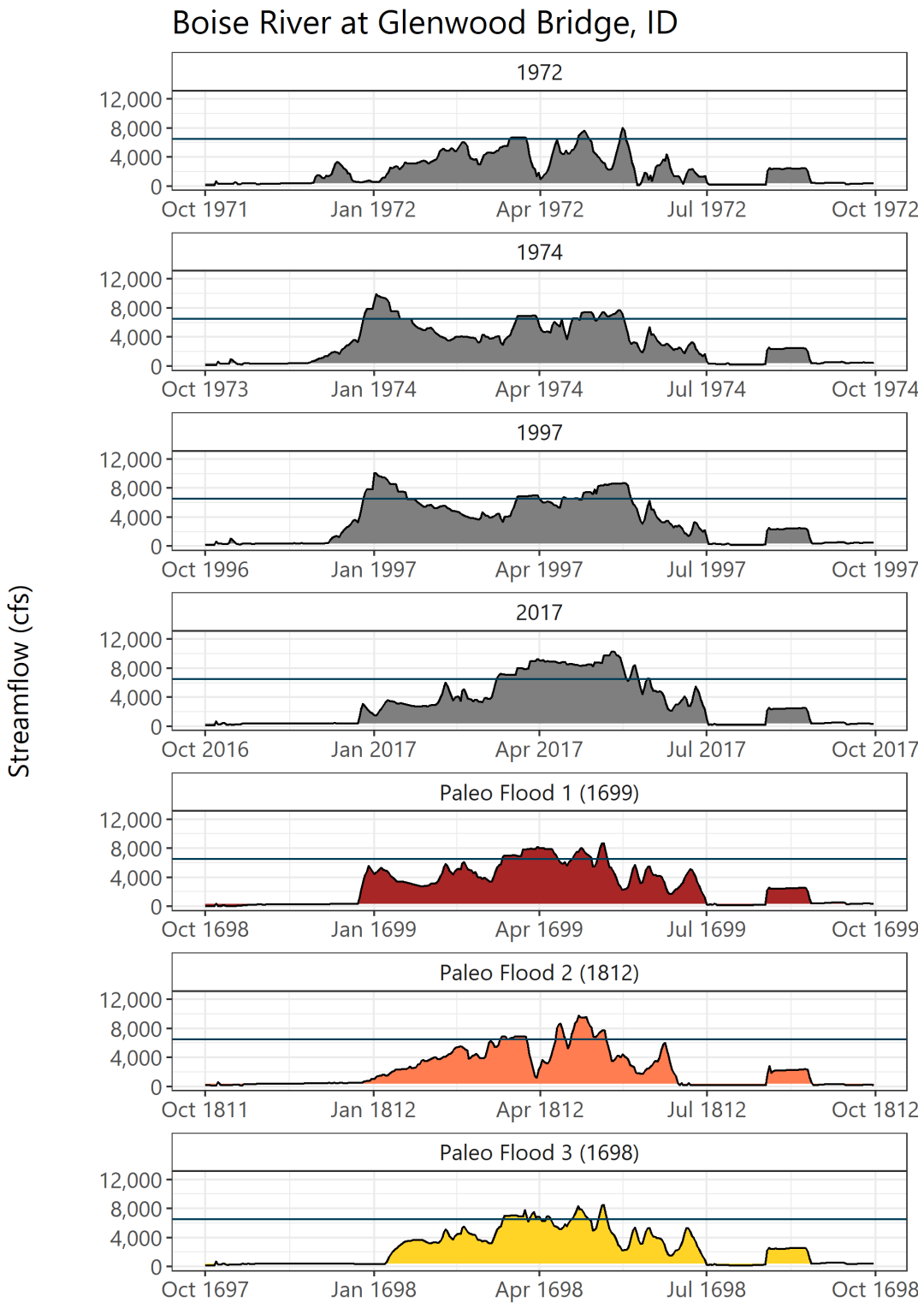

Figure 119. Modeled daily streamflow for the Boise River at Glenwood Bridge, ID for identified flood events.

Note: Streamflow during four historical years that experienced flood events (top 4 panels) are shown in gray. Three paleo years with flood events (bottom three panels) are shown in red, orange, and yellow.

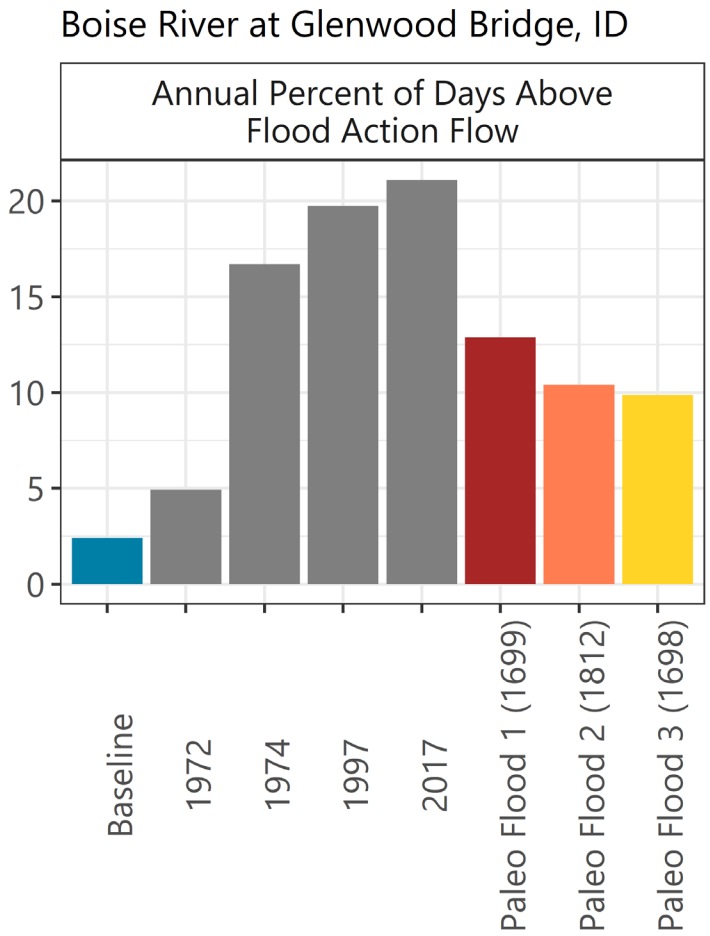

Figure 120. Average exceedance above Flood Action Flows at Boise River at Glenwood Bridge, ID for identified flood events.

Note: Average exceedance computed for the baseline period is shown in blue. Those computed for four historical years are shown in gray and the three paleo years are shown red, orange, and yellow.

To further understanding of potential future flood events, the River Management Joint Operating Committee (RMJOC) RMJOC-II effort evaluated future flood risk management using future climate projections. To focus the analysis on flood volumes, U.S. Army Corps of Engineers analyzed the projections for winter and spring separately. For each projection and 30-year epoch (historical period, 2030s, 2070s), the top five flood events by volume were identified for each flood season. One historical baseline was used for comparison purposes. In the lower Snake River basin, the average April to August runoff volume of the five largest events is projected to be similar or possibly decrease by the 2070s according to a range of future projections; whereas, the runoff volume contributing to the largest winter floods is projected to increase in the 2030s, and more so in the 2070s, for most of the future projections considered (RMJOC-II, 2020; refer to study report for more details about future projections used and the approach for analysis).

6.4 Klamath River Basin

The Klamath River Basin encompasses around 15,700 square miles and extends from southern Oregon into northern California. The Klamath River headwaters are predominantly located in the southern Cascade Mountain range just south of Crater Lake. The upper portion of the Klamath River Basin contains the Klamath Project, one of the first Projects constructed by Reclamation. The Klamath Project provides irrigation water supply to 210,000 acres of farmland. Upper Klamath Lake serves as the primary storage reservoir for the Klamath Project and has a total capacity of 561,838 acre-feet. The mainstem Klamath River originates from Upper Klamath Lake and in the upper basin is joined by the Lost River. Keno Dam and four dams downstream are operated by PacifiCorp for the generation of hydroelectricity, the most downstream dam being Iron Gate Dam. Below Iron Gate Dam is the lower basin where the Klamath River is joined by the Shasta, Scott, Salmon, and Trinity Rivers as major tributaries before arriving at its mouth on the Pacific Ocean near Klamath, California. Reclamation manages the Klamath River for water supply and to meet responsibilities under the Endangered Species Act. These include maintaining specified lake levels in Upper Klamath Lake, and meeting instream flow targets along the Klamath River.

6.4.1 Paleohydrology Scenario Development

Paleohydrology scenarios for the Klamath River Basin were developed using the annual streamflow reconstruction for the Klamath River at Keno, OR (USGS ID 11509500) and the Trinity River at Lewiston, CA (USGS ID 11525500). Additional information including references for these reconstructions can be found in Chapter 2.

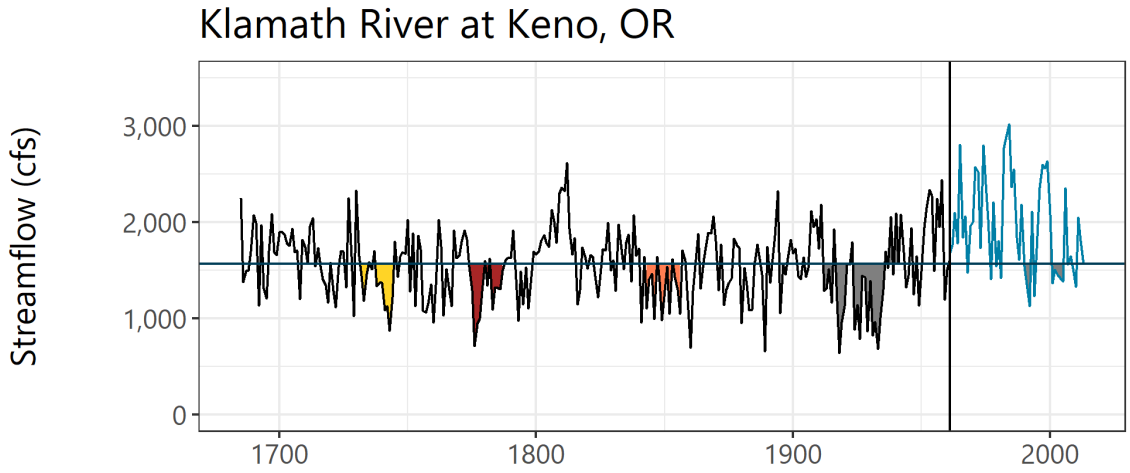

Figure 121. Annual streamflow for the Klamath River at Keno, OR showing droughts in the paleo-reconstructed and observed historical periods.

Note: Paleo-reconstructed streamflow is in black and historical streamflow is in blue. The horizontal line shows long-term median streamflow. Drought events are shaded (red, orange, and yellow for Paleo Droughts 1, 2, and 3, respectively, and gray for historical droughts).

cfs = cubic feet per second

Figure 121 shows the Klamath River at Keno, OR streamflow reconstruction and naturalized (i.e, unimpaired) streamflow over the observed historical period and identifies the six drought events examined in the Klamath River Basin in this report. The Klamath River Basin has experienced three notable droughts in the observed historical period. The first, which can be considered the most impactful drought in the basin, occurred between 1912 and 1941, lasting 29 years (Historical Drought 1). Two droughts occurred in the more recent past, one lasting 6 years between 1990 and 1995 (Historical Drought 2), and the second lasting 6 years between 2000 and 2005 (Historical Drought 3). Historical Drought 1 falls outside the observed historical period used as a baseline, water years 1960 to 2013, which is due to a lack of complete observational records with which to run the river system model prior to 1960. This drought was still identified by water managers in the basin as an important event to consider and was simulated using the paleo-reconstructed data. These three droughts represent three of the most severe droughts to occur in the Klamath River Basin based on streamflow records for the Klamath River at Keno, Oregon. In the paleo-reconstructed period, three droughts were identified using the "largest cumulative deficit" definition, and these three events lasted between 13 and 14 years. The largest paleo drought (Paleo Drought 1) sees decreases in streamflow comparable to the largest historical drought. All three paleo droughts are more impactful than the two more recent historical droughts, as measured by streamflow, but do not match the largest historical drought.

6.4.2 River Systems Model Overview

The Klamath River Basin Study (KRBS) model was developed to support the Klamath River Basin Study (Reclamation, 2016a). The KRBS model was developed using the RiverWare software package and simulates the managed river system, including reservoir operations, water diversions and return flows, irrigation deliveries, and municipal and industrial water use, in accordance with the management policy specified in the 2013 Biological Opinion (NMFS and USFWS, 2013).

The KRBS model is a daily timestep model that was built upon existing models for the Klamath River Basin. One existing model is commonly referred to as the Klamath Basin Planning Model (KBPM), which was developed to support the Endangered Species Act consultations over the impacts of Klamath Project operations on the threatened Southern Oregon/Northern California Coast coho salmon (*Oncorhynchus kisutch*), as well as the endangered Lost River (*Deltistes luxatus*) and shortnose suckers (*Chasmistes brevirostris*) (Reclamation, 2016a). The other existing model was developed to support the environmental impact assessment for removal of four of the mainstem Klamath River dams (U.S. Department of the Interior and California Department of Fish and Game, 2011).

The KRBS model encompasses the entire watershed, including tributaries of Upper Klamath Lake, the Lost River system, and major Klamath River tributaries. It was developed over a historical time period of water years 1961 through 2013 to facilitate comparison of results with the KBPM model. The model incorporated 2010 crop information, observed municipal and industrial demands, and modeled historical irrigation demands from the Klamath River Basin Study. Initial reservoir conditions were set at observed long-term averages over the historical period.

6.4.3 Water Resource Metrics

The Klamath River as simulated by the KRBS model uses the water management policy specified in the 2013 Biological Opinion. At present, the Klamath River is currently managed according to an updated Biological Opinion issued in 2019, with the re-initiation of consultation anticipated in 2021. Results presented below, including the water resource metrics identified in Table 31, are reflective of the management specified in the 2013 Biological Opinion and would potentially show different results were a different policy to be used. Average end-of-water-year reservoir storage is presented for consistency in analysis with other basins. Annual Klamath Project supply is also an important metric to illustrate Reclamation's ability to meet one of its management objectives.

Table 31. Metrics for quantifying water supply reliability in the Klamath River Basin

Storage Metric
Average percent of capacity on September 30 for Upper Klamath Lake
Other Metric
Average annual Klamath Project supply

6.4.4 Summary

Drought events from the observed historical period and the paleo-reconstructed period were selected to examine whether paleo droughts were more impactful than those from the observed historical period and from average historical conditions. In looking at storage in Upper Klamath Lake over each of the droughts (Figure 122), only in Historical Drought 1 of the three historical droughts does storage appear to remain substantially below full pool for multiple years. In the paleo droughts, Paleo Drought 1 results in reservoir drawdown greater than during other paleo drought events. In looking at September 30 storage in Upper Klamath Lake (Figure 123), on average, over the water years 1961 to 2013, the observed historical baseline period for Upper Klamath Lake was at 44 percent of capacity. For Historical Drought 1, this drops to 30 percent of capacity. Interestingly, the three paleo drought events each have similar percent capacity at the end of the water year, between 31 percent and 32 percent.

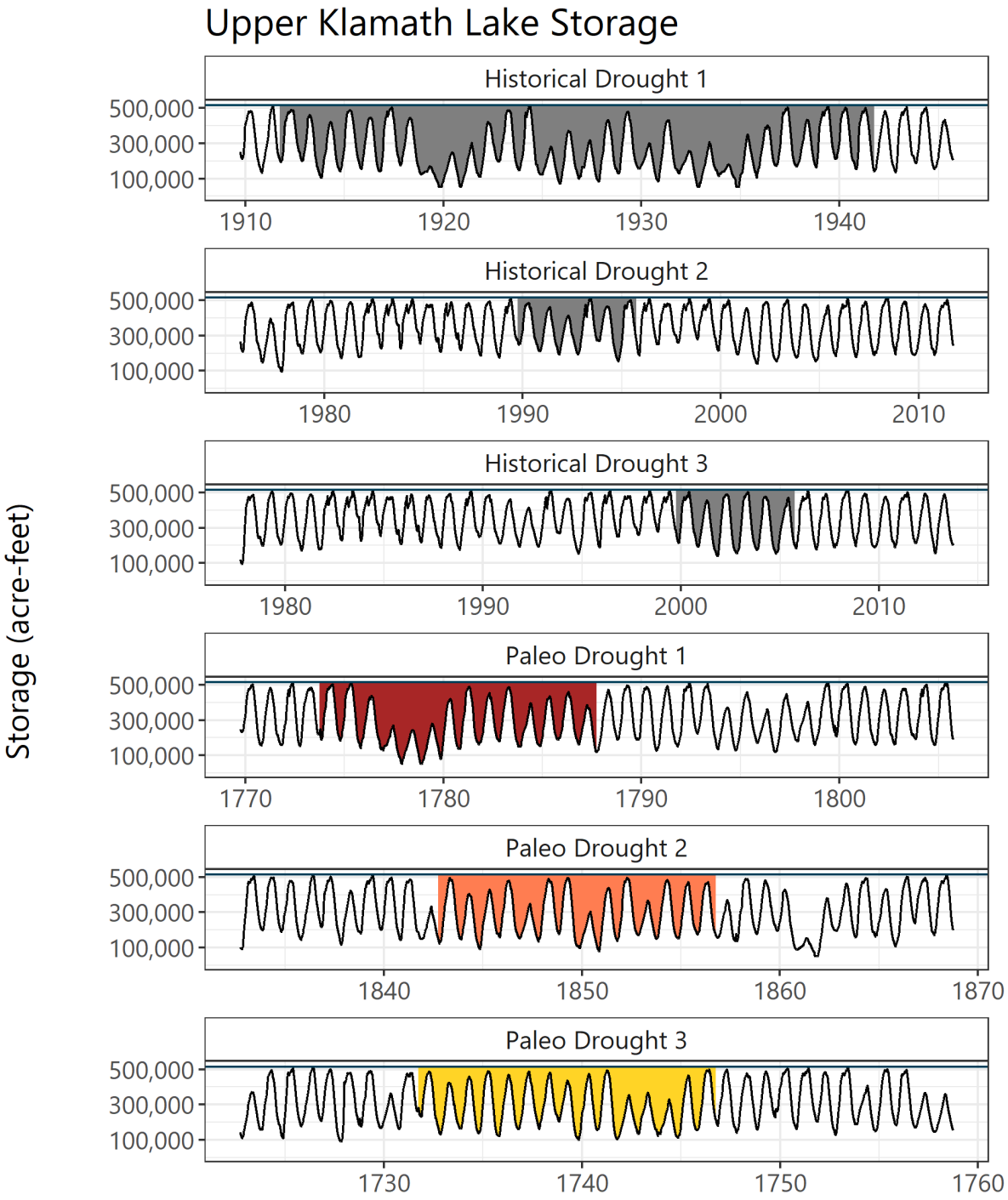

Figure 122. Daily modeled storage for Upper Klamath Lake for each drought event (panels).

Note: The solid horizontal line shows the top of total storage (514,950 acre-feet). Drought events are shaded.

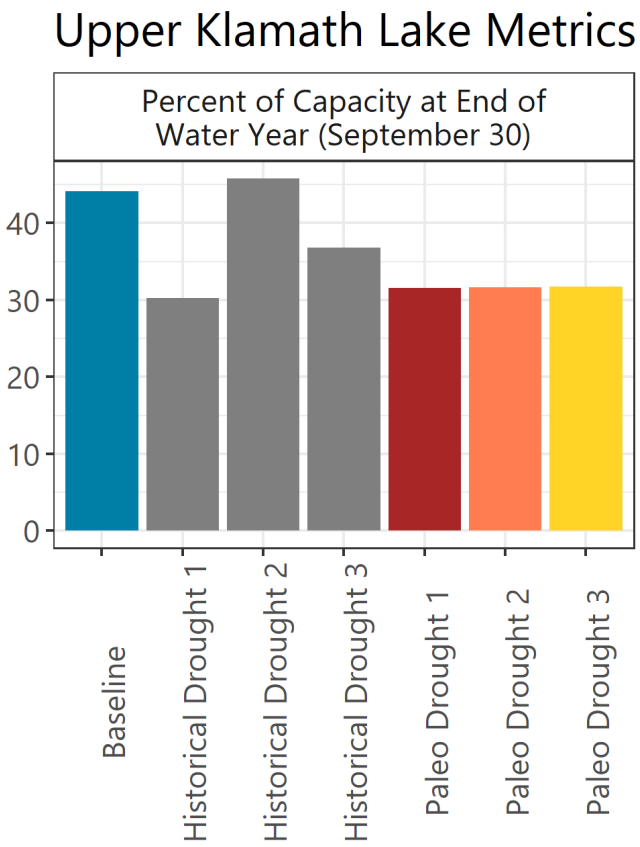

Figure 123. Upper Klamath Lake storage metric showing mean baseline conditions (blue), historical droughts (gray), and paleo droughts (red, orange, and yellow).

The impact of drought on the annual water supply allocated to the Klamath Project was also investigated. Figure 124 shows these impacts as average annual allocations for the 1960 to 2013 historical baseline period against each of the drought events. Over the baseline period, the Klamath Project had an average annual supply of 358,248 acre-feet. Historical Drought 1 greatly impacted Project supply, reducing this average to 203,606 acre-feet. This low Project supply is almost matched by Paleo Drought 1, which had an average Project supply of 219,792 acre-feet. The two remaining paleo droughts, Paleo Drought 2 and Paleo Drought 3, while not as impactful to Project supply as either Historical Drought 1 or Paleo Drought 1, still greatly reduced Project supply to 243,691 acre-feet and 255,043 acre-feet, respectively.

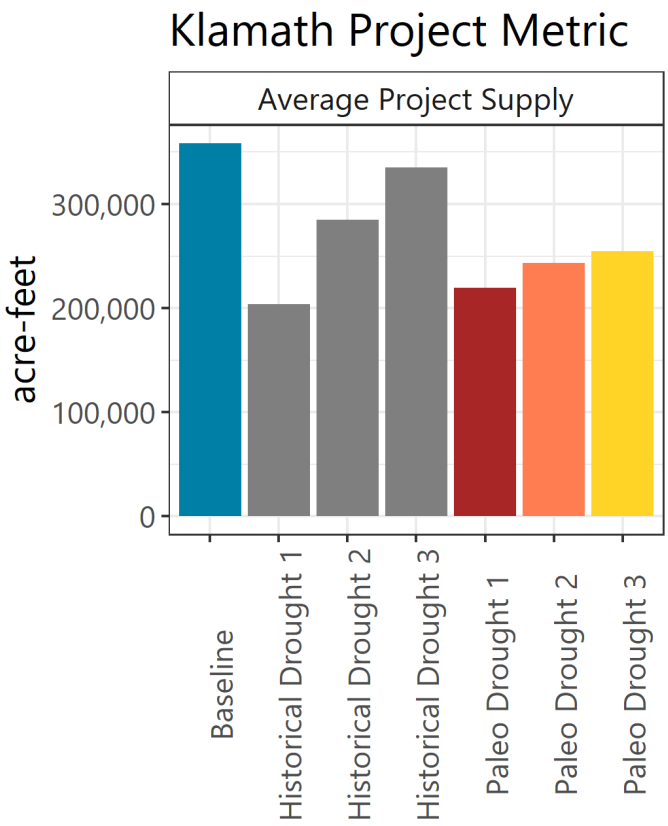

Figure 124. Klamath Project annual supply showing mean baseline conditions (blue), historical droughts (gray), and paleo droughts (red, orange, and yellow).

To explore how more recent historical and paleo drought events compare against projected future events, LOCA downscaled CMIP5 RCP4.5 and RCP8.5 hydrologic traces were used to identify drought events. Figure 125 shows droughts from the observed historical period, the paleo-reconstructed period, and for the future period covering 2006 to 2099. Droughts are shown with average annual deficit by volume (in thousand acre-feet) and duration (in years), with future events showing the drought with the largest cumulative deficit for each projected hydrology trace.

The grey circles represent notable droughts in the instrumental record identified by Reclamation's regional partners. The colored diamonds represent the three largest paleo drought events. The green triangles represent the drought events for each future hydrologic projection. These droughts are based on natural streamflow for the Klamath River at Keno, OR and do not reflect water management effects. The figure illustrates that the paleo drought events had a similar intensity, but much shorter duration than Historical Drought 1, and that the remaining two historical droughts had much lower intensities and durations. Future droughts of equal severity to Historical Drought 1, but with durations of up to 50 years instead of the 30 years for the historical drought, are possible. Droughts with much greater severity are also possible.

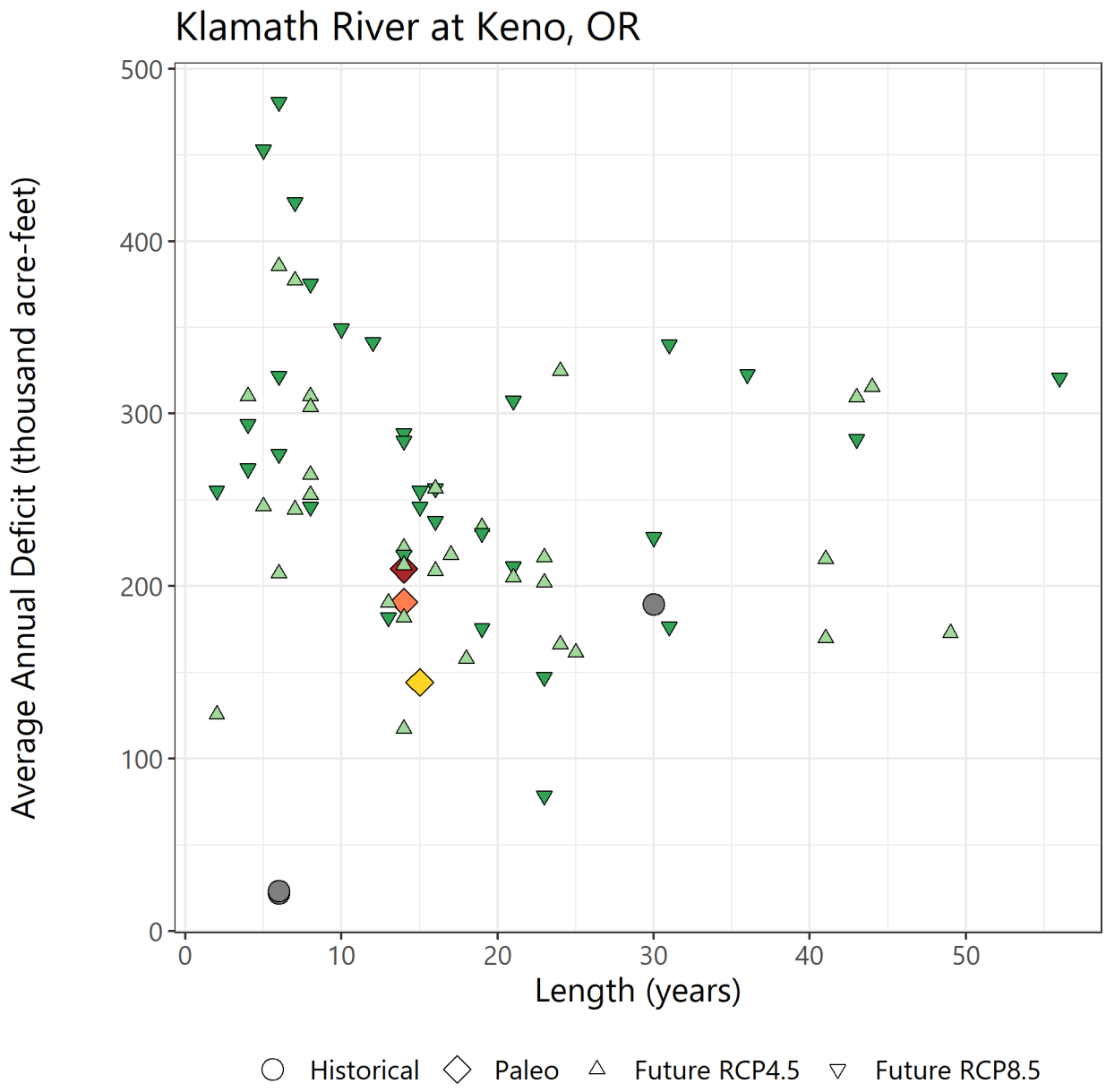

Figure 125. Drought length and average annual drought deficit for drought events at the Klamath River at Keno, OR.

Note: Circles represent historical droughts, diamonds represent paleo droughts, and triangles represent the largest drought from each projection in the LOCA dataset for RCP4.5 and RCP8.5.

6.5 Missouri River Basin (Upper Missouri)

The Upper Missouri River Basin upstream of Fort Peck Reservoir encompasses an area of about 50,000 square miles. The Missouri River is formed at the confluence of the Jefferson, Madison, and Gallatin Rivers, which flow out of the mountain ranges of southwest Montana. Tributaries to the Missouri River downstream of this confluence flow out of the Rocky Mountain Front and include the Sun, Teton, and Marias Rivers. The Upper Missouri River Basin also includes the

Smith, Judith, and Musselshell Rivers. Within the Upper Missouri River Basin, Reclamation manages several units of the Pick-Sloan Missouri Basin Program, including the East Bench Unit, Canyon Ferry Unit, Helena Valley Unit, and Lower Marias Unit. In addition, Reclamation manages the Sun River Project. In total, including Reclamation and non-Reclamation facilities, the Upper Missouri River supplies water to 1.1 million acres of irrigated land and 320,000 people in the basin.

6.5.1 Paleohydrology Scenario Development

Paleohydrology scenarios for the Upper Missouri River Basin were developed using annual streamflow reconstructions for the Missouri River at Fort Benton, MT (USGS ID 06090800) and the Musselshell River at Mosby, MT (USGS ID 06130500). Additional information including references for these reconstructions can be found in Chapter 2.

Figure 126 shows the Missouri River at Fort Benton, MT streamflow reconstruction and naturalized (i.e., unimpaired) streamflow over the observed historical period and identifies the six drought events examined in this study. Three drought periods from the observed historical period were selected for analysis—the first lasting 17 years from 1930 to 1946 (Historical Drought 1), the second lasting 11 years from 1954 to 1964 (Historical Drought 2), and the third lasting 8 years from 1985 to 1992 (Historical Drought 3). Analyses of managed streamflow and reservoir storage for these drought periods were compared with results for an overall historical baseline simulation period, in this case, 1950 to 1999. Additionally, results were compared with those from paleohydrology scenarios, which are described in the next section.

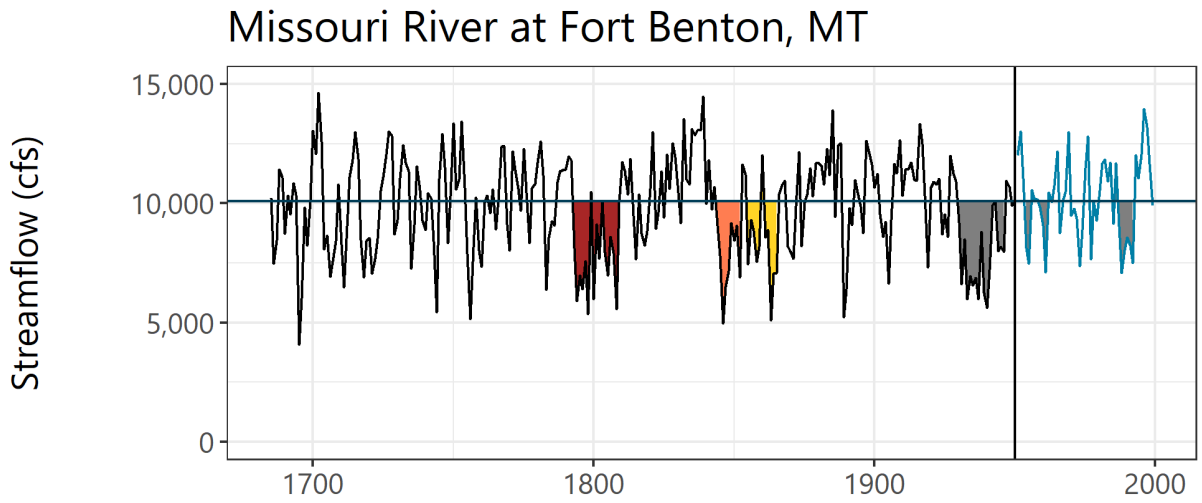

Figure 126. Annual streamflow for the Missouri River at Fort Benton, MT showing droughts in the paleo-reconstructed and observed historical periods.

Note: Paleo-reconstructed streamflow is in black and historical streamflow is in blue. The horizontal line shows long-term median streamflow. Drought events are shaded (red, orange, and yellow for Paleo Droughts 1, 2, and 3, respectively, and gray for historical droughts).

cfs = cubic feet per second

It is important to note that major drought events have occurred in the Upper Missouri River Basin beyond those evaluated in this report. Due to the objective of providing a West-wide analysis with greatest possible consistency in methods across regions, these additional drought events were not evaluated in the modeling framework described here. However, results from existing studies may provide additional context. Across the Upper Missouri River Basin, the recent drought of 2000 to 2010, known as the "Turn-of-the-Century Drought," was likely more severe than any in the instrumental record including the Dust Bowl Drought (Martin et al., 2020). Additional severe droughts were identified in the late 13th century (overlapping with the start of the severe and sustained "Great Drought" period in the American Southwest) and in the late 15th century (consistent with the timing of the 16th century North American megadrought). The same streamflow reconstructions were used in the Upper Missouri River Basin as used in this report. In terms of drought events with decadal persistence in streamflow, two of the four most severe droughts in the last 1,200 years appear to have occurred within the last century (Martin et al., 2020).

6.5.2 River Systems Model Overview

The Upper Missouri Basin Impacts Assessment (UMBIA) RiverWare model was originally developed using the RiverWare software package (Zagona et al., 2001) to support the Upper Missouri Basin Impacts Assessment (Reclamation, 2019) and the Missouri Headwaters Basin Study (Reclamation, 2020c). The model represents the Missouri River and its tributaries upstream of Fort Peck Reservoir and including the Musselshell River. The UMBIA model simulates the managed river system, including Reclamation and non-Reclamation reservoirs and irrigation projects, and agricultural, municipal, and industrial water uses. The model simulates using 2016 water management policy and current river regulatory constraints. The model runs at a daily timestep, with the historical baseline period beginning on January 1, 1950, and ending on December 31, 1999. Historical model inputs were developed using a suite of models. The VIC hydrology model was used to develop a majority of the inflows; however, some inflows and local inflows were calculated through mass balance or set to a fixed value in the case of springs. Reservoir evaporation was calculated using the Complementary Relationship Lake Evaporation (CRLE) model (Morton et al., 1985) and crop water demands were calculated using the ET demands model (Reclamation, 2015a). Crop water demands were set using current cropping patterns and acreages based on Reclamation (2012a) and Montana DNRC (2015).

Municipal and industrial water demands were represented for four cities in the Upper Missouri River Basin, and demands were identified using each city's water use plan or conversations with city officials—Bozeman (AEES, 2013), Helena (City of Helena, 2011), Great Falls (City of Great Falls, 2013), and Butte (Larson, 2013). River system initial conditions, primarily reservoir storage, at the start of each model run were set to mean historical conditions (i.e., each reservoir storage volume for January 1, 1950, was set to its mean storage volume between January 1, 1950, and December 31, 1999).

6.5.3 Water Resource Metrics

The largest Reclamation reservoir in the Upper Missouri River Basin is Canyon Ferry Reservoir, located along the mainstem Missouri River near Helena, Montana. Results from this analysis

focused on the effects of drought on storage of water in Canyon Ferry Reservoir. Downstream of Canyon Ferry Reservoir the abilty to meet summer and winter streamflow targets for the Missouri River at Toston, MT were examined. In addition, impacts of drought on two other Reclamation facilities, the Sun River Project and the East Bench Unit of the Pick-Sloan Missouri Basin Program, were investigated by looking at water users supplied by each facility—Fort Shaw Irrigation District (FSID), along with Broken O Ranch, and Greenfields Irrigation District (GID) for the Sun River Project; and the Clark Canyon Water Supply Company and East Bench Water Users for the East Bench Unit. These metrics are summarized in Table 32.

Table 32. Metrics for quantifying water supply reliability in the Upper Missouri River Basin

Storage Metrics
Percent of years during drought event that Canyon Ferry Reservoir reaches top of joint-use storage (1,891,888 acre-feet).
Percent of days during drought event that Canyon Ferry Reservoir falls below joint-use storage pool (1,097,599 acre-feet).
Average percent of Canyon Ferry Reservoir joint-use storage capacity on September 30.
Flow Metrics
Average percent of days each year meeting Missouri River at Toston summer (May 1 to June 15; 4,000 cfs) streamflow target.
Average percent of days each year meeting Missouri River at Toston winter (September 15 to December 31; 3,000 cfs) streamflow target.
Other Metrics
Average annual water shortage, in acre-feet, to Fort Shaw Irrigation District and Broken O Ranch.
Average annual water shortage, in acre-feet, to Greenfields Irrigation District.
Average annual water allocation percent to Clark Canyon Water Supply Company.
Average annual water allocation percent to East Bench Water Users.

6.5.4 Summary

Drought events from the observed historical period and the paleo-reconstruction period were selected to examine whether paleo droughts were more impactful than those from the observed period and from average historical conditions. Figure 126 shows the drought events and, qualitatively, it can be seen that Historical Drought 1 is the most sustained and severe drought. This drought, commonly referred to in the basin as the "Dustbowl Drought," is still often considered the drought of record and used in water supply planning studies. Paleo Drought 1 is

similar in length, but does not see the same sustained level of severity as the Dustbowl Drought. The other two paleo droughts are less severe than either the Dustbowl Drought or Paleo Drought 1, but appear more severe than the other two historical droughts—the late 1950s and early 1960s drought and the late 1980s and early 1990s drought, which are also used in water supply planning studies.

Reclamation currently has unallocated water supply in Canyon Ferry Reservoir, which provides a measure of support against drought conditions (Figure 127). This is evident in the drought storage metrics shown in Figure 128. Over the 1950 to 1999 observed historical baseline period, the reservoir refilled to the top of joint-use storage in 94 percent of the years (47 years out of 50). In the individual drought events, the reservoir refilled each year during Paleo Drought 2 and Paleo Drought 3. Over Paleo Drought 1, which is the longest paleo drought evaluated, the reservoir did not fill in 2 of the 17 years. For the other droughts evaluated, the reservoir did not refill in only 1 year within each drought event.

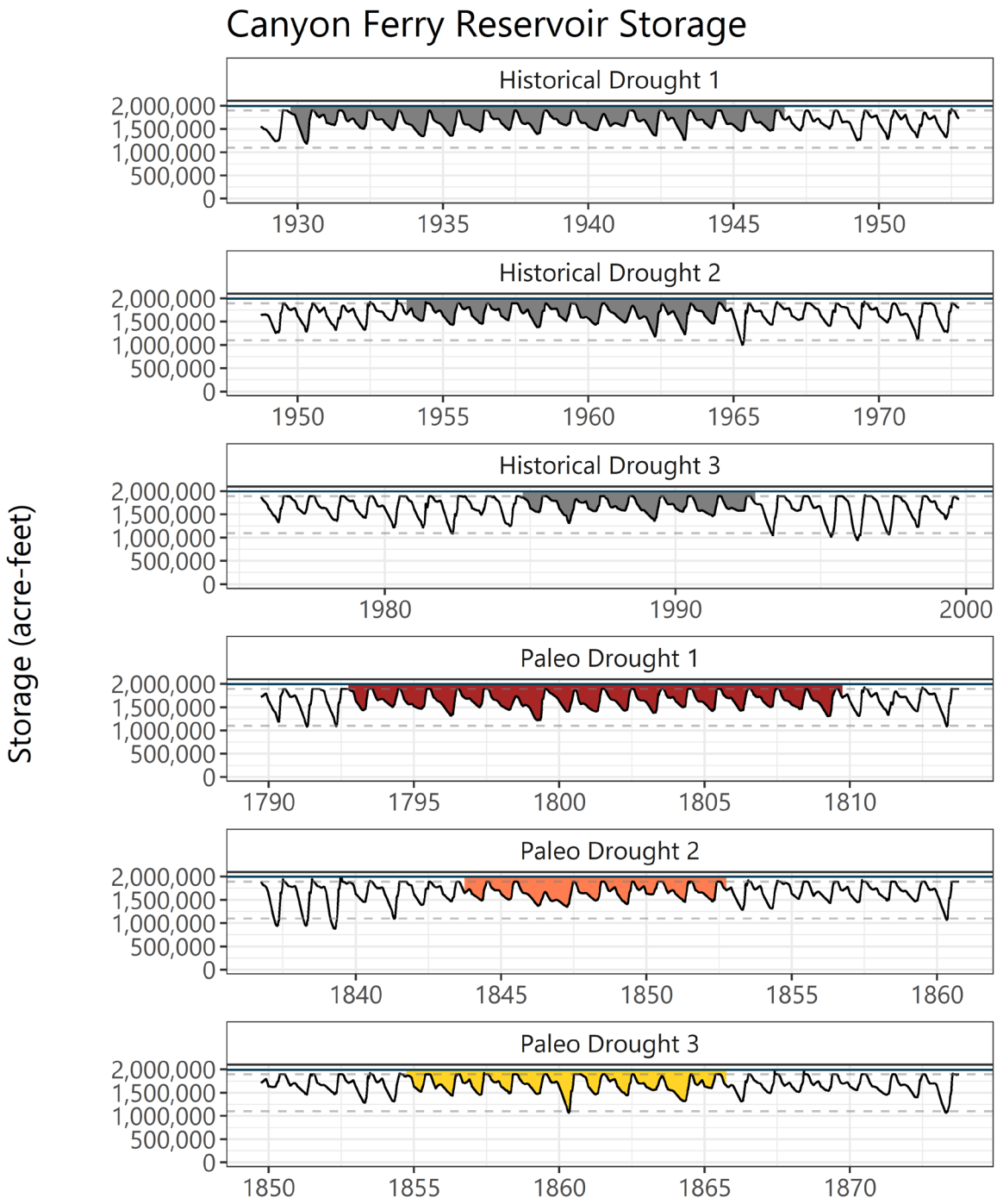

Figure 127. Daily modeled storage for Canyon Ferry Reservoir for each drought event (panels).

Note: The solid horizontal line shows the top of joint-use storage (1,891,888 acre-feet) and the dashed horizontal line shows the bottom of joint use storage (1,097,599 acre-feet). Drought events are shaded.

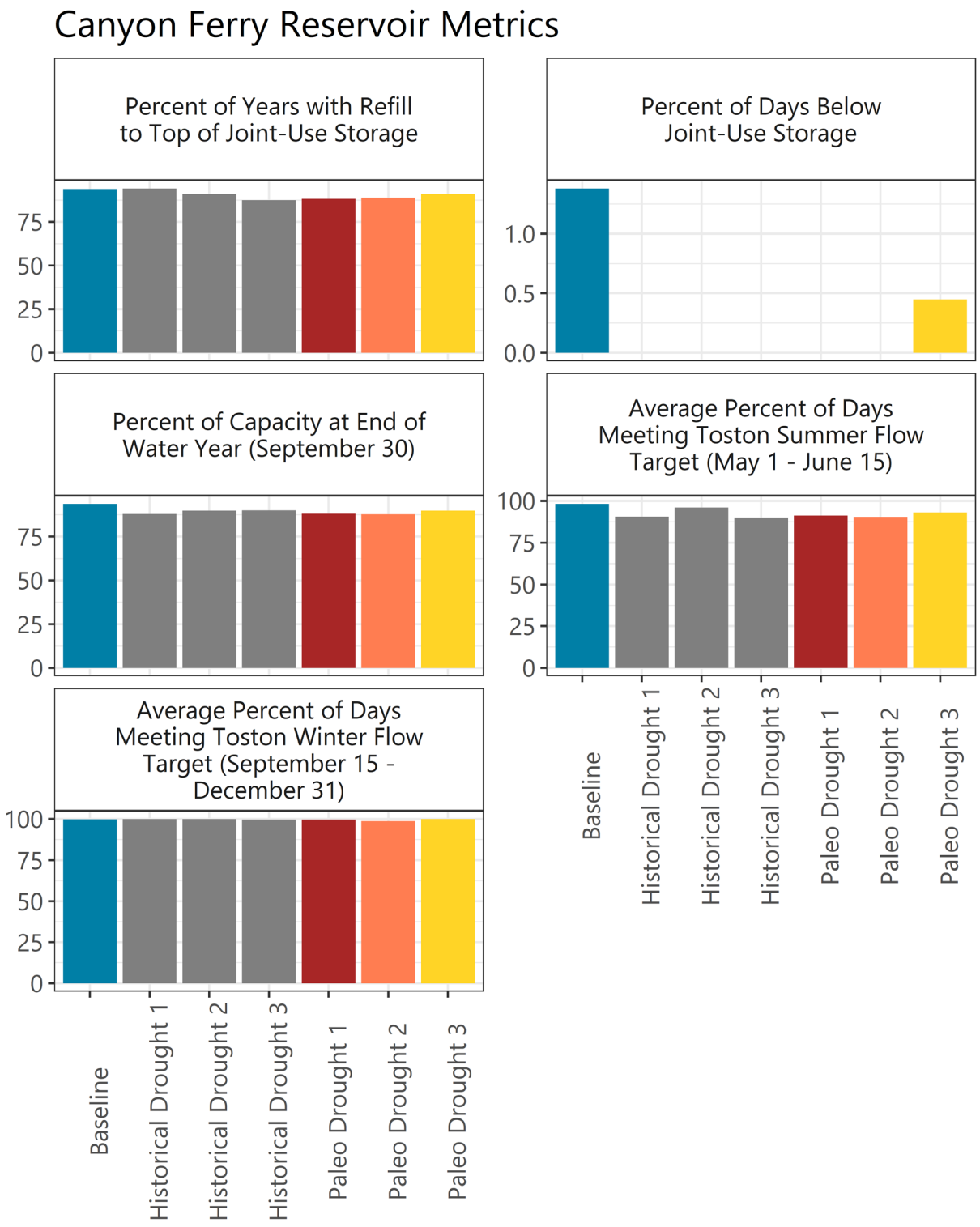

Figure 128. Canyon Ferry Reservoir storage and downstream streamflow metrics showing mean baseline conditions (blue), historical droughts (gray), and paleo droughts (red, orange, and yellow).

In addition to Canyon Ferry Reservoir, the impact of drought on two additional Reclamation facilities were examined: the Sun River Project and the East Bench Unit of the Pick-Sloan Missouri Basin Program. The Sun River Project is located west of Great Falls, Montana, and supplies irrigation water to about 93,000 acres of land in the Sun River basin. The Sun River is a tributary to the Missouri River, flowing out of the Rocky Mountain front region before joining with the Missouri River in Great Falls, Montana (refer to the basin map at the front of the Missouri River Basin document of the Water Reliability in the West - 2021 SECURE Water Act Report). Two irrigation districts receive water from the Sun River Project, primarily Fort Shaw Irrigation District, along with Broken O Ranch, and Greenfields Irrigation District. Figure 129 shows shortages to FSID and Broken O and GID on average over the 1950 to 1999 observed historical baseline period, and over each of the observed historical and paleo droughts. Shortages for FSID over the baseline period average almost 70 acre-feet (i.e., this irrigation district has senior water rights within the Sun River basin) and shortages for GID over the same period average 3,355 acre-feet. Shortages are substantially higher for each irrigation district for all drought events. Particularly notable are Paleo Drought 1 and Paleo Drought 3, which have more substantial shortages for FSID and Broken O than any historical drought. For GID, shortages over these droughts are more comparable to historical drought shortages, but are still larger than any historical drought.

The East Bench Unit in southwest Montana provides irrigation water to 21,800 acres in the Beaverhead River basin. The Beaverhead River basin is in the headwaters of the Upper Missouri River Basin, upstream of Three Forks, Montana. Shortages to water users are presented as a percentage of full allocation and are shown in Figure 130. The Clark Canyon Water Supply Company (CCWSC) and East Bench Water Users both receive water from the East Bench Unit and, over the historical baseline period, receive on average 93 percent and 82 percent of their allocations, respectively. The CCWSC, the more senior water user, is less impacted by drought and sees smaller decreases in allocations during drought. The lowest allocation is seen during Paleo Drought 1, when allocations averaged 84 percent. The East Bench Water Users are a junior water user and their allocations are more impacted by drought. Under Historical Drought 1, they receive an allocation of 67 percent. More notably, under Paleo Drought 1, they receive a 60 percent allocation and, under Paleo Drought 2, a 56 percent allocation.

The two examples from the Sun River Project and East Bench Unit show that, while the analyzed drought events have minimal impacts on Canyon Ferry Reservoir on average (likely because of the unallocated water supply), they do impact other Reclamation Projects in the Upper Missouri River Basin.

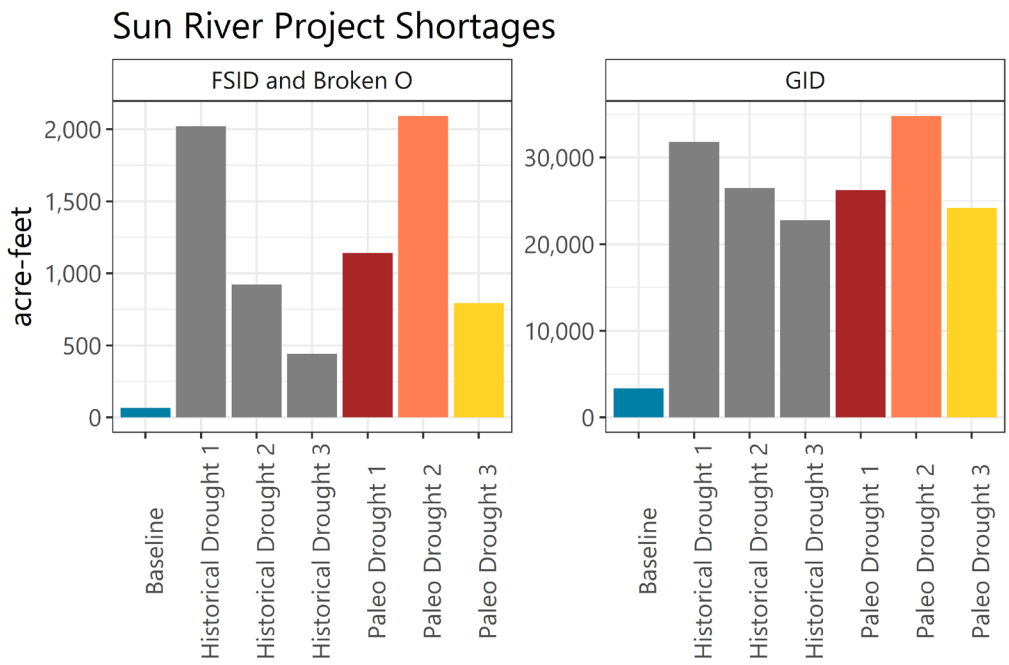

Figure 129. Shortages to Sun River Project Fort Shaw Irrigation District (FSID) and Broken O Ranch (left), and Greenfields Irrigation District (GID; right) showing mean baseline shortage (blue), historical droughts (gray), and paleo droughts (red, orange, and yellow).

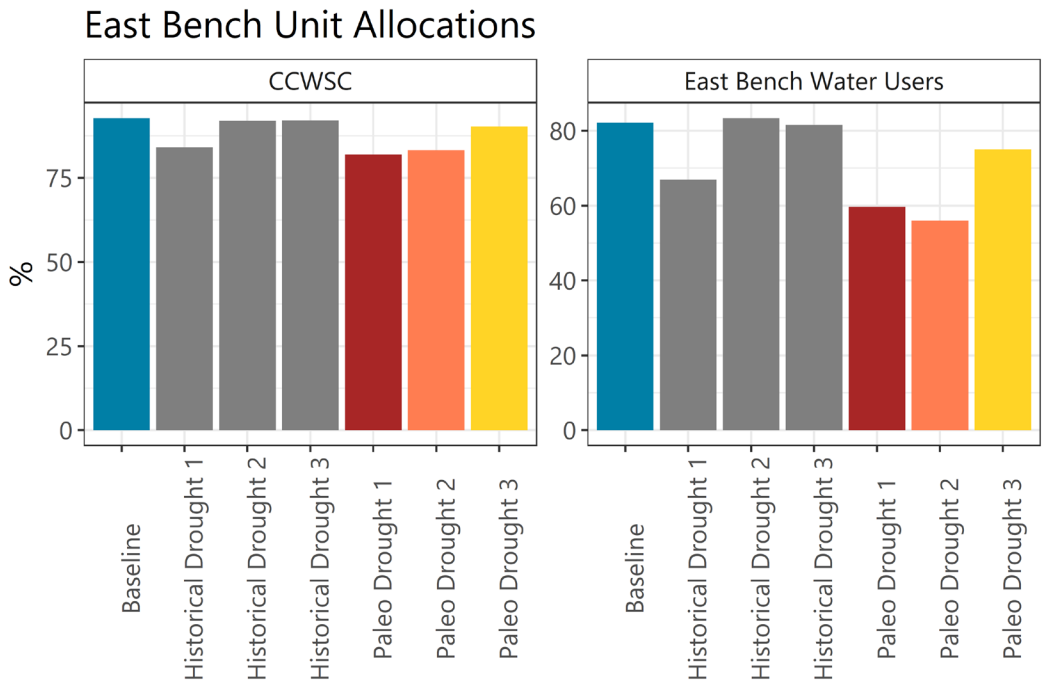

Figure 130. Allocations to East Bench Unit water users, Clark Canyon Water Supply Company (CCWSC; left), and East Bench Water Users (right) showing mean baseline allocation (blue), historical droughts (gray), and paleo droughts (red, orange, and yellow).

To explore how more recent historical and paleo drought events may be different from projected drought events using the LOCA downscaled CMIP5 RCP4.5 and RCP8.5 hydrologic traces from 2006 to 2099, average annual deficit by volume (acre-feet) and duration (length in years) are plotted for the drought events discussed in this section (drought events in the observed historical period and the paleo-reconstructed period), as well as for the largest cumulative deficit events for each projected hydrology trace. Figure 131 illustrates these events relative to each other.

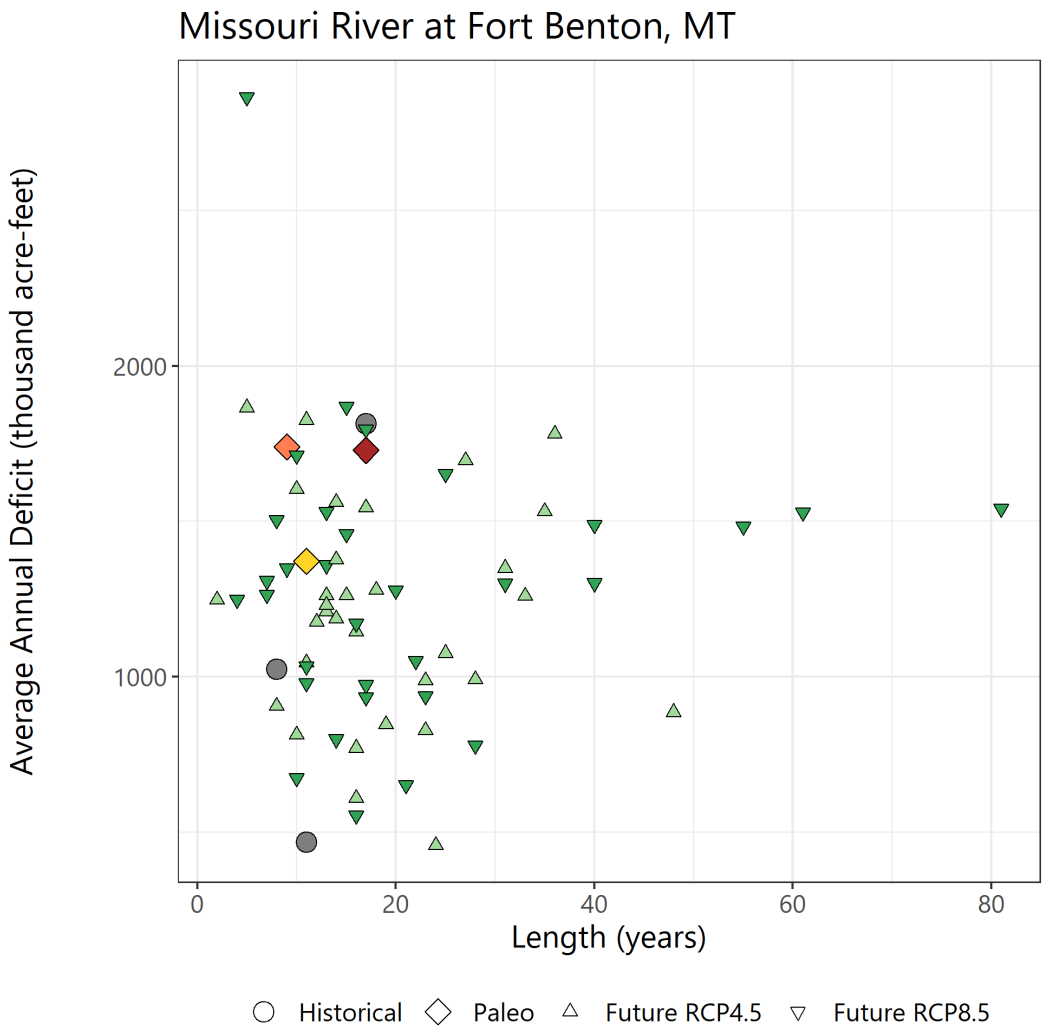

Figure 131. Drought length and average annual drought deficit for drought events at the Missouri River at Fort Benton, MT.

Note: Circles represent historical droughts, diamonds represent paleo droughts, and triangles represent the largest drought from each projection in the LOCA dataset for RCP4.5 and RCP8.5.

The grey circles represent notable droughts in the instrumental record identified by Reclamation's regional partners. The colored diamonds represent the three largest paleo drought events. The green triangles represent the drought events for each future hydrologic projection. These droughts are based on natural streamflow for the Missouri River at Fort Benton and do not reflect water management effects. The figure illustrates that the paleo drought events were

similar in length to the observed historical droughts and had a severity (as represented by average annual deficit) comparable to the Dustbowl Drought. Future droughts generally reflect the same range of severity seen in the historical and paleo droughts, with one notable exception, but indicate the possibility of much longer droughts, upwards of 40 to 60 years, and with one drought with a length of 81 years.

6.6 Rio Grande Basin

For the Rio Grande Basin, this report focuses on the Upper Rio Grande from the headwaters in the San Juan Mountains of southern Colorado to the Rio Grande at Caballo Reservoir in New Mexico. In the headwaters of the San Luis Valley of Colorado, the Conejos River joins the Rio Grande and the Rio Grande receives pumped groundwater from Reclamation's Closed Basin Project. Additional major tributaries of the Rio Grande include the Rio Chama and the Jemez River. Imported water comes from tributaries of the San Juan River in Colorado to the Rio Chama by means of Reclamation's San Juan-Chama Project, which constitutes a portion of New Mexico's allocation under the 1922 Colorado River Compact. The entire amount imported from the San Juan system (historically about 90,000 acre-feet per year) must be consumed upstream of Elephant Butte Reservoir, as defined under the Rio Grande Compact (e.g., Littlefield, 1991). Reclamation maintains this water in a project pool at Heron Reservoir on the Rio Chama. The amount allocated and the timing of allocation depends on the available supply in Heron Reservoir.

The Rio Grande serves as the primary source of water for agriculture throughout the Rio Grande Valley, as well as for municipal use by the major municipalities along the river corridor (including the cities of Albuquerque and Las Cruces, New Mexico; El Paso, Texas; and Ciudad Juarez, Mexico), and environmental and recreational uses in the States of Colorado, New Mexico, and Texas, as well as in Mexico. The basin also supports critical habitat for the federally endangered Southwestern Willow Flycatcher (*Empidonax traillii extimus*) and Rio Grande silvery minnow (*Hybognathus amarus*). Downstream of Elephant Butte Reservoir, the Rio Grande only flows during the Rio Grande Project's irrigation water deliveries or in rare floods. In El Paso, Texas, water is diverted for required deliveries to Mexico. Streamflow supports river and reservoir recreation, as well as vital environmentally sensitive areas.

The analysis of water supply risks related to drought events was performed by identifying notable historic drought events, as well as drought events in the paleo-reconstructed period, and comparing the managed system, under current operations and demands, with an observed historical baseline period. Two drought periods from the observed historical period were selected for analysis—the first lasting 6 years from 1950 to 1956 (Historical Drought 1), and the second lasting 4 years from 2011 to 2015 (Historical Drought 2). Analysis of managed streamflow and reservoir storage for these drought periods were compared with results for an overall historical baseline simulation period, in this case 1950 to 2015. Additionally, results were compared with those from paleohydrology scenarios, which are described in the next section.

6.6.1 Paleohydrology Scenario Development

Paleohydrology scenarios for the Rio Grande River were informed by annual streamflow reconstructions at the Conejos River near Mogote, CO (USGS ID 08246500); Rio Grande near Del Norte, CO (USGS ID 8220000); and, Rio Grande at Otowi Bridge, NM (USGS ID 08313000). Additional information including references for these reconstructions can be found in Chapter 2. These developed scenarios encompass the three most highly ranked drought events with the largest cumulative deficit. According to this drought definition, the largest drought occurred over a 14-year period from 1870 to 1883. The second largest drought occurred over a 11-year period from 1772 to 1782. The third largest drought occurred over a 10-year period from 1728 to 1737.

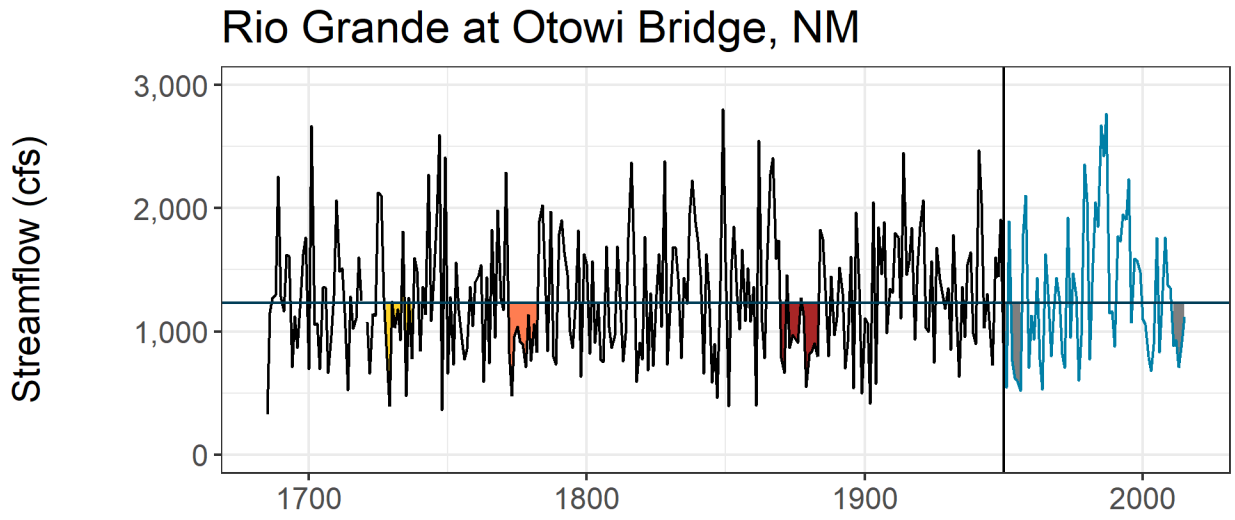

Figure 132. Annual streamflow for the Rio Grande River at Otowi Bridge, NM showing droughts in the paleo-reconstructed and observed historical periods.

Note: Paleo-reconstructed streamflow is in black and historical streamflow is in blue. The horizontal line shows long-term median streamflow. Drought events are shaded (red, orange, and yellow for Paleo Droughts 1, 2, and 3, respectively, and gray for historical droughts).

cfs = cubic feet per second

Figure 132 shows the annual streamflow reconstruction for the Rio Grande at Otowi Bridge, New Mexico in black, with the historical naturalized streamflow over the observed historical period shown in blue. Drought events of interest are shaded and include the three "largest cumulative deficit" droughts from the paleo-reconstruction period, the 1950s drought and the 2010s drought from the observed historical period. Streamflow at Otowi Bridge is presented because it is an integration of streamflow in the Upper Rio Grande headwater tributaries and representative of streamflow variability in the modeled region. Qualitatively, the three largest droughts in the paleo-reconstructed period were longer than the notable droughts in the observed period. Additionally, there were years with above average streamflow during drought events that did not meet the criteria to end the drought event.

Paleohydrology scenarios encompassing the five identified drought events were used to investigate impacts to reservoir storage in Elephant Butte Reservoir, as well as impacts to several other metrics that are important water supply indicators.

6.6.2 River Systems Model Overview

Daily operations and long-term planning are performed using simulations by the Upper Rio Grande Water Operations Model (URGWOM) developed in RiverWare. URGWOM is the tool central to coordinated river management in the basin and its use and development is supported via a memorandum of understanding among the managing agencies, including Reclamation, the U.S. Army Corps of Engineers, and the New Mexico Interstate Stream Commission. URGWOM contains data from an observed historical period of January 1950 through December 2015. The model was used as the basis for analysis of impacts of drought events, including historical events that have occurred over the observed record, as well as reconstructed events based on tree-rings, termed paleohydrology scenarios.

URGWOM is used to complete simulations based on policy for operations of all the facilities in the Rio Grande Basin from its headwaters in Colorado to Hudspeth County, Texas, and involves the use of complex accounting to track water specifically allocated for different water users. It applies the principals of mass conservation to simulate the physical processes of the hydrologic system. In addition, the URGWOM policy includes major legal constraints, such as reservoir and project authorization and the Rio Grande Compact. The primary purpose of URGWOM is to facilitate more efficient and effective accounting and management of water in the Upper Rio Grande Basin. However, URGWOM has been used for a variety of applications over the years, including accounting of native and trans-basin (San Juan-Chama Project) water in the system, daily operations according to the Annual Operating Plan, and long-term planning for specific projects, such as environmental or biological assessments, impact statements, and modified operations of specific elements (reservoir or project) of the system.

For this analysis, the model was implemented by Reclamation's Albuquerque Area Office in coordination with Technical Service Center staff who developed scenario inputs and performed analysis of model results. The model was run in Annual Operation Planning (AOP) mode, where URGWOM can be run in a flexible way to re-sequence historical data, if needed, as well as to vary the order of years. This AOP mode allows the use of the three sequences of years based on locations that TSC provided to be used in URGWOM.

Initial reservoir conditions in the model were identical for each scenario simulation. Initial storage for each reservoir was computed as the median of 1974 to 2019 historical storage, except for Platoro Reservoir that began operating in 1983. To estimate water demand from Elephant Butte and Caballo Reservoirs, an approach was taken that relates demand to current reservoir storage, reservoir inflow, and Caballo Reservoir releases.

6.6.3 Water Resource Metrics

In the Rio Grande Basin, storage at reservoirs such as El Vado and Heron on the Rio Chama, as well as Elephant Butte on the mainstem Rio Grande, provide insights to water supply reliability. Several metrics related to reservoir storage were selected to evaluate how these reservoirs are

impacted by drought events compared with an average historical baseline condition. The storage metrics evaluated for the Rio Grande are similar to storage metrics evaluated in other basins to inform a West-wide analysis of droughts and reservoir storage. One storage metric is the percent of years during a drought that storage reaches the top of active storage (in some cases full pool). Another storage metric is the percent of days over the drought duration that storage falls below the minimum conservation pool. Yet another storage metric is the average percent of capacity at the end of the water year (September 30). Again, this average is computed over each drought duration.

Table 33 summarizes the metrics evaluated in the Rio Grande Basin. For Elephant Butte storage, URGWOM has dead pool storage of 2,000 acre-feet. However, water managers generally try to maintain minimum storage at 50,000 acre-feet. Therefore, 50,000 acre-feet is used as the minimum storage threshold for Elephant Butte Reservoir. Storage metrics for Elephant Butte Reservoir are discussed in this section.

Table 33. Metrics for quantifying water supply reliability in the Rio Grande Basin

Storage Metrics
Percent of years during drought event that Elephant Butte Reservoir reaches top of active storage (2,010,900 acre-feet)
Percent of days during drought event that Elephant Butte Reservoir falls below conservation pool (50,000 acre-feet)
Average percent of capacity on September 30 at Elephant Butte Reservoir
Other Metrics
Average percent of days Middle Rio Grande Conservation District receives full demand (i.e., Cochiti Reservoir release is greater than or equal to Middle Rio Grande Conservation District demand)
Average percent of days for which Article VII of the Rio Grande Compact between Colorado, New Mexico, and Texas (i.e., when Rio Grande Project storage water in Elephant Butte and Caballo Reservoirs is less than 400,000 acre-feet) is in effect

Metrics listed in Table 33 in the "Other" category include additional metrics that are specific to the Rio Grande Basin. One such metric is the average percent of days the Middle Rio Grande Conservation District receives its full demand. To calculate this metric, if Cochiti Reservoir outflow is greater than or equal to Middle Rio Grande Conservation District demand on a given day (generally between March and October), then the full demand is met.

Another metric is the average percent of days during a drought event that the Rio Grande Compact Article VII restrictions are in effect, which occurs if reservoir storage for the Rio Grande Project (simplified as the sum of Elephant Butte Reservoir storage and Caballo Reservoir storage) is less than 400,000 acre-feet. When Article VII restrictions are in place, upstream

States (Colorado and New Mexico) are not allowed to store native water in reservoirs constructed after 1929.

Another important metric for water supply in the basin is whether contractors of San Juan-Chama Project water in Heron Reservoir receive their full annual allocation, which totals 96,200 acre-feet for all of the contractors. The metric is computed based on the available storage in Heron Reservoir plus the amount diverted from tributaries to the San Juan River. Results for this metric were evaluated in this report, but are not shown because, during the identified drought events in this analysis, there were not computed shortages. Interestingly, the results show that the configuration of the modeling experiment in terms of identified droughts and in terms of model initial conditions have a substantial impact on the results. Therefore, additional analysis is needed to fully investigate these impacts and may be seen as a useful next step for this work.

6.6.4 Summary

Drought events from the observed historical period and the paleo-reconstruction period were selected to examine whether paleo droughts were more impactful than those from the observed period and from average historical conditions. If droughts were more severe in the paleo-reconstructed period than the observed period, water managers may choose to make more conservative decisions with the additional understanding that water supplies may take longer to be replenished than previously thought.

Figure 133 illustrates modeled daily storage at Elephant Butte Reservoir over select time periods that encompass selected drought events. Dashed lines indicate the minimum storage of 50,000 acre-feet (based on agreement) and maximum active capacity of 2,010,900 acre-feet. It is notable that storage never reaches the top of active capacity in the drought event simulations. Storage does fall below the minimum storage target.

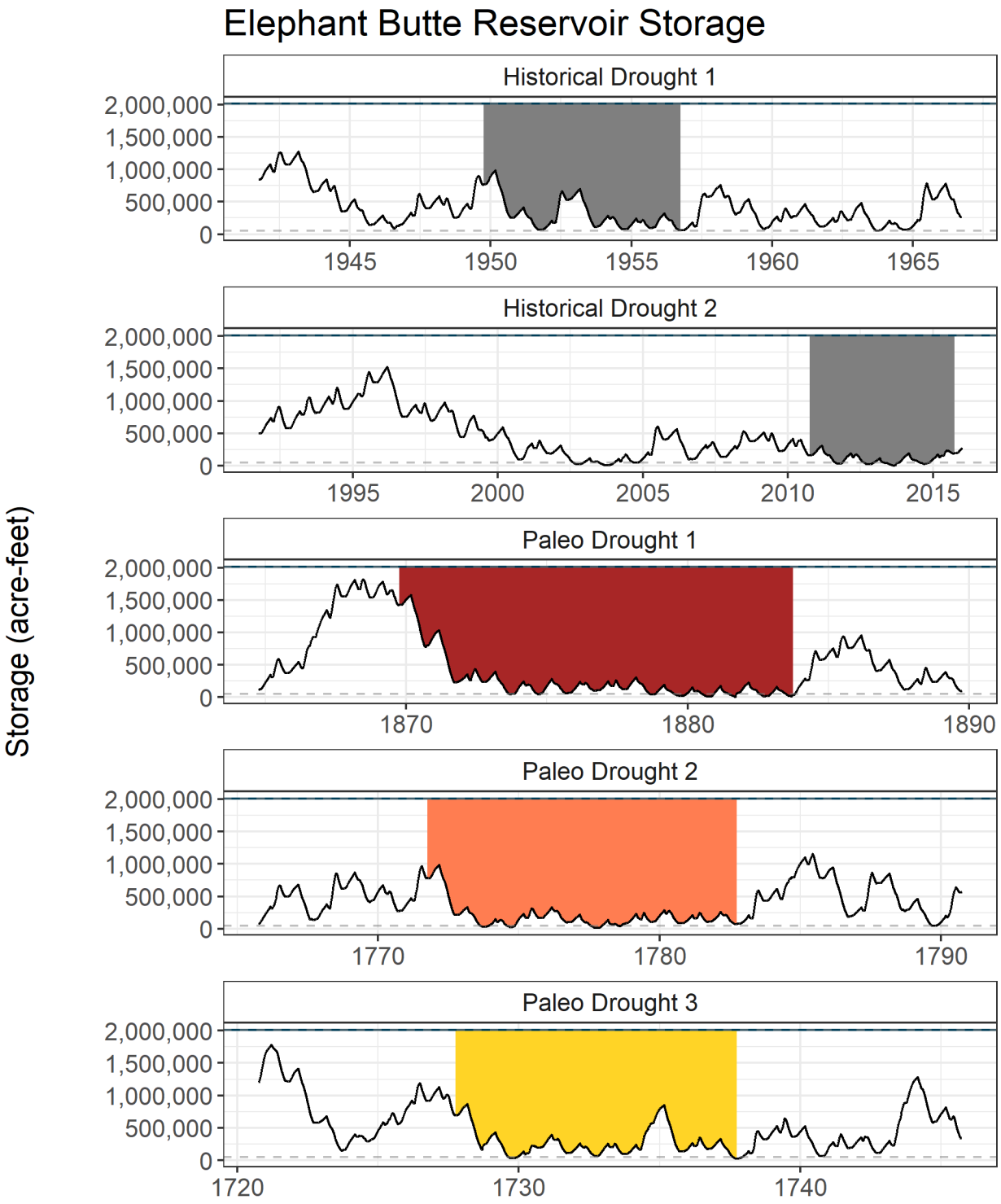

Figure 133. Daily modeled storage for Elephant Butte Reservoir for each drought event (panels).

Note: The solid horizontal line shows the top of active storage (2,010,900 acre-feet) and the dashed horizontal line shows the bottom of conservation pool storage (50,000 acre-feet by agreement). Drought events are shaded.

Figure 134 summarizes some aspects of the timeseries information presented in Figure 133. For the observed historical baseline period, Elephant Butte Reservoir reached top of active storage in only 1 year over the 1950 to 2015 period—in May 1987 (figure not shown). There were almost 8 percent of days out of about 66 years of record where reservoir storage dipped below the agreed 50,000 acre-feet minimum. Interestingly, during the 1950s drought (Historical Drought 1), storage came close, but never fell below, the minimum while in other drought events the percent of days below the minimum was higher than the historical baseline (about 28 percent for Historical Drought 2; 15 percent for Paleo Drought 1; 10 percent for Paleo Drought 2; and 4 percent for Paleo Drought 3). This metric appears to show that Historical Drought 2 was much worse compared with Paleo Drought 1; however, upon review of the timeseries of storage, both droughts have substantial impact on water supply with Paleo Drought 1 showing minimal storage lasting a decade or more.

End-of-water-year storage at Elephant Butte Reservoir was 21 percent of capacity on average, which represents approximately one average year of inflow, over the observed historical baseline period. Generally, the irrigation districts served by the Rio Grande Project may not use their full surface water allocation in order to have reservoir storage available for the following year. In addition, the districts served by the Rio Grande Project also have access to groundwater, so they may use groundwater to make up for any needed surface water left in the reservoir. In comparison over the drought events, Historical Drought 1 (1950s) had about 9 percent of capacity on average; Historical Drought 2 (2010s) had about 3 percent of capacity on average; Paleo Drought 1 had 7 percent of capacity on average; Paleo Drought 2 had 5 percent of capacity on average; and Paleo Drought 3 had 8 percent of capacity on average. Therefore, the end-of-water-year storage is lower in these historical and paleo drought simulations than it is, on average, in the historic baseline.

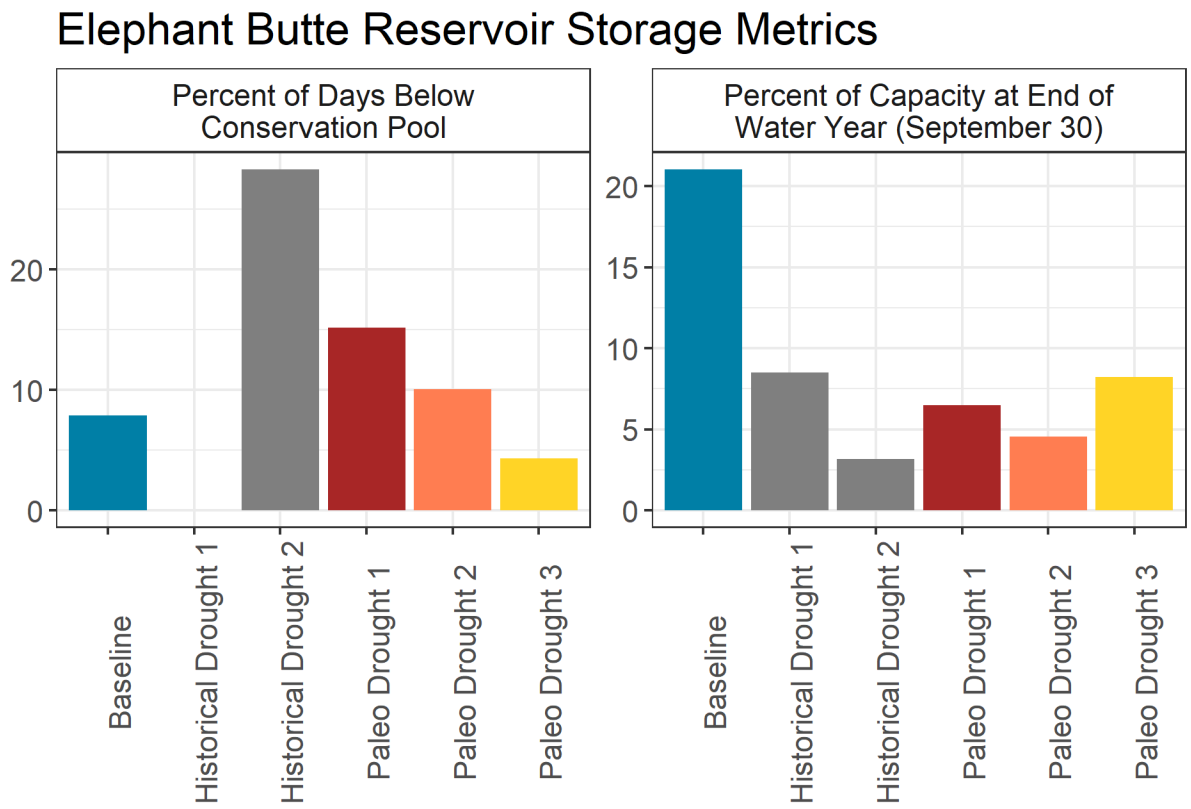

Figure 134. Elephant Butte Reservoir storage metrics showing mean baseline conditions (blue), historical droughts (gray), and paleo droughts (red, orange, and yellow).

Figure 135 summarizes results of the drought analysis for metrics meaningful in the Upper Rio Grande Basin. Over the observed historical baseline period of 1950 to 2015, the model simulates that the basin is under Article VII restrictions 49 percent of the days. This increased to 70 percent over the 1950s drought (Historical Drought 1) and to 100 percent over the 2010s drought (Historical Drought 2). For the paleo droughts, the basin was generally in Article VII more often—84 percent of days over Paleo Drought 1; 92 percent of days over Paleo Drought 2; and 76 percent of days over Paleo Drought 3.

Over the observed historical baseline period, the average percent of days the Middle Rio Grande Conservation District received its full demand is 66 percent. For the historical droughts, this was similar or slightly lower—61 percent over the 1950s drought and 58 percent over the 2010s drought. Results were also slightly lower over the paleo droughts—52 percent over Paleo Drought 1; 52 percent also over Paleo Drought 2; and 51 percent over Paleo Drought 3. Generally, the drought events show slightly more days in shortage on average.

Over the observed historical baseline period, the average percent of years the San Juan-Chama Project contractors received their full allocation was 88 percent. Interestingly, for all of the drought events (more recent historical droughts and paleo drought events), San-Juan Chama Project contractors did not have shortages.

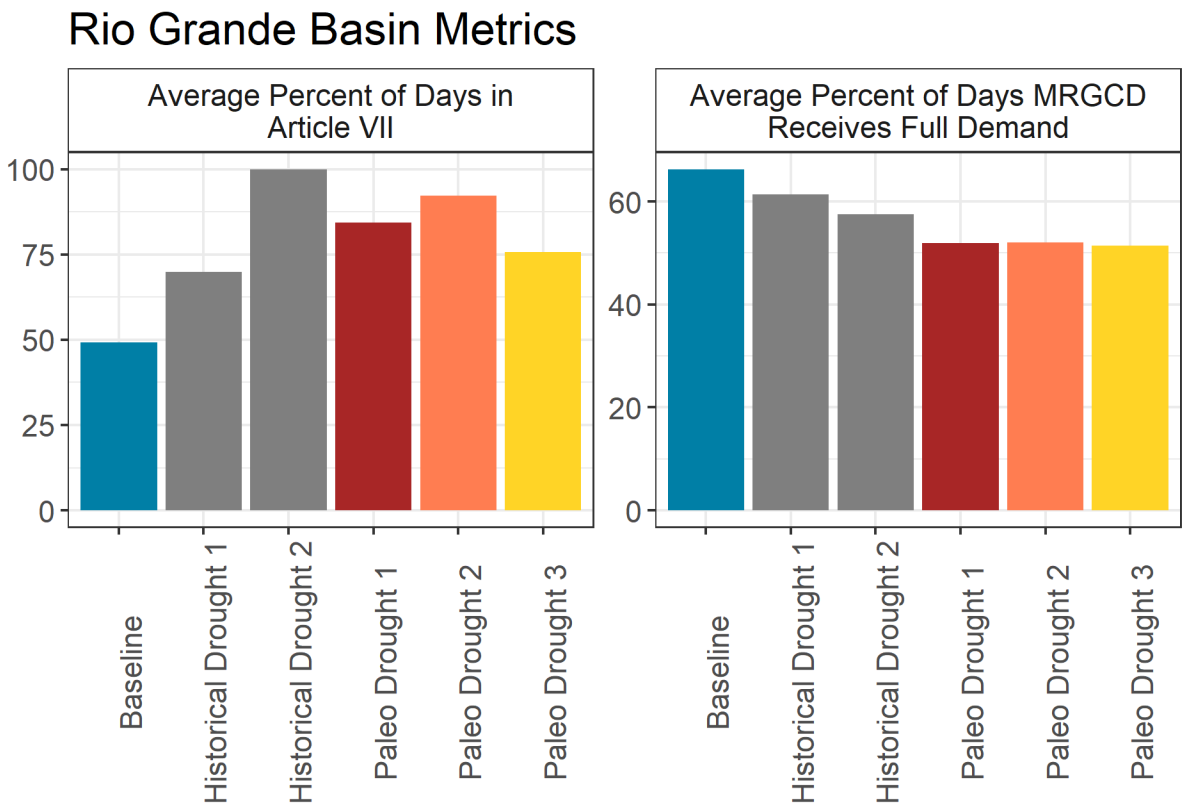

Figure 135. Relevant Rio Grande Basin metrics showing mean baseline conditions (blue), historical droughts (gray), and paleo droughts (red, orange, and yellow).

To explore how more recent historical and paleo drought events may be different from projected drought events via LOCA downscaled CMIP5 RCP4.5 and RCP8.5 hydrologic traces from 2006 to 2099, average annual deficit by volume (acre-feet) and duration (length in years) are plotted for the drought events discussed in this section (drought events in the observed historical period and the paleo-reconstructed period), as well as for the largest cumulative deficit events for each projected hydrology trace. Figure 136 illustrates these events relative to each other.

The grey circles represent notable droughts in the instrumental record identified by Reclamation's regional partners. The colored diamonds represent the three largest paleo drought events. The green triangles represent the drought events for each future hydrologic projection. These droughts are based on natural streamflow at Rio Grande at Otowi Bridge and do not reflect water management effects. The figure illustrates that the paleo drought events were longer than the observed historical drought events of interest, but also encompass a similar range of severity (as represented by average annual deficit). However, future drought events may be longer and more severe than what has been either observed or reconstructed by tree-ring records of the distant past.

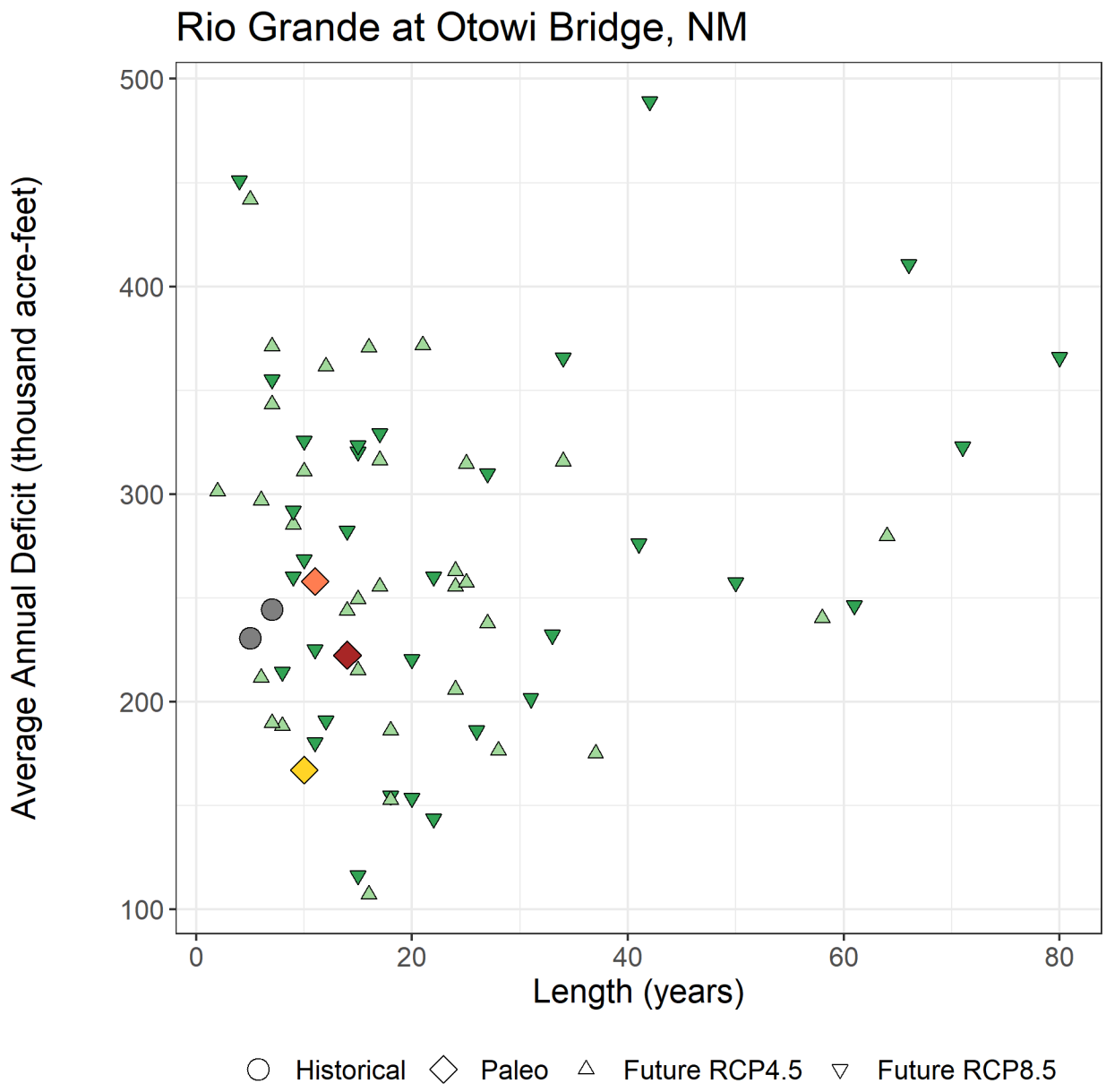

Figure 136. Drought length and average annual drought deficit for drought events at the Rio Grande at Otowi Bridge, NM.

Note: Circles represent historical droughts, diamonds represent paleo droughts, and triangles represent the largest drought from each projection in the LOCA dataset for RCP4.5 and RCP8.5.

6.7 Sacramento and San Joaquin River Basins

The Sacramento and San Joaquin Rivers are the two largest rivers in California. Together with the Central Valley Project (CVP) operated by Reclamation and California State Water Project operated by the State of California, they represent one of the most complex water management systems in the world. The Sacramento River originates in the Klamath Mountains in northern California and flows about 400 miles to its mouth at the Sacramento-San Joaquin Rivers Delta

(Delta). The San Joaquin River originates on the western slope of the Sierra Nevada Mountains and its tributaries drain a large portion of the Sierra Nevada Range. The CVP provides water for agriculture (on average 5,000,000 acre-feet), for municipal and industrial use (on average 600,000 acre-feet), and for environmental purposes (on average 1,210,000 acre-feet). The California State Water Project provides municipal and industrial water use for more than 23 million people.

The analysis of water supply risks related to drought events was performed by identifying notable historic drought events, as well as drought events in the paleo-reconstructed period, and comparing the managed system, under current operations and demands, with an observed historical baseline period. Two drought periods from the observed historical period were selected for analysis—the first lasting 7 years from 1928 to 1934 (Historical Drought 1), and the second lasting 6 years from 1987 to 1992 (Historical Drought 2). A third drought, lasting from 2013 to 2015 was of interest given its recent occurrence and the awareness of the general public to this drought; however, the management model simulation period did not allow for the inclusion of this drought in this study. Analysis of managed streamflow and reservoir storage for these drought periods were compared with results for an overall historical baseline simulation period, in this case 1922 to 2003. Additionally, results were compared with those from paleohydrology scenarios, which are described in the next section.

6.7.1 Paleohydrology Scenario Development

Paleohydrology scenarios for the Sacramento and San Joaquin River Basins were developed using 11 streamflow reconstructions shown in Figure 3. Detailed results for four of these reconstructions—the Sacramento River at Bend Bridge, CA (USGS ID 11377100); the Feather River at Oroville, CA (USGS ID 11407000); the American River at Fair Oaks, CA (USGS ID 11446500); and the San Joaquin River at Millerton, CA (USGS ID 11250100)—are presented below. These two reconstructions represent hydrology in close proximity to four of the key reservoirs in the Sacramento and San Joaquin River Basins—Shasta Reservoir, Oroville Reservoir, Folsom Reservoir, and Millerton Lake. Droughts from the observed historical period are the same for all four of these reconstructions; however, droughts from the paleohydrology period were identified for each reconstruction individually. Similar to identified drought events in other basins, the identification of drought is dependent on the reconstructions used and the drought definition applied, as discussed in Chapter 2.

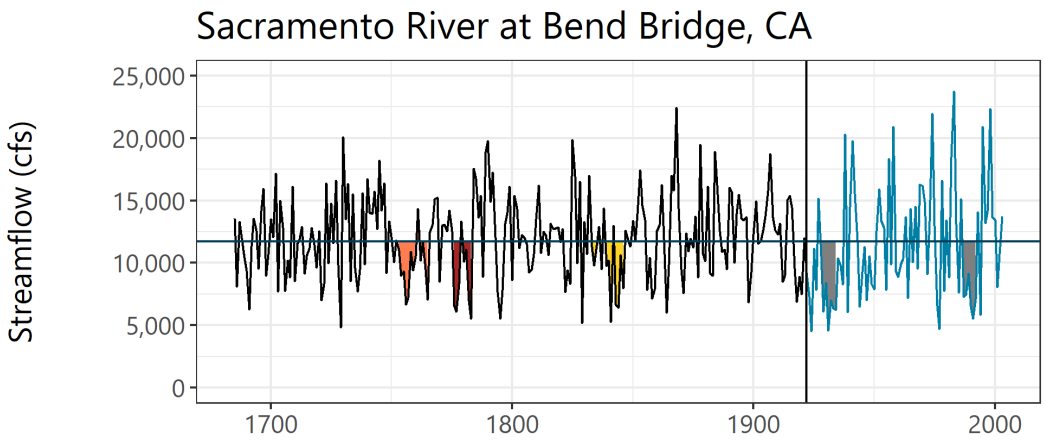

Figure 137. Annual streamflow for the Sacramento River at Bend Bridge, CA showing droughts in the paleo-reconstructed and observed historical periods.

Note: Paleo-reconstructed streamflow is in black and historical streamflow is in blue. The horizontal line shows long-term median streamflow. Drought events are shaded (red, orange, and yellow for Paleo Droughts 1, 2, and 3, respectively, and gray for historical droughts).

cfs = cubic feet per second

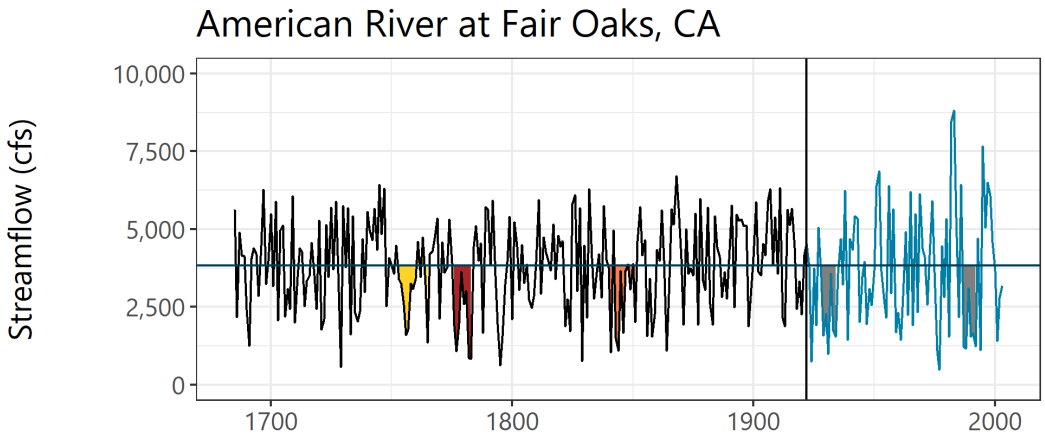

Figure 138. Annual streamflow for the American River at Fair Oaks, CA showing droughts in the paleo-reconstructed and observed historical periods.

Note: Paleo-reconstructed streamflow is in black and historical streamflow is in blue. The horizontal line shows long-term median streamflow. Drought events are shaded (red, orange, and yellow for Paleo Droughts 1, 2, and 3, respectively, and gray for historical droughts).

cfs = cubic feet per second

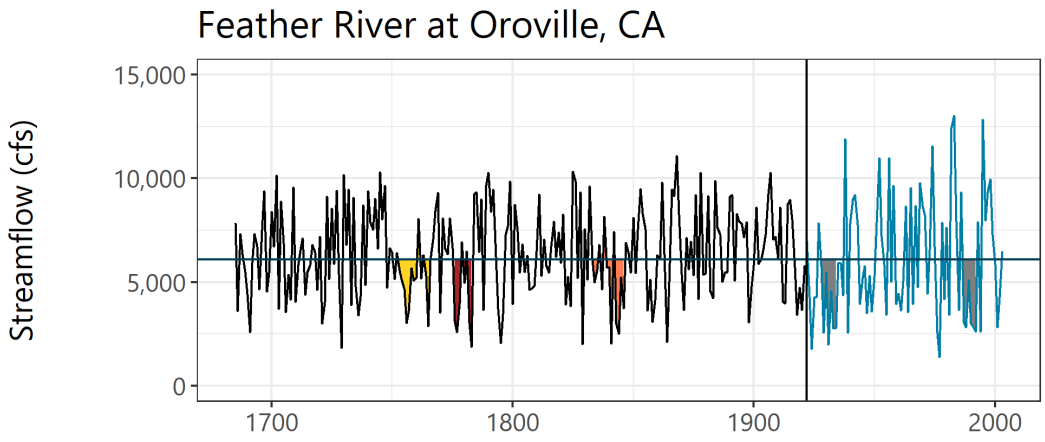

Figure 139. Annual streamflow for the Feather River at Oroville, CA showing droughts in the paleo-reconstructed and observed historical periods.

Note: Paleo-reconstructed streamflow is in black and historical streamflow is in blue. The horizontal line shows long-term median streamflow. Drought events are shaded (red, orange, and yellow for Paleo Droughts 1, 2, and 3, respectively, and gray for historical droughts).

cfs = cubic feet per second

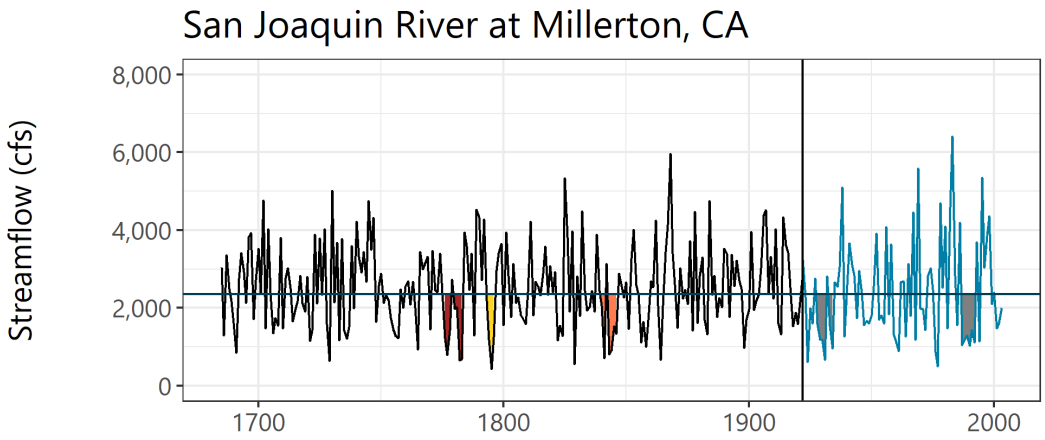

Figure 140. Annual streamflow for the San Joaquin River at Millerton, CA showing droughts in the paleo-reconstructed and observed historical periods.

Note: Paleo-reconstructed streamflow is in black and historical streamflow is in blue. The horizontal line shows long-term median streamflow. Drought events are shaded (red, orange, and yellow for Paleo Droughts 1, 2, and 3, respectively, and gray for historical droughts).

cfs = cubic feet per second

These four reconstructions highlight how drought events impacting the Sacramento and San Joaquin River Basins often affect the entire region, and that there are also spatial differences in the drought events. Across the four reconstructions, the largest drought from the paleo-reconstruction period (identified in Figure 137 to Figure 140 by the red shading) are the same,

lasting 8 years from 1776 to 1783. The second largest drought in the paleo-reconstruction period differs across reconstructions. Both the American River at Fair Oaks and the San Joaquin River at Millerton have droughts that begin in 1840; however, while the San Joaquin River drought only lasts for 7 years, until 1846, the American River drought extends 12 years to 1851.

The second largest drought for the Feather River at Oroville begins earlier, in 1833, and overlaps with both the American River and San Joaquin River droughts, lasting 14 years until 1846. The Sacramento River at Bend Bridge also experiences a drought during this time, but it ranks as the third largest drought. By contrast, the second largest drought seen for the Sacramento River at Bend Bridge corresponds with the third largest drought seen for the American River and the Feather River, all beginning in 1753 and ending in 1765 or 1766. The third largest drought seen for the San Joaquin River is distinct from the other three reconstructions, beginning in 1793 and lasting 4 years to 1796. In presenting results, individual reservoirs use the paleo-reconstruction period droughts unique to the corresponding reconstruction location. Results for overall system metrics use the drought events for the Sacramento River at Bend Bridge.

6.7.2 River Systems Model Overview

The managed river system within the Sacramento and San Joaquin River Basins, including the CVP and the California State Water Project, are modeled using the CalSim2 model. CalSim2 is built using the Water Resource Integrated Modeling System (WRIMS model engine, or WRIMS), a generalized water resources modeling system for evaluating operational alternatives for large, complex river basins. WRIMS integrates a simulation language for flexible operational criteria specification with a linear programming solver for efficient water allocation decisions. CalSim2 is a long-term planning model which simulates CVP and California State Water Project operations under a specified set of regulatory criteria. WRIMS and CalSim2 are products of joint development between the State of California Department of Water Resources and Reclamation (Close et al., 2003; Draper et al., 2004). The version of CalSim2 used for this study is an adaptation of the model used as the basis for the February 18, 2020, Record of Decision on Re-initiation of Consultation on Coordinated Long-Term Operations of the CVP and the California State Water Project (Reclamation, 2020b).

6.7.3 Water Resource Metrics

Results for the Sacramento and San Joaquin River Basins are presented to highlight four key reservoir locations—Shasta Reservoir, Oroville Reservoir, Folsom Reservoir, and Millerton Lake. These four reservoirs represent major storage facilities that support Reclamation's CVP and the California State Water Project. Water Resources metrics related to reservoir storage are listed in Table 34. At Shasta Reservoir, a May 1 storage volume of 4,100 thousand acre-feet is considered a threshold that can support Sacramento River temperature requirements through the summer, although numerous other conditions affect the accrual of cold water pool. End-of-September carryover has historically been as low as 1,400 thousand acre-feet; both 1,900 thousand acre-feet and 2,200 thousand acre-feet have been key thresholds for desired carryover to promote subsequent year refill. At Folsom Reservoir, an end-of-December storage threshold of 230 thousand acre-feet is the assumption used in current operations under the American River Flow Management Standard. At Oroville Reservoir,

carryover threshold of 1,600 thousand acre-feet is used in calculating allocations to the California State Water Project. That said, end-of-year storage conditions can be lower than that, depending on California State Water Project obligations for meeting environmental and other regulatory criteria.

In addition to storage metrics, the combined CVP and California State Water Project system is evaluated using two system metrics—total Delta outflow and total exports. These are also listed in Table 34. Total Delta outflow is a measure of freshwater flow from the Sacramento and San Joaquin Rivers into the Sacramento-San Joaquin Rivers Delta. Freshwater outflow is important in preserving habitat in the Delta, as well as preventing saline water intrusion upstream of the Delta. Total exports quantify the water supply provided by the CVP and California State Water Project to South-of-Delta delivery areas and demonstrate the range of project operations capabilities given regulatory export restrictions in the Delta.

Table 34. Metrics for quantifying water supply reliability in the Sacramento and San Joaquin River Basins

Storage Metrics
Average percent of years during drought event above 4,100 thousand acre-feet in Shasta Reservoir on May 1
Average percent of years during drought event above 1,900 thousand acre-feet in Shasta Reservoir on September 30
Average percent of capacity in Shasta Reservoir at the end of the water year (September 30)
Average percent of capacity in Millerton Lake at the end of the water year (September 30)
Other Metrics
Total Delta outflow in mean thousand acre-feet per year
Total exports, the sum of exports from Banks and Jones Pumping Plants, in mean thousand acre-feet per year

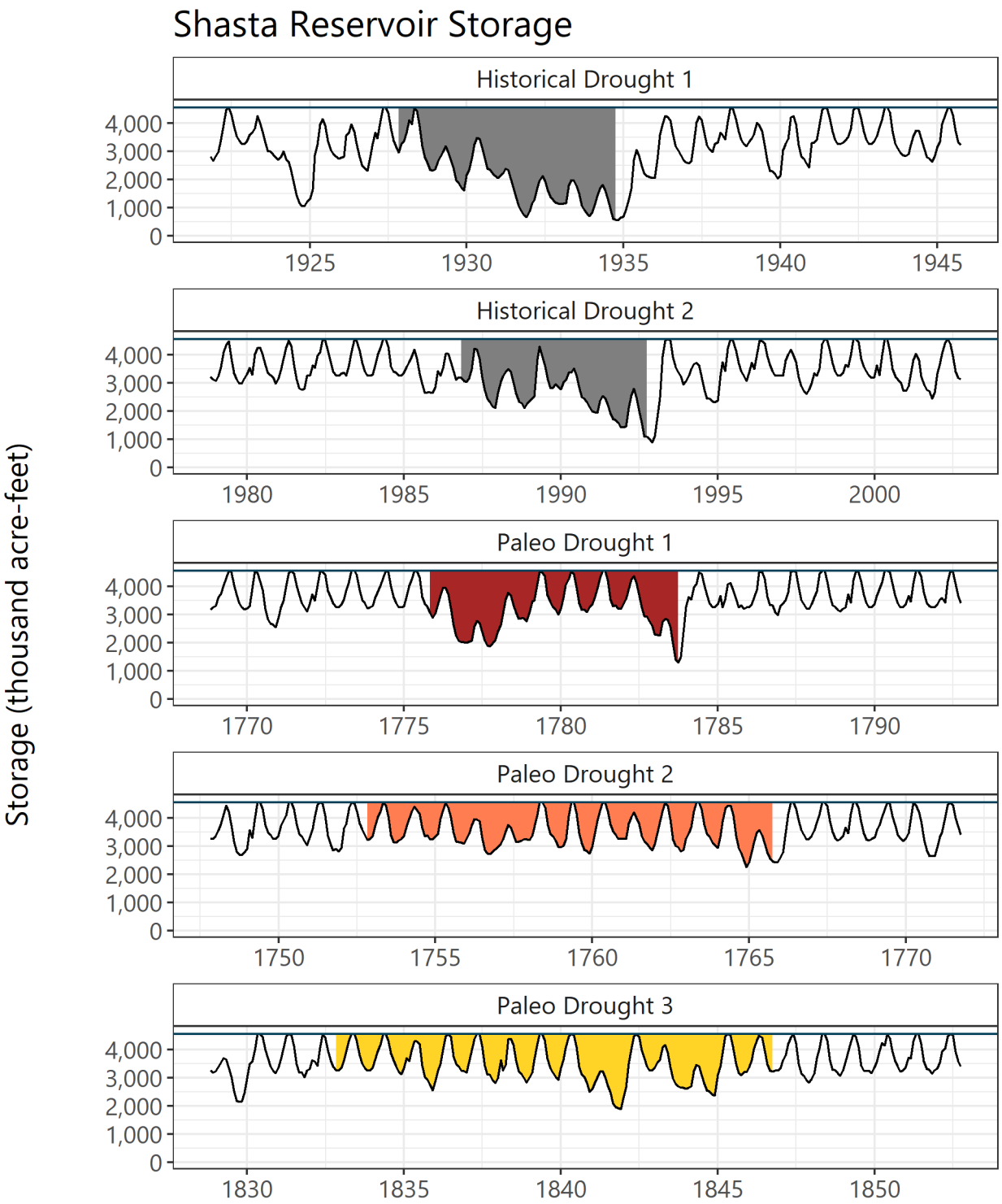

Figure 141. Monthly modeled storage for Shasta Reservoir for each drought event (panels).

Note: The solid horizontal line shows the top of storage (4,552,000 acre-feet). Drought events are shaded.

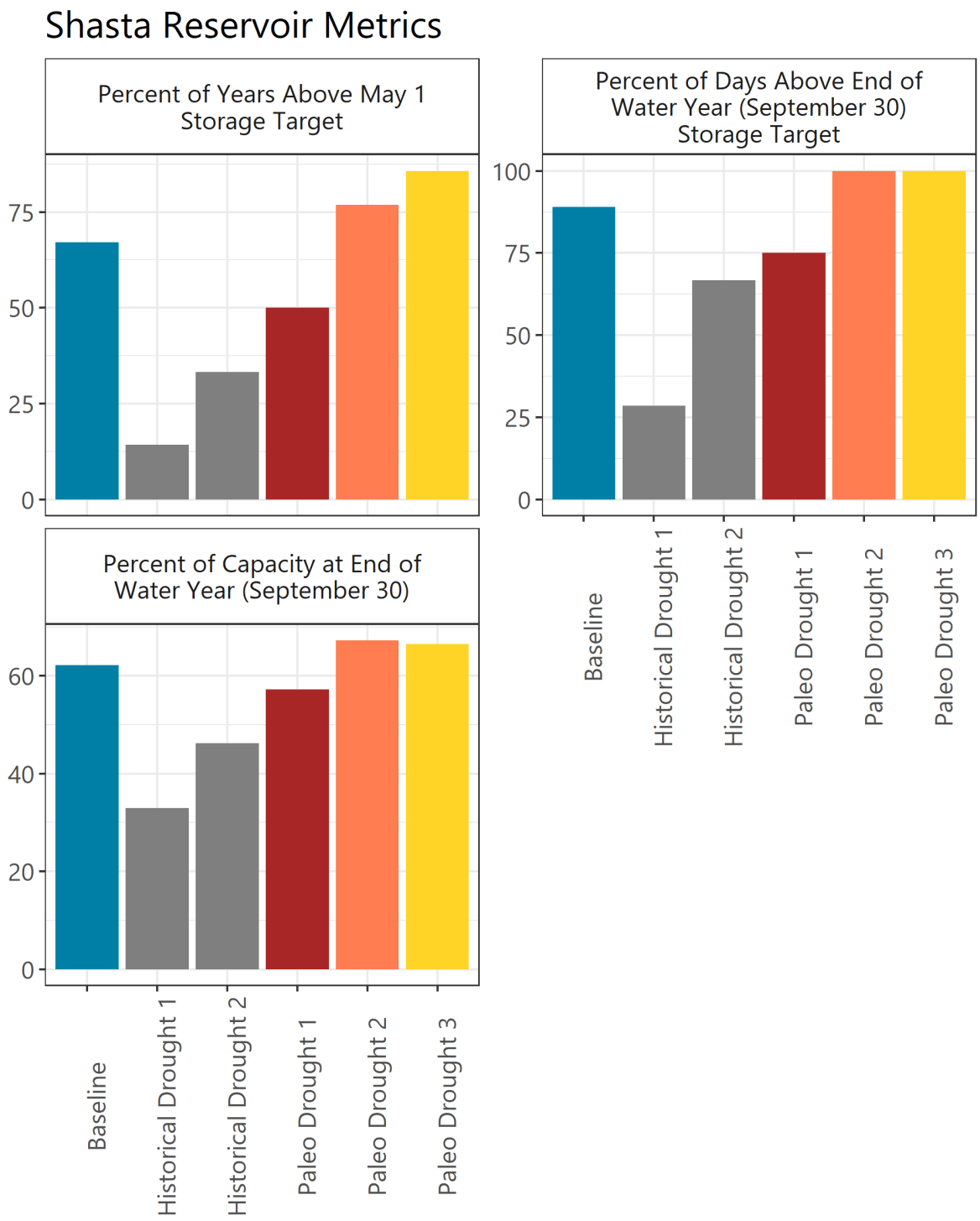

Figure 142. Shasta Reservoir storage and metrics showing mean baseline conditions (blue), historical droughts (gray), and paleo droughts (red, orange, and yellow).

6.7.4 Summary

6.7.4.1 Shasta Reservoir

Shasta Reservoir is located at the north end of the Sacramento Valley along the mainstem of the Sacramento River. It is a major storage reservoir for Reclamation's CVP. Figure 141 shows modeled storage in Shasta Reservoir for each drought event. The two historical drought events impact storage to a much greater extent than any of the three paleo droughts, with storage reaching their lowest levels in Historical Drought 1, lasting from 1928 to 1934. During this drought, the reservoir can refill to full pool in the first year of the drought, but then drops considerably over the subsequent years. It takes several years following the end of the drought before storage returns to full pool. In Historical Drought 2, storage also remains below full pool for multiple years, but sees a moderate recovery midway through the drought, and a rapid recovery following the end of the drought.

By contrast, of the three paleo drought events, only Paleo Drought 1 shows storage remaining substantially below full pool for multiple years. The second half of Paleo Drought 1 and the other two paleo droughts show storages that are mostly able to recover to full pool or close to it each year. Figure 142 shows storage metrics for Shasta Reservoir and they reiterate that the two more recent historical droughts had a much larger impact on the reservoir than the three paleo droughts. However, Figure 141 illustrates that the paleo droughts, although perhaps less severe, lasted much longer. Two metrics for Shasta Reservoir are a May 1 storage volume of 4,100 thousand acre-feet and 1,900 thousand acre-feet on September 30, at the end of the water year. Over the 1922 to 2003 baseline period, the May 1st 4,100 thousand-acre-foot threshold is achieved 67 percent of the time and the September 30 carryover of 1,900 thousand acre-feet is seen 62 percent of the time. During Historical Drought 1, the May 1 value is exceeded just 14 percent of years over the drought, and the September 30 value is exceeded just 28 percent of years over the drought. Historical Drought 2 and Paleo Drought 1 show some decrease frequency of exceeding these thresholds, but, during the remaining two paleo droughts, these storage levels are seen with even greater frequency than over the baseline period.

6.7.4.2 Millerton Lake

Millerton Lake impounds water from the Upper San Joaquin River, near the town of Friant, California. It supplies water to the Friant Division of the CVP and regulates streamflow releases for San Joaquin River restoration.

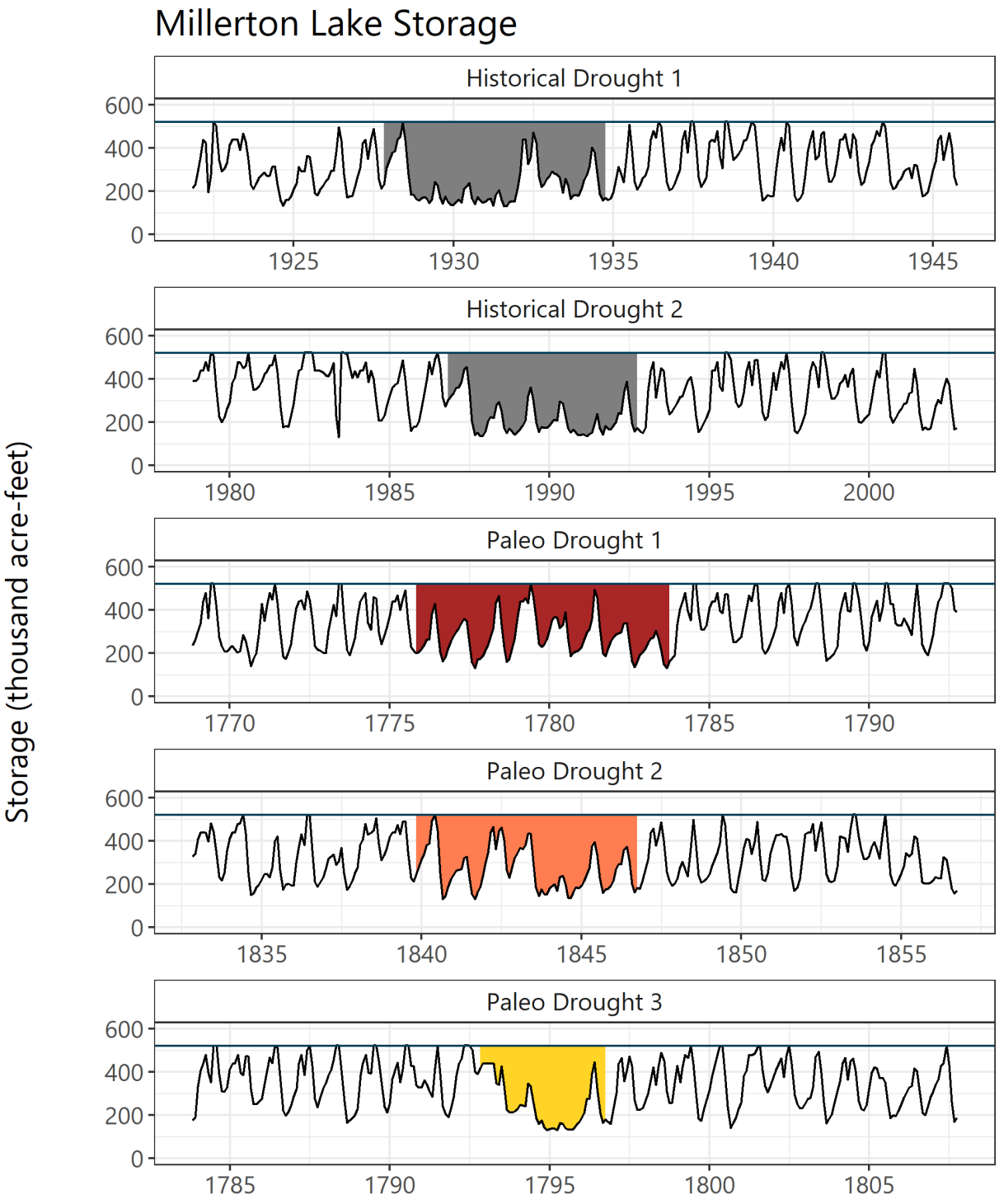

Figure 143. Monthly modeled storage for Millerton Lake for each drought event (panels).

Note: The solid horizontal line shows the top of storage (520,500 acre-feet). Drought events are shaded.

Millerton Lake storage exhibits similar impacts to Shasta Reservoir storage (Figure 143) where the two most impactful droughts appear to be the two historical droughts. During these events, storage drops substantially and remains well below full pool for multiple years. While the three paleo drought events show storages below full pool, there is moderate recovery year-to-year through the drought, with storages rebounding to full pool or close to full pool fairly often. Millerton Lake does not have explicit storage targets, so storage was only examined using September 30 or end-of-water-year storage percent, as shown in Figure 144. Over the 1922 to 2003 baseline period, Millerton Lake was at 42 percent of capacity. All drought events appear to have similar impacts and percent capacity ranges between 33 and 35 percent. While informative, the monthly timeseries of storage shown in Figure 143 provides a clearer picture of the impact of drought on Millerton Lake.

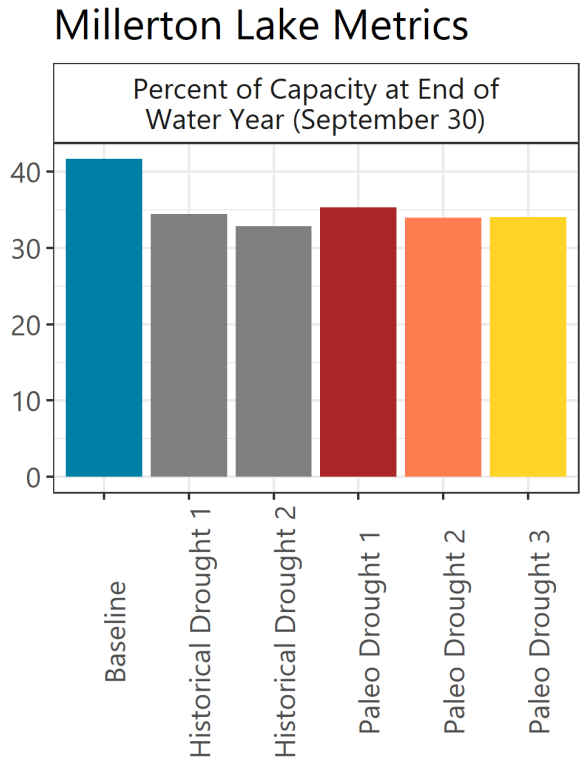

Figure 144. Millerton Lake storage metric showing mean baseline conditions (blue), historical droughts (gray), and paleo droughts (red, orange, and yellow).

6.7.4.3 Delta Outflow and Total Exports

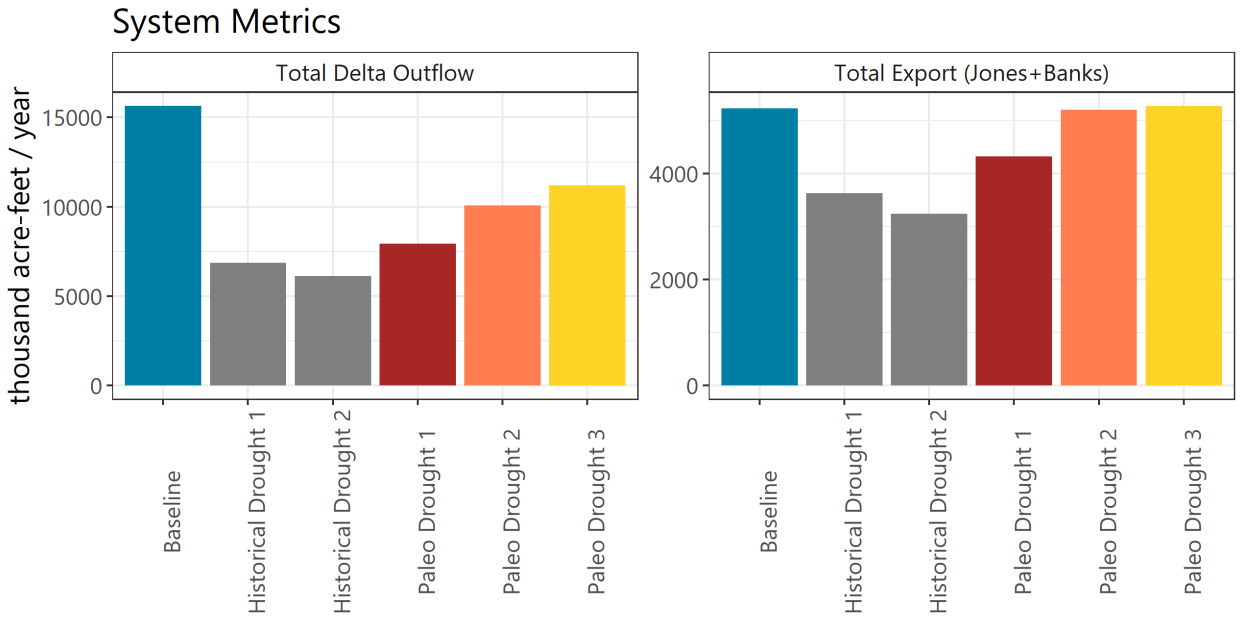

Figure 145. Key metrics of Reclamation's Central Valley Project and California's State Water Project showing mean annual total Sacramento-San Joaquin Rivers Delta outflow (in thousand acre-feet) and mean annual total exports for baseline conditions (blue) against historical droughts (gray) and paleo droughts (red, orange, and yellow).

To examine the impact of drought on the entire Sacramento and San Joaquin River Basins, and the interconnected CVP and California State Water Project systems, two metrics were selected. Total Delta Outflow is a measure of the water exiting the river basins and entering the Sacramento-San Joaquin Rivers Delta. Delta outflow of freshwater from the Sacramento River and San Joaquin River are critical to the maintenance of habitat and wildlife within the Delta, and also provide a buffer against the intrusion of saline water into the river basins. Total Exports is a sum of water pumped by the Jones Pumping Plant and Banks Pumping Plant, supplying water into the CVP and California State Water Project systems.

Figure 145 shows these two metrics including their average conditions over the 1922 to 2003 baseline period and over each of the drought events. Over the baseline period, Total Delta Outflow averaged 15,600,000 acre-feet per year. This drops to only 6,900,000 acre-feet per year for Historical Drought 1 and 6,100,000 acre-feet per year for Historical Drought 2. For the most impactful paleo drought, Paleo Drought 1, Total Delta Outflow averaged 7,900,000 acre-feet per year. While these results show that the two historical droughts were still more impactful with respect to Delta outflow than any of the paleo droughts, Paleo Drought 1 appears to impact the overall system in a greater way than it does just on Shasta Reservoir.

Over the baseline period, Total Exports averaged 5,200,000 acre-feet per year. Historical Drought 1 and Historical Drought 2 reduce these exports on average to 3,600,000 acre-feet and 3,200,000 acre-feet, respectively. Paleo Drought 1 also reduces exports to 4,300,000 acre-feet on average. It is interesting to note that, for both Total Delta Outflow and Total Exports, Historical

Drought 2, which lasted from 1987 to 1992, saw greater reductions in both metrics than Historical Drought 1. This is in contrast to the results presented above which show that Historical Drought 1 had a much greater impact on Shasta Reservoir than Historical Drought 2.

6.7.4.4 Future Drought

To explore how projected future events compare against more recent historical and paleo drought events, droughts were identified for each projection using the LOCA downscaled CMIP5 RCP4.5 and RCP8.5 hydrologic traces from 2006 to 2099. The largest drought for each projection was identified using the largest cumulative deficit measure used to identify paleo drought events. Figure 146 and Figure 147 show these projected future droughts against paleo droughts and historical droughts by plotting average annual deficit by volume (acre-feet) against duration (length in years).

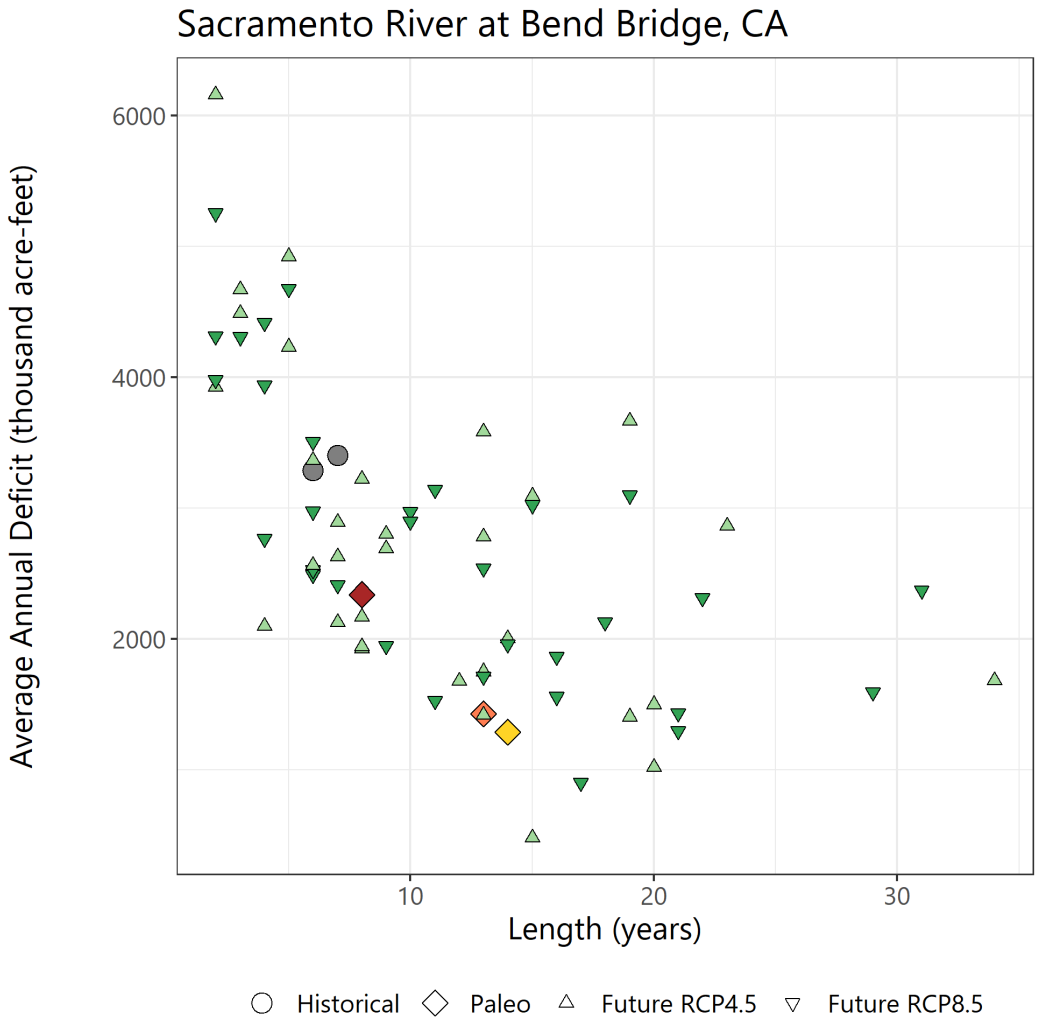

Figure 146. Drought length and average annual drought deficit for drought events at the Sacramento River at Bend Bridge, CA.

Note: Circles represent historical droughts, diamonds represent paleo droughts, and triangles represent the largest drought from each projection in the LOCA dataset for RCP4.5 and RCP8.5.

The grey circles represent notable droughts in the instrumental record identified by Reclamation's regional partners. The colored diamonds represent the three largest paleo drought events. The green triangles represent the drought events for each future hydrologic projection. These droughts are based on natural streamflow and do not reflect the impact of management for either the Sacramento River at Bend Bridge or the San Joaquin River at Millerton. Figure 146, showing events for the Sacramento River at Bend Bridge, reaffirms that the two historical droughts examined in this study were more severe, as measured by average annual deficit, than the three paleo droughts examined.

The future projected droughts indicate the possibility of more severe, but shorter, droughts, as well as droughts of equal severity to the historical droughts, but lasting as long as 18 years. They also indicate the possibility of droughts equal in severity to the largest paleo drought, but lasting as long as 30 years. Figure 147, showing events for the San Joaquin River at Millerton, has similar findings. Here, the future projected droughts could be of equal to greater severity than the historical droughts, but lasting as long as 19 years. Some projections also indicate the possibility of long-duration (over 30 years), but mild-severity droughts.

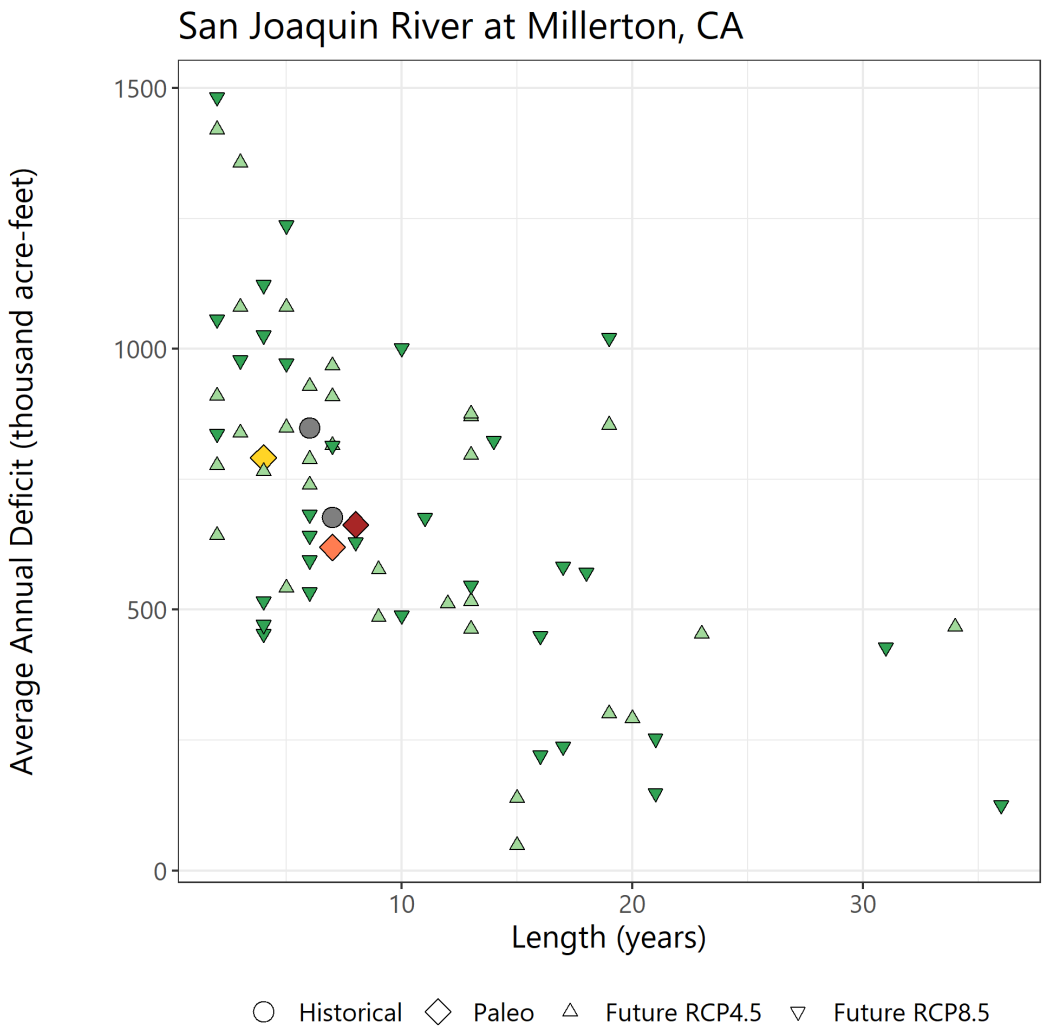

Figure 147. Drought length and average annual drought deficit for drought events at the San Joaquin River at Millerton, CA.

Note: Circles represent historical droughts, diamonds represent paleo droughts, and triangles represent the largest drought from each projection in the LOCA dataset for RCP4.5 and RCP8.5.

6.8 Truckee and Carson River Basins

The Truckee and Carson River Basins support natural ecosystems and are a vital water source for more than 400,000 people. Tributaries high in the Sierra Nevada Mountains of California flow into Lake Tahoe, which is the source of the Truckee River. From its outlet at Lake Tahoe Dam, the Truckee River gains additional streamflow from several tributaries including Martis Creek, Prosser Creek, and the Little Truckee River in California, and Steamboat Creek in Nevada. This streamflow is an important source of municipal, agricultural, and environmental water for inhabitants of the Truckee River Basin, as well as the neighboring Carson River basin where some Truckee River streamflow is diverted via the Truckee Canal to support the Newlands Project, Stillwater National Wildlife Refuge, and the Fallon Paiute-Shoshone Indian Reservation

and Community. Remaining streamflow enters the Pyramid Lake Paiute Indian Reservation and discharges into Pyramid Lake where two endangered endemic fish species, cui-ui (*Chasmistes cujus*) and the Lahontan Cutthroat Trout (*Oncorhynchus clarkii henshawi*), are found and the Anaho Island National Wildlife Refuge provides breeding habitat for pelicans. Pyramid Lake is the terminal point of the Truckee River. The lake and its water elevation reflect the balance among the availability of water supplies, the high rate of evaporative losses experienced in the basin, and diversions to meet human demand.

While the greater portion of the Truckee and Carson River Basins and most of the corresponding demands for water resources lie in Nevada, most of the precipitation and virtually all of the water storage from the Truckee and Carson River Basins lies in California.

The analysis of water supply risks related to drought events was performed by identifying notable historical drought events, as well as drought events in the paleo-reconstructed period, and comparing the managed system, under current operations and demands, with an observed historical baseline period. Two drought periods from the observed historical period were selected for analysis—the first lasting 14 years from 1923 to 1936 (Historical Drought 1), and the second lasting 5 years from 2012 to 2016 (Historical Drought 2). Analysis of managed streamflow and reservoir storage for these drought periods were compared with results for an overall historical baseline simulation period, in this case 1901 to 2017. Additionally, results were compared with those from paleohydrology scenarios, which are described in the next section.

6.8.1 Paleohydrology Scenario Development

Paleohydrology scenarios for the Truckee and Carson Rivers were developed using the annual streamflow reconstruction for the Carson River near Fort Churchill, NV (USGS ID 10312000). Additional information including references for these reconstructions can be found in Chapter 2. These developed scenarios encompass the three most highly ranked drought events with the largest cumulative deficit. According to this definition, the largest drought occurred over an 11-year period from 1841 to 1851. The second largest drought occurred over an 8-year period from 1776 to 1783. The third largest drought occurred over a 10-year period from 1856 to 1865.

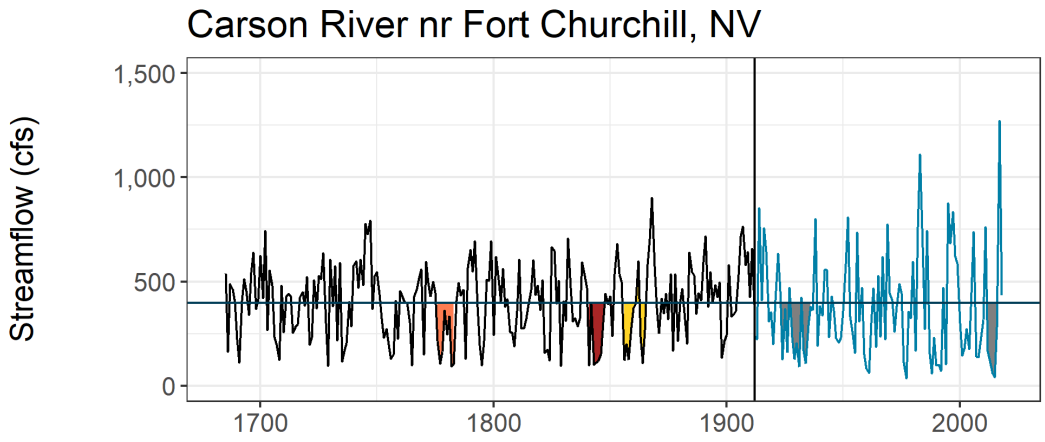

Figure 148. Annual streamflow for the Carson River near Fort Churchill, NV showing droughts in the paleo-reconstructed and observed historical periods.

Note: Paleo-reconstructed streamflow is in black and historical streamflow is in blue. The horizontal line shows long-term median streamflow. Drought events are shaded (red, orange, and yellow for Paleo Droughts 1, 2, and 3, respectively, and gray for historical droughts).

cfs = cubic feet per second

Figure 148 shows the annual streamflow reconstruction for the Carson River near Fort Churchill, NV in black, with the historical naturalized (i.e., unimpaired) streamflow over the observed historical period shown in blue. Drought events of interest are shaded and include the three "largest cumulative deficit" droughts from the paleo-reconstruction period, and the 1920s drought and the 2010s drought from the observed historical period. Qualitatively, Historical Drought 1 (1923 to 1936 shaded in grey) was longer than any of the three largest droughts in the paleo-reconstructed period (as defined by the largest cumulative deficit). Additionally, only during Paleo Drought 3 (shaded in yellow) was there a substantial wet year during the drought event. Paleohydrology scenarios encompassing the five identified drought events were used to investigate impacts to reservoir storage in Lake Tahoe, Lahontan Reservoir, and Stampede Reservoir, as well as impacts to several other metrics that are important water supply indicators.

6.8.2 River Systems Model Overview

The Truckee River Operating Agreement, signed in 2008 (Reclamation, 2008) and implemented in December 2015, is an agreement developed by Federal, State, Tribal, and local agencies and organizations, and required by Public Law 101-618, for operation of the Truckee and Carson River Basins. The Truckee River Operating Agreement creates flexibility in water use and storage while ensuring that existing water rights are served, and flood control and dam safety requirements are met. Principally, the Truckee River Operating Agreement provides for more effective coordination of reservoir operations on the Truckee River. As such, the agreement allows for more stable water supply for Reno, Sparks, and Washoe County, Nevada; enhances streamflow in the Truckee River below Derby Dam for threatened and endangered fish species; and improves water quality.

Truckee River Operating Agreement operations is a complex blend of legal requirements and stakeholder input to determine Truckee River operational needs. To aid in the process, the Truckee River Operating Agreement Operations Model (TROA Operations Model) was collaboratively built in RiverWare to guide daily operations. The model contains the Truckee River Operating Agreement governing regulations and allows stakeholders to provide input into how they would like to manage their water. The operations model is managed by the Truckee River Operating Agreement administrator and is regularly updated to meet operational needs. Along with the operations model, Reclamation's Lahontan Basin Area Office manages a collaboratively developed TROA Planning Model. The TROA Planning Model is logic-driven and simulates Truckee River and Carson River operations over the last 117-year period (1901 to 2017). The planning model is regularly used by stakeholders to complete long-term studies (e.g., Safety of Dams studies, water supply studies, and drought contingency planning).

With assistance from the Lahontan Basin Area Office, Technical Service Center staff developed scenario inputs, implemented the model, and performed analysis of model results for this report. Initial conditions in the model were identical for each scenario simulation and were set at water year 2018 levels, as recommended by the Lahontan Basin Area Office. Similarly, demands were set at 2018 levels and remained the same for each year throughout the runs.

6.8.3 Water Resource Metrics

In the Truckee and Carson River Basins, storage at reservoirs such as Lake Tahoe, Lahontan, and Stampede provide insights into water supply reliability. Several metrics related to reservoir storage were selected to evaluate how these reservoirs are impacted by drought events compared with an average historical baseline condition from 1901 to 2017. The storage metrics evaluated for the Truckee and Carson River Basins are similar to storage metrics evaluated in other basins to inform a West-wide analysis of droughts and reservoir storage. One storage metric is the percent of years during a drought that storage reaches an identified upper storage target. For Lahontan, that is the current end-of-month storage objective (LSOCM) for June. For Tahoe, that is the legal filling limit.

Another storage metric is the percent of days over the drought duration that storage falls below the minimum storage. In the case of Tahoe, this is the rim of the natural lake. Yet another storage metric is the average percent of capacity at the end of the water year (September 30). In the case of Tahoe, a more meaningful target is the percent of capacity on April 1, when allocations are set. These averages are computed over the drought duration. Table 35 summarizes the metrics evaluated in the Truckee and Carson River Basins.

Table 35. Metrics for quantifying water supply reliability in the Truckee and Carson River Basins

Storage Metrics
Percent of years during drought event that Lahontan Reservoir reaches the end-of-June storage objective (LSOCM)
Pool Elevation Metrics
Average percent of years during drought event that Lake Tahoe reaches the legal filling limit (6,229.2 feet)
Average percent of days during drought event that Lake Tahoe falls below the rim of the lake (6,223 feet)
Flow Metrics
Average percent of days during flood event that the Truckee River at Reno streamflow is above 5,500 cfs daily average (recognizing 6,000 cfs instantaneous maximum)
Other Metrics
Average percent of days Floriston Rates are met (400 cfs November through March; 500 cfs April through October)
Average percent of days over the drought duration that Carson Division of the Newlands Project demand is met

Metrics listed in Table 35 in the "Other" category include additional metrics that are specific to the Truckee and Carson River Basins. One such metric is the average number of days during a drought that the Floriston Rates are met. This is a top operational priority in the basin. This rate is a designated flow rate required to flow past Floriston, California, on a daily basis. The target rate is typically 400 cfs from November through March and 500 cfs from April through October. The Floriston Rate can be reduced based upon the designated drought status of the basin determined on April 1 or April 15 using the Lake Tahoe elevation and predicted inflow. Another important metric is the average number of days during a drought that the Carson Division of the Newlands Project has a shortage (i.e., does not receive its full allocation).

6.8.4 Summary

Drought events from the observed historical period and the paleo-reconstruction period were selected to examine whether paleo droughts were more impactful than those from the observed period and from average historical conditions. If droughts were more severe in the paleo-reconstructed period than the observed historical period, water managers may choose to make more conservative decisions with the additional understanding that water supplies may take longer to be replenished than previously thought.

Figure 149 illustrates modeled daily storage over select time periods that encompass selected drought events. The shaded regions in the figure illustrate the difference between actual storage and the top of conservation pool. However, for Lahontan Reservoir, the more important metric is whether LSOCM end-of-month targets are met, particularly at the end of June when storage is typically at its highest to provide the season's irrigation water supply. Periods during which the dark blue dashed line are above the solid black line are indicative of not meeting the monthly storage target.

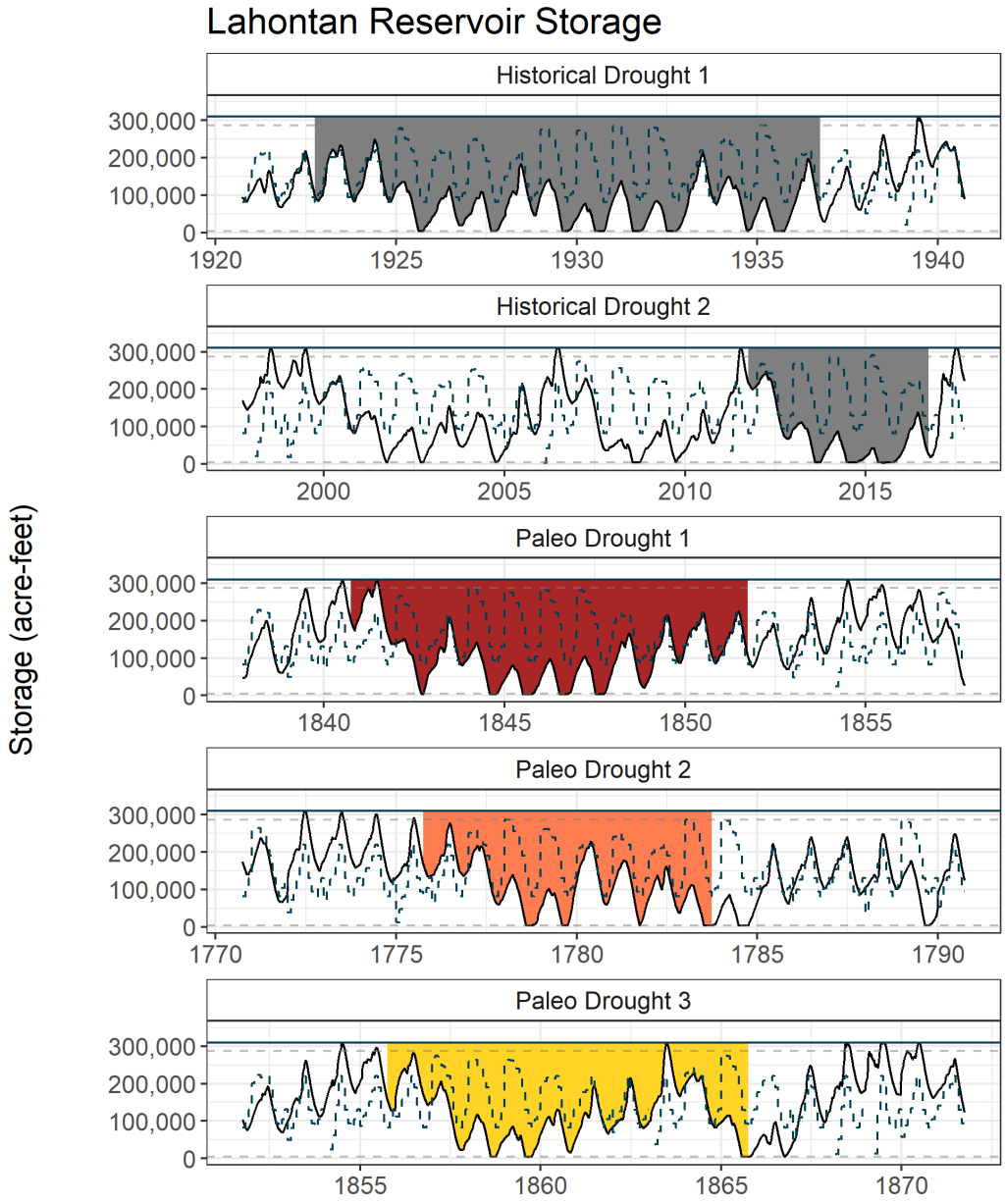

Figure 149. Daily modeled storage for Lahontan Reservoir for each drought event (panels).

Note: The horizontal lines show the top of active storage (dashed, upper at 286,978 acre-feet) and bottom of conservation pool (dashed, bottom at 4,000 acre-feet) storages. The dark blue dashed line indicates the end-of-month storage target, LSOCM. Drought events are shaded.

Figure 150 summarizes what is difficult to visualize in Figure 149. For the observed historical baseline period, storage in Lahontan Reservoir met the end-of-June storage target (LSOCM) in 40 percent of years over the 1901 to 2017 period. Over Historical Drought 1 (1923 to 1936), the reservoir met this target only 1 year of the 14-year drought (or 7 percent). Over Historical Drought 2 (2012 to 2016), the reservoir never met the end-of-June target. Over the three largest paleo droughts, the reservoir met this end-of-June target 27 percent, 13 percent, and 20 percent of years, respectively, for Paleo Drought 1 (3 out of 11 years), Paleo Drought 2 (1 out of 8 years), and Paleo Drought 3 (2 out of 10 years).

Over the instrumental historical baseline period, Lahontan Reservoir end-of-water-year storage (on September 30) was about 34 percent of active capacity on average. For the drought periods, the average percentage of capacity was lower, around 12 percent and 8 percent for Historical Drought 1 and Historical Drought 2, and 20 percent, 16 percent, and 25 percent, respectively, for Paleo Droughts 1 through 3. Lahontan Reservoir has the capacity to hold approximately 1 year of inflow volume.

Collectively, these results indicate the droughts identified over the observed historical period, using the drought definition described in Chapter 2, were as severe as or more severe than the largest paleo droughts in terms of their impact on Lahontan Reservoir storage.

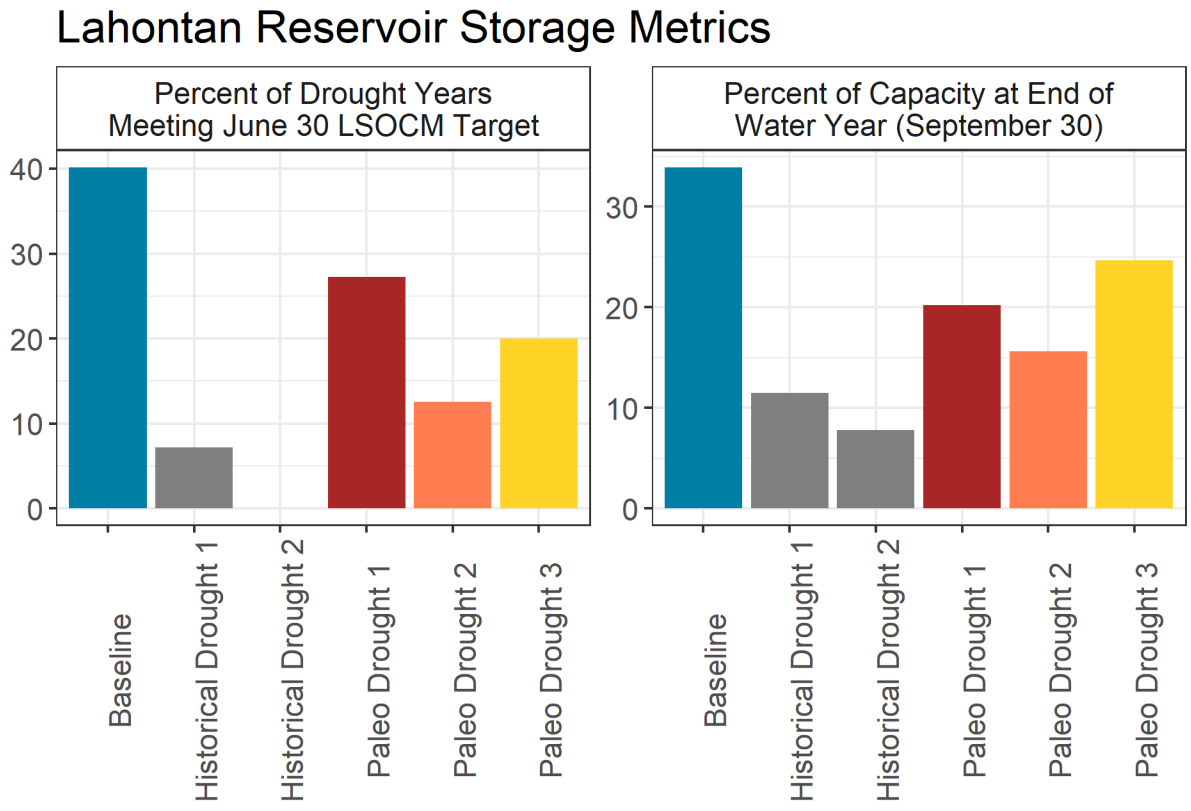

Figure 150. Lahontan Reservoir storage and downstream streamflow metrics showing mean baseline conditions (blue), historical droughts (gray), and paleo droughts (red, orange, and yellow).

Important metrics for evaluating water supply risk with respect to Lake Tahoe include lake storage between the original natural lake level and the legal filling limit of the overlying reservoir. In addition, allocations from Lake Tahoe are set on April 1, so storage at that time is also an important metric for seasonal water supply. Figure 151 illustrates daily Lake Tahoe storage over the same drought events (in the observed historical period and paleo-reconstructed period) reported on for Lahontan Reservoir. Over Historical Drought 1 (1923 to 1936), Lake Tahoe pool elevation generally decreased over the drought duration and even dipped below the rim of the natural lake. Storage cannot be released below the rim of the natural lake (6,223 feet); therefore, the reduction in pool elevation below this level is likely due to lake evaporation over the course of the drought event. The lake was not reduced to elevation much below the rim of the natural lake during Historical Drought 2; however, the drought duration was also much shorter (5 years as opposed to 14 years). Over Paleo Droughts 1, 2, and 3, the lake also dipped below the natural rim, likely due to lake evaporation. After Paleo Drought 2, it took about 7 years for the lake to return to elevations in the operable range (6,223 to 6,229.2 feet).

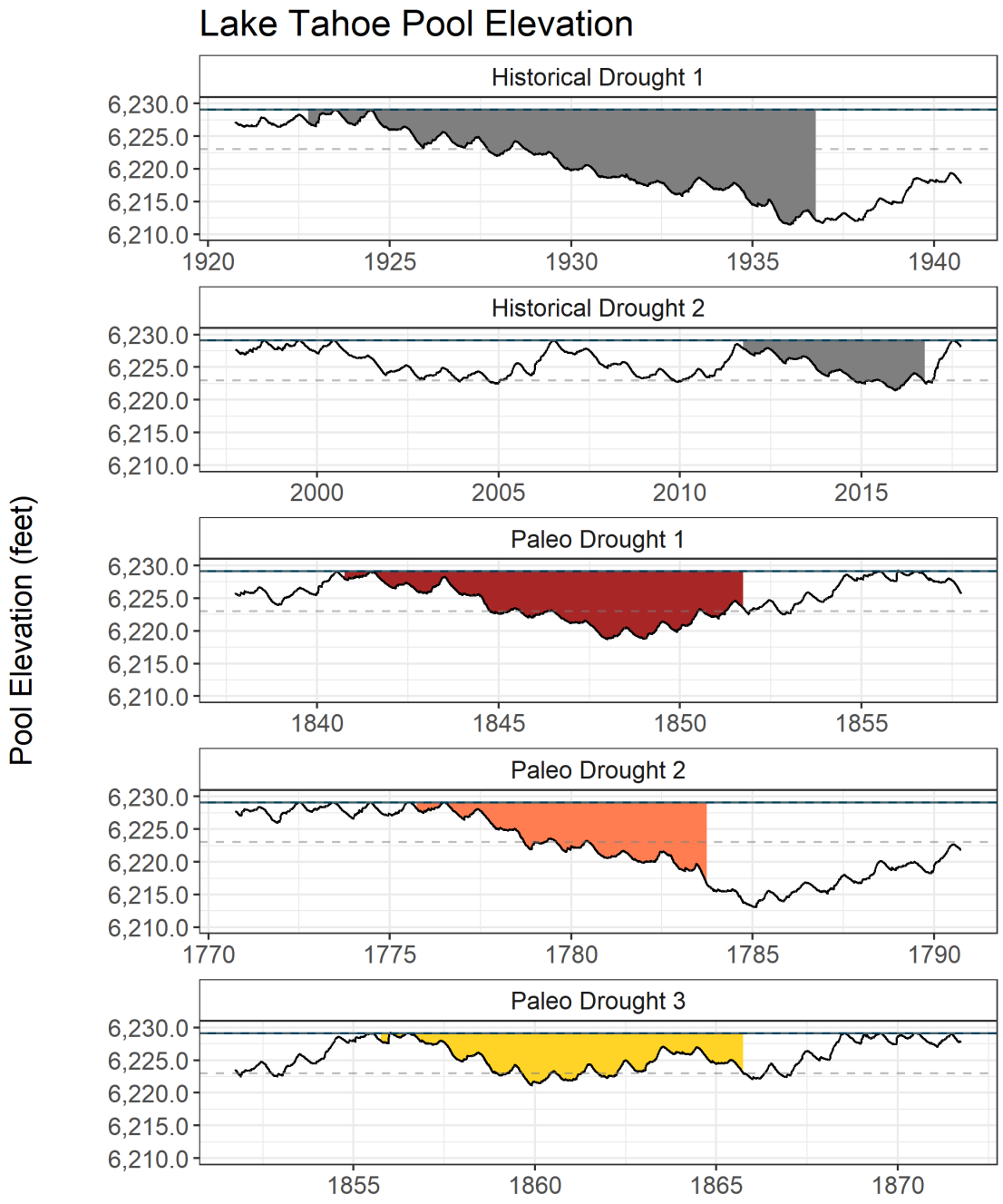

Figure 151. Daily modeled pool elevation for Lake Tahoe for each drought event (panels).

Note: The horizontal lines show the legal filling limit (upper) and natural lake rim (bottom) storages. Drought events are shaded.

Figure 152 summarizes metrics illustrative of the progression of Lake Tahoe pool elevation shown in Figure 150. Over the instrumental historical baseline period, Lake Tahoe filled to its legal limit 36 percent of years between 1901 and 2017. Over the course of the 14-year Historical Drought 1, it refilled in one of those years. Over the course of the 5-year Historical Drought 2, it did not refill to the legal limit. Over Paleo Droughts 1, 2, and 3, it refilled once over each drought and, in each case, this was in the first year after the start of the drought.

The upper right panel of Figure 152 illustrates the percent of days, on average, the lake dipped below the natural elevation of the lake (i.e., the rim). Over the 117-year observed historical period, this occurred about 9 percent of days. Over the 14-year Historical Drought 1, this occurred about 61 percent of days and over the 5-year Historical Drought 2, this occurred about 16 percent of days. Over the paleo-reconstruction period droughts (1, 2, and 3), this occurred 53 percent, 57 percent, and 23 percent of days, respectively, over the course of these drought events. This result highlights the likelihood of lake evaporation being a larger factor in the loss of water supply in the future.

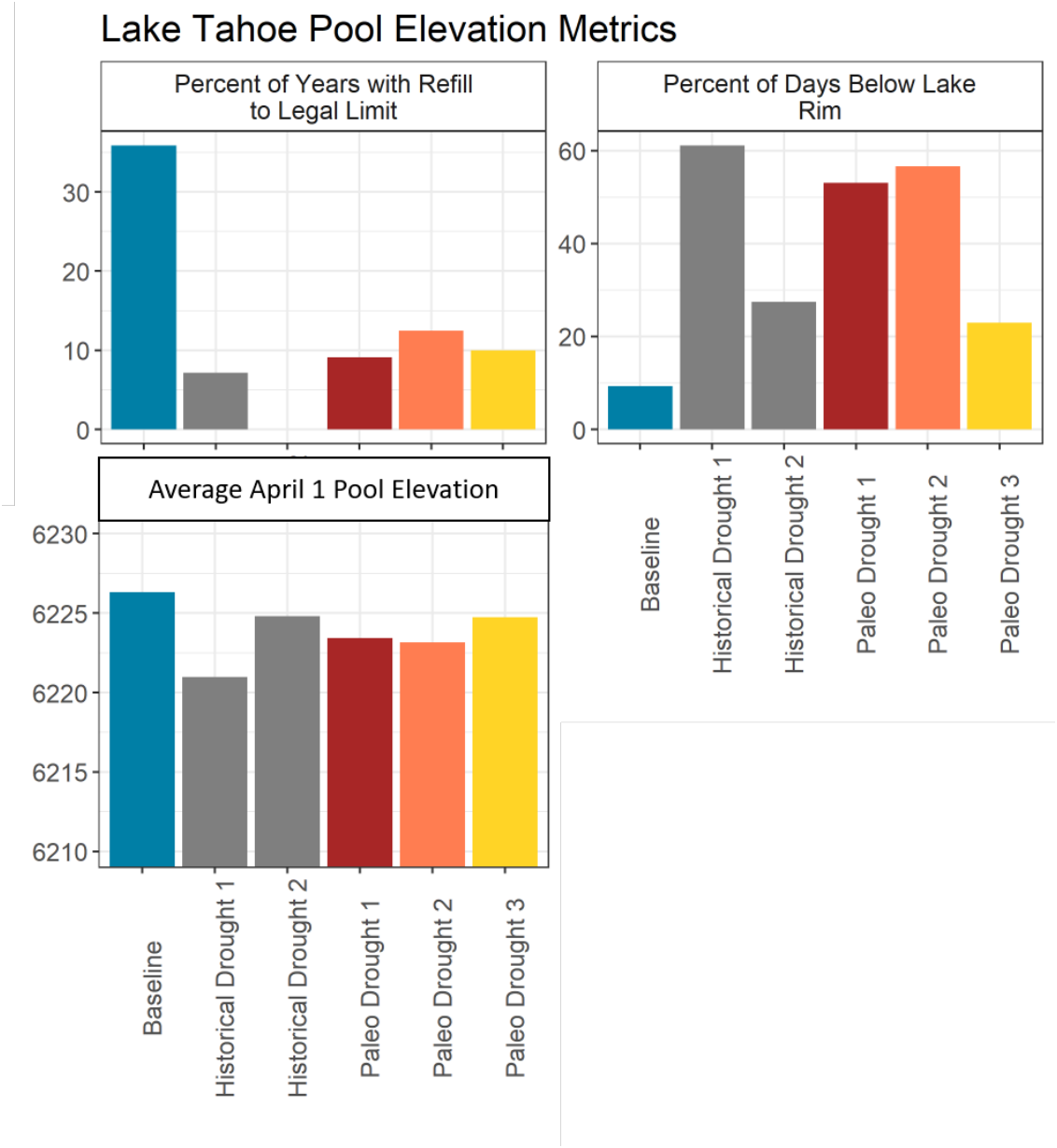

Figure 152. Lake Tahoe pool elevation metrics showing mean baseline conditions (blue), historical droughts (gray), and paleo droughts (red, orange, and yellow).

April 1 pool elevation is an important metric for seasonal water supply. On average, the April 1 pool elevation of the lake was 6,226 feet as simulated by the Truckee River Operating Agreement model from 1901 to 2017 water years. Over the course of Historical Droughts 1 and 2, the average April 1 pool elevation is 6,221 feet and 6,225 feet, respectively, over the course of these droughts (14 years and 5 years in duration). Over the course of Paleo Drought 1 and Paleo Drought 2, the average April 1 pool elevation is similarly about 6,223 feet. For Paleo Drought 3, the average April 1 pool elevation is 6,225 feet.

Additional metrics considered for the Truckee and Carson River Basins include the percent of days Floriston Rates are met and the average frequency of Carson Division water demand of the Newlands Project (CDD) being fully met (computed as a percent of days during the drought). Over the instrumental historical baseline period, Floriston Rates are met 83 percent of days and the average percent of days that CDD is met is about 93 percent.

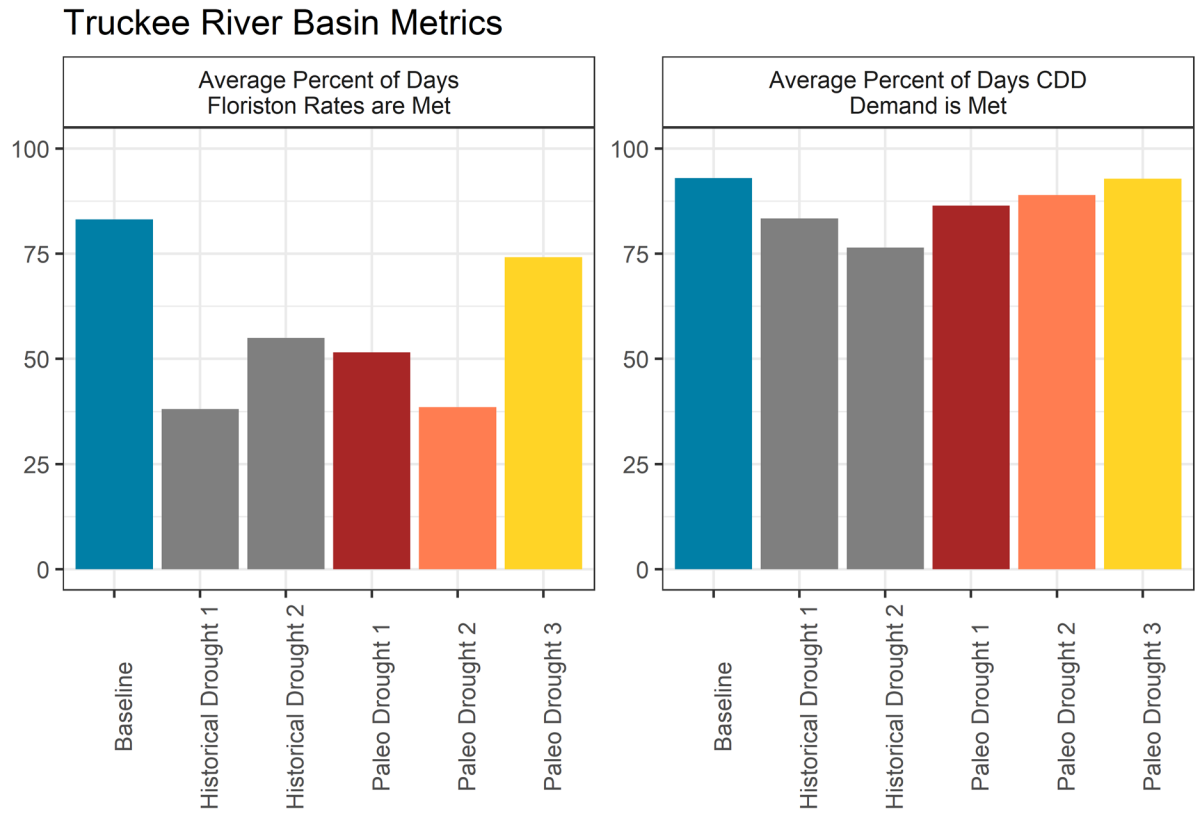

Figure 153. Relevant metrics for the Truckee and Carson River Basins showing mean baseline conditions (blue), historical droughts (gray), and paleo droughts (red, orange, and yellow).

By contrast, the average percent of days the Floriston Rates are met is much lower over the 14-year Historical Drought 1 (about 38 percent), while over Paleo Drought 3, the percent of days is about 74 percent. The percent of days CDD demand is met is not substantially reduced under any of the drought scenarios; however, Historical Drought 2 seemed to impact the frequency of meeting CDD demand the most.

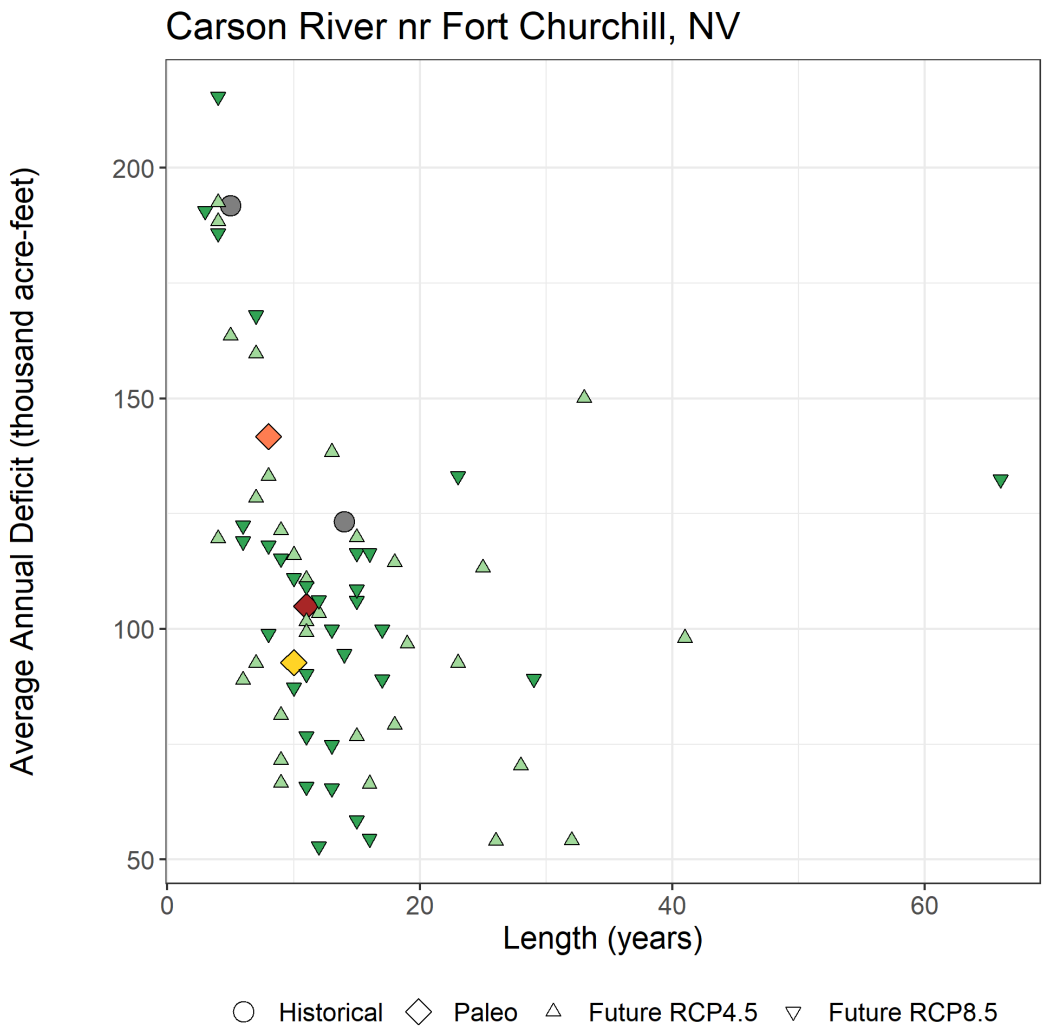

Figure 154. Drought length and average annual drought deficit for drought events at the Carson River near Fort Churchill, NV.

Note: Circles represent historical droughts, diamonds represent paleo droughts, and triangles represent the largest drought from each projection in the LOCA dataset for RCP4.5 and RCP8.5.

To explore how more recent historical and paleo drought events may be different from projected drought events via LOCA downscaled CMIP5 RCP4.5 and RCP8.5 hydrologic traces from 2006 to 2099, average annual deficit by volume (acre-feet) and duration (length in years) are plotted for the drought events discussed in this section (drought events in the observed historical period and the paleo-reconstructed period), as well as for the largest cumulative deficit events for each projected hydrology trace. Figure 154 illustrates these events relative to each other.

The grey circles represent notable droughts in the instrumental record identified by Reclamation's regional partners. The colored diamonds represent the three largest paleo drought events. The green triangles represent the drought events for each future hydrologic projection. These droughts are based on natural streamflow at Carson River near Fort Churchill and do not reflect water management effects. The figure illustrates that the historical drought events are among the longest and most severe events when compared with the events from the paleo-

reconstruction period (as represented by average annual deficit). However, the future drought events that were identified as having the largest cumulative deficit could be longer, but probably not more severe, than historical drought events.

6.8.4.1 Analysis of Flood Events – Case Study for the Truckee and Carson River Basins

In the Truckee and Carson River Basins, flooding is an important consideration, particularly due to the combined effects of atmospheric river precipitation events as well as snowpack storage. A maximum streamflow target of 5,500 cfs daily average exists for the Truckee River at Reno, Nevada (USGS ID 10348000). Historical flood events occurred in 1928, 1983, 1997, and 2017. Figure 155 shows daily modeled streamflow for the Truckee River at Reno, NV for these four historical flood events, as well as for 3 years in the paleo record that also experienced flood events.

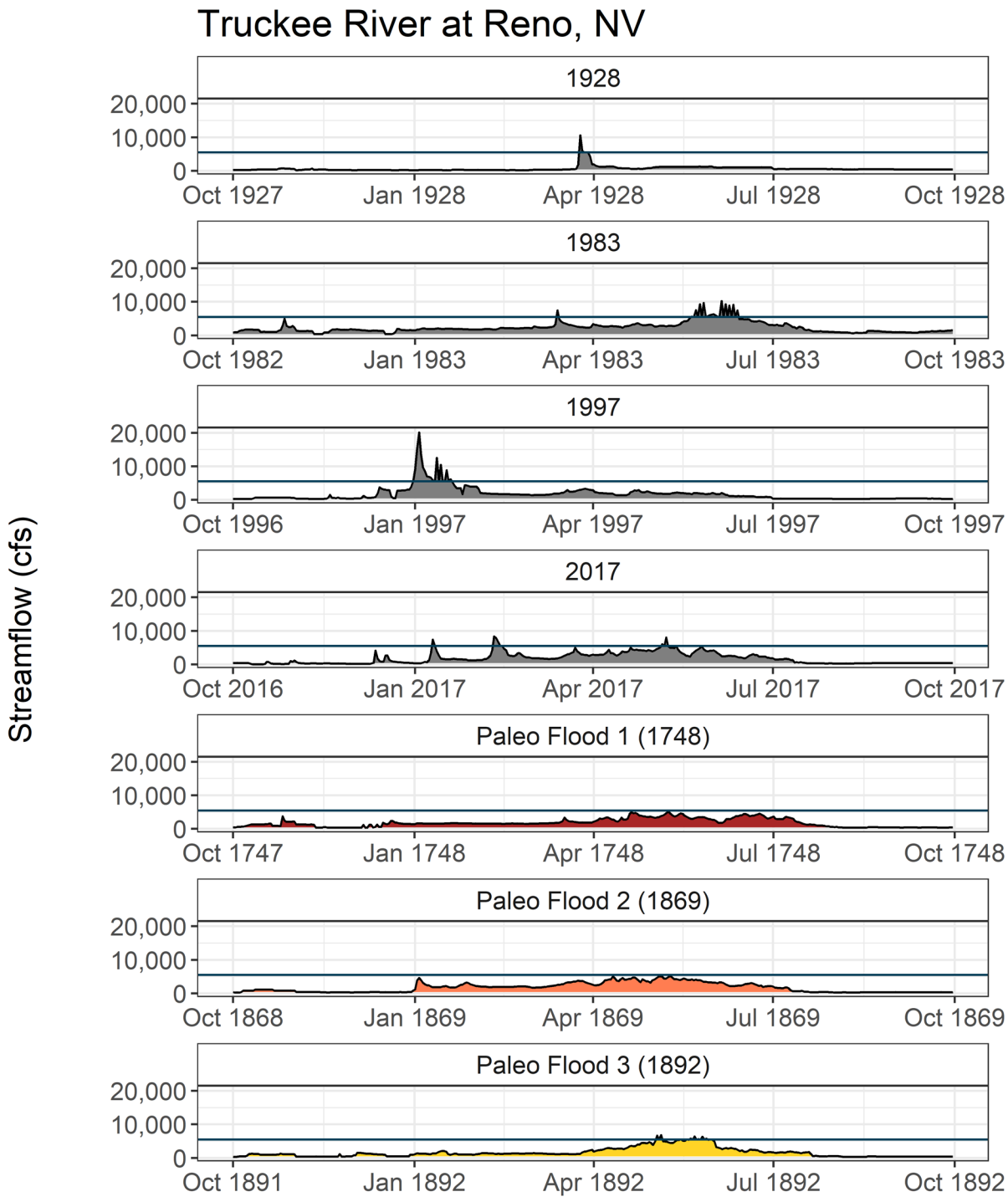

Figure 155. Modeled daily streamflow for the Truckee River at Reno, NV for identified flood events.

Note: Streamflow during four historical years that experienced flood events (top 4 panels) are shown in gray. Three paleo years with flood events (bottom three panels) are shown in red, orange, and yellow.

The observed historical baseline simulation period resulted in few days with streamflow in the Truckee River at Reno above the maximum flood threshold. Notable flood events are illustrated in the figure as well to highlight specific flood years. However, the percent of flood days over the course of the 117-year observed historical period is very low.

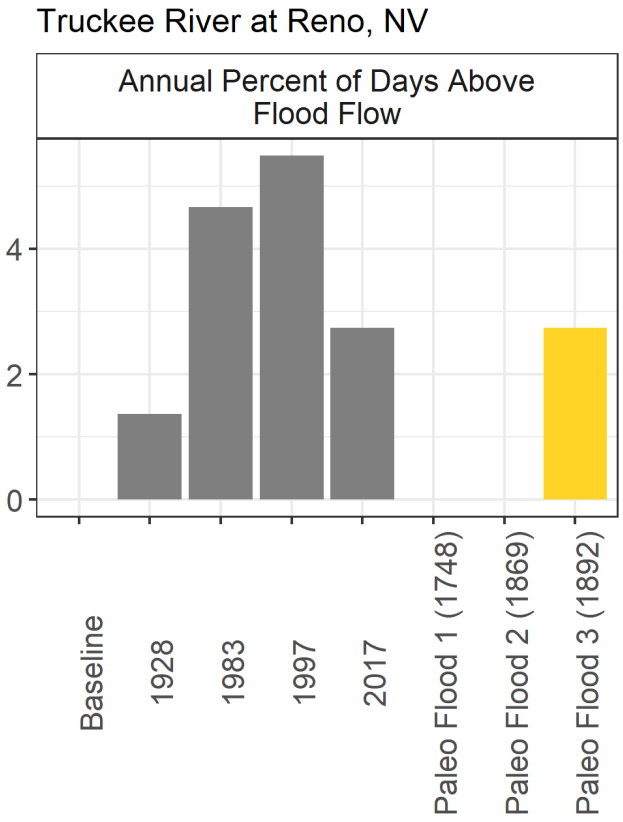

Figure 156. Average exceedance above Flood Action Flows at Boise River at Truckee River at Reno, NV for identified flood events.

Note: Average exceedance computed for the baseline period is shown in blue (if values are greater than zero). Those computed for four historical years are shown in gray and the three paleo years are shown red, orange, and yellow (if values are greater than zero).

6.9 Key Findings

This report has provided a comprehensive evaluation of the implication of drought events on the management of water across Reclamation's operational domain. This work has allowed for collaboration with the country's experts in dendrochronology and paleohydrology. In addition, it has facilitated the compilation of a vast database of paleo-reconstructed streamflow data. Use of paleohydrology information to inform water management is not new, but this Water Supply Reliability Assessment has provided the opportunity to perform a consistent set of modeling experiments across the eight major Reclamation river basins and explore the impacts of observed

historical droughts and droughts of the distant past on river systems. This work has allowed exploration of the question: *How might a river basin respond if the same droughts were to occur today under current operating policies and water demands?*

6.9.1 Hydrologic Variability Across the West

The use of paleohydrology scenarios allows for an examination of conditions within each river basin in the more distant past as compared to the observed historical period. This analysis can put more recent basin conditions in a broader historical context and identify whether these more recent conditions were particularly dry or wet, and whether the basin experienced more or less hydrologic variability than the more distant past.

In both the Boise River basin and the Klamath River Basin, the observed historical period appears wetter overall than the paleo-reconstructed period and appears to have more variability. The Colorado River Basin experienced more variability, though wetter conditions, in the paleo-reconstructed period. Previous studies investigating the Colorado River Basin using reconstructions extending further back in time do show drier periods in the more distant past. The period known as the Medieval Climate Anomaly (~800 to 1400 across the West) was defined by both more severe and sustained droughts and pluvial events than what is known as the Little Ice Age period (1500 to 1850). Our analysis timeframe falls within the Little Ice Age, so we are not testing the most severe recorded paleo droughts in any of these records. That said, we are relating recent historical droughts to the period over which the paleohydrology data (streamflow and PDSI) are highest quality. In the Rio Grande Basin, streamflow variability in the paleo-reconstructed period is similar to the observed historical period, with slightly more persistent periods of low streamflow than is seen in the more recent past. The Sacramento and San Joaquin River Basins show slightly more streamflow variability in the observed historical period compared with the paleo-reconstructed period and more persistent periods of low streamflow more recently. Though there are some regional differences, the multiple reconstruction locations examined in this basin indicate similar behavior. The Truckee River Basin shows slightly higher variability in observed historical period, comparable to the Sacramento and San Joaquin River Basins.

6.9.2 Drought Events

Through this analysis, notable drought events in the observed historical period were identified by water managers for each basin. Droughts in the more distant past were identified using the paleo-reconstructed streamflow data for each basin. In the observed historical period, some droughts have broader regional impacts that extend across river basins. This includes the 1930s drought, which was substantial in every basin modeled, with slightly varying years, except for the Rio Grande Basin. In the late 1980s to early 1990s, the northern and coastal regions of the Western United States also experienced drought, including the Upper Missouri River Basin, the Boise River basin, the Klamath River Basin, and the Sacramento and San Joaquin River Basins. Similarly, in the late 2000s, the Southwestern United States, including the Colorado River Basin, Rio Grande Basin, and Truckee River Basin, also experienced drought.

The severity of droughts in the paleo-reconstructed period as compared to the observed historical period varied from basin to basin. In the Boise River basin, paleo droughts were both longer and more severe than historical droughts. This was the only basin where this behavior was seen. In the Upper Missouri River Basin, Rio Grande Basin, and Truckee and Carson River Basins, paleo droughts were comparable to historical droughts in their length and severity. The Klamath River Basin was mixed, where the 1930s historical drought was the most impactful, but the three paleo droughts then exceeded the remaining historical droughts in both length and severity. In both the Colorado River Basin and Sacramento and San Joaquin River Basins, historical droughts were both longer and more severe than the paleo droughts. As has been mentioned, in the Colorado River Basin and across the West, there are longer and more severe droughts that occur outside the 1685 to 1977 West-wide common reconstruction period.

Examining the droughts in the paleo-reconstructed period, similar regional patterns exist as those discussed in the observed historical period. Across the greater Pacific Northwest region, including the Boise River basin, Klamath River Basin, and Upper Missouri River Basin, the 1730s appear to be a substantial drought period. Similarly, the 1840s and 1850s saw droughts across the Sacramento and San Joaquin, Truckee, Colorado, Klamath, and Upper Missouri River Basins.

It is interesting to note that while there are drought periods that have impacted a majority of the Western United States in both the paleo period and the historical period, the impact to local basin conditions has varied, as has the severity of paleo droughts relative to historical droughts.

6.9.3 Water Management Impacts of Drought Events

The relative effect of drought on water management in each of the basins for droughts in the paleo-reconstructed period relative to the observed historical period generally reflect the severity of the drought as viewed from its impact to streamflow. Compared to historical droughts, the Boise River basin was more impacted by paleo droughts, with these droughts showing a greater impact to streamflow in the Boise River than during any of the historical droughts. This is also seen when looking at reservoirs along the Boise River. Anderson Ranch Reservoir has difficulty refilling during two of the three paleo droughts examined, with reservoir storage remaining at critically low levels for multiple years in a row. These droughts have a similar impact on storage in Lucky Peak Reservoir, with storage remaining low for multiple years in a row, and even falling close to empty for several years on one of the events. For these two reservoirs there are no historical droughts that impact reservoir storage to the same extent.

For Lake Powell, pool elevation thresholds at 3,575 feet (below which Lake Powell enters into the Mid-Elevation Release Tier) and elevation 3,490 feet (below which Lake Powell enters into the Lower Elevation Balancing Tier) are important for management under the 2007 Interim Guidelines which manage the Colorado River system during drought. During Historical Drought 2, Lake Powell elevation fell below the lower minimum threshold early in the drought, recovered and remained close to the upper minimum threshold, and then fell below the lower minimum threshold again at the end of the drought. The paleo droughts considered showed Lake Powell falling below the lower minimum threshold for a longer period of time than the

historical droughts, but then refilling faster than this drought. According to the simulations, the three paleo droughts are impactful, but relatively short-lived relative to the historical droughts. It is important to note that in the Colorado River system, as well as others across the West, droughts prior to 1685 (which is the beginning of the paleo-reconstructed period used in this report) did rank as some of the most severe droughts, if not the most severe, ever recorded.

For Lake Mead, 1,025-foot pool elevation is important because below this elevation Lake Mead is in a shortage condition where deliveries to Lower Division States are reduced to 7.0 million acre-feet. The 1,000-foot elevation is important for management because, below this elevation, drinking water supply can no longer be conveyed to Las Vegas, Nevada. Historical Drought 2 shows Lake Mead elevation remaining between these low elevation thresholds, while pool elevation generally fared better in paleo drought event years. The 12-year paleo drought from 1772 to 1783 shows greater impacts, with lake elevation dropping below the 1,000-foot threshold for several years before recovering following the end of the drought. Interestingly for Lake Mead and Lake Powell, while the pool elevation thresholds show greater impacts to the Colorado River Basin during the paleo droughts, average reservoir releases show greater impacts during observed historical droughts.

In the Klamath River Basin, the extended drought in the first half of the 1900s remains the most impactful drought when looking at historical and paleo droughts considered in this report. It is only during this event, and the top ranked paleo drought, that Upper Klamath Lake fails to refill for multiple years in a row. Upper Klamath Lake levels are highly constrained by the current Biological Opinion. The lake must maintain a minimum elevation for endangered Lost River and shortnose suckers and maintain storage for fall Klamath River flows to support threatened Klamath River coho salmon. These minimum elevations somewhat buffer the impact of droughts on Upper Klamath Lake storage, but impact irrigators substantially, as illustrated by impacts to seasonal Klamath Project supply. It is interesting that the 2000s historical drought event (Historical Drought 3) did not result in greater impact to Klamath Project supply according to the river systems model simulations.

The managed Upper Missouri River Basin is resilient to drought, particularly Canyon Ferry Reservoir, because of unallocated storage that can provide a buffer against water demand. Results show that over the 1950 to 1999 observed historical baseline period, the reservoir refilled to the top of joint-use storage in 47 out of 50 years. There is only a slightly greater impact on Canyon Ferry Reservoir storage under paleo drought events. Other Reclamation Projects in the basin, including the Sun River Project and the East Bench Unit of the Pick-Sloan Missouri Basin Program, are more impacted by drought, particularly the Sun River Project. Water users in these two basins both experience shortages during historical and paleo drought events. The top ranked paleo drought impacts water users in both Projects more than any historical drought, though to a similar degree.

In the Rio Grande Basin, it appears that the largest cumulative deficit drought events in the paleo-reconstruction period similarly impacted water supply metrics, such as the average percent of days Article VII restrictions of the Rio Grande Project are in place and the average percent of days the Middle Rio Grande Conservation District receives its full demand, as the observed

historical drought events. However, Historical Drought 2 (2011 to 2015) appears to have the largest impact on average for Article VII restrictions. Also, individual reservoirs, such as Elephant Butte Reservoir, were similarly impacted by the largest paleo drought event and by observed historical droughts in terms of end-of-water-year storage deficits, but the 2011 to 2015 drought appears among the most impactful. It is notable that storage in Elephant Butte Reservoir reached the top of active capacity in the observed historical period only once, in May 1987. Over the entire simulated paleo-reconstructed period, the reservoir never reaches this level. Due to the capacity of the reservoir relative to streamflow in the Rio Grande, drought has less of an impact on the reservoir when storage is already low, but can reduce even moderate storage in the reservoir in the years following the start of a drought. Over the observed historical baseline period, the average percent of years the San Juan-Chama Project contractors received their full allocation is 88 percent. Interestingly, for all of the drought events, more recent historical droughts and paleo drought events, San Juan-Chama Project contractors did not have shortages; however, more exploration is needed to understand how the study experiment might impact this result.

In the Sacramento and San Joaquin River Basins, modeled storage in Shasta Reservoir and Millerton Lake shows that the two historical drought events impact storage to a much greater extent than any of the three paleo droughts, with storage reaching their lowest levels in the 1928 to 1934 drought event. During this drought, Shasta Reservoir storage falls considerably, and it takes several years following the end of the drought before storages recovers. Similar behavior is seen at Millerton Lake, where storage remains considerably below full pool for multiple years. In the paleo droughts, storage at both Shasta Reservoir and Millerton Lake are less impacted and generally able to recover to at least moderate storage levels each year. Looking at the system as a whole, the two historical droughts evaluated have the greatest impact on both Total Delta Outflow and Total Exports. Interestingly, the top ranked paleo drought has a fairly substantial impact on Total Delta Outflow and a less severe, but still substantial, impact on Total Exports. This is in contrast to the much more minimal impact this drought had on storage at Shasta Reservoir and Millerton Lake.

In the Truckee and Carson River Basins, the drought events from the observed historical period were as impactful, or possibly more impactful, to water management than the largest cumulative deficit drought events of the paleo-reconstruction period. During each drought event, Lahontan Reservoir was largely not able to meet monthly LSOCM storage targets. In fact, the reservoir also did not meet the LSOCM storage target the year following the end of each drought. Collectively, these results indicate the identified droughts over the observed historical period were as severe as or more than the largest paleo droughts in terms of their impact on Lahontan Reservoir storage. For Lake Tahoe, the 1923 to 1936 drought saw pool elevation generally decrease over the drought duration and even below the rim of the natural lake. Storage cannot be released below the rim of the natural lake (6,223 feet), so the reduction in pool elevation below this level is likely due to lake evaporation over the course of the drought event. This result highlights the likelihood of lake evaporation being a larger factor in the loss of water supply in the future. Over the observed historical period, Lake Tahoe filled to its legal limit 36 percent of years between 1901 and 2017. Over the course of the 14-year Historical Drought 1, it refilled in

one of those years. Over the course of the 5-year Historical Drought 2, it did not refill to the legal limit. Results from the analysis show that the ability to meet Floriston Rates may be substantially impacted during drought events; however, the Carson Division demands appear less impacted. Interestingly, drought events did not substantially impact CDD demand compared to the overall instrumental historical baseline period, at least in terms of frequency of shortages.

Figure 157 summarizes the average percent of reservoir capacity at the end of the water year (i.e., on September 30) for each of the key reservoirs discussed in this chapter. Results are summarized over the historical baseline simulation period for each river basin, as well as for observed historical drought events and the largest cumulative deficit drought events in each basin. It should be noted that averages were computed across the duration of each identified period and that these differ across basins. Further, these metrics do not necessarily illustrate cumulative impacts due to prolonged drought. Also, the percent of capacity at the end of the water year is dependent not only on hydrology conditions, but also how each reservoir is managed. For example, Elephant Butte Reservoir in the Rio Grande Basin can hold approximately 4.5 times its mean annual inflow, while Lucky Peak Reservoir in the Boise River basin can only hold about 15 percent of its mean annual streamflow.

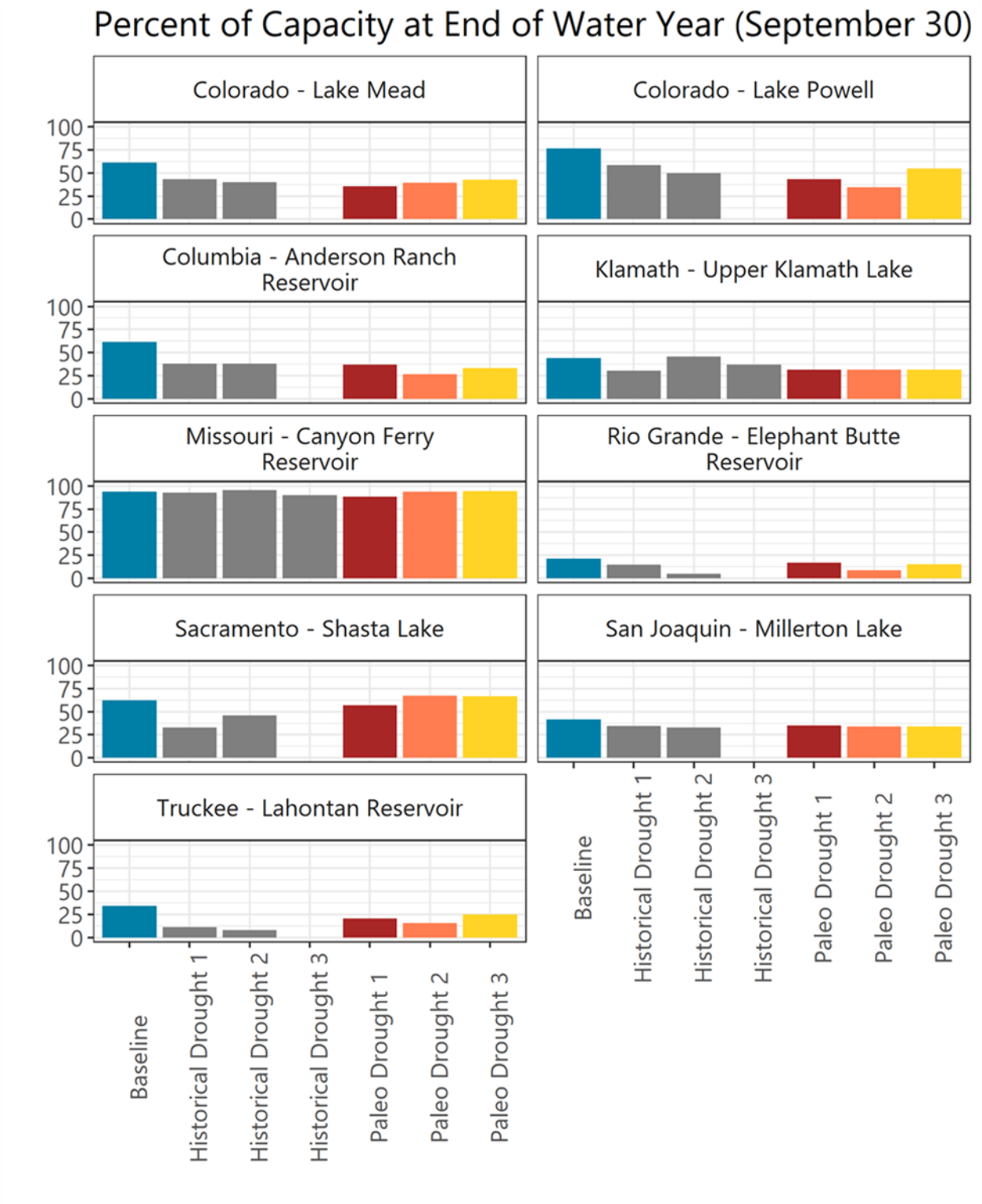

Figure 157. Average percent of capacity at the end of the water year (i.e., September 30) for key reservoirs in each of Reclamation's eight major river basins under baseline historical and identified drought events.

6.9.4 Pluvial Events

Pluvial events were not extensively investigated in this study. In two of the basins, the Boise River basin and the Truckee and Carson River Basins, individual years in the observed historical period where substantial flood events occurred were examined and compared to individual years in the paleo-reconstructed period that experienced high streamflow. Water year 2017 was a significant wet year in both the Truckee and Carson River Basins and the Boise River basin. This event appears in both river basins as a wet spring event, due to high snowmelt runoff. Similarly, 1997 appeared as a substantial pluvial event in both of these river basins. In the Truckee and Carson River Basins, the event caused flooding mostly in January. In the Boise River basin, the event was substantial in January, but it seemed to persist into the spring and was further complicated by cooler and wetter weather that resulted in lower-than-normal irrigation diversions from the river. Precipitation in both snowfall and rain set numerous records in the Truckee River Basin in 2017; Lahontan Dam made flood releases from February 15, 2017, until July 17, 2017. For the Boise River, there is a Flood Action Flow at the Glenwood Bridge, Idaho gage. The four historical years investigated, 1972, 1974, 1997, and 2017, exceeded this streamflow between 5 and 22 percent of days according to model simulations summarized in this report. The 3 event years from the paleo-reconstructed period exceeded this target between 9 and 12 percent of days suggesting that, while impactful, more severe conditions with respect to flooding have been seen in the recent past. For the Truckee River, there is a Flood Action Flow for the Reno, Nevada gage. The four historical years investigated, 1928, 1993, 1997, and 2017, exceeded this target between 1 and 5 percent of days. Only 1 year in the paleo-reconstructed period exceeded this target and saw flows above the Flood Action Flow for 3 percent of days. This suggests that more severe conditions with respect to flooding have been seen in the recent past in the Truckee and Carson River Basins as well.

6.9.5 Projected Future Drought Events

Using hydrology simulations developed from the LOCA downscaled climate projection dataset, the most impactful hydrologic drought, as measured by cumulative deficit (refer to Chapter 2 for definition), was identified for each climate projection. These hydrologic droughts were then compared with droughts from the observed historical period and paleo-reconstructed period. This analysis only examined drought through its impact on streamflow, looking at the length of drought and the average annual deficit in streamflow. These future hydrologic drought projections generally indicate the possibility of droughts of greater severity (as measured by average annual deficit) and greater length as compared to both historical and paleo droughts. There are basin-specific differences, however.

In the Boise River basin, where the paleo droughts were much more severe than the historical droughts, the future drought projections indicate the possibility of more severe, but shorter duration events as compared to the paleo events, or longer, but less severe events. In the Klamath River Basin, hydrologic droughts of greater severity and of longer duration are evident in the future projections, as well as shorter duration events of much greater severity. In the Missouri River Basin, the future hydrologic drought projections generally are comparable to the historical and paleo events, but suggested the possibility of a more moderate, but extremely long duration

event. In the Rio Grande Basin, future hydrologic drought projections suggest droughts of greater severity and longer duration than any of the historical or paleo events. In the Sacramento and San Joaquin River Basins, future hydrologic drought projections were generally of equal severity to historical or paleo events, but of greater length, or of shorter length but greater severity. Finally, in the Truckee and Carson River Basins, the future hydrologic drought projections generally were comparable to historical or paleo events, with the exception of a few projections that indicated the possibility of events of comparable severity, but of much longer duration.

6.10 Summary and Next Steps

The analysis presented in this chapter represents the first standardized and comprehensive use of paleohydrology information across Reclamation's operational domain. It is hoped that the information presented will be directly useful to water managers in each of the basins included. However, it is also acknowledged that this is a preliminary analysis and could be greatly expanded upon in a number of ways. Additional results from the river systems models used in this analysis exist and could be used to examine a broader set of water resource metrics to better understand the impacts of droughts and pluvial events from the paleo-reconstructed period.

A more rigorous assessment of the impacts of different drought and pluvial events using the existing set of metrics could also provide a more complete picture of the impacts of these events. To provide consistency across all basins considered, a standard paleo-reconstructed period of 1685 to 1977 was selected. There exists streamflow reconstruction information for individual basins that extend beyond these dates that could be used to develop additional paleohydrology scenarios. Additional river basins could be considered and paleohydrology scenarios could be developed for other river systems models. Particularly for pluvial events, and specifically considering flood events, a more in-depth review of the methods used to develop the paleohydrology scenarios could be performed. This review could evaluate whether these methods are appropriate to events that occur at much shorter timescales, on the order of days to weeks typically, and if there are improvements that would provide better scenarios to examine these events in the paleo-reconstructed period.

7 Urban Landscape Demands Analysis

Urban landscapes throughout the Western United States are a substantial consumer of water resources; however, limited spatial and temporal information exists on the evapotranspiration (ET) rates and consumptive use of these systems. Typical urban landscapes are comprised of a variety of plants and designs with turfgrass serving as the major surface cover component for most irrigated urban environments. Previous studies have estimated that irrigated turfgrass is the largest irrigated crop in the United States, covering up to 1.9 percent of the land area within the United States (Milesi et al., 2005).

Reclamation developed estimates of historical and future agricultural irrigation and reservoir evaporation water demands through the West-wide Baseline Assessments Program (Reclamation, 2015a), and this chapter contains companion estimates for turfgrass irrigation water demands for major urban areas in the Western United States. Demand estimates were developed as rates (in inches per day; in/day), with the volume of water demand estimated for select urban areas.

7.1 Turfgrass Demand Areas

Sixty-eight urban demand areas were selected using the urban area boundaries defined by the 2010 United States Census and urban area populations from the 2010 United States Census (U.S. Census Bureau, 2010). A population threshold of 200,000 was used to identify major urban areas in the 17 States in the Western United States within Reclamation's authority, and an additional nine cities were selected in the northern Great Plains and northern Rockies as no cities in these regions met the population threshold. Figure 158 illustrates urban areas assessed in this study.

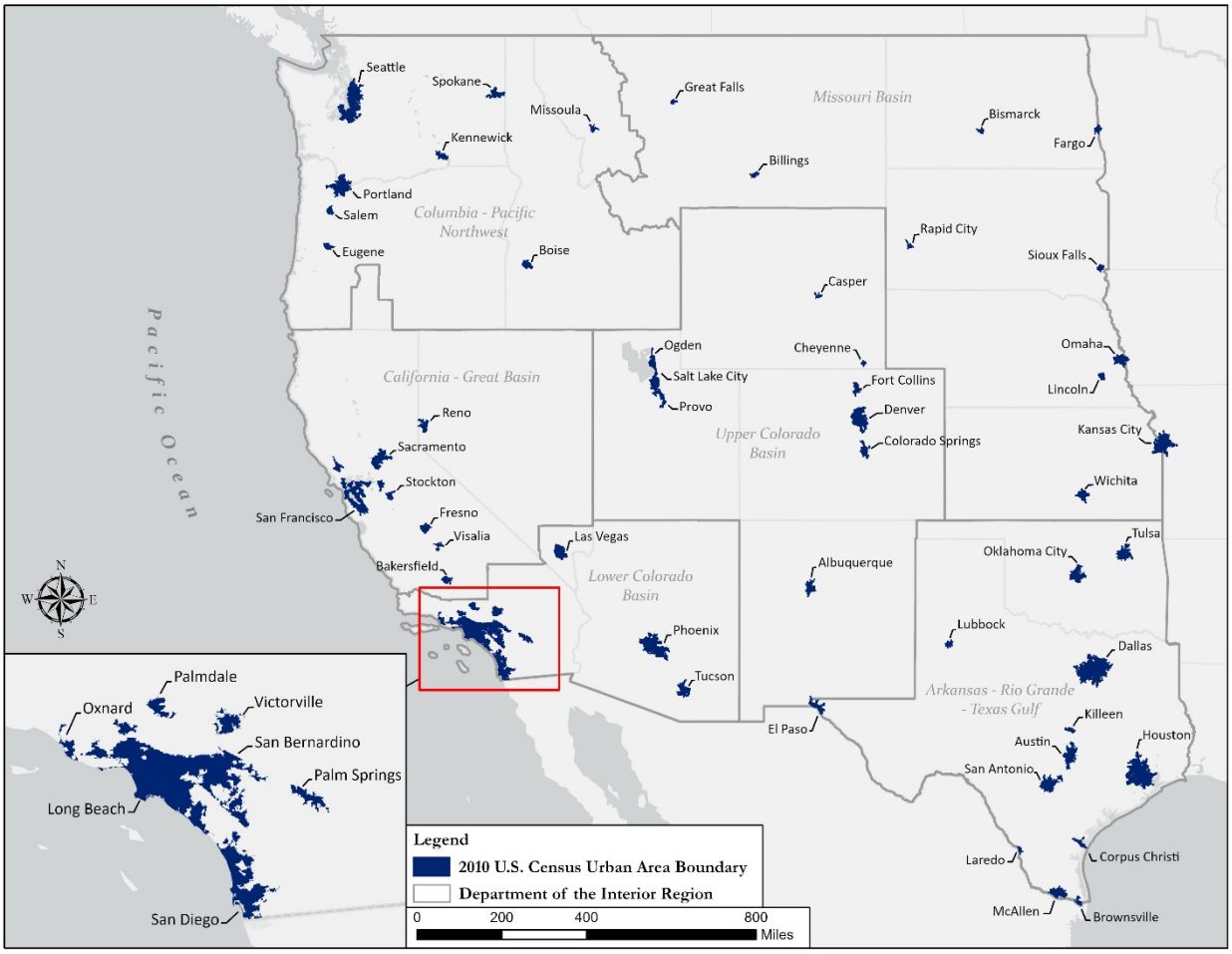

Figure 158. Urban areas analyzed throughout the Western United States.

7.2 Turfgrass Demands Modeling

7.2.1 ET Demands Model

Turfgrass water demands were estimated using an ET and irrigation water requirements model, ET Demands (Allen et al., 1998; Allen et al., 2005; Allen and Robison, 2009; Huntington and Allen, 2010; Reclamation, 2015a). The ET Demands model estimates crop evapotranspiration (ETc) and net irrigation water requirements (NIWR), and is based on the common reference ET and crop coefficient approach, where the reference ET (ETo) is multiplied by time-varying crop coefficients to estimate the actual ET of a vegetated area (Allen et al., 1998). ETo refers to the ET from a cool season clipped grass reference crop that is actively growing, not limited by soil moisture, and is continuously maintained at full cover and peak height. The professional and scientific communities generally recognize the FAO-56 (Allen et al., 1998) and American Society of Civil Engineers' Environmental and Water Resources Institute Standardized Penman-Monteith method (ASCE-PM; ASCE-EWRI, 2005) as the most appropriate and recommended ETo method for estimating crop ET since it is physically based, and is a function of solar

radiation, temperature, humidity, and wind speed. Prevailing meteorological and radiative conditions are incorporated into the ETo, whereas crop coefficients account for variations from the reference condition due to factors such as crop type, phenological development, harvests, and stress.

In this study, the standardized ASCE-PM method was applied with the dual crop coefficient approach for estimating turfgrass ETc and NIWR, where the crop coefficient is separated into a transpiration or basal crop coefficient (Kcb) and an evaporation coefficient (Ke). The dual crop coefficient is preferred over the single crop coefficient approach since it allows for separate accounting of transpiration and evaporation to better quantify evaporation from precipitation and simulated irrigation events, and in turn allows for accounting of soil moisture gains and losses both during the growing and non-growing seasons. Accounting for non-growing season soil moisture gains and losses is important for accurate estimation of effective precipitation and annual NIWR. The NIWR is defined as the annual ETc less the effective precipitation entering the root zone that is available for evaporation or transpiration. NIWR is synonymous with the terms "irrigation demand," "net consumptive use," and "precipitation deficit" (Allen and Robison, 2009; Huntington and Allen, 2010). A detailed description of the ET Demands model is provided in Reclamation (2015a).

Time series of Kcb values typically range from 0 to ~1.2 and are referred to as crop coefficient curves. They represent impacts of changes in vegetation phenology on crop ET, which can vary from year to year depending on the start, duration, and termination of the growing season, all of which are dependent on temperature conditions during spring, summer, and fall periods. Rather than assuming fixed time intervals and growth points of Kcb curves as is traditionally done with the FAO-56 approach, thermal parameters of 30 day moving average air temperature and daily minimum air temperature were used to simulate the effects of air and soil temperature on Kcb start, duration, and termination of annual growing season and non-growing season periods.

This approach allows for the length and shape of Kcb curves to be a function of thermal units rather than specified or constant calendar dates, which is necessary for integrating the effects of year-to-year variability and long-term trends in air temperature into growing-season length and crop phenology. Three sets of Kcb values as a function of percent time from green-up to effective full cover were developed for turfgrass in this study: warm, intermediate, and cool season. These categories represent the predominant turfgrass varieties grown in the Western United States—Bermuda (warm season), Kentucky Bluegrass (cool season), and Perennial Rye and Tall Fescue (intermediate season).

Typical growing season dates for the predominant variety of turfgrass in each urban area were researched through inquiries with local agricultural extension offices, municipalities, and local sod farms. Acquired green-up and dormancy dates were used to calibrate temperature parameters that control the shape and length of ET Demands crop coefficient curves based on historical simulations.

7.2.2 Meteorological Data

Historical meteorological data of daily solar radiation, maximum and minimum air temperature, humidity, wind speed, and precipitation used for historical ET Demands simulations and model calibration were acquired from gridMET (Abatzoglou, 2013) for the period of 2009 through 2019. gridMET is a 4 kilometer (km) spatial resolution hybrid dataset of the North American Land Data Assimilation System (NLDAS; Mitchell et. al., 2004) and Parameter-elevation Regressions on Independent Slopes Model (PRISM; Daly et al., 1994). For each urban area, daily gridMET meteorological data and computed ETo were spatially averaged across coincident gridMET cells resulting in single time series of meteorological forcings.

Future meteorological data of daily solar radiation, maximum and minimum air temperature, humidity, wind speed, and precipitation used for baseline and future ET Demands projections were obtained from the Multivariate Adaptive Constructed Analogs (MACA) dataset (Abatzoglou and Brown, 2012) for the same gridMET cells and spatially averaged for each urban area for the period of 1950 to 2100. The MACA dataset is a downscaled future gridded climate dataset consistent with the gridMET grid and is ideal for estimating physically based evaporative demand using the ASCE-PM equation since it provides downscaled solar radiation, air temperature, humidity, wind speed, and precipitation at daily time steps. MACA relies on adapted constructed analogs of multiple variables from gridMET, in this case daily maximum and minimum air temperature, solar radiation, humidity, wind speed, and precipitation.

The MACA approach includes bias correction by mapping daily global climate model (GCM) data to aggregated gridded observations (Maurer et al., 2010); epoch adjustment for no analogs under future climate scenarios (Hidalgo et al., 2008); constructed analogs by finding predictor patterns using gridded observation data; and, bias correction using quantile mapping to gridMET data[19]. The full suite of MACA data includes climate projections from 20 different models that participated in Coupled Model Inter-Comparison Project Phase 5 efforts (CMIP5; Taylor et al., 2012) (i.e., only 20 CMIP5 models archived daily outputs). MACA data includes GCM outputs from the historical CMIP5 experiment for the years 1950 to 2005 and GCM outputs from two future experiments for Representative Concentration Pathways (RCPs) (Moss et al., 2010) of 4.5 and 8.5 for 2006 to 2100.

RCP4.5 refers to the experiment where an additional radiative forcing of 4.5 Watts per square meter (W/m^2) is simulated by 2100 compared to pre-industrial conditions, which is a future scenario of moderate climate action and controlled greenhouse emissions. RCP8.5 refers to the experiment where an additional radiative forcing of 8.5 W/m^2 is simulated by 2100 and represents a future with no climate action and increased greenhouse emissions. In total, 40 MACA transient projections were obtained for gridMET cells coincident with urban areas and were spatially averaged resulting in single time series projections of meteorological forcings and computed ETo for each urban area.

[19] Refer to MACA documentation at https://www.climatologylab.org/maca.html.

7.2.3 ET Demands Model Parameterization and Application

The ET Demands model was parameterized with urban area latitude and longitude, elevation, soil type, turfgrass type(s), and respective meteorological data. Based on communication with local agricultural extension offices, local sod farms, and literature review, a typical silt-loam soil type was assumed with percent sand, silt, and clay of 20, 60, and 20, respectively; available water capacity of 0.2 inches per inch; initial rooting depth of 12 inches; and maximum rooting depth of 24 inches (Koenig and Isaman, 2010; USDA-NRCS, 1998; Allen and Robison, 2009).

Impacts of increased carbon dioxide (CO_2) on ETc were considered following methods of Kruijt et al. (2008), which result in scaled Kcb values based on sensitivity functions of CO_2 concentration, stomatal conductance, and transpiration. Kruijt et al. (2008) summarized results from over 30 studies and developed general CO_2 - stomatal conductance sensitivity functions for different crop types. There are numerous irrigation water requirement uncertainties associated with sensitivities of stomatal conductance, transpiration, and leaf area index to increased CO_2, and unknown land surface energy balance feedbacks from increased leaf temperatures and vapor pressure deficits (Allen et al., 1991; Jacobs and De Bruin, 1992, 1997; Islam et al., 2012); however, the approach of Kruijt et al. (2008) is practical in that it is physically based and considers primary CO_2 affects that ultimately reduce transpiration and ETc. Application of the generalized grass and herb sensitivity formula developed by Kruijt et al. (2008) resulted in Kcb scale factors ranging from 0.99 to 0.94 and 0.99 to 0.84 for the period of 2006 to 2100 for RCP scenarios 4.5 and 8.5, respectively. These scale factors were applied in time to simulated Kcb values within ET Demands according to an annual timeseries of CO_2 concentrations from 4.5 and 8.5 RCPs.

The ET Demands model was run with historical gridMET time series representative of observed climate histories from 2009 to 2019 for Kcb curve calibration. Once calibrated, ET Demands was then run with 40 individual MACA climate projection time series from 1950 to 2100 to derive and illustrate baseline (1950 to 2005) and projected (2006 to 2100) estimates of annual average temperature, solar radiation, humidity, wind speed, total precipitation, ETo, ETc, and NIWR for each urban area using program scripts[20]. While the ET Demands results from running the model with historical gridMET data are not summarized in this report, the digital files are available. The ET Demands model simulates ETo, growing season and non-growing-season soil and root zone water balance components, irrigation, and ETc and NIWR, all at daily time-steps (e.g., Figure 159). Where turf area estimates are available, projected changes in volumes of turfgrass ETc and NIWR can also be calculated using turfgrass to highlight volumetric changes. Annual and mean daily time series of ETc and NIWR and associated meteorological variables for historical and future time periods are presented in the results section.

[20] Refer to Python programs that can be found on GitHub at https://github.com/usbr/et-demands. Any use of trade, firm, or product names is for descriptive purposes only and does not imply endorsement by the United States Government.

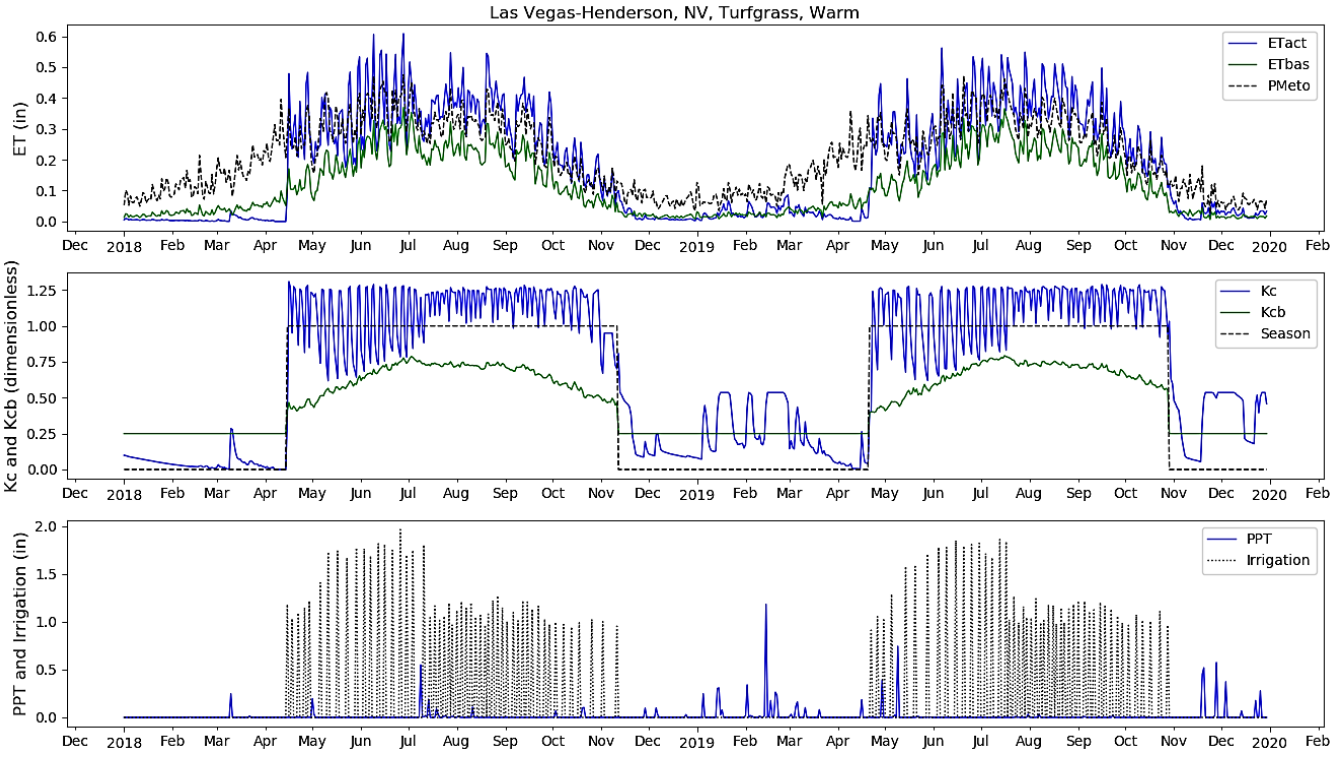

Figure 159. Example ET Demands model simulation with selected parameters and inputs.

Note: ET Demands model simulation of gridMET derived ETo, warm season turfgrass ETc, basal ET (ETbas), basal crop coefficient curve (Kcb), total crop coefficient curve (Kc), simulated irrigations, and estimated gridMET precipitation for Las Vegas, NV. The simulated Kc curve, irrigations, and estimated precipitation are shown to illustrate the development of the Kc curve, and response of the Kc curve and ETc due to wetting events from precipitation and simulated irrigation events.

ET = evapotranspiration; in = inches; PPT = precipitation; PMeto = Penman-Monteith reference evapotranspiration; ETact = evapotranspiration actual

Statistics for future turfgrass water demand estimates were calculated for three future time periods, the 2020s defined as 2010 to 2039, the 2050s defined as 2040 to 2069, and the 2080s defined as 2070 to 2099. These three future time periods correspond to those that have commonly been used by Reclamation in long-term planning studies, including for the Baseline Assessments *Irrigation Demand and Reservoir Evaporation Projections* (Reclamation, 2015a). The study authors acknowledge the decade of overlap between the 2020s future time period and the present (2020 at the time of writing), but its inclusion is warranted given that the time period extends through 2039, and it offers a comparison with other Reclamation long-term planning studies.

7.3 Results

Future projections for all urban areas throughout the West predict increases in average annual temperature, which in turn lead to large increases in evaporative demand. In addition to increased evapotranspiration rates, increased temperatures also allow for longer growing seasons which

increases the total number of days that plants consume water. Annual plant water consumption is a function of both the evaporation rate and total time a plant is active. Projections and relative change of solar radiation, temperature, humidity, wind speed, and precipitation are region-specific causing spatially variable changes in ETc and NIWR.

The following sections discuss results for three urban areas from different regions throughout the Western United States. Results are summarized using 5th, 25th, 50th (median), 75th, and 95th percentile statistics of model output from all 40 climate projection datasets (RCP4.5 and RCP8.5 scenarios; 20 models).

Baseline estimates (1951 to 2005) generated using historical MACA data are not meant to represent actual historical conditions for each specific year. Historical MACA data were trained using the gridMET data from 1979 to 2009 and have the same overlying statistics as the training data, but are not a hindcast. Historical MACA estimates are used for comparison with future time periods to provide estimates of relative change.

7.3.1 Las Vegas, Nevada – Warm Season Turfgrass

Future projections of ETc and NIWR for warm season turfgrass in Las Vegas, Nevada, show increases of 13.9 inches/year and 13.7 inches/year, respectively, by the 2080s (Figure 160). Notably, median windspeed in this region is expected to decrease; however, these decreases are not enough to offset the temperature-driven increases in PM ETo. Future projections of precipitation in the region remains close to the historical baseline.

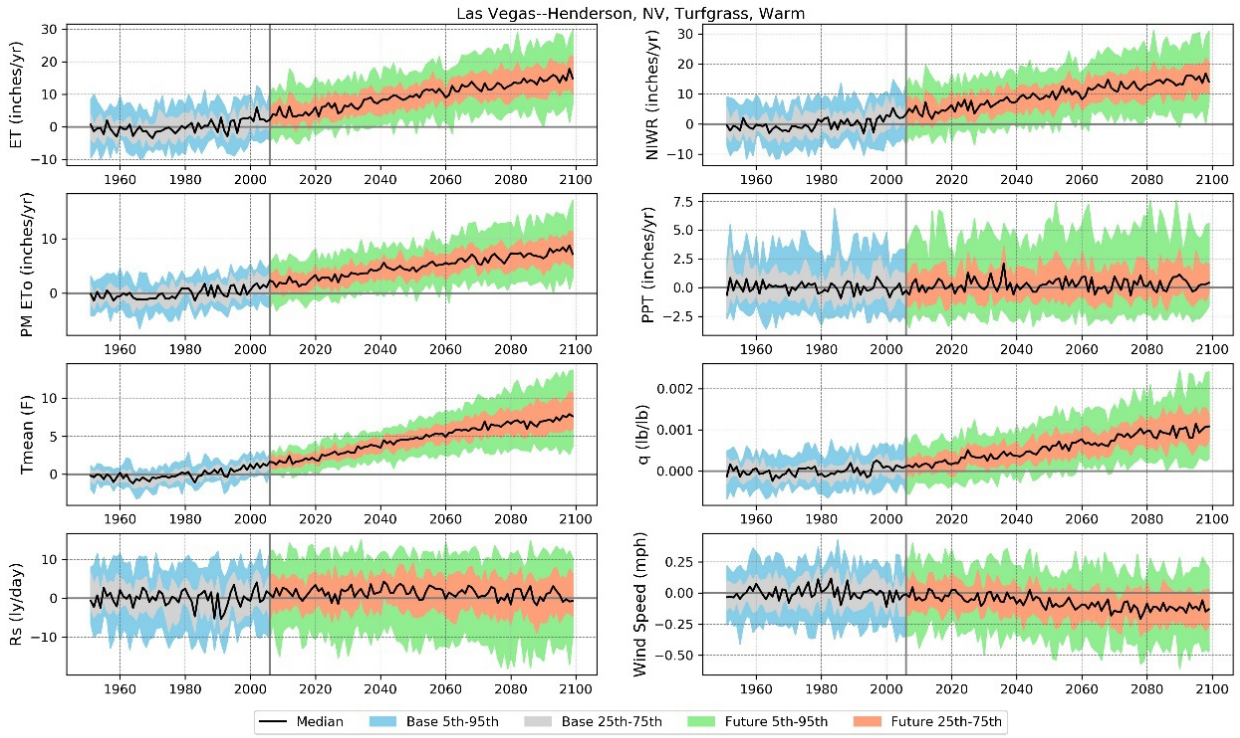

Figure 160. Anomaly from baseline (1951 to 2005) time series plots of climate, ET, and NIWR estimates for Las Vegas--Henderson, Nevada.

Annual estimates of ETc show increases beyond PM ETo due to substantial lengthening of the growing season (Figure 161; ~50 days total: ~30-day earlier onset, ~20-day later end). Projected shifts in growing season are based on earlier commencement of typical emergence temperatures (i.e., T30) and later onset of killing frost temperatures.

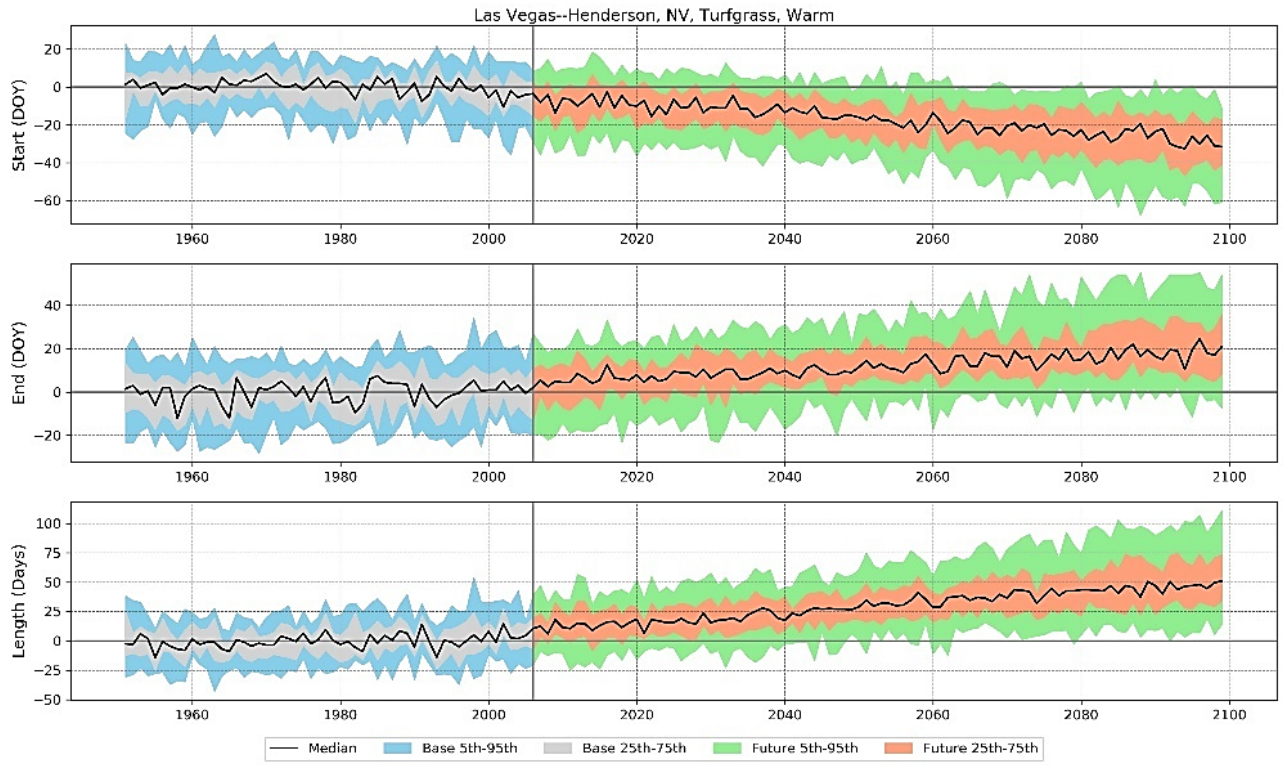

Figure 161. Anomaly from baseline (1951 to 2005) time series plots for growing season start day of year (DOY), end day of year, and total length for Las Vegas--Henderson, Nevada.

Investigation into monthly evaporation patterns show substantial changes in the growing season shoulder month ET and NIWR (largely driven by growing season length changes), as well as an overall increase in the magnitude of summer ET and NIWR. For example, baseline estimates of ET and NIWR for March and April are close to zero for most projections, but future scenarios show earlier startup and substantial evaporation occurring in these months by the 2080s for most climate scenarios.

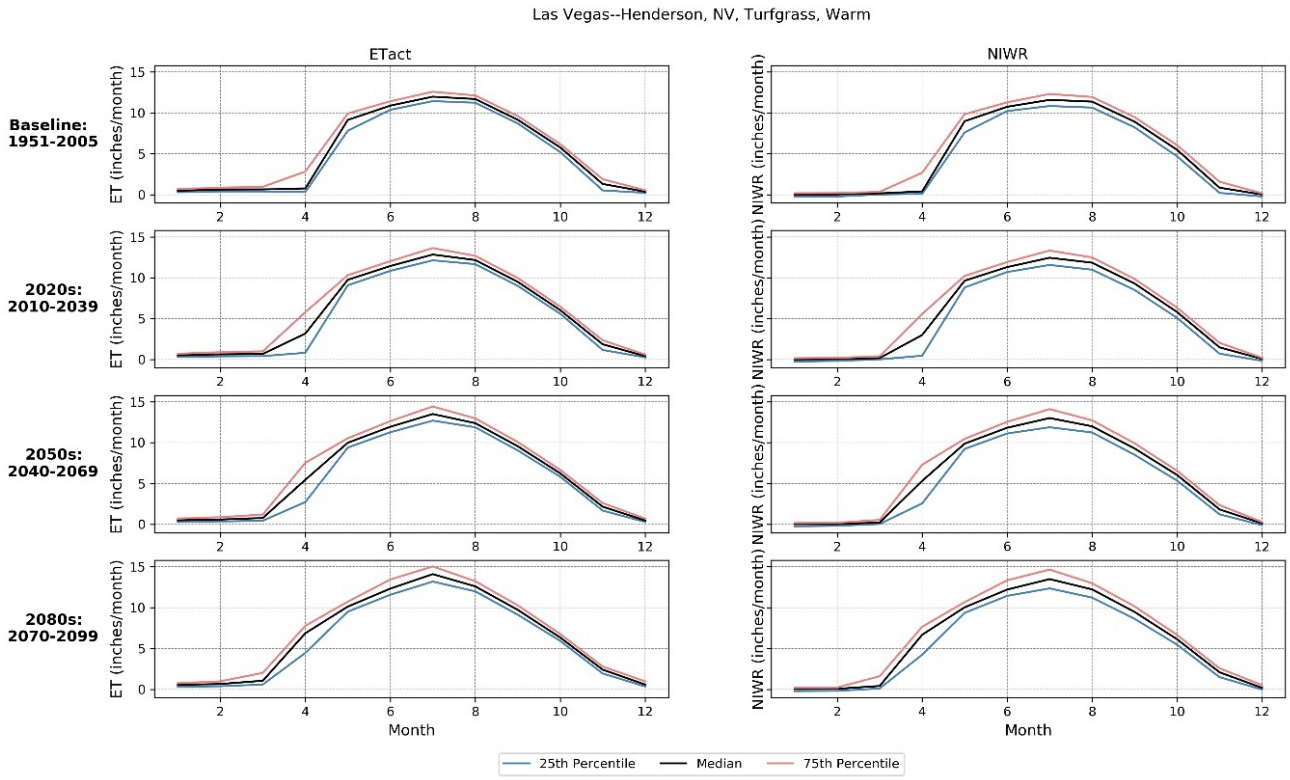

Figure 162. Monthly evaporation and NIWR percentile summary plots for baseline (1951 to 2005), 2020s (2010 to 2039), 2050s (2040 to 2069), and 2080s (2070 to 2099) for Las Vegas--Henderson, Nevada.

Note: ET = evapotranspiration; ETact = evapotranspiration actual; NIWR = net irrigation water requirements

7.3.2 Los Angeles, California – Intermediate Style Turfgrass

Los Angeles, California, along with the majority of urban areas throughout California, use Dwarf Tall Fescue turfgrass varieties for urban landscaping (Huntington, 2020). An intermediate turfgrass Kcb curve (average of cool and warm season turfgrass crop coefficient curves) was developed for ET estimation in these areas. Typical management practices throughout California allow for a complete year growing season with limited to no dormancy.

Results for Los Angeles show projected increases in median ETc of ~5.1 inches/year by the 2080s with increases of median NIWR of ~5.4 inches/year by 2080 compared to the average 1951 to 2005 baseline (Figure 163). Larger increases in NIWR compared to ETc are due to small decreases in average annual precipitation.

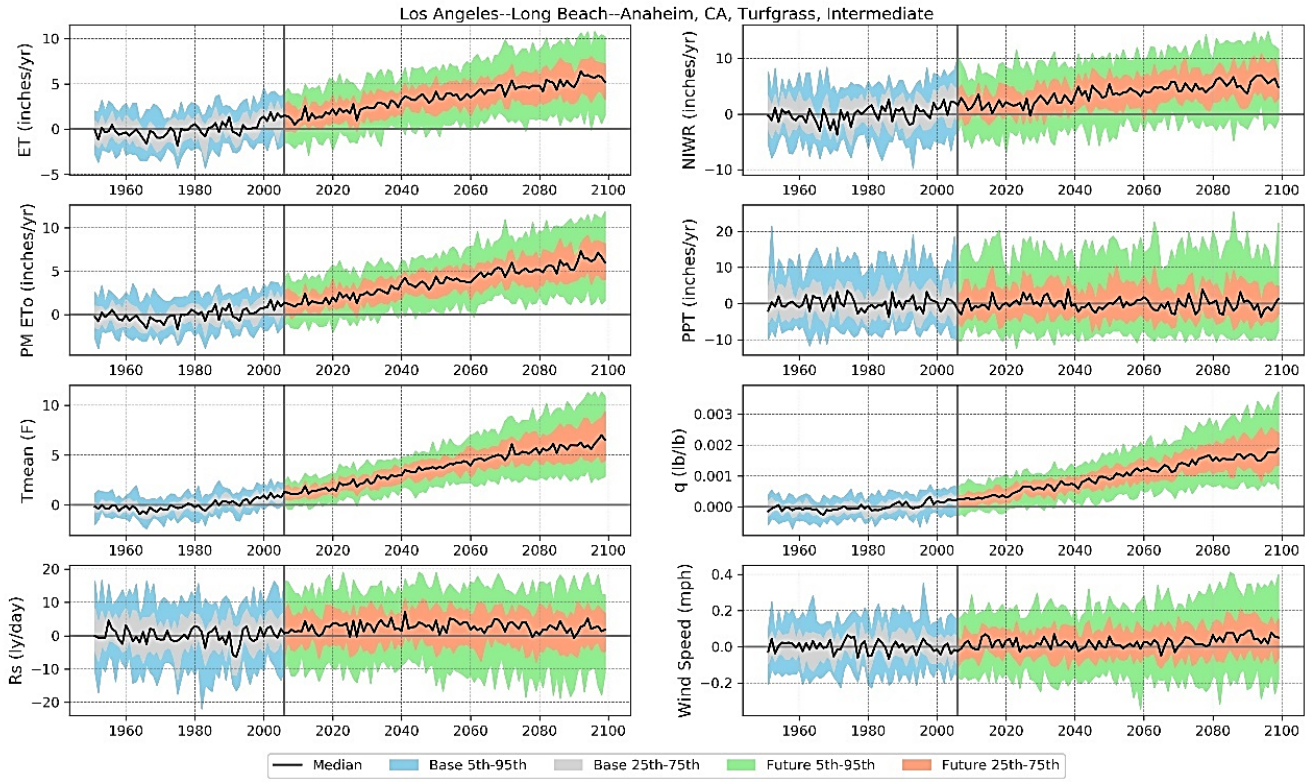

Figure 163. Anomaly from baseline (1951 to 2005) time series plots of climate, ET, and NIWR estimates for Los Angeles--Long Beach--Anaheim, California.

Further investigation into monthly ETc and NIWR rates shows that annual patterns remain relatively unchanged due to current year-round growing practices. ETc and NIWR increases appear to be evenly distributed with no specific season or month showing more substantial changes than others (Figure 164).

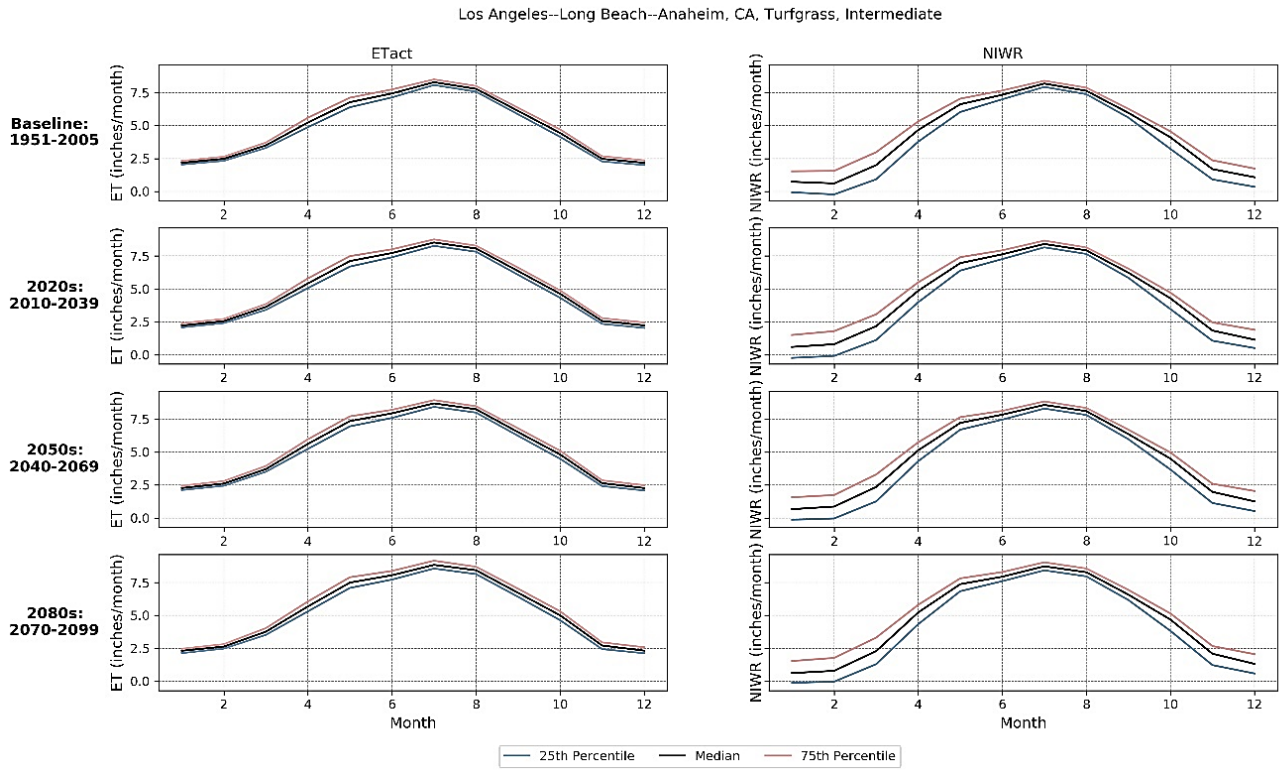

Figure 164. Monthly evaporation and NIWR percentile summary plots for baseline (1951 to 2005), 2020s (2010 to 2039), 2050s (2040 to 2069), and 2080s (2070 to 2099) for Los Angeles--Long Beach--Anaheim, California.

Note: ET = evapotranspiration; ETact = evapotranspiration actual; NIWR = net irrigation water requirements

7.3.3 Denver, Colorado – Cool Season Turfgrass

Median projected changes by the 2080s in the Denver, Colorado region for cool season turfgrass (Kentucky Bluegrass) are 11.1 inches/year for ETc and 9.9 inches/year for NIWR (Figure 165). Increases in NIWR are slightly lower than increases in ETc due to projected increases in annual precipitation. Increases in ETo remain relatively high, even though wind speed is projected to decrease by ~0.5 miles per hour (mph) for median level climate scenarios.

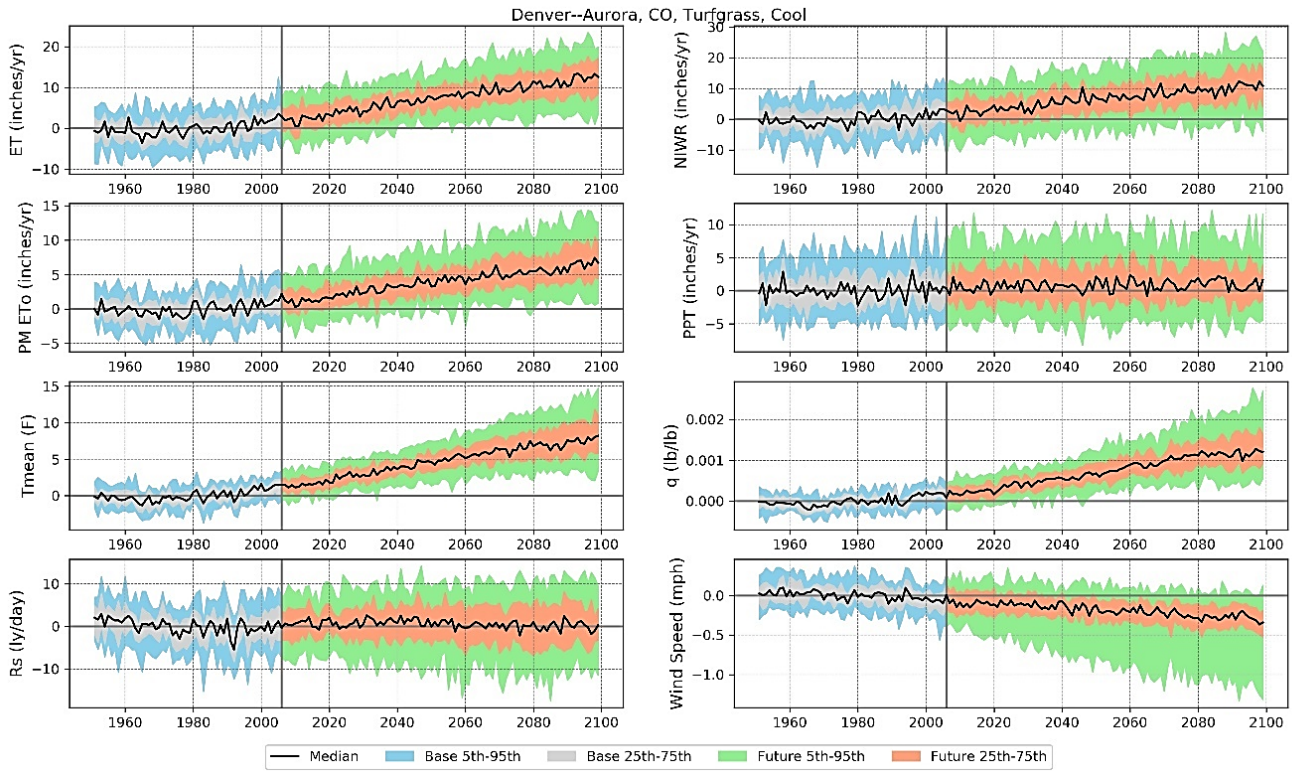

Figure 165. Anomaly from baseline (1951 to 2005) time series plots of climate, ET, and NIWR estimates for Denver--Aurora, Colorado.

Temperature-based growing season start and end dates show an increase of approximately 90 days by the 2080s, with the majority of lengthening driven by earlier green-up (Figure 166). Lengthening of the growing season is reflected in the monthly ET and NIWR rates where shoulder months show shifts from limited to no ETc and NIWR to rates of 2 to 3 inches per month (Figure 165). Peak summertime ETc and NIWR rates are also increased under future projections. Increases in NIWR occur despite slight increases in projected precipitation for this region.

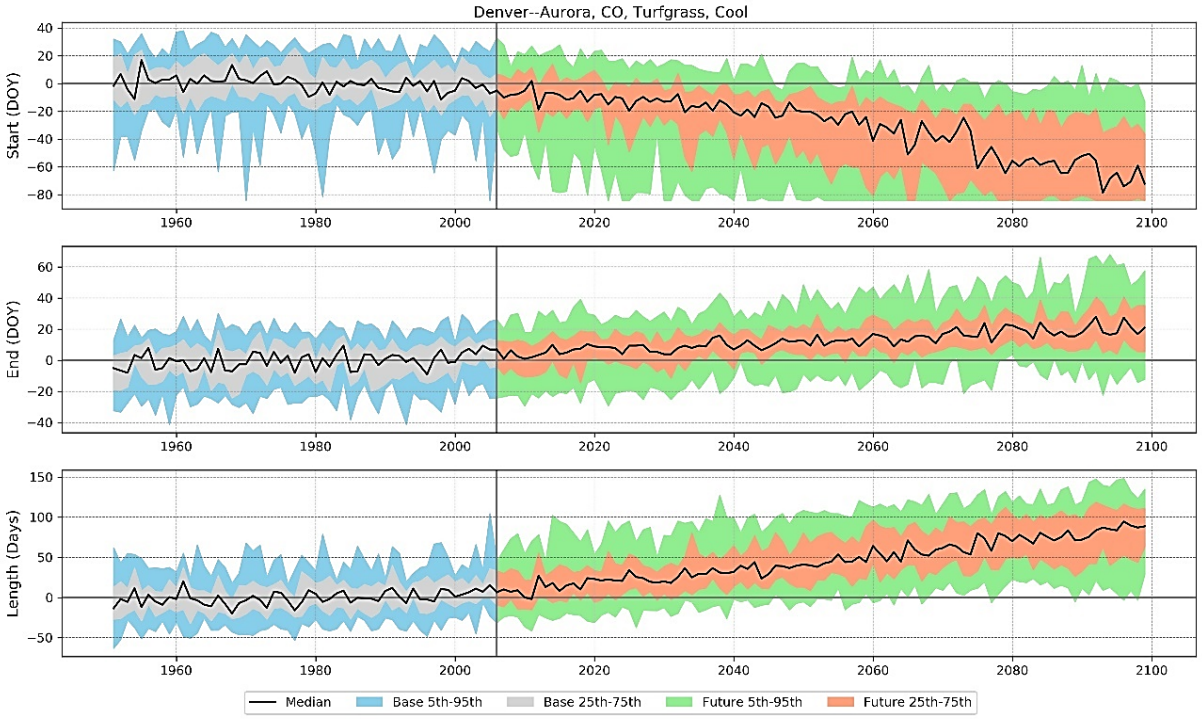

Figure 166. Anomaly from baseline (1951 to 2005) time series plots for growing season start day of year (DOY), end day of year, and total length for Denver--Aurora, Colorado.

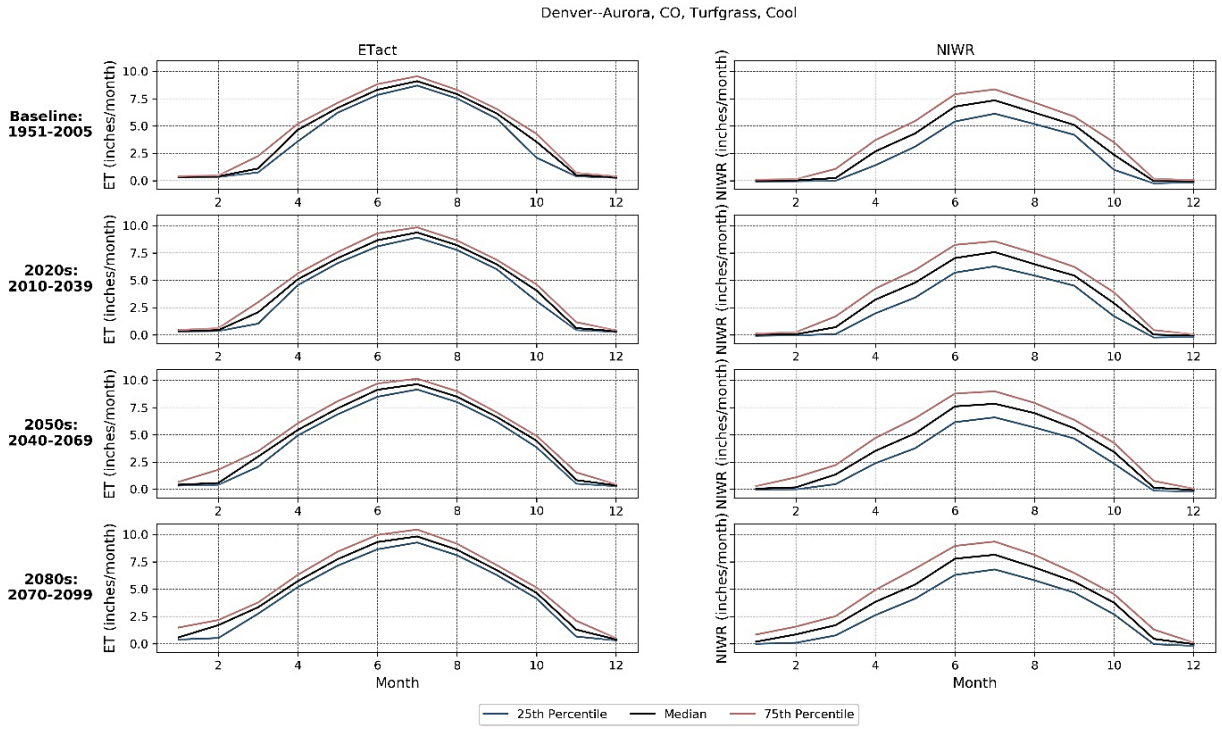

Figure 167. Monthly evaporation and net irrigation water requirement percentile summary plots for baseline (1951 to 2005), 2020s (2010 to 2039), 2050s (2040 to 2069), and 2080s (2070 to 2099) for Denver--Aurora, Colorado.

Note: ET = evapotranspiration; ETact = evapotranspiration actual; NIWR = net irrigation water requirements

7.3.4 Volume Estimates

Volumetric estimates of turfgrass water consumption are a function of both the ETc and NIWR rates and respective surface area. The ET Demands model simulates ETc and NIWR estimates as rates and is not dependent on areal extents. Current estimates of turfgrass areas were available for a limited number of urban areas, and these estimates were used to calculate ETc and NIWR volume estimates by pairing each water district with its intersecting urban area. Table 36 lists turfgrass area estimates, along with current and future estimates of ETc and NIWR, in acre-feet per year based on projected rates estimated by ET Demands. Results are presented for three quantiles q25, q50, and q75 corresponding to the three percentiles, 25th, 50th, and 75th respectively, and for the baseline period (1951 to 2005), along with the three future periods 2020s (2010 to 2039), 2050s (2040 to 2069), and 2080s (2070 to 2099).

Table 36. Baseline (1951 to 2005) and future urban irrigation evaporation volume estimates for select water districts in the Western United States

Water Authority or District	ET Demands Urban Area	Irrigated Acres*	Variable	NIWR	NIWR	NIWR	ETc	ETc	ETc	NIWR	NIWR	NIWR	ETc	ETc	ETc
			Quantile	q25	q50	q75	q25	q50	q75	q25	q50	q75	q25	q50	q75
			Estimate Type	Baseline (1951-2005)	Baseline (1951-2005)	Baseline (1951-2005)	Baseline (1951-2005)	Baseline (1951-2005)	Baseline (1951-2005)	2020s	2020s	2020s	2020s	2020s	2020s
Southern Nevada Water Authority	Las Vegas—Henderson, NV	11,547	Rate (in/year)	59.21	61.79	64.33	64.51	66.60	68.49	63.26	66.05	68.85	68.85	70.86	73.13
			Volume (acre-ft/year)	56,975	59,458	61,900	62,072	64,085	65,901	60,867	63,555	66,254	66,248	68,180	70,365
Western Municipal	Riverside—San Bernardino, CA	4,776	Rate (in/year)	51.16	53.94	56.71	60.35	61.97	63.50	53.24	55.99	58.91	62.40	64.07	65.89
			Volume (acre-ft/year)	20,364	21,467	22,572	24,018	24,666	25,275	21,189	22,283	23,448	24,834	25,501	26,226
Eastern Municipal Water District	Murrieta—Temecula—Menifee, CA	12,051	Rate (in/year)	48.92	51.89	55.00	59.10	60.80	62.48	51.05	53.89	56.95	61.02	62.83	64.80
			Volume (acre-ft/year)	49,126	52,106	55,234	59,349	61,060	62,743	51,262	54,122	57,189	61,283	63,092	65,074
Water Authority or District	**ET Demands Urban Area**	**Irrigated Acres***	**Variable**	**NIWR**	**NIWR**	**NIWR**	**ETc**	**ETc**	**ETc**	**NIWR**	**NIWR**	**NIWR**	**ETc**	**ETc**	**ETc**
			Quantile	**q25**	**q50**	**q75**	**q25**	**q50**	**q75**	**q25**	**q50**	**q75**	**q25**	**q50**	**q75**
			Estimate Type	**2050s**	**2050s**	**2050s**	**2050s**	**2050s**	**2050s**	**2080s**	**2080s**	**2080s**	**2080s**	**2080s**	**2080s**
Southern Nevada Water Authority	Las Vegas—Henderson, NV	11,547	Rate (in/year)	66.31	69.43	72.73	71.91	74.47	76.93	68.09	71.97	75.79	74.02	76.99	80.59
			Volume (acre-ft/year)	63,811	66,807	69,982	69,200	71,657	74,029	65,524	69,252	72,929	71,224	74,087	77,552
Western Municipal	Riverside—San Bernardino, CA	4,776	Rate (in/year)	55.44	58.60	61.54	64.48	66.27	68.13	56.64	60.07	63.27	65.70	67.65	70.00
			Volume (acre-ft/year)	22,066	23,324	24,493	25,664	26,374	27,115	22,543	23,908	25,180	26,147	26,923	27,861
Eastern Municipal Water District	Murrieta—Temecula—Menifee, CA	12,051	Rate (in/year)	53.18	56.43	59.73	63.16	64.94	66.92	54.33	57.77	61.23	64.29	66.36	68.70
			Volume (acre-ft/year)	53,408	56,668	59,986	63,432	65,215	67,206	54,557	58,018	61,486	64,564	66,638	68,991

* Note: Urban irrigated acres are based on 2020 estimates provided by each water authority or district. Future volumes consider climate driven rate changes only and do not account for changes in total acreages, turfgrass type, or irrigation practices.

7.4 Summary and Next Steps

Projections of future ETc and NIWR for urban turfgrass throughout the Western United States show substantial increases in water demand by the 2080s. Increases in median projected ETc and NIWR from baseline conditions ranged from 8 to 36 percent and 9 to 54 percent, respectively. Increases in ETc are largely driven by increased temperatures and the accompanying increase in both ETo and growing season length. Large changes in either the growing season start, or end, dates has the potential to stress water supply systems during time periods when historical demands for water are typically low. Increases in precipitation in some regions provides some offset for increased annual ET, but, is typically not enough to completely compensate for the total increase in plant water demand. Spatially varying changes in projected windspeed and solar radiation lead to variable changes in ETo throughout the West.

Current turfgrass species selection and management practices (e.g., year-round growth in California) may not reflect future practices and should be investigated for their potential to reduce total water consumption under future climate. Further research on plant phenology and growth dynamics related to energy-limited versus temperature-limited growth should be performed. Refinement of weather datasets for urban environments through comparison of gridded products with local station datasets will help improve the accuracy of ET estimates and overall water demand. Improved estimates and tracking of the spatial coverage and total acreage of urban turfgrass through the use of remote sensing and high-resolution imagery can help translate ET rate estimates to total volumes.

7.5 Key Findings

A listing of key findings from the urban landscape demand analysis and for the selected urban areas analyzed are given below:

- Future projections for all urban areas throughout the West predict increases in average annual temperature, which in turn lead to large increases in evaporative demand.
- In addition to increased evapotranspiration rates, increased temperatures also allow for longer growing seasons, which increases the total number of days that plants consume water.
- Annual plant water consumption is a function of both the evaporation rate and the total time a plant is active.
- For Las Vegas, Nevada, investigation into monthly evaporation patterns shows substantial changes in the growing season shoulder month ET and NIWR (largely driven by growing season length changes), as well as an overall increase in the magnitude of summer ET and NIWR.

- For Los Angeles, California, investigation into monthly ET for turf grass (ETc) and NIWR rates shows that annual patterns remain relatively unchanged due to current year-round growing practices. ETc and NIWR increases appear to be evenly distributed with no specific season or month showing substantial changes.
- For Denver, Colorado, increases in NIWR are slightly lower than increases in ETc due to projected increases in annual precipitation.

8 Climate Impacts on Groundwater

The SECURE Water Act (SWA) identifies the critical need to improve understanding of water cycle variability and water use in part through the continued assessment of the availability of surface and groundwater supplies to meet the future needs of the United States. Assessment of groundwater is particularly challenging due to the changing equilibrium between recharge and discharge. This chapter provides a literature review of the impacts of climate on groundwater recharge and discharge and summarizes findings from recent studies (approximately over the last 5 years) conducted by Reclamation.

8.1 Impact of Climate on Groundwater Recharge and Discharge

Recharge, or the replenishment of groundwater in aquifers, represents the amount of precipitation or applied water that remains to percolate into the subsurface after surface processes, such as evapotranspiration, snowmelt, and runoff. Recharge calculations often aggregate the errors from these surface processes, including the uncertainty and variability in precipitation, vegetation, and soil properties. Meixner et al. (2016) categorize recharge into four mechanisms as follows:

- Diffuse recharge, or the precipitation that percolates directly to the water table.
- Focused recharge, which comes from concentrated areas, such as streams and playas.
- Mountain system recharge, which includes focused stream recharge along the mountain front, as well as water transported to the aquifer system from the mountain block.
- Irrigation recharge, which is the infiltration and percolation of excess irrigation water.

The relative importance of these mechanisms varies with regional climate, topography, land use, and aquifer properties. The Central Valley of California, for example, is dominated by irrigation recharge, while the High Plains Aquifer spanning from Nebraska to Texas is predominately diffuse recharge (Meixner et al., 2016; Gurdak et al., 2007). Mountain system recharge is an important mechanism in aquifers in the Rocky Mountain and Intermountain regions, such as the San Pedro and Wasatch Front systems (Meixner et al., 2016), as well as the Lower Santa Cruz River basin.

Generally, as wet areas get more wet and dry areas get drier (Trenberth, 2011), diffuse recharge will mimic these regional patterns, with some buffering and intensification, respectively, from increased evapotranspiration driven by widespread anticipated temperature increases. Mountain system recharge may similarly reflect changes in high elevation precipitation, with decreases anticipated in the Central Valley and San Pedro (Meixner et al., 2016); however, mountain aquifers are poorly understood and are an active area of research. Focused recharge may also increase with projected increases in precipitation intensity, despite decreased totals in

precipitation. Changes in focused recharge, however, are highly uncertain, as the ability to model precipitation intensity is largely dependent on modeling climate processes at high spatial resolution to topographic effects and convective events. Finally, irrigation recharge will largely depend on water demands, and the response of farming practices and technology to meet these demands.

Discharge, or the return of groundwater to the surface water system, requires characterization of subsurface processes that are hard to observe, but that determine the flow paths along which recharged water returns to the surface. Due to the nature of groundwater aquifers as storage systems, discharge is often a complex mix of water that recharged at different locations and traveled along variable paths with variable travel times before returning to the surface.

Climate-driven changes in recharge and discharge continue to be an active area of research (e.g., Taylor et al., 2013) and this chapter broadly summarizes the state of knowledge on the topic and some of the recent work and case studies from Reclamation and its partners, and Federal and non-Federal collaborations (Figure 168).

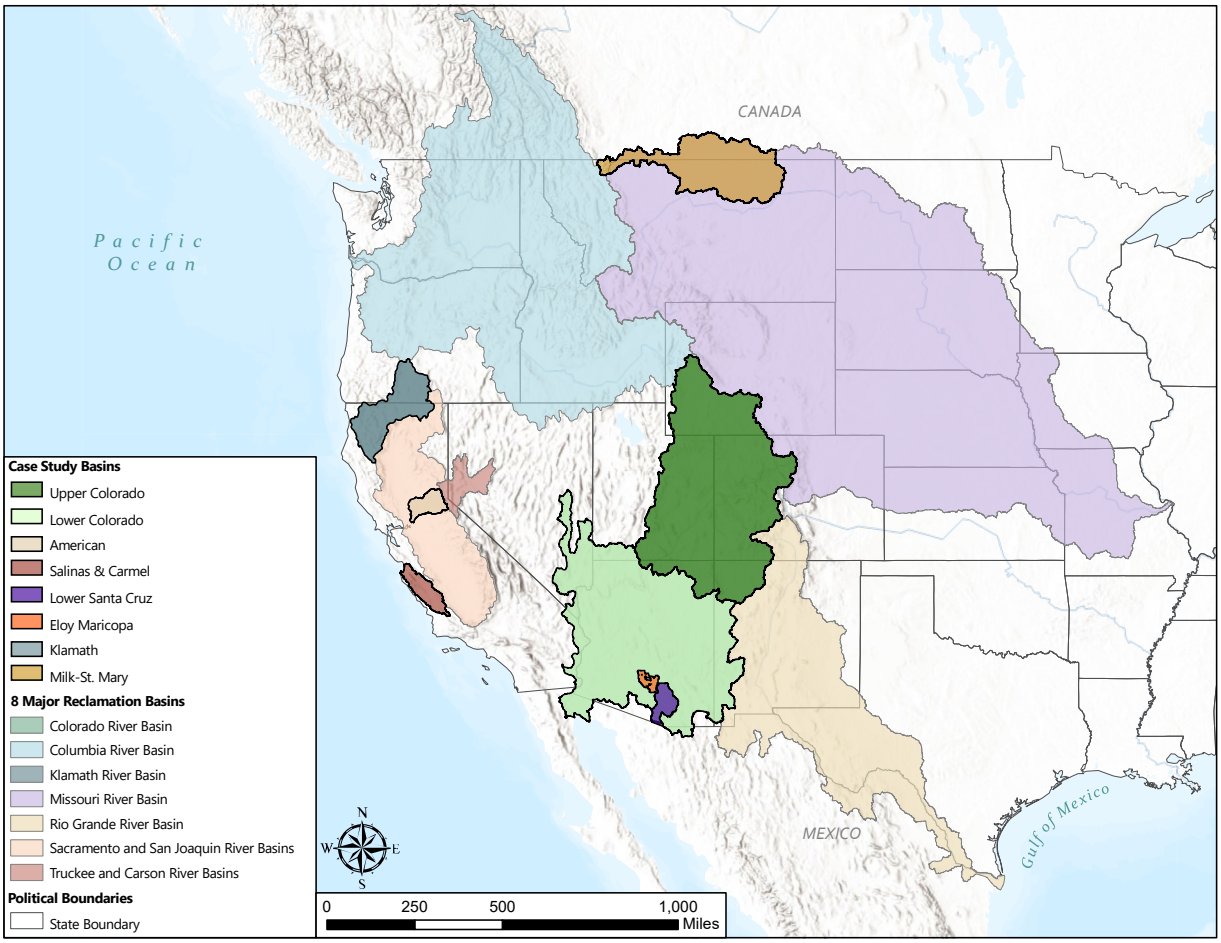

Figure 168. Location of groundwater case study basins across the West.

8.1.1 Large-scale Hydrologic Events and Recharge

Groundwater recharge is dependent on many factors, including subsurface hydrogeology, topography, and climate. In the arid and semi-arid Western United States, recharge primarily occurs after large, infrequent hydrologic events. These events must contain enough precipitation to surpass soil moisture and evaporation demands and thus excess water can infiltrate into the subsurface. In a recent study, it was hypothesized that these large recharge events only occur on a quasi-decadal scale (i.e., every, one to two decades) and contribute the majority of recharge to aquifers in arid and semi-arid environments (Masbruch et al., 2016). To investigate this hypothesis, groundwater records were analyzed with precipitation, temperature, and snow water equivalent (SWE) records from 1960 to 2013 in the northern Utah portion of the Great Basin. In addition, existing groundwater models were used to assess the impact of different recharge events on subsurface storage, and to investigate how changing the magnitude and timing of these events might alter aquifer recharge.

Large recharge events were identified five times over the 53 years analyzed and were defined as time periods where the normalized groundwater level increased for three consecutive years. Multivariate timeseries analysis identified that these large recharge events occur, on average, every 11 to 13 years. On average, the annual precipitation during these large recharge events was 131 millimeters[21] higher than the average annual precipitation, and the annual SWE was 71 millimeters higher. Seasonal trends indicated that the largest increases in precipitation were observed in spring during these large recharge events and the smallest increases were observed during the summer months. While average annual temperatures did not appear to be driving these large recharge events, it was found that most of the large recharge events corresponded to winters with warmer than average temperatures and springs with colder than average temperatures. Cooler spring temperatures slow snowpack melt and increase infiltration while reducing runoff leading to larger subsurface recharge amounts.

Using the groundwater models to simulate these large recharge events suggested that each event recharges 115 to 205 cubic millimeters per basin. The study also used these models to change the frequency and magnitude of one large recharge event to an average event. This not only decreased the amount of recharge entering the aquifer during those 3 years, but also increased the amount of time between large recharge events. Comparing those two simulations showed that aquifer stress and depletion occurred 2 years earlier when one large recharge event was replaced with an average recharge event. This study not only showed the crucial role climate plays in groundwater recharge in the West, but also highlights the importance of understanding how these large recharge events and climatic drivers will change in the future.

8.1.2 Spatial Distribution of Groundwater Recharge

Given the direct coupling between groundwater recharge and climate, recent focus has turned towards understanding how climate change will alter groundwater resources. Future recharge projections are normally developed through forcing a hydrologic model with climate data from

[21] 1 inch = 25.4 millimeters

global climate models (GCMs) (e.g., Allen et al., 2010; Crosbie et al., 2011). GCMs climate output is typically at a daily or monthly timescale and provided at a coarse spatial resolution of around 100 to 200 kilometer (km) per grid cell side and is then downscaled to a finer resolution anywhere between 6 to 12 km. In groundwater resource studies, a finer spatial scale allows for a more realistic representation of topography, land use, and geology, which all factor into how recharge is incorporated to underlying aquifers. In addition, groundwater recharge can occur on daily or even sub-daily timescales. However, considerable effort goes into downscaling the GCM climate data and understanding the spatial and temporal uncertainty associated with the downscaling method. Given the temporal and spatial scales associated with natural aquifer recharge, a study by Tillman et al. (2018) investigated the effects of scale on simulating historic recharge in the Upper Colorado River Basin (UCRB). The study used a Soil Water Balance (SWB) model to simulate recharge and forced the model with historic climate datasets at three spatial resolutions (800 meters, 4 km, and 12 km) and two temporal scales (daily and monthly).

When using daily climate data, Tillman et al. (2018) found that there are very few differences in the average annual recharge from 1982 to 2014 when modeling recharge at the three different spatial scales. However, there were substantial differences when modeling seasonal recharge trends, where the 4 km resolution resulted in 21 percent and 38 percent higher recharge during the summer months than the 800 m and 12 km resolutions, respectively. The difference in recharge during these months between scales was not explained by differences in precipitation, but by differences in snowpack and temperature during the winter months. Using monthly climate data to model recharge produced similar trends between spatial scales as the daily climate data did, where annual averages and trends were similar between spatial scales and the largest differences were seen when looking at recharge during the summer months. In addition, there were very few differences when directly comparing temporal scales, which suggests monthly models may be sufficient to capture seasonal and annual groundwater recharge dynamics.

Scale has always been an important issue to consider in hydrologic modeling, and the study by Tillman et al. (2018) further highlights how differences in spatial and temporal scale may or may not alter simulated groundwater recharge trends. The results from the study suggest that for water resource managers interested in long-term annual or decadal recharge estimates, using a coarser timescale and spatial resolution is most likely sufficient and timesaving. However, if seasonal dynamics are of interest, a finer temporal and spatial scale might be useful, as long as consideration is given to the uncertainties associated with finer-scale data.

8.2 Climate Change and Groundwater Case Studies

Reclamation-funded studies focusing on recharge and groundwater dynamics have been focused on the Upper Colorado River Basin, as summarized below. Other Reclamation studies address groundwater changes, many through the supply and demand imbalance planning efforts referred to as “basin studies.” Studies—such as the Lower Santa Cruz River and Eloy-Maricopa Basin Studies in Arizona, the Salinas and Carmel River Basin Study and the American River Basin

Study, both in California, and Klamath River Basin Study spanning from Oregon into California—explicitly model changes in groundwater processes under future climate conditions. These studies are also summarized below. Other basin studies, such as those in the Upper Missouri and Milk St. Mary River basins have incorporated groundwater changes inferred from external studies into their planning methodology. The response of groundwater systems to changes in climate varies across Reclamation's regions as outlined by the following case studies.

8.2.1 Upper Colorado River Basin

8.2.1.1 Groundwater Recharge

The Colorado River provides water for more than 38 million people and traverses more than 2,200 km from its headwaters in the Rocky Mountains through seven States and into Mexico. Given the large expanse of the Colorado River Basin, it has been divided into two separate basins, where the upper basin is north of Lees Ferry, Arizona, and the lower basin is south of Lees Ferry. The discharge of groundwater into the Upper Colorado River Basin is estimated to provide between 21 to 58 percent of streamflow (Miller et al., 2014), with higher percentages during low-flow years.

Given the importance of groundwater in the Upper Colorado River Basin, a recent study quantified projected changes in the UCRB between the recent historical (1950 to 2015) and future (2016 to 2099) time periods (Tillman et al., 2016a). The study used the SWB groundwater recharge model that estimates recharge by direct infiltration after calculating each water balance component (i.e., rainfall, snowmelt, interception, evapotranspiration (ET), and streamflow in between model cells). SWB was then forced with gridded climate data derived from 97 different climate projections from the Coupled Model Intercomparison Project Phase 5 (CMIP5) model archive. The 97 projections represented four different Representative Concentration Pathways (RCP) with radiative forcing levels of 8.5, 6, 4.5, and 2.6 Watts per square meter (W/m^2) and were downscaled using the Bias Correction and Spatial Disaggregation (BCSD) method into monthly temperature and precipitation grids. The monthly values were further disaggregated into daily values using a historical resampling and scaling technique. Results were presented from 1950 to 2099 on a 10-year moving average basis to smooth out the variability of extreme years and its effects are integrated over time in groundwater systems.

Tillman et al. (2016a) found that simulated future groundwater recharge is anticipated to be greater than the historical average in most future decades (Figure 169). The median simulated groundwater recharge in the future moving 10-year annual averages are projected to be between 73 to 88 percent greater than the historical averages, depending on the RCP of each simulation. Despite projected increases in temperature and thus ET, recharge is projected to increase due to projected increases in precipitation over the basin from the BCSD downscaled data.

In addition to estimating the overall change to groundwater recharge in the UCRB as described in the above study, Tillman et al. (2017) investigated how the spatial and seasonal recharge dynamics might shift in the future. Using the same methods and datasets as Tillman et al. (2016a), it was found that projected changes in future recharge are not spatially homogenous

across the UCRB. Recharge in the northern part of the UCRB is projected to increase while recharge in the more southern areas is projected to decrease. Seasonal changes in recharge are also anticipated across the entire UCRB, as projected recharge is estimated to decrease by approximately 50 percent in the summer while increasing by around 50 percent during the winter.

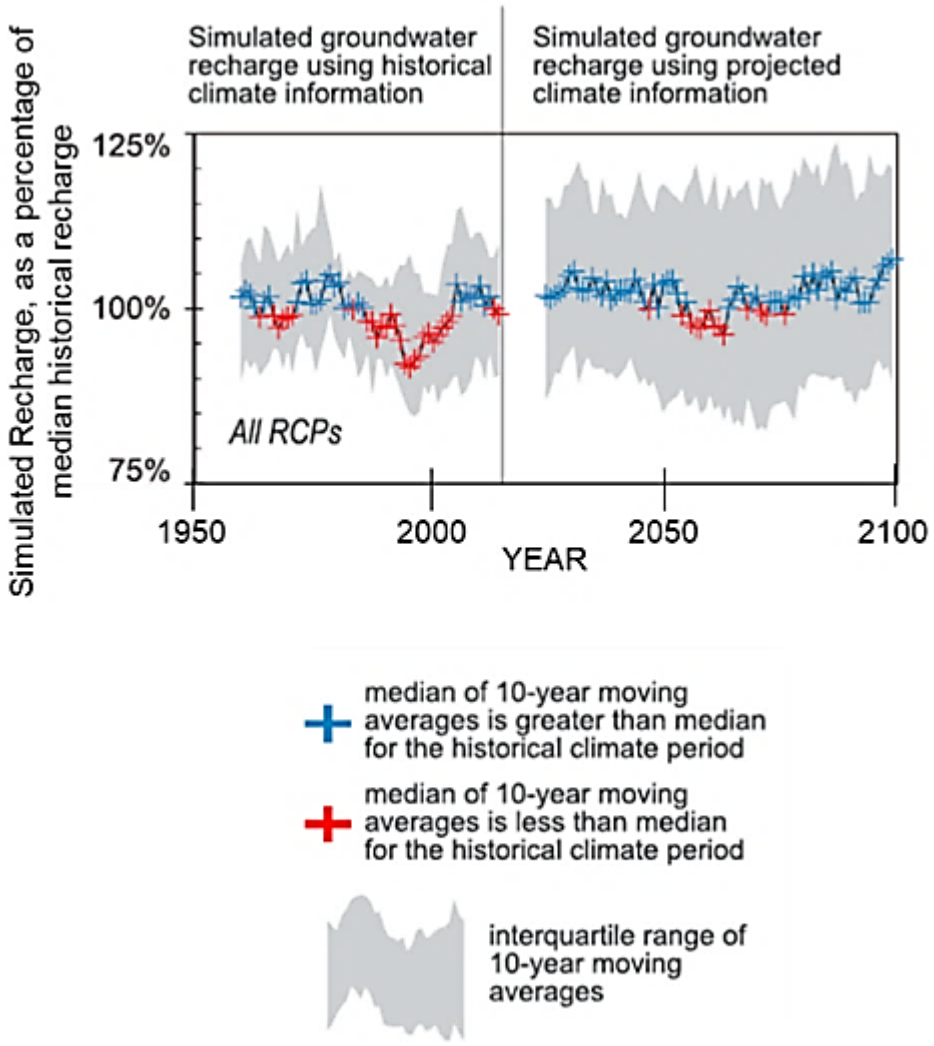

Figure 169. Median of 10-year moving averages of simulated annual recharge from RCPs.

Note: SWB model simulated annual groundwater recharge from BCSD downscaled projections using all CMIP5 RCPs (2.6, 4.5, 6.0 and 8.5). Figure modified from Tillman et al. (2016a).

While the study by Tillman et al. (2016a) compared recharge in simulated historical and future time periods, it did not investigate how closely the simulated historical periods from each of the 97 projections actually matched observed climate data. This comparison is described in Tillman et al. (2016b). Even though the 97 modeled projections were bias corrected using observed data from Maurer et al. (2002), they were constrained using only monthly statistics. Thus, for any

given year, there can be substantial differences between the observed historical value and the bias-corrected modeled value of precipitation or temperature. In addition, those differences are magnified when using precipitation and temperature as inputs to a recharge model. To this end, a subsequent study (Tillman et al., 2016b) investigated the difference between estimating historical recharge using the 97 modeled climate projections as Tillman et al. (2016a) did and estimating historical recharge using the observed climate dataset that the 97 climate projections were bias-corrected following Maurer et al. (2002). Historic recharge was modeled from 1951 to 2010 using the same SWB model as the above Tillman et al. (2016a) study, and forced with precipitation, maximum and minimum temperatures from actual climate observations, and the 97 CMIP5 model results. Results compared simulated historic recharge between the observed and modeled input datasets on an average monthly, average annual, and moving 10-year average basis.

Results from the Tillman et al. (2016b) study indicate that using the modeled climate projections preserve the historic monthly recharge dynamics seen when using observational data. The months of March through June account for over 88 percent of the mean annual recharge in the UCRB using both datasets. The largest differences between historic recharge simulated using observed or modeled climate data are seen in the months of July and August; however, each of these months only accounts for 1 percent of the mean annual recharge in the basin.

Similarly, the modeled input data preserves the annual trends and dynamics in historic recharge values that are seen when using observed input data. The biggest difference is seen when comparing the 10-year moving average of historic recharge between the observed and CMIP5 modeled data. It is worth noting that, when using observed climate data to simulate historic and future recharge, analysis of the 10-year moving averages suggests that there will be less recharge in the future than historically. This is opposite of the trend found when using the CMIP5 model data to compare historic recharge to future time periods.

Overall, these studies conducted in the UCRB highlight the uncertainty with future recharge projections. There is considerable spatial heterogeneity throughout the UCRB with future recharge estimations, in addition to seasonal dynamics. However, projected increases in precipitation and temperature alone do not fully explain the spatially diverse projected changes in recharge and it would be useful to better understand the different drivers behind anticipated increases or decreases to future recharge.

8.2.1.2 Groundwater Discharge

The return of groundwater to the surface as discharge sustains rivers between precipitation events. This non-event portion of streamflow is often called baseflow and is important for river ecological health and water supply, particularly during drought periods. Since this water has passed through the subsurface, it is both older and more chemically complex than the streamflow derived directly from precipitation events. These characteristics of discharge are commonly used to quantify the fraction of streamflow derived from groundwater using age-dating and chemical separation techniques.

Recent studies indicate that, on average, greater than half of the annual streamflow in the UCRB comes from shallow subsurface flow paths or larger-scale groundwater flow paths (Miller et al., 2016). This estimate was from a combined modeling approach using site-specific conductivity mass balance results to calibrate a hybrid statistical-deterministic-geospatial model, called SPARROW (SPAtially Referenced Regression On Watershed attributes). The SPARROW models were then driven by statistically downscaled projections of future climate and runoff to estimate future baseflow (Miller et al., 2019).

Future baseflow delivered to local stream reaches decreased by approximately 10 percent under hot/dry climate scenarios; remained unchanged for median climate scenarios; and increased by approximately 10 percent for warm/wet scenarios. However, across climate scenarios, the models projected decreases in baseflow delivered to the outlet of the UCRB at Lees Ferry. Relative to historical conditions, baseflow at Lees Ferry decreases by 30 to 40 percent by the 2080s. These regional-scale decreases in baseflow are driven largely by increases in evapotranspiration associated with increased temperatures, offsetting any local-scale increases in baseflow due to increased precipitation (Miller et al., 2019). Further analysis of the dynamic watershed processes that drive these changes in discharge could be assessed using process-based models that explicitly account for groundwater/surface water interactions (Miller et al., 2016).

8.2.2 Lower Colorado River Basin

Projected changes to groundwater recharge in the Lower Colorado River Basin (LCRB) are quite different than those in the UCRB. The LCRB extends south from Lees Ferry, Arizona, all the way down into Mexico. A recent study (Tillman et al., 2020) investigated how future recharge patterns in the LCRB compared to the UCRB using the 97 CMIP5 projection ensemble and the SWB model as was done in Tillman et al. (2016a). Due to the unavailability of data in Mexico, Tillman et al. (2020) only included the portion of the LCRB that resides in the United States. The LCRB is substantially more arid than the UCRB with annual precipitation as little as 70 millimeters near Yuma, Arizona, and temperatures 45 to 50 degrees Fahrenheit warmer than the UCRB. In addition, seasonal precipitation patterns in the LCRB are very different than those in the UCRB where precipitation is fairly uniform throughout the year. In the LCRB, the majority of precipitation falls from the monsoonal storms in July and August, with the remaining precipitation falling from September to March.

In addition to climate, the principle aquifers in the UCRB and LCRB consist of different geologies. The principle aquifers in the UCRB are composed of permeable, moderately- to well-consolidated sedimentary rocks while the principle aquifers in the LCRB are basin-fill aquifers consisting of unconsolidated gravel, sand, silt and clay, or partially consolidated sedimentary or volcanic material (Tillman et al., 2020). Given these differences in the geologic attributes and the climate of the UCRB and LCRB, it is not surprising that substantial differences in projected recharge patterns were found between the two areas.

Historical climate data in the LCRB suggests a weak decreasing trend in precipitation from 1951 to 2015 (Tillman et al., 2020). Along these same lines, future projected precipitation in the LCRB is estimated to be the same as or slightly lower than precipitation during the historical

period through most of the rest of this century. Similar to projected temperature trends in the UCRB, temperature is projected to increase substantially throughout the remainder of this century. Therefore, with the combined projections of increased temperature (and increased ET) and decreased precipitation, groundwater recharge is projected to be substantially less than historic levels in the LCRB. Out of the 71 remaining decades (calculated as 10-year moving averages) in this century, 55 of those decades are projected to have less than the historical 25th percentile of recharge, which equates to 77 percent of the time (Tillman et al., 2020).

However, an important uncertainty projecting groundwater recharge using SWB is the lack of vegetation feedback to climate change. In particular, the SWB model does not simulate responses to changes in atmospheric CO_2 in terms of stomatal conductance and carbon assimilation, which may have various compensating effects on the ET response to temperature change (e.g., Dieleman et al., 2012).

8.2.3 American River Basin

The American River Basin Study (ARBS) is a project by Reclamation and a diverse set of partners that aims to identify vulnerabilities to future water resources under a changing climate in the American River basin. The American River basin is located from Sacramento, California east to the Sierra Nevada mountains and bounded by Bear River on the north and Cosumnes River to the south. Groundwater resources were investigated in two subbasins at the bottom of the foothills adjacent to Sacramento (the North and South American groundwater subbasins). Changes to groundwater storage were simulated using CalSim3 (CA-DWR, 2017), a water resources planning model, coupled to C2VSim (Brush et al., 2013), which is a spatially distributed groundwater model specific to the Central Valley. Calsim3 receives hydrologic inputs from the Variable Infiltration Capacity (VIC) model (Liang et al., 1994, 1996; Nijssen et al., 1997), which is a large-scale, semi-distributed hydrologic model that simulates the surface water balance at each grid cell, including infiltration and soil moisture storage, evaporation and transpiration, and surface runoff and baseflow. VIC was forced with five different climate scenarios, which were created using the same downscaled LOCA projections and hybrid-delta ensemble (HDe) methodology as the Eloy-Maricopa Stanfield Basin Study mentioned below (Reclamation, 2020a).

All of the developed climate scenarios for the ARBS indicate increasing temperatures through the end of the next century while the projected change in precipitation is less certain with wet scenarios projecting small increases in annual precipitation and dry scenarios projecting small decreases in annual precipitation. Due to the projected rise in temperatures, SWE, and potential evapotranspiration are predicted to decrease and increase, respectively. On the other hand, runoff is more similar to projected precipitation patterns, where the dry scenarios indicate a decrease in annual runoff while the wet scenarios suggest an increase in annual runoff by the end of the next century. These coupled changes between climate and hydrology in the ARBS study area will lead to projected changes in groundwater storage in the two lower elevation groundwater subbasins. Groundwater model results suggest that, under all future climate scenarios, the North American groundwater subbasin will experience a decline in groundwater storage. In the

South American groundwater subbasin, groundwater storage is projected to increase under wet climate scenarios and decrease under dry climate scenarios with the central tendency scenario suggesting a net loss of 300,000 acre-feet of storage by the end of the 20th century.

8.2.4 Salinas and Carmel River Basins

The Salinas and Carmel Rivers Basin Study (SCRBS) is similar to the ARBS described above, where Reclamation collaborated with other Federal agencies and local partners to identify water resource vulnerability under a changing future climate in the Salinas River basin and the Carmel River basin. The SCRBS also created multiple strategic portfolios demonstrating different water resource adaptations to combat potential imbalances between projected water availability and demand. The study area for the SCRBS is located along the coastline in central California and encompasses both the Salinas and Carmel River basins in addition to the Monterey Peninsula. Overall, the study area is approximately 4,500 square miles and has a population of around 370,00 people. The area is primarily known for its tourism and agriculture and is one of the most prominent agricultural areas across the Western United States. Despite multiple reservoirs and rivers in the study area, groundwater is a prominent source of water in the area. For example, San Luis Obispo sources nearly 80 percent of its water demand from groundwater and a recent transition from cattle ranching to irrigated agriculture has increased the groundwater demand. These supply and demand imbalances have led to declining groundwater levels and water supply challenges.

To address these water imbalances and plan for the future, the SCRBS developed five future climate scenarios (Reclamation and U.S. Geological Survey, 2020a) coupled to three future socioeconomic scenarios and modeled the change in groundwater levels under these future scenarios through the end of the 21st century (Reclamation and U.S. Geological Survey, 2020b). The SCRBS also modeled projected sea level rise as it has the potential to impact saltwater intrusion into adjacent groundwater aquifers within the study area. Future climate scenarios were developed using the transient HDe approach, which is similar to the HDe approach used in the ARBS and the Eloy-Maricopa Stanfield Basin Study, except that it also accounts for the time-varying evolution of projected changes in precipitation and temperature over the study area. The transient HDe methodology was developed and applied as part of the Sacramento and San Joaquin Rivers Impacts Assessment (Reclamation, 2014) and Basin Study (Reclamation, 2016b). The future sea level scenario was created by using one GCM projection that represented a conservative (“worst-case”) estimate of sea level rise in the area.

The future climate and sea level rise scenarios were used as input into four different hydrologic models that were used to analyze future groundwater conditions across three distinct areas within the study area. The first model used is called the Basin Characterization Model (BCM; Flint et al., 2013), which is a watershed model that can calculate daily watershed budgets. BCM includes a suite of pre- and post-processing tools that are used to map historical climate data and GCM projected climates onto a smaller grid using spatial-interpolation and downscaling methods. In this study, BCM is used to spatially-interpolate and downscale the climate scenarios and estimate potential evapotranspiration for the following three models.

The second model used is called the Hydrologic Simulation Program-Fortran (HSPF). HSPF is a semi-distributed, lumped-parameter model that simulates watershed flow and transport processes (Bicknell et al., 1997). HSPF simulates streamflow hydrographs, soil moisture, surface runoff, interflow, baseflow, evapotranspiration, groundwater recharge, channel routing, sediment and nutrient fluxes, and reservoir routing. The third model used is the MODFLOW – One-Water Hydrologic Model (MF-OWHM; Harbaugh, 2005). MF-OWHM integrates physically based flow processes, both natural and human-influenced, into a supply and demand framework. This software is well-suited to address conjunctive use, water management, water-food-security, and climate-crop-water scenario analyses. The fourth model used was GS-FLOW: Coupled Groundwater Surface-Water Flow Model (Leavesley et al., 1983). GS-FLOW is an integrated groundwater and surface water model that couples the U.S. Geological Survey (USGS) Precipitation-Runoff Modeling System (PRMS; Markstrom et al., 2015) with the USGS Modular Ground-Water Flow Model (MODFLOW-NWT; Niswonger et al., 2011).

Different models were used for three distinct areas within the study domain based on what models were already available for those areas: the Carmel River basin, the Salinas River basin, and the Paso Robles basin. GS-FLOW was used to model groundwater and surface water interactions in the Carmel River basin.

To simulate hydrology in the Salinas River basin, two different models were developed based on the four models outlined above. The first model is called the Salinas Valley Watershed Model (SVWM), which is a hydrologic modeling tool developed by the USGS to simulate streamflow responses to climate inputs across the Salinas Valley watershed, several smaller watersheds along the Monterey Bay coastline, and the Monterey Peninsula. In general, the SVWM combines the BCM and HSPF models to simulate the climate and hydrology for the upland areas and tributaries draining into the alluvial valleys, which are simulated by the following two models.

The second model is called Salinas Valley Integrated Hydrologic Model (SVIHM). The SVIHM was created by coupling the SVWM to MF-OWHM to create an integrated hydrologic model that accounts for the movement of water, including water management systems that re-distribute water supplies to meet urban, agriculture, environmental, and industrial needs.

Last, to model groundwater resources in the Paso Robles basin, the SCRBS used an existing integrated hydrologic model called the Paso Robles Basin Model (PRBM) and coupled it to SVWM to create the Paso Robles Integrated Hydrologic Model (PRIHM). This approach provided a consistent framework for addressing rainfall and runoff processes throughout the Salinas Valley watershed and presents future opportunities for evaluating sediment and nutrient transport processes. Similar to the SVIHM, the SVWM was used to develop inflows to the PRIHM stream network for each climate simulation. In addition, PRIHM was used with MF-OWHM to dynamically simulate climate and land use and associated agricultural demands, groundwater pumpage, and recharge.

Similar to the ARBS, all future climate scenarios in the SCRBS suggest an increase in annual average temperatures. Precipitation is less certain, with two dry scenarios indicating a decrease of up to 10 percent in annual precipitation and two wet scenarios indicating an increase of 10 to

20 percent in annual precipitation. In addition, the three future socioeconomic scenarios all suggest an increase in population and water demand of varying degrees. Sea level rise is also projected to increase substantially along the coastal regions, which could lead to saltwater intrusion among adjacent groundwater aquifers. Coupling these future climate results to the three socioeconomic scenarios and taking into account future sea level rise suggests that water resources, including groundwater, will become scarcer over the next century and imbalances between supply and demand will continue to grow. Groundwater modeling results using these future scenarios for the SCRBS are still being carried out and will lend insight into how different adaptation strategies might help mitigate future groundwater vulnerabilities.

8.2.5 Lower Santa Cruz River Basin

The Lower Santa Cruz River passes through Tucson, Arizona. The climate is hot and arid with recharge dominated by infrequent rain events during the fall monsoon season or winter months. Natural recharge in the area is not spatially distributed; but, is mostly confined to stream channels as rain events often cause surface runoff into channels rather than direct infiltration. The agricultural, municipal, and industrial water supply is dependent on groundwater and the Central Arizona Project, which imports Colorado River water to the region. Reclamation (2020a) studied changes in climate, streamflow, evapotranspiration, and soil moisture under two future climate scenarios using CMIP5 RCP4.5 and RCP8.5 emissions scenarios to span a range of possible future emissions. The study used these future estimates of precipitation and temperature to produce streamflow changes using the Colorado Basin River Forecast Center's Sac-SMA model. The streamflow projections are used to calculate changes in streamflow recharge for groundwater modeling efforts that assess the combined effects of changes in artificial and natural recharge, as well as other anthropogenic factors, such as groundwater pumping.

Climate scenarios consistently identify increases in temperature in the future in the Lower Santa Cruz River basin, with higher increases under the higher emission scenario. Precipitation changes are more variable than temperature. Under the lower emissions scenario, relatively minimal and inconsistent changes are projected in seasonal precipitation. In the worse-case scenario, total precipitation decreases in the monsoon and winter wet seasons. Precipitation becomes increasingly variable under projected future conditions. Soil moisture decreases, with the largest decreases in the spring months preceding the dry season under the higher emissions scenarios. Despite increases in temperature, evapotranspiration decreases due to limited soil moisture. The combination of these findings suggests a range of changes in streamflow and related risks to the sustainability of groundwater, infrastructure, and environmental systems.

The groundwater system in the area of the Lower Santa Cruz River basin is part of the Tucson Active Management Area. The groundwater model for the Tucson Active Management Area requires inputs of recharge, including recharge facilities, stream recharge, and mountain front recharge. While mountain front recharge will change with climate-driven changes in snow, precipitation, and evaporation, it was not the focus of this study and continues to be an active area of research. Preliminary estimates of stream recharge across the basin decreased by 40 percent under future climate conditions, although the change varies by stream. The basin

study did not explicitly address groundwater discharge to streams, but the number of days with no streamflow per month from the Sac-SMA model consistently increases in the higher emissions scenario, especially in April, May, and August. The loss of baseflow suggests decreases in groundwater returning to the stream under future climate scenarios. While the study basin largely consists of ephemeral or intermittent streams, these waterways are critical for supporting riparian vegetation and the associated wildlife habitat in the region. Longer periods without streamflow and potentially deeper groundwater levels would negatively impact these natural systems.

8.2.6 Eloy-Maricopa-Stanfield Basins

The Eloy-Maricopa Stanfield Basin Study is a project investigating the projected change in natural recharge in southern Arizona (Reclamation, 2020a). The study area is located south of Phoenix and north of Tucson and has a climate similar to the Lower Santa Cruz River basin. The two rivers of interest that contribute to natural recharge in the study area are the Gila River that enters on the northeastern part of the domain and leaves on the northwestern part of the domain and the Santa Cruz River that enters from the south with all flow infiltrating within the study area. Recharge from the Gila River is assumed to be the volume of water entering the domain minus the volume of water leaving the domain, while all water entering the domain from the Santa Cruz River is assumed to recharge. The challenge of modeling recharge from these two rivers lies in the fact that the Gila River flow is regulated by discharge from an upstream dam and the Santa Cruz River flow is primarily effluent dominated, except during large precipitation events.

In order to model future recharge in the Eloy-Maricopa Stanfield Basin Study area, a statistical relationship between historic annual streamflow and precipitation was developed for each river. Changes in annual temperatures did not explain any of the annual variation in streamflow, probably due to the flashy nature of the system and evaporation not playing an important role. However, a power function relationship (e.g., Crosbie et al., 2013) with annual precipitation was able to best explain the variance in streamflow for the Santa Cruz River. For the Gila River, it was found that a power law relationship with annual precipitation, combined with a linear relationship with total precipitation from the largest annual event, best explained the managed streamflow response. These relationships were then coupled to projected climate data to estimate the magnitude and trends in future natural recharge within the study area. Projected climate data was developed by using 64 downscaled LOCA climate projections (Pierce et al., 2014) of precipitation and temperature to develop five future climate scenarios using the HDe methodology (Hamlet et al., 2010).

Projected changes in climate in this southern Arizona basin suggest that, while the average annual change in precipitation over the next 80 years ranges between -1 to 2 inches, all climate scenarios indicate an increase in extremely wet or extremely dry years (above the 90^{th} percentile or below the 10^{th} percentile of annual precipitation, respectively). Given the power law relationship that was found between recharge events and annual precipitation, it is apparent that recharge events in this area primarily occur only during years with extremely high amounts of

precipitation. Therefore, in the future, there appears to be more years where natural recharge from streamflow infiltration contributes to aquifer storage for both wet scenarios. On the other hand, there are also more years where there is no natural groundwater recharge from streamflow due to the increase in extremely dry years in both dry scenarios. However, when using the HDe methodology to develop climate scenarios, the historic sequencing of events is preserved while the relative magnitude of the climate data is adjusted. That means the results from this basin study do not delve into whether or not there will be more consecutive wet years or more consecutive dry years. Future investigations should focus on investigating whether or not the sequencing of events might change and how this will contribute to aquifer storage.

8.2.7 Klamath River Basin

The Klamath River flows from south-central Oregon to the Pacific Ocean on the coast of California. The Klamath River Basin has many competing water uses resulting in imbalances in water supply and demand. Since 2001, groundwater pumping in the basin has increased to meet the range of water needs in the basin. As part of the Klamath River Basin Study (Reclamation, 2016a), Reclamation and partners evaluated the effects of climate variability and change on three groundwater basins in the Klamath River Basin. The study relied on global climate model (GCM) outputs from both Coupled Model Intercomparison Projects phases—phase 3, CMIP3 and phase 5, CMIP5. These projects include model results that encompass a range of potential futures. This study selected five climate scenarios to span this range, pairing temperature ranges from warm to hot with precipitation changes from wet to dry while including the central tendency of the projections.

In the Upper Klamath Basin, the groundwater evaluation used a previously developed groundwater model (MODFLOW) driven by perturbed inputs of recharge to groundwater and maximum evapotranspiration from groundwater. Maximum evapotranspiration consistently increased under a range of possible future scenarios, driven by increases in temperature. Recharge, calculated based on relationships with precipitation, also increased under the wetter precipitation scenarios, but suggested slight decreases under some dry scenarios. The scenario representing the central tendency of the available set of CMIP3 or CMIP5-BCSD-downscaled futures indicated increases in recharge from 3 to 11 percent. Increased precipitation drives the increase in recharge, with larger changes under the CMIP5 modeling scenarios and into the farther future. The groundwater system combines these compensatory effects of more water leaving the system through evapotranspiration and more water entering the system through increase recharge. For the central tendency, the increased recharge exceeded the increased losses, resulting in increased groundwater storage and discharge to streams, although some drier projections did indicate storage losses.

Storage increases were greater around the mountainous edges of the basin, with little projected change in the agricultural valleys. The two remaining basins (Scott Valley and Shasta) did not have groundwater models available at the time of the study. The study developed a groundwater screening tool which considers changes in basin-average groundwater elevation from changes in water availability, water demand, and management practices. The results of this statistical tool

similarly indicate that the increase in recharge from increased precipitation under future climate conditions may offset increases in evapotranspiration driven by higher future temperatures.

Neither the modeling approach nor the assessment tool fully account for changes in groundwater demands in the system. Furthermore, the study identified shifts in the timing and volume of snowmelt runoff and surface water flows. Feedbacks between the surface and groundwater systems are complex and challenging to capture. As a result, the study identified the development of a coupled groundwater-surface water model as a possible effort that would enhance understanding of climate change impacts on the Klamath River Basin.

8.2.8 Milk and St. Mary River Basins

The Milk and St. Mary River basins lie in northern Montana and southern Canada and are mostly comprised of rural and agricultural lands with numerous small towns scattered throughout. The climate in the area is typical of the northern Great Plains, with large seasonal variations. Summers are cooler and wetter in the higher elevations of the western part where snow can be observed during every month of the year. In 2012, Reclamation completed a basin study on the Milk and St. Mary River basins to address the imbalances in water demand and supply, which are mostly due to irrigation shortages (Reclamation, 2012c). In addition, the 2012 study investigated future climate projections and how changing climate conditions might alter future water demands and supplies in the region. Currently, Reclamation is updating the 2012 Milk and St. Mary Basin Study with the latest climate projections and surface hydrology models.

The Milk and St. Mary Basin Study uses a scenario approach to quantify water supply, demand, and management risk under current operating policies. Similar to other basin studies, these scenarios included projected future climate conditions compared to historical conditions; however, they also included paleo-reconstructed conditions that represented periods of extreme drought and pluvial events (extremely wet periods). Future climate scenarios were developed similarly to those in the Eloy-Maricopa Stanfield Basin Study and the ARBS in that they were developed using the HDe methodology and used the ensemble of 64 CMIP5-LOCA climate projections.

Streamflow calculated from each climate scenario were then input into a RiverWare model (Zagona et al., 2001) to evaluate current and future activities and conditions in the St. Mary River and Milk River basins. Groundwater was incorporated into the study analysis by way of return flows to rivers and streams in the RiverWare model. Return flows were calculated using unit response functions that are based on diversions and consumptive use by crops and phreatophytes. Therefore, return flows were connected to the different climate scenarios only in the sense that diversions and consumptive use are impacted by changes in precipitation and temperature. Results from the update to the Milk and St. Mary Basin Study are still pending at the time of this report.

8.3 Summary and Next Steps

Many of the studies highlighted in this report relied on multiple models, each capturing only portions of the hydrologic cycle (e.g., weather patterns, land surface processes, groundwater fluxes). This approach limits the ability to holistically investigate feedbacks between these systems. One such example is drawn from the Lower Santa Cruz River Basin Study, whose stakeholders were interested in climate-driven changes in riparian evapotranspiration. The amount of water returned to the atmosphere by near-stream vegetation will depend on climatic influences on the near-surface atmosphere, river levels, and groundwater depths. Models that couple these systems have large computational and input data requirements, often inhibiting the long runs needed to analyze climate trends.

Future work should address the need to bring the strengths of integrated modeling to climate change studies. One such program that aims to close this gap is the National Science Foundation's Convergence Accelerator program that funds projects that shorten the time between research and practice. As part of the Convergence Accelerator program, Reclamation is working on an upcoming project to couple machine learning around an integrated groundwater-surface model. This effort aims to facilitate long-term simulations of the hydrologic cycle from the land surface through the groundwater system.

Improvements in estimations of projected precipitation will undoubtedly improve estimates of the influence of climate on groundwater systems. In addition, models used, for example the SWB to estimate groundwater recharge, lack vegetation feedback effects on climate change. A full literature review on combined effects of atmospheric CO_2 and temperature on transpiration from different plant types would point to the need to address this topic in future regional projections of ET and associated groundwater recharge. As mentioned above, this includes higher resolution climate modeling to capture convective events that drive both diffuse and convective events. This also includes better understanding of mountain precipitation and flow paths to valley aquifer systems. As modeling of future precipitation and temperature improves, the groundwater community must keep pace to improve estimates of groundwater storage in the Western United States.

8.4 Key Findings

Consistent groundwater recharge and discharge analysis West-wide is not available; therefore, only case study-specific findings were documented in this chapter. However, for the Colorado River Basin—Upper Colorado River Basin (UCRB) and Lower Colorado River Basin (LCRB)—results from a multi-year collaboration effort with the USGS are available. This analysis was completed using the 97 CMIP5 projections that were statistically downscaled using the Bias Correction and Spatial Disaggregation (BCSD) method. Key findings from the studies in the Colorado River Basin are listed below:

- Historical (1896 to 2019) precipitation and temperature data for the Upper and Lower Colorado River Basins were analyzed to better understand recent trends in climate data that may affect groundwater resources in the area.
    - Historical data indicate multidecadal-scale cyclical patterns in precipitation in both the UCRB and LCRB. Although UCRB precipitation had no statistical trend over the recent historical period, the LCRB had a weak negative trend over this period. Multidecadal-scale cyclical patterns in temperature also are observed in historical climate data in both the UCRB and LCRB, at least until the early 1970s. Beginning at that time, both the UCRB and LCRB experienced strong, monotonic positive trends in temperature.
- Projected climate data from 97 CMIP5 ensemble members across the full range of RCPs from water years 1951 through 2099 were evaluated to understand what current climate models are projecting about future conditions in the Colorado River Basin, and what this might mean for groundwater systems in the region.
    - Precipitation in the UCRB is projected to increase throughout the rest of the century, rising to 6 percent above the 1951 to 2015 historical period by mid-century and to 9 percent above the historical period by the end of this century.
    - Temperature in the UCRB also is projected to be above the recent historical median throughout the rest of the century, with steady warming in decadal average temperatures expected until the last quarter of this century.
    - In contrast to projected precipitation in the UCRB, precipitation in the LCRB is projected to be the same as, or slightly less than, the historical period throughout most of the rest of this century.
    - Like projected temperature in the UCRB, temperature in the LCRB also is projected to be above the recent historical median throughout the rest of the century.
    - Comparing median projections for all future decades with median results from all historical decades, future precipitation is expected to be greater than that of the past in the UCRB, though no significant difference is projected for precipitation in the LCRB. Significant (at 5 percent significance level) increases are expected in temperature in both the UCRB and LCRB. In general, projections of future precipitation are more variable and less certain than those for future temperature.
- To estimate the effects of projected precipitation and temperature on groundwater systems in the region, results from the 97 member CMIP5 climate projection ensembles were used as input in a Soil-Water Balance (SWB) groundwater infiltration model for the Colorado River Basin.
    - SWB simulation results indicate that the UCRB is expected to experience decades of above-historical-average groundwater infiltration through the end of the century.

  - For the LCRB, simulated groundwater infiltration is projected to be consistently less than the recent (1951 to 2015) historical period for most of the remaining century.
  - A comparison of the distribution of all median simulated groundwater infiltration results between recent historical and future periods indicates projected groundwater infiltration in the UCRB is significantly (at 5 percent significance level) greater over the combined 2020 to 2099 future period than the recent (1951 to 2015) historical period. Moreover, in 41 of 71 (58 percent) possible future decades (calculated as 10-year moving averages) in this century, groundwater infiltration is projected to be greater than the 75th percentile of historical simulated groundwater infiltration.
  - Projected groundwater infiltration in the LCRB across all future decades is significantly less than in the historical period. Of the 71 future decades in the century, projected groundwater infiltration in the LCRB is expected to be less than the 25th percentile of historical infiltration in 55 (77 percent) of the 10-year periods.
  - Important differences in projected precipitation between the upper (increasing precipitation) and lower (decreasing precipitation) basins largely drive the different responses of simulated groundwater infiltration in the upper (increasing infiltration) and lower (decreasing infiltration) basins.

- Finally, considering the uncertainty inherent in projected climate data, coarser spatial and longer temporal scale input data may be sufficient for water resources managers who need to understand changes in trends in groundwater recharge over water-year or longer time periods.

9 Uncertainties

Water managers make decisions every day that are based on less-than-perfect knowledge of future conditions. Drawing on these experiences, while knowing more about the nature of the uncertainties of the information (described throughout this chapter), can help in navigating future change—an effort broadly classified as decision-making under uncertainty.

It is helpful to recognize at the onset that within science uncertainty analysis is a process that helps identify a range of possible outcomes, adding important context and understanding to information presented. It is often categorized in two ways: uncertainty that will always exist (e.g., inherent randomness natural to a process), known as aleatory uncertainty, and uncertainty that can be reduced with improved process understanding or data (e.g., improving model structures or parameters, improving quality of observations), known as epistemic uncertainty (O'Hagan, 2004). Climate and hydrologic evaluations, including those in this report, have both types of uncertainty; therefore, one should not expect that advances in climate, hydrology and paleohydrology science can entirely eliminate uncertainty. However, there is inherent value in knowing more about the possible range of the decision variables (e.g., annual or seasonal streamflow magnitudes) for water managers, which is what uncertainty analysis can provide.

This chapter provides perspective on potential sources of uncertainty in this report's climate and hydrologic projections and paleohydrology evaluations. This perspective builds on past reports. Since the first SECURE Water Act Report, the data, and tools available for evaluating impacts of projected future climate on water supplies throughout the West have evolved and improved in many ways. Reclamation has consistently pursued evaluations using current science that provide updated models accompanied by a range of projections that characterize certain aspects of uncertainty. This started in 2011 with CMIP3 climate projections using a single statistical downscaling approach, the BCSD approach (Reclamation, 2011b). In 2016, this evaluation broadened to using CMIP5 projections and the same BCSD statistical downscaling approach (Reclamation, 2016c). In 2021, as outlined in this report, CMIP5 projections were used with an alternative statistical downscaling approach called LOCA, in conjunction with other assessment methods, including ones that leverage paleohydrology data.

The assessment methods used in this report provide many robust insights into hydroclimatic variability in the recent past, the more distant past through paleohydrology, and changes projected for the future. This diversity of techniques to evaluate water supply reliability collectively provide a more robust analysis, especially when these different techniques reveal similar conclusions. For example, future climate projections and paleohydrology are two complementary types of information that both help to understand and prepare for conditions outside of those seen in the instrumental period. Future projections of streamflow rely on a suite of models—GCMs, downscaling methods, hydrology models, and river routing models—to reveal how increases in greenhouse gas concentrations influence hydroclimate processes. Alternatively, paleohydrology reconstructions use dendrochronology—the science of using tree-

rings to better understand the climate of the distant past. These reconstructions analyze tree-ring cores, correlate those cores to stream gage and hydroclimate records via statistical models and estimate what this reveal about past hydroclimate across the Western United States.

Together, these approaches can give broader context to the questions of what hydroclimate states have occurred in the recent or distant past that could occur again, and what do future projections suggest, outside of hydroclimate conditions experienced in the recent or distant past. Both of these analyses (paleohydrology and future projections) require unique tools and models, which have associated uncertainties across the analysis steps. Collectively, using multiple approaches broadens the understanding of possible future conditions and allows for a more informed risk-informed decision-making framework to support robust water resources planning in the West.

The analyses in this report are designed to be used in a risk-informed decision-making framework. They follow methods documented in peer-reviewed literature and are supported by leading researchers and practitioners in Federal agencies and research institutes across the United States. Because of the amount and nature of the uncertainty in future hydroclimate projections, however, it is also appropriate to consider concepts and techniques that provide decision makers with actionable information that does not rely on probabilities, using a subfield of decision science that deals with a deeply uncertain future. Deep uncertainty arises when, among other factors, the likelihoods of future conditions cannot be stated with confidence, and when experts do not agree on the most appropriate way to represent complex interactions between factors influencing a planning context (Lempert et al., 2003; Marchau et al., 2019).

In essence, the scientific and engineering knowledge base contributing to impact assessment methods is steadily evolving. Ongoing research, described throughout this chapter, offers insights into the potential uncertainties of the methods used in this report and should be considered as findings are interpreted.

9.1 Future Projections

Chapters 2 and 3 describe the future projections used in this report. These projections use GCMs generated as part of CMIP5, multiple emission scenarios (RCP4.5, RCP8.5), and are downscaled using the LOCA statistical downscaling approach. This section provides additional context on the implications of these model choices within climate science broadly and describes the uncertainties inherent in projecting future hydroclimate conditions.

Uncertainties in future projections stem from the inability to predict future global sociopolitical developments, incomplete understanding of complex system processes, imperfect representation of those processes in models, and irreducible natural variability. Numerous decisions must be made to generate usable projections, and each has associated uncertainties: choice in scenarios of greenhouse gases (uncertainties in human behavior); choice of models used for global climate simulation; choice of model initial conditions; choice of climate downscaling techniques; and, choice, configuration, and calibration of hydrologic models, as examples. The quantitative implications of all of these decisions aggregate to represent the overall uncertainty in

characterizing projected future climate impacts. Clark et al. (2016) presents the steps in developing hydrologic projections, starting with climate modeling, moving through climate downscaling, and finally applying hydrologic modeling and identifying areas of uncertainty.

The next sections provide an overview of characterizing and analyzing uncertainty in four broad areas, namely, (1) climate modeling, including use of GCMs, scenarios of greenhouse gas concentrations, and internal climate variability, (2) climate downscaling, (3) hydrologic modeling, and (4) highlights from ongoing research aimed at mitigating the challenges of planning under deep uncertainty.

9.1.1 Climate Modeling

Climate modeling includes multiple sources of uncertainty, which are often described as GCMs, greenhouse gas concentrations scenarios (also referred to as emission scenarios), and internal variability, described in detail below. The influence these uncertainties have on future projections varies depending on region and time horizon. For example, when analyzing regional temperatures from CMIP3 models, Hawkins and Sutton (2009) found uncertainty in future projections related to internal climate variability is greater in the near future, whereas uncertainties due to greenhouse gas concentrations and climate model selection is larger at the end of the 21st century.

9.1.1.1 Global Climate Models

A key source of uncertainty in climate impacts assessments lies in the structure of global climate models, or GCMs. This report relies on the same GCMs that were used to inform the West-Wide Climate Risk Assessment of the 2016 SECURE Water Act Report (Reclamation, 2016c). This generation of GCMs, namely CMIP5, have more detailed representations of Earth systems in terms of spatial detail and representation of physical and biogeochemical processes than the CMIP3 generation of GCMs used in the West-Wide Climate Risk Assessment of the 2011 SECURE Water Act Report (Reclamation, 2016c). For that reason, many GCMs have come to be termed Earth System Models.

While the CMIP5 generation of GCMs agree better with global observations of temperature and precipitation (Knutti et al., 2013), Earth System Models continue to have irreducible uncertainties like internal climate variability (Bishop and Abramowitz, 2013; Knutti and Sedlácek, 2013). Diversity in GCMs offers an information resource that can be used to define alternative climate change narratives for the water resources sector (Brekke et al., 2009).

GCM projections are based upon initial model states, assumptions of future greenhouse gas concentrations in the atmosphere, and internal as well as external forcings, such as solar radiation and volcanic activity to name just a few. Changes in land surface, atmosphere, and ocean dynamics, as well as how such changes are best modeled in GCMs, continue to be areas of active research. Depending on how these and other factors are represented within each GCM, projected future conditions, such as the magnitude of temperature and precipitation changes, may vary.

However, the degree to which the magnitude of GCM-simulated warming agrees with historical observations varies based on the data, methods, and time periods used for making such comparisons, where some studies find more GCM warming (Santer et al., 2017) while others show warming rates more in line with observations (Lin et al., 2016; Richardson et al., 2016). GCMs continue to be refined, including how to characterize model outputs and observations, and how measurement errors, internal variability, and model forcings can be improved to enhance future model performance (Lin et al., 2016).

Climate modeling is inherently uncertain due to climate system feedbacks and the chaotic evolution of system states. As such, inter-model differences are expected (Hawkins and Sutton, 2009), and multi-model estimates of uncertainty are a critical component of many climate impact assessments (Brekke et al., 2009). Not all models are created equal and carefully rejecting, or giving less weight to, models that have an inadequate representation of Earth-system processes or climate system dynamics is often desired, but challenging to do (Knutti, 2010; Knutti et al., 2010) and does not necessarily lead to a reduced range in projections. The research community is working to develop methods for meaningful multi-model combinations (Mote et al., 2011; Bishop and Abramowitz, 2013; Evans et al., 2013; Abramowitz et al., 2019), but this effort is a complicated, application-specific challenge because some models have more relevance and skill depending on assessment questions.

9.1.1.2 Scenarios of Greenhouse Gas Concentrations

While there is inherent uncertainty in future projections, there is high confidence in the science community's understanding of the greenhouse effect and the knowledge that human activities are changing the climate in unprecedented ways. Reclamation has consistently relied on a broad range of possible climate scenarios when assessing the risks and impacts from climate change. The NCA4 identified RCP4.5 and RCP8.5 as the core scenarios representing an appropriate range of future conditions, stating "NCA4 focuses on RCP8.5 as a 'higher' scenario, associated with more warming, and RCP4.5 as a 'lower' scenario with less warming. Other RCP scenarios (e.g., RCP2.6, a 'very low' scenario) are used where instructive, such as in analyses of mitigation of science issues" (USGCRP, 2018).

Reclamation's use of a range of RCPs—without assigning probabilities to any individual climate modeling experiment—reflects Reclamation's commitment to understand uncertainties associated with future projections and identify a range of possible outcomes consistent with the current state of the practice in water resources climate impact assessments. This adheres to the requirements in P.L.111-11 (§9503(b)(1)) to use, "the best available scientific information with respect to presently observed and projected future impacts of global climate change on water resources. …" Furthermore, NCA4 future projections currently constitute nationally available scientific information that has been extensively reviewed by Federal and non-Federal experts.

9.1.1.3 Internal Climate Variability

Another source of uncertainty stems from internal climate variability, which is often thought of as equivalent to year-to-year and decade-to-decade natural variability. It has long been

recognized that the climate system evolves in a chaotic way (Lorenz, 1963), meaning that small perturbations in atmospheric initial conditions cause large differences in the trajectory of future climate simulations (Deser et al., 2012a; Deser et al., 2012b). The differences among different initializations of the same model can be attributed to internal climate variability, as distinct from any model error (Tebaldi et al., 2011). In most climate impact assessments, internal climate variability is represented using the ensemble of opportunity described as individual simulations by various GCMs and often several simulations of the same GCM with differing initial conditions.

In an effort to explore and understand the consequences of relying on such ensembles, Kay et al. (2015) explicitly characterized the uncertainties associated with internal climate variability in a series of simulations of the Community Earth Systems Model (one of many Earth Systems Models included in CMIP5). Early results demonstrated the influence of internal climate variability on 20th to 21st century climate trajectories. Internal climate variability, as seen in multiple runs of a single GCM, can produce projection spread comparable to that in CMIP5 GCMs collectively. While internal variability can have a big influence on values in a particular year or decade, the overall climate change signals are not changed, establishing that GCMs work properly in their overall response to climate change.

9.1.2 Climate Downscaling

It is important to recognize that many of the outputs from climate models validate better against observations at continental to global scales than at local to regional scales and may not capture regional or watershed-level metrics well. For example, because their spatial grid resolution may be on the order of one-degree latitude/longitude, some GCMs may not capture the orographic effects associated with certain mountain ranges (e.g., the Cascade Mountains of Washington). Accordingly, techniques must be employed to localize or "downscale" GCM output for applications such as basin-specific water resources planning studies. Ultimately, the downscaled projections of climate are used as inputs to hydrologic models to produce projected streamflow, which are then used to assess impacts to the water resource system in question.

Of note, the primary difference in future climate projections presented in this report compared to the West-Wide Climate Risk Assessment of the 2016 SECURE Water Act Report is the use of the statistical downscaling method called LOCA (LOcalized Constructed Analogs) as a compliment to the BCSD (Bias Correction and Spatial Disaggregation) statistical downscaling approach used in earlier reports.

Uncertainties exist at each of the steps necessary to translate GCM output to water resources impacts. Uncertainties in the downscaling process can result in variations depending on the modeling technique used. While the current and past SECURE reports have focused on two statistical approaches (see Vano et al., 2020 for a detailed comparison), a large variety of downscaling methods exist, including: (1) statistical methods that make use of the climate model circulation patterns (Fowler et al., 2007; Wilby et al., 2014) or incorporate physically based dynamical considerations (Jarosch et al., 2012); (2) dynamical downscaling approaches

(Giorgi, 1990; Rasmussen et al., 2014), and, more recently, (3) hybrid approaches that combine elements of statistical and dynamical methods (e.g., Gutmann et al., 2016).

The statistical downscaling methods traditionally used by the water resources sector in the United States, as in this report, have involved rescaling the precipitation and temperature outputs from the climate model using a statistical model (Wood et al., 2004; Hidalgo et al., 2008; Stoner et al., 2013). Such methods vary in the degree to which they preserve the change signal produced by the climate model itself (Pierce et al., 2015), which some users view as a requirement. These statistical approaches often have weaknesses in their representation of hydrologically important meteorological features, such as the time-space scaling of storm characteristics (Maraun, 2013; Gutmann et al., 2014).

Reducing uncertainty in the downscaling process will be difficult, but progress can be made through improvements in computational power, systematic evaluation of existing downscaling methods, and the removal of poorly performing methods. For example, for an application that depends on the proper representation of precipitation in the mountains, it may be reasonable to remove methods that rely on climate model precipitation if that climate model does not have a representation of those mountains due to its coarse spatial resolution. If, in this case, multiple downscaling methods that provide a better representation of orographic effects all provide a similar answer, the resulting uncertainty can reasonably be reduced.

Depending on the application, it is also possible to select methods for their ability to produce either unbiased information (Teutschbein and Seibert, 2012), or a proper representation of extreme events or spatial scaling characteristics (Gutmann et al., 2014). Improvements in computational capacity also have the potential to reduce uncertainties in regional climate modeling as these improvements lead to the ability to run models with convection permitting scales (Kendon et al., 2014; Rasmussen et al., 2014). At these scales, it is possible to explicitly resolve convection, thus reducing one source of uncertainty. Finally, one of the most important pieces to evaluate for any climate change assessment is the ability of the methods to represent the changes most relevant to identified management concerns, though how best to do this is still not yet established.

Differences between future projections presented here based on the LOCA downscaling method and in the 2016 SECURE Water Act Report based on the BCSD method are described in detail in a Technical Memorandum, *Comparing Downscaled LOCA and BCSD CMIP5 Climate and Hydrology Projections* (Vano et al., 2020). In general, these two methods provide generally similar results, both in relation to their historical comparisons and future projections. There are, however, locations and variables where differences arise. For example, in the Canadian portion of the Columbia, precipitation declines in LOCA relative to BCSD result in lower ET, runoff, and SWE in hydrologic model output, which can be attributed to the observation datasets used.

9.1.3 Hydrologic Modeling

Hydrologic models translate downscaled temperature and precipitation into relevant water management variables like snowpack and runoff. In this report, Reclamation presents a range of projected future hydroclimate variables measured using the central tendency (ensemble median), and the 10th and 90th percentile bounds from the 64-projection ensemble. These help in providing a lower and upper bound of hydroclimatic change possibilities through time for this analysis. The 2011, 2016, and 2021 SECURE Water Act reports all use the Variable Infiltration Capacity (VIC) macroscale hydrology model, although the model version has advanced and spatial resolution has been further refined over the years. Relative to changes in emission scenarios, GCMs, and downscaling techniques, the differences in future projections because of VIC versions or resolutions between the 2016 and 2021 reports are small (Vano et al., 2020).

Choices made in hydrological modeling can influence results and are being researched at Reclamation and elsewhere. Commonly for long-term water supply planning studies (e.g., basin studies) performed by Reclamation, an evaluation is done to select an appropriate surface hydrologic model to use to simulate runoff (Broman and McGuire 2020; Brekke, 2010). A selection may be made based on available existing models for a region or the ability of a model to represent relevant hydrologic processes, though results of these processes have not been highlighted in this or past SECURE reports.

An important result in research on the hydrologic impacts of climate change is that the portrayal of climate change impacts depends on the decisions made on the selection, configuration, and calibration of hydrologic models (Wilby, 2005; Miller et al., 2012; Vano et al., 2014; Mendoza et al., 2015). In one of the earliest studies, Wilby (2005) demonstrated that parameter uncertainties have a large impact on the portrayal of climate change impacts. Subsequent work has demonstrated that the portrayal of climate change impacts also depends on the choice of hydrologic models and on specific decisions made in model calibration (Miller et al., 2012; Vano et al., 2014; Mendoza et al., 2015). For a variety of reasons, hydrologic model calibration often receives inadequate attention in climate change impact assessments, with potential first-order effects on the estimation of future hydrologic responses.

The uncertainties in hydrologic modeling stem from both algorithmic simplifications of hydrologic theory and data limitations (Clark et al., 2016). Considerations of parsimony may compel modelers to neglect specific processes (e.g., groundwater-surface water interactions, carbon fertilization). Moreover, data limitations constrain the extent that it is possible to adequately capture the details of the landscape, and especially, define appropriate model parameter values. Specifically, inter-model differences occur because different modelers have made model development decisions in different ways, as manifested in different spatial discretizations, process parameterizations, model parameter values, and time-stepping schemes (Clark et al., 2011). It is now possible to use multiple hypothesis-modeling frameworks to deliberately and systematically characterize uncertainties in physically motivated hydrologic models (Clark et al., 2015a; Clark et al., 2015b; Clark et al., 2015c), and such work will be important to improve the realism of the portrayal of climate risk.

It is important to acknowledge that the current analytical approach used provides only a limited view of the uncertainty space. For example, the trend toward using multiple hydrologic models rather than a single model (the standard approach for many prior studies, as well as this one) has confirmed that a single hydrologic model selection erroneously narrows the final projection uncertainty space by failing to represent the hydrologic sensitivities that would be estimated through different modeling choices. As the impact assessment community continues to formulate strategies toward reducing projection uncertainty, it is nonetheless important to better understand the possible sources of uncertainty, which likely are more substantial than the present approach assumes.

The opportunities to reduce uncertainty in hydrologic modeling relate to the configuration and calibration of hydrologic models. Reducing uncertainties associated with model configuration requires that models appropriately represent dominant processes, because neglecting processes (e.g., groundwater-surface water interactions, or carbon fertilization) or over-simplifying process representations (e.g., temperature index snow models, or temperature-based representations of potential evapotranspiration), can lead to biased portrayals of climate change impacts (Milly and Dunne 2011; Lofgren et al., 2013). For example, Sheffield et al. (2012) demonstrated that trends in global drought are exaggerated when using temperature-based representations of potential evapotranspiration. Efforts to reduce uncertainties through increases in model complexity may in fact increase inter-model differences. Such changes in the portrayal of uncertainty should not be viewed as an increase in uncertainty, but, rather, increases in inter-model differences simply reveal uncertainties that have always been present.

The most accessible opportunity to reduce uncertainties is through the judicious selection of model parameter values (i.e., parameter values that are either specified *a priori* or inferred through model calibration). Yet, there are two challenges associated with this task, other than the investment of time and effort. The first challenge is the realism of calibrated models for individual basins. Mendoza et al. (2016) demonstrated that model calibration can substantially reduce projected change uncertainty and is an important aspect of hydrologic simulation. However, decisions made during model calibration can lead to appreciable differences in the portrayal of climate change impacts. These problems stem from parameter interactions and compensatory errors associated with traditional calibration objectives (e.g., a singular focus on daily streamflow errors), suggesting that more work should be focused on diagnostic, multivariate, and multi-objective approaches to parameter estimation so models get the right answers for the right reasons (Gupta et al., 2008).

The second challenge is the difficulty in defining spatially consistent model parameters over large geographic domains (Archfield et al., 2016) in the face of sparse hydrologic observations. In many continental domain applications, estimates of model parameters can be highly uncertain (Mizukami et al., 2017), where parameters are typically specified *a priori* to default values, or parameter maps are patched together from independent, uncoordinated calibration efforts. Such continental-domain parameter estimates can be improved substantially through the application of scale-aware parameter regionalization methodologies (Samaniego et al., 2010), a notable research advance.

Another hydrologic modeling element worth mentioning is that the choice of historical meteorological dataset, the dataset on which a hydrologic model is calibrated, can also play a role in how sensitive different locations are to changes in temperature and precipitation (Elsner et al., 20l4; Vano et al., 2020).

In summary, the consideration of hydrologic model selection, individual basin calibration and large-domain parameter estimation techniques, and an awareness of meteorological datasets used in the modeling process support considerations for multiple sources of uncertainty in long-term planning studies. An awareness of how these choices affect modeling results can build knowledge of, and at times reduce, uncertainties associated with representing hydrologic processes.

9.1.4 Deep Uncertainty in Hydroclimate Projections

The content above describes the implications of, and research into, processes and choices required to translate global climate projections into practical inputs to system planning models. The purpose of this work is to enable exploration of how potential future changes may challenge water resources management. This approach to impacts assessment can be considered "top-down" (Dessai and Hulme, 2004), wherein a set of futures is developed as a representation of the range of potential future conditions and used to probabilistically describe future system risks. Under climate change, and the complicated steps necessary to translate climate change signals to regional streamflow, relying on probabilistic analyses to make decisions can be problematic. These systems are subject to conditions of deep uncertainty, described as situations where conditions external to, but impacted by, a planning context cannot be confidently described as more or less likely, and there is disagreement among experts about how to represent complex interactions that affect planning (Lempert et al., 2003; Marchau et al., 2019), and thus it is prudent to recognize the need to explore alternative planning paradigms.

In the case of projecting future climate risks to water resources systems, the first factor, difficulties in placing likelihoods, is applicable because of the impossibility of determining the most probable future trajectory of global greenhouse gas concentrations. The second factor, disagreement among experts, is demonstrated by the large number of GCMs that do not agree and the subsequent downscaling steps that are all subject to philosophical and methodological choices and are undergoing continual research and development.

Due to this unresolvable deep uncertainty, it is advantageous to use a "bottom-up" approach in planning with climate change data. Bottom-up approaches (Dessai and Hulme, 2004) begin with a foundation of extensively testing a system to determine external conditions that result in poor or unacceptable performance (i.e., identifying vulnerabilities). In water resources planning, vulnerabilities could be tied to, for example, a certain reduction in streamflow compared to historical volumes, a certain level of demand growth, and specific downstream flow constraints, among others. Through various processes and types of analysis, and with varying levels of certainty, these can be translated into monitorable conditions or scenarios, such as, temperature increases, wildfires, or policy developments.

A critical advantage of "bottom-up" approaches is that planning outcomes and risk perceptions are not contingent on assumptions made at the beginning of a planning process about modeling inputs, which rely on imperfect data at best, or deeply uncertain data at worst. Instead, planning is based on actionable information that more readily supports monitoring and incrementalism with the goal of making robust decisions that perform acceptably well across a wide range of potential futures.

Decision-making under deep uncertainty (DMDU) is a subfield of decision science that has developed methods, processes, and tools to implement the bottom-up paradigm and mitigate the challenges of planning under deep uncertainty. DMDU is an active area of research and practice (DMDU Society, 2021), with applications across many sectors including defense, energy policy, and disaster preparedness (Marchau et al., 2019; DMDU Society, 2021). Water resources planning and management is one of the most prominent focus areas (Lempert and Groves 2010; Herman et al., 2015; Kasprzyk et al., 2013; Brown et al., 2012; Haasnoot et al., 2003; Groves et al., 2021), and Reclamation has undertaken several studies that explore or apply DMDU methods (Reclamation, 2012b; Alexander, 2018). Expanding awareness of deep uncertainty and increasing knowledge and applications of DMDU methods will be an important component of Reclamation's future activities related to assessing and adapting to climate change impacts.

9.2 Paleohydrology Information and Reconstructions

Chapters 4, 5, and 6 highlight the use of paleohydrology in this report. Paleohydrology uses climate information recorded as growth variability in tree rings to reconstruct variability in past climate.

Here, tree ring measurements serve as proxy records for moisture conditions of the past that allow estimations of streamflow through a statistical relationship between observed tree growth and naturalized records of gaged streamflow. Incorporating long paleohydrologic records into water resource studies can inform decision-making by adding important information on past conditions that are not captured in recent observational records; however, some uncertainties arise when using paleohydrology. This uncertainty stems from both methodological choices inherent to the technique as well as a limited understanding of how past variability characteristics will persist under changing future climate conditions. These uncertainties are discussed in greater detail below.

Two sets of paleohydrology information based on tree-ring chronologies were used in this report. The two sets are: reconstructed drought index, summer (June-July-August) season Palmer Drought Severity Index (PDSI) (Cook et al., 2010), and water-year annual reconstructed streamflow (Rice et al., 2009; Martin et al., 2019; Littell et al., 2016). These reconstructions of PDSI and streamflow were used in conjunction with instrumental (mostly 20th century) and climate projection (21st century) information in a range of analyses. The analyses included using the PDSI index directly in a long-term drought analysis (Chapter 4), analyzing severe sustained and flash droughts using reconstructed streamflow (Chapter 5), and identifying significant

drought events in the reconstructed streamflow record that reflect particularly challenging conditions that can be used to assess water supply reliability with water resources system models (Chapter 6). In the following paragraphs, uncertainties related to developing and assessing reconstructions broadly, and streamflow reconstructions specifically, are discussed.

Fundamentally, there is uncertainty associated with correlating tree-rings with annual streamflow using a statistical model. The steps in developing the chronologies include, selecting appropriate sites for trees, developing the tree-ring chronologies from the sampled trees' annual tree-rings, and developing the empirical models between chronologies and annual flows.

The chronology development methods, going from interpreting raw measured ring widths (from tree stands and even wood laying on the ground) to representative chronologies have methodological choices associated with them, and those choices are not universal. Though the tree-ring chronologies developed by the team that worked on this report largely use approaches consistent with the common practices in dendrochronology, there are some differences in the broader dendrochronology community in terms of objective approaches to building chronologies.

The choice of statistical modeling approaches also vary, and the observational data of natural streamflows used in the statistical modeling can be uncertain. For some locations, model-derived natural streamflow is also used, and such reconstructions inherit the uncertainties present in the hydrology models used to develop the natural flow estimates. Other factors that contribute to uncertainty can also include the fact that as one goes further and further back in time, the number of trees available to develop chronologies decreases. Thus, there is a sample-size consideration that factors into developing the reconstructions. Potential uncertainty associated with low sample sizes are typically addressed by first assessing the climate signal quality over the length of chronologies themselves (Briffa and Jones, 1990) and secondly by choosing the starting year of the reconstruction based on adequate verification skill of the reconstruction model as determined by the availability of chronologies over time. In this report, the drought analysis with reconstructed PDSI used 1473 as the starting year and analyses with streamflow data used 1685 as the beginning year to identify drought events. While this study uses previously published reconstructions, it is standard practice to thoroughly describe the methodological choices made and both minimize and provide the uncertainty bounds for all reconstructed values. While the reconstructions listed in Table 2 were not yet published at the time of this report, streamflow reconstructions in the Milk and St. Mary River basins were developed following the approach described in Martin et al. (2020) and reconstructions in the Columbia River Basin were developed following the approach of Gedalof et al. (2004).

In addition to the analytical aspects of developing reconstructions, there are fundamental environmental aspects to the growth of the trees. The sensitivity of tree growth to climate can fluctuate over time and some trees switch between temperature and moisture sensitivity. In the case of streamflow, trees tend to be more skillful at recording dry conditions than very wet conditions. These challenges can be partially addressed by first screening chronologies prior to their use in reconstruction models to ensure they contain a consistent climate signal of interest (for example, are well correlated with local precipitation records, e.g., Martin et al., 2019).

Issues of switching climate sensitivities can also be partially addressed in the model verification process by identifying models that fail to capture defined shifts in climate conditions (Briffa et al., 1988).

Furthermore, some regions have better coupling between tree growth and climate than others across the West. For example, the Upper Colorado River Basin has a strong tree growth-climate relationship (e.g., higher skill, measured using correlation), but in the Missouri River Basin, this relationship can be less direct, resulting in skill that is not uniform across the West. The uncertainty associated with the strength of the climate-growth relationship of a region can largely be understood using the reconstruction statistics that quantify reconstruction skill.

Events such as wildfires, floods, and particular insect activity leading to defoliation can be hard to detect and differentiate from climate. However, stand-level uncertainties like fire or insect activity are minimized as much as possible starting at the level of producing a climate sensitive chronology, but also in the statistical methods employed to develop the reconstructions. The most robust methods against stand level disturbance usually employ linear multi-variate methods like Principal Component Analysis (PCA) to summarize common growth signals across many chronologies. The least robust methods to this potential problem use only a few individual chronologies in a regression-based reconstruction framework. However, generally, before final reconstructions are accepted, the selected predictor chronologies are checked for obvious signs of stand-level disturbance. In summary, uncertainty from stand-wide disturbances in any individual streamflow reconstruction would be expected to be quite small.

Probabilistic interpretations of flow reconstructions are needed because of uncertainty stemming from limitations of the basic data, from the reconstruction process itself, and from the choice of analytical methods. Important differences in reconstructions can largely be traced to differences in basic tree-ring data, hydrologic data, and modeling choices. Short calibration periods with inadequate natural flow records are considered the largest sources of uncertainty and, especially, if the record only exists over a single sustained wet, dry, or average period. When possible, this uncertainty is addressed by developing or extending natural flow estimates over the longest time period possible.

Statistical reconstruction methods, such as multiple linear regression, yield an estimate of the reconstruction uncertainty in terms of the error variance. The error variance reflects the goodness of fit of the reconstruction model and is critical to the interpretation of the reconstructed streamflow statistics. Such statistics are typically developed from both calibration and verification estimates of error and goodness of fit. The biases and standard errors of reconstructed streamflow drought statistics have been found to depend on degree of the goodness-of-fit, calibration sample length, reconstruction sample length, and autocorrelation of the reconstructed flows (Brockway and Bradley, 1995). Gangopadhyay et al. (2009) presents a non-parametric reconstruction methodology to develop an ensemble of streamflow reconstructions to support probabilistic interpretations. The uncertainties related to reconstructing streamflows, such as developing chronologies and methodological choices, largely apply to uncertainties for reconstructing the PDSI timeseries (Cook et al., 2010).

Finally, the use of paleohydrology as a tool for estimating possible future conditions relies at least in part on an assumption of stationary hydrologic variability through time. Given projections of changing future climate conditions outlined in this report, some uncertainty exists in that assumption itself (Milly et. al., 2008). As a result, some characteristics of hydrologic variability evident in paleohydrologic records may or may not be possible under future climate conditions. However, given this uncertainty and the knowledge that such variability has occurred in the past, the most prudent course of action remains to plan for the full range of possibilities evident from the past, a task for which the use of paleohydrology is uniquely suited.

9.3 West-wide Drought Analyses

Chapter 4 of this report details a long-term drought analysis of both the distant past and future projections. These West-wide analyses use both reconstructed Palmer Drought Severity Index (PDSI) (Cook et al., 2010) and projections of PDSI developed using precipitation and temperature data from the CMIP5-LOCA archive. The PDSI data was broadly defined over two periods for the analyses—historical period (1473 to 2005) and projection period (2006 to 2099).

Though PDSI was developed by Palmer (1965) and continues to be used and even underlies the U.S. Drought Monitor, the use of it as an index to identify droughts, especially in the context of a climate change analysis has been debated (e.g., Ault, 2020). Dai (2011a; 2011b) and Dai et al. (2004) provide discussions on the choice of using PDSI in drought analysis and note that PDSI has been reasonably successful at quantifying long-term drought (Dai and NCAR, 2019). Assessing impacts, such as droughts, adds a level of complexity and, therefore, additional uncertainty in characterizing such impacts from GCM data. GCM-based projections have known uncertainties, yet practitioners who are familiar with those uncertainties still use them. Using GCM output for additional analysis can be useful, although it requires further effort and expertise as uncertainties are compounded.

Analyses of drought characteristics over the common period (1950 to 2005) largely show that climate models encompass the observed drought characteristics and that the climate model simulations can be useful in understanding droughts under future conditions across the Western United States. One key source of uncertainty in this analysis is drought interarrival time, the details of which are presented in Chapter 4. To date, not all sources of uncertainty have been analyzed, but, all distributional model parameter estimates, and associated standard errors or confidence bounds of model parameters, were retained and can be used to further explore uncertainties in future studies.

9.4 Water Supply Reliability Assessments

In Chapter 6 of this report, paleohydrology scenarios were developed and run through river systems models to identify how current river management might be affected by some of the substantial droughts of the distant past, in comparison with more recent historical droughts

(and floods in two cases). Along with scenarios of streamflow, various assumptions were made to inform other inputs, such as water demand, reservoir evaporation, model initial conditions, and duration of model run before the drought event or flood event occurs. All of these choices inform the event-based scenario approach taken in this assessment and ultimately contribute to outcome uncertainties.

Where possible, sensitivity analyses were performed to inform methodological choices. One example is the model initial conditions and duration of the model simulation before the selected drought (pluvial) event takes place. For each simulated river basin (refer to Chapter 6), the sensitivity of the results to initial conditions (e.g., reservoir storage) and duration prior to drought events was either explicitly evaluated using the system model or was discussed with water managers in the basin where selections were made according to on-the-ground experience. Although these choices may be seen as sources of uncertainty, they were coordinated with regional water managers and are therefore documented and transparent. Similarly, water demand model inputs were based on discussions with water managers and typically corresponded with static demands at set levels (2018 demands for example) throughout the model simulations. In most cases, these choices were made to coincide with previous existing planning studies performed in the respective river basins.

Other river system model inputs such as reservoir evaporation and inflows were computed based on available physically based models. Uncertainties associated with those methods inherently cascade into the water supply reliability assessment modeling.

Moreover, a river system model itself is a representation of a river system and how it is managed. Therefore, this representation introduces additional uncertainties into the estimation of drought impacts on water supply and river management. For example, river and reservoir operations that actually occur on the ground are translated into logic statements within a river system model. How operational policies are interpreted and thereby how the logic statements are composed may vary depending on the modeler. However, there may be uncertainty associated with the development of the river management logic within a model. In this report, to reduce river system model uncertainty, the analyses relied upon existing models that have been calibrated, reviewed, and used in previous regional long-term planning studies.

9.5 Urban Landscape Demands Analysis

In Chapter 7, the ET Demands model (Reclamation, 2015a) was used to estimate turf grass evapotranspiration demands to quantify outdoor urban landscape water demand given that turfgrass is the most extensive urban vegetation type. In this analysis, there are numerous irrigation water requirement uncertainties for historical and future climate periods.

For historical periods, primary uncertainties include those associated with accuracy of gridded weather data, turf grass crop coefficients, and simplifying assumptions, parameterizations, and model processes within ET Demands, such as thermal based functions for simulating turfgrass

phenology, root depth and seasonal root growth, soil water balance and runoff, and irrigation amount and frequency.

For future periods, primary uncertainties include those for historical periods, in addition to those associated with accuracy of weather data under future climate (using the Multivariate Adaptive Constructed Analogs (MACA) downscaling method), potential changes in turfgrass varieties, and effects of increased CO_2. Uncertainties associated with increased CO_2 include sensitivities of stomatal conductance, transpiration, and leaf area index, and unknown land surface energy balance feedbacks from increased leaf temperatures and vapor pressure deficits (Allen et al., 1991; Jacobs and De Bruin, 1992, 1997; Islam et al., 2012). While it is acknowledged that there are numerous uncertainties associated with estimating historical and future water requirements using ET Demands, more complex plant growth models (PGMs) have similar uncertainties given they are highly parameterized and require detailed input data and calibration, often times calibrated to empirical crop coefficient curves used in the ET Demands model.

Therefore, the principle of parsimony was followed in this study given the limited information available and uncertainties associated with gridded weather, model input data, and calibration information. ET Demands and the approach of Kruijt et al. (2008) used in this assessment is practical and justified in that it is physically based, accepted and endorsed by the American Society of Civil Engineers (ASCE) and Food and Agricultural Organization (FAO), and considers primary CO_2 effects that ultimately reduce transpiration and crop evapotranspiration (ETc) under future climate scenarios.

9.6 Climate Impacts on Groundwater

Changes in focused groundwater recharge are highly uncertain since the ability to model precipitation intensity is largely dependent on modeling climate processes at high spatial resolution to capture topographic effects and convective events. This report provides an overview of existing studies, each of which have elements of uncertainty. For example, studies conducted in the Upper Colorado River Basin highlight the uncertainty with future recharge projections. There is considerable spatial heterogeneity throughout the Upper Colorado River Basin with future recharge estimations, in addition to seasonal dynamics. However, projected increases in precipitation and temperature alone do not fully explain the spatially diverse projected changes in recharge and it would be useful to better understand the different drivers behind anticipated increases or decreases to future recharge.

9.7 Summary

This report was designed to take advantage of the best available information and techniques in a risk-informed decision-making framework, following methods documented in peer-reviewed literature and supported by collaboration with leading researchers in other Federal agencies and research institutes across the United States. This report focuses on demonstrating what is

possible to assess across a West-wide domain. And, while each method could be further refined, the diversity of approaches is not intended to be all encompassing, but rather a research effort that provides useful context and prompts further inquiries.

The complexities of the climate system, of physical processes in nature, of human behaviors dictating greenhouse gas concentrations, and of computing tools, all ultimately lead to uncertainties in the results of long-term planning studies. Reclamation commonly considers risks in water resources planning associated with these uncertainties and continues planning with these insights in mind, recognizing both the value and shortcomings of the information, and also recognizing the need to explore alternative planning paradigms to consider decision-making under deep uncertainty.

Future scenarios encompass uncertainties associated with climate modeling, climate downscaling, and hydrologic modeling (Wilby and Harris, 2006; Davie et al., 2013; Addor et al., 2014; Schewe et al., 2014; Vano et al., 2014; Mendoza et al., 2015). Although these methods were widely accepted as a reasonable strategy toward this objective, there is a growing awareness that many of these choices would affect assessment findings. Where once climate changes were based on a single GCM (e.g., Wood et al., 2004; and associated Western United States assessments, such as Christensen et al., 2004), the recognition of uncertainty in GCM choice has standardized the use of more than a dozen GCMs today. The approach taken in this study relies on numerous climate projections to understand future climate and hydrology, though it primarily relies on the LOCA downscaling method (and MACA downscaling for urban water demand) and a single hydrology model using *a priori* parameter set for the hydroclimate analysis. Thus, current future hydroclimate projections provide a limited view of the uncertainty space. For example, the trend toward using multiple hydrologic models rather than a single model has confirmed that a single hydrologic model selection artificially narrows the range by not representing the hydrologic sensitivities that would be estimated through different modeling choices.

Furthermore, a problem confronting practitioners and decision-makers in the progress of climate science is that the projection uncertainty space (i.e., the combined uncertainty arising from uncertainties present at each step in the analysis) has expanded as research reveals a fuller range of uncertainties associated with the identified modeling steps. Therefore, it is important that the impact assessment community continues to formulate strategies toward reducing projection uncertainty. It is nonetheless critical now to gain a better understanding of the multiple sources of uncertainty, which likely are more substantial than the present approach suggests.

Similar to development of future scenarios for analysis, there is uncertainty associated with paleo information used and developed in this report, as discussed above. The drought analysis conducted in this report used a range of methods spanning degrees of complexity. The field is continuing to progress towards new, expanded uncertainty paradigms, just as it did in the past for the hydroclimate analysis. At the time of this report, work is still underway to identify and/or pragmatic and scientifically sound strategies for doing so.

While it is important to acknowledge limitations in the analyses presented in this report and to make an initial effort to more fully characterize and better reveal that uncertainty space, ongoing research should also keep the computational requirements in perspective. There is a need for guidance to make specific methodological choices such that users are able to understand and communicate the implications of those choices for their respective applications. It is also important to consider impacts beyond those captured in simulations, such as the impact of wildfires on water availability and quality.

Additionally, it is important to recognize that a diversity of techniques collectively provides a more robust analysis, especially when different techniques reveal similar conclusions. For example, future climate projections and paleohydrology provide complementary information that help to understand and prepare for conditions outside those seen in the observed period. Collectively, paleo analysis and analysis using future projections both reveal scenarios and likelihoods which extend understanding, allow for a more informed risk-informed decision-making framework, and can help promote more resilient planning.

As research continues to characterize and, where possible, reduce uncertainties inherent in projecting hydroclimate impacts of climate change, the water resources management community should also be aware that future conditions are ultimately deeply uncertain. This means that risk-informed analyses alone may not provide appropriate practical information for planning, and that bottom-up approaches using decision-making under deep uncertainty (DMDU) methods or similar approaches should be more broadly explored. Such bottom-up methods can help mitigate the challenges of planning under deep uncertainty and reduce the influence of imperfect, often limiting, up-front assumptions during planning processes. These methods likely present a prudent future direction for water resources planning and management.

10 References

Abatzoglou, J.T., (2013). Development of gridded surface meteorological data for ecological applications and modelling. International Journal of Climatology, 33(1):121–131.

Abatzoglou, J.T. and T.J. Brown, (2012). A comparison of statistical downscaling methods suited for wildfire applications. International Journal of Climatology, 32(5):772–780.

Abramowitz, G., N. Herger, E. Gutmann, D. Hammerling, R. Knutti, M. Leduc, R. Lorenz, R. Pincus, and G.A. Schmidt, (2019). ESD Reviews: Model dependence in multi-model climate ensembles: weighting, sub-selection and out-of-sample testing. Earth System Dynamics, 10(1):91–105, doi:10.5194/esd-10-91-2019.

Addor, N., O. Rössler, N. Köplin, M. Huss, R. Weingartner, and J. Seibert, (2014). Robust changes and sources of uncertainty in the projected hydrological regimes of Swiss catchments. Water Resources Research, 50:7541–7562.

Advanced Engineering and Environmental Services, Inc. (AEES), (2013). Bozeman Integrated Water Resources Plan. Bozeman, Montana.

Alexander, E.A., (2018). Searching for a Robust Operation of Lake Mead. M.S. Thesis, University of Colorado, Boulder, Colorado.

Allen, R.G. and C.W. Robison, (2009). Evapotranspiration and Consumptive Irrigation Water Requirements for Idaho. University of Idaho Report, 222 p. Available at: http://www.kimberly.uidaho.edu/ETIdaho/ (last accessed October 26, 2020)

Allen, R.G., F.N. Gichuki, C. Rosenzweig, (1991). CO2 Induced Climatic Changes and Irrigation Water Requirements. Journal of Water Resources Planning and Management, 117(2):157–178.

Allen, R.G., L.S. Pereira, D. Raes, and M. Smith, (1998). Crop Evapotranspiration: Guidelines for Computing Crop Water Requirements, Irrigation and Drainage Paper 56. Food and Agriculture Organization of the United Nations, Rome, 300 p.

Allen, R.G., L.S. Pereira, M. Smith, D. Raes, and J.L. Wright, (2005). FAO-56 Dual Crop Coefficient Method for Estimating Evaporation from Soil and Application Extensions. Journal of Irrigation and Drainage Engineering, ASCE, 131(1):2–13.

Allen, D.M., A.J. Cannon, M.W. Toews, and J. Scibek, (2010). Variability in simulated recharge using different GCMs. Water Resources Research, 46, doi:10.1029/2009WR008932.

Allen, E.B., T.M. Rittenour, R.J. DeRose, M.F. Bekker, R. Kjelgren, and B.M. Buckley, (2013). A tree-ring based reconstruction of Logan River streamflow, northern Utah. Water Resources Research, 49, doi:10.1002/2013WR014273.

American Society of Civil Engineers-Environmental and Water Resources Institute (ASCE-EWRI), (2005). The ASCE Standardized Reference Evapotranspiration Equation, Report 0-7844-0805-X. ASCE Task Committee on Standardization of Reference Evapotranspiration, Reston, Virginia. American Society of Civil Engineers.

Archfield, S.A., M.P. Clark, B. Arheimer, L.E. Hay, H. McMillan, J.E. Kiang, J. Seibert, K. Hakala, A. Bock, T. Wagener, W.H. Farmer, V. Andreassian, S. Attinger, A. Viglione, R. Knight, S. Markstrom, and T. Over, (2016). Accelerating advances in continental domain hydrologic modeling. Water Resources Research, 51:10078–10091, doi:10.1002/2015WR017498.

Ault, T.R., (2020). On the essentials of drought in a changing climate. Science, 368:256–260.

Bicknell, B.R., J.C. Imhoff, J.L. Kittle, A.S. Donigian, and R.C. Johanson, (1997). Hydrological Simulation Program–Fortran: User's manual for version 11: U.S. Environmental Protection Agency, National Exposure Research Laboratory. Athens, Georgia. EPA/600/R-97/080, 755.

Bishop, C.H., and G. Abramowitz, (2013). Climate model dependence and the replicate Earth paradigm. Climate Dynamics, 41:885–900.

Brekke, L.D., E.P. Maurer, J.D. Anderson, M.D. Dettinger, E.S. Townsley, A. Harrison, and T. Pruitt, (2009). Assessing reservoir operations risk under climate change. Water Resources Research, 45:W04411, doi:10.1029/2008WR006941.

Brekke, L.D., (2010). Preferences among Hydrologic Models for Studies involving Climate Change. Presentation at California Water and Environmental Modeling Forum, Annual Meeting Pacific Grove, California, 23 February 2010. https://www.cwemf.org/Asilomar/LBrekkeHydroModelsComparison.pdf

Briffa K.R., P.D. Jones, J.R. Pilcher, and M.K. Hughes, (1988). Reconstructing summer temperatures in northern Fennoscandinavia back to A.D. 1700 using tree-ring data from Scots pine. Arctic and Alpine Research, 20(4):385–394, doi:10.1080/00040851.1988.12002691.

Briffa K.R. and P.D. Jones, (1990). Basic Chronology Statistics and Assessment. In Cook E.R., Kairiukstis L.A. (eds), Methods of Dendrochronology: Applications in the Environmental Sciences. Dordrecht: Kluwer Academic Publishers, 137–152.

Brockway, C.G. and A.A. Bradley, (1995). Errors in streamflow drought statistics reconstructed from tree-ring data. Water Resources Research, 31(9):2279–2293, doi:10.1029/95WR01141.

Broman, D.P and M. McGuire, (2020). Hydrologic Model Comparison in Support of Water Resources Planning and Operations Studies. Technical Memorandum No. ENV-2020-071, Technical Service Center, Denver, Colorado, 27 p.

Brown C., Y. Ghile, M. Laverty, and K. Li, (2012). Decision scaling: Linking bottom-up vulnerability analysis with climate projections in the water sector. Water Resources Research, 48:W09537, doi:10.1029/2011WR011212.

Brush, C.F., E.C. Dogrul, and T.N. Kadir, (2013). Development and calibration of the California Central Valley groundwater-surface water simulation model (C2VSim), version 3.02-CG. Bay-Delta Office, California Department of Water Resources. Available at: https://water.ca.gov/Library/Modeling-and-Analysis/Central-Valley-models-and-tools/C2VSim (last accessed October 16, 2020)

California Department of Water Resources (CA-DWR), (2017). A Water Resources System Planning Model for State Water Project (SWP) and Central Valley Project (CVP): CalSim 3.0 Draft Report. California Department of Water Resources. Sacramento, California (Vol. December).

——— (2015). Perspectives and Guidance for Climate Change Analysis. CA-DWR Climate Change Technical Advisory Group. 142 p. Available at: https://water.ca.gov/-/media/DWR-Website/Web-Pages/Programs/All-Programs/Climate-Change-Program/Climate-Program-Activities/Files/Reports/Perspectives-Guidance-Climate-Change-Analysis.pdf (last accessed October 26, 2020)

Christensen, N.S., A.W. Wood, N. Voisin, D.P. Lettenmaier, and R.N. Palmer, (2004). The effects of climate change on the hydrology and water resources of the Colorado River basin. Climatic Change, 62:337–363.

City of Great Falls, (2013). City of Great Falls Growth Policy Update. Great Falls, Montana.

City of Helena, (2011). City of Helena 2011 Growth Policy. Helena, Montana.

Clark, M.P., D. Kavetski, and F. Fenicia, (2011). Pursuing the method of multiple working hypotheses for hydrological modeling. Water Resources Research, 47, doi:10.1029/2010WR009827.

Clark, M.P., Y. Fan, D.L. Lawrence, J.C. Adam, D. Bolster, D. Gochis, R.L. Hooper, M. Kumar, L.R. Leung, D.S. Mackay, R.M. Maxwell, C. Shen, S.C. Swenson, and X. Zeng, (2015a). Improving the representation of hydrologic processes in Earth System Models. Water Resources Research, 51:5929–5956, doi:10.1002/2015WR017096.

Clark, M.P., B. Nijssen, J. Lundquist, D. Kavetski, D. Rupp, R. Woods, E. Gutmann, A. Wood, L. Brekke, J. Arnold, D. Gochis, and R. Rasmussen, (2015b). A unified approach to process-based hydrologic modeling. Part 1: Modeling concept. Water Resources Research, 51, doi:10.1002/2015WR017198.

Clark, M.P., B. Nijssen, J. Lundquist, D. Kavetski, D. Rupp, R. Woods, E. Gutmann, A. Wood, D. Gochis, R. Rasmussen, D. Tarboton, V. Mahat, G. Flerchinger, and D. Marks, (2015c). A unified approach for process-based hydrologic modeling: Part 2. Model implementation and example applications. Water Resources Research, 51, doi:10.1002/2015WR017200.

Clark, M.P., R.L. Wilby, E.D. Gutmann, J.A. Vano, S. Gangopadhyay, A.W. Wood, H.J. Fowler, C. Prudhomme, J.R. Arnold, and L.D. Brekke, (2016). Characterizing uncertainty of the hydrologic impacts of climate change. Climate Change Reports, 2(2):55–64, doi:10.1007/s40641-016-0034-x.

Close, A., W.M. Haneman, J.W. Labadie, D.P. Loucks, J.R. Lund, D.C. McKinney, and J.R. Stedinger, (2003). A strategic review of CALSIM II and its use for water planning, management, and operations in Central California. California Bay Delta Authority Science Program Association of Bay Governments, Oakland, California.

CME Group, (2020). News Release--CME Group to Launch First-Ever Water Futures Based on Nasdaq Veles California Water Index (NQH2O). Available at: https://www.cmegroup.com/media-room/press-releases/2020/9/17/cme_group_to_launchfirst-everwaterfuturesbasedonnasdaqvelescalif.html (last accessed October 26, 2020)

Cook, E.R., R. Seager, R.R. Heim, R.S. Vose, C. Herweijer, and C. Woodhouse, (2010). Megadroughts in North America: Placing IPCC projections of hydroclimatic change in a long-term paleoclimate context. Journal of Quaternary Science, 25(1):48–61, doi:10.1002/jqs.1303.

Crosbie, R.S., W.R. Dawes, S.P. Charles, F.S. Mpelasoka, S. Aryal, O. Barron, and G.K. Summerell, (2011). Differences in future recharge estimates due to GCMs, down-scaling methods and hydrological models. Geophysical Research Letters, 38(11), doi:10.1029/2011GL047657.

Crosbie, R.S., B.R. Scanlon, F.S. Mpelasoka, R.C. Reedy, J.B. Gates, and L. Zhang, (2013). Potential climate change effects on groundwater recharge in the High Plains Aquifer, USA. Water Resources Research, 49:3936–3951, doi:10.1002/wrcr.20292.

Dai, A., K.E. Trenberth, and T. Qian, (2004). A global data set of Palmer Drought Severity Index for 1870–2002: Relationship with soil moisture and effects of surface warming. Journal of Hydrometeorology, 5(6):1117–1130, doi:10.1175/JHM-386.1.

Dai, A., (2011a). Characteristics and trends in various forms of the Palmer Drought Severity Index (PDSI) during 1900–2008. J. Geophysical Research–Atmospheres, 116, D12115, doi:10.1029/2010JD015541.

Dai, A., (2011b). Drought under global warming: A review. Wiley Interdisciplinary Reviews: Climate Change, 2:45–65, doi:10.1002/wcc.81.

Dai, A. and National Center for Atmospheric Research (NCAR) Staff (Eds), (2019). The Climate Data Guide: Palmer Drought Severity Index (PDSI). Available at: https://climatedataguide.ucar.edu/climate-data/palmer-drought-severity-index-pdsi (last accessed February 2, 2021)

Daly, C., R.P. Neilson, and D.L. Phillips, (1994). A statistical-topographic model for mapping climatological precipitation over mountainous terrain. Journal of Applied Meteorology, 33(2):140–158.

Davie, J., P. Falloon, R. Kahana, R. Dankers, R. Betts, F. Portmann, D. Wisser, D. Clark, A. Ito, and Y. Masaki, (2013). Comparing projections of future changes in runoff from hydrological and biome models in ISI-MIP. Earth System Dynamics, 4:359–374.

Deser, C., R. Knutti, S. Solomon, and A.S. Phillips, (2012a). Communication of the role of natural variability in future North American climate. Nature Climate Change, 2:775–779.

Deser, C., A. Phillips, V. Bourdette, and H. Teng, (2012b). Uncertainty in climate change projections: the role of internal variability. Climate Dynamics, 38:527–546.

Dessai, S., and M. Hulme (2004). Does climate adaptation policy need probabilities? Climate Policy, 4(2):107–128, doi:10.1080/14693062.2004.9685515.

Dieleman, W.I., S. Vicca, F.A. Dijkstra, F. Hagedorn, M.J. Hovenden, K.S. Larsen, J.A. Morgan, A. Volder, C. Beier, J.S. Dukes, J. King, S. Leuzinger, S. Linder, Y. Luo, R. Oren, P. De Angelis, D. Tingey, M.R. Hoosbeek, and I.A. Janssens, (2012). Simple additive effects are rare: a quantitative review of plant biomass and soil process responses to combined manipulations of CO_2 and temperature. Global Change Biology, 18(9):2681–2693, doi:10.1111/j.1365-2486.2012.02745.x.

DMDU (Decision Making Under Deep Uncertainty) Society, (2021). The Society for Decision Making Under Deep Uncertainty. Available at: https://www.deepuncertainty.org/ (last accessed February 9, 2021)

Doss-Gollin, J., (2020). Sequential adaptation through prediction of structured climate risk. Doctoral dissertation. Columbia University, New York, New York.

Doss-Gollin, J., D.J. Farnham, S. Steinschneider, and U. Lall, (2019). Robust adaptation to multiscale climate variability. Earth's Future, 7(7):734–747.

Douglass, A., (1941). Crossdating in dendrochronology. Journal of Forestry, 39(10):825–831.

Draper, A.J., A. Munevar, S.K. Arora, E. Reyes, N.L. Parker, F.I. Chung, and L.E. Peterson, (2004). CalSim: Generalized model for reservoir system analysis. Journal of Water Resources Planning and Management, 130(6):480–489.

Elsner, M.M., S. Gangopadhyay, T. Pruitt, L.D. Brekke, N. Mizukami, and M.P. Clark, (2014). How Does the Choice of Distributed Meteorological Data Affect Hydrologic Model Calibration and Streamflow Simulations? Journal of Hydrometeorology, 15(4):1384–1403, doi:10.1175/JHM-D-13-083.1.

Erkyihun, S.T., B. Rajagopalan, E. Zagona, U. Lall, and K. Nowak, (2016). Wavelet-based time series bootstrap model for multidecadal streamflow simulation using climate indicators. Water Resources Research, 52(5):4061–4077, doi:10.1002/2016WR018696.

Evans, J.P., F. Ji, G. Abramowitz, and M. Ekström, (2013). Optimally choosing small ensemble members to produce robust climate simulations. Environmental Research Letters, 8, 044050.

Flint, L.E., A.L. Flint, J.H. Thorne, and R. Boynton, (2013). Fine-scale hydrologic modeling for regional landscape applications: the California Basin Characterization Model development and performance. Ecological Processes, 2(25), doi:10.1186/2192-1709-2-25.

Fowler, H., S. Blenkinsop, and C. Tebaldi, (2007). Linking climate change modelling to impacts studies: recent advances in downscaling techniques for hydrological modelling. International Journal of Climatology, 27:1547–1578.

Fritts, H.C., (1976). Tree-rings and climate. Academic Press, San Diego, California.

Gangopadhyay, S., B.L. Harding, B. Rajagopalan, J.J. Lukas, and T.J. Fulp, (2009). A nonparametric approach for paleohydrologic reconstruction of annual streamflow ensembles. Water Resources Research, 45(6):W06417, doi:10.1029/2008WR007201.

Gangopadhyay, S., and G.J. McCabe, (2010). Predicting regime shifts in flow of the Colorado River. Geophysical Research Letters, 37:L20706, doi:10.1029/2010GL044513.

Gangopadhyay, S., G. McCabe, G. Pederson, J. Martin, and J.S. Littell, (2019). Risks of hydroclimatic regime shifts across the Western United States. Scientific Reports, 9(1), doi:10.1038/s41598-019-42692-y.

Gedalof, Z., D.L. Peterson, and N.J. Mantua, (2004). Columbia River flow and drought since 1750. Journal of the American Water Resources Association. 40:1579–1592.

Giorgi, F., (1990). Simulation of regional climate using a limited area model nested in a general circulation model. Journal of Climate, 3:941–963, doi:10.1175/1520-0442(1990)003<0941:SORCUA>2.0.CO;2.

Groves, D.G., N. Kalra, J. Syme, E. Molina-Perez, and C. Garber, (2021). Water Planning for the Uncertain Future: An Interactive Guide to the Use of Methods for Decision-making Under Deep Uncertainty (DMDU) for U.S. Bureau of Reclamation Water Resources Planning. RAND, Santa Monica, California. Available at: https://www.rand.org/pubs/tools/TL320.html (last accessed March 16, 2021)

Gupta, H.V., T. Wagener, and Y.Q. Liu, (2008). Reconciling theory with observations: elements of a diagnostic approach to model evaluation. Hydrological Processes, 22:3802–3813, doi:10.1002/hyp.6989.

Gurdak, J.J., R.T. Hanson, P.B. McMahon, B.W. Bruce, J.E. McCray, G.D. Thyne, and R.C. Reedy, (2007). Climate Variability Controls on Unsaturated Water and Chemical Movement, High Plains Aquifer, USA. Vadose Zone Journal, 6(3):533–547, doi:10.2136/vzj2006.0087.

Gutmann, E., T. Pruitt, M.P. Clark, L. Brekke, J. Arnold, D. Raff, and R. Rasmussen, (2014). An intercomparison of statistical downscaling methods used for water resource assessments in the United States. Water Resources Research, 50:7167–7186, doi:10.1002/2014WR015559.

Gutmann, E., I. Barstad, M.P. Clark, J.R. Arnold, and R.M. Rasmussen, (2016). The Intermediate Complexity Atmospheric Research Model. Journal of Hydrometeorology, 17(3):957–973, doi:10.1175/JHM-D-15-0155.1.

Hamlet, A.F., P. Carrasco, J. Deems, M.M. Elsner, T. Kamstra, C. Lee, S.-Y. Lee, G.S. Mauger, E.P. Salathé, I. Tohver, and L.W. Binder, (2010). Final project report for the Columbia Basin Climate change scenarios project. Available at: https://warm.atmos.washington.edu/2860/report/ (last accessed October 16, 2020)

Harbaugh, A.W, (2005). MODFLOW-2005: the U.S. Geological Survey modular ground-water model--the ground-water flow process: U.S. Geological Survey Techniques and Methods 6-A16, variously paginated.

Haasnoot, M., J.H. Kwakkel, W.E. Walker, J. ter Maat, (2003). Dynamic adaptive policy pathways: A method for crafting robust decisions for a deeply uncertain world. Global Environmental Change, 23(2):485–498, doi:10.1016/j.gloenvcha.2012.12.006.

Hawkins, E., and R. Sutton, (2009). The potential to narrow uncertainty in regional climate predictions. Bulletin of the American Meteorological Society, 90:1095-1107.

Herman, J.D., P.M. Reed, H.B. Zeff, and G.W. Characklis, (2015). How should robustness be defined for water systems planning under change? Journal of Water Resources Planning and Management, 141(10):04015012, doi:10.1061/(ASCE)WR.1943-5452.0000509.

Hidalgo, H.G., T.C. Piechota, and J.A. Dracup, (2000). Alternative principal components regression procedures for dendrohydrologic reconstructions. Water Resources Research, 36(11):3241–3249.

Hidalgo, H.G., M.D. Dettinger, and D.R. Cayan, (2008). Downscaling with constructed analogues: Daily precipitation and temperature fields over the United States. California Energy Commission PIER Final Project Report CEC-500-2007-123, 48 p.

Hosking, J.R.M. and J.R. Wallis, (1997). Regional Frequency Analysis. Cambridge University Press, 224 p.

Huntington, J., (2020). Personal communication between Justin Huntington, Ph.D., Desert Research Institute (https://www.dri.edu/directory/justin-huntington/; last accessed October 28, 2020) and Ali Harivandi, Ph.D., University of California Cooperative Extension (https://ucanr.edu/?facultyid=926; last accessed October 28, 2020)

Huntington, J.L. and R. Allen, (2010). Evapotranspiration and Net Irrigation Water Requirements for Nevada. Nevada State Engineer’s Office Publication, 266 p.

Intergovernmental Panel on Climate Change (IPCC), (2001). Climate Change 2001–IPCC Third Assessment Report. Available at: https://www.ipcc.ch/reports/ (last accessed October 26, 2020)

_____ (2007). Climate Change 2007–IPCC Fourth Assessment Report. Available at: https://www.ipcc.ch/reports/ (last accessed October 26, 2020)

_____ (2014). Climate Change 2014–IPCC Fifth Assessment Report. Available at: https://www.ipcc.ch/reports/ (last accessed October 26, 2020)

Islam, A., L. Ahuja, L. Garcia, L.M, Anapalli, S. Saseendran, and T. Trout, (2012). Modeling the impacts of climate change on irrigated corn production in the Central Great Plains. Agricultural Water Management, 110(C):94–108.

Jacobs, C.M.J. and H.A.R. De Bruin, (1992). The sensitivity of regional transpiration to land-surface characteristics – significance of feedback. Journal of Climate 5(7):683–698.

Jacobs, C.M.J. and H.A.R. De Bruin, (1997). Predicting regional transpiration at elevated atmospheric CO2: influence of the PBL-vegetation interaction. Journal of Applied Meteorology, 36:1663–1675.

Jarosch, A.H., F.S. Anslow, and G.K. Clarke, (2012). High-resolution precipitation and temperature downscaling for glacier models. Climate Dynamics, 38:391–409.

Kasprzyk, J.R., S. Nataraj, P.M. Reed, and R.J. Lempert, (2013). Many objective robust decision making for complex environmental systems undergoing change. Environmental Modelling & Software, 42:55–71, doi:10.1016/j.envsoft.2012.12.007.

Kay, J., C. Deser, A. Phillips, A. Mai, C. Hannay, G. Strand, J. Arblaster, S. Bates, G. Danabasoglu, J. Edwards, M. Holland, P. Kushner, J.-F. Lamarque, D. Lawrence, K. Lindsay, A. Middleton, E. Munoz, R. Neale, K. Oleson, L. Polvani, and M. Vertenstein, (2015). The Community Earth System Model (CESM) large ensemble project: A community resource for studying climate change in the presence of internal climate variability. Bulletin of the American Meteorological Society, 96(8):1333–1349, doi:10.1175/BAMS-D-13-00255.1.

Kendon, E.J., N.M. Roberts, H.J. Fowler, M.J. Roberts, S.C. Chan, and C.A. Senior, (2014), Heavier summer downpours with climate change revealed by weather forecast resolution model. Nature Climate Change, 4:570–576, doi:10.1038/nclimate2258.

Knutti, R., (2010). The end of model democracy? Climatic Change, 102:395–404.

Knutti, R., D. Masson, and A. Gettelman, (2013). Climate model genealogy: Generation CMIP5 and how we got there. Geophysical Research Letters, 40:1194–1199.

Knutti, R. and J. Sedláček, (2013). Robustness and uncertainties in the new CMIP5 climate model projections. Nature Climate Change, 3(4):369–373, doi:10.1038/nclimate1716.

Knutti, R., R. Furrer, C. Tebaldi, J. Cermak, and G.A. Meehl, (2010). Challenges in combining projections from multiple climate models. Journal of Climate, 23, 2739–2758.

Koenig, R. and V. Isaman, (2010). Topsoil Quality Guidelines for Landscaping. Utah State University Cooperative Extension Report, 4 p.

Kojadinovic I. and J. Yan, (2010). Modeling Multivariate Distributions with Continuous Margins Using the copula R Package. Journal of Statistical Software, 34(9):1–20, doi:10.18637/jss.v034.i09.

Kruijt B., J.P.M. Witte, C.M.J. Jacobs, T. Kroon, (2008). Effects of rising atmospheric CO2 on evapotranspiration and soil moisture: A practical approach for the Netherlands. Journal of Hydrology, 349(3-4):257–267.

Kwon, H-H. and U. Lall, (2016). A copula-based nonstationary frequency analysis for the 2012–2015 drought in California. Water Resources Research, 52:5662–5675, doi:10.1002/2016WR018959.

Larson, R., (2013). Personal Communication between Rick Larson, Planning Manager, City of Butte, Montana and Aaron Fiaschetti, Surface Water Hydrologist, Montana Department of Natural Resources and Conservation.

Leavesley, G.H., R.W. Lichty, B.M. Troutman, and L.G. Saindon, (1983). Precipitation-runoff modeling system; user's manual. U.S. Geological Survey Techniques and Methods, Water-Resources Investigations Report 83-4238, 207 p., doi:10.3133/wri834238.

Lempert, R.J., S. Popper, and S. Bankes, (2003). Shaping the Next One Hundred Years: New Methods for Quantitative, Long Term Policy Analysis. Report MR-1626-RPC, RAND, Santa Monica, California.

Lempert, R. J., and D.G. Groves, (2010). Identifying and evaluating robust adaptive policy responses to climate change for water management agencies in the American west. Technological Forecasting and Social Change, 77(6):960–974.

Liang, X., D.P. Lettenmaier, E.F. Wood, and S.J. Burges, (1994). A simple hydrologically based model of land surface water and energy fluxes for general circulation models. Journal of Geophysical Research, 99(D7):14415–14428.

Liang, X., E.F. Wood, and D.P. Lettenmaier, (1996). Surface soil moisture parameterization of the VIC-2L model: evaluation and modifications. Global Planetary Change, 13:195–206.

Lin, L., Z. Wang, Y. Xu, and Q. Fu, (2016). Sensitivity of precipitation extremes to radiative forcing of greenhouse gases and aerosols. Geophysical Research Letters, 43(18):9860–9868.

Littell, J.S., G.T. Pederson, S.T. Gray, M. Tjoelker, A.F. Hamlet, and C.A. Woodhouse, (2016). Reconstructions of Columbia River Streamflow from Tree-Ring Chronologies in the Pacific Northwest, USA. Journal of the American Water Resources Association, 52(5):1121–1141, doi:10.1111/1752-1688.12442.

Littlefield, D., (1991). The Rio Grande Compact of 1929: A Truce in an Interstate River War. Pacific Historical Review, 60(4):497–515.

Livneh B., E.A. Rosenberg, C. Lin, B. Nijssen, V. Mishra, K.M. Andreadis, E.P. Maurer, D.P. Lettenmaier, (2013). A Long-Term Hydrologically Based Dataset of Land Surface Fluxes and States for the Conterminous United States: Update and Extensions. Journal of Climate, 26(23):9384–9392, doi:10.1175/JCLI-D-12-00508.1.

Livneh, B., T.J. Bohn, D.W. Pierce, F. Munoz-Arriola, B. Nijssen, R. Vose, D.R. Cayan, and L. Brekke, (2015). A spatially comprehensive, hydrometeorological data set for Mexico, the U.S., and Southern Canada 1950–2013. Scientific Data, 2, 150042, doi:10.1038/sdata.2015.42.

Loáiciga, H., (2005). On the probability of droughts: The compound renewal model. Water Resources Research, 41:W01009, doi:10.1029/2004WR003075.

Lofgren, B.M., A.D. Gronewold, A. Acciaioli, J. Cherry, A. Steiner, and D. Watkins, (2013). Methodological approaches to projecting the hydrologic impacts of climate change. Earth Interactions, 17(19), doi:10.1175/2013ei000532.1.

Lorenz, E.N., (1963). Deterministic nonperiodic flow. Journal of the Atmospheric Sciences, 20:130-141.

Lukas, J., and E. Payton, eds., (2020). Colorado River Basin Climate and Hydrology: State of the Science. Western Water Assessment, University of Colorado Boulder. doi:10.25810/3hcv-w477.

Malevich, S.B., C.A. Woodhouse, and D.M. Meko, (2013). Tree-ring reconstructed hydroclimate of the Upper Klamath basin. Journal of Hydrology, doi:10.1016/j.jhydrol.2013.04.048.

Maraun, D., (2013). Bias correction, quantile mapping, and downscaling: Revisiting the inflation issue. Journal of Climate, 26:2137–2143.

Marchau, V.A., W.E. Walker, P.J. Bloemen, and S.W. Popper, (2019). Decision Making under Deep Uncertainty: From Theory to Practice. Springer, 405 p.

Margolis, E.Q., Meko, D.M., and R. Touchan, (2011). A tree-ring reconstruction of streamflow in the Santa Fe River, New Mexico. Journal of Hydrology, 397(1-2):118–127.

Markstrom, S.L., R.S. Regan, L.E. Hay, R.J. Viger, R.M. Webb, R.A. Payn, and J.H. LaFontaine, (2015). PRMS-IV, the precipitation-runoff modeling system, version 4. U.S. Geological Survey Techniques and Methods, 6(B7).

Martin, J.T., G.T. Pederson, C.A. Woodhouse, E.R. Cook, G.J. McCabe, E.K. Wise, P. Erger, L. Dolan, M. McGuire, S. Gangopadhyay, K. Chase, J.S. Littell, S.T. Gray, S. St. George, J. Friedman, D. Sauchyn, J. St. Jacques, and J. King, (2019). A network of 31 Upper Missouri River Basin naturalized water-year (Oct-Sep) streamflow reconstructions spanning years 800-1998 CE: U.S. Geological Survey data release, doi:10.5066/P9FC7ILX.

Martin, J.T., G.T. Pederson, C.A. Woodhouse, E.R. Cook, G.J. McCabe, K.J. Anchukaitis, E.K. Wise, P. Erger, L. Dolan, M. McGuire, S. Gangopadhyay, K. Chase, J.S. Littell, S.T. Gray, S. St. George, J. Friedman, D. Sauchyn, J. St. Jacques, J. King, (2020). Increased drought severity tracks warming in the United States' largest river basin. Proceedings of the National Academy of Sciences of the United States of America, 117(21):11328–11336.

Masbruch, M.D., C.A. Rumsey, S. Gangopadhyay, D.D. Susong, and T. Pruitt, (2016). Analyses of infrequent (quasi-decadal) large groundwater recharge events in the northern Great Basin: Their importance for groundwater availability, use, and management. Water Resources Research, 52(10):7819–7836, doi:10.1002/2016WR019060.

Matthew F., R. Bekker, J. DeRose, B.M. Buckley, R.K. Kjelgren, and N.S. Gill, (2014). A 576-Year Weber River Streamflow Reconstruction from Tree Rings for Water Resource Risk Assessment in the Wasatch Front, Utah. Journal of the American Water Resources Association 50:1338–1348, doi:10.1111/jawr.12191.

Maurer, E., A. Wood, J. Adam, D. Lettenmaier, and B. Nijssen, (2002). A long-term hydrologically-based data set of land surface fluxes and states for the conterminous United States. Journal of Climate, 15(22):3237–3251.

Maurer, E.P., H.G. Hidalgo, T. Das, M.D. Dettinger, and D.R. Cayan, (2010). The utility of daily large-scale climate data in the assessment of climate change impacts on daily streamflow in California. Hydrology and Earth System Sciences, 14:1125–1138, doi:10.5194/hess-14-1125-2010.

Maurer, E.P., L. Brekke, T. Pruitt, B. Thrasher, J. Long, P. Duffy, M. Dettinger, D. Cayan, and J. Arnold, (2014). An enhanced archive facilitating climate impacts and adaptation analysis. Bulletin of the American Meteorological Society, 95:1011–1019, doi:10.1175/BAMS-D-13-00126.1.

Meixner, T., A.H. Manning, D.A. Stonestrom, D.M. Allen, H. Ajami, K.W. Blasch, A.E. Brookfield, C.L. Castro, J.F. Clark, D.J. Gochis, A.L. Flint, K.L. Neff, R. Niraula, M. Rodell, B.R. Scanlon, K. Singha, M.A. Walvoord, (2016). Implications of projected climate change for groundwater recharge in the Western United States. Journal of Hydrology, 534:124–138, doi:10.1016/j.jhydrol.2015.12.027.

Meko, D.M. and D.A. Graybill, (1995). Tree-ring reconstruction of Upper Gila River discharge. Water Resources Bulletin, 31(4):605–616.

Meko, D.M., C.A. Woodhouse, C.A. Baisan, T. Knight, J.J. Lukas, M.K. Hughes, and M.W. Salzer, (2007). Medieval drought in the upper Colorado River Basin. Geophysical Research Letter, 34(10):1–5, doi:10.1029/2007GL029988.

Meko, D.M., (2008). New Streamflow Reconstructions for the Rio Grande and Canadian River. A Follow-up on Tree-Ring-Based Streamflow Reconstructions for the Rio Grande Basin Workshop. NMSU Extension, Albuquerque, New Mexico. May 20, 2008.

Meko, D. M., C.A. Woodhouse, and R. Touchan, (2014). Klamath/San Joaquin/Sacramento hydroclimatic reconstructions from tree rings. Draft Final Report to the California Department of Water Resources, University of Arizona: Tucson, Arizona. 117 p.

Mendoza, P.A., M.P Clark, N. Mizukami, A. Newman, M. Barlage, E. Gutmann, R.M Rasmussen, B. Rajagopalan, L. Brekke, J.R Arnold, (2015). Effects of hydrologic model choice and calibration on the portrayal of climate change impacts. Journal of Hydrometeorology, 16(2):762–780, doi:10.1175/JHM-D-14-0104.1.

Mendoza, P.A., M.P. Clark, N. Mizukami, E.D. Gutmann, J.R. Arnold, L.D. Brekke, and B. Rajagopalan, (2016). How do hydrologic modeling decisions affect the portrayal of climate change impacts? Hydrological Processes, 30(7):1071–1095, doi:10.1002/hyp.10684.

Milesi, C., S.W. Running, C.D. Elvidge, J.B. Dietz, B.T. Tuttle, and R.R Nemani, (2005). Mapping and modeling the biogeochemical cycling of turf grasses in the United States. Environmental Management, 36(3):426–438, doi:10.1007/s00267-004-0316-2.

Miller, W.P., R.A. Butler, T. Piechota, J. Prairie, K. Grantz, and G. DeRosa, (2012). Water management decisions using multiple hydrologic models within the San Juan River basin under changing climate conditions. Journal of Water Resources Planning and Management,138:412–420, doi:10.1061/(ASCE)WR.1943-5452.0000237.

Miller, M.P., D.D. Susong, C.L. Shope, V.M. Heilweil, and B.J. Stolp, (2014). Continuous estimation of baseflow in snowmelt-dominated streams and rivers in the Upper Colorado River Basin: A chemical hydrograph separation approach. Water Resources Research, 50:6986–6999, doi:10.1002/2013WR014939.

Miller, M.P., S.G. Buto, D.D. Susong, and C.A. Rumsey, (2016). The importance of base flow in sustaining surface water flow in the Upper Colorado River Basin. Water Resources Research, 52(5):3547–3562.

Miller, M.P., D.K. Jones, L.A. Bearup, J.R. Alder, O.L. Miller, and C. Rumsey, (2019). Forecasting the changing importance of baseflow in sustaining streamflow in the Upper Colorado River Basin, Present-2080. AGUFM Abstract, H33M-2145.

Milly, P.C.D. and K.A. Dunne, (2011). On the hydrologic adjustment of climate-model projections: The potential pitfall of potential evapotranspiration. Earth Interactions, 15:1–14, doi:10.1175/2010EI363.1.

Milly, P.C.D, J. Betancourt, M. Falkenmark, R.M. Hirsch, Z.W. Kundzewicz, D.P. Lettenmaier, and R.J. Stouffer, (2008). Stationarity Is Dead: Whither Water Management? Science, 319:573–574, doi:10.1126/science.1151915.

Mitchell, K.E., D. Lohmann, P.R. Houser, E.F. Wood, J.C. Schaake, A. Robock, and A.A. Bailey, (2004). The multi-institution North American Land Data Assimilation System (NLDAS): Utilizing multiple GCIP products and partners in a continental distributed hydrological modeling system. Journal of Geophysical Research–Atmospheres 109(D7):1984–2012.

Mizukami N., M.P. Clark, K. Sampson, B. Nijssen, Y. Mao, H. McMillan, R.J. Viger, S.L. Markstrom, L.E. Hay, R. Woods, J.R. Arnold, and L.D. Brekke, (2016). Mizu Route version 1: A river network routing tool for a continental domain water resources applications. Geoscientific Model Development, 9:2223–2238, doi:10.5194/gmd-9-2223-2016.

Mizukami, N., M.P. Clark, A.J. Newman, A.W. Wood, E.D. Gutmann, B. Nijssen, O. Rakovec, and L. Samaniego, (2017). Towards seamless large-domain parameter estimation for hydrologic models, Water Resources Research, 53:8020–8040, doi:10.1002/2017WR020401.

Montana Department of Natural Resources and Conservation (Montana DNRC), (2015). The Montana State Water Plan 2015. 64 p.

Morton, F.I., F. Ricard, and S. Fogarasi, (1985). Operational estimates of areal evapotranspiration and lake evaporation. Program WREVAP, Pap. 24, 75 p. Natl. Hydrol. Res. Inst. Ottawa, Ontario, Canada.

Moss, R.H., J.A. Edmonds, K.A. Hibbard, M.R. Manning, S.K. Rose, D.P. Van Vuuren, T.R. Carter, S. Emori, M. Kainuma, T. Kram, and G.A. Meehl, (2010). The next generation of scenarios for climate change research and assessment. Nature, 463(7282):747–756, doi:10.1038/nature08823.

Mote, P., L. Brekke, P.B. Duffy, and E. Maurer, (2011). Guidelines for constructing climate scenarios. Eos, Transactions American Geophysical Union, 92:257–258.

National Institute of Standards and Technology (NIST), (2012). Engineering Statistics Handbook, doi:10.18434/M32189.

National Marine Fisheries Service and U.S. Fish and Wildlife Service (NMFS and USFWS), (2013). Biological Opinions on the Effects of Proposed Klamath Project Operations from May 31, 2013, through March 31, 2023, on Five Federally Listed Threatened and Endangered Species. Southwest Region. May 2013.

Nijssen, B.N., D.P. Lettenmaier, X. Liang, S.W. Wetzel, and E.F. Wood, (1997). Streamflow simulation for continental-scale river basins. Water Resources Research, 33(4):711–724, doi:10.1029/96WR03517.

Niswonger, R.G., S. Panday, and M. Ibaraki, (2011). MODFLOW-NWT, A Newton formulation for MODFLOW-2005: U.S. Geological Survey Techniques and Methods, book 6, ch, 44. No. 68-68210-2014-01. February 2015. 222 p.

Nowak, K., J. Prairie, B. Rajagopalan, and U. Lall, (2010). A nonparametric stochastic approach for multisite disaggregation of annual to daily streamflow. Water Resources Research, 46(8):W08529, doi:10.1029/2009WR008530.

O'Hagan, T., (2004). Dicing with the unknown. Significance, 1(3):132–133, doi:10.1111/j.1740-9713.2004.00050.x.

Palmer, W.C., (1965). Meteorological drought. Research Paper No. 45. U.S. Weather Bureau. NOAA Library and Information Services Division. Washington, D.C. Available at: https://www.ncdc.noaa.gov/temp-and-precip/drought/docs/palmer.pdf (last accessed October 16, 2020)

Pierce, D.W., D.R. Cayan, and B.L. Thrasher, (2014). Statistical downscaling using localized constructed analogs (LOCA). Journal of Hydrometeorology, 15(6):2558–2585, doi:10.1175/JHM-D-14-0082.1.

Pierce, D.W., D.R. Cayan, E.P. Maurer, J.T. Abatzoglou, and K.C. Hegewisch, (2015). Improved Bias Correction Techniques for Hydrological Simulations of Climate Change. Journal of Hydrometeorology, 16(6):2421–2442, doi:10.1175/JHM-D-14-0236.1.

Pierce, D.W., J.F. Kalansky, and D.R. Cayan, (Scripps Institution of Oceanography), (2018). Climate, Drought, and Sea Level Rise Scenarios for the Fourth California Climate Assessment. California's Fourth Climate Change Assessment, California Energy Commission. Publication Number: CNRA-CEC-2018-006, 78 p. Available at: https://www.energy.ca.gov/sites/default/files/2019-11/Projections_CCCA4-CEC-2018-006_ADA.pdf (last accessed October 26, 2020)

Prairie, J., K. Nowak, B. Rajagopalan, U. Lall, and T. Fulp, (2008). A stochastic nonparametric approach for streamflow generation combining observational and paleoreconstructed data. Water Resources Research, 44(6):W06423, doi:10.1029/2007WR006684.

R Core Team, (2019). R: A language and environment for statistical computing. R Foundation for Statistical Computing. Vienna, Austria. Available at: https://www.R-project.org/ (last accessed October 16, 2020)

Rajagopalan, B., S.T. Erkyihun, U. Lall, E. Zagona, and K. Nowak, (2019). A nonlinear dynamical systems-based modeling approach for stochastic simulation of streamflow and understanding predictability. Water Resources Research, 55(7):6268–6284.

Rasmussen, R., K. Ikeda, C.H. Liu, D. Gochis, M.P. Clark, A. Dai, E. Gutmann, J. Dudhia, F. Chen, M. Barlage, D. Yates, and G. Zhang, (2014). Climate change impacts on the water balance of the Colorado headwaters: High-resolution regional climate model simulations. Journal of Hydrometeorology, 15(3):1091–1116, doi:10.1175/JHM-D-13-0118.1.

Ravindranath, A., N. Devineni, U. Lall, E.R. Cook, G. Pederson, J. Martin, and C. Woodhouse, (2019). Streamflow reconstruction in the upper Missouri River basin using a novel Bayesian network model. Water Resources Research, 55(9):7694–7716, doi:10.1029/2019WR024901.

Reclamation (Bureau of Reclamation), (2007). Colorado River Interim Guidelines for Lower Basin Shortages and Coordinated Operations for Lake Powell and Lake Mead. U.S. Department of the Interior, Bureau of Reclamation. Available at: https://www.usbr.gov/lc/region/programs/strategies/FEIS/index.html (last accessed October 26, 2020)

——— (2008). Truckee River Operating Agreement and Related Documents. Available at: https://www.usbr.gov/mp/troa/ (last accessed October 27, 2020)

——— (2011a). Reclamation, SECURE Water Act Section 9503(c)—Reclamation Climate Change and Water, Report to Congress, 2011. Policy and Administration, Denver, Colorado, 206 p.

——— (2011b). West-Wide Climate Risk Assessments: Bias-Corrected and Spatially Downscaled Surface Water Projections. Technical Memorandum No. 86-68210-2011-01, Technical Service Center, Denver, Colorado, 138 p.

——— (2012a). Missouri River Basin Depletions Database. U.S. Department of the Interior, Bureau of Reclamation, Great Plains Region, Billings, Montana. September 2012. 97 p.

_____ (2012b). Colorado River Basin Water Supply and Demand Study: Executive Summary. U.S. Department of the Interior, Bureau of Reclamation. Available at: https://www.usbr.gov/watersmart/bsp/docs/finalreport/ColoradoRiver/CRBS_Executive_Summary_FINAL.pdf (last accessed October 16, 2020)

_____ (2012c). St. Mary River and Milk River Basins Study Technical Report. U.S. Department of the Interior, Bureau of Reclamation, Milk River Project, Montana, Great Plains Region, Billings, Montana.

_____ (2014). West-Wide Climate Risk Assessment: Sacramento and San Joaquin Basins Climate Impact Assessment. U.S. Department of the Interior, Bureau of Reclamation. Available at: https://www.usbr.gov/watersmart/baseline/docs/ssjbia/ssjbia.pdf (last accessed October 16, 2020)

_____ (2015a). West-Wide Climate Risk Assessments: Irrigation Demand and Reservoir Evaporation Projections. Technical Memorandum. Technical Memorandum No. 86-68210-2014-01. U.S. Department of the Interior, Bureau of Reclamation, Technical Services Center, Denver, Colorado.

_____ (2015b). Colorado River Basin Stakeholders Moving Forward to Address Challenges Identified in the Colorado River Basin Water Supply and Demand Study – Phase 1 Report: Executive Summary. U.S. Department of the Interior, Bureau of Reclamation. Available at: https://www.usbr.gov/lc/region/programs/crbstudy/MovingForward/Phase1Report/ExecSumm.pdf (last accessed March 1, 2021)

_____ (2016a). Klamath River Basin Study. Technical Memorandum 86-68210-2016-06. U.S. Department of the Interior, Bureau of Reclamation. Available at: https://www.usbr.gov/watersmart/bsp/docs/klamath/fullreport.pdf (last accessed October 16, 2020)

_____ (2016b). Sacramento and San Joaquin Basins Study, Report to Congress 2015. Prepared for: U.S. Department of the Interior, Bureau of Reclamation, Mid-Pacific Region, Sacramento, California. Available at: https://www.usbr.gov/watersmart/bsp/docs/finalreport/sacramento-sj/Sacramento_SanJoaquin_TechnicalReport.pdf (last accessed October 16, 2020)

_____ (2016c). West-Wide Climate Risk Assessments: Hydroclimate Projections. Technical Memorandum No. 86-68210-2016-01, Technical Service Center, Denver, Colorado, 140 p.

_____ (2016d). SECURE Water Act Section 9503(c) – Reclamation Climate Change and Water 2016. Policy and Administration, Denver, Colorado.

_____ (2018). Upper Missouri Basin Impacts Assessment. Summary Report. U.S. Department of the Interior, Bureau of Reclamation, Technical Services Center, Denver, Colorado.

_____ (2019). Risk and Reliability Assessment for the Upper Missouri River Basin Impacts Assessment. Technical Memorandum No. 86-68210-2018-01. U.S. Department of the Interior, Bureau of Reclamation.

_____ (2020a). Eloy-Maricopa Stanfield Basin Study: The development of future climate and recharge scenarios. Report No. ENV-2020-064. U.S. Department of the Interior, Bureau of Reclamation, Technical Service Center, Denver, Colorado.

_____ (2020b). Record of Decision. Reinitiation of Consultation on the Coordinated Long-Term Modified Operations of the Central Valley Project and State Water Project. U.S. Department of the Interior, Bureau of Reclamation. Interior Region 10, California-Great Basin. February 19, 2020.

_____ (2020c). Missouri Headwaters Basin Study. Report No. ENV-2020-081. U.S. Department of the Interior, Bureau of Reclamation, Technical Service Center, Denver, Colorado.

_____ (2020d). Upper Snake RiverWare Model: Model Documentation. U.S. Department of the Interior, Bureau of Reclamation, Columbia-Pacific Northwest Region, Boise, Idaho. May 2020 Draft.

Reclamation and U.S. Geological Survey (2020a). Salinas and Carmel Rivers Basin Study: development of future climate and sea level scenarios. U.S. Department of the Interior, Bureau of Reclamation and U.S. Geological Survey. Technical Memorandum No. 2. July 23, 2019.

_____ (2020b). Salinas and Carmel Rivers Basin Study: Modeling tools overview. U.S. Department of the Interior, Bureau of Reclamation and U.S. Geological Survey. Technical Memorandum No. 4. July 2019.

Rice, J., C. Woodhouse, and J. Lukas, (2009). Science and decision-making: Water management and tree-ring data in the western United States. Journal of the American Water Resources Association, 45(5):1248–1259.

Richardson, M., K. Cowtan, E. Hawkins, and M.B. Stolpe, (2016). Reconciled climate response estimates from climate models and the energy budget of Earth. Nature Climate Change, 6(10):931–935, doi:10.1038/nclimate3066.

RMJOC (River Management Joint Operating Committee), (2018). Climate and Hydrology Datasets for RMJOC Long-Term Planning Studies: Second Edition (RMJOC-II), Part I: Hydroclimate Projections and Analyses. Portland, Oregon: River Management Joint Operating Committee. Available at: https://www.bpa.gov/p/Generation/Hydro/hydro/cc/RMJOC-II-Report-Part-I.pdf (last accessed February 7, 2021)

Salehabadi, H., D. Tarboton, E. Kuhn, B. Udall, K. Wheeler, D. Rosenberg, S. Goeking, J.C. Schmidt, (2020). The future hydrology of the Colorado River Basin. The Future of the Colorado River Project, Center for Colorado River Studies, Quinney College of Natural Resources, Utah State University. White Paper No. 4.

Samaniego, L., R. Kumar, and S. Attinger, (2010). Multiscale parameter regionalization of a grid-based hydrologic model at the mesoscale. Water Resources Research, 46:W05523, doi:10.1029/2008WR007327.

Santer, B.D., S. Solomon, G. Pallotta, C. Mears, S. Po-Chedley, Q. Fu, F. Wentz, C.-Z. Zou, J. Painter, I. Cvijanovic , and C. Bonfils, (2017). Comparing tropospheric warming in climate models and satellite data. Journal of Climate, 30(1):373–392, doi:10.1175/JCLI-D-16-0333.1.

Schewe, J., and Coauthors, (2014). Multimodel assessment of water scarcity under climate change. Proceedings of the National Academy of Sciences of the United States of America, 111(9):3245–3250, doi:10.1073/pnas.1222460110.

Seaber, P.R., F.P. Kapinos, and G.L. Knapp, (1987). Hydrologic Unit Maps: U.S. Geological Survey Water-Supply Paper 2294, 63 p.

Sheffield, J., E. Wood, and M. Roderick, (2012). Little change in global drought over the past 60 years. Nature, 491:435–438, doi:10.1038/nature11575.

Shiau, J.T., (2006). Fitting drought duration and severity with two-dimensional copulas. Water Resources Management, 20:795–815, doi:10.1007/s11269-005-9008-9.

Stokes M.A. and T.L. Smiley, (1968). An introduction to tree-ring dating. University of Chicago Press. Chicago, Illinois.

Stoner, A.M.K., K. Hayhoe, X. Yang, and D. J. Wuebbles, (2013). An asynchronous regional regression model for statistical downscaling of daily climate variables. International Journal of Climatology, 33(11):2473–2494, doi:10.1002/joc.3603.

Taylor, K.E., R.J. Stouffer, and G.A. Meehl, (2012). An overview of CMIP5 and the experiment design. Bulletin of the American Meteorological Society, 93:485–498, doi:10.1175/BAMS-D-11-00094.1.

Taylor, R.G., B. Scanlon, P. Döll, M. Rodell, R. van Beek, Y. Wada,L. Longuevergne, M. Leblanc, J.S. Famiglietti, M. Edmunds, L. Konikow, T.R. Green, J. Chen, M. Taniguchi, M.F. Bierkens, A. MacDonald, Y. Fan, R.M. Maxwell, Y. Yechieli, J.J. Gurdak, D.M. Allen, M. Shamsudduha, K. Hiscock, P.J. Yeh, I. Holman, and H. Treidel, (2013). Ground water and climate change. Nature Climate Change, 3:322–329, doi:10.1038/nclimate1744.

Tebaldi, C., J.M. Arblaster, and R. Knutti, (2011). Mapping model agreement on future climate projections. Geophysical Research Letters, 38:L23701, doi:10.1029/2011GL049863.

Teutschbein, C., and J. Seibert, (2012). Bias correction of regional climate model simulations for hydrological climate-change impact studies: Review and evaluation of different methods. Journal of Hydrology, 456:12–29, doi:10.1016/j.jhydrol.2012.05.052.

Thomas, N., (2018). Cal-Adapt: Linking climate science with practitioner need. UC Berkeley's Geospatial Innovation Facility, Webinar. Available at: https://www.climateassessment.ca.gov/events/docs/20181206-Slides_Thomas_Cal-Adapt.pdf (last accessed October 26, 2020)

Tillman, F.D., S. Gangopadhyay, and T. Pruitt, (2016a). Changes in groundwater recharge under projected climate in the Upper Colorado River Basin. Geophysical Research Letters, 43, doi:10.1002/2016GL069714.

——— (2016b). Understanding the past to interpret the future: comparison of simulated groundwater recharge in the Upper Colorado River Basin (USA) using observed and general-circulation-model historical climate data. Hydrogeology Journal, 25(2):347–358, doi:10.1007/s10040-016-1481-0.

_____ (2017). Changes in projected spatial and seasonal groundwater recharge in the Upper Colorado River Basin. Groundwater, 55(4):506–518, doi:10.1111/gwat.12507.

_____ (2018). Effect of spatial and temporal scale on simulated groundwater recharge investigations. Advances in Water Resources, 119:257–270, doi:10.1016/j.advwatres.2018.07.014.

_____ (2020). Trends in recent historical and projected climate data for the Colorado River Basin and potential effects on groundwater availability. U.S. Geological Survey Scientific Investigations Report, 2020–5107, 24 p., doi:10.3133/sir20205107.

Trenberth, K., (2011). Changes in precipitation with climate change. Climate Research, 47, 123–138, doi:10.3354/cr00953.

U.S. Census Bureau, (2010). Cenpop2010. Available at: https://www2.census.gov/geo/docs/reference/ua/ua_st_list_all.txt (last accessed October 27, 2020)

U.S. Department of Agriculture (USDA)–Natural Resources Conservation Service (NRCS), (1998). Soil Quality Resource Concerns: Available Water Capacity. Soil Quality Information Sheet, 2 p. Available at: https://www.nrcs.usda.gov/Internet/FSE_DOCUMENTS/nrcs142p2_051279.pdf (last accessed October 27, 2020)

U.S. Department of the Interior and California Department of Fish and Game, (2011). Klamath Facilities Removal Public Draft Environmental Impact Statement/Environmental Impact Report. State Clearinghouse No. 2010062060.

U.S. Global Change Research Program (USGCRP), (2018). Impacts, risks, and adaptation in the United States: Fourth National Climate Assessment, Volume II [Reidmiller, D.R., C.W. Avery, D.R. Easterling, K.E. Kunkel, K.L.M. Lewis, T.K. Maycock, and B.C. Stewart (eds.)]. U.S. Global Change Research Program, Washington, DC, USA. 1515 p., doi:10.7930/NCA4.2018.

Vano, J.A., B. Udall, D.R. Cayan, J.T. Overpeck, L.D. Brekke, T. Das, H.C. Hartmann, H.G. Hidalgo, M. Hoerling, and G.J. McCabe, (2014). Understanding uncertainties in future Colorado River streamflow. Bulletin of the American Meteorological Society, 95(1):59–78, doi:10.1175/BAMS-D-12-00228.1.

Vano, J., J. Hamman, E. Gutmann, A. Wood, N. Mizukami, M. Clark, D.W. Pierce, D.R. Cayan, C. Wobus, K. Nowak, and J. Arnold, (2020). Comparing downscaled LOCA and BCSD CMIP5 climate and hydrology projections – Release of downscaled LOCA CMIP5 hydrology, 96 p.

Venables, W.N. and B.D. Ripley, (2002). Modern applied statistics with S. Fourth edition. Springer.

Viger, R.J., (2014). Preliminary spatial parameters for PRMS based on the Geospatial Fabric, NLCD2001 and SSURGO. US Geological Survey, doi:10.5066/F7WM1BF7.

Webb, R., C.E. Rosenzweig, and E.R. Levine, (2000). Global soil texture and derived water-holding capacities. ORNL DAAC. Oak Ridge, Tennessee, doi:10.3334/ORNLDAAC/548.

Wells, N., (2003). PDSI User's Manual–Version 2.0, 17 p. Available at: https://greenleaf.unl.edu/downloads/scPDSI_Manual.pdf (last accessed October 27, 2020)

Wilby, R.L., (2005). Uncertainty in water resource model parameters used for climate change impact assessment. Hydrological Processes, 19:3201–3219.

Wilby, R.L. and I. Harris, (2006). A framework for assessing uncertainties in climate change impacts: Low-flow scenarios for the River Thames, UK. Water Resources Research, 42:W02419, doi:10.1029/2005WR004065.

Wilby, R.L., C.W. Dawson, C. Murphy, P. O'Connor, and E. Hawkins, (2014). The statistical downscaling model–decision centric (SDSM-DC): conceptual basis and applications. Climate Research, 61:259–276, doi:10.3354/cr01254.

Wise, E.K., (2010). Tree ring record of streamflow and drought in the upper Snake River. Water Resources Research, 46:W11529, doi:10.1029/2010WR009282.

Wood, A.W., L.R. Leung, V. Sridhar, and D. Lettenmaier, (2004). Hydrologic implications of dynamical and statistical approaches to downscaling climate model outputs. Climatic Change, 62:189–216.

Woodhouse, C.A., (2001). A tree-ring reconstruction of streamflow for the Colorado Front Range. Journal of the American Water Resources Association, 37(3):561–569.

Woodhouse, C.A., S.T. Gray, and D.M. Meko, (2006). Updated streamflow reconstructions for the Upper Colorado River Basin. Water Resources Research, 42:W05415.

Woodhouse, C.A., D.M. Meko, G.M. MacDonald, D.W. Stahle, and E.R. Cook, (2010). A 1,200-year perspective of 21st century drought in southwestern North America. Proceedings of the National Academy of Sciences of the United States of America, 107(50):21283–21288.

Woodhouse, C.A., (2010). Dendrochronological Reconstruction of the Arkansas River at Salida, Report to Colorado Spring Utilities, Colorado Spring, Colorado. September 6, 2010.

Woodhouse, C.A., G.T. Pederson, and S.T. Gray, (2011). An 1800-year record of decadal-scale hydroclimatic variability in the Upper Arkansas River basin from bristlecone pine. Quaternary Research. 75:483–490, doi:10.1016/j.yqres.2010.12.007.

Woodhouse, C.A. and J.J. Lukas, (2006). Multi-century tree-ring reconstructions of Colorado streamflow for water resource planning. Climatic Change 78:293–315.

Woodhouse, C.A., D.W. Stahle, and J. Villanueva-D'az, (2012). Rio Grande and Rio Conchos water supply variability from instrumental and paleoclimatic records. Climate Research, 51:125–136, doi:10.3354/cr01059.

Ye, W., B.C. Bates, N.R. Viney, and M. Sivapalan, (1997). Performance of conceptual rainfall-runoff models in low-yielding ephemeral catchments. Water Resources Research, 33(1):153–166.

Yeager, S.G., G. Danabasoglu, N.A. Rosenbloom, W. Strand, S.C. Bates, G.A. Meehl, and N.S. Lovenduski, (2018). Predicting near-term changes in the Earth System: A large ensemble of initialized decadal prediction simulations using the Community Earth System Model. Bulletin of the American Meteorological Society, 99(9):1867–1886.

Zagona, E.A., T.J. Fulp, R. Shane, T. Magee, and H.M. Goranflo, (2001). Riverware: A generalized tool for complex reservoir system modeling. Journal of the American Water Resources Association, 37(4):913–929, doi:10.1111/j.1752-1688.2001.tb05522.x.